Reanalysis of the Settlement of a Levee on Soft Bay Mud

By

Hoang Q. Nguyen

B.S. Civil Engineering (2002)
University of Civil Engineering, Hanoi, Vietnam

Submitted to the Department of Civil and Environmental Engineering in Partial Fulfillment of the Requirements for the Degree of

Master of Science in Civil and Environmental Engineering
at the
Massachusetts Institute of Technology

February 2007

Signature of Author _____

Department of Civil and Environmental Engineering
September 14, 2006

Certified by _____

Andrew J. Whittle
Professor of Civil and Environmental Engineering
Thesis Supervisor

_____

Charles C. Ladd
Edmund K. Turner Professor of Civil and Environmental Engineering, Emeritus
Thesis Co-supervisor

Accepted by _____

Andrew J. Whittle
Chairman, Departmental Committee for Graduate Students

Reanalysis of the Settlement of a Levee on Soft Bay Mud

By
Hoang Q. Nguyen

Submitted to the Department of Civil and Environmental Engineering on September 14, 2006 in partial fulfillment of the requirements for the degree of Master of Science in Civil and Environmental Engineering

Abstract

Staged construction of embankments on soft ground remains one of the most challenging topics in geotechnical engineering due to the complex shear and consolidation behavior of clays. This thesis presents a case study on the performance of the New Hamilton Partnership (NHP) levee in Novato, California. This 11ft high levee was constructed over 30 ft – 40 ft thick layer of San Francisco Bay Mud during a six-month period in 1996. Settlements along the levee crest were monitored over a period of 5.2 years after the end of construction (until early 2002), at which time URS installed piezometers to measure the existing consolidation stresses (σ'_{vc}) within the Bay Mud. URS also conducted state-of-the art field and laboratory test programs to develop well-defined values of preconsolidation stress (σ'_{p}) and compressibility parameters for the Bay Mud. However, conventional 1-D consolidation analyses greatly underestimated the measured levee settlements. Hence URS reduced σ'_{p} by 20% for the Plaxis FE analyses with the Soft Soil Model (SSM) used to replicate the performance of the existing NHP levee and then to design an expanded levee system.

This thesis presents a detailed re-evaluation of the NHP levee performance and of the stress history, strength, and consolidation properties of the Bay Mud obtained during the URS geotechnical site investigation. New conventional 1-D consolidation analyses with higher values of the recompression ratio and revised profiles of σ'_{vc} indicate that the measured levee settlements at 5.2 years can be matched when σ'_{p} is reduced by 10% to 15%. The thesis also presents two series of Plaxis analyses with the Soft Soil Model. The first evaluated SSM parameters to better model results from the laboratory consolidation and K_0-consolidated undrained shear tests on the Bay Mud. The second series conducted 2-D FE analyses to identify the most important variables effecting the predicted performance of the levee during and after construction. These parametric analyses show that the measured settlements during the 5.2 year period and the excess pore pressures measured in early 2002 can be consistently described only after careful definition of four major variables: the recompression ratio, RR, the normally consolidated coefficient of consolidation, c_v(NC), and the preconsolidation stress, σ'_{p}, of the Bay Mud; and the boundary drainage conditions. The measured performance is best matched by using values of c_v(NC) and σ'_{p} that are less than measured by the laboratory CRSC tests.

Analyses with more sophisticated soil models are needed before definitive conclusions can be reached regarding the in situ properties of the Bay Mud and whether no not secondary compression (creep) plays an important role during primary consolidation (i.e., Hypothesis A versus Hypothesis B).

Thesis Supervisor: **Dr. Andrew J. Whittle**
Title: Professor of Civil and Environmental Engineering
Thesis Co-supervisor: **Dr. Charles C. Ladd**
Title: Edmund K. Turner Professor of Civil and Environmental Engineering, Emeritus

ACKNOWLEDGMENTS

I am very thankful to have had the opportunity to work with Professor Andrew J. Whittle and Professor Charles C. Ladd at MIT. This thesis would not have been possible without their helps.

I gratefully acknowledge and thank Professor Whittle for giving me a great opportunity to do research in soil modeling. Under his supervision, I have learned many things in theoretical soil mechanics and soil modeling. I am indebted to him for all the knowledge he has taught me both in classes and in our research, and especially his contributions throughout my research and writing this thesis.

I gratefully acknowledge and thank Professor Ladd for his tremendous contributions, support, and thorough guidance on my work. My experiences with him changed the way I look at myself and the way I work as a geotechnical engineer. He has given me "uncountable" many long hours guiding my research, reviewing and correcting the thesis. It was truly the "most difficult and the most fulfilling experience" (Germaine et. al., 2003) in my career.

I would like to thank Dr. John Germaine for providing me with all the results of MIT laboratory tests on San Francisco Bay Mud, for spending many hours of invaluable discussions of the test results. It has been always joyful asking him questions. I am very thankful to have his encouragement, and inspiration to my study.

I also have to thank my professors from Vietnam, especially Dr. Vu C. Ngu, Dr. Nguyen A. Dung, Dr. Vo Q. Bao and Dr. Le Nguyen M. Quang for all of their supports in my professional development.

I am very much indebted to the Vietnam Education Foundation for awarding me the fellowship to study at MIT. This thesis is not big enough to contain all the reasons that I have to be thankful to the VEF.

I want to thank all my colleagues and friends at MIT for all the love, support, and help in my research throughout these years: Matt Chattier, Maria - Katerina Nikolinakou, Vytiniotis Antonios , Prasad Anamika, Abdulhadi Naeem, Rita Sousa, Constantinos Tsoucalas, Agarwal Anna, Pei Jianyong, Dung T. Nguyen, Vinh X. Doan, and Son T. Nguyen.

I am forever indebted to my parents, my brothers, and his family (Phi-Ngoc-Anh). They have given me all their love, support, and hope in every single step of my life, that I could never repay them back.

Of course, I am truly indebted to my wife, Hai Anh, for keeping me strong all the time, and for constantly believing in me. I could not have made it without her. Not only did she generally care and scarify for me in everyday life, but also, my writing the thesis got her busy helping me out with a lot of editing work. She has really contributed a great part of work on this thesis. I am very thankful and very proud of marrying a PhD candidate in environmental engineering, who can share so many things in life, such as our engineering professionals. I also appreciate the love and support given by my sister and parents-in-law throughout the years.

Nguyen Q. Hoang (BA)

Dedication to my wife and my family

BA

TABLE OF CONTENTS

Abstract **3**

Acknowledgments **5**

Index of Tables **11**

Index of Figures **14**

Glossary **23**

CHAPTER 1 INTRODUCTION **28**

1.1 Settlement of Embankments on Soft Ground 28

1.2 Hypothesis A vs. Hypothesis B 32

1.3 New Hamilton Partnership Levee (NHPL) Project 35

1.4 Objectives and Scope of Thesis 38

CHAPTER 2 PRIOR GEOTECHNICAL STUDIES OF THE NHPL EMBANKMENT ... 45

2.1 Introduction 45

2.2 URS Field and Laboratory Test Programs 46

2.2.1 Field Test Program 46

2.2.2 Laboratory Test Program 49

2.2.3 Unit Weight of Fill and Natural Soils 50

2.3 Measured Settlement of NHPL 51

2.4 Stress History of Bay Mud 53

2.4.1 Virgin Ground (Free Field) 53

2.4.2 Beneath NHP Levee 54

2.5 Consolidation Properties of Bay Mud 55

2.5.1 Virgin Compressibility, CR 55

2.5.2 Recompression 56

2.5.3 Coefficient of Consolidation (NC) 56
2.5.4 Coefficient of Permeability 57
2.6 Undrained Strength Properties of Bay Mud 57
2.6.1 Overview of MIT CK_0U Test Program 57
2.6.2 CK_0UDSS 58
2.6.3 CK_0UTX 58
2.7 Settlement Analyses by URS 59
2.7.1 Methodology 59
2.7.2 Analyses at TS3, TS5 and Other Locations 60
2.8 Discussion 63
CHAPTER 3 REANALYSIS OF THE CONSOLIDATION AND DEFORMATION BEHAVIOR OF THE NHP LEVEE 89
3.1 Introduction 89
3.2 Reexamination on Soil Properties for Bay Mud 90
3.2.1 Soil Profile and Stress History for Reanalysis 91
3.2.2 Index, Permeability and Compressibility Properties of Bay Mud 96
Index properties 96
Hydraulic Conductivity 97
Compressibility properties 98
Recompression Ratio from Normalized CRSC Stress-Strain Plots 99
3.2.3 Coefficient of Consolidation – C_v(NC) 102
3.2.4 Coefficient of Earth Pressure at Rest, Ko 103
3.2.5 Strength Properties 103

3.3 Conventional 1-D Consolidation Settlement Analysis 105

3.3.1 Final Consolidation Stress, σ'_{vf} 105

3.3.2 Measured Excess Pore Pressure at TS3 and TS5 on Feb-Mar, 2002 108

3.3.3 Consolidation Stress Profiles, σ'_{vc} at TS3 and TS5 109

3.3.4 Stress History Profiles for 1-D Settlement Calculation 110

3.3.5 One-Dimensional Consolidation Settlement Calculations with Varying Preconsolidation Stress Profiles 111

3.3.6 1-D Final Consolidation Settlements, ρ_{cf} Computed for SH2 113

3.3.7 Summary and Conclusions 113

3.4 Element Analysis on Bay Mud with PLAXIS Soft Soil Model 116

3.4.1 Summary of SSM 116

3.4.2 One-Dimensional Consolidation 119

3.4.3 CKoU PSC/E Tests Simulation 121

3.4.4 CK_0PS-DSS Tests Simulation 122

3.4.5 Summary and Conclusions 124

3.5 NHPL Reanalysis Using Soft Soil Model in Finite Element Code PLAXIS 126

3.5.1 Geometry and Mesh of NHPL Model 126

3.5.2 Defined Cases for FE Analyses of the NHPL 127

3.5.3 Selection of Material Parameters for FE Plaxis Analyses 129

3.5.4 Simulation and Calculation Procedures 129

3.5.5 Results from Cases A1 and A2 131

3.5.6 Results from Case B Compared to Case A2 135

3.5.7 Results from Cases C1, C2, and C3 Compared to Case A2 136

3.5.8 Results from Cases D1 and D2 Compared to Case A2 and URS (2003) 137

3.5.9 Results from Case D3 Analysis and Comparison with Cases A1, C1 and D2 140

3.5.10 Results from Case D4 Analysis 141

3.5.11 Discussion on Computed Arching Effects during Consolidation 142

3.5.12 Summary and Conclusions 143

CHAPTER 4 SUMMARY, CONCLUSIONS AND RECOMMENDATIONS 249

4.1 Summary and Conclusions 249

4.1.1 Overview of Project 250

4.1.2 URS Site Characterization and Settlement Analyses 251

4.1.3 Hypothesis A versus Hypothesis B 253

4.1.4 Reanalysis of One-Dimensional (1-D) Consolidation Settlements 254

4.1.5 Simulated Bay Mud Behavior in Plaxis SSM 256

4.1.6 Two-Dimensional (2-D) Finite Element Analyses 257

4.2 Recommendations for Further Research 260

CHAPTER 5 REFERENCES 261

CHAPTER 6 APPENDIXES 265

6.1 Appendix A: MIT Laboratory Tests on Bay Mud 265

6.1.1 CRSC Tests on Bay Mud at TS3-B1(From Germaine, 2002) 265

6.1.2 CK_0U-DSS Tests at OCR =1, 2, & 3 on Bay Mud (From Germaine, 2002 & 2004) 298

6.1.3 CK_0UTC/TE tests on Bay Mud at OCR =1 (From Germaine, 2002) 318

6.2 Appendix B: 1-D Consolidation Settlement Calculation 334

6.3 Appendix C: NHPL Plaxis Analysis Control Parameters 344

6.4 Appendix D: Author's Replication of URS (2003) Plaxis Analysis of NHPL 357

INDEX OF TABLES

Table 2.1 Summary of Field Tests – Geotechnical Exploration and Measurements for NHP Levee 66

Table 2.2 Laboratory Testing on Bay Mud for NHP Levee 67

Table 2.3 Summary of Index Tests on Levee Fill and Natural Soils (From URS 2003) 68

Table 3.1 Summary of Laboratory CRSC Tests on Virgin Ground at TS3-B1 (Free Field Condition) 146

Table 3.2 Summary of Field Vane Shear Test Results at Virgin Ground Condition 147

Table 3.3a Summary of Recompression Ratio Evaluation 148

Table 3.3b Selected RR for 1-D Analysis 148

Table 3.4 NC Coefficient of Consolidation of Bay Mud 149

Table 3.5a Summary of Undrained Strength Ratio of Bay Mud from DSS Tests 150

at NHP, N1 and N2 Levees 150

Table 3.5b Summary of Direct Simple Shear Results for NHPL BAY MUD 150

Table 3.6 Summary of Triaxial Tests on Bay Mud from NHP Levee 151

Table 3.7a Selected Values of Parameters for Computing σ'_{vf} Using PLAXIS - **CASE A**: Stiff and Uncracked, Continuous Pavement and Stiff Crust 152

[Properties other than Bay Mud = Table 4.1 URS/ARUP Test Fill (2005)] 152

Table 3.7b Properties of Soils Used in σ'_{vf} Analyses for **CASE B**: Stiff Cracked Pavement and Stiff Crust 153

Table 3.7c Properties of Soils Used in σ'_{vf} Analyses for **CASE C**: Weaker Cracked Pavement and Crust 154

Table 3.7d Selected Undrained Shear Strength and Young's Modulus for Bay Mud for σ'_{vf} Calculation 155

Table 3.8a Measured Excess Pore Pressure Data at TS3 156

Table 3.8b Measured Excess Pore Pressure Data at TS5 157

Table 3.9a Summary Results of 1-D Consolidation Settlement Calculations [SH1, SH2, and URS (2003)] 158

Table 3.9b Comparison of Computed 1- D Consolidation Settlements (Computed with SH2) and Measured Settlements 158

Table 3.10 Parameters for Simulations of Consolidation and Undrained Shear - Bay Mud 159

Table 3.11 Calculation Scheme for 1-D Consolidation Simulation of Incremental Oedometer Test 160

Table 3.12 Summary Results of PSC Simulations 161

Table 3.13 Summary Results of DSS Simulations 163

Table 3.14 Definition of Cases for NHPL FE Analyses 164

Table 3.15 Soil and Pavement Properties Used in NHPL FE Analyses 165

Table 3.16 Imposed Initial OCR and K_0 in the Subsoil Layers for Plaxis Analyses of the NHP Levee 166

Table 3.17 Calculation phases in PLAXIS 167

Table 3.18 Summary of Results of All Plaxis Analyses of the NHP Levee 168

Table A1 Summary of CRSC Tests at TS3-B1 265

Table A2 Details of Direct Simple Shear Test Results of Bay Mud at NHPL and North Levees (N1 and N2) 299

Table A3 Detail Results of CK_0U Triaxial Tests on Bay Mud at NHPL 319

Table B-1 1-D Consolidation Settlement Prediction at TS3 (computed with σ'_p profile) 335

Table B-2 1-D Consolidation Settlement Prediction at TS3 (computed with $0.9\sigma'_p$ profile) 336

Table B-3 1-D Consolidation Settlement Prediction at TS3 (computed with $0.8\sigma'_p$ profile) 337

Table B-4 1-D Consolidation Settlement Prediction at TS5 (computed with σ'_p profile) 338

Table B-5 1-D Consolidation Settlement Prediction at TS5 (computed with $0.9\sigma'_p$ profile) 339

Table B-6 1-D Consolidation Settlement Prediction at TS5 (computed with $0.8\sigma'_p$ profile) 340

Table B-7 1-D Final Consolidation Settlement Prediction at TS3 & TS5 (computed with σ'_p profile) 341

Table B-8 1-D Final Consolidation Settlement Prediction at TS3 & TS5 (computed with $0.9\sigma'_p$ profile) 342

Table B-9 1-D Final Consolidation Settlement Prediction at TS3 & TS5 (computed with $0.8\sigma'_p$ profile) 343

INDEX OF FIGURES

Figure 1.1 Consolidation Behavior of Saturated Soil and 1-D Consolidation Settlement Calculation 40

Figure 1.2 Comparison of Hypotheses A and B and Effect of Sample Thickness on 41

1-D Strain 41

Figure 1.3 Application of Hypothesis B in Predicting Final Consolidation Settlement 41

Figure 1.4 Location Plan of HAAF Wetlands Restoration Project 42

Figure 1.5 - Typical Cross Section at NHPL – TS3 43

Figure 1.6 Plasticity Chart for Bay Mud at NHPL 44

Figure 2.1 Plan of NHPL with Location of Test Sections 69

Figure 2.2 Plan of Test Section Area with Borings, Field Tests and Instrumentation 70

Figure 2.3 Settlement Data, Thickness of Bay Mud, Test Section Locations and Settlement Survey Points along NHP Levee 71

Figure 2.4a Settlements vs Log[time] at Survey Points Near Test Section TS3&TS5 72

Figure 2.4b Settlements vs. Log[time] at Survey Points Near Test Section TS3&TS5 (Modified Plot) 73

Figure 2.5 Summary of NHPL Free Field σ'_p(FV) for μ=0.8 and Laboratory σ'_p 74

Figure 2.6a Stress History at TS3, Comparison of μ =0.8 σ'_p(FV) vs. σ'_p(CRSC) 75

Figure 2.6b Comparison of μ=0.8 σ'_p(FV) with σ'_p from CRSC 76

and Oedometer Tests at S2-B3 (South Levee) 76

Figure 2.7 Excess Pore Pressure Measured at TS3 & TS5 [From URS (2003) for Period, Jan-Mar, 2002] 77

Figure 2.8a Stress History under Crest of Levee at TS3 78

Figure 2.8b Stress History of under Crest of Levee at TS5 79

Figure 2.9a Water Content and Virgin Compressibility of NHPL Bay Mud vs. Elevation 80

Figure 2.9b Virgin Compression Ratio vs. Natural Water Content of NHPL Bay Mud 81

Figure 2.10a Recompression Ratio, RR vs. Elevation and CR (Virgin + Under Levee Crest) 82

Figure 2.10b Swelling Ratio, SR vs. Elevation and RR 83

Figure 2.11 Coefficient of Consolidation vs. Liquid Limit for Bay Mud at NHPL and Other Levees 84

Figure 2.12 Coefficient of Permeability: Typical e-logσ'_{vc}-logk Curves from MIT CRSC Tests on NHPL Bay Mud 85

Figure 2.13 Stress History for Settlement Analyses 86

at TS3 for Mean Profile σ'_p(FV) at Two Different Correction Factors, μ = 0.8 and 0.6 86

Figure 2.14 Field Vane Correction Factor vs. Computed Settlement for Mean σ'_p(FV) Profiles: TS3 and TS5 87

Figure 2.15 Comparison of Cross-Sections and Measured vs. Predicted Settlements for Mean σ'_p(FV) Profile at TS1 Through TS5 88

Figure 3.1 NHPL, Line 1 Average Soil Profile and Stress History – Free Field Conditions 170

Figure 3.2 Index Properties of Bay Mud at Free Field Condition, TS3-B1 171

Figure 3.3a Hydraulic Conductivity Property of Bay Mud at TS3-B1 172

Figure 3.3b Selected Consolidation Properties for Virgin Bay Mud 173

Figure 3.4a CRS431 Normalized Compression Curve in Log-Scale ($\sigma'_p \approx \sigma'_{vc}$) 174

Figure 3.4b CRS443 Normalized Compression Curve in Log-scale ($\sigma'_{vc} \approx \sigma'_p$) 175

Figure 3.4c CRS444 Normalized Compression Curve in Log-scale ($\sigma'_{vc} \approx \sigma'_p$) 176

Figure 3.4d CRS432 Normalized Compression Curve in Log-scale ($\sigma'_{vc} > \sigma'_p$) 177

Figure 3.4e CRS441 Normalized Compression Curve in Log-scale ($\sigma'_{vc} > \sigma'_p$) 178

Figure 3.4f CRS440 Normalized Compression Curve in Log-scale ($\sigma'_{vc} < \sigma'_p$) 179

Figure 3.4g CRS435 Normalized Compression Curve in Log-scale ($\sigma'_{vc} < \sigma'_p$) 180

Figure 3.5 Comparison of NC Coefficient of Consolidation of Bay Mud with NAVFAC DM-7.1 (May1982) Chart 181

Figure 3.6 Coefficient of Earth Pressure at Rest for Normally Consolidated Bay Mud, K_0^{NC} 182

Figure 3.7 Undrained Strength Ratio vs. Overconsolidation Ratio (Log s_u/σ'_{vc} vs. Log OCR) 183

Figure 3.8 Typical Results of CK_0UDSS Tests on Bay Mud at OCR = 1, 2 and 3 184

Figure 3.9a Results of CK_0UTX Tests on Bay Mud at OCR =1: Stress-Strain and Stress Path 185

Figure 3.9b Results of CK_0UTX Tests on Bay Mud at OCR =1: Undrained Young's Modulus 186

Figure 3.10 Influence of Young's Modulus and Strength of Uncracked, Continuous Concrete Pavement on Final Vertical Effective Stress Distribution in Bay Mud 187

Figure 3.11a Geometry for CASE B&C Analyses of Final Vertical Stress, σ'_{vf} 188

Figure 3.11b PLAXIS Predicted Final Consolidation Vertical Effective Stress at Centerline and Toe of Levee 189
(Cases A, B and C) 189
Figure 3.12a Selected Excess Pore Pressure Profiles under Centerline of Levee at TS3 and TS5 190
Figure 3.12b TS3 & TS5, Line 3 Stress Histories for One-Dimensional Consolidation Analysis (SH1) 191
Figure 3.12c TS3 & TS5, Line 3 Stress Histories for One –Dimensional Consolidation Analysis (SH2) 192
Figure 3.13a One-Dimensional Consolidation Settlements and Measured Settlements at TS3 & TS5 up to 01/31/02 (SH1) 193
Figure 3.13b One-Dimensional Consolidation Settlements and Measured Settlements at TS3 & TS5 up to 01/31/02 (SH2) 194
Figure 3.13c Comparison of 1-D Consolidation Settlements at TS3 and TS5 at 1/31/02 [SH1, SH2, and URS (2003)] 195
Figure 3.13d Predicted 1-D Consolidation Settlements at 1/02 and Final Consolidation Settlements with SH2 196
Figure 3.14a Stress-Strain Log Scale, 1-D Consolidation Model Test on Bay Mud SSM 197
Figure 3.14b Stress-Strain Natural Scale, 1-D Consolidation Model Test on Bay Mud SSM 197
Figure 3.14c Coefficient of Consolidation, 1-D Consolidation Model Test on Bay Mud SSM 198

Figure 3.14d Change in Permeability, Case 1 1-D Consolidation Model Test on Bay Mud SSM 199
Figure 3.14e Change in Permeability, Case 2 1-D Consolidation Model Test on Bay Mud SSM 199
Figure 3.15 Undrained Shear Strength Ratio vs. OCR, CK_0U PSC/E Tests Simulation with SSM for Bay Mud 200
Figure 3.16 Undrained Strength Ratio vs. OCR, DSS Simulation 201
for Bay Mud (SSM), $\kappa^* = 0.104$ and 0.002 201
Figure 3.17a Normalized Undrained Shear Stress vs. Shear Strain, DSS Simulation on Bay Mud (SSM), $\kappa^*=0.104$ 202
Figure 3.17b Normalized Undrained Modulus vs. Shear Strain, DSS Simulation on Bay Mud (SSM), $\kappa^*=0.104$ 203
Figure 3.18a Normalized Undrained Shear Stress vs. Shear Strain, DSS Simulation on Bay Mud (SSM), $\kappa^*=0.002$ 204
Figure 3.18b Normalized Undrained Modulus vs. Shear Strain, DSS Simulations on Bay Mud (SSM), $\kappa^*=0.002$ 205
Figure 3.19 Geometry of NHP Levee Model with FE Mesh and Soil Materials for Cracked Pavement 206
Figure 3.20 Staged Construction Modeling of NHP Levee 207
Figure 3.21a Predicted and Measured Consolidation Settlements of NHPL for Cases A1 and A2 Analyses: Effect of Pavement Cracking 208
Figure 3.21b Predicted and Measured Excess Pore Pressure at Feb., 2002 under Centerline for Cases A1 and A2 Analyses: Effect of Pavement Cracking 209

Figure 3.21c Predicted and Measured Excess Pore Pressure at Feb., 2002 under Toe for Cases A1 and A2 Analyses: Effect of Pavement Cracking.....210
Figure 3.21d Comparison of Predicted and Measured Stress Histories under Centerline of NHPL at Feb. 2002 for Cases A1 and A2 Analyses: Effect of Pavement Cracking.....211
Figure 3.21e Predicted Total Settlement Profiles at CD180 and CD2115 under Centerline of the NHPL for Case A2 Analysis.....212
Figure 3.21f Predicted Settlement Profiles at CD180 and CD2115 of the Ground under the NHPL for Case A2 Analysis.....213
Figure 3.21g Predicted Settlement vs. logt for Case A2 Analysis 214
Figure 3.21h Predicted Excess Pore Pressure at Mid-point of Bay Mud vs. logt for Case A2 Analysis.....215
Figure 3.21i Horizontal Displacements at Toe of the NHPL for Case A2 Analysis.....216
Figure 3.22a Predicted and Measured Consolidation Settlements of the NHPL for Cases A2 and B Analyses: Effect of Free Draining Alluvium 217
Figure 3.22b Predicted and Measured Excess Pore Pressure under Centerline of the NHPL at Feb. 2002 for Cases A2 and B Analyses: Effect of Free Draining at the Alluvium 218
Figure 3.22c Predicted and Measured Excess Pore Pressure at Toe of the NHPL at Feb. 2002 for Cases A2 and B Analyses: Effect of Free Draining at the Alluvium 219

Figure 3.22d Comparison of Predicted and Measured Stress Histories under Centerline of the NHPL at Feb. 2002 for Cases A2 and B Analyses: Effect of Free Draining Alluvium 220
Figure 3.23a Predicted and Measured Consolidation Settlements of the NHPL for Cases A2, C1, C2, and C3 Analyses: Effect of c_v(NC) of Bay Mud 221
Figure 3.23b Predicted and Measured Excess Pore Pressure at Centerline of the NHPL for Cases A2, C1, C2 and C3 Analyses: Effect of c_v(NC) of Bay Mud 222
Figure 3.23c Predicted and Measured Excess Pore Pressure at Toe of the NHPL for Cases A2, C1, C2, and C3 Analyses: Effect of c_v(NC) of Bay Mud 223
Figure 3.23d Comparison of Predicted and Measured Stress Histories for Cases A2, C1 and C3 Analyses: Effect of c_v(NC) of Bay Mud 224
Figure 3.24a Predicted and Measured Consolidation Settlements of the NHPL for Case A2, D1, D2 and URS(2003) Analyses: Effect of Preconsolidation Stress 225
Figure 3.24b Predicted and Measured Excess Pore Pressure at Centerline of the NHPL for Cases A2, D1, D2 and URS (2003) Analyses: Effect of Preconsolidation Stress 226
Figure 3.24c Predicted and Measured Excess Pore Pressure at Toe of the NHPL for Cases A2, D1, and D2 Analyses: Effect of Preconsolidation Stress 227
Figure 3.24d Predicted and Measured Stress Histories for Cases A2, D1 and D2 Analyses: Effect of Preconsolidation Stress 228
Figure 3.24e Predicted Settlement Profiles under Centerline of the NHPL for Case D2 Analysis: Effect of Preconsolidation Stress 229

Figure 3.24f Predicted Settlement Profiles of the Ground under the NHPL for Cases D2 and URS (2003) Analyses....230
Figure 3.24g Predicted Settlement vs. logt for Case D2 Analysis: Effect of Preconsolidation Stress....231
Figure 3.24h Predicted Excess Pore Pressure at Mid-point of Bay Mud vs. logt for Case D2 Analysis....232
Figure 3.24i Predicted Horizontal Displacements at Toe of the NHPL for Case D2 Analysis....233
Figure 3.25a Predicted and Measured Consolidation Settlements of the NHPL for Cases A2, C1, D2 and D3 Analyses: Combined Effects of Preconsolidation Stress and Bay Mud c_v(NC)....234
Figure 3.25b Predicted and Measured Excess Pore Pressure at Centerline of the NHPL for Cases A2, C1, D2 and D3 Analyses: Combined Effects of Preconsolidation Stress and Bay Mud c_v(NC)....235
Figure 3.25c Predicted and Measured Excess Pore Pressure at Toe of the NHPL for Cases A2, C1, D2 and D3 Analyses: Combined Effects of Preconsolidation Stress and Bay Mud c_v(NC)....236
Figure 3.25d Predicted Stress Histories for Cases A2, C1, D2 and D3 Analyses....237
Figure 3.26a Predicted and Measured Consolidation Settlements of the NHPL for Case D4 and URS (2003): Combined Effects of Bay Mud c_v(NC), σ'_p Profile and Permeability of BM Crust and Alluvium....238

Figure 3.26b Predicted and Measured Excess Pore Pressure at Centerline of the NHPL at CD2115 for Case D4 and URS (2003): Effects of Bay Mud c_v(NC), σ'_p Profile and Permeability of BM Crust and Alluvium 239

Figure 3.26c Predicted and Measured Excess Pore Pressure at Toe of the NHPL at CD2115 for Case D4 240

Figure 3.26d Predicted Stress Histories for Case D4 241

Figure 3.27a Predicted Reduction in Total Vertical Stress at Centerline of NHPL during Consolidation from CD180 (EOC) to CD2115 for Case A2 Analysis 242

Figure 3.27b Predicted Reduction in Total Vertical Stress at Centerline of NHPL during Consolidation from CD180 (EOC) to CD2115 for Case C1 Analysis 243

Figure 3.27c Predicted Reduction in Total Vertical Stress at Centerline of NHPL during Consolidation from CD180 (EOC) to CD2115 for Case D2 Analysis 244

Figure 3.27d Predicted Changes in Total Vertical Stress ("Arching Effect") under the NHPL at El. -29.7 ft for Case D2 Analysis 245

Figure 3.28a Summary and Comparison of Plaxis Predicted Consolidation Settlements at Feb. 2002 with URS (2003) and 1-D ρ_c Results 246

Figure 3.28b Summary and Comparison of Plaxis Predicted Maximum Excess Pore Pressure within Bay Mud at Feb. 2002 247

GLOSSARY

$C_{\alpha\varepsilon}$, $C_{\alpha e}$	Secondary Compression Index ($d\log\varepsilon_v/d\log t$, $de/d\log t$)
C_c	Compression index, $C_c = de/d\log\sigma'_v$ in virgin compression range
$C_{c\,max}$	Maximum compression index C_c
C_k	Coefficient of change in permeability, $C_k = de/d\log k_v$
C_r	Recompression index, $C_r = de/d\log\sigma'_v$ in recompression range
CR	Virgin compression ratio, $CR = C_c/(1+e_0)$, $= d\log\varepsilon_v/d\log\sigma'_v$
CR_{max}	Maximum virgin compression ratio
c_v(NC)	Coefficient of consolidation for normally consolidated clay
c_v(OC)	Coefficient of consolidation for over-consolidated clay
e, e_0	Void ratio, initial void ratio
E_{oed}	Oedometer loading modulus
E_u	Undrained shear modulus
H_d	Drainage Height
H_i	Height of soil layer *i*
H	Horizontal displacement
h_{max}	Maximum horizontal displacement
I_p	Plastic index
K_{0NC}	Coefficient of earth pressure at rest for normally consolidated soil
K_{0OC}	Coefficient of earth pressure at rest for overconsolidated soil
k_x, k_y=k_h, k_v	Hydraulic conductivity in horizontal, vertical direction
k_{h0}	Initial horizontal hydraulic conductivity
k_{v0}	Initial vertical hydraulic conductivity
LL	Liquid limit
M	Coefficient, $m = d\log(s_u/\sigma'_{vc})/d\log(OCR)$
OCR	Over consolidation Ratio, $OCR = \sigma'_p/\sigma'_{vo}$
PI	Plasticity index
p'	Mean effective stress ($=\sigma'_{oct}$)
p_p	Preconsolidation stress
q	Shear stress ($=\sigma_1 - \sigma_3$)
r_k	Coefficient of permeability anisotropy
RR	Recompression ratio, $RR = d\log\varepsilon_v/d\log\sigma'_v = C_r/(1+e_0)$
RR_{max}	Maximum recompression ratio
RR_{min}	Minimum recompression ratio

S	Undrained shear strength ratio for normally consolidated soil
S_c	Undrained shear strength ratio in TC for NC clay
S_d	Undrained shear strength ratio in DSS for NC clay
S_e	Undrained shear strength ratio in TE for NC clay
S_{FV}	Undrained shear ratio for field vane as a function of plasticity index
S_i	Degree of saturation
s_u	Undrained shear strength
$s_u(FV)$	Field vane undrained shear strength
t_c	Consolidation time
t_o	Zero time (from middle of loading period)
t_p	Time to end of primary (at $u_e = 0$)
u_0	Initial excess pore pressure due to loading (at $t = 0$)
u_e	Excess pore pressure at time t
$\bar{U}$	Average degree of consolidation
w_L	Liquid limit
w_n	Natural water content
w_p	Plastic limit
$\bar{f}$	Function of the stress state *(p', q)*
μ	Field vane correction factor
ε_a	Axial strain, %
ε_v	Volumetric strain
ε_{vo}	Vertical strain at overburden stress
$\lvert\varepsilon_a\rvert$	Absolute axial strain, %.
λ^*	Modified compression index = CR/2.3
κ^*	Modified swelling index = 2RR/2.3
ϕ'_{tc}	Friction angle in TC
σ'_p	Preconsolidation stress for 1-D vertical consolidation
$\sigma'_{p(CRSC)}$	Preconsolidation stress from CRSC test
$\sigma'_{p(FV)}$	Preconsolidation stress from field vane test
σ'_{ps}	Reduced preconsolidation stress (due to creep occurring before EOP)
σ'_{v0}	In-situ overburden stress
σ'_{vc}	Vertical consolidation effective stress
σ'_{vf}	Ultimate drained equilibrium vertical effective stress (final stress): σ'_{vf} =

	$\sigma'_{vo} + \Delta\sigma_v$
$\Delta\sigma_v$	Change in total vertical stress
γ_b	Buoyant unit weight
γ_t	Total unit weight
ρ_c	Consolidation settlement
ρ_{cf}	Final consolidation settlement
ρ_{cr}	Settlement due to creep during primary consolidation
ρ_i	Initial settlement
ρ_m	Measured settlement
ρ_s	Secondary compression settlement
ρ_t	Total settlement
ν_{ur}	Poisson's ratio in which the subscript *ur* denotes unloading/reloading

Abbreviations

ARUP	Geotechnical consulting firm for the HAAF project
BM	Bay Mud
CCL	Professor C.C Ladd
CD	Construction days
CK_0UDSS	K_0 consolidated-undrained direct simple shear
CK_0UPSC/E	K_0 consolidated-undrained plane strain compression/extension shear
CK_0UTC	K_0 consolidated-undrained triaxial compression shear
CK_0UTE	K_0 consolidated-undrained triaxial extension shear
CK_0UTX	K_0 consolidated-undrained triaxial test
CPTU	Piezo-Cone penetration test
CRSC	Constant rate of strain consolidation
DSS	Direct simple shear
EL.	Elevation
EOC	End of Construction
EOP	End of Primary
FE	Finite Element Method
FVT	Field vane test
HAAF	Hamilton Army Air Field
HQN	The author
MC	Mohr-Coulomb
MSL	Mean sea level
NHPL	New Hamilton Partnership Levee
OED	Oedometer test
SFBM	San Francisco Bay Mud
SHANSEP	Stress history and normalized soil engineering properties
SSM	Soft Soil Model for Plaxis
TC	Triaxial compression
TE	Triaxial extension

TS	Test section
TX	Triaxial test
URS	Geotechnical consulting firm for the HAAF project
VCL	Virgin compression line
WT	Water table

CHAPTER 1

INTRODUCTION

1.1 Settlement of Embankments on Soft Ground

Ground conditions can be divided into two situations, "stiff" or "soft", with respect to the applied embankment loading. A 'soft ground' condition denotes cohesive, compressible soils that undergo both recompression and virgin compression during consolidation. In other words, soft ground conditions occur when σ'_{vf}, the ultimate drained equilibrium vertical stress (i.e., $\sigma'_{vf} = \sigma'_{vo} + \Delta\sigma_v$, where σ'_{vo} is the initial in situ effective stress, and $\Delta\sigma_v$ is the change in total vertical stress), exceeds σ'_p, the vertical preconsolidation (yield) stress within the soil profile. Hence, normally consolidated and slightly overconsolidated clay deposits correspond to soft-ground conditions, where relatively large consolidation settlements can be expected. In contrast, 'stiff ground' conditions occur if σ'_{vf} is less than σ'_p throughout the soil profile. This means the ground will experience only recompression behavior, leading to relatively small settlements.

There are many geotechnical structures built on soft ground conditions such as embankments for transportation facilities, flood-control levees, embankment dams, land fills, storage tanks and offshore gravity platforms. Figure 1.1 presents the typical scenario for a soft ground condition. In this example, the soil profile comprises a layer about 30 feet deep of a saturated, slightly over-consolidated clay (with a typical overconsolidation ratio $OCR = \sigma'_p/\sigma'_{vo} \approx 1.5$). The final consolidation stress profile exceeds the preconsolidation profile through most of the depth of the deposit except for a relatively thin crust layer at the surface. In the zone from the ground surface to the point where the preconsolidation stress profile intersects the final stress profile (marked X in Fig. 1.1a), the soil remains over-consolidated and undergoes only recompression from the initial in

situ stress (σ'_{vo}) to the final stress (σ'_{vf}), because σ'_p is larger than σ'_{vf}. Below X, the soil will experience recompression from σ'_{v0} to σ'_p and then virgin compression from σ'_p to σ'_{vf}.

Problems associated with soft ground conditions are large total settlements, a slow rate of consolidation leading to long-term consolidation settlements, and low undrained shear strength leading to possible failures during loading. Large lateral deformations may also occur during loading and can increase during subsequent consolidation. Soft ground construction therefore requires comprehensive site characterization and understanding of soil properties and soil behavior issues, e.g., stress history of the ground with σ'_p, σ'_{vo}, σ'_{vc} , and σ'_{vf} profiles, rate of consolidation with coefficients of consolidation c_v(NC) and c_v(OC), compressibility of soil (RR, CR), and undrained shear strength (s_u) for stability analyses.

There are three components of settlement that contribute to the total settlement:

1) Initial settlement, ρ_i: settlement due to undrained shear deformation of the ground when initially applying $\Delta\sigma_v$. This type of settlement is called an undrained settlement by Foott and Ladd (1981): "*When a load is rapidly applied over a limited area above a clay soil deposit, the shear stresses induced in the clay cause lateral deformation of the soil resulting in settlement. This settlement is commonly considered an instantaneous response to the applied loading, therefore, occurring under undrained conditions and known as initial settlement, ρ_i.*"

2) Consolidation settlement, ρ_c: Settlement due to drainage of pore water which occurs during the increase in effective stress in the soil. The rate of this type of settlement is

often computed by Terzaghi's consolidation theory: $\rho_c = \bar{U}\,\rho_{cf}$, where $\bar{U}$ is the average degree of consolidation, and ρ_{cf} is the final consolidation settlement predicted at t = t_p, where t_p is the time to reach the end of primary consolidation (EOP).

Conventional practice usually assumes that the overall total ρ_t at EOP is equal to final consolidation settlement, ρ_{cf}, for a one-dimensional (1-D) strain condition:

$$\rho_{cf} = \sum \left[H_i \left(RR \log \frac{\sigma_p^{'}}{\sigma_{vo}^{'}} + CR \log \frac{\sigma_{vf}^{'}}{\sigma_p^{'}} \right) \right] \qquad (1.1)$$

where:

- H_i = initial thickness for the i^{th} sub-layer of the compressible foundation soil;
- $\sigma'_{vf} = \sigma'_{vo} + \Delta\sigma_v$ = final vertical effective stress, which is the ultimate drained equilibrium vertical stress;
- $\Delta\sigma_v$ is the change in total vertical stress due to the applied surface loading, and usually is computed from an elastic stress distribution method;
- σ'_p is the preconsolidation stress interpreted from 1-D laboratory consolidation tests, such as the incremental loading Oedometer test (OED) or the Constant Rate of Strain Consolidation test (CRSC, Wissa et. al. 1971), or correlated from in situ tests such as the Field Vane or Piezocone;
- *RR, CR* are the Recompression and Virgin Compression Ratio (properties of the clay that are defined in conventional ε_v-logσ_v' space, Fig.1.1b):

$$RR = \frac{\Delta\varepsilon_v}{\Delta \log \sigma_v^{'}} = \frac{C_r}{1+e_0},$$

$$\text{and } CR = \frac{\Delta\varepsilon_v}{\Delta \log \sigma_v^{'}} = \frac{C_c}{1+e_0}$$

where C_r, C_c are the compression indices for overconsolidated and normally consolidated clay, and e_0 is the initial void ratio.

Figure 1.1 summarizes the computation of the final consolidation settlement and associated parameters for a one-dimensional (1-D) loading condition, which is typically assumed in conventional practice (even though the actual loading is two- or three-dimensional).

3) Drained creep settlement, ρ_s: settlement due to secondary compression of soil that occurs after the end of primary consolidation ($t = t_p$ at EOP, excess pore pressure $u_e = 0$):

$$\rho_s = \sum \left[H_i \left(C_\alpha \log \frac{t}{t_p} \right) \right] \qquad (1.2)$$

where C_α is the rate of secondary compression = $d\varepsilon_v/dlogt$

Figure 1.1.c illustrates how the three components of settlement occur in sequence. In general, the total settlement is computed as follows:

$$\rho_t = \rho_i + \rho_c, \qquad \text{(Before EOP)} \qquad (1.3a)$$

$$\text{and,} \quad \rho_t = \rho_i + \rho_{cf} + \rho_s, \qquad \text{(After EOP)} \qquad (1.3b)$$

Creep may also occur during primary consolidation, which leads to an increased ρ_{cf} at EOP. This problem is discussed in Section 1.2.

The assumption of using Equation 1.1 for estimating the total settlement at the end of consolidation ignores the initial settlement, ρ_i. For some cases of highly plastic (CH) or organic (OH) soil deposits, especially where there is a low factor of safety against undrained shear instability, the initial settlement due to undrained shear deformations

(i.e., lateral deformation) may become significant. In addition to the initial settlement, continued lateral deformations of clay also occur during consolidation, thus adding a certain amount of creep settlement, ρ_{cr}, to the total settlement (Foott and Ladd, 1981). Hence, a settlement estimate using Equation 1.1 that ignores ρ_i and ρ_{cr} is one controversy for CH-OH soils. The other controversy concerns the appropriate preconsolidation stress (σ'_p) to use in Equation 1.1. Should σ'_p corresponds to the value measured in the laboratory test at EOP ($t_{increment} = t_p$) or at a reference time such as $t_{increment}$ = 24 hours used in many conventional oedometer tests. Alternatively, some suggest that σ'_p is much lower in the field, due to the increased drainage path length (H_d) and much larger time to end of primary, due to the occurrence of significant secondary compression during the primary consolidation. This controversy is discussed in more detail in Section 1.2.

1.2 Hypothesis A vs. Hypothesis B

Ladd et al. (1977) first defined this controversy in terms of Hypothesis A versus Hypothesis B as illustrated in Figure 1.2. The two competing hypotheses are illustrated by the relationship between strains measured in a thin lab test specimen and a thick field deposit of the same clay. Hypothesis A (curve A, Fig.1.2) essentially assumes that significant secondary compression (drained creep) occurs only after EOP [after $t=t_p$(field), where $t_p(field) = t_p(lab).H_d(field)^2/H_d(lab)^2$]. Proponents of this hypothesis believe that the physical mechanisms causing secondary compression are similar to those responsible for volume change due to an increase in effective stress (e.g., elastic deformation of particles; slippage at contacts and reorientation of particles; double layer compression and displacement of adsorbed water and particle crushing), [e.g., Mesri and

Godlewski (1977), and Ladd et al. (1977)]. Hypothesis A assumes that there is a unique location of the EOP compression curve independent of increases in sample thickness (i.e., drainage height, H_d) and hence the soil has a unique value of σ'_p [e.g., Mesri (2003)]. In contrast, Hypothesis B (curve B, Fig.1.2) assumes that significant creep occurs during primary consolidation and has the same rate as measured in standard laboratory oedometer tests. Hence the strain at the end of primary consolidation increases, causing a downward shift in the EOP compression curve. This corresponds to a reduction in σ'_p in the field compared to the laboratory EOP value of σ'_p [e.g., Leroueil et al. (1985) used lab and field data on Champain "quick" clays of Canada to support Hypothesis B]. The mechanisms responsible for secondary compression occurring during primary consolidation are often thought to be due to some type of "structural viscosity" or time dependent deformation of adsorbed water films [Bjerrum (1973)].

The ε_v - $\log\sigma'_v$ plot in Fig.1.3 illustrates the reduction in the field σ'_p according to Hypothesis B (dashed line) as compared to Hypothesis A (solid line), which explains the increase in strain predicted at the end of consolidation, ε_{cf}(B), Fig. 1.2. Hypothesis B often assumes that the strain due to secondary compression (ε_s) which occurs during primary consolidation in the field can be computed as

$$\varepsilon_s = C_\alpha . \log(\frac{t_p}{t_1}), \qquad (1.4)$$

where t_1 is the reference time measured in 1 day (t_1=1 day), and $t_p = t_p$(field) is the time to end of primary consolidation at field scale. This is equivalent to using Equation 1.1 with a reduced $\sigma'_p = \sigma'_{ps}$ (reduced preconsolidation stress), where:

$$\varepsilon_s = CR \log \frac{\sigma'_p}{\sigma'_{ps}}, \qquad (1.5)$$

Hence, we have the following relationship:

$$\log \frac{\sigma'_p}{\sigma'_{ps}} = \frac{C_\alpha}{CR} \log \frac{t_p}{t_1} \qquad (1.6)$$

with t_1 = 1day.

Thus the value of σ'_{ps} in the field depends on the time, t_p, which is the field EOP consolidation time [t_p(field)] during which secondary compression occurs, and the ratio C_α/CR of the clay. Note that Eq. 1.6 neglects the difference in the values of the lab EOP σ'_p and that measured at t_c = 1 day.

Terzaghi, Peck and Mesri (1996) quote typical values of C_α/CR as 0.04 ±0.1 for inorganic soft clays and 0.05 ± 0.01 for highly plastic organic clays [e.g., Mesri and Feng (1986)]. For an average C_α/CR = 0.045, the reduction ratio in preconsolidation stress in the field becomes

t_p (year)	σ'_{ps}/σ'_p
5	0.71
10	0.69
50	0.64

The use of Hypothesis B therefore leads to a significant increase in the predicted ρ_{cf} due to the reduced σ'_{ps}, especially for low values of σ'_{vf}/σ'_p and large values of t_p.

1.3 New Hamilton Partnership Levee (NHPL) Project

The New Hamilton Partnership Levee (NHPL) is one of several existing levees that surround the Hamilton Army Air Field (HAAF) Base Wetlands Restoration project (Fig.1.4). The location of this site is within the City of Novato, north of San Francisco, California. The location of the Hamilton Army Air Field used to be a part of an extensive tidal wetlands area adjacent to the San Francisco Bay. As part of a federal program to convert military bases to civilian use, an area of about 900 acres is being restored to tidal and seasonal wetlands after the closure of the Air Base in 1994 (URS, 2003).

The plan of the HAAF Wetlands Restoration project is to create a system of seasonal and tidal wetlands by placing approximately 10.6 million cubic yards of dredged material to raise site elevation, which is now several feet below sea level. Also a new levee system is required to protect neighboring residential, agricultural and industrial areas from flooding. Therefore, the project would require construction of levees all around the perimeter of the new wetlands, including enlargement of the existing NHPL by constructing a new embankment overlapping the outboard (east) side of the levee. An intensive site investigation program, a new instrumentation and monitoring program, and an analysis program of the behavior of NHPL were conducted in 2002 by URS - the geotechnical consulting firm - to calibrate analytical and finite element (FE) models for further use in design of this and other levees.

The existing NHPL alignment is located on a thick layer (30-40 ft) of recent San Francisco Bay Mud (SFBM). The NHPL was built between March and October 1996, and is approximately 7,200 feet long and 12 feet high as a flood-control embankment structure for the New Hamilton Partnership residential area.

Figure 1.5 shows a typical cross-section of the embankment, which has a height of about 12 ± 1 ft. The water table varies seasonally and is typically located several feet below the ground surface. The embankment consists of well-compacted, slightly cohesive granular fill and is underlain by:

- 3.0 to 4.5 feet air-field concrete pavement slab (or occasionally fill material);
- Several feet of stiff clay called Bay Mud Crust. The crust is composed of desiccated Bay Mud over the entire area;
- 30 to 40 ft layer of soft, compressible marine clay known as Recent Bay Mud (or San Francisco Bay Mud)
- Various essentially incompressible soil strata (sand, stiff clay, etc.) overlying bedrock.

The Bay Mud is a highly plastic, organic clay (CH-OH) with Atterberg limits plotted in Fig. 1.6. It is slightly over-consolidated (OCR is about 1.5), and has a high virgin compressibility, low undrained shear strength, and low hydraulic conductivity. The settlement and stability of levees are primarily controlled by the soft Recent Bay Mud layer.

The City of Novato conducted a program to monitor the settlement along the crest of the NHP levee at 200 ft intervals shortly after it was constructed[1]. In January 2002, approximately 5.2 years after construction, the settlement of the levee (ρ_m) = 2.0 ± 0.5 ft along most of the levee alignment. The settlement data also show that the soft Bay Mud is still in primary consolidation, which is estimated to take 50 years.

[1] The Novato program does not include measurements of pore water pressure and lateral deformation in the foundation soils.

In 2002, a comprehensive geotechnical site investigation was conducted by URS with "state of the art" field and laboratory testing programs to evaluate the performance of the NHPL and investigate the site geotechnical conditions for further developments of the project. The site investigation included both in situ Field Vane (FV) and Piezocone Penetration (CPTU) tests and laboratory consolidation and strength tests (OED, CRSC, CK_0UTX, CK_0UDSS) on undisturbed clay. The testing program resulted in a well-defined stress history profile, compressibility and flow properties. In addition, URS installed instrumentation (sondex profilers, piezometers and inclinometers) at several locations designated as test sections (TS), both under the levee and beyond its toe (i.e., virgin ground).

URS calculated the settlements of the NHP levee using the conventional 1-D consolidation method via Equation 1.1 with profiles of current consolidation stress $\sigma'_{vc} = \sigma'_{vo} + \Delta\sigma_v$ (levee) $- u_e$ (measured from piezometers), and found a large discrepancy between measured and predicted settlements. At test sections TS3 and TS5 (which are typical conditions along the NHP levee) the best-estimate of σ'_p from laboratory EOP curves, produced a consolidation settlement, $\rho_c \approx 0.6$ ft, whereas the measured settlement at about 5.2 yr after construction, $\rho_m \approx 1.6$ ft. Hence, the prediction seriously underestimated the measured settlement. For the design of the wetland restoration project, URS reduced the lab best-estimate σ'_p(EOP) profile by a factor of 0.8 in order to obtain agreement between calculated and measured settlements of the existing NHP levee.

Professor C.C. Ladd, as a consultant to URS, prepared a memo (Ladd, 2002) that evaluated possible reasons for the large discrepancy between the calculated and measured settlements. He concluded that use of Hypothesis B was consistent with the larger measured settlement. However, he also thought that the plastic nature of clay might have caused a large initial settlement, $\rho_{i,}$ plus ongoing creep, and thus increased settlement due to lateral deformation [e.g., Foott and Ladd (1981)]. The writer notes that Mesri and Choi (1985) [Fig.23 in Jamiolkowski et al. (1985)] ran consolidation tests on San Francisco Bay Mud with varying sample thickness (H_d) and concluded that this clay had an unique EOP compression curve and that it followed Hypothesis A, (i.e., no reduction in σ'_p with increase in time to the end of primary, t_p).

1.4 Objectives and Scope of Thesis

In an attempt to try to understand and be able to explain the discrepancy in settlements of the NHPL, the thesis has three prime objectives:

1) Re-evaluate the consolidation properties of the Bay Mud selected by URS and make new 1-D settlement calculations.

2) Perform 2-D FE consolidation analysis using the Soft Soil Model (SSM), which is essentially the Modified Cam Clay, with PLAXIS, first to replicate similar analyses made by URS, and second to perform analyses with the author's properties.

3) Evaluate the importance of ρ_i and the effect of varying σ'_p on predicted settlements.

Chapter 2 of the thesis presents a summary of the site characterization and previous analyses of the NHPL embankment project by URS, in which the author synthesizes the work of URS (2003) and Ladd (2002).

Chapter 3 presents re-examination of soil properties at test sections TS3 and TS5, 1-D consolidation analyses of the NHPL, simulations of consolidation and undrained strength behaviors of Bay Mud using FE PLAXIS code with Soft Soil Model (SSM), and PLAXIS analyses of the NHPL using SSM.

Chapter 4 presents summary, conclusions and recommendations of the thesis.

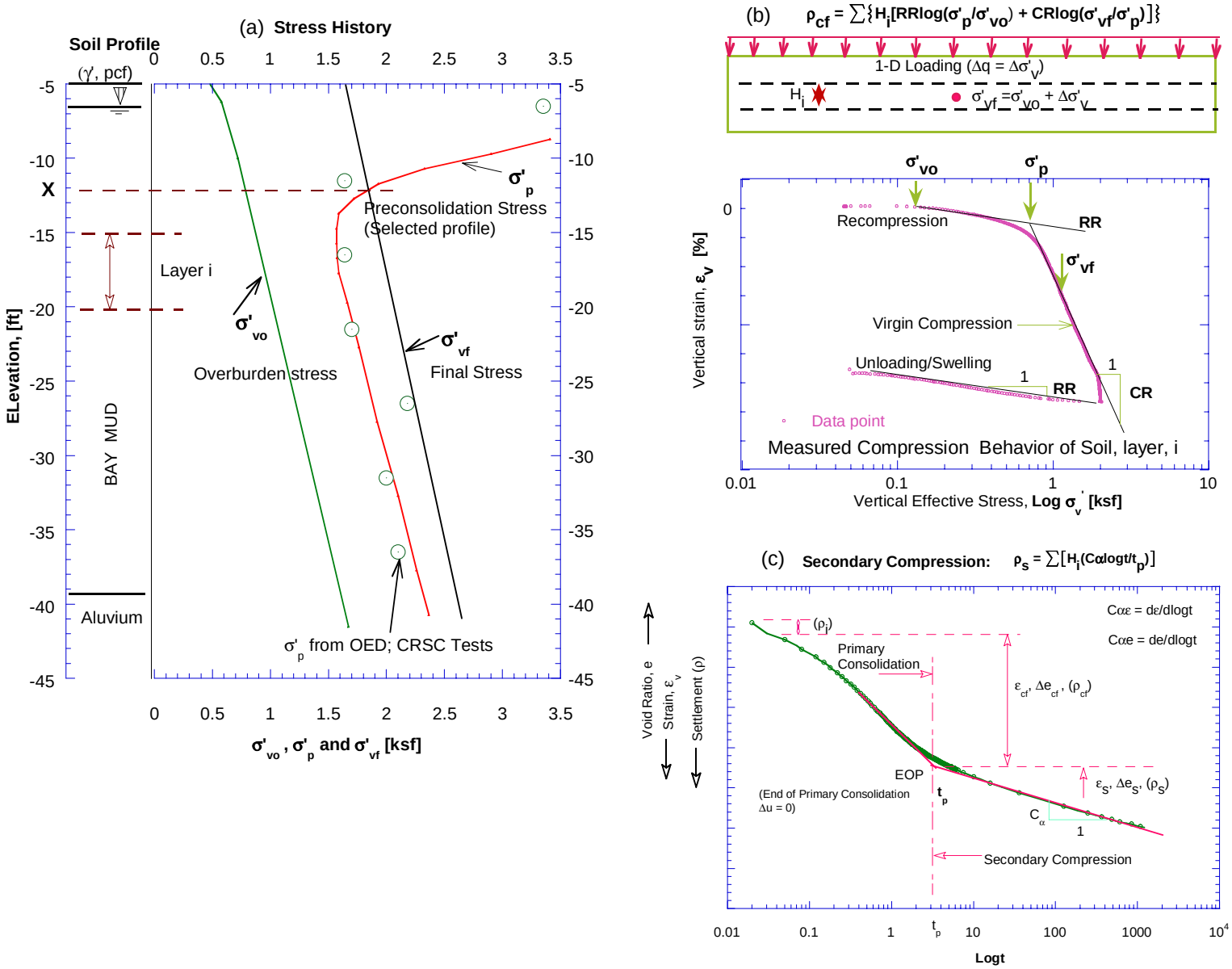

Figure 1.1 Consolidation Behavior of Saturated Soil and 1-D Consolidation Settlement Calculation

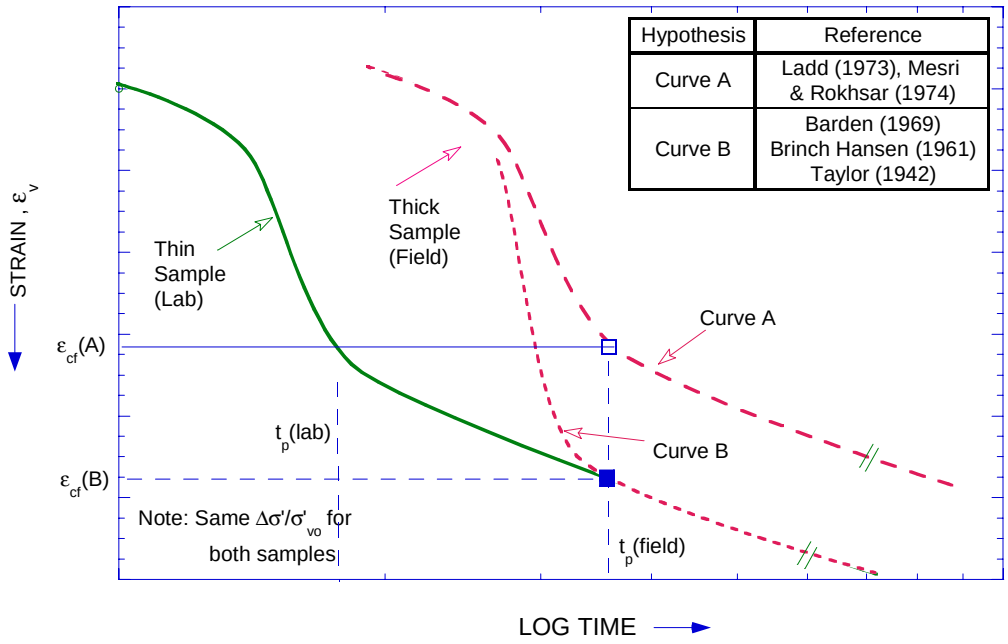

Figure 1.2 Comparison of Hypotheses A and B and Effect of Sample Thickness on 1-D Strain

[From Ladd et al. (1977)]

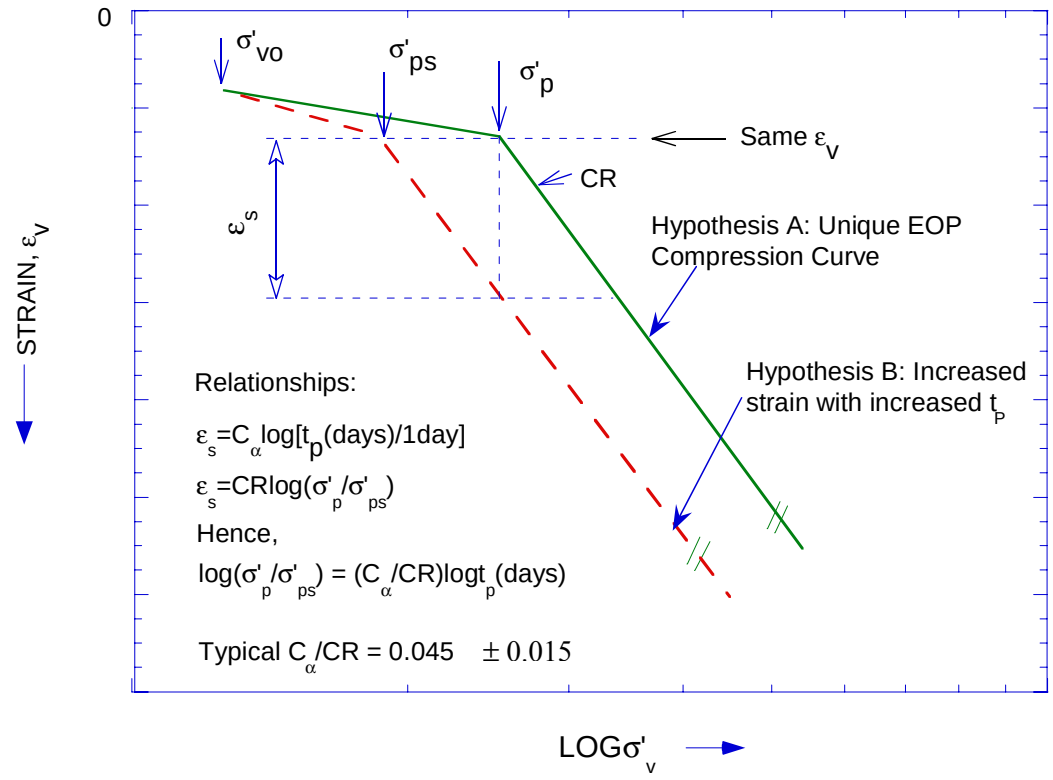

Figure 1.3 Application of Hypothesis B in Predicting Final Consolidation Settlement

[From Ladd, 2002]

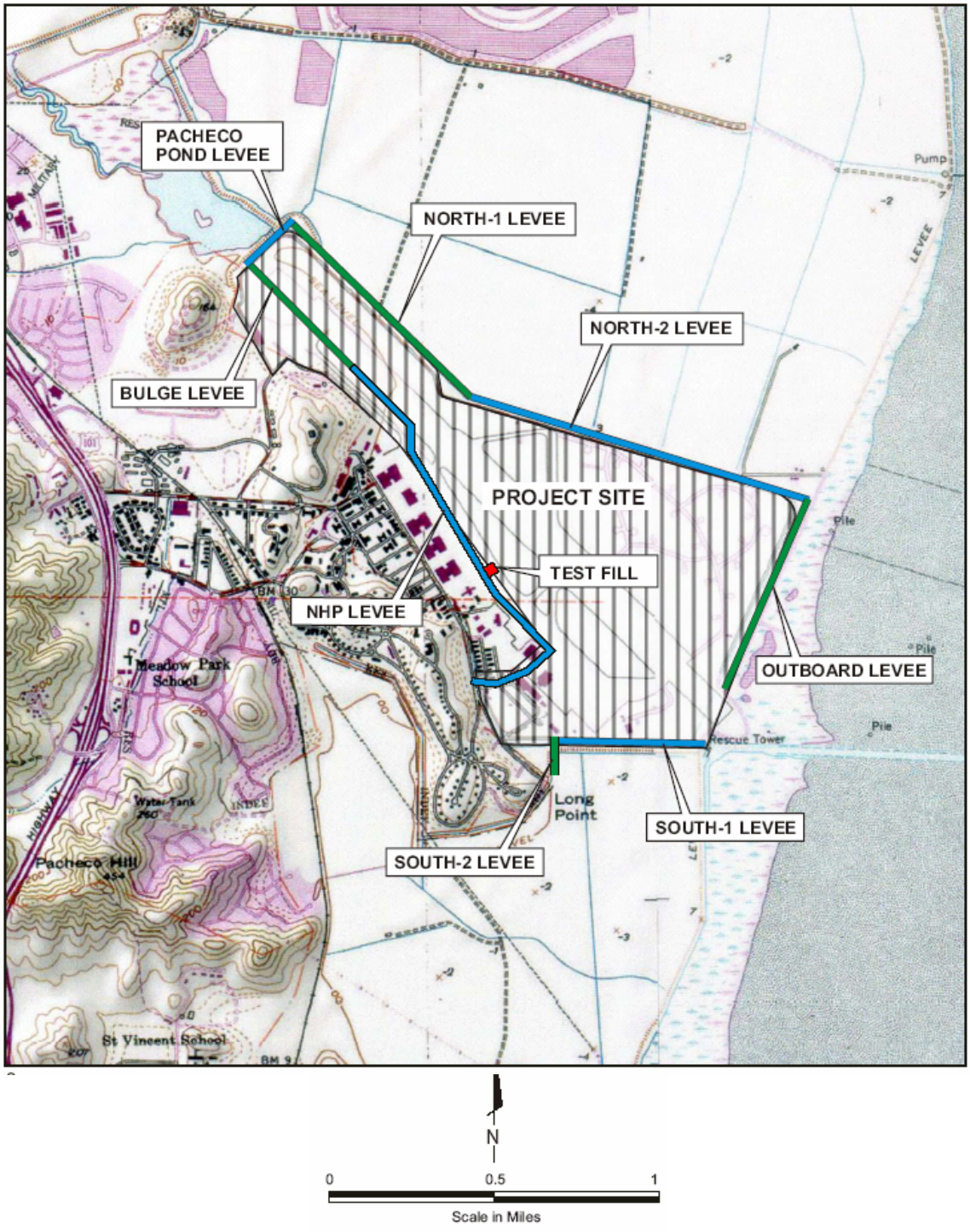

Figure 1.4 Location Plan of HAAF Wetlands Restoration Project
[From URS (2003)]

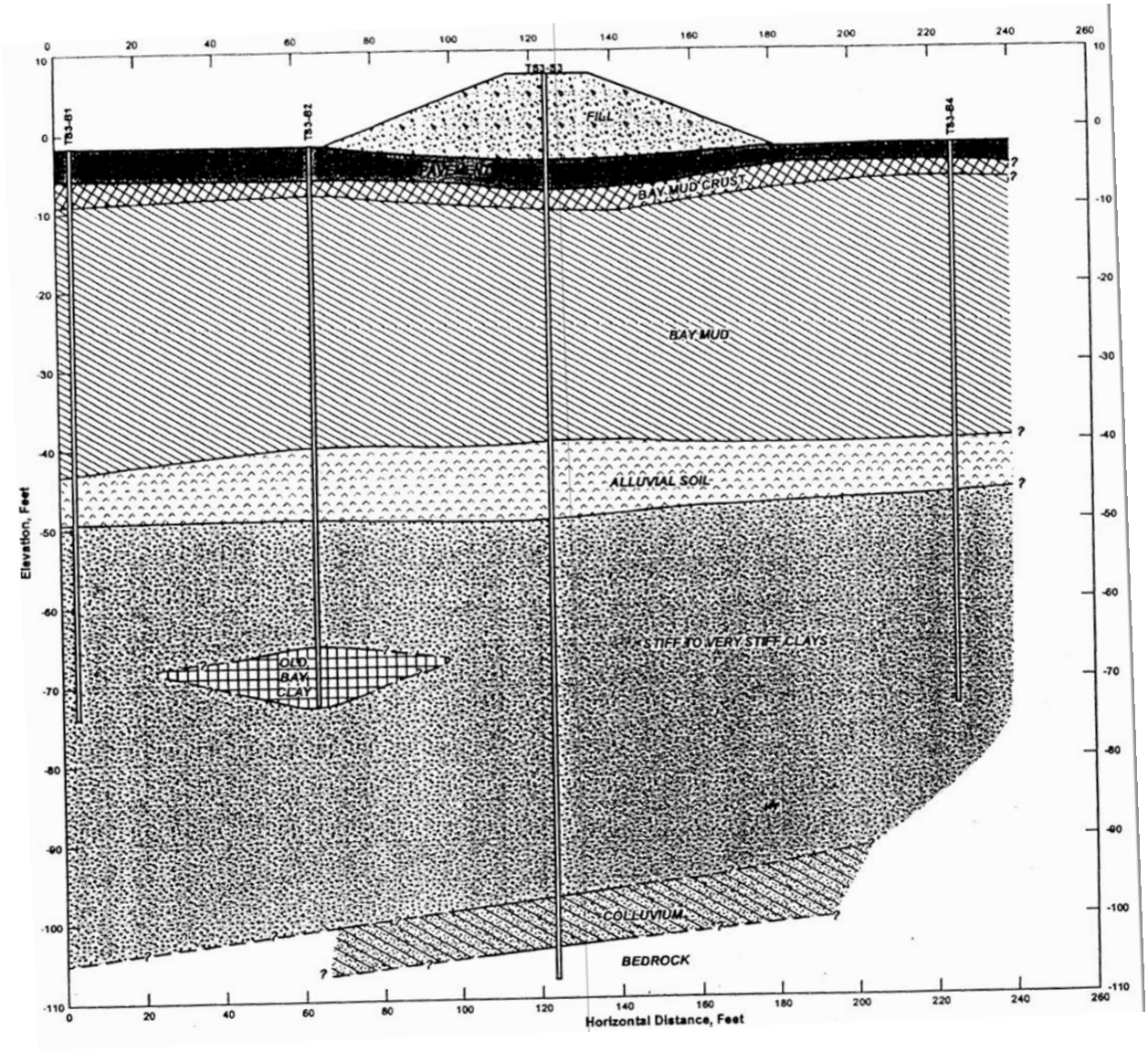

Datum: Mean Sea Level (MSL)

Figure 1.5 - Typical Cross Section at NHPL – TS3
[From URS (2003)]

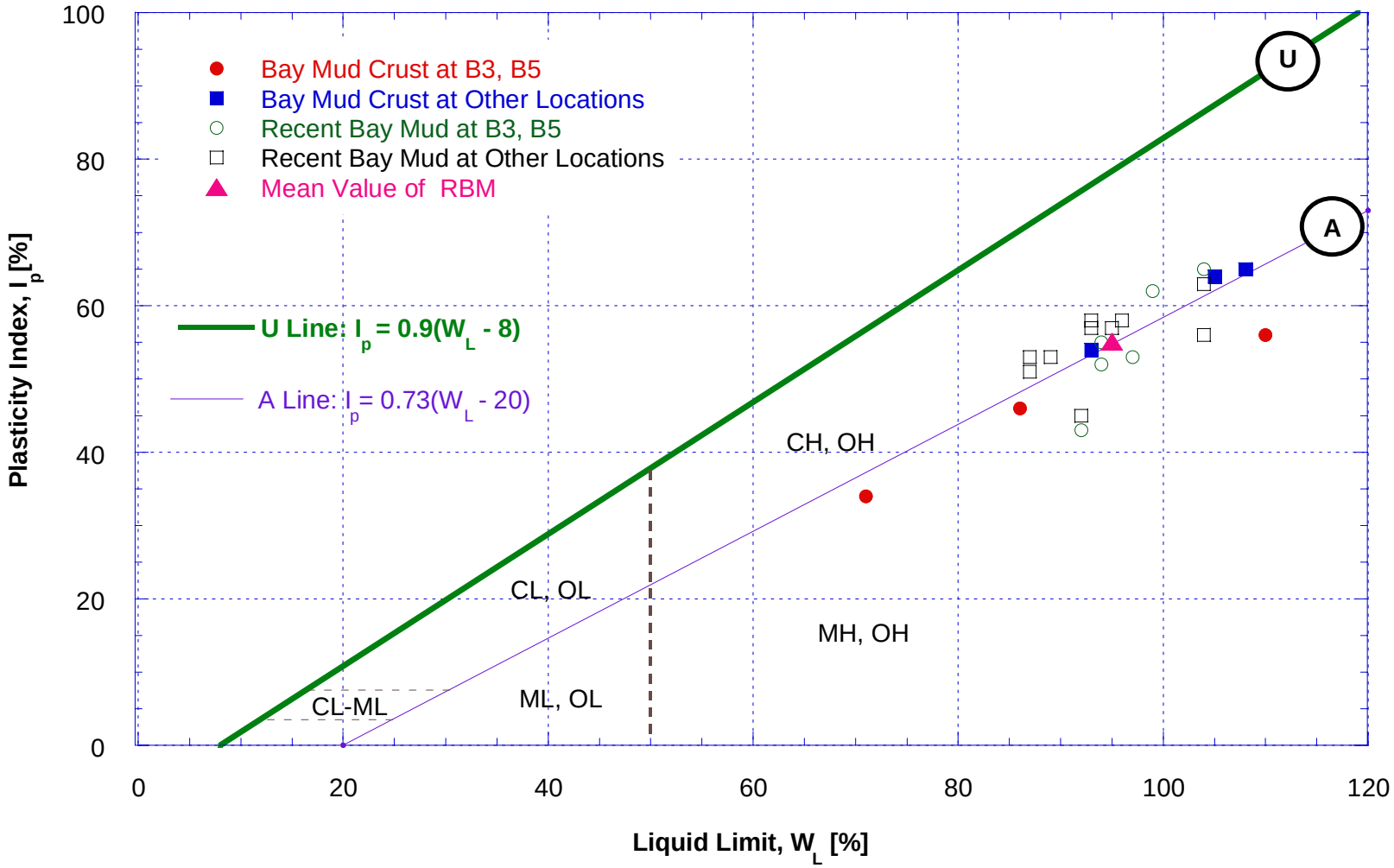

Figure 1.6 Plasticity Chart for Bay Mud at NHPL

CHAPTER 2

PRIOR GEOTECHNICAL STUDIES OF THE NHPL EMBANKMENT

2.1 Introduction

Section 1.3 discussed the overall layout of the project, including a typical soil profile and levee cross-section (e.g., Fig. 1.5). Figure 2.1 shows a plan view of the project with the alignment of the existing NHP levee, and the locations of test and exploration sections designated as TS (i.e., borings, in situ tests and instrumentations). TS3 and TS5, shown in Fig. 2.2, are of prime interest for this study.

The existing NHP levee was built between March and October in 1996 next to the New Hamilton Partnership residential area. There is lack of detailed information about the construction history in the URS reports. The recorded settlement measurements by City of Novato were dated "since November 11, 1996" at points 16, 17, 18 and 19, which are closest to test section TS3 and TS5. The last recorded data presented in URS (2003) was dated January 31, 2002.

The URS comprehensive site investigation took place from December 19, 2001 to February, 2003. The "state-of-the art" site investigation program included borings with tube samples for laboratory tests, in situ field vane and cone penetration tests, and installation of field instrumentation to measure pore pressure, settlements and lateral deformations. The results from this program and from consolidation analyses at the test sections are presented in this chapter.

Chapter 2 of this thesis covers the following material:

- Description of URS field and laboratory test programs and results of settlement monitoring by the City of Novato
- Evaluation of soil properties, especially for the Bay Mud with emphasis on stress history of both virgin (free field) ground and conditions under the levee
- Results of URS consolidation analyses and comparison with measured settlements
- Discussion of using a reduced σ'_p in order to match the measured settlements.

2.2 URS Field and Laboratory Test Programs

2.2.1 Field Test Program

Table 2.1 summarizes the field testing program. The field tests included borings and sampling, field vane tests (FVT), piezocone penetration soundings (CPTU), and downhole geophysical tests. In addition, field instrumentation at test sections included peizometers to measure in situ pore water pressures, inclinometers to measure lateral deformations, and Sondex devices to measure subsurface vertical settlement profiles.

- Borings and Sampling: 19 boreholes were drilled at different locations along the levee alignment (at the crest, toe and in virgin ground) by Pitcher Drilling of Palo Alto, California – a subcontractor of URS. Rotary wash drilling procedures were used for advancing the boreholes. Figure 2.2 shows a plan location of borings and instrumentation and field tests at the main test section area of NHPL. The average ground surface elevation is EL. – 1.6 feet (NGVD) for the free field, and EL. + 6.9 feet (NGVD) for the

crest of levee (Line 3). The ground water table elevation is about EL. – 4.5 feet (NGVD). Note that NGVD elevation zero approximates mean sea level (MSL).

At test section TS3, boring TS3-B1 and TS3-B4 are located about 30 ft away from the toe of the levee. They were assumed to have no affect from the existing NHPL in term of change in soil properties due to the construction and consolidation of the levee, and thus represent virgin ground conditions (or 'free field' conditions). Samples for laboratory consolidation and strength tests on virgin Bay Mud are from boring TS3-B1. Dames and Moore 2.5" diameter, 18" long, fixed piston, brass thin-wall samplers were used to extract most soil samples. This type of sampling technique is close to best practice for getting high quality undisturbed samples (Ladd and DeGroot, 2003). Results of radiography (X-Ray) of the samples at MIT and recorded vertical strains at overburden stress of laboratory test samples show that most of the samples are high-quality.

- **Geonor FV:** In situ preconsolidation stress, σ'_p profiles and undrained shear strength, s_u profiles were obtained from Geonor field vane tests using SHANSEP equation and Bjerrum's field vane correction method (Ladd and DeGroot, 2003):

$$OCR = \frac{\sigma'_p}{\sigma'_v} = \left(\frac{\mu s_u(FV)/\sigma'_v}{S} \right)^{1/m} \qquad (2.1)$$

where OCR = Overconsolidation Ratio, σ'_p = preconsolidation stress, σ'_v = either σ'_{v0} (free field) or σ'_{vc} (under levee), s_u(FV) = measured peak field vane strength, coefficient μ = Bjerrum (1972)'s field vane correction factor empirically correlated with Plasticity Index -I_p, coefficient S = undrained strength ratio for normally consolidated soil, and m = exponent giving increase in undrained shear strength ratio with OCR. URS selected μ =

0.8 based on an average I_p= 50% for BM, S = 0.25 based on prior experience with San Francisco Bay Mud and results of direct simple shear tests, and m = 0.85.

Figure 2.2 also shows the locations where the FVT were conducted at the area of main interest. There are FV tests located at free field (Line 1), toe of levee (Line 2) and under the crest of levee, (Line 3) at each test section TS3 and TS5, for a total of six FV profiles.

- **CPTU and Geophysical tests**: The cone penetration tests with pore pressure measurement (piezocone penetration soundings - CPTU) were also conducted at the site at some locations. The CPTU test gives a continuous log of cone tip resistance, cone side friction, and pore pressures near the tip of the cone. The CPTU was used to evaluate the spatial variation in s_u [$s_u = (q_c - \sigma'_{vo})/N_c$ with N_c = 16]. In addition, excess pore pressures generated during penetration and dissipated when holding the cone give an indication of hydraulic conductivity of soil layers. URS (2003) state that the undrained shear strength profiles estimated from CPTU test results are very close to those estimated by FVT.

Four downhole geophysical tests were performed in the area of test sections to obtain shear wave and compression wave velocities through soil layers as means to extrapolate the spatial variation of soil properties. The shear wave velocity can also serve as a mean for estimating the maximum shear modulus of soils.

- **Instrumentation at TS3&TS5:** Figure 2.2 also shows locations of instrumentation at the two test sections. The instrumentation by URS was started on January 25, 2002 and measured data were available in URS (2003) report until April 20,

2003. Four piezometers clusters (TS3-P4, TS3-P1, TS5-P1 and TS6-P4) were installed at Line 1 and Line 4 (free field locations) to measure the in situ pore pressure of virgin ground and the results show hydrostatic water pressures. The results also show variation in groundwater table (WT) elevation. URS (2003) state that the groundwater table varies between elevations EL. -4.0 and -5.0 feet (i.e., WT at EL. -4.0 ft for TS3 and WT at EL. -4.5 ft for TS5). Two piezometers clusters were installed at Line 3 (TS3-P3 and TS5-P3) and three clusters at the toe of the levee, Line 4' and Line 2 (TS3-P2, TS5-P2 and TS6-P4A) to measure pore pressures under the crest and the toe of the levee. These piezometers showed excess pore pressures, especially at Line 3 where the ground under the levee is still being consolidated.

In addition, two Sondex Profiler devices were installed at TS3, TS3-S1 at Line 1 and TS3-S3 at Line 3, to measure the vertical settlement profile with depth (Note: the Sondex at TS3-S1 was for the test fill that was subsequently constructed during 2005). Two inclinometers were installed at the toe of levee in Line 4'(TS3-I4' and TS5-I4'), one inclinometer (TS6-I4) installed at Line 4 test section TS6, and also two at Line 3 (TS3-I3 and TS5-I3). These inclinometers are to monitor lateral deformations. Measured data of the Sondex Profilers and Inclinometers were dated from February 06, 2002 to November 20, 2002 in URS (2003).

2.2.2 Laboratory Test Program

Table 2.2 shows all laboratory tests performed on the Bay Mud at TS3 and TS5. Good to excellent sampling practices were used to obtain high quality undisturbed samples for laboratory engineering property tests. Sample tube radiography (X-Rays), constant rate of strain consolidation (CRSC), K_0 consolidated - undrained direct simple

shear (CK_0UDSS) and K_0 consolidated - undrained triaxial compression/extension shear (CK_0UTC/TE) tests were all performed at MIT. In addition, conventional incremental oedometer (OED) tests were performed by Signet for URS.

Consolidation tests included 22 CRSC and 16 OED on the Bay Mud to evaluate the preconsolidation stress profile, σ'_p and consolidation engineering properties, e.g., compressibility properties (RR, CR, C_r, C_c, SR, C_α), hydraulic conductivity ($k_{v0,}$ C_k), coefficients of consolidation [c_v(NC), c_v(OC)]. Among the 22 CRSC tests, seven were on samples at boring TS3-B1, which represents the virgin ground. The other CRSC tests are for samples under the crest and toe of the levee.

Undrained shear tests, including CK_0UDSS (7 tests), CK_0UC (3 tests) and CK_0UE (2 tests), were performed using the SHANSEP procedure (Ladd et al., 1977) to evaluate undrained shear strength and modulus properties of Bay Mud (all samples are under the NHP levee). DSS tests were performed at OCR=1 and 2, while all 5 triaxial shear tests were performed at OCR=1.

In addition, many CRSC and CK_0UDSS tests were also run on samples from the South and North Levees with similar index properties, but different stress history.

2.2.3 Unit Weight of Fill and Natural Soils

Table 2.3 summarizes the mean values with standard deviations for total unit weight, water content, liquid limit and plasticity index of the embankment fill and the natural soil layers under the NHPL embankment. Total unit weight of the embankment fill varies between 98 pcf to 144 pcf, with an average value of 126.3 pcf, from 46 density tests. A slightly higher value of 130 pcf was chosen for the fill by URS for settlement

analyses. Three to 4.5 feet of concrete pavement material above the Bay Mud crust was assumed to have a total unit weight of 150 pcf. Bay Mud crust layer unit weight varies from 93 pcf to 106 pcf, with an average value of 100 pcf. The Bay Mud below the Crust has a total unit weight range from 79 pcf to 97 pcf, with an average value of 92.4 pcf. URS selected 92 pcf for the Bay Mud for analysis.

2.3 Measured Settlement of NHPL

Post-construction settlement data of NHPL are provided by City of Novato from 32 settlement markers on the flood wall (levee wall), which is located about 10 ft from the centerline of the levee. Figure 2.3 shows profiles of the thickness of the SFBM and recorded wall settlements (ρ_m or s_m) along the NHPL about 3.8 and 5.2 years after construction. Typical thickness of SFBM layer along the NHPL alignment ranges from 30 to 40 ft. The settlements readings on 1/31/02 generally range from 20 to 30 inches, with a maximum of 32 inches near test section TS1 and a minimum of 13 inches south of TS4.

Figure 2.4 shows plots of settlement vs. log time at survey points 16, 17, 18 and 19, which are near the TS3&5 test section locations. The increasing slope of the curves indicates that the soil layer is still consolidating with a significant zone of virgin compression. The data in the figures also show that settlements were recorded more frequently during the first year (i.e., from 01/07/97 to 07/09/97). After that, only four subsequent readings were taken and scattered roughly once per year. Zero time, t_0 is assumed by the author to occur at mid-point of the embankment construction (approximately 4 months after construction started). Settlements at the survey points 16,

17, 18, and 19 measured on 1/31/02 (about 5 years plus 2 months after construction) are about 20 ± 2 inches (equal to 1.5 to 1.8 ft). Measured settlements at test section TS3 and TS5 are $\rho_m = s_m$ = 1.65 and 1.57 ft respectively (Ladd, 2002). Note that these measured settlements were recorded on the flood wall, which was constructed after the end of placement of embankment fill.

However, changes in elevation of the Concrete Pavement indicate that the actual total settlement at TS3 and TS5 is about 1 to 1.5 ft larger than the measured wall settlements. At TS3, boring B3/I3 at centerline of NHPL shows the elevation of the top of the pavement in February 2002 at -4.1 ft, while for virgin ground (on Line 1 and 4) the elevation of the pavement top is -1.5 ft. Therefore, the difference in pavement elevation is estimated to be about 2.6 ft, and this is considered the actual total settlement. Similar data gives an actual settlement at TS5 of about 3.2 ft.

Borings at Line 3&1	TS3	TS5
Top Pavement elevation Line 3 (ft)	-4.1	-5.0
Top Pavement elevation Line 1 (ft)	-1.5	-1.8
Change in elevation (ft)	- 2.6	- 3.2

Therefore, about 1 to 1.5 ft of settlement is believed to have occurred prior to the first reading of wall settlements. This added settlement occurred either during placement of the levee fill (initial settlement due to undrained shear deformation) or between completion of the levee and the first elevation reading on the levee wall (consolidation settlement) or a combination of both sources of settlement (Ladd, 2002).

2.4 Stress History of Bay Mud

2.4.1 Virgin Ground (Free Field)

The vertical preconsolidation stress profile for virgin ground was investigated at many locations along the NHPL using in situ field vane (FVT) data and at two locations with laboratory consolidation tests. Figure 2.5 shows all results of σ'_p(FV) and laboratory σ'_p for the free field condition. The σ'_p (FV) profile was estimated using the SHANSEP technique in Equation 2.1 with coefficients S= 0.25, m = 0.85 and Bjerrum's field vane correction factor μ=0.8 (for an average Bay Mud I_p=50%). The σ'_p results from CRSC tests on samples at TS3-B1 and OED tests on samples at ES2A-B1.5 are also plotted in the figure to compare with field vane data. The figure also shows a typical overburden vertical effective stress profile, σ'_{vo} for reference.

The data in the figure shows that the σ'_p(FV) profiles at the different locations along the levee are very consistent, except at TS4 where the σ'_p(FV) profile is higher than typical, especially above elevation -20 ft. Figure 2.1 shows that TS4 is located at the far south-end of the NHPL, far from TS3 and TS5. The mean σ'_p(FV) profile for the free field condition therefore excluded data from TS4. Figure 2.5 and Figure 2.6 show that σ'_p data from CRSC tests are in good agreement with the mean σ'_p(FV) profile, whereas OED data at two locations are significantly less than the mean σ'_p(FV) profile (the lower σ'_p from OED tests probably resulted from a combination of lower sample quality and use of 24 hr load increments). On the other hand, the CRSC σ'_p may be about 10% too high due to the strain rate ($d\varepsilon/dt$ = 0.72 %/hr) used to run the CRSC tests as suggested by Mesri and Feng (1992) [Ladd, 2002].

The data on Fig. 2.5 show that the Bay Mud Crust (top few feet of Bay Mud) is highly overconsolidated with OCR in the range of about 6.5 down to 2.5. The soft Bay Mud at greater depth is slightly overconsolidated with OCR = 1.5 - 2.0.

2.4.2 Beneath NHP Levee

The stress history of the Bay Mud under the levee considers: values of σ'_p from lab consolidation tests and field vane tests and the current consolidation stress (σ'_{vc}) determined by subtracting the excess pore pressure (u_e) measured by piezometers from the final consolidation stress (σ'_{vf}) computed by a 2-D finite element analysis. Figure 2.7 shows the u_e profiles selected by URS (2003) at TS3 and TS5. The figure also plots values of u_e computed by the Author from the piezometer data presented in Appendix H of the URS (2003) report. Note that u_e is close to zero at the top and bottom of the soft Bay Mud.

URS computed the current consolidation stress as follows:

$$\sigma'_{vc} = \sigma'_{vo} + \Delta\sigma_v - u_e \qquad (2.2)$$

Where

- σ'_{vo} = initial overburden stress;
- $\Delta\sigma_v$ = change in total stress due to loading of embankment fill (stress distribution $\Delta\sigma_v$ is computed using 2-D finite element – Plaxis code);
- u_e = selected excess pore water pressure profiles shown in Fig. 2.7

Figures 2.8 a, b plot approximate profiles of preconsolidation stresses [σ'_p(FV), σ'_p (CRSC) and σ'_p(DSS)], current consolidation stress (σ'_{vc}), and final consolidation stress (σ'_{vf}) at TS3 and TS5, respectively. The results show that σ'_p from the CRSC and DSS tests are highly scattered about σ'_{vc}, suggesting that the center of the Bay Mud is still consolidating with virgin compression. The σ'_p(FV) data for μ = 0.8 are generally scattered about σ'_{vc} within the central zone, but are much higher near the top and bottom of the clay.

2.5 Consolidation Properties of Bay Mud

2.5.1 Virgin Compressibility, CR

Compressibility parameters of the Bay Mud were evaluated from the most reliable laboratory consolidation tests (i.e., the CRSC and CK_0UDSS tests). Figure 2.9a summarizes URS reported values of virgin compression ratio, CR from these tests (not necessarily for the maximum slope) on Bay Mud at test section TS3 and TS5 both under the levee crest and for virgin ground (TS3-B1). The Compression Ratio, plotted as a function of elevation, for the Bay Mud Crust ranges from about 0.23 to 0.26 and CR of the Bay Mud ranges from about 0.25 to 0.45. URS selected CR=0.41 for consolidation analysis for both Bay Mud and Bay Mud Crust layers.

Figure 2.9.b shows the variation of CR with water content. The data are scattered, but still show a reasonably consistent trend for increasing values of CR with increasing value of water content.

2.5.2 Recompression

Figure 2.10a plots URS reported results of Recompression Ratio, RR from CRSC and DSS tests on Bay Mud as functions of elevation and Virgin Compression Ratio. There is considerable scatter in the data, with values of RR ranging from 0.019 to 0.038. URS selected RR = 0.04 for calculation of recompression settlements based on the empirical correlation RR = 0.1CR (typical range, RR/CR = 0.05 - 0.10, for many clays).However, the RR versus CR plot shows that the data are scattered about RR/CR= 0.075CR.

In Table 2-A of URS (2003), URS reported RR as well Swelling Ratio (SR) separately. Figure 2.10b plots SR data versus elevation and compares SR with RR from the CRSC tests. It should be noted that the CRSC tests did not have unload/reload cycles.[2] Also, independent interpretations by Professor Ladd and the Author of RR from CRSC tests at boring TS3-B1 (virgin ground) as a function of σ'_{vc}/σ'_{p} are presented in Chapter 3.

2.5.3 Coefficient of Consolidation (NC)

Figure 2.11 plots Bay Mud coefficients of vertical consolidation, c_v versus Liquid Limit compared with the commonly used correlation from DM-7.1 (NAVFAC 1982). Data are shown from CRSC and OED tests on samples from the NHPL levee and from other levees of the project. The plot shows c_v values for both normally consolidated and overconsolidated Bay Mud. c_v(NC) values of Bay Mud are highly scattered and

[2] The author assumes that URS interpreted RR from the slope of the first loading curve in the DSS and CRSC tests.

generally fall on to well above the DM-7 mean-line. The average c_v(NC) is roughly 10 ft^2/yr and most c_v(OC) values are about 100 ft^2/yr or higher.

2.5.4 Coefficient of Permeability

Figure 2.12 shows a typical plot of void ratio versus logarithm of vertical consolidation stress and hydraulic conductivity (permeability) from CRSC tests on Bay Mud during 1-D compression. The slope of e-logk curve defines the coefficient $C_k = \Delta e/\Delta \log k$. The intersection between the C_k slope and the line of constant e_0 defines the initial vertical hydraulic conductivity (k_{v0}).

URS selected C_k = 1.143 and initial values of hydraulic conductivities of $k_{v0} = 4.0 \times 10^{-4}$ ft/day and $k_{h0} = 8.0 \times 10^{-4}$ ft/day for their Plaxis consolidation analyses of the NHP levee.

2.6 Undrained Strength Properties of Bay Mud

2.6.1 Overview of MIT CK_0U Test Program

Undrained shear properties of the Bay Mud were evaluated in the MIT laboratory using state-of-the-art testing techniques. The MIT testing program included many K_0 Consolidated - Undrained Direct Simple Shear (CK_0UDSS) tests and several K_0 Consolidated - Undrained Triaxial Compression and Extension (CK_0UTC/TE) tests to evaluate the anisotropic strength and deformation properties of Bay Mud. Undisturbed soil samples were consolidated using the SHANSEP technique (Ladd, and Foott, 1974) to simulate in situ anisotropic stress conditions (i.e., K_0 condition) and then sheared

undrained in different modes of shearing (e.g., direct simple shear, DSS; triaxial compression, TC or triaxial extension, TE) to evaluate the stress-strain anisotropic properties of the Bay Mud.

2.6.2 CK_0UDSS

Many DSS tests were run on Bay Mud at NHP levee and other levee segments around the entire project site. There were 7 tests run on Bay Mud samples at NHPL, one of them with OCR = 2 and the rest with OCR=1. In addition, DSS tests were run on samples taken along the alignment of North Levees 1 and 2 (N1, N2), which included tests at OCR = 2 and 3. For NC Bay Mud (OCR =1), all tests show fairly consistent normalized undrained strength ratios, τ/σ'_{vc} at maximum stress ranging from 0.23 to 0.26. At OCR = 2 and 3, the average undrained strength ratios increased to 0.47 and 0.57 respectively. Detailed interpretation of the CK_0UDSS tests will be presented in Chapter 3.

2.6.3 CK_0UTX

Five CK_0UTX tests were run on Bay Mud at NHP levee. Three of them were triaxial compression (CK_0UTC) and the other two were triaxial extension (CK_0UTE). The test samples were taken at the middle zone of Bay Mud layer, namely at El. -18.1 ft at TS5 (under the levee crest) and at EL. -21.1 ft at TS3 (virgin ground). All five samples were tested at OCR = 1. The results from the tests show that the undrained strength ratio in compression mode (TC) is 0.348 ± 0.032 and in extension mode (TE) is 0.274 ± 0.016. For the three compression tests, the minimum value of friction angle is $\phi'_{tc} = 38.7^0$ and the maximum value is $\phi'_{tc} = 54^0$. The friction angle measured at ε_a = 10% for the two

extension tests are ϕ'_{te} equal to 60^0 and 78^0. Detailed results of the triaxial tests will be presented in Chapter 3.

In summary, two of the three TC tests and both TE tests gave undrained strength ratios and friction angles much higher than expected based on typical behavior as summarized in Ladd and DeGroot (2003).

2.7 Settlement Analyses by URS

2.7.1 Methodology

URS used the same format and principles in Equation 1.1 to calculate consolidation settlements of the NHPL, namely:

$$\rho_c = \sum H_i \left[RR \log \frac{\sigma'_p}{\sigma'_{vo}} + CR \log \frac{\sigma'_{vc}}{\sigma'_p} \right] \qquad (2.3)$$

where ρ_c = predicted consolidation settlement at current vertical effective consolidation stress σ'_{vc} , H_i = initial layer thickness, σ'_{v0} = initial vertical effective stress, σ'_p = preconsolidation stress, RR = Recompression Ratio, CR = Virgin Compression Ratio.

In Equation 2.3, $\sigma'_{vc} = \sigma'_{vf} - u_e$, where $\sigma'_{vf} = \sigma'_{v0} + \Delta\sigma_v$. Also note that σ'_{vc} replaces σ'_p if the soil remains overconsolidated. The current vertical consolidation stress, σ'_{vc} is computed as in Equation 2.2.

The soil properties selected by URS for predicting settlements at 5 test sections (TS1 to TS5) using Equation 2.3 are:

- Recompression Ratio: RR = 0.04;

- Virgin Compression Ratio: CR=0.41;
- Bjerrum's correction factor μ = 0.8 for PI = 50% selected based on agreement between the computed $\sigma'_{p(FV)}$ and σ'_p data from CRSC tests;
- Preconsolidation stress profile: σ'_p= mean $\sigma'_{p(FV)}$ profile at 7 test locations for the free field condition (see Fig.2.5);
- Total unit weights used to calculate the initial and final stresses: Levee Fill = 129 pcf, Pavement Slab = 150 pcf, Riprap =135 pcf, Fill = 130 pcf, Bay Mud Crust = 100 pcf, and BM = 92 pcf;
- Water table at EL. = - 5.0 ft.

The URS (2003) report does not show the soil profiles used for the 1-D consolidation settlement analyses at the 5 test section locations. However, Professor Ladd was provided the spreadsheets used for the settlement calculation from which he developed the soil profiles shown in Fig. 2.15.

2.7.2 Analyses at TS3, TS5 and Other Locations

Stress histories used in settlement calculations are evaluated in Fig. 2.13 for TS3 as follows:

- Line No.1 = Preconsolidation stress σ'_p(FV) computed with correction factors μ=0.8 and 0.6 based on the mean FV data of test locations along the NHPL levee (free field condition);

- Line No.2 = Current vertical consolidation effective stress σ'_{vc} (= σ'_{vf} - u_e), where σ'_{vf} is the final consolidation stress ($\sigma'_{vf} = \sigma'_{vo} + \Delta\sigma_v$) computed with Plaxis, u_e = current

excess pore water pressure measured from the field piezometers data (e.g., the URS profiles in Fig. 2.7);

- Line No.3 = initial effective overburden stress (σ'_{vo});

- Line No.4 = Final consolidation stress (σ'_{vf}) computed from Plaxis accounting for fill stiffness and increased modulus of the concrete slab and the Bay Mud Crust;

- Line No.5 = Current σ'_p(FV) computed with μ=0.8 and 0.6 from FV tests run under the crest of the levee. This line is not used for calculating ρ_c, but is shown for perspective since it theoretically should not exceed Line 1, except where σ'_{vc} is greater than Line 1 (Ladd, 2002).

The shaded zones are where the soil is normally consolidated because the current consolidation stress profile (σ'_{vc}) surpasses the virgin preconsolidation stress σ'_p(FV) profile. For μ=0.8, this virgin compression zone occurs near the top of the Bay Mud and is roughly only about one third of the Bay Mud thickness. Therefore, about 2/3 of the Bay Mud thickness would be in recompression range, and some 60% of the computed ρ_c for the mean μ=0.8 profile comes from recompression rather than virgin compression (Ladd, 2002).

The virgin compression zone is significantly increased, as shown in Figure 2.13b, when reducing μ =0.8 to μ=0.6, which decreases the estimated σ'_p (FV) profile by 29%. This reduced σ'_p profile is significantly lower than the laboratory σ'_p results from high quality undisturbed samples and high quality lab CRSC tests. In addition, using μ = 0.6 also predicts a σ'_p(FV) profile under the levee that is less than the current effective consolidation stress (σ'_{vc}), which is not consistent with reality.

Figure 2.14 shows the correlation between the field vane correction factor, μ versus computed settlement for mean σ'_p(FV) profiles at TS3 and TS5. Computed settlements corresponding to three values of μ (0.8, 0.7 and 0.6) are plotted to establish a line from which one can determine the value of $\mu = \mu_a$, at which the measured settlement, ρ_m equals the computed settlement, ρ_c. The results show that, in order to match the measured and the computed settlements, the required FV correction factors are $\mu_a = 0.66$ for TS3 and $\mu_a = 0.65$ for TS5.

Figure 2.15 summarizes the results of measured versus predicted settlements for mean σ'_p(FV) profiles at TS1 through TS5. The figure shows, at each test section, the soil profile, measured settlement ($s_m = \rho_m$) at 01/31/02, computed consolidation settlement for μ=0.8 (ρ_c), and the derived value of μ_a leading to agreement between measured and predicted settlement (Ladd, 2002).

For the TS3 levee with thickness H=11.0 ft, elevation of the bottom of the crust = -9.5 ft, and thickness of the soft Bay Mud T=32 ft: the measured settlement $\rho_m = 1.65$ ft, computed settlement for μ =0.8 $\rho_c = 0.61$ ft, meaning the measured settlement equals 2.7 times the computed settlement, and the derived $\mu_a = 0.66$.

For the TS5 levee with thickness H=11.5 ft, elevation of the bottom of the crust = -10 ft, thickness of the soft BM T=30 ft: the measured settlement $\rho_m = 1.57$ ft, computed settlement for μ=0.8 $\rho_c = 0.58$ ft, meaning the measured settlement again equals 2.7 times the computed settlement and the derived $\mu_a = 0.65$. Figure 2.15 also shows values of μ_a at the three other locations, these being lower than computed for TS3 and TS5 with μ_a = 0.57 to 0.60 (latter based on σ'_p (FV) at TS4 rather than the mean for NHPL).

2.8 Discussion

In general, for all test sections, the computed settlements for σ'_p(FV) using μ=0.8 are some three to four times less than the measured settlements. Note that: (1) the measured settlements had not even taken into account the 1.0 to 1.5 ft of settlement that probably occurred before measuring the wall settlement; and (2) μ = 0.8 presents the "best estimate" σ'_p profile. In conclusion, the very large discrepancy between measured and calculated settlement was "entirely unexpected" (Ladd, 2002).

To proceed with the design of the new Containment Dike and Hydraulic Fill, URS selected a reduced preconsolidation stress profile equal to 80% of the μ = 0.8 field vane preconsolidation stress profile, i.e., a design $\sigma'_p = 0.8\sigma'_p$(FV), which corresponds to using μ_a = 0.662. The consolidation – deformation analyses were done using the finite element code Plaxis with the Soft Soil Model.

It was highly unusual and unexpected that the measured settlements of the NHP levee were several times larger than predicted from conventional one-dimensional settlements calculations given the comprehensive, state-of-the art field and laboratory testing programs that had been used to characterize the stress history and compressibility parameters of the soft Bay Mud layer.

Professor Ladd in his 2002 report thoroughly assessed potential reasons that might have caused this large discrepancy. His assessment and discussion focused on: (1) potential errors in parameter selection for settlement calculations using Equation 2.3 assuming Hypothesis A and that the measured wall settlements closely approximate 1-D

consolidation of the Bay Mud below the levee (i.e., ignoring settlement due to lateral deformations); (2) the decrease in σ'_p when applying Equation 2.3 according to Hypothesis B; and (3) potential increases in the total settlement of the levee due to lateral shear induced deformations because of undrained shear strains during initial loading (initial settlement), which also would continue to increase with time due to undrained or partially drained creep.

As noted above, to achieve agreement between predictions and the measured settlements, URS reduced the best estimate preconsolidation stress (σ'_p) profile derived from field vane tests by 20%, which corresponds to $\mu_a = 0.65$. This reduction in σ'_p, which significantly increases the predicted settlement due to virgin compression, is consistent with proponents of Hypothesis B for $C_\alpha/CR = 0.045$ and assuming that creep starts at one day. Hypothesis B assumes that secondary compression (1-D creep) occurs throughout primary consolidation, which displaces the in situ compression curve to the left of the laboratory curve, and therefore reduces the in situ σ'_p.

According to Ladd (2002), although Hypothesis B provides a theoretical basis for reducing σ'_p in settlement predictions, a "more likely explanation" lies in lateral deformations of the Bay Mud. It is well established that two-dimensional loads on soft clays, similar to the NHPL, will produce undrained shear deformations that can be significant with highly plastic, organic clays such as the Bay Mud (e.g., Foott and Ladd, 1981). These soil types also are likely to be highly creep susceptible, meaning that the lateral deformations continue to increase during the consolidation process, and therefore generate settlements greater than predicted for 1-D consolidation. However, increased settlements due to creep-type lateral deformations cannot be reliably predicted.

The thesis therefore will perform finite element analyses using a simple soil model to evaluate the potential values of initial settlements during construction, to look at rates of consolidation settlement, and to assess the effect of varying preconsolidation stress profile. It also will re-evaluate the soil properties and soil profiles selected by URS (2003), both for simple 1-D consolidation analyses and the more complex finite element analyses.

Table 2.1 Summary of Field Tests – Geotechnical Exploration and Measurements for NHP Levee

Tasks	**Technique/contractor**	**Quantity**	**Remarks**
FIELD WORK			
Borings with sampling along the alignment of NHPL	Rotary wash drilling; Dames Moore U-sampler, Pitcher sampler, Dames & Moore Piston Sampler, and SPT	19 bore holes	Taking undisturbed samples typically at 5 ft depth intervals in Bay Mud borehole logs; Dames&More Piston Sampler used to get undisturbed sample (2.5 inches in diameter and 18 inches long –brass tubes) for laboratory tests. Also some 3" ϕ Osterberg sampler for MIT DSS tests.
Field vane tests	Geonor device	20 locations	- Undrained shear strength and stress history spatial variations under and adjacent to levee; - Field vane correction factor $\mu = 0.8$.
CPTU tests (piezocone penetration tests)	$N_k = 16$	7 locations	- Tip resistance, side friction, pore pressures used mainly to provide information on stratigraphy and strength; - Pore pressure dissipation proved the sandy layer under the BayMud is a draining layer.
Downhole geophysical tests	Redpath Geophysics of Murphys, California	4 locations, in the area of the proposed new test fill	- Compression and shear wave velocities; SFBM has shear wave velocity = 255 to 270 ft/sec (free field) -Deposit stratigraphy.
Instrumentation: Piezometers, inclinometers and Sondex devices	URS	6 test sections, 26 piezometers, 2 inclinometers, 2 Sondex systems	- Pore pressures, lateral deformation, vertical settlement profiles; -TS3 and 5 at proposed test fill area.
Prior settlement monitoring program after construction of NHPL From Oct. 96 to Jan. 31, 2002	City of Novato	32 points, 200-foot spacing along the NHPL alignment	- Settlement markers were installed on the floodwall (about 3.0 ft away from center of the levee crest) - Baseline readings were taken between Oct. 7 and Dec. 4, 1996 - Between baseline and Jan. 2002, 11 sets of readings were taken

Table 2.2 Laboratory Testing on Bay Mud for NHP Levee

Tasks	**Technique/contractor**	**Quantity**	**Remarks**
LAB WORK	MIT Signet Testing Lab (URS)		
Index tests (Atterberg limits, grain size analyses, moisture content, specific gravity and density)	- ASTM D422, D 1140, D 4318, D 2216, D2937	All tubes	
X-rays	MIT	All tubes tested at MIT	All tubes sent to MIT for X-rays for assessing microfabric and sample quality
Consolidation tests (CRSC) Conventional incremental Oedometer tests	ASTM D 4186, MIT ASTM D 2435, Signet	22 CRSC 16 OED	Compressibility and hydraulic conductivity parameters and stress history Casagrande and Becker et al. (1987) strain energy techniques for σ'_p
CK_0U-DSS	ASTM D 6528, MIT	7 DSS	SHANSEP technique with values of S & m; DSS also provided compressibility and σ'_p
CK_0UTC/TE	ASTM D 4767, MIT	3 TC 2 TE	

Table 2.3 Summary of Index Tests on Levee Fill and Natural Soils (From URS 2003)

Soil unit	**Total Unit weight γ_t, [pcf]**	**Total Unit weight Chosen for Analysis by URS γ_t, [pcf]**	**Moisture Content ω_n [%]**	**Liquid Limit ω_L [%]**	**Plasticity Index I_p [%]**
Levee Fill	126.3 ± 9.8	130	16.8 ± 11.4		
Concrete Pavement		150			
Bay Mud Crust	99.8 ± 4.5	100	65.3 ± 16.5	95.5 ± 15.2	53.2 ± 11.7
Bay Mud	92.4 ± 4.1	92	93.7 ± 22.4	109.8 ± 43.4 (1)	62.6 ± 22.7 (2)
Alluvial Soils (Stiff Clays)	120.7 ± 9.0	120	33.6 ± 14.0	45.8 ± 20.7	23.7 ± 15.2
Dense Sand		130			
Old Bay Mud		130			

(1) Includes 2 tests with w_L = 220 and 236. If these are excluded, mean w_L = 95.0%.

(2) Includes 2 tests with I_P = 114 and 131. If these are excluded, mean I_P = 55.1%.

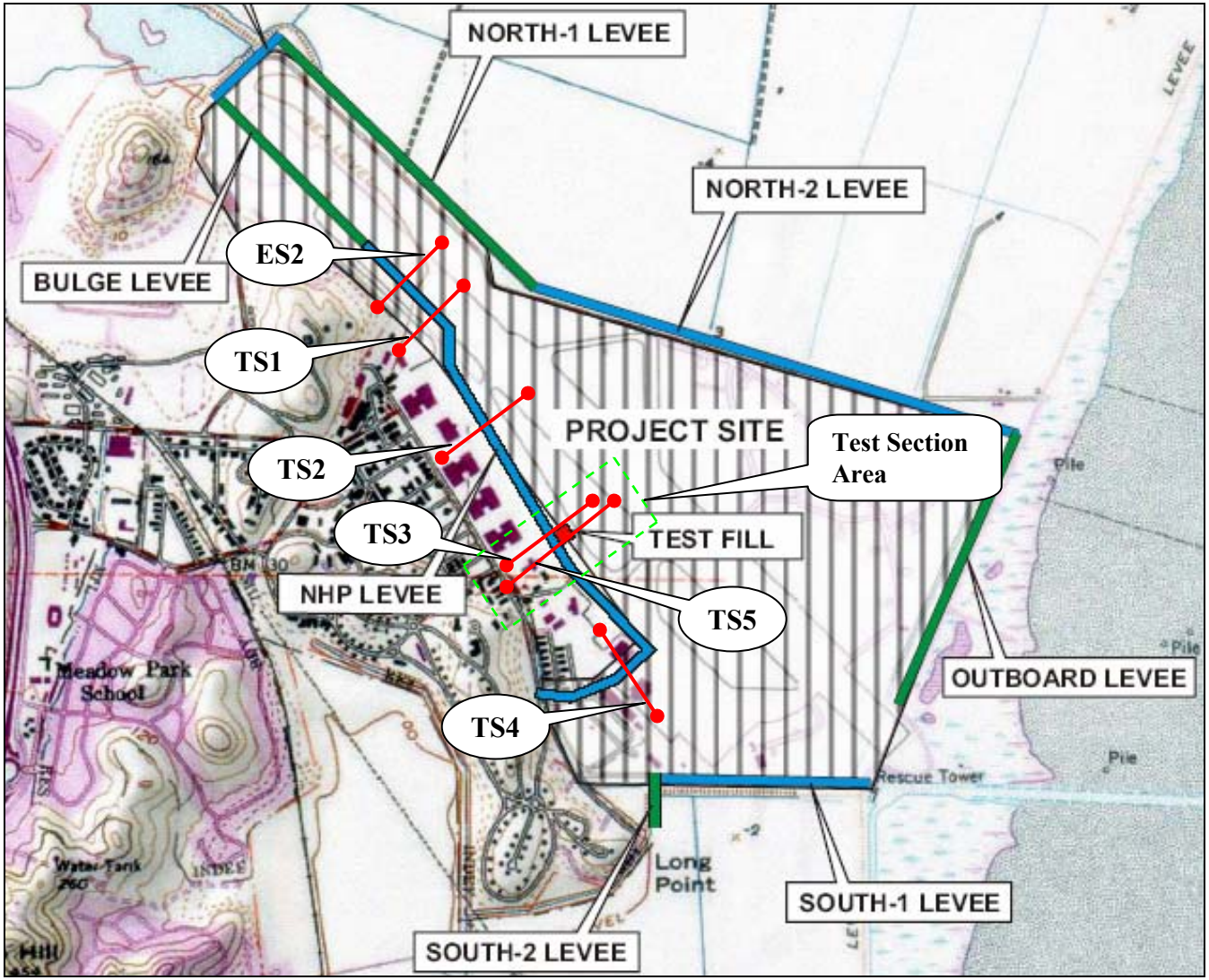

Figure 2.1 Plan of NHPL with Location of Test Sections
[Modified from URS (2003)]

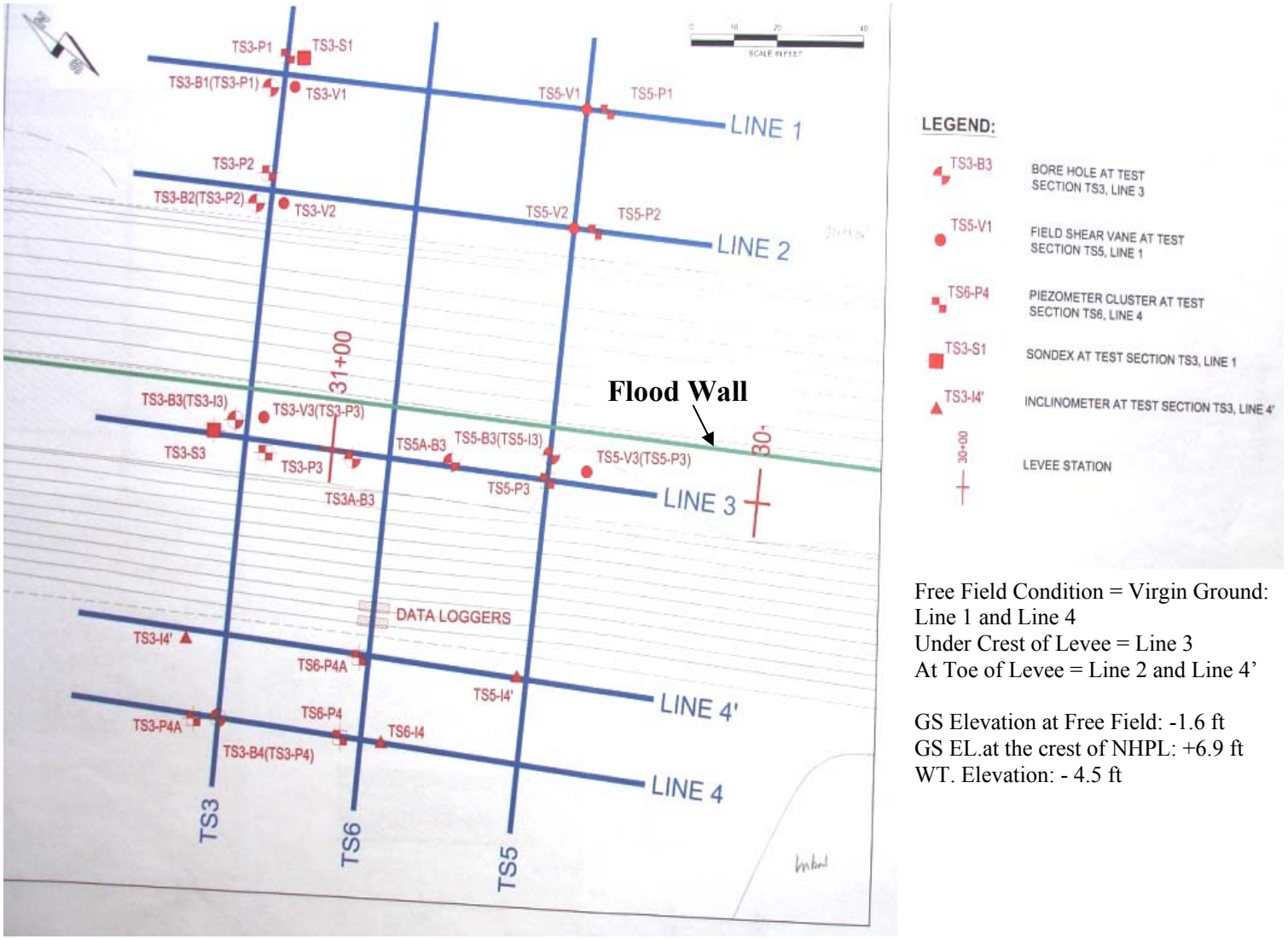

Free Field Condition = Virgin Ground:
Line 1 and Line 4
Under Crest of Levee = Line 3
At Toe of Levee = Line 2 and Line 4'

GS Elevation at Free Field: -1.6 ft
GS EL.at the crest of NHPL: +6.9 ft
WT. Elevation: - 4.5 ft

Figure 2.2 Plan of Test Section Area with Borings, Field Tests and Instrumentation
[From URS, 2003]

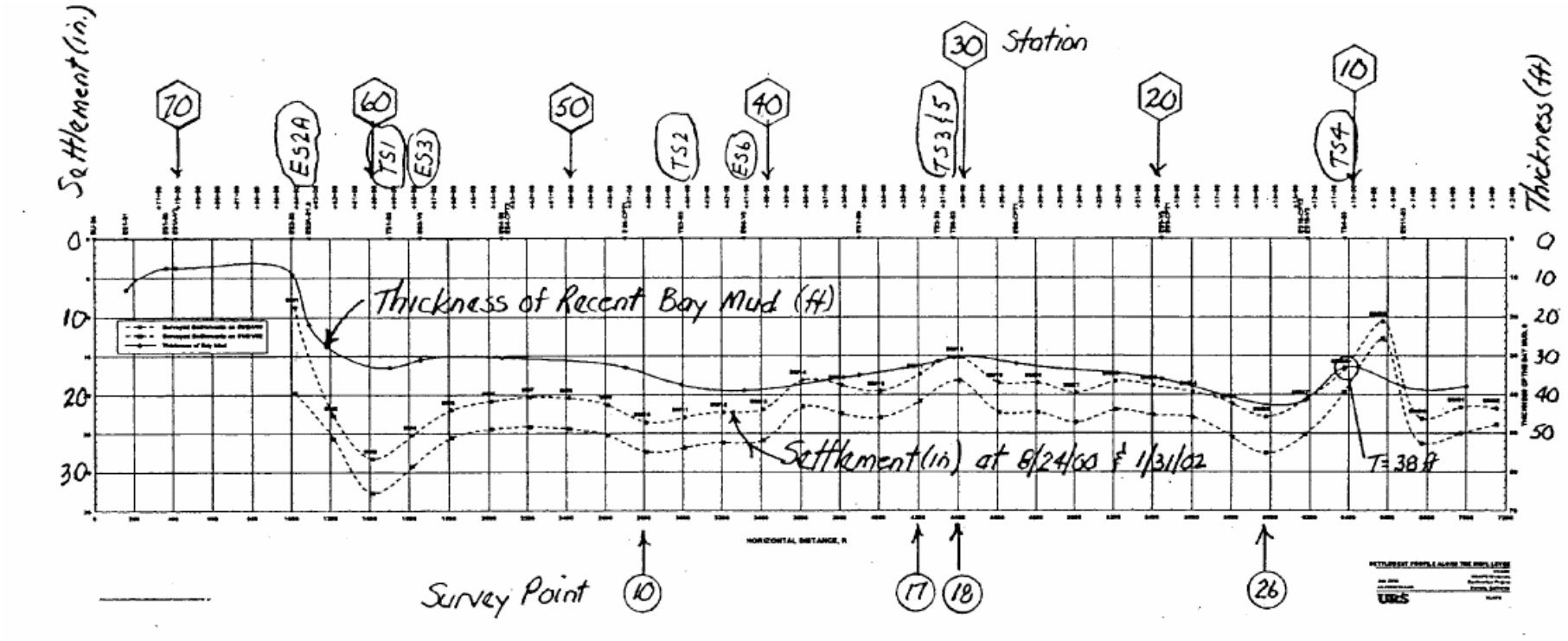

Figure 2.3 Settlement Data, Thickness of Bay Mud, Test Section Locations and Settlement Survey Points along NHP Levee

[From URS, 2003 and Ladd, 2002]

Note: Time zero equals 10/07/96 to 12/04/96 for points 1 to 32

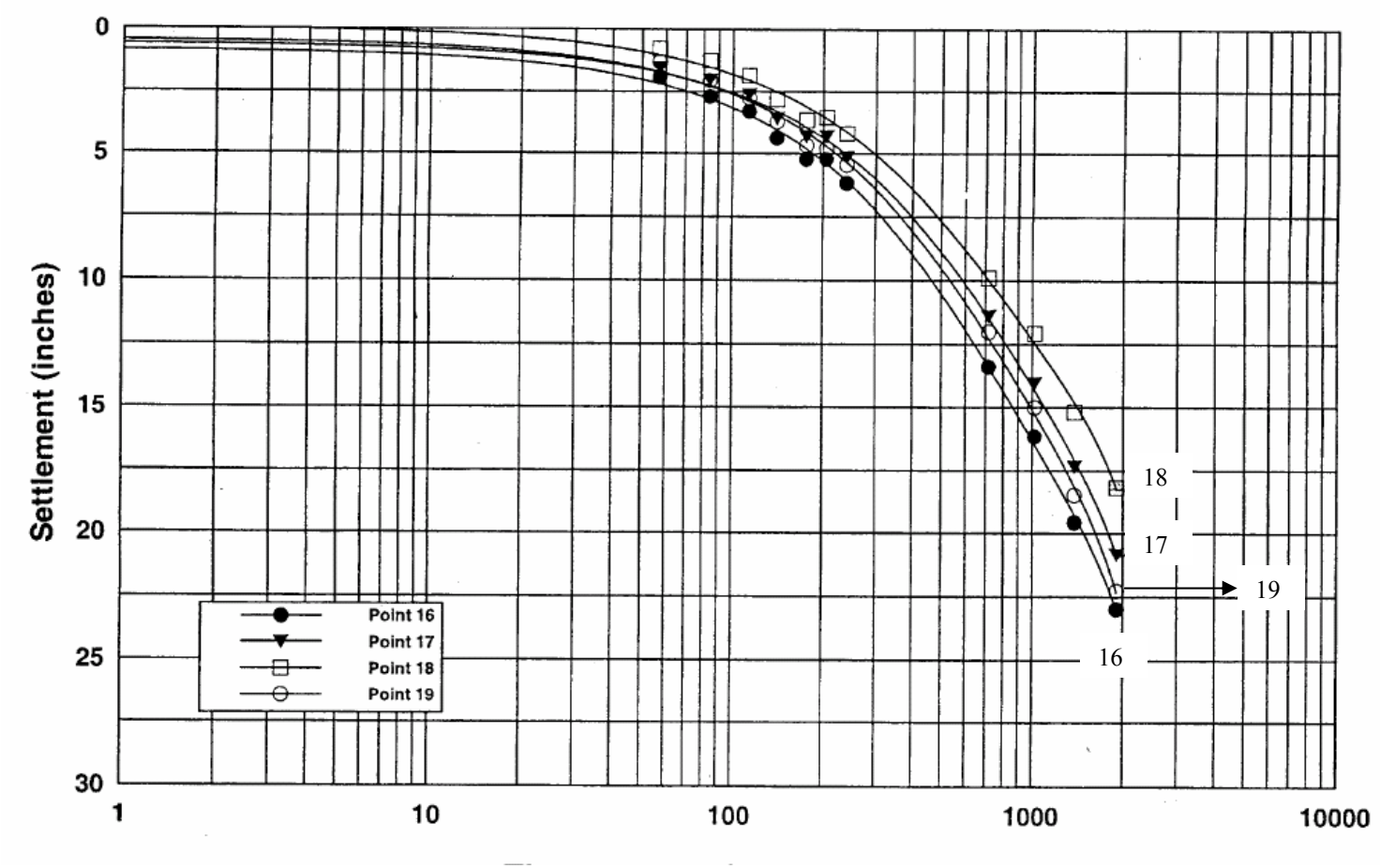

Figure 2.4a Settlements vs Log[time] at Survey Points Near Test Section TS3&TS5
(From URS, 2003)

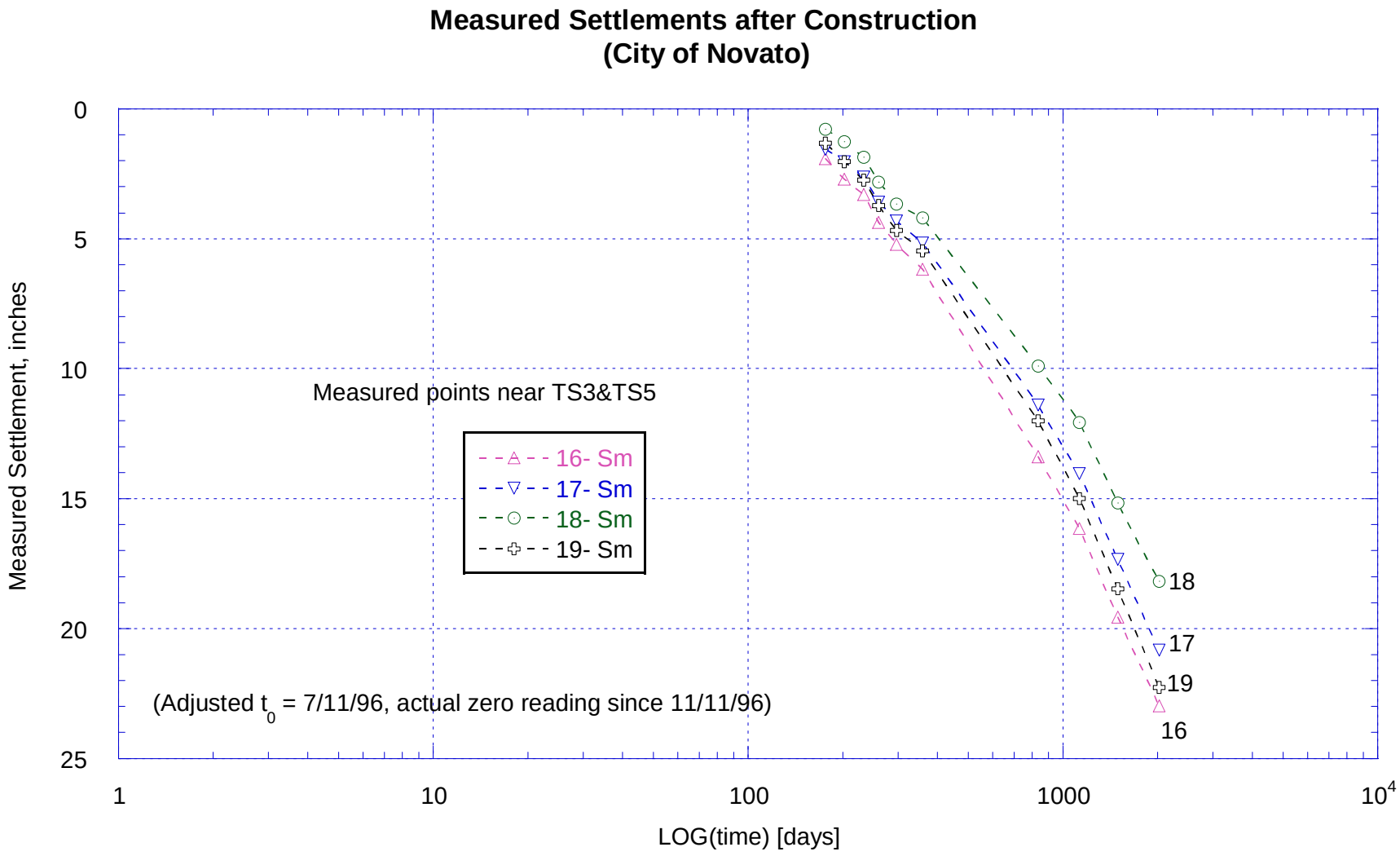

Figure 2.4b Settlements vs. Log[time] at Survey Points Near Test Section TS3&TS5 (Modified Plot)
(Modified from URS, 2003)

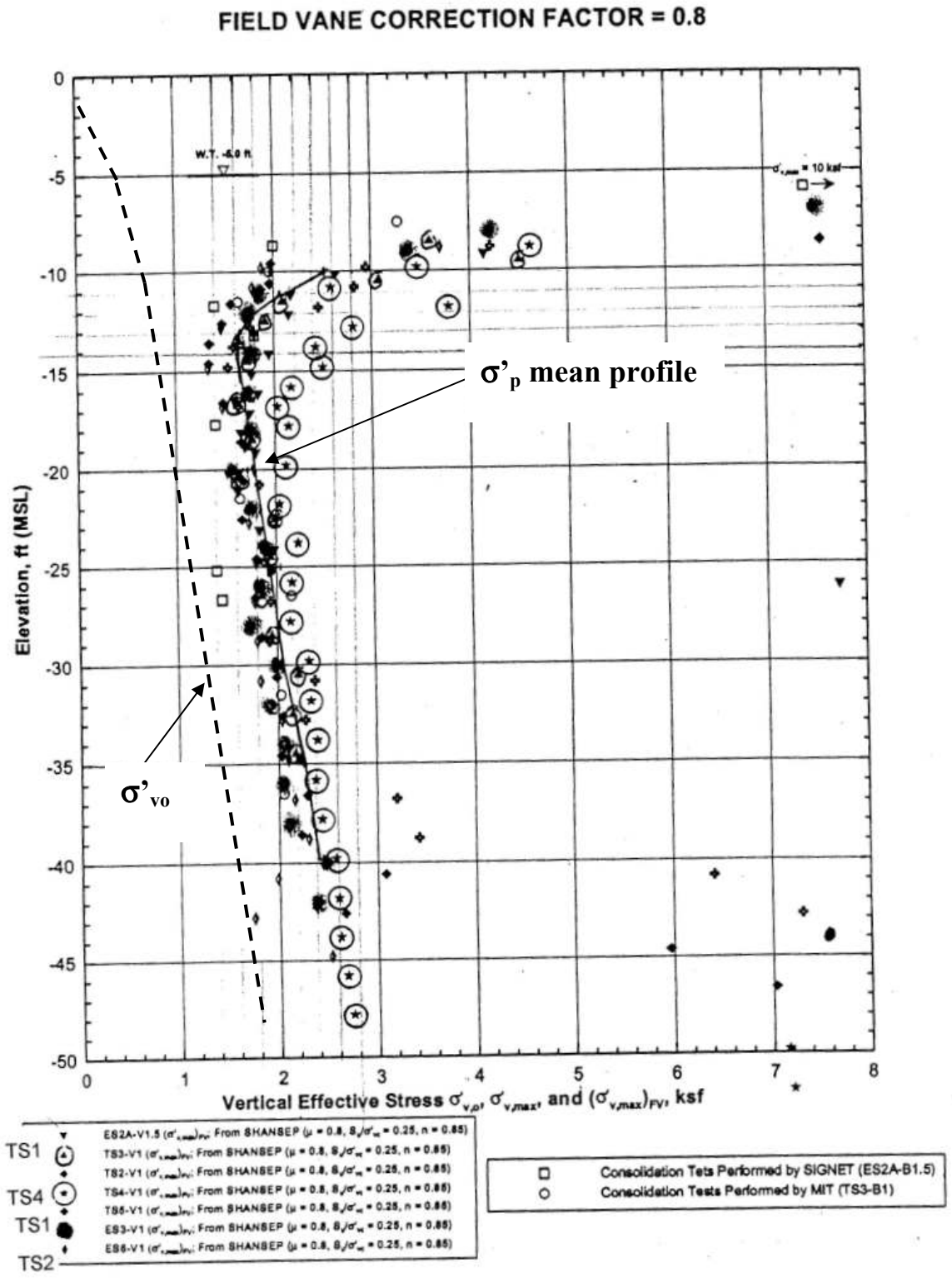

Figure 2.5 Summary of NHPL Free Field σ'_p(FV) for μ=0.8 and Laboratory σ'_p

[From URS (2003) and Ladd (2002)]

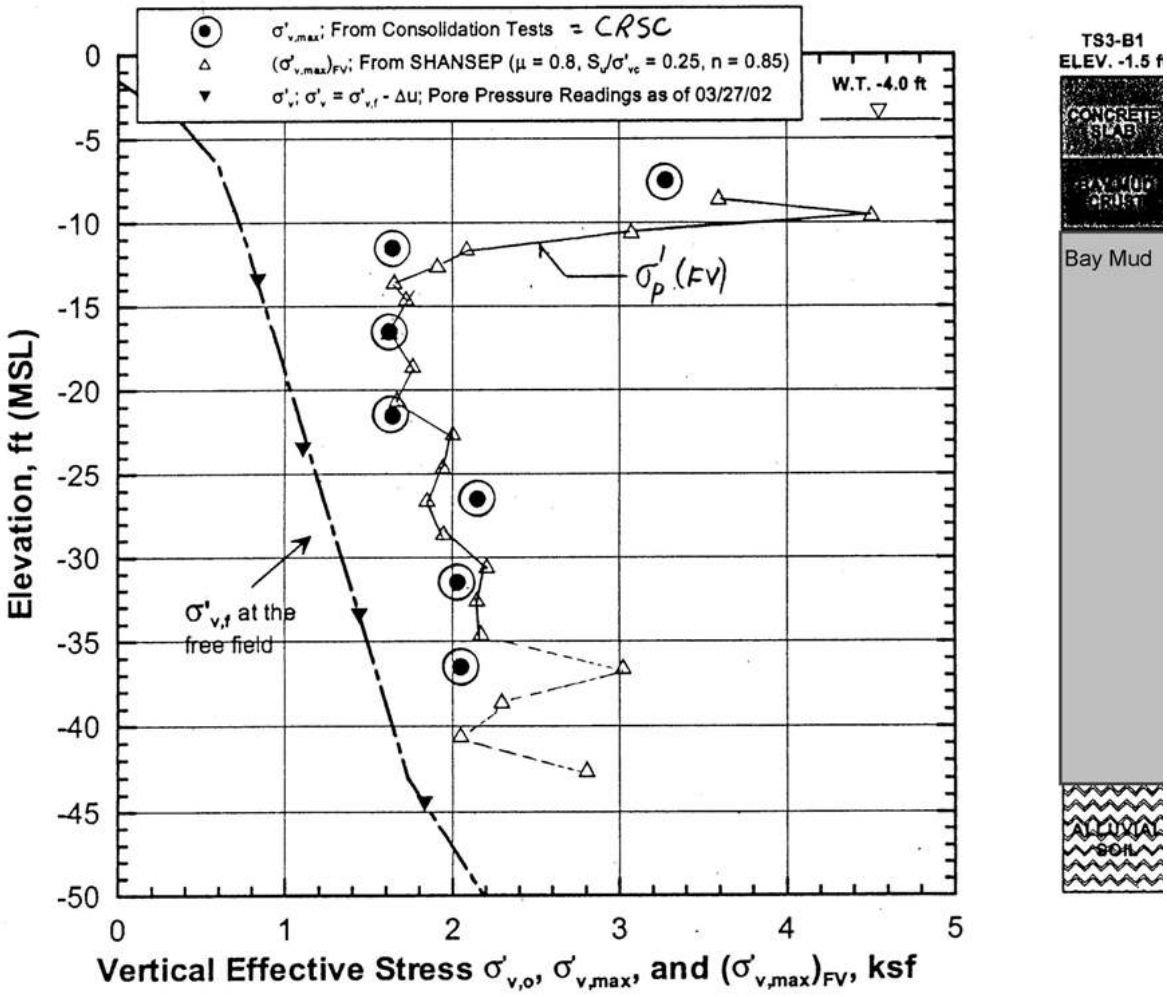

Figure 2.6a Stress History at TS3, Comparison of μ =0.8 σ'$_p$(FV) vs. σ'$_p$(CRSC)

[From URS (2003) and Ladd (2002)]

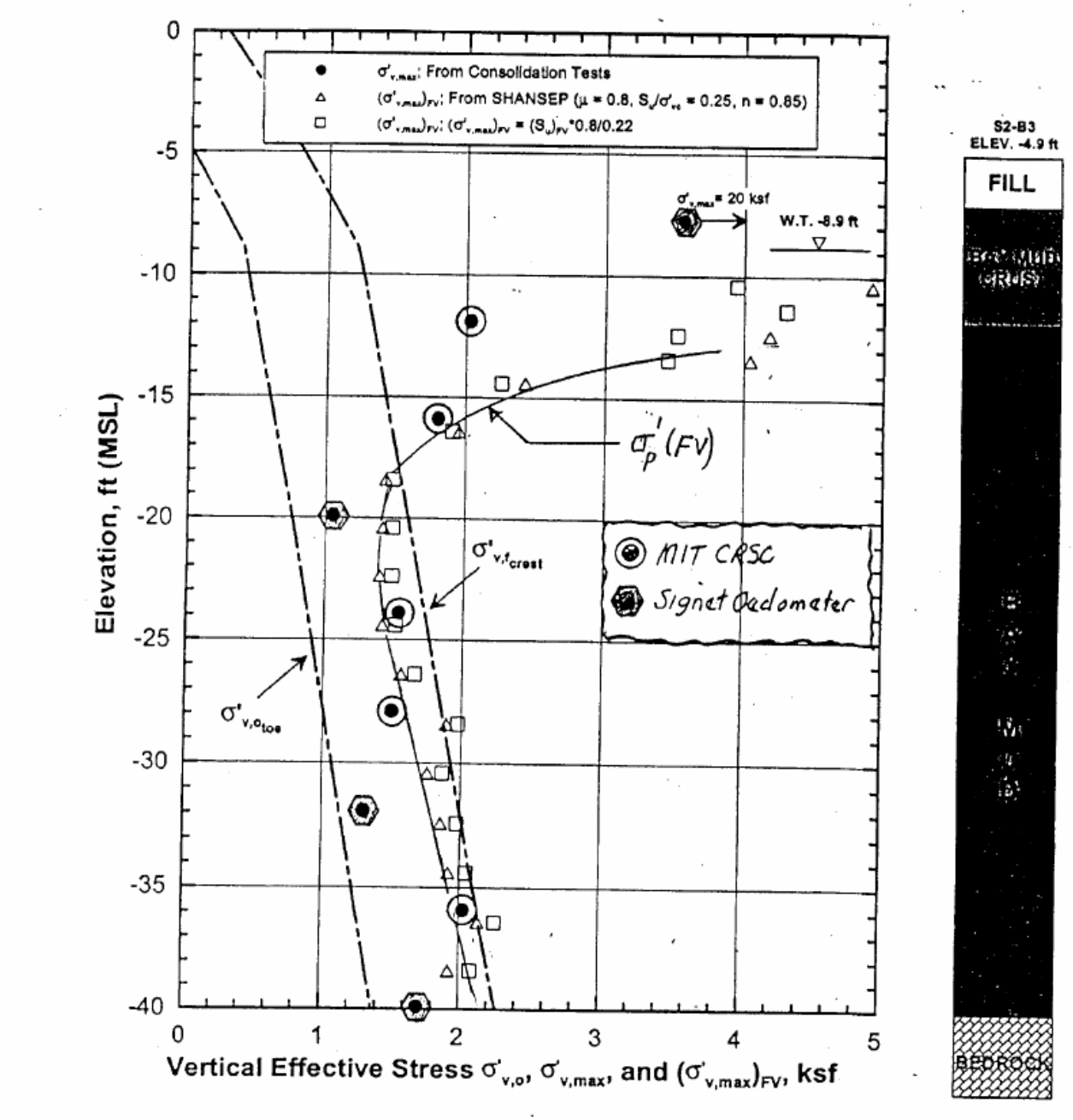

Figure 2.6b Comparison of μ=0.8 σ'$_p$(FV) with σ'$_p$ from CRSC and Oedometer Tests at S2-B3 (South Levee)

[From URS (2003) and Ladd (2002)]

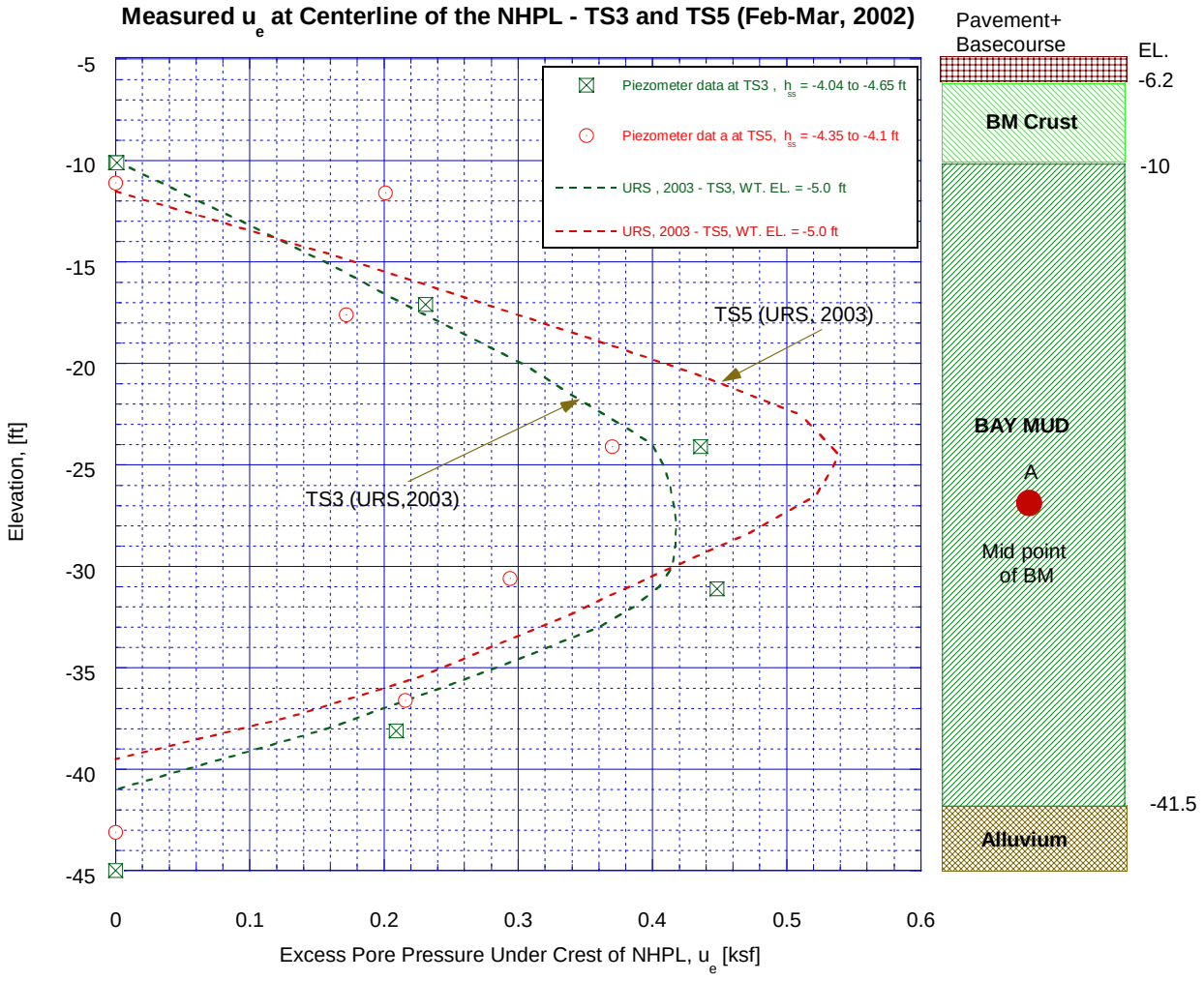

Figure 2.7 Excess Pore Pressure Measured at TS3 & TS5 [From URS (2003) for Period, Jan-Mar, 2002]

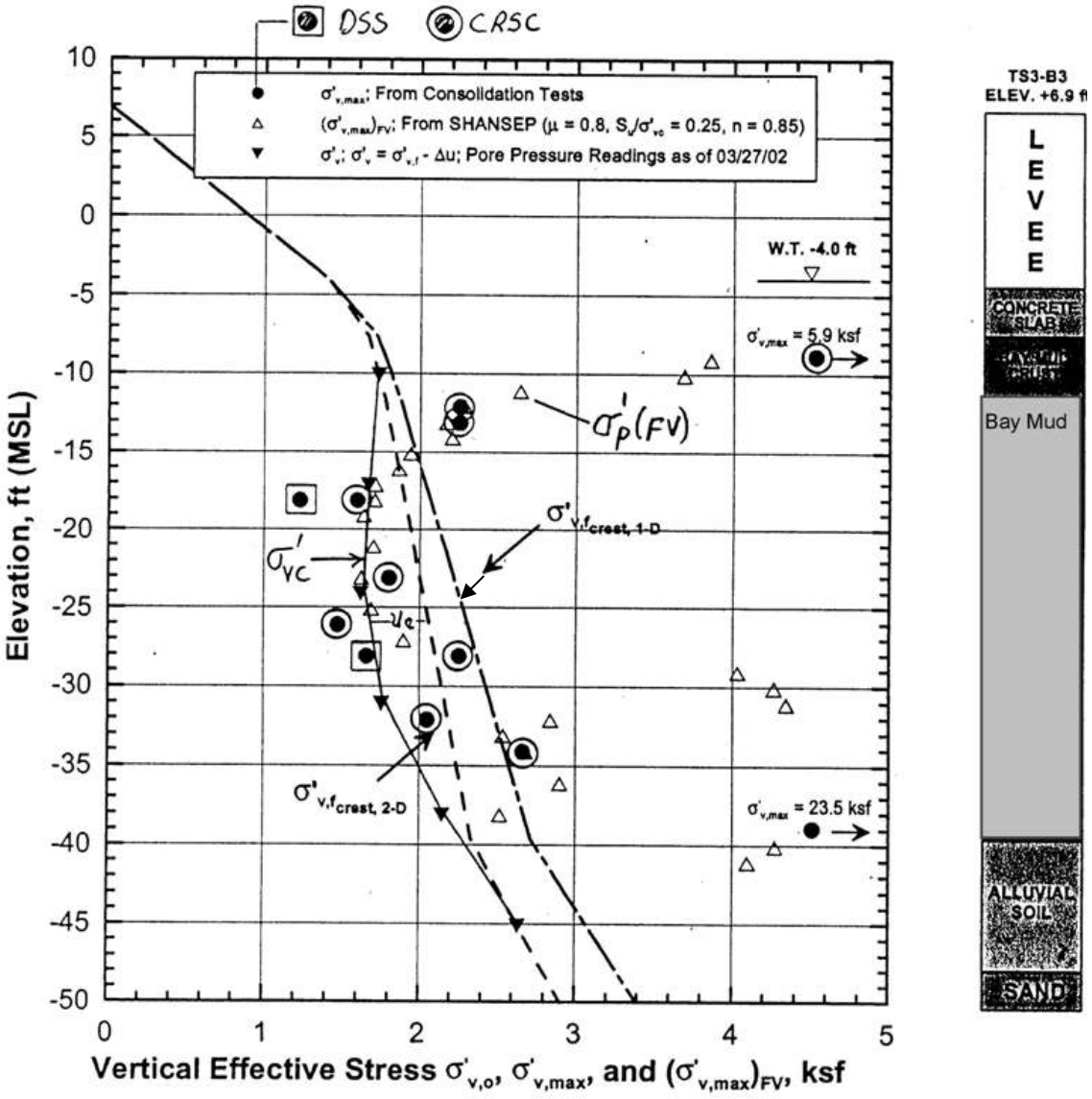

Figure 2.8a Stress History under Crest of Levee at TS3
[From URS (2003) and Ladd (2002)]

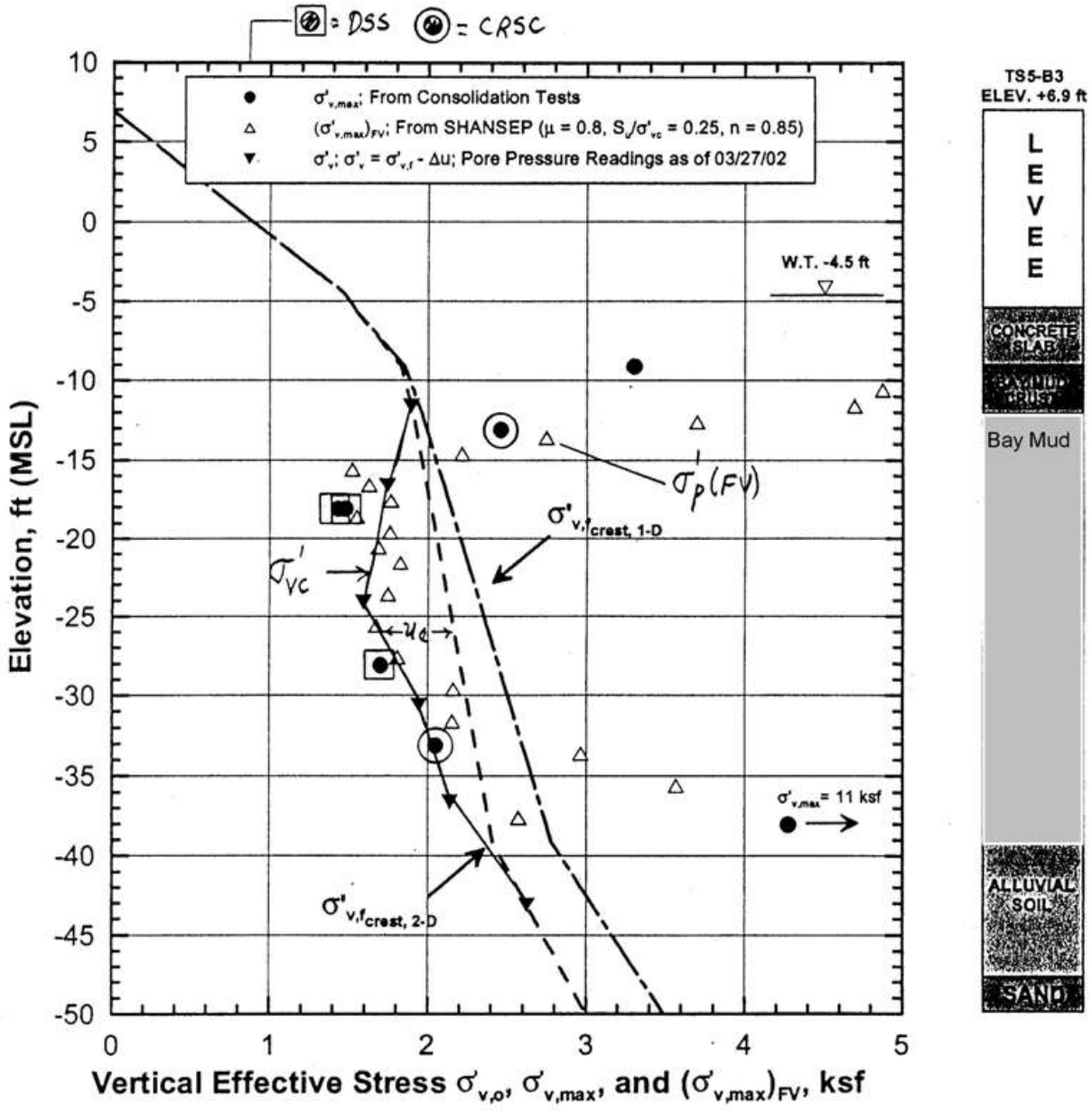

Figure 2.8b Stress History of under Crest of Levee at TS5

[From URS (2003) and Ladd (2002)]

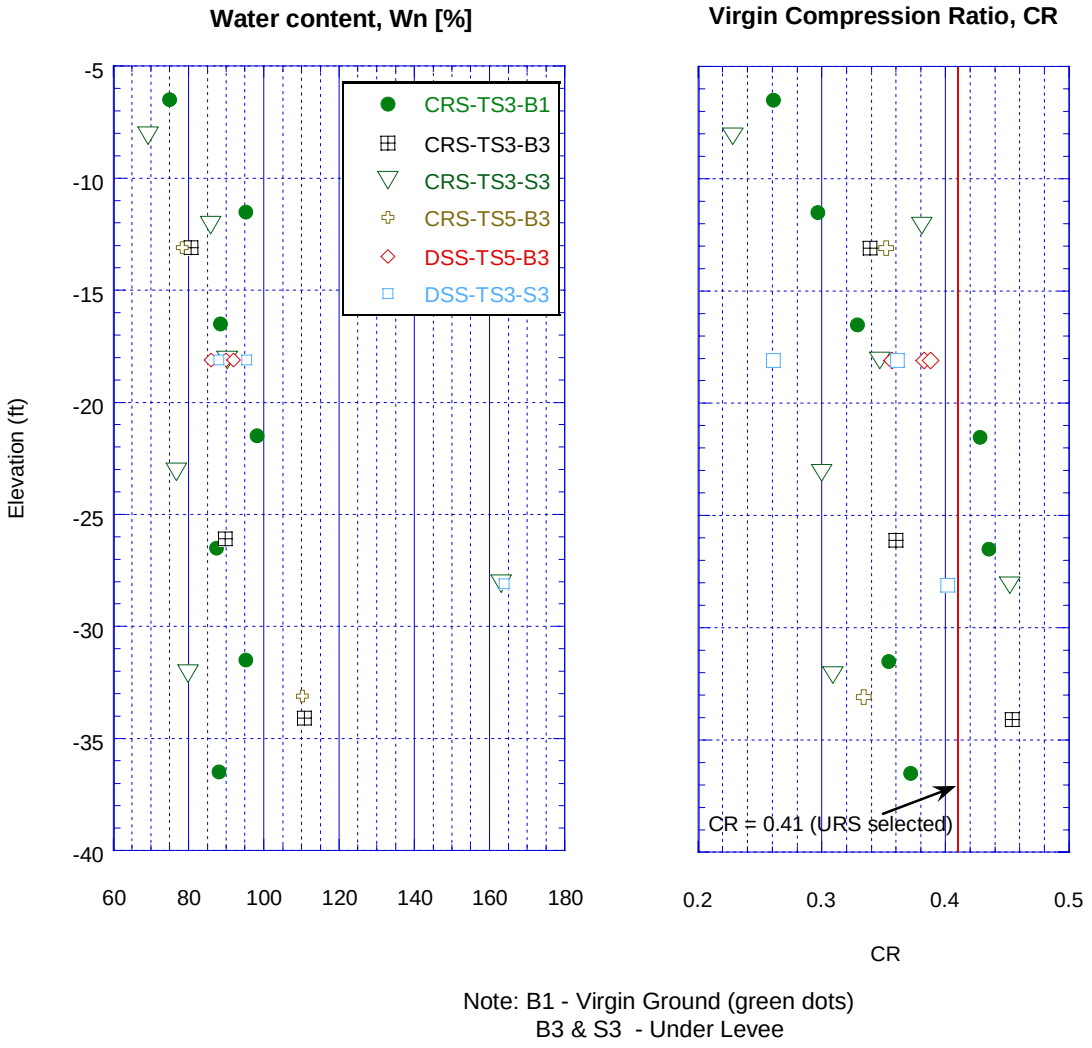

Figure 2.9a Water Content and Virgin Compressibility of NHPL Bay Mud vs. Elevation
[Data from URS (2003)]

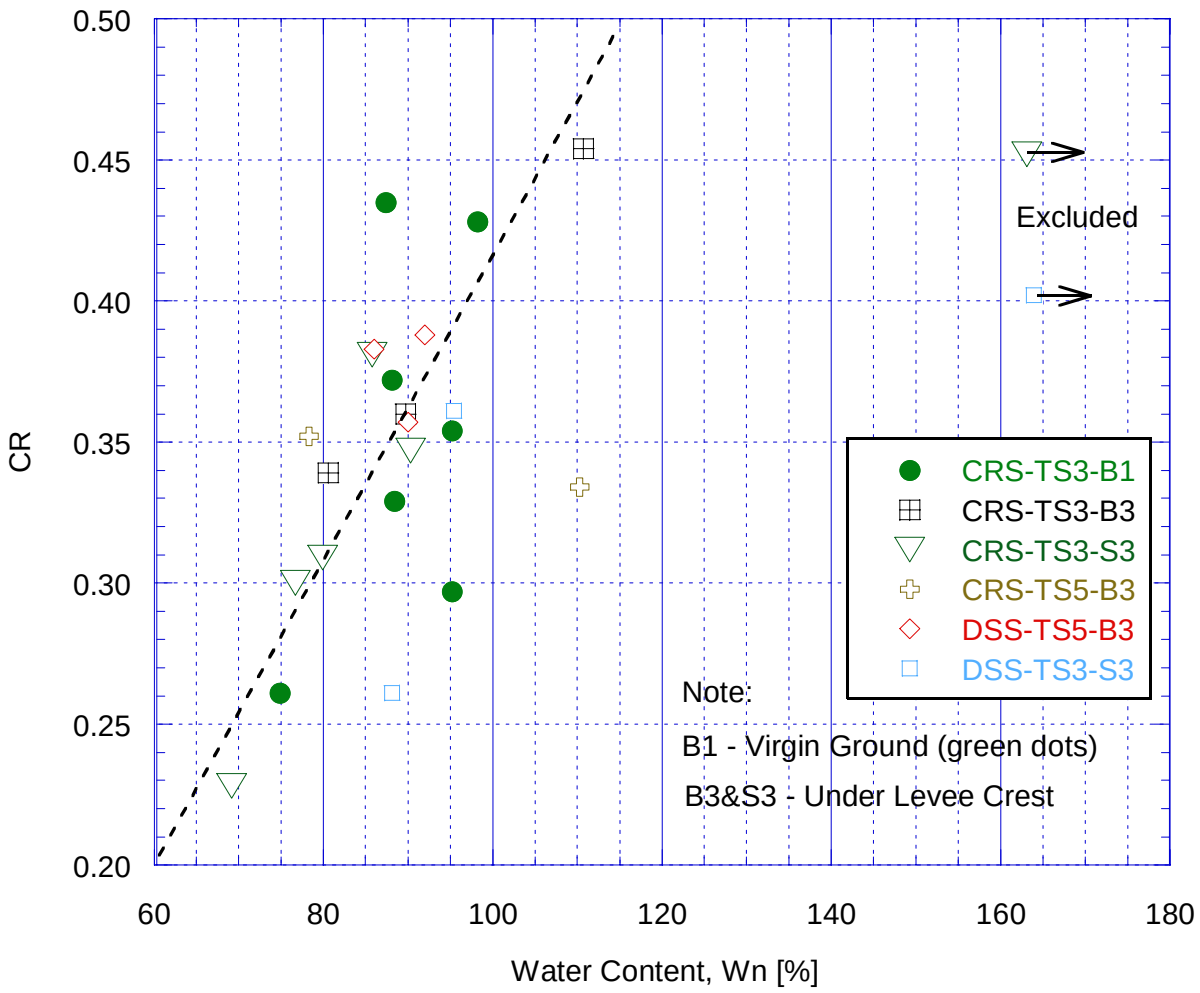

Figure 2.9b Virgin Compression Ratio vs. Natural Water Content of NHPL Bay Mud
[Data from URS (2003)]

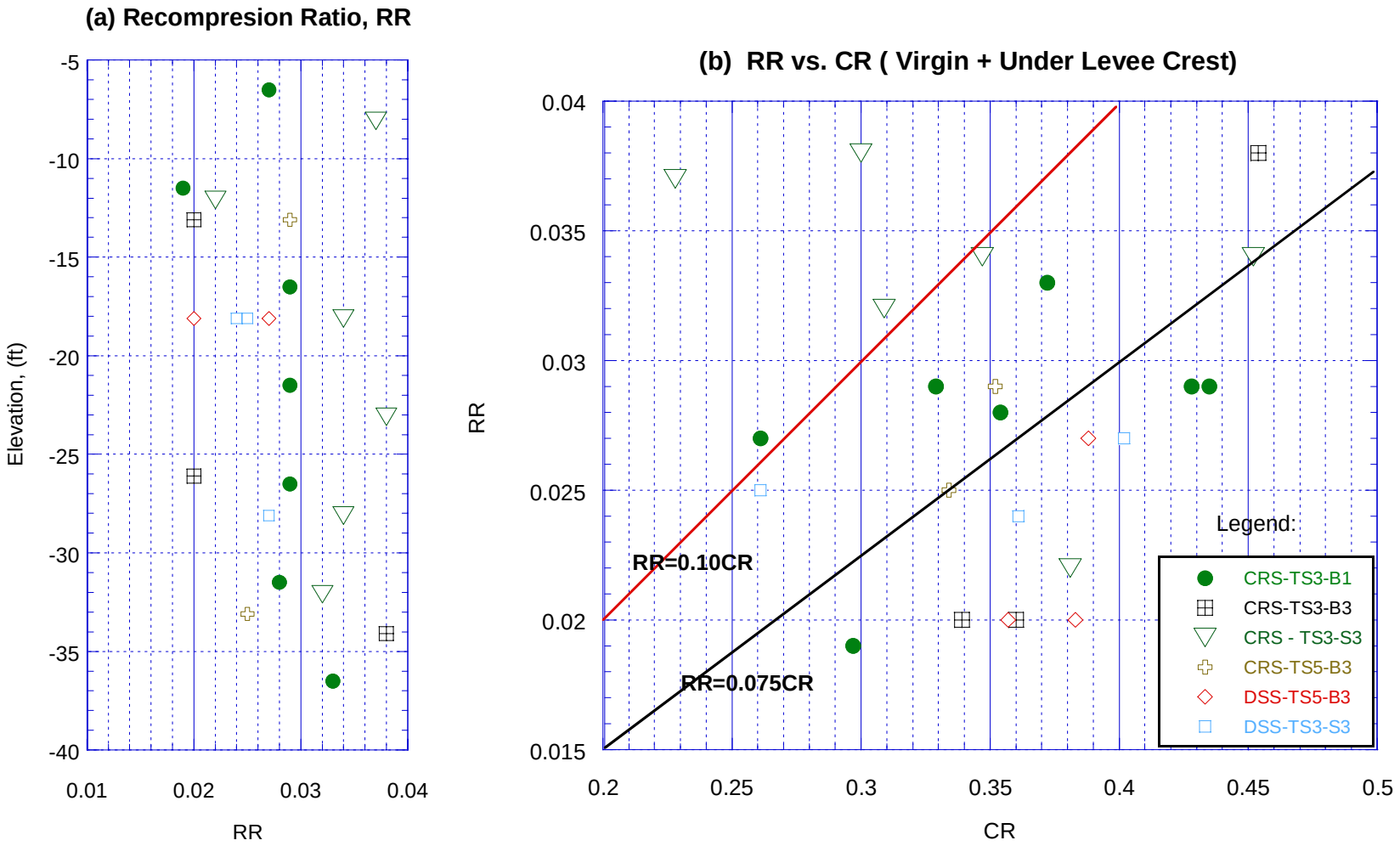

(b)

Note: B1- Virgin Ground (green dots); B3 & S3 – Under Levee Crest

Figure 2.10a Recompression Ratio, RR vs. Elevation and CR (Virgin + Under Levee Crest)
[Data from Table 2-A, URS (2003)]

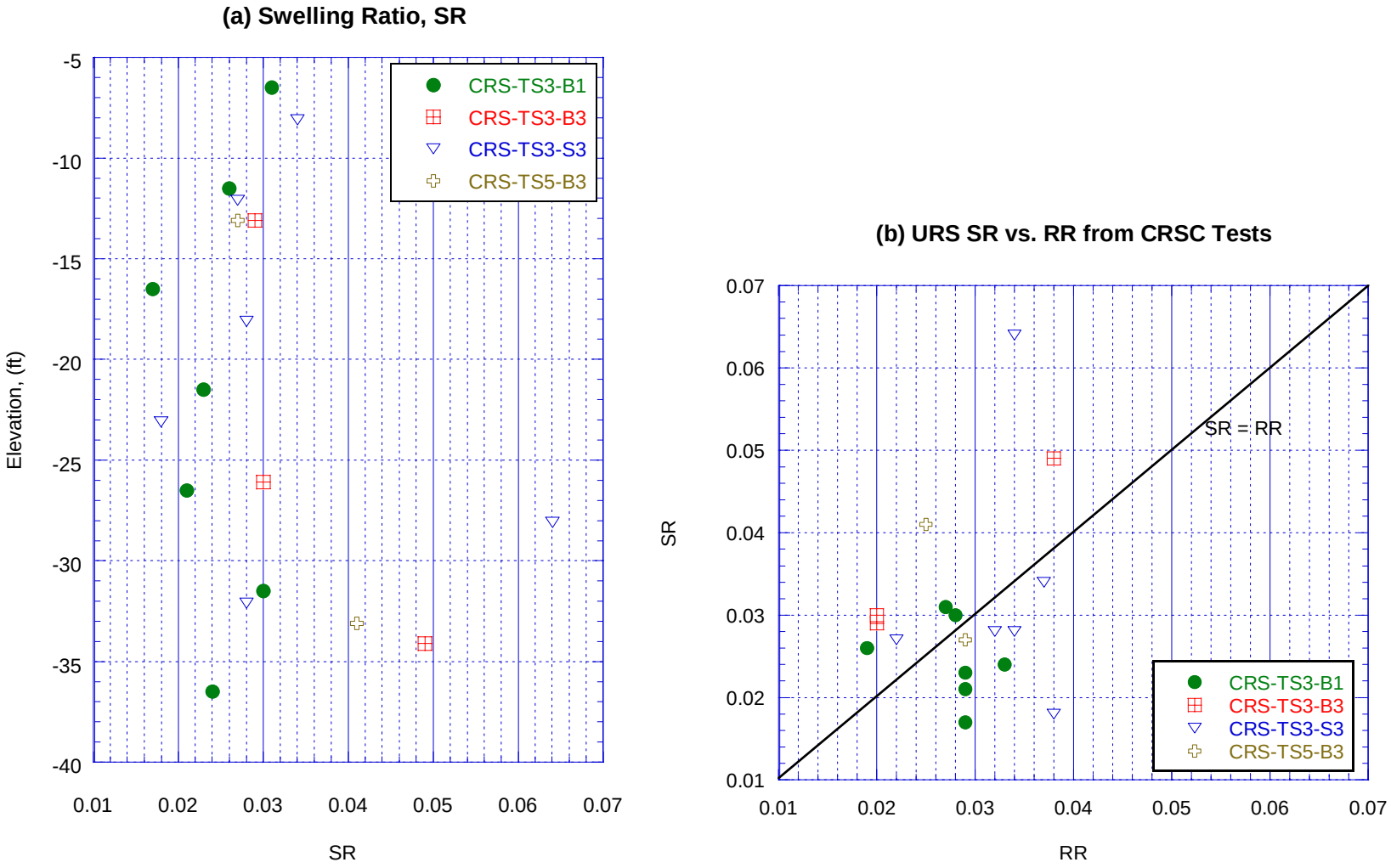

Figure 2.10b Swelling Ratio, SR vs. Elevation and RR
[Data from Table 2-A, URS (2003)]

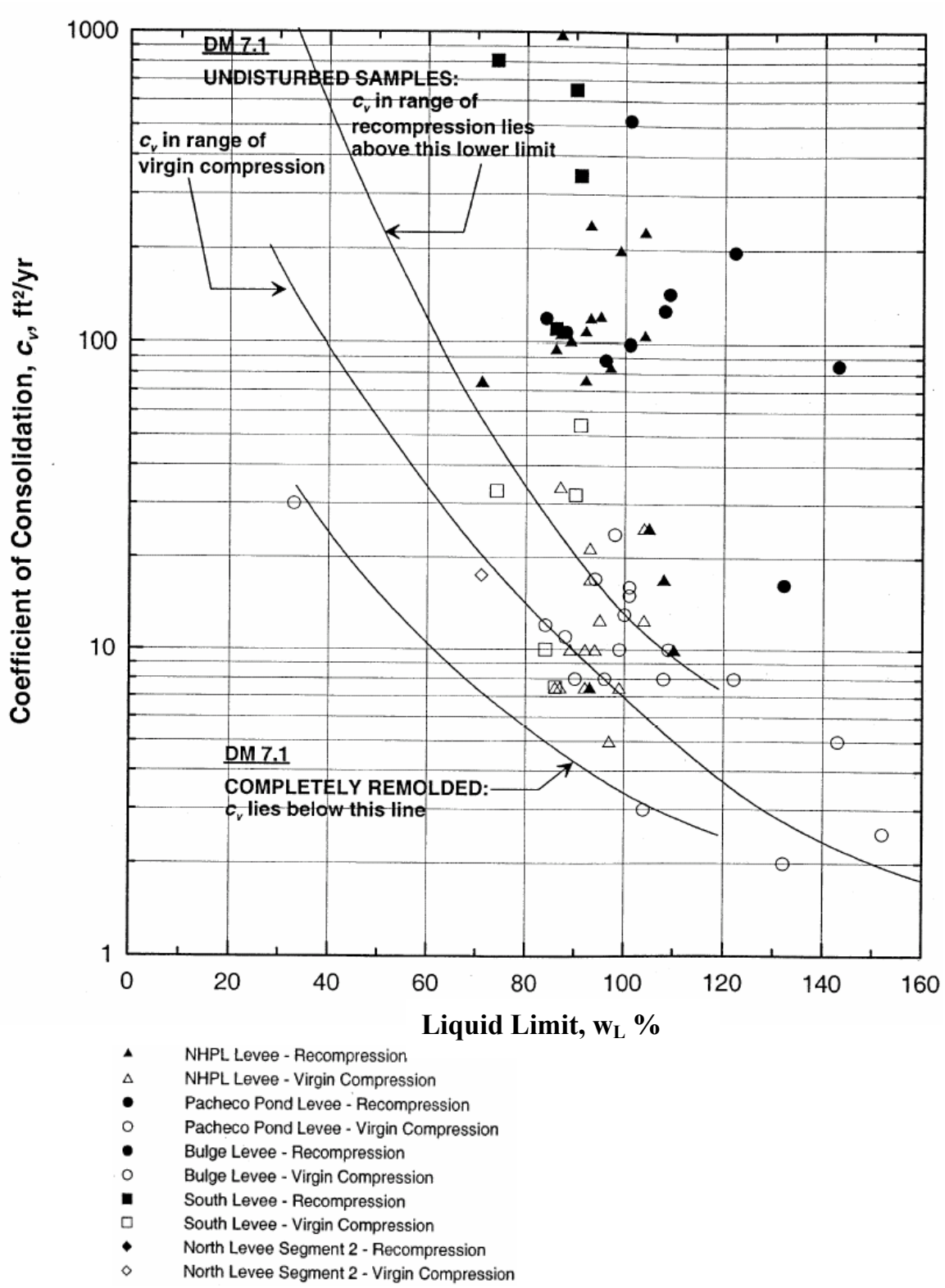

Figure 2.11 Coefficient of Consolidation vs. Liquid Limit for Bay Mud at NHPL and Other Levees
[From URS (2003)]

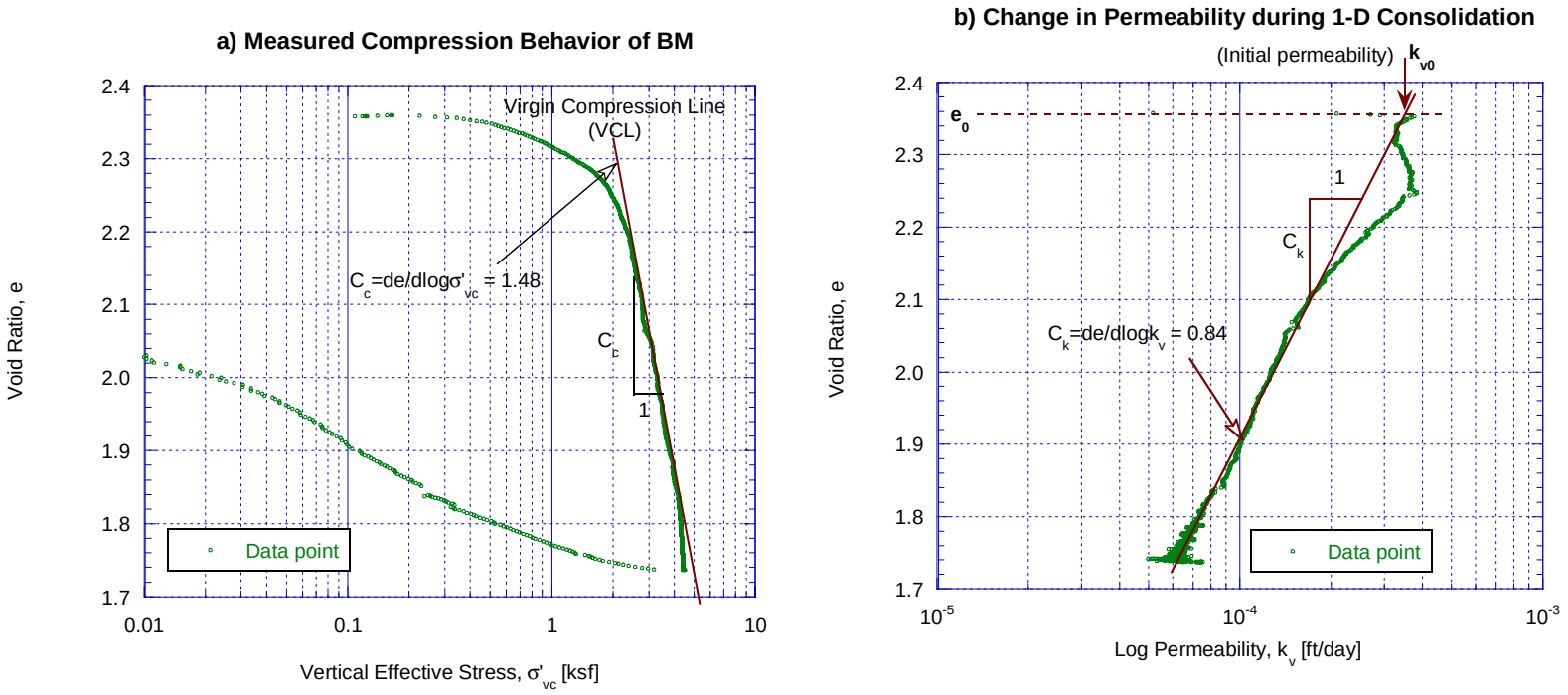

Figure 2.12 Coefficient of Permeability: Typical e-logσ'_{vc}-logk Curves from MIT CRSC Tests on NHPL Bay Mud
(For CRS435, TS3-B1, El. – 26.5 ft)

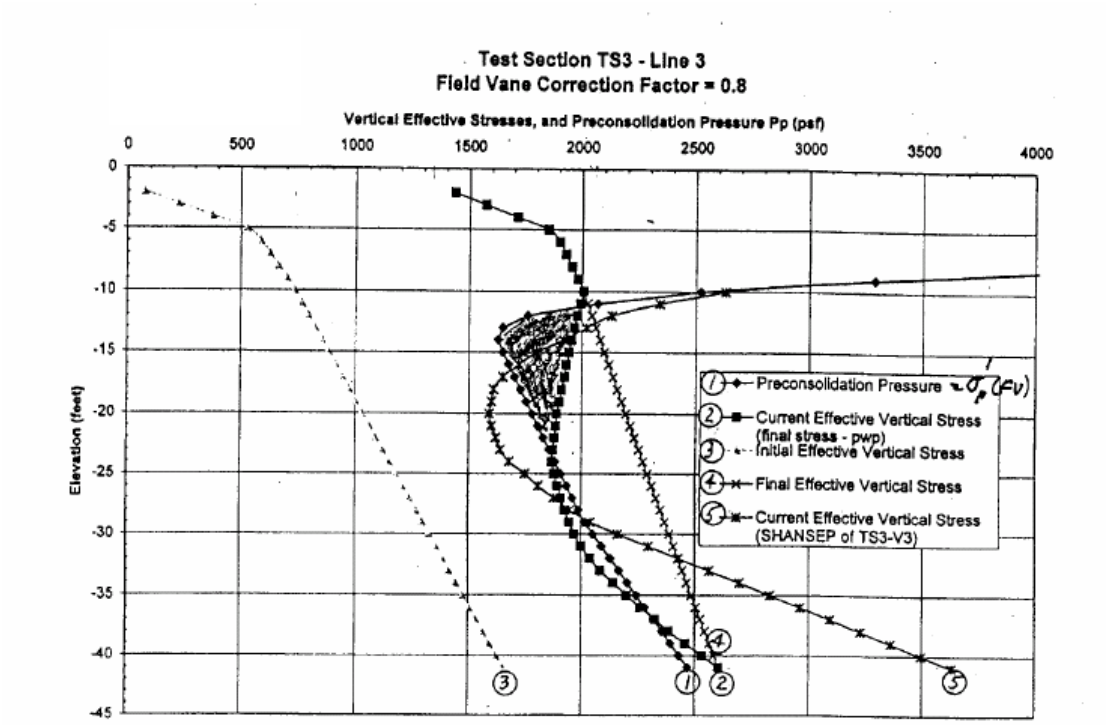

a) μ = 0.8

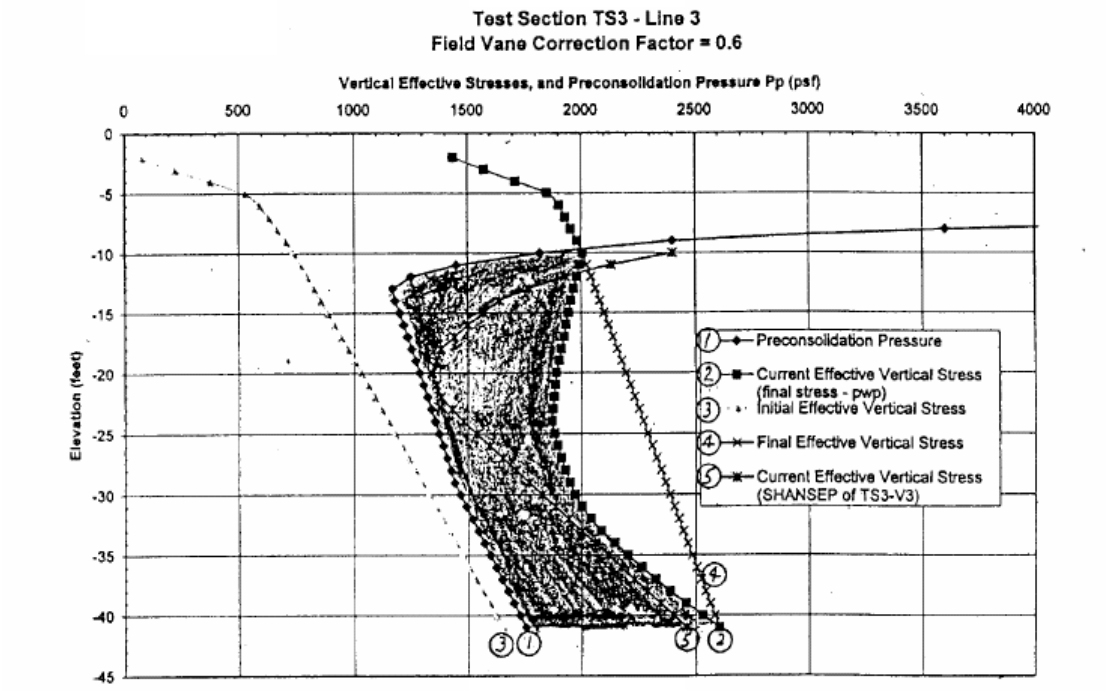

b) μ = 0.6

Figure 2.13 Stress History for Settlement Analyses at TS3 for Mean Profile σ'_p(FV) at Two Different Correction Factors, μ = 0.8 and 0.6
[From URS (2003) and Ladd (2002)]

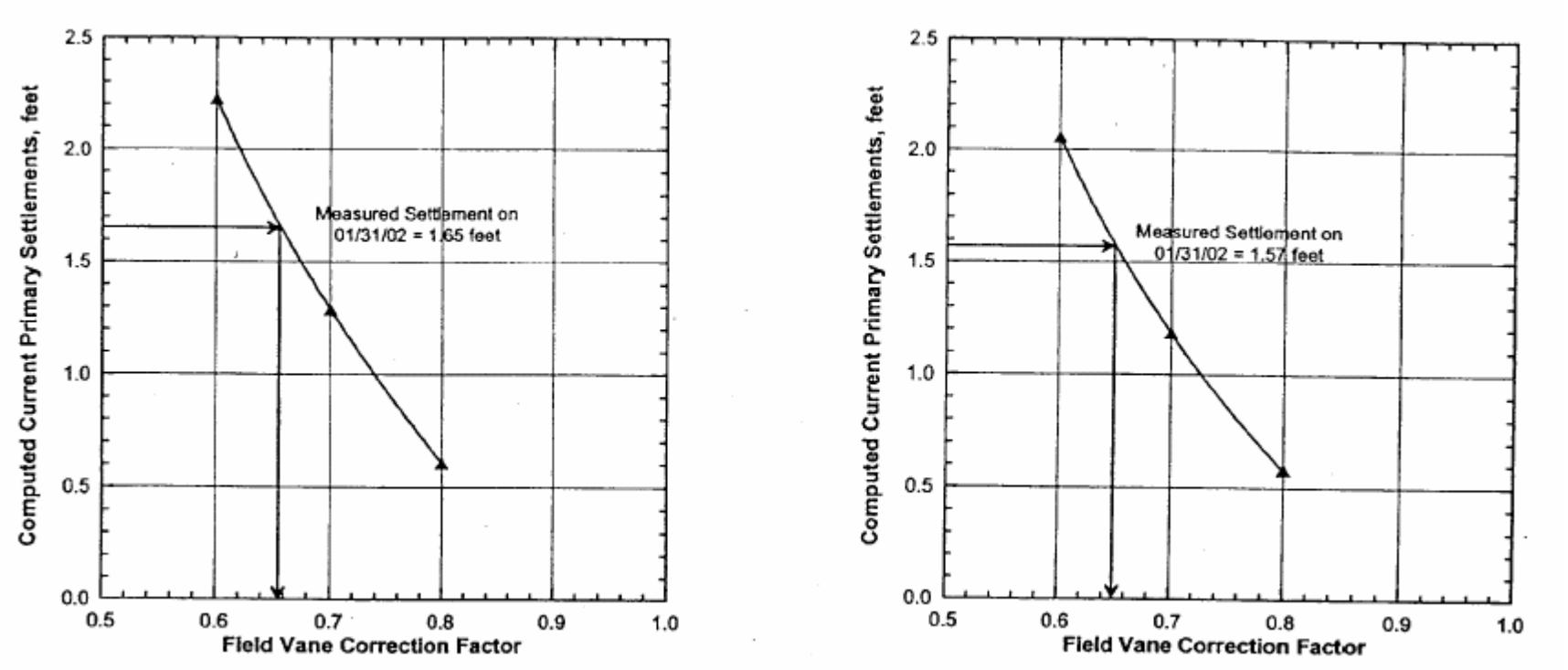

Figure 2.14 Field Vane Correction Factor vs. Computed Settlement for Mean σ'_p(FV) Profiles: TS3 and TS5

[From URS (2003) and Ladd (2002)]

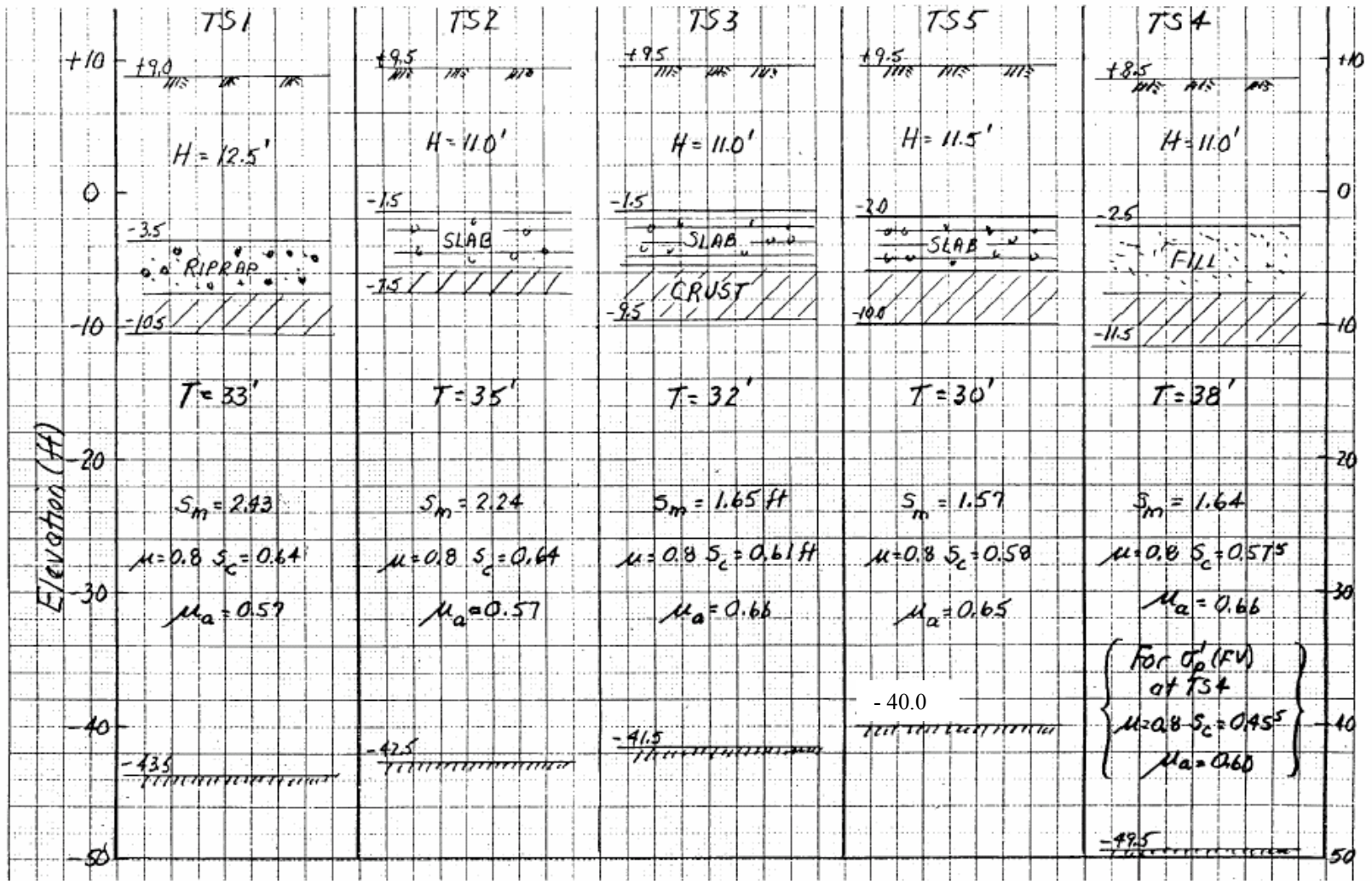

Figure 2.15 Comparison of Cross-Sections and Measured vs. Predicted Settlements for Mean σ'_p(FV) Profile at TS1 Through TS5

[From URS (2003) and Ladd (2002)]

CHAPTER 3

REANALYSIS OF THE CONSOLIDATION AND DEFORMATION BEHAVIOR OF THE NHP LEVEE

3.1 Introduction

This chapter presents a detailed independent reanalysis of the settlement of the NHP levee using the same techniques as URS (2003). The Author reexamines the soil properties; makes conventional 1-D consolidation settlement calculations; and performs parametric, 2-D non-linear, finite element analyses using the Plaxis code.

Section 3.2 interprets mechanical properties of the Bay Mud from available field and laboratory data for use in the subsequent 1-D and 2-D settlement analyses. In this section, the Author re-evaluates the soil profile and stress history for virgin ground at two test sections, TS3 and TS5, and revises the interpretation of the consolidation and undrained shear strength properties of the soft Bay Mud.

Section 3.3 focuses on reanalysis of the settlement of the NHP levee using the same 1-D consolidation settlement calculation procedures as URS, but with revised soil properties. The calculations are based on a direct estimate of the vertical effective stress profile obtained from the in-situ pore pressures measured in early 2002 (i.e., 5.2 years after the end of construction) and the total vertical stress at the end of consolidation based on fully drained 2-D finite element analyses. One-dimensional consolidation settlement calculations are then presented using both the best estimate and reduced preconsolidation stress profiles.

Section 3.4 introduces the Soft Soil Model (SSM) in PLAXIS to characterize the behavior of Bay Mud in nonlinear FE analyses. One-dimensional consolidation and undrained strength behavior of Bay Mud were simulated with SSM and compared with laboratory results from consolidation and CK_0U shear tests.

Section 3.5 presents results of the 2-D reanalysis of the NHP levee performance, including consolidation settlement, undrained shear induced settlement, horizontal displacement, excess pore pressure and consolidation stress using PLAXIS with SSM for the Bay Mud.

In addition, there are four appendixes, that include data on laboratory tests on Bay Mud, the Author's 1-D consolidation calculations, PLAXIS calculation of boundary conditions for the NHPL levee analyses, and details of an analysis to replicate the URS calculations.

3.2 Reexamination on Soil Properties for Bay Mud

A detailed study of the engineering properties of Bay Mud was carried out to check the interpretations presented by URS (2003), and to provide a more reliable basis for reanalyzing the settlement of the NHP levee. The main focus is on the properties that control the consolidation settlement of the ground including stress history, compressibility, hydraulic conductivity, and strength properties of Bay Mud. The reexamination combines previously published results on Bay Mud properties, including the URS (2003) geotechnical site investigation report, and data from an extensive program of tests carried out at MIT (Germaine, 2002, 2004).

3.2.1 Soil Profile and Stress History for Reanalysis

In Chapter 2, the Author summarized the URS soil profile (URS, 2003) and stress history of the Bay Mud beneath the crest and in the free field along the NHP levee alignment, focusing on the two instrumented test sections TS3 and TS5. In this section, the Author presents an independent assessment of the soil profile and stress history of virgin ground at TS3 and TS5 for the reanalysis.

Figure 3.1 shows the selected soil profile and stress history for the free field condition. The soil profile was based on careful evaluation of all boring logs in the area, which include those presented in URS(2003) plus additional borings made for instrumentation installed for the test fill constructed in 2005 [URS/ARUP (2005)]. The ground surface is at elevation, EL. -1.6 ft with respect to the Mean Sea Level (MSL) datum[3]. The average water table is at EL. -4.5 ft. The profile comprises (Fig. 3.1):

- 4.6 ft thick stiff old concrete pavement (EL. -1.6 ft to -6.2 ft) subdivided into:
    + 2.9 ft thick layer of concrete (EL. -1.6 ft to -4.5 ft) with total unit weight, γ_t = 150 pcf;
    + 1.7 ft thick layer of basecoarse (EL. -4.5 ft to -6.2 ft) with total unit weight, γ_t = 145 pcf; and buoyant unit weight[4], γ_b = 82.6 pcf;
- 3.8 ft thick Bay Mud Crust layer (EL. -6.2 ft to -10.0 ft) with total unit weight, γ_t = 99.8 pcf, (γ_b = 37.4 pcf). The Bay Mud crust is stiff;
- 31.5 ft thick of Bay Mud layer (El. -10.0 ft to -41.5 ft) with total unit weight, γ_t = 92.7 pcf, (γ_b = 30.3 pcf). The Bay Mud is soft, highly compressible, with high void ratio, low hydraulic conductivity and low undrained shear strength;

[3] MSL datum = Old (NGVD) used by URS (2002, 2003)
After 2003, URS uses new datum = NAVD(1988) = Old (NGVD) + 2.70 ft
[4] Assuming fresh water γ_w = 62.4 pcf.

- Alluvium (below El.-41.5 ft), very stiff, considered incompressible. The Alluvium probably has a higher hydraulic conductivity than the overlying Bay Mud.

The right hand side of Fig. 3.1 shows:

(1) In-situ overburden stress profile, σ'_{v0}, assuming hydrostatic pore pressure conditions as measured by piezometers in free field conditions (URS, 2003);

(2) Preconsolidation stress data computed from CRSC tests, σ'_{p}*(CRSC)* at test section TS3;

(3) Preconsolidation stress data computed from Field Vane tests, σ'_{p}*(FV)* at test sections TS3 and TS5 based on the method proposed by Chandler (1988);

(4) The selected mean profile of the preconsolidation stress, σ'_{p}*(average)* represented by the dashed line. This average profile also equals the mean profile that URS selected for their analyses. It is important to note that this selected mean profile of the preconsolidation stress is consistent with the Field Vane data in the BM Crust, but is biased towards the lower bound of the FV data within the Bay Mud. The CRSC preconsolidation stresses are lower than the mean FV profile in BM Crust, but are scattered about the mean profile at depth. Given the high quality of the CRSC test samples and testing techniques, and the good agreement with the mean σ'_{p} (FV) line, this profile has been selected as the "best estimate".

Table 3.1 summarizes laboratory results for CRSC tests at TS3 in free field condition. There are seven samples located at depth intervals of approximately 5 feet from boring TS3-B1, including one sample in the Bay Mud Crust and six samples in the Bay Mud itself. The first three columns of Table 3.1 present *Specimen Location* information including test number, sample elevation, and in situ overburden stress (from Fig.3.1). The

following columns present *Specimen Data* with information on the specimen initial conditions, including natural water content (w_n), total unit weight (γ_t), void ratio (e_0), degree of saturation (S), liquid and plastic limit (ω_L, ω_p), plasticity index (I_p), and vertical strain measured for reconsolidation to the vertical overburden stress ($\varepsilon_v\%@\sigma'_{v0}$). Values of the vertical strain at the vertical overburden stress are an index that has been proposed for assessing sample disturbance, and hence test quality (e.g., Ladd and DeGroot, 2003). The strains at vertical overburden stresses of the tests are generally less than 2 %, indicating high quality samples. The other columns in the table present main results selected by the Author from the CRSC tests including compressibility parameters (RR, CR_{max}, and $C_{c\ max}$), preconsolidation stress (σ'_p), vertical initial hydraulic conductivity (k_{v0}), coefficient of change in permeability (C_k), and coefficient of consolidation for normally consolidated Bay Mud c_v(NC). The shaded cells show values of compressibility parameters and σ'_p selected by URS for comparison. The Author used the both the Casagrande (1936) and the Strain Energy method by Becker et al. (1987) to select values of the preconsolidation stress. Methods for selecting RR_{max}, C_k and k_{v0} are discussed in the following sections. Detailed data and plots of the CRSC tests are presented in Appendix A.

Table 3.2 summarizes the reevaluation of field vane test data to characterize the in-situ undrained strength profile and preconsolidation stress profile using the URS method based on the SHANSEP equation and that proposed by Chandler (1988). Measured field vane shear strengths, s_u(FV) at two test locations TS3-V1 and TS5-V1 were tabulated in URS(2003).

URS used the SHANSEP equation (Ladd and Foott, 1974) to calculate overconsolidation ratio of the clay. Calculations of preconsolidation stress are based on Equations 3.1 to 3.3.

$$\sigma'_{vo}(ksf) = 0.3436 + 0.0374(-EL.) \quad \text{in BM Crust} \qquad (3.1a)$$

$$\sigma'_{vo}(ksf) = 0.4145 + 0.0303(-EL.) \quad \text{in Bay Mud} \qquad (3.1b)$$

$$OCR = \left(\frac{\mu S_u(FV) / \sigma'_{vo}}{S} \right)^{1/m} \qquad (3.2)$$

$$\sigma'_p(FV) = (OCR).\sigma'_{vo} \qquad (3.3)$$

where:

EL. = elevation in feet (NGVD datum ≈ MSL);

μ = Field vane correction factor, URS selected $\mu = 0.8$ as a function of I_p as discussed in Chapter 2;

S = Undrained strength ratio for normally consolidated soil; URS selected S = 0.25 as discussed in Chapter 2 based on DSS test results;

m = Empirical coefficient [$m = dlog(s_u/\sigma'_{vc})/dlog(OCR)$], URS selected m = 0.85.

The Chandler (1988) method was also used to determine preconsolidation stress profiles from the two field vane test locations TS3-V1 and TS5-V1 for comparison with the URS method. Calculations using Chandler (1988) are based on Equation 3.4.

$$OCR = \left(\frac{S_u(FV) / \sigma'_{vo}}{S_{FV}} \right)^{1.05} \qquad (3.4)$$

where:

S_{FV} = Coefficient as a function of plasticity index, $S_{FV} = f(I_p)$; selected $S_{FV} = 0.297$ for Bay Mud $I_p = 58.5\%$. These results for σ'_p were plotted in Figure 3.1 to characterize preconsolidation stress profile of the virgin ground.

The last column in Table 3.2 presents the ratio of σ'_p computed by the URS and Chandler(1988) methods. In the BM Crust and several feet below the Crust, URS obtained higher values than Chandler by about 10% to 15% and reducing to 2% to 5% several feet below the Crust. Within soft Bay Mud below the crust from EL. -15 ft to -41.5 ft, the two methods give very similar values of preconsolidation stress.

In summary, reevaluating the stress history of the virgin ground has led to the following conclusions:

1) Use of the Chandler (1988) method decreases σ'_p(FV) by about 10 % at top Bay Mud (EL. -10 ft), but has negligible effect below EL. -15 ft with OCR generally ≤ 1.75.

2) Within the soft Bay Mud, URS selected σ'_p(FV) mean profile tends to be at the lower end of field vane data, except near EL. -14± 1 ft, where σ'_p(FV) equals the selected mean profile.

3) Within soft Bay Mud, three of the six CRSC σ'_p are very close to the URS selected σ'_p profile;

4) Since the CRSC σ'_p may be too high (since the strain rate used in these tests is higher than the strain rate at the EOP, $\dot{\varepsilon}_v > \dot{\varepsilon}_p$) by 7.5 ±3% (Ladd, 2002), there is some justification for using a lower mean σ'_p below EL. -10 ft:

- Approximately by ≈ 10 -15% at top of Bay Mud based on Chandler and one CRSC;

- Approximately by ≈ 7.5 % below El. -15 ft based on reduced σ'_p (CRSC) from 3 or 4 of the 5 tests.

3.2.2 Index, Permeability and Compressibility Properties of Bay Mud

Index properties

Figure 3.2 summarizes the index properties of Bay Mud in the free field condition based on data from seven CRSC tests at boring TS3-B1. Index properties of Bay Mud plotted versus elevation include Atterberg limits (ω_n, ω_L, ω_p), unit weight (γ_t) and initial void ratio (e_0).

The plot of Atterberg limits versus elevation shows that only four Atterberg limits are available, with one in the Crust. Average values from the four tests give Liquid Limit, ω_L= 97 ± 9 %, and Plasticity Index, I_p = 59.5 ±5 %. Note: if Atterberg limit data for Bay Mud below the NHPL Crest are included, one obtains ω_L = 96 ±6%; I_p =58.5 ±4%. Average natural water content from six tests below the Crust is ω_n =91.2±4.7%. Hence, the natural water content is close to the liquid limit in the soft Bay Mud.

The plot of total unit weight versus elevation (Fig.3.2) shows that the measured values within the Bay Mud are very consistent. The Bay Mud average total unit weight of 92.1 pcf is slightly lower than the 92.7 pcf selected, which was computed from the average ω_N for S_i = 100% and G_s = 2.70.

Initial void ratio of the Bay Mud (Fig.3.2c) is relatively high and consistent through the Bay Mud depth, with an average e_0 = 2.5 ±0.15.

Hydraulic Conductivity

Figure 3.3a presents the in-situ vertical hydraulic conductivity properties of Bay Mud. Data for the three plots were interpreted from the 7 CRSC tests at TS3-B1 on virgin Bay Mud. The technique for estimation of k_{vo} was discussed in Chapter 2 (Fig. 2.12). The average in-situ vertical hydraulic conductivity, $k_{v0} = 4.75 \pm 1.5x10^{-4}$ ft/day, while the data range from $3x10^{-4}$ ft/day to $6x10^{-4}$ ft/day, Fig. 3.3a.

Horizontal hydraulic conductivity, k_{h0} for anisotropic marine clays is typically estimated based on:

$$r_k = k_h/k_v \qquad (3.5)$$

where $r_k \approx (1.0 – 1.5)$ for marine clays (Ladd, 1998).

The high salt content in the pore fluid of marine clays produces a flocculated micro-structure, with low values of r_k approximating nearly isotropic flow properties. For the Bay Mud, the Author generally selected $k_h \approx 1.5\ k_v$ (upper bound) to estimate k_{h0}, while URS used r_k =2.0 in their analyses.

It is noted that the hydraulic conductivity values computed from the CRSC tests are “intact” values on discrete samples, (i.e., they are representative for small uniform specimens of Bay Mud). Due to the fact that the CRSC tested samples were usually selected at “best quality” portions from a sample tube, the tested samples do not take into account possible effects of layers of more permeable soil and other aspects of macro-fabric affecting hydraulic conductivity of a deposit. Thus, the in situ hydraulic conductivity of the deposit at macro-scale can have a higher values, r_k and k_{h0} than selected by the Author.

The middle plot in Fig. 3.3a presents permeability index (C_k) values interpreted from the same seven CRSC tests. By definition, C_k defines changes in the hydraulic conductivity with decreasing void ratio due to consolidation:

$$C_k = \frac{de}{d\log k} \qquad (3.6)$$

Results from seven CRSC tests show C_k =0.8 ±0.3.

The last plot in Fig. 3.3a compares C_k to C_c and e_0. The ratio of C_k/C_c is less than 1.0 (about 0.5 on average), which indicates that c_v(NC) decreases with increasing consolidation stress (Mesri and Rokhar, 1974). However, the CRSC tests on Bay Mud (Appendix A) show that c_v(NC) generally remains constant. The ratio $C_k/e_0 \approx 0.3$, which is less than the lower limit of usual range of $C_k/e_0 = 0.33 – 0.50$ (Ladd, 1998).

The low values of C_k for Bay Mud may, in part, be related to the interpretation of the CRSC tests. These data generally do not show well-defined linear plots of e vs. $\log k_v$, which complicated selection of C_k (See Appendix A).

Compressibility properties

Figure 3.3b summarizes the compressibility properties of the Bay Mud including the maximum virgin compression ratio, CR_{max}, and recompression ratio, RR. Note: The coefficient of consolidation for NC clay [C_v(NC)] will be discussed later. Data on the plots were obtained from the 7 CRSC tests on Bay Mud at TS3-B1. Values of CR = 0.40, RR = 0.06 above El. -20 ft; and RR = 0.12 at depth were initially selected by the Author for the 1-D settlement analyses of the NHP levee at sections TS3 and TS5.

URS (2003) and the Author have used very similar values for CR (CR = 0.41 and 0.40, respectively) in their 1-D settlement analyses, but very different RR values throughout. URS (2003) assumed RR = 0.1 CR = 0.04 throughout the Bay Mud, while the Author selected much higher values based on a re-evaluation of the recompression behavior of the Bay Mud.

As will be seen, the measured vertical consolidation stress, σ'_{vc}, under the crest of the levee in early 2002 is close to the mean σ'_p profile within most of the Bay Mud. Hence, there is a little virgin compression occurring within the clay, and the recompression parameter, RR, is critical in calculation of settlements. The next section describes the Author's reevaluation of RR.

Recompression Ratio from Normalized CRSC Stress-Strain Plots

The approach assumes that sample disturbance did not affect the recompression behavior measured in CRSC tests at stresses greater than the overburden stress, σ'_{v0}. In reality, disturbance does tend to increase the measured strains to some degree and hence, the derived values of RR from the CRSC tests represent an upper limit to the presumed in situ 1-D compression. However, since the CRSC tests did not include unload-reload cycles, and were run on high quality samples, this was the only reasonable approach for assessing RR.

The Author plotted compression curves normalized by the overburden stress in both logarithmic and natural scales for the 7 CRSC tests at TS3-B1 to evaluate the recompression ratio for the Bay Mud. Figures 3.4a-g present the normalized CRSC stress-strain plots in the recompression range in ε_v versus log $\sigma'_{vc}/\sigma'_{v0}$ space. The plots start at $\varepsilon_0 = 0$ at σ'_{v0} and end at $\sigma'_{vc} = 1.3\ \sigma'_p$. These normalized plots allow one to

interpret and select appropriate values of RR by considering the value of the "current" σ'_{vc} (i.e., that measured in early 2002) in relationship to the value of σ'_p. Note that the "current" σ'_{vc} is the average of the two profiles measured at TS3 and TS5. The first evaluation of RR used the mean σ'_p(FV), leading to three conditions: (1) all recompression to $\sigma'_{vc} \approx \sigma'_p$; (2) both recompression and virgin compression to $\sigma'_{vc} > \sigma'_p$; and (3) recompression to $\sigma'_{vc} < \sigma'_p$. Since settlement analyses were also made with reduced σ'_p profiles, values of RR were also computed for σ'_p = 0.8 and/or 0.9 times the mean σ'_p(FV).

The Author divided the seven CRSC tests into three categories as follows.

(1) At locations where $\sigma'_{vc} \approx \sigma'_p$: Three tests (CRS431, CRS443, and CRS444) at locations where the preconsolidation stresses are very close to the current in-situ vertical consolidation effective stress, σ'_{vc} under the Levee (refer to the stress history plot for consolidation settlement calculation in Fig. 3.12b, c). In detail, the normalized plots of the three tests (Fig. 3.4.a to 3.4c) show:

- Line 1 = Selected virgin compression line (VCL);

- Line 2 = Maximum slope recompression line – this line goes from the overburden stress σ'_{v0} with zero strain through ε_v at the preconsolidation stress, $\sigma'_p = \sigma'_{vc}$;

- Line 3 = Minimum slope recompression line – this line is tangent to the curve near the overburden stress, which gives the minimum value for recompression ratio (RR_{min}).

(2) At locations where $\sigma'_{vc} > \sigma'_p$, i.e. the in-situ vertical consolidation effective stresses are larger than the preconsolidation stress (CRS432 and CRS441 as in Figs 3.4d and 3.4e), the plots show:

- Line 1 = Virgin Compression line (VCL);

- Line 2 = Recompression line for all recompression – this line goes through σ'_{vc} (this line is not used);

- Line 3 = Recompression line for recompression and virgin compression – this line goes through intersection between σ'_p and the VCL;

- Line 4 = Minimum Recompression line – this line is the tangent line near the overburden stress.

(3) At locations where $\sigma'_{vc} < \sigma'_p$ as in Figs 3.4f and 3.4g, the soil experiences all recompression. The plots of the two tests CRS440 and CRS435 show:

- Line 1 = Virgin compression line (VCL);

- Line 2 = Recompression line – this line goes through σ'_{vc};

- Line 3 = Minimum recompression line – this line is tangent to the curve near the overburden stress.

Table 3.3a summarizes the evaluations and results of the recompression ratios for all seven tests, and Table 3.3b shows the selected values of RR for the 1-D and 2-D settlement analyses using both the mean σ'_p(FV) and the reduced σ'_p profiles.

Conclusions

- Vertical strains at the overburden stress for the CRSC tests are ≤ 2 % (except for one test), indicating high quality samples.
- CR selected by the Author (CR = 0.40) is essentially the same as that selected by URS (CR = 0.41).
- It is critical to investigate recompression behavior by considering the current in-situ effective consolidation stress compared to the preconsolidation stress since $\sigma'_{vc} \approx \sigma'_{p}$ within most of the deposit. In other words, the stress history in Fig.3.12b and c shows that settlement due to recompression plays a critical role in the overall recompression and virgin compression settlements of the clay.
- Reevaluation of the 7 CRSC developed RR values generally much larger than RR = 0.04 selected by URS (2003).

3.2.3 Coefficient of Consolidation – C_v(NC)

Figure 3.5 summarizes the values of coefficient of consolidation for normally consolidated Bay Mud [c_v(NC)] from CRSC tests at TS3 and TS5 (Table 3.4, also see Fig. 3.3b for c_v(NC) for the CRSC tests on virgin Bay Mud) in comparison to the established DM-7 correlation.

The results show that Bay Mud has very high values of c_v(NC) that, exceed the DM-7 mean line for an average Liquid Limit ≈ 95 %. In fact, the data are scattered about the lower limit line for OC clay. The average value for the Bay Mud c_v(NC) ≈ 22 ft^2/yr. The high values of c_v(NC) suggest that the Bay Mud deposit will have a faster rate of

consolidation and a shorter time to end of primary consolidation (t_p) than other comparable clays (i.e., having similar thickness and index properties).

Plots of c_v(NC) versus logσ'_{vc} from the CRSC tests at TS3-B1 are shown in Appendix A for reference. These plots generally show that c_v(NC) of Bay Mud is approximately constant with increasing σ'_{vc}. This contradicts the data in Fig.3.3a since a C_k/C_c ratio less than unity predicts that c_v(NC) decreases with increasing σ'_{vc}.

3.2.4 Coefficient of Earth Pressure at Rest, Ko

Figure 3.6 plots K_0 versus σ'_{vc} (at both log and natural scales) from consolidation phases of five CK_0U triaxial shear tests on specimens of Bay Mud. Individual plots of K_0 versus σ'_{vc} of each test are shown in Appendix A.

The plots show K_0 decreases as the specimens are reconsolidated into the normally consolidated range. Within the normally consolidated range of effective stress K_0(NC) = 0.44 to 0.50. The author selected K_0(NC) = 0.47 as the mean value for the Bay Mud. In comparison, URS (2003) used K_0(NC) = 0.62 for the Bay Mud in their analyses based on results of research done by University of California at Berkeley (URS, 2003).

3.2.5 Strength Properties

Figure 3.7 summarizes results of the undrained shear strength versus OCR from 2 CK_0UE, 3 CK_0UC and 16 CK_0UDSS tests on the Bay Mud from the NHP, N1 and N2

levees. Table 3.5 summarizes the results for the CK_0UDSS tests and Table 3.6 summarizes results for the triaxial shear tests[5].

At OCR =1, the mean value for the undrained shear strength ratio in DSS tests is $S_{uDSS}/\sigma'_{vc} = S_d = 0.25$; in TE tests, $S_e = 0.274$, and in TC, $S_c = 0.348$. It is very unusual to measure a lower undrained strength ratio in the simple shear mode (S_d) than in triaxial extension.

Interpretation of SHANSEP parameters (S and m) from results of the DSS tests shows that S =0.25 and m = 0.8. In comparison, URS used reasonable values of S = 0.25 and m = 0.85 in their calculation of the preconsolidation stress from the field vane tests.

Figure 3.8 presents typical results of CK_0UDSS tests on Bay Mud including normalized shear stress versus shear strain, (Fig.3.8a), effective stress paths (σ'_v/σ'_{vc} vs. τ/σ'_{vc}, Fig. 3.8b), and normalized modulus versus shear strain (E_u/σ'_{vc} vs. γ; Fig. 3.8c). The three plots show results of three DSS tests at OCR = 1, 2, and 3. The two tests at OCR = 1 and 2 are at TS5-B3 location, while the DSS test at OCR = 3 is for the North Levee 1.

Figures 3.9a and 3.9b plot results from all of the available CK_0UC/E tests on K_0-consolidated specimens. The results of the tests are also summarized in Table 3.6. Two of the three CK_0UC tests show a very high peak undrained strength ratio, $s_u/\sigma'_{vc} \approx 0.37$. The Bay Mud shows some softening in TC at axial strain exceeding 2-3%. The tests also give very high friction angles, especially in the extension shear mode. The author selected an average value of $\phi'_{tc} = 47^0$ for the Bay Mud.

[5] DSS test data on the Bay Mud are available at OCR = 1,2, and 3, but only tests at OCR =1 are available for the TX tests. Noted that the figure uses the DSS tests at OCR=3 from the BM samples at the North levees because there was no sample from the NHP levee tested at OCR = 3 or higher.

Figure 3.9b plots results of undrained Young's modulus from the same triaxial tests (E_u/σ'_{vc} vs. $|\varepsilon_a|$%). The results show that Young's modulus decreases sharply as the strain increases beyond $\varepsilon_a \approx 0.1\%$. At small strains (i.e., $\varepsilon_a \approx 0.001\%$) $E_u/\sigma'_{vc} = 170$ to 600. Thus, at $\varepsilon_a = 0.001\%$, a minimum ratio of undrained Young's modulus to strength (E_u/s_u) for normally consolidated Bay Mud is 680 for $s_u/\sigma'_{vc} = 0.25$.

3.3 Conventional 1-D Consolidation Settlement Analysis

One of the efforts in the reanalysis of the NHP levee settlements is to calculate conventional 1-D consolidation settlements of the levee for comparison with the measured settlements. The Author computed 1-D consolidation settlements for the NHP levee using the same basic methodology as URS that was described in Section 2.7 of Chapter 2. This section presents the Author's work on characterizing stress history for consolidation settlement reanalysis and recalculation of conventional 1-D consolidation settlements using the revised compressibility parameters (RR, CR).

3.3.1 Final Consolidation Stress, σ'_{vf}

As described in Section 2.7, URS determined the consolidation vertical effective stress (σ'_{vc}) based on measured excess pore pressures, u_e recorded in early 2002, as $\sigma'_{vc} = \sigma'_{vf} - u_e$. This section describes the process to get the σ'_{vf} profile using finite element analysis code PLAXIS.

The Author began FE analysis by assessing the effects of Young's modulus and strength of the overlying concrete pavement on the final stress distribution under the

levee. A series of simulations were carried out assuming different elastic stiffness and strength properties for the pavement.

Figure 3.10 summarizes the computed vertical stress distributions beneath the centerline and toe of the NHP levee using different assumptions for the stiffness and shear strength of the pavement material. The 'base case' calculations consider $E = 2x10^5$ ksf and compare solutions for an elastic pavement with those for an elasto-plastic pavement using the Mohr-Coulomb (MC) model (c = 4960 psf, $\phi' = 35^0$, $\psi = 2^0$). The results show that yielding of the concrete pavement causes a significant increase in the centerline vertical effective stress, while reducing the stress beneath the toe of the levee. Further analyses were performed using reduced elastic stiffness for MC pavements with E = 2000 ksf and 500 ksf. These produce small changes in the computed stress fields (Fig. 3.10).

A further three analysis cases (A, B and C) were carried out to evaluate the effects of the layers above the Bay Mud (i.e., Pavement, Base Course and Bay Mud Crust) on the overall stress distribution within the Bay Mud.

Case A analysis was carried out with an uncracked, continuous, and very stiff pavement and a stiff BM Crust under the NHPL. Table 3.7a presents properties used in Case A analysis, including layers of the soil deposit under the NHP levee, and corresponding selected values of material parameters used in PLAXIS for calculating σ'_{vf}. For soils other than Bay Mud, the Author used values from URS/ARUP (2005). The Mohr-Coulomb (MC) soil model was used for the levee Fill, Crust and Bay Mud layers while the Alluvium is assumed to be elastic. The Bay Mud profile was subdivided into 5 ft sublayers with undrained strengths estimated based on SHANSEP with S = 0.25 and m

= 0.85. The undrained Young's modulus profile for the Bay Mud was then estimated using the correlation, $E_u = 200s_u$. The calculations to obtain undrained shear strength and Young's modulus for the Bay Mud in the analysis are presented in Table 3.7d.

Case B analysis was carried out with a cracked pavement and a stiff BM Crust under the NHPL. Table 3.7b presents the selected properties for Case B, which are the same as Case A except for the cracked pavement having a much lower cohesion (25 psf versus 4960 psf) and a slightly lower modulus.

Case C analysis was carried out with much lower strength parameters for the levee fill, cracked pavement, and BM Crust under the NHPL [i.e., properties in Table 6, URS (2003)]. Table 3.7c presents the selected properties used for Case C.

Figure 3.11a shows the geometry of the NHPL in Plaxis analyses for Case B and Case C, which has a cracked pavement under the levee and fill material at the toes of the levee. For Case A, there is only an uncracked and continuous pavement under the NHPL.

Figure 3.11b shows vertical profiles of σ'_{vf} below the toe and centerline of the NHP levee from the there analysis cases (and also shows the URS (2003) σ'_{vf} profile). The results show that Case C, with lower values of E and c' for the BM Crust and the cracked pavement compared with Case A and Case B, produces higher stresses at centerline and lower stresses at toe of the levee. These changes in σ'_{vf} (i.e., $\Delta\sigma'_{vf}$ =0.1 – 0.2 ksf) within the Bay Mud are due to the fact that the stronger pavement and fill in Case A & B causes more spreading of the load from the levee fill.

The Author selected the Case C centerline σ'_{vf} profile for calculating σ'_{vc} for his 1-D consolidation analyses. This profile is very similar to that used by URS (2003) in their spreadsheet analyses sent to Professor Ladd.

3.3.2 Measured Excess Pore Pressure at TS3 and TS5 on Feb-Mar, 2002

Figure 3.12a presents the measured excess pore pressure data at the centerline of the NHPL at TS3 and TS5 as computed by the Author in Table 3.8a. The figure also shows three u_e profiles at TS3 and TS5 as follows.

1) u_e profiles selected by URS (2003) for their 1-D consolidation settlement calculations;
2) First estimates by the Author using u_e values scaled from URS (2003) report and labeled SH1. These were used for computing σ'_{vc} as shown in Fig. 3.12b;
3) Best estimates of u_e profiles based on the piezometer data, SH2, used to compute σ'_{vc} as in Fig. 3.12c (SH2).

There are significant differences in the interpreted u_e at TS3 and TS5 between URS (2003) and the Author's SH1 and SH2. For example, the maximum u_e values at TS3 and TS5 are summarized and compared in the table following.

Profile No.	Name	Max. u_e (ksf)	
		TS3	TS5
1	URS(2003)	0.42	0.54
2	SH1	0.53	0.39
3	SH2	0.48	0.365

There are uncertainties in the measured u_e data due to variable water table (or h_s) assumptions and scatter in the data (e.g., u_e within the upper Bay Mud at TS5) at the two test sections. Thus, it is difficult to define u_e at TS3 and TS5 precisely. The Author and Professor C.C. Ladd developed the measured piezometer data during February to March, 2002, as presented in Table 3.8a and 3.8b, for TS3 and TS5 respectively. The Author concludes that profiles SH2, which are based on these values of u_e, should be the most realistic.

3.3.3 Consolidation Stress Profiles, σ'_{vc} at TS3 and TS5

Vertical consolidation effective stress profiles (σ'_{vc}) were calculated from the computed final vertical consolidation effective stress profiles (i.e., σ'_{vf} in Fig. 3.11b) by subtracting the u_e profiles plotted in Fig. 3.12a as follows.

Figure 3.12b shows σ'_{vc} profiles at TS3 and TS5 computed with the lower σ'_{vf} (i.e., Case A&B σ'_{vf} analysis) and the higher SH1 for u_e.

Figure 3.12c shows σ'_{vc} profiles at TS3 and TS5 computed with the higher σ'_{vf} (i.e., Case C σ'_{vf} analysis) and the lower SH2 for u_e.

Therefore, the consolidation stress profile σ'_{vc} at TS3 and TS5 for SH2 (Fig. 3.12c) are higher than those of SH1 (Fig.3.12b). In addition, consolidation stress profiles at TS3 and TS5 used by URS (2003) are shown in Fig.3.12c for comparison.

3.3.4 Stress History Profiles for 1-D Settlement Calculation

Figures 3.12b and 3.12c present two consolidation effective stress history profiles (SH1 and SH2) for 1-D settlement calculations.

SH1 in Fig.3.12b summarizes the initial overburden stress profile for virgin ground (σ'_{v0}); the selected preconsolidation stress profiles (σ'_p; $0.9\sigma'_p$; and $0.8\sigma'_p$); the computed final consolidation stress profile (σ'_{vf}) from Case A; and the vertical consolidation effective stress profiles at TS3 and TS5 at time 1/31/02 (σ'_{vc}) computed from the SH1 u_e data. The figure shows that for the best estimate σ'_p profile, there is only a small zone of virgin compression in the Bay Mud (i.e., from EL. -12.5 to - 20 ft for TS3 and -12 to -23.5 ft for TS5 where $\sigma'_{vc} > \sigma'_p$), while the rest of the deposit has only recompression. Hence, a large portion of the levee settlement would be due to recompression settlements. Reducing the preconsolidation stress profile will obviously increase the virgin compression zone in the deposit, and therefore increase the predicted consolidation settlement. The selected soil profile and values of RR and CR are presented in the figure for reference.

Figure 3.12c shows the same information, but the σ'_{vc} profiles are now higher due to the large σ'_{vf} (Case C) and smaller values of u_e based on the SH2 profiles (Fig. 3.12a). This presents the Author's best estimate of consolidation stress conditions for use in settlement calculations.

3.3.5 One-Dimensional Consolidation Settlement Calculations with Varying Preconsolidation Stress Profiles

The Author used the same methodology as URS to compute 1-D consolidation settlements at TS3 and TS5 of the NHP levee, which was described in Section 2.7. Consolidation settlements (ρ_c) were computed for three preconsolidation stress profiles: the best estimate profile of preconsolidation stress based on the mean σ'_p (from FV data); and reduced values equal to $0.9\sigma'_p$ and $0.8\sigma'_p$.

Calculation sheets are presented in Appendix B for the stress histories in Fig. 3.12c. The Author assumed that consolidation settlements of the deposit under the NHP levee occur only in the BM Crust and Bay Mud layers (from EL. -6.2 ft = top of BM Crust to EL. -41.5 ft = bottom of Bay Mud). The soil from EL. -6.2 to -41.5 ft is divided into small sub-layers (usually one foot thick). Each sub-layer has a constant strain, which is computed at the mid-point of each sub-layer, due to change in vertical effective stress from σ'_{v0} to σ'_{vc}. Settlement of each sub-layer is the multiplication of the strain and the sub-layer thickness. Total consolidation settlement of the levee is the addition of all sub-layer settlements. Similar calculations with $0.9\sigma'_p$ and $0.8\sigma'_p$ profiles at TS3 and TS5 are presented in Appendix B.

Compressibility parameter RR was selected as a function of σ'_{vc}/σ'_p, leading to the selected values shown in Table 3.3b. In all cases, the selected value of CR = 0.40 throughout the depth of the BM Crust and Bay Mud.

Figure 3.13a plots results of the 1-D consolidation settlement calculations for SH1 stress history (i.e., Fig.3.12b), which are also summarized in Table 3.9a. The measured

consolidation settlements after the end of construction, ρ_m at TS3 and TS5 are also shown for comparison. The computed ρ_c with the σ'_p profile shows that $\rho_c/\rho_m \approx 46\%$ ρ_m at TS3 and 52% at TS5. For cases with $0.9\sigma'_p$, $\rho_c/\rho_m \approx 58\%$ at TS3 and 75% at TS5, while the $0.8\sigma'_p$ profile, $\rho_c/\rho_m \approx 75\%$ at TS3 and 96% at TS5. Calculations for SH1 result in values of ρ_c that are much too low, presumably due to the fact that SH1 underestimates σ'_{vc}.

Figure 3.13b plots results of the 1-D consolidation settlement calculations for the SH2 consolidation stresses (i.e., Fig.3.12c). Calculation sheets for SH2 are presented in Appendix B and Table 3.9b summarizes the computed results. At TS3, ρ_c/ρ_m increases from 63% to 104% as the preconsolidation stress is reduced from σ'_p to $0.8\sigma'_p$. For TS5, the corresponding ratios are 73% and 119%. According to these results, the 1-D consolidation analyses with the SH2 stress history predict satisfactorily the measured settlement using a reduced preconsolidation stress profile of $0.9\sigma'_p$.

Figure 3.13c plots ρ_c versus the selected σ'_p profile for the Author's SH1 and SH2 stress histories, plus the results presented in URS (2003). Note that ρ_c computed with the Author's SH2 stress history is much larger than computed by URS (2003), who concluded that the measured σ'_p should be reduced by 20% for design calculations of levee settlements along the NHPL alignment. The principal reason for the large differences in ρ_c lies in the much higher values of RR used by the Author (0.06 and 0.12 versus only 0.04). The Author's selected u_e profile at TS5 also is significantly lower than selected by URS (2003).

3.3.6 1-D Final Consolidation Settlements, ρ_{cf} Computed for SH2

Figure 3.13d plots predictions of final consolidation settlements (ρ_{cf}) at TS3 and TS5 computed for σ'_p, $0.9\sigma'_p$, and $0.8\sigma'_p$ using the same RR and CR selected for the ρ_c calculations with σ'_p and $0.9\sigma'_p$ profiles. The figure also shows computed profiles of ρ_c for comparison. The results show that ρ_{cf} = 1.76 ft for σ'_p profile, and increasing to ρ_{cf} = 2.63 ft for the $0.8\sigma'_p$ profile. The corresponding degrees of consolidation at TS3 and TS5 equal 59% and 65%, respectively, for ρ_c and ρ_{cf} computed for the measured σ'_p; and equal 65% and 71%, respectively, for ρ_c and ρ_{cf} computed with $0.9\sigma'_p$ or $0.8\sigma'_p$. Appendix B presents the calculation sheets for ρ_{cf}. Table 3.9b also summarizes these results, as well as the corresponding values of ρ_c/ρ_m.

3.3.7 Summary and Conclusions

Application of the conventional 1-D consolidation method to predict the amount of consolidation settlement (ρ_c) of the NHP levee at 5 plus years after the end of construction at two test section locations (TS3 and TS5) with extensive piezometer data is complicated by several factors, the most important being:

1) The strength and modulus of the levee fill [very different properties where selected in the URS (2003) and URS/ARUP (2005) reports];
2) The strength of the overlying pavement and whether or not the pavement has undergone extensive cracking. Factors 1 and 2 can significantly affect the magnitude of the final vertical effective stress (σ'_{vf});

3) Selection of profiles of excess pore pressure (u_e) from the piezometer data due to uncertainties in the equilibrium pore pressure (i.e., location of water table) and scatter in the readings) needed to computed profiles of $\sigma'_{vc} = \sigma'_{vf} - u_e$; and

4) Selection of appropriate values for the recompression ratio (RR) when the computed σ'_{vc} is either slightly less or slightly greater than the well defined mean preconsolidation stress (σ'_p), such as occurs throughout most of the soft Bay Mud.

Most of Sections 3.2 and 3.3 have focused on the above issues, leading to the Author's "best estimate" of RR [with values several times larger than selected by URS (2003)] and the stress history (denoted as SH2) presented in Fig. 3.12c. The remaining comments are based on estimates of ρ_c using that figure, unless otherwise noted.

It is evident that the conventional 1-D consolidation method significantly under-predicts the measured consolidation settlement (ρ_m) of the NHP levee when computed with the "best estimate" σ'_p(FV) profile (i.e., $\rho_c = 63\%\ \rho_m$ at TS3 and $\rho_c = 73\%\ \rho_m$ at TS5 as per Table 3.9b). Reducing the preconsolidation stress profile by 10% results in good agreement with the measured ρ_m, especially at TS5 (where ρ_c equals ρ_m). As concluded in Section 3.2.1, there is some justification for using a lower mean σ'_p within the Bay Mud deposit (i.e., "high" strain rate of $d\varepsilon/dt$ = 0.73%/hr for the CRSC tests, and σ'_p(CRSC)/σ'_p(FV) < 1 in four of the 7 tests at TS3-B1).

In contrast, URS (2003) concluded that σ'_p(FV) should be reduced by 20% for settlement predictions.

It is clearly not satisfactory to arbitrarily reduce the preconsolidation stress by 10% or 20% to match field measurements, especially since the field and lab tests were

done using "state-of-the-art" practices and the σ'_p profiles from the Field Vane and lab CRSC tests are in good agreement (Fig.3.1). Therefore, two questions remain: (1) Will a 2-D consolidation settlement analysis help to improve the agreement between predicted and measured settlements? (2) Or does Hypothesis B apply for the consolidation behavior of the Bay Mud? Further 2-D analyses of the NHP levee using a Finite Element code have been carried out to address these questions.

3.4 Element Analysis on Bay Mud with PLAXIS Soft Soil Model

This section describes the application of the Soft Soil Model (SSM) in Plaxis for characterizing the elemental behavior of Bay Mud, and the calibration of SSM soil parameters from the field and laboratory tests. The model parameters are based on simulations of:

1) 1-D consolidation tests to evaluate coefficient of consolidation and other consolidation properties;

2) Undrained plane strain shear tests (CK_0PSC/E); and

3) Undrained direct simple shear (CK_0DSS) model test

These model test exercises are to calibrate SSM material parameters for Bay Mud to obtain reasonable soil behavior in term of consolidation [i.e., c_v(NC), k_{v0}, and C_k] and undrained shear strength [i.e., s_u(DSS), c', ϕ', and K_{0NC}]. This work also identifies problems with using the SSM in Plaxis to predict undrained shear deformations.

3.4.1 Summary of SSM

Soft Soil Model (SSM) in Plaxis is formulated based on the modified Cam-Clay isotropic soil model. The model assumes a logarithmic relationship between the volumetric strain ε_v and the mean effective stress *p'* as in Equations 3.6 and 3.7:

$$\varepsilon_v - \varepsilon_{v0} = \lambda^* . \ln(\frac{p'}{p_0'}) \qquad \text{(For isotropic virgin compression)} \qquad (3.6)$$

$$\varepsilon_v^e - \varepsilon_{v0}^e = \kappa^* . \ln(\frac{p'}{p_0'}) \qquad \text{(For isotropic unloading/reloading)} \qquad (3.7)$$

where λ^* is the modified compression index, which is related to the virgin compression ratio CR as in Equation 3.8; and κ^* is the modified swelling index, which is related to the recompression ratio as in Equation 3.9.

$$\lambda^* = \frac{CR}{2.3} \tag{3.8}$$

$$\kappa^* \approx \frac{2RR}{2.3} \tag{3.9}$$

The superscript *e* in Equation 3.7 implies elastic behavior in recompression and swelling (unloading/reloading) as formulated in Equation 3.10.

$$E_{ur} = 3(1-2\nu_{ur}).\frac{p'}{\kappa^*} \tag{3.10}$$

where E_{ur} is the elastic Young's modulus and ν_{ur} is the Poisson's ratio in which the subscript *ur* denotes unloading/reloading. In SSM, ν_{ur} and κ^* are input parameters to compute elastic strains.

The SSM is capable of simulating soil behavior under general states of stress. For triaxial stress states for which $\sigma'_2 = \sigma'_3$, the SSM yield function is defined as:

$$f = \overline{f} - p_p \tag{3.11}$$

where $\overline{f}$ is a function of the stress state *(p', q)* and the preconsolidation stress p_p is a function of plastic strain such that:

$$\bar{f} = \frac{q^2}{M^2(p'+c'.\cot\varphi')} + p' \tag{3.12a}$$

$$\text{where } M \approx 3\sqrt{\frac{(1-K_0^{NC})^2}{(1+2K_0^{NC})^2} + \frac{(1-K_0^{NC})(1-2\nu_{ur})(\frac{\lambda^*}{\kappa^*}-1)}{(1+2K_0^{NC})(1-2\nu_{ur})\frac{\lambda^*}{\kappa^*} - (1-K_0^{NC})(1+\nu_{ur})}} \tag{3.12b}$$

is the slope of the critical state line used in Modified Cam-Clay models;

$$p' = -\frac{1}{3}\left(\sigma_1' + 2\sigma_3'\right) \tag{3.13}$$

is the isotropic effective stress, or mean effective stress;

$$q = \left|\sigma_1' - \sigma_3'\right| \tag{3.14}$$

is the equivalent shear stress;

and,

$$p_p = p_p^0 \exp\left(\frac{\Delta\varepsilon_v^p}{\lambda^* - \kappa^*}\right) \tag{3.15}$$

The vertical preconsolidation stress σ'_p is used to compute p_p^0, which determines the initial position of the yield surface as follows:

$$\sigma'_1 = \sigma'_p \tag{3.16}$$

$$\sigma'_2 = \sigma'_3 = K_{0NC}.\sigma'_p \tag{3.17}$$

$$OCR = \frac{\sigma_p'}{\sigma_{v0}'} \tag{3.18}$$

where K_{0NC} is the coefficient of lateral earth pressure at rest for normally consolidated soil. In the SSM, the default setting of K_{0NC} is the Jaky formula ($K_{0NC} = 1\text{-}\sin\varphi$). But one can impose a specified value for K_{0NC}. OCR is the overconsolidation ratio.

It should be noted that SSM uses the conventional Mohr-Coulomb criterion, (φ', *c'*) and K_{0NC} as model input parameters, while the critical state line (slope, M) is not used directly.

3.4.2 One-Dimensional Consolidation

The aim of this exercise is to examine the computed coefficient of consolidation for normally consolidated clay [c_v(NC)] of Bay Mud at OCR = 1.5 using SSM, and then to select appropriate parameters for the hydraulic conductivity properties (k_{v0} and C_k) such that SSM produces c_v(NC) ≈ 0.06 ft^2/day, which is the average measured value of c_v(NC) for the Bay Mud.

Table 3.10 shows two sets of SSM input parameters used in the 1-D consolidation simulations. Case 1 uses parameters selected by URS (2003) in their analyses on the NHP levee. Case 2 corresponds to the set of parameters selected by the Author for which: λ^*, κ^* and e_0 are best estimates from the laboratory data; C_k is selected equal C_c =1.40; k_x, k_y are calibrated values of initial horizontal and vertical hydraulic conductivities to get c_v(NC) ≈ 0.06 ft^2/day. The other input parameters remain the same as Case 1. Initial conditions were set up so that the preconsolidation stress σ'_p = 1.5 ksf and the over-consolidation ratio OCR = 1.5. In addition, the coefficient of lateral earth pressure at rest for the Bay Mud was selected as K_{0OC} = 0.73 for OCR =1.5 (e.g., for OCR = 1.5, K_{0NC} = 0.62 and $K_{0OC} = K_{0NC}.(OCR)^n$, where n = 0.4).

Table 3.11 shows the calculation scheme for the 1-D load incremental oedometer consolidation simulation on SSM having a drainage height H_d = 3 inches. The scheme simulates a conventional incremental loading consolidation test in laboratory. The model was loaded from recompression to virgin compression to examine the variation of c_v in SSM. c_v was backcalculated using the relationship in Equation 3.19a to 3.19d.

$$c_v = \frac{k_y E_{oed}}{\gamma_w}, \qquad (3.19a)$$

where $E_{oed} = \frac{\Delta\sigma'_{vc}}{\Delta\varepsilon_v}$ is the equivalent oedometer loading modulus; (3.19b)

$$k = k_0 10^{\left(\frac{\Delta e}{C_k}\right)} \quad (3.19c)$$

$$\Delta e = (1 + e_0).\varepsilon_v \quad (3.19d)$$

Figure 3.14a plots the stress-strain relationship in logarithmic scale for Case 1 and Case 2 analyses. Figure 3.14b plots the same results in natural scale in order to determine the equivalent oedometer loading modulus, E_{oed}. Figure 3.14c plots variations of backcalculated c_v for the simulations and the measured c_v(NC) from the CRSC tests. In addition, Figures 3.14d and 3.14e show changes in permeability for the two cases.

In Case 1, the URS selected set of SSM parameters produces c_v(NC) = 0.04 ft^2/ft, which underestimates the measured value of c_v(NC) = 0.06 ft^2/day of the Bay Mud. Hence, this set of SSM parameters would presumably underestimate the rate of consolidation for virgin compression at field scale. In contrast, the Author's Case 2, with the higher k_{v0} = 9x10^{-4} ft/day and consistent values of C_c and C_k = 1.40, obtains c_v(NC) from SSM = c_v(NC) measured from CRSC tests. These parameters are selected as best estimates for the analysis of the NHP levee in Section 3.5. Note, however, that predictions of the rate of consolidation during recompression will be less rapid than for the URS Case 1 due to the decrease in c_v(OC) [but less so for the Bay Mud having lower values of RR as per Figs. 3.12b and c].

3.4.3 CKoU PSC/E Tests Simulation

One- dimensionally (K_0) consolidated plane strain compression undrained shear tests were simulated in Plaxis using SSM in order to calibrate the model parameters, K_{0NC} and ϕ'for Bay Mud. SSM parameters for Bay Mud used in the analyses are presented in Table 3.10. The simulations were carried out with two values of K_{0NC} for Bay Mud (i.e., the URS selected K_{0NC}=0.62 and the MIT lab measured K_{0NC} = 0.47). Simulations of varying friction angles (ϕ' = 20^0, 25^0, 30^0 and 46^0) were carried out for each of the two specified K_{0NC} values. For each pair of $K_{0NC,}$ ϕ' values, five CK_0U PSC tests were simulated at OCR = 1, 1.5, 2, 3, and 5. For simulations with overconsolidated samples (OCR > 1), K_0 conditions are imposed using the Schmidt (1966) empirical relationship, $K_0 = K_{0NC}.(OCR)^n$, where n = 0.4.

The pair of K_{0NC} = 0.62, ϕ' = 30^0 are the URS selected parameters, and K_{0NC} = 0.47, ϕ'=46^0 are the MIT measured values for the Bay Mud in TX tests. Table 3.12 summarizes results of all the PSC simulations. The undrained shear strength at each OCR is the same in both compression and extension in the plane strain shear mode with SSM.

Figure 3.15 plots the results of undrained shear strength ratio, s_u/σ'_{vc} versus OCR for all of the CK_0U PSC simulations and compares them with the laboratory measured CK_0U DSS, TC and TE data. Line 2a presents results of the SSM undrained shear strength of the pair of parameters (K_{0NC} = 0.62, ϕ'=30^0) that was used by URS (2003). The URS pair of parameters underestimate the undrained shear strength at OCR >3 and overestimate it at OCR <2. At OCR = 1.5, where most of the soil below Bay Mud crust experiences (i.e., Fig. 3.1), Line 2a shows s_u/σ'_{vc} = 0.44, which is 25% higher than the

measured CK_0UDSS value (DSS s_u/σ'_{vc} = 0.35). In addition, Line 2a gives S_d = 0.38, which is 50% higher than measured S_d = 0.25.

Results from SSM with K_{0NC} = 0.47, ϕ' = 46^0 (i.e., Line 3b) correspond to properties measured ≈ the MIT triaxial shear tests, result in much too high S_d = 0.52 (i.e., 108% higher than the measured S_d) and greatly overestimate s_u at OCR=1.5 [6][i.e., s_u(SSM) ≈ 166% of measured s_u(DSS) at OCR =1.5].

The figure shows that Line 1b (K_{0NC} = 0.47, $\phi'=20^0$) gives S_d (SSM) = S_d (lab), but underestimates the measured undrained shear strength at the average in situ OCR ≈ 1.5.

To get agreement of s_u(DSS) versus s_u(SSM) at OCR = 1.5, the best selected pair of parameters are $\phi'=25^0$, K_{0NC} = 0.47.

3.4.4 CK_0PS-DSS Tests Simulation

Plane strain direct simple shear (PS-DSS) tests were simulated with SSM for Bay Mud at OCR = 1, 1.5, 2, and 4. Selected SSM parameters for the Bay Mud in the analyses are presented in Table 3.10.

K_0 consolidation was simulated using a distributed load system and a prescribed displacement at the top and at both sides of the soil element. The element was first K_0 consolidated to 1.5 ksf into the virgin compression range. In every test, the element was then unloaded to a specified OCR prior to shearing. Shearing process was simulated by imposing no displacement in the vertical direction (Y-axis) while straining the element by a prescribed displacement at the top to 30% shear strain in horizontal direction (X-axis).

[6] This result reflects limitations of the SSM soil model, not in the values of ϕ', K_{0NC} themselves.

The DSS simulations were carried out with two values of the modified swelling index, $\kappa^* = 0.104$ (i.e., the lab measured κ^* for getting realistic recompression behavior to predict consolidation settlement, ρ_c), and $\kappa^* = 0.002$ (i.e., the reduced κ^* for getting realistic undrained modulus, E_u to predict shear induced settlement or initial settlement, ρ_i). Eq.3.10 shows the relationship between E_u and κ^* .

Figures 3.16 presents the results of undrained shear strength ratio, s_u/σ'_{vc} versus OCR from the DSS simulations for the cases where $K_{0NC} = 0.47$, $\phi' = 25^0$, and $\kappa^* = 0.104$ and 0.002. Simulations with both values of κ^* generally result in the same undrained shear strength at a given OCR. In addition, the results from the DSS simulations are essentially the same with the PSC/E (i.e. Fig.3.15 Selected Line). Table 3.13 summarizes results of all the DSS simulations.

Figure 3.17a, b present results of the DSS simulations for the cases where the modified swelling index, $\kappa^* = 0.104$ (i.e., selected maximum value of RR = 0.12). Figure 3.17a plots stress-strain curves for the DSS simulations at OCR = 1, 1.5, 2 and 4. The undrained strength ratios at failures are then plotted versus OCR to establish the best fitting line as shown in Figure 3.16 (i.e., FE Simulation line).

Figure 3.17b plots the normalized undrained modulus, E_u/σ'_{vc} versus shear strain, $\gamma\%$. E_u values were computed from the undrained shear modulus, G_u based on the relationship $E_u = 3G_u$, where $G_u = \Delta\tau/\Delta\gamma$. Measured data from the laboratory DSS tests are shown for comparison with the SSM simulation results. As shown in the figure, using the selected maximum κ^* value greatly underestimates the undrained modulus, E_u by a factor of 45 to 50 at OCR = 1.5. The measured $E_u/\sigma'_{vc} \approx 500$ (at OCR =1) to 1000 (at OCR=2, 3), and the averaged ratio at OCR = 1.5, $E_u/\sigma'_{vc} \approx 750$. On the other hand, the

DSS simulation at OCR =1.5 gives E_u/σ'_{vc} = 16, which is much too low (by a factor of 47) compared with the measured data. Therefore, using the SSM, one cannot use a selected κ^* for realistic prediction of initial settlement during embankment construction, ρ_i. Prediction of ρ_i needs a realistic E_u, which requires a reduced value of κ^* (i.e., κ^* = 0.002, by a factor of 47 compared with the lab κ^*).

Figures 3.18a,b present results of the DSS simulations with the reduced κ^* = 0.002. Realistic values of E_u at very small strain (i.e., at $\gamma = 1x10^{-5}$ %) and at γ = 0.1 to 0.2 % are achieved by the reduced κ^* = 0.002 (i.e., Fig.3.18b).

3.4.5 Summary and Conclusions

SSM s_u and E_u simulations have shown the following results.

1) The SSM predicted values of s_u at OCR = 1 depend primarily on the selected values of ϕ' and to a lesser degree on K_{0NC}, whereas E_u depends primarily on κ^*.
2) SSM needs a low value of friction angle, ϕ' to predict a reasonable DSS undrained shear strength ratio for NC clay, S_d, but the low ϕ' results values of s_u(DSS) that are two low at OCR >1.
3) SSM with $\phi' = 25^0$ gives reasonable agreement between the measured and computed s_u(DSS) at OCR = 1.5 for the Bay Mud.
4) SSM with the "best selected" $\phi'=25^0$ greatly underestimates s_u at OCR >2.
5) Using κ^* in SSM based on lab data results in much too low E_u (by a factor of 50 at OCR =1.5 for κ^* = 0.104 corresponding to RR = 0.12). To obtain a reasonable E_u, and therefore reasonable predictions of the initial settlement ρ_i, one has to reduce κ^* to values an order of magnitude less than appropriate for consolidation analyses.

6) Hence, we cannot use the same value of κ^* for realistic prediction of both ρ_i and ρ_c. But one can use two values of κ^*, one to predict ρ_i and another much higher value to predict ρ_c.

7) SSM predicts the same undrained shear strength in plane strain compression, extension and DSS shear modes since it is an isotropic model.

8) Because the Bay Mud has OCR ≈ 1.5 within most of the deposit (below EL. -12 ft), the SSM strength parameters selected by the Author for the Bay Mud are $\phi' = 25^0$ and $K_{0NC} = 0.47$.

3.5 NHPL Reanalysis Using Soft Soil Model in Finite Element Code PLAXIS

Using a finite element code to model and predict deformations of the NHP levee allows one to address the 2-D effects that a 1-D consolidation analysis cannot take into account. This section presents 2-D finite element analyses for the NHP levee using the commercial finite element code PLAXIS v.8.2. The built-in Soft Soil Model (SSM) in PLAXIS was used to represent the Bay Mud Crust and the Bay Mud. The Author ran PLAXIS analyses with varying sets of SSM parameters for the Bay Mud to predict the performance of the NHP levee, including vertical settlements, horizontal displacements, and excess pore pressures. The results from PLAXIS analyses are then compared with the measured data to evaluate the capabilities of the 2-D FE analyses.

3.5.1 Geometry and Mesh of NHPL Model

Geometry of the NHP levee fill and the soil deposit were set up in layers, which are called to soil clusters in the model. Splitting the fill and the materials under the fill into clusters help one to model different material properties and simulate staged construction. Figure 3.19 presents the NHP levee model geometry. Pavement and soil layers and the water table elevation are shown in the figure. All elevations of material layers were set up in the model as follows:

- Levee fill was from elevation of the levee crest at 9.4 ft down to the levee base at -1.6 ft, giving a 11 ft levee height. The widths of the levee fill were 23.0 ft an the top and 89.0 ft at the bottom. The levee fill was divided into six clusters (sub-layers). Each levee fill

cluster is 2 ft thick, except for the top one having thickness of 1 ft (Note that URS used only two layers for the levee fill).

- Concrete pavement (or cracked pavement, i.e., in cases where analyses are run with a cracked pavement under the NHPL) from elevation -1.6 ft to -4.5 ft = one cluster;
- Base course from elevation -4.5 ft to -6.2 ft = one cluster;
- Bay Mud Crust from elevation -6.2 ft to -10 ft equivalent to = one cluster;
- Bay Mud from elevation -10 ft to -41.5 ft divided into 8 clusters (sub-layers) to model the changes in the stress history (OCR), and the corresponding coefficient of earth pressure at rest (K_0), plus changes in compressibility; and
- Alluvial soil layer from elevation – 41.5 to -60 ft = one cluster.

Fig. 3.19 also plots the mesh of the NHP levee model (i.e., the mesh type of *Very-Fine* in the *Global Coarseness* was selected in the meshing type). The geometry, which had a total width of 325 ft, with frictionless ends, was meshed into 1231 triangle-15-moded elements with total 10079 nodes and 14772 stress points. The average element size is 4.28 ft. A twelve-point Gauss integration was used in each element. Note that finer and coarser meshes were also evaluated during the analysis process of the NHP levee and there was almost no change in the analysis results due to changes in the selection of mesh types.

3.5.2 Defined Cases for FE Analyses of the NHPL

Table 3.14 presents four groups of cases (A, B, C and D) for the FE analyses of the NHPL. Cases A1 and A2 are analyses using same best estimates of material

properties for all soil layers. Case A1 assumes a continuous uncracked pavement, while Case A2 assumes cracked pavement (properties extending to the toe of the levee).

Case A2 is identified as the base analysis (i.e., for comparisons with all other cases). The soil properties used in A1 and A2 can be summarized as follows: Preconsolidation stress profile σ'_p = mean σ'_p(FV) profile. K_{0NC} and ϕ' were selected for Bay Mud that give s_u(SSM) = s_u(DSS) at OCR =1.5 (i.e., K_{0NC} = 0.47 and $\phi' = 25^0$). Compressibility parameters used the best estimate RR and CR values for Bay Mud and Bay Mud Crust (i.e., CR = 0.40; RR = 0.06 from EL. = - 6.2 to -20 ft and RR = 0.12 from EL. = -20 to -41.4 ft). The hydraulic conductivity properties were selected for Bay Mud that gives lab measured average c_v(NC) = 0.06 ft^2/day (i.e., $k_{v0} = 9x10^{-4}$ ft/day, $k_{h0} = 12x10^{-4}$ ft/day, and C_k = 1.40). And $k_{v0} = k_{h0}$ = 0.001 ft/day within the Alluvial soil below the Bay Mud.

Case B assumes that the underlying Alluvium layer is effectively free draining (i.e., $k_{v0} = k_{h0}$ = 1.0 ft/day), and hence the excess pore pressure u_e = 0 throughout this stratum by early 2002.

Cases C1, C2, and C3 were carried out to evaluate the effects of c_v(NC) for the Bay Mud. Each analysis case varies the hydraulic conductivity properties (i.e., k_{v0}, k_{h0}, and C_k) such that c_v(NC) is in the range of c_v(NC) = 0.04 to 0.06 ft^2/day [i.e., Case C1 = URS (2003) parameters that gives c_v(NC) = 0.04 ft^2/day; C2 = 0.045 ft^2/day; and C3 = 0.05 ft^2/day].

Finally, Cases D1 and D2 analyses were carried out with reduced preconsolidation profiles; $0.9\sigma'_p$ and $0.8\sigma'_p$ respectively, and with c_v(NC) = 0.06 ft^2/day to evaluate the effect of the preconsolidation stress profile on the consolidation behavior of the NHP

levee. Case D3 uses a reduced c_v(NC) for comparison with D2. Case D4 uses a reduced hydraulic conductivity values for the BM Crust and Alluvium (i.e., 0.005 ft/day) in order to improve agreement with measured profiles of excess pore pressure at TS3 and TS5.

3.5.3 Selection of Material Parameters for FE Plaxis Analyses

The material parameters for the FE Plaxis analyses were selected both from URS (2003) and from the Author's reevaluation of soil properties in the previous sections of this chapter. Table 3.15 gives a complete summary of the material models and input parameters used for the Plaxis analyses of the NHP levee.

The Mohr-Coulomb (MC) material model was used for the Levee fill, the uncracked Pavement, cracked Pavement and Base Coarse layers, while Linear Elasticity was assumed for the underlying Alluvium layer. The material parameters for the materials above the Bay Mud were selected from Table 6 of URS (2003) after being evaluated by the Author in Section 3.3.1 (i.e., to get best estimated σ'_{vf} profile).

Soft Soil Model (SSM) was used for the Bay Mud and Bay Mud Crust layers. Within the Bay Mud, the soil from EL. = -10 ft to EL. = -20 ft is identified as Bay Mud 1 and the soil from EL. = -20 ft to EL. = -41.5 ft is Bay Mud 2, where the recompression ratio is varied according to values shown at the bottom of Table 3.14.

3.5.4 Simulation and Calculation Procedures

The four groups of analysis cases (A, B, C and D) were run following the same simulation and calculation procedures.

Initial conditions of the ground with unit weight, water table elevation, stress history and coefficient of earth pressure at rest (K_0) selected for the Plaxis analyses are shown in Tables 3.15 and 3.16. Table 3.16 shows overconsolidation ratio (OCR) profiles selected by the author based on the best estimated preconsolidation stress profile (σ'_p) as in Fig. 3.1. Based on the OCR data, the K_0 profile of the ground was estimated using the following formula [Ladd et al. (1997)]:

$$K_{0OC} = K_{0NC}.(OCR)^m \quad , \qquad (3.20)$$

where K_{0OC} and K_{0NC} are coefficients of earth pressure at rest for overconsolidated and normally consolidated soils, respectively; *m* is a coefficient depending on plasticity index of soil (I_p) (i.e., for I_p = 50%, $m \approx 0.35$); K_{0NC} = 0.47 for the Bay Mud from the laboratory triaxial tests.

Figure 3.20 shows the sequence assumed in the FE simulations for which was the staged embankment construction (the actual schedule of loading is not known). The figure shows a key assumption that the consolidation time for the settlement monitoring stated at CD90, which is midway through the estimated construction period. URS (2003) reported that the NHP levee was built between March and October 1996, whereas measurements of settlements were initiated only after the end of construction (11/11/96; CD210).

Table 3.17 lists all the calculation phases for the FE model. Each loading step was calculated as a *Plastic Loading* phase (with undrained response in the Bay Mud and Bay Mud crust), followed by *Consolidation*. For the first two fill layers, each was loaded instantaneously with *Plastic Calculation* and then *Consolidation* for 45 days. Each of the four consecutive layers was then loaded and consolidated for 30 days. In the final phase,

after completing the levee fill, the NHP levee was consolidated about 5 years and 2 months to the date when both measured settlements and pore pressures were available (i.e., at CD2115 = 01/31/02).

3.5.5 Results from Cases A1 and A2

These analyses used the best estimate set of parameters for soils below the levee. Case A1 used Young's modulus E = 1000 ksf for the uncracked pavement while Case A2 used E = 200 ksf for the cracked pavement.

Figure 3.21a plots the predicted consolidation settlement, ρ_c versus logt for analysis Cases A1 and A2 compared with the measured data (ρ_m) from settlement points P16 to P19. The results show that the curves of ρ_c from both cases are essentially the same. Hence, there is minimal effect of the pavement on the computed consolidation settlements between the two cases. Figures 3.21b to 3.21d show comparisons of the excess pore pressures and stress histories at CD2115 for the analysis Cases A1 and A2. The results also show no difference in the predicted u_e and σ'_{vc} between the two cases. Therefore, one can conclude that the difference in Young's modulus E of the pavement in the two cases has no effect on the consolidation behavior of the NHPL.

Comparison of the predicted consolidation settlement (ρ_c) with the measured consolidation settlements (ρ_m) at measured points near TS3 and TS5 (i.e., 16, 17, 18 and 19) are shown in the Fig. 3.21a assuming that $\rho_m = 0$ shortly after the assumed EOC (CD210). The results show that at CD2115 (1/31/02), $\rho_c \approx \rho_m$ at point 18, and $\rho_c \approx 75\%$

ρ_m at point 17. At CD2115, Cases A1 and A2 predict $\rho_c \approx 1.47$ ft, while URS (2003) reported that $\rho_m = 1.65$ ft at TS3 and $\rho_m = 1.57$ ft at TS5. In general, the analyses underestimate the measured rate of consolidation recorded at P16 – P19.

Figure 3.21b shows comparison of the predicted excess pore pressures at CD2115 versus elevation at centerline of the NHPL with the measured data. Cases A1 and A2 both under-predict the maximum u_e at the mid-depth of the Bay Mud by about 38% and 50% compared to u_e measured at TS5 and TS3, respectively. In addition, the two cases predict excess pore pressures in the BM Crust (from EL. -6.2 to -10 ft) and in the Alluvium below Bay Mud (below EL. -44 ft). In contrast, the measured data show $u_e = 0$ at both locations. Figure 3.21c shows a similar comparison of excess pore pressure at toe of the levee. The figure shows that Case A1 and A2 are in good agreement with measurements within the Bay Mud layer, but again overestimate u_e at the BM Crust and Alluvium interfaces.

Figure 3.21d shows a comparison of the predicted vertical consolidation stress σ'_{vc} for Cases A1 and A2 with the selected σ'_p profile, and the "measured SH2" σ'_{vc} at TS3 and TS5 under the centerline of the NHPL. Comparison of σ'_p and the predicted σ'_{vc} shows that σ'_{vc} is larger than σ'_p from EL. -12 to - 35 ft, creating a relatively large zone of virgin compression in the Bay Mud. But, a large fraction of ρ_c still comes from recompression. The figure also shows that the predicted σ'_{vc} profile is close to the measured σ'_{vc} at TS5 from EL. = -15 ft to -32 ft, but higher than σ'_{vc} at TS3 from EL. = -20 to -35 ft. The predicted $\sigma'_{vf} = \sigma'_{vc} + u_e$ at CD2115 for the two cases is plotted in the figure to compare with σ'_{vf} for 1-D SH2 case presented in Fig.3.12c. There is a significant reduction in σ'_{vf} due to decreases in the total vertical stress σ_v during

consolidation under the centerline of the levee. This "arching effect" is due to coupled consolidation with SSM (Ladd et. al , 1994). This arching effect is evaluated further in Section 3.5.11.

Figure 3.21e plots profiles of the predicted total settlement (ρ_t) at CD180 (EOC), and CD2115 (1/31/02) and the resulting consolidation settlement after EOC (ρ_c) versus elevation at centerline of the NHPL for the Case A2 analysis. The ρ_t line at CD180 presents the total settlement profile at the end of construction (i.e., comprising undrained shear induced settlements, which are much too high due to the very low SSM E_u values for the Bay Mud, plus consolidation settlements during construction of the levee). Line ρ_t at CD2115 is the total settlement profile at 1/31/02. Hence, the predicted consolidation settlement of the NHPL after the EOC is $\rho_c = \rho_t$ (CD2115) - ρ_t (CD180). The results show a constant $\rho_c \approx 1.40$ ft from EL. = 9.4 (levee crest) to EL. = -10 (bottom of BM Crust). Thus, all of the predicted ρ_c occurs within the soft Bay Mud, which is reasonable. In comparison, the measured settlements of are 1.65 ft at TS3 and 1.57 ft at TS5.

The results in Fig. 3.21e show an amount of 0.4 ft of compression occurring within the Base Course and Cracked Pavement layers at CD180 and CD2115. This corresponds to an axial strain of approximately 5%. This is not very realistic, but is due to the relatively low stiffness (E = 200 ksf) recommended by URS (2003) for these layers.

Figure 3.21f plots the computed settlement for the pavement on top of the BM Crust from the Case A2 analysis at CD180 and CD2115. The maximum settlement occurs at the centerline of the levee, while there is an upward movement (heave) beyond the toe of the levee. The heave pattern reflects undrained shear-induced strains, which are too large because of the low E_u used in the analysis for the Bay Mud.

Figure 3.21g plots settlement versus logarithm of time at Point A located at the centerline of NHP levee for the cracked pavement Case A2 analysis. The plot shows that for each loading step, there is an undrained shear induced settlement occurring instantly during each loading step, followed by a consolidation settlement. The undrained shear induced settlements contribute a significant fraction of the predicted total settlement during construction of the fill. These large undrained shear induced settlements occurred because the analyses used very low values of undrained modulus E_u, that are much lower than measured in the lab CK_0U DSS tests (i.e., see Section 3.4.4). Therefore, these large "initial" settlements are not realistic. The predicted consolidation settlement (ρ_c) is computed from end of construction (CD180) to CD2115 (01/31/02), and was compared with the measured settlements after EOC (i.e., in Fig. 3.21a). Note that about 0.3 ft of predicted consolidation settlement occurred during construction of the levee compared to a total settlement of 2.4 ft.

Figure 3.21h plots the centerline excess pore pressure (u_e) versus logarithm of construction day near the mid-point of the soft Bay Mud for Case A2. The figure shows the excess pore pressure response during and after construction, in which u_e builds up during each loading step and then dissipates, especially after EOC. The excess pore pressure at the mid-point is $u_e \approx 0.94$ ksf at CD180, and $u_e = 0.23$ ksf at CD2115 (5.2 years after EOC), with very little u_e dissipation during construction.

One of the advantages of a 2-D analysis compared with a 1-D analysis is the capability to compute and take into account both horizontal and vertical deformations within the soil mass. Two-dimensional (2-D) effects could be important for the NHP

levee where the ratio of the thickness of the deposit to the width of the levee, H/B is about 0.6.

Figure 3.21i plots the predicted horizontal displacements versus elevation at the toe and 20 ft away from the toe of the levee at time CD180 (end of construction) and CD2115 (1/31/02). The maximum horizontal displacement is 1.14 ft located at EL. = -20 ft within the Bay Mud. Much less horizontal displacement is predicted within the Bay Mud near the ground surface as shown in the figure. It is likely due to the high stiffness of the upper layers (i.e., the BM Crust, pavement and levee fill).

It is noted that the analysis predicts slightly decreasing horizontal displacements during consolidation after EOC. This prediction is not realistic since extensive field data show that horizontal displacements always increase during consolidation (i.e., Ladd, 1991). In addition, the measured data for the Test Fill (URS/ARUP, 2005) proved that the horizontal displacements were increasing during consolidation after EOC. Thus, predicting decreased horizontal displacement during consolidation is one of the limitations of the SSM in Plaxis.

3.5.6 Results from Case B Compared to Case A2

The Case B analysis evaluates the effect of the hydraulic conductivity of the Alluvium below the Bay Mud. The input parameters for Case B are the same as Case A2, except for a 1000 fold increase in the hydraulic conductivity of the Alluvium (i.e., k_{v0} = k_{h0} = 1.0 ft/day) such that there is effectively free drainage below the Bay Mud.

Figure 3.22a compares the computed ρ_c versus logt from analysis Cases B and A2 with measured data ρ_m at points 16, 17, 18 and 19 near TS3 and TS5. Case B predicts a

faster rate of consolidation than Case A2. From CD180 to about CD1200, the Case B predicted ρ_c closely matches with the measured values of settlement point 17, but then has a much slower rate of settlement. Case B analysis predicts $\rho_c \approx 1.5$ ft at CD2115 (1/31/02), which is equivalent to 95% the measured ρ_m at TS5 and 90% ρ_m at TS3.

Figures 3.22b and 3.22c plot the predicted u_e at the centerline and toe of the NHPL compared with the measured u_e at TS3 and TS5. Case B predicts much less u_e at CD2115 than the measured data or Case A2 at both the centerline and toe locations. The figures also show that $u_e = 0$ below the bottom of the Bay Mud for Case B.

Figure 3.22d plots stress histories for the two analyses. The figure shows comparison of the predicted σ'_{vc} at the centerline of the NHPL for Case B along with σ'_p, σ'_{vc} from Case A2, and the "measured SH2" σ'_{vc} profiles at TS3 and TS5. The predicted σ'_{vc} for Case B is higher than σ'_{vc} below El. -12ft for Case A2. Although this results in a much larger zone of virgin compression in Bay Mud compared to Case A2, the predicted ρ_c for Case B at CD2115 is just slightly higher than that of Case A2. Therefore, The very small increase in ρ_c is not consistent with the relatively large increase in σ'_{vc}, which the Author cannot explain.

3.5.7 Results from Cases C1, C2, and C3 Compared to Case A2

Case C1, C2 and C3 evaluate the effect of c_v(NC) of Bay Mud on the consolidation behavior of the NHPL compared with Case A2. Case C1 used URS input parameters ($k_{v0} = 4x10^{-4}$ ft/day, $k_{h0} = 8x10^{-4}$ ft/day and $C_k = 1.143$), which are equivalent to c_v(NC) = 0.04 ft^2/day in SSM 1-D consolidation, while c_v(NC) = 0.045 and 0.05 ft^2/day in cases C2 and C3.

Figure 3.23a plots the predicted ρ_c versus logt from the four analyses, along with the measured ρ_m. The Case C1 ρ_c curve shows a much slower rate of settlement compared with the measured and Case A2 curves. At CD2115, Case C1 predicts ρ_c = 1.25 ft, and Case C3 predicts ρ_c = 1.34 ft; both being less much less than measured.

Figure 3.23b and Figure 3.23c plot results of excess pore pressure versus elevation at centerline and toe of the NHPL, respectively, for Cases C analyses compared with the measured u_e and those from Case A2. Case C1 predicts much higher u_e profiles compared to Case A2, and agree quite well with the measured centerline data from EL. = -24 to -34 ft at TS3 (Fig. 3.23b). Cases C1 and C2 seem to encompass the range of measured u_e at the centerline of TS3 and TS5, but overpredict those at the toe (Fig.3.23c).

Figure 3.23d shows predicted σ'_{vc} at CD2115 for Cases C1 and C3 and compares them with the σ'_p profile, σ'_{vc} from Case A2 and the "measured SH2" σ'_{vc} profiles at TS3 and TS5. Case C1 predicts a very small virgin compression zone (from EL. -12.5 to -22 ft) and therefore, the main source of ρ_c in this case comes from recompression. The higher c_v(NC) for Case 3 predicts σ'_{vc} moderately less than σ'_{vc} from Case A2.

3.5.8 Results from Cases D1 and D2 Compared to Case A2 and URS (2003)

The Case D1 and D2 analyses use reduced (scaled) preconsolidation stress profiles in the Bay Mud ($0.9\sigma'_p$ and $0.8\sigma'_p$, respectively). Input parameters for Cases D1 and D2 are the same as Case A2, except for lower RR values (Table 3.14) and the reduced OCR and K_0 profiles (Table 3.16).

Figure 3.24a plots the predicted ρ_c versus logt for Cases D1 and D2 and compares them with the base Case A2, as well as with prior analysis by URS (2003), and the measured ρ_m at points near TS3 and TS5. The Case D1 and D2 curves show higher rates of settlement compared to Case A2, and they bracket very well the measured ρ_m curves. The D2 analysis (with $0.8\sigma'_p$) gives much higher settlements than those reported by URS (2003) using the same preconsolidation profile. The larger Case D2 prediction of ρ_c is probably mainly due to the fact that URS used c_v(NC) = 0.04 ft^2/day, which is smaller than the Case D2 c_v(NC) = 0.06 ft^2/day and predicted a much higher centerline u_e profile (Fig. 3.24b). In addition, URS (2003) used RR = 0.04 for Bay Mud, while Case D2 used a higher RR = 0.08 from EL. -20 to EL. -41.5.

Figure 3.24b shows comparisons of u_e at the centerline of the NHPL. Cases D1 and D2 predict much less excess pore pressure than measured at TS3 and TS5, but similar to Case A2. The predicted maximum excess pore pressure at mid-point of the Bay Mud is roughly 50% of the averaged measured u_e at TS3 and TS5. In contrast, the URS (2003) u_e is in much better agreement with the measured data, and also predicts a smaller u_e within the Alluvium.

Figure 3.24c compares u_e at the toe of the NHPL. The figure shows that the predicted u_e agrees quite well with the measured data above EL. -38 ft, but overpredicts u_e below EL. -38 ft.

Figure 3.24d plots the predicted stress histories from Cases A2, D1 and D2, which shows relatively small differences in the σ'_{vc} profiles. Case D2 with the $0.8\sigma'_p$ profile has a very large zone of virgin compression, and thus the main source of ρ_c comes from

virgin compression. The figure also shows a reduction of about 0.1 ksf in σ'_{vf} profiles of Cases D1 and D2 due to the arching effect.

Figure 3.24e plots the predicted total settlements (ρ_t) versus elevation at the centerline of the levee from the Case D2 analysis at CD180 and CD2115. The predicted consolidation settlement (ρ_c) from CD180 to CD2115 is also shown.

Figure 3.24f shows plots of horizontal profiles of the predicted ρ_t (at CD180 and CD2115), predicted ρ_c (from CD180 to CD2115) from Case D2 analysis, and ρ_c from URS (2003). Case D2 predicts a maximum ρ_c about 0.3 ft higher than URS (2003).

Figure 3.24g plots settlement at EL.- 3.0 ft versus logt of Point A at the centerline of the levee from Case D2. Note that the total settlement is reset to zero at CD180 prior to consolidation after loading of the last fill layer. The figure shows that there is about 0.3 ft of consolidation settlement, and about 1.5 ft of undrained shear induced settlement during construction of the levee. The consolidation settlement after EOC from CD180 to CD2115 is ≈ 1.9 ft.

Figure 3.24h plots the predicted excess pore pressure of Case D2 versus logt at the mid-point of Bay Mud (EL. = -26 ft).

Figure 3.24i plots the horizontal displacement at toe versus elevation at CD180 and CD2115. From the top of the cracked pavement to EL. -11ft, the horizontal displacement slightly decreases from CD180 to CD2115, and then remains essentially constant at greater depths. In contrast, the A2 analysis predicted a decrease in horizontal displacement of about 0.1 ft through most of the BM during consolidation (Fig.3.21i).

3.5.9 Results from Case D3 Analysis and Comparison with Cases A1, C1 and D2

The Case D3 analysis was carried out with a reduced preconsolidation stress profile ($0.8\sigma'_p$) and c_v(NC) = 0.04 ft^2/day to further evaluate the combined effects of the preconsolidation stress and c_v(NC) of Bay Mud on the NHPL performance.

Figure 3.25a plots the predicted ρ_c versus logt for Case D3 and compares it with Case A2, Case C1, and Case D2, along with the measured settlements, ρ_m at points near TS3 and TS5. Case D3 predicts a much higher rate of settlement compared with Case C1 having the same c_v(NC) and its consolidation settlement curve matches very well with the ρ_m of point 18. The figure shows that Cases D2 and D3, both with the $0.8\sigma'_p$ profile, encompass the four measured settlement curves. The figure also shows that a reduction in c_v(NC) causes a large decrease in the predicted ρ_c, especially when σ'_p is reduced by 20%.

Figures 3.25b and 3.25c show predictions of excess pore pressures at the centerline and the toe of the NHP levee for the same four analysis Cases. These results confirm the importance of c_v(NC) in controlling magnitudes of u_e at the end of the monitoring period, CD2115, whereas σ'_p has relatively little effect.

Figure 3.25d shows comparison of the predicted σ'_{vc} at centerline of NHPL for the same four analyses. The figure shows that the predicted zone of virgin compression is significantly effected by both c_v(NC) and σ'_p, although the later variable has a larger effect on ρ_c at CD2115.

3.5.10 Results from Case D4 Analysis

This case attempted to improve the predicted excess pore pressures u_e at the centerline of NHP levee at CD2115. Therefore, the hydraulic conductivities of the BM Crust and the Alluvium are selected such that the analysis gives high value of u_e within the soft Bay Mud, along with $u_e \approx 0$ in the Bay Mud Crust and Alluvium. The selected hydraulic conductivities for the soils are $k_{v0} = k_{h0} = 0.005$ ft/day in both the BM Crust and Alluvium.

Figure 3.26a plots ρ_c versus logt for Case D4 and the predicted ρ_c of URS (2003). The selected c_v(NC) for Bay Mud and the hydraulic conductivities of BM Crust and the Alluvium in Case D4 and URS(2003) are also shown for comparison. URS(2003) analysis used a sand layer below a thin stiff clay under the Bay Mud with very high permeability ($k_{v0}=k_{h0}$ =1 ft/day) as a draining layer.

Figure 3.26b shows comparisons of u_e vs. elevation at centerline of Case D4, URS (2003) and the measured data at TS3 and TS5. The plot shows that URS (2003) overpredicts u_e above El. -20 ft because URS (2003) used very low hydraulic conductivities for BM Crust (i.e., $k_{v0} = 4x10^{-4}$ ft/day and $k_{h0} = 8x10^{-4}$ ft/day). The predicted u_e from Case D4, as shown in the figure, perfectly matches the measured data at TS5, but underpredict the high u_e measured at TS3.

Figure 3.26c shows comparison of the predicted u_e vs. elevation at toe from Case D4 with measured u_e data. Case D4 predicted u_e at toe again matches very well with the measured data at TS5, but now overpredicts the data at TS3.

Figure 3.26d shows predicted stress histories for Case D4, which are about 0.1 ksf lower than measured (due to the lower σ'_{vf}).

3.5.11 Discussion on Computed Arching Effects during Consolidation

Ladd et. al. (1994) investigated the "arching effect" behavior of an embankment on Boston Blue clay in which FE analyses using the MCC and MIT-E3 soil models predicted a decrease in σ_v at centerline and an increase of σ_v beyond the toe of the embankment during consolidation.

Figure 3.27a plots the net stress, $\sigma'_v = \sigma_v - u_{hydrostatic}$ versus elevation at centerline of the levee computed at CD180 and CD2115 for the base Case analysis. The results are compared with the final effective stress profile σ'_{vf} used in 1-D settlement calculations [i.e., 1-D (SH2) σ'_{vf}]. The figure shows that σ'_v of Case A2 at CD180 is slightly higher than that used for the 1-D ρ_c calculation presented in Section 3.3. Importantly, the figure shows that $\sigma'_v = (\sigma_v - u_{hydro})$ at CD2115 is reduced significantly from that at CD180, i.e., $\Delta\sigma_v \approx 0.05$ ksf from top of BM Crust at El -6.2 down to El. -20 ft, and $\Delta\sigma_v \approx 0.1$ to 0.13 ksf from El. -20 ft to the bottom of the Bay Mud at El. -41.5 ft.

Figures 3.27b and 3.27c presents similar results from the Case C1 and Case D2 analyses. Case C1 has $\Delta\sigma_v \approx 0.05$ ksf at top of BM Crust, and $\Delta\sigma_v \approx 0.1$ ksf within most of the Bay Mud. Case D2 has the largest reduction of $\Delta\sigma_v \approx 0.13$ from CD180 to CD2115 at centerline.

Figure 3.27d plots $\Delta\sigma_v$ from CD180 to CD2115 versus distance from centerline of the NHPL at El. = -29.7 ft. The result shows that σ_v decreases 0.135 ksf at centerline and increases by the same amount at toe of the levee.

The decrease in the total vertical stress under an embankment is contrary to the common assumption that σ_v remains constant during consolidation.

3.5.12 Summary and Conclusions

Table 3.18 summarizes the ten analysis cases of the NHPL. Table 3.18a presents comparison of the predicted ρ_c and u_e with measured data at TS3 and TS5 and with the URS (2003) analysis. Table 3.18b lists the total settlements at CD180 (EOC) and CD2115 (1/31/02), the consolidation settlement (ρ_c) at 5.2 years after end of construction (i.e., from CD180 to CD2115) and the maximum horizontal displacement (h_{max}) and the maximum excess pore pressure (u_e) predicted at CD2115.

Figure 3.28a plots the predicted consolidation settlements from the 2-D FE analyses for 8 cases and compares them with the URS (2003) value and with the 1-D ρ_c calculation results from 1- D SH1, 1-D SH2 and 1- D URS (2003). The figure plots the predicted ρ_c versus the σ'_p profile used in the analyses. Results from the Plaxis analyses are divided into two groups: (1) those analysis cases with c_v(NC) = 0.06 ft^2/day (i.e., A1, A2, B, D1 and D2); and (2) those analysis cases with c_v(NC) = 0.04 ft^2/day (i.e., C1, D3, and D4).

For the Author's Plaxis analyses, an increase in c_v(NC) and a decrease in σ'_p both increase ρ_c, as would be expected. The effect of c_v(NC) on ρ_c is most pronounced for the $0.8\sigma'_p$ profile. Note that RR was reduced from 0.06 and 0.12 to 0.04 and 0.08 for the $0.9\sigma'_p$ and $0.8\sigma'_p$ profiles, which explain the smaller increase in ρ_c for a 10% reduction in σ'_p compared to the 20% reduction (i.e., the results from the A2, D1 and D2 Cases). The effect of reducing u_e to zero at the top and bottom of the soft Bay Mud is also important

for the $0.8\sigma'_p$ profile (Cases D3 and D4). Note that the D4 analysis predicts a ρ_c very close to that reported by URS (2003).

Overall, the results of the Plaxis analyses are in reasonable agreement with the SH2 1-D ρ_c calculations for the two lower σ'_p profiles, especially when considering the results for Cases D1, D2 and D4.

Figure 3.28b plots the predicted maximum u_e versus Bay Mud c_v(NC) from the analyses, along with the measured data at TS3 and TS5, and the URS (2003) analysis. The results show that Cases C1, D3 and D4 with c_v(NC) = 0.04 ft^2/day predict u_e in the range of the measured data. Analyses using higher c_v(NC) values underestimate the maximum u_e below the centerline, but can still achieve reasonable agreement with maximum values beneath the toe.

The combined results of the conventional 1-D consolidation analysis (SH2) and the Plaxis analyses indicate that the preconsolidation stress (σ'_p) of the Bay Mud is lower than the σ'_p(FV) profile developed by URS (2003) and checked by the Author. The CRSC σ'_p data also were in reasonable agreement with σ'_p(FV). One must also reduce σ'_p, and also c_v(NC) compared to the lab CRSC data, in order to achieve reasonable agreement between predicted and measured values of both ρ_c and u_e. A 10% reduction in σ'_p can be explained by the fact that the CRSC tests overpredict σ'_p due to the higher strain rate than occurs at the EOP in incremental oedometer tests. And a 20% reduction in σ'_p would support Hypothesis B.

Unrealistic undrained shear induced settlements (initial settlements) are predicted (therefore the horizontal displacements) when using SSM with the best selected parameters to predict ρ_c. This is due to the fact that reasonable values of κ^* for

consolidation analyses result in values of E_u that are much too low (i.e., as discussed in Section 3.4.4). In addition, the SSM cannot predict increasing horizontal displacements during consolidation after the EOC.

Table 3.1 Summary of Laboratory CRSC Tests on Virgin Ground at TS3-B1 (Free Field Condition)

Spec. Location TS3-B1 @GL=-1.5 ft			**Specimen Data**								**Compressibility Parameters**					**Preconsolidation Stress**		**Flow Properties** by HQN		
											CR		**RR**		**C_c max**	**σ'_p[ksf]**		k_{vo}	C_k	**c_v(NC)**
CRSC Test #	EL. [ft]	σ'_{vo} [ksf]	w_n [%]	γ_t [pcf]	e_0 [Gs=2.70]	S [%]	ω_p [%]	ω_L [%]	I_P	ε_v% @σ'_{vo}	URS	CCL/ HQN CRmax	URS	CCL/ HQN RRmax		URS	CCL/ HQN	[10^{-4} ft/day]		[ft^2/yr]
440	-6.5	0.59	74.9	97.3	2.025	99.8	41	105	64	0.8	0.261	0.255	0.027	0.036	0.772	3.28	3.35	1.1	0.664	17.0±3.4
441	-11.5	0.76	95.2	92.0	2.575	99.8				1.1	0.297	0.480	0.019	0.055	1.715	1.64	1.64	5.7	0.676	16.6
432	-16.5	0.91	88.4	93.2	2.41	100	34	87	53	1.3	0.329	0.373	0.029	0.071	1.27	1.62	1.64	6.2	0.587	30.9
431	-21.5	1.07	98.2	90.8	2.68	99				2.0	0.428	0.420	0.029	0.117	1.545	1.64	1.70	5.7	0.830	13.2
435	-26.5	1.22	87.4	94.0	2.36	100	35	93	58	1.5	0.435	0.440	0.029	0.065	1.48	2.15	2.18	2.8	0.838	18.7
443	-31.5	1.37	95.2	89.3	2.685	95.8				2.2	0.354	0.340	0.028	0.131	1.253	2.03	2.00	5.1	0.477	30.5 ± 7.5
444	-36.5	1.52	88.1	93.4	2.395	99.4	41	104	63	1.5	0.372	0.390	0.033	0.119	1.325	2.05	2.10	3.1	1.127	25.1

Notes:

URS from Appendix E table E-2-1A, 2A

NQH & CCL used plots from Germaine (2002)

All tests are run at a strain rate of 0.72 % per hour

σ'_{vo}[ksf] = 0.3436+0.0374(-EL.) for BM Crust

σ'_{vo}[ksf] = 0.4145+0.0303(-EL.) for Recent Bay Mud

Water Table Elevation = -4.5 ft

Table 3.2 Summary of Field Vane Shear Test Results at Virgin Ground Condition

URS= SHANSEP (Ladd&Foott, 1974): μ=0.80; S=0.25; m=0.85

$$OCR = \left(\frac{\mu S_u(FV)/\sigma'_{vo}}{S}\right)^{1/m}$$

Chandler(88) - Select S_{FV}=0.297 for I_p = 58.5%

$$OCR = \left(\frac{s_u(FV)/\sigma'_{vo}}{S_{FV}}\right)^{1.05}; S_{FV} = f(PI)$$

Vane Sounding No.	Test No.	MSL EL. [ft]	Soil	σ'_{vo} [ksf]	S_u(FV) [ksf]	S_u(FV)/ σ'_{vo}	OCR		σ'_p(FV) [ksf]		Ratio
							URS	Chandler(88)	URS	Chandler (88)	URS/ Chandler(88) x100%
TS3-V1 GSEL. -1.5 ft	1	-8.5	BM Crust	0.662	0.873	1.320	5.445	4.788	3.602	3.167	113.7
	2	-9.5	BM Crust	0.699	1.066	1.525	6.456	5.573	4.512	3.895	115.8
	3	-10.5	BM	0.733	0.776	1.059	4.204	3.800	3.080	2.784	110.6
	4	-11.5	BM	0.763	0.562	0.737	2.742	2.595	2.092	1.980	105.7
	5	-12.5	BM	0.793	0.524	0.661	2.412	2.315	1.914	1.836	104.2
	6	-13.5	BM	0.824	0.465	0.565	2.006	1.963	1.652	1.617	102.2
	7	-14.5	BM	0.854	0.485	0.568	2.020	1.976	1.725	1.687	102.2
	8	-16.5	BM	0.914	0.465	0.509	1.773	1.759	1.621	1.608	100.8
	9	-18.5	BM	0.975	0.504	0.517	1.808	1.789	1.762	1.745	101.0
	10	-20.5	BM	1.036	0.485	0.468	1.609	1.613	1.667	1.671	99.8
	11	-22.5	BM	1.096	0.572	0.522	1.828	1.807	2.004	1.981	101.1
	12	-24.5	BM	1.157	0.562	0.486	1.680	1.676	1.944	1.939	100.2
	13	-26.5	BM	1.217	0.543	0.446	1.520	1.533	1.850	1.866	99.2
	14	-28.5	BM	1.278	0.572	0.448	1.526	1.538	1.950	1.966	99.2
	15	-30.5	BM	1.339	0.640	0.478	1.649	1.649	2.207	2.207	100.0
	16	-32.5	BM	1.399	0.630	0.450	1.537	1.548	2.150	2.166	99.3
	17	-34.5	BM	1.460	0.640	0.438	1.489	1.505	2.174	2.197	98.9
	18	-36.5	BM	1.520	0.853	0.561	1.990	1.950	3.026	2.965	102.1
	19	-38.5	BM	1.581	0.679	0.429	1.454	1.473	2.298	2.329	98.7
	20	-40.5	BM	1.642	0.620	0.378	1.250	1.287	2.051	2.113	97.1
	21	-42.5	BM	1.702	0.814	0.478	1.649	1.649	2.808	2.807	100.0
	22	-45.5	Alluvium	1.793	>1.80						
TS5-V1 GSEL. -1.8 ft	1	-8.8	BM Crust	0.673	0.989	1.470	6.183	5.362	4.159	3.607	115.3
	2	-9.8	BM Crust	0.710	0.737	1.038	4.105	3.720	2.915	2.642	110.3
	3	-10.8	BM	0.742	0.717	0.967	3.775	3.453	2.800	2.561	109.3
	4	-11.8	BM	0.772	0.640	0.829	3.151	2.938	2.433	2.268	107.2
	5	-12.8	BM	0.802	0.485	0.604	2.173	2.109	1.744	1.692	103.0
	6	-13.8	BM	0.833	0.446	0.536	1.885	1.857	1.570	1.547	101.5
	7	-14.8	BM	0.863	0.436	0.505	1.760	1.747	1.519	1.508	100.7
	8	-16.8	BM	0.924	0.465	0.503	1.753	1.741	1.619	1.608	100.7
	9	-18.8	BM	0.984	0.485	0.493	1.709	1.702	1.682	1.675	100.4
	10	-20.8	BM	1.045	0.524	0.502	1.745	1.734	1.823	1.811	100.6
	11	-22.8	BM	1.105	0.562	0.508	1.773	1.759	1.960	1.944	100.8
	12	-24.8	BM	1.166	0.543	0.466	1.599	1.604	1.864	1.870	99.7
	13	-26.8	BM	1.227	0.562	0.458	1.569	1.577	1.924	1.934	99.5
	14	-28.8	BM	1.287	0.562	0.437	1.482	1.499	1.908	1.929	98.9
	15	-30.8	BM	1.348	0.679	0.504	1.754	1.742	2.364	2.347	100.7
	16	-32.8	BM	1.408	0.659	0.468	1.608	1.612	2.264	2.270	99.8
	17	-34.8	BM	1.469	0.650	0.442	1.506	1.520	2.212	2.233	99.1
	18	-36.8	BM	1.530	0.892	0.583	2.083	2.031	3.186	3.106	102.6
	19	-38.8	BM	1.590	0.950	0.597	2.143	2.083	3.408	3.312	102.9
	20	-40.8	Alluvium	1.651	1.692						

Table 3.3a Summary of Recompression Ratio Evaluation

Status	CRS#	El. [ft]	σ'_{vo} [ksf]	σ'_{p} [ksf]	Ave. σ'_{vc} [ksf]	σ'_{vc}/σ'_{p}	σ'_{p}/σ'_{vo} [OCR]	$\sigma'_{vc}/\sigma'_{vo}$	CR_{max}	RR	RR_{min}	Remarks
$\sigma'_{vc} \approx \sigma'_{p}$	431	-21.5	1.065	1.70	1.70	1.0	1.6	1.6	0.42	0.117	0.045	$\sigma'_{v0} \rightarrow \sigma'_{vc}$
	443	-31.5	1.370	2.00	1.93	0.97	1.46	1.41	0.34	0.131	0.084	
	444	-36.5	1.52	2.10	2.10	1.0	1.38	1.38	0.39	0.119	0.075	
$\sigma'_{vc} > \sigma'_{p}$ (Virgin Compression)	432	-16.5	0.915	1.64	1.73	1.05	1.79	1.9	0.373	0.071	0.045	For CR = 0.375
										0.108		For all Recomp.
	441	-11.5	0.763	1.64	1.8	1.10	2.15	2.36	0.48	0.055	0.037	For CR = 0.48
										0.098		For all Recomp.
$\sigma'_{vc} < \sigma'_{p}$ All Recompression	440	-6.5	0.58	3.35	1.70	0.51	5.8	2.93	0.255	0.036	0.020	
	435	-26.5	1.22	2.18	1.86	0.85	1.8	1.525	0.44	0.065	0.045	

Table 3.3b Selected RR for 1-D Analysis

Preconsolidation Profile	El.	RR Selected
For σ'_{p} & $0.9\sigma'_{p}$	From -6 to -20 ft	0.06
	From -20 to -41.5 ft	0.12
For $0.8\sigma'_{p}$	From -6 to -20 ft	0.04
	From -20 to -41.5 ft	0.08

Table 3.4 NC Coefficient of Consolidation of Bay Mud

Condition	Boring GSE.	EL. [ft]	ω_N [%]	ω_L [%]	I_p [%]	CRSC#	C_v(NC) [x10^{-4}cm^2/s]	C_v(NC) [ft^2/yr]
Free Field	TS3-B1	-11.5	91.1			441	4.9	16.6
		-16.5	88.2	87	53	432	9.1	30.9
	-1.5 ft	-21.5	96.0			431	3.9	13.2
		-26.5	86.7	93	58	435	5.5	18.7
		-31.5	100.5			443	9.0	30.6
		-36.5	86.6	104	63	444	7.4	25.1
Under Crest of NHPL Levee	TS3-B3							
	+6.9 ft	-13.1	79.3			451	4.1	13.9
		-26.1	89.7			450	3.9	13.2
		-34.1	127.1			442	4.2	14.3
	TS3-S3	-12.1	85.5			437	3.9	13.2
	+6.9 ft	-18.1	87.1	96	58	439	4.5	15.3
		-23.1	76.8			433	7.6	25.8
		-28.1	171.8			438	2.2	7.5
		-32.1	80.9	93	57	434	5.6	19.0
	TS5-B3	-13.1	77.9			445	4.2	14.3
	+6.9 ft	-33.1	107.2			449	4.7	16.0

Index & Boring Log data from Appendix A&E (URS, 2003)
C_v(NC) data from Germaine (2002)

Table 3.5a Summary of Undrained Strength Ratio of Bay Mud from DSS Tests at NHP, N1 and N2 Levees

DSS Test #	Location	ω_n [%]	El. [ft]	OCR	τ/σ'_{vc}
583	N2-B7(S5)	77.4		1	0.2653
584	N2-B7(S5)	78.0		1	0.242
585	N2-B7 (S9)	78.1		1	0.2532
586	N2-B7 (S9)	69.7		1	0.2448
587	N2-B7 (S13)	93.7		1	0.2654
588	TS5-B3 (S6)	86.0	-18.1	1	0.2533
589	TS5-B3(S8)	88.1	-28.1	1	0.2295
590	TS3-S3(S3)	95.4	-18.1	1	0.2383
591	TS3-S3(S5)	163.9	-28.1	1	0.3205
592	TS5-B3(S6)	90.6	-18.1	1	0.2306
593	TS5-B3(S6)	92.0	-18.1	1.96	0.4828
594	N2-B7 (S7)	76.7		1.96	0.4589
596	N2-B7(S13)	89.7		1.97	0.4546
601	TS3-S3(S3)	94.5	-18.1	1	0.2366
621	N1-B9(S6)	85.4		2.89	0.5999
622	N1-B4(S9)	86.0		2.94	0.5454

Table 3.5b Summary of Direct Simple Shear Results for NHPL BAY MUD

OCR	Types of Analysis	# of tests	Mean of max. τ/σ'_{vc}	SD
1	All DSS tests	11	0.2527	0.0171
	All Tests at TS3&TS5	6	0.2515	0.0236
	All tests at TS3&TS5 except DSS591	5	0.2377	0.0065
2	All tests	3	0.4654	0.0116
	Only at TS5 & TS3	1	0.4828	0.0000
3	All tests	2	0.5727	0.0273

Table 3.6 Summary of Triaxial Tests on Bay Mud from NHP Levee						
TX Test #	Mode	Location	El. [ft]	q/σ'vc	ε_a[%]	OCR
575	TC	TS5-B3(S6)	-18.1	0.3757	1.53	1
576	TE	TS5-B3(S6)	-18.1	-0.2908	-15	1
584	TC	TS5-B3(S6)	-18.1	0.3725	2.41	1
590	TC	TS3-S3(S6)	-18.1	0.3009	3.84	1
603	TE	TS3-B1(S4)	-21.1	-0.258	-14.5	1
Average of TC mode (n=3):				*0.3479 ± 0.0325*	*2.59±0.831*	
Average of TE mode (n=2)				*0.2744 ± 0.0164*	*14.75 ± 0.25*	

Table 3.7a Selected Values of Parameters for Computing σ'_{vf} Using PLAXIS - **CASE A**: Stiff and Uncracked, Continuous Pavement and Stiff Crust
[Properties other than Bay Mud = Table 4.1 URS/ARUP Test Fill (2005)]

Layer No.	**Material**	**El.[ft]**	**Model**	**γ_t[pcf]**	**ϕ' [deg]**	**c or s_u [ksf]**	**Eu[ksf]**	**ν**	**k_h [ft/day]**	**k_v [ft/day]**
1	Levee Fill	From 9.4 to -1.6	MC	130.0	37	0.300	300	0.3	0.1	0.1
2	Pavement	From -1.6 to -4.5	MC	150.0	35	4.960	2000	0.15	1	1
3	Base Course	From -4.5 to -6.2	MC	145.0	45	0.025	1500	0.2	1	1
4	BM Crust	From -6.2 to -10	MC	99.8	0	0.800	300	0.29	6.E-04	4.E-04
5	BM1	From -10 to -15	MC	92.7	0	0.392	78.3	0.26	6.E-04	4.E-04
6	BM2	From -15 to -20	MC	92.7	0	0.366	73.1	0.26	6.E-04	4.E-04
7	BM3	From -20 to -25	MC	92.7	0	0.406	81.2	0.26	6.E-04	4.E-04
8	BM4	From -25 to -30	MC	92.7	0	0.450	90.0	0.26	6.E-04	4.E-04
9	BM5	From -30 to -35	MC	92.7	0	0.491	98.1	0.26	6.E-04	4.E-04
10	BM6	From -35 t0 -40	MC	92.7	0	0.533	106.5	0.26	6.E-04	4.E-04
11	BM7	From -40 to -41.5	MC	92.7	0	0.559	111.8	0.26	6.E-04	4.E-04
12	Below BM	From -41.5 below	Linear Elastic	120.0			3000	0.3		

Note: The Author replaced the lower portion of the pavement used by URS/ARUP (2005) with a granular base course (Layer 3)

Table 3.7b Properties of Soils Used in σ'_{vf} Analyses for **CASE B**: Stiff Cracked Pavement and Stiff Crust

[Properties other than Bay Mud = Table 4.1 – URS/ARUP Test Fill (2005)]

Layer No.	**Material**	**El.[ft]**	**Model**	**γ_t[pcf]**	**ϕ' [deg]**	**c or s_u [ksf]**	**Eu[ksf]**	**ν**	**k_h [ft/day]**	**k_v [ft/day]**
1	Levee Fill	From 9.4 to -1.6	MC	Values are the same as Table 3.7a					0.1	0.1
2	Cracked Pavement	From -1.6 to -4.5	MC	150.0	35	**0.025**	**1500**	**0.2**	1	1
3	Base Course	From -4.5 to -6.2	MC	Values are the same as Table 3.7a					1	1
4	BM Crust	From -6.2 to -10	MC						8.E-04	4.E-04
5	BM1	From -10 to -15	MC						8.E-04	4.E-04
6	BM2	From -15 to -20	MC						8.E-04	4.E-04
7	BM3	From -20 to -25	MC						8.E-04	4.E-04
8	BM4	From -25 to -30	MC						8.E-04	4.E-04
9	BM5	From -30 to -35	MC						8.E-04	4.E-04
10	BM6	From -35 t0 -40	MC						8.E-04	4.E-04
11	BM7	From -40 to -41.5	MC						8.E-04	4.E-04
12	Below BM	From -41.5 below	Linear Elastic							

Note: The Author replaced the lower portion of the pavement used by URS/ARUP (2005) with a granular base course (Layer 3)

Table 3.7c Properties of Soils Used in σ'_{vf} Analyses for **CASE C**: Weaker Cracked Pavement and Crust

[Properties other than BM and BM Crust = Table 6, URS (2003)]

Layer No.	**Material**	**El.[ft]**	**Model**	**γ_t[pcf]**	**ϕ' [deg]**	**c or s_u [ksf]**	**Eu[ksf]**	**ν**	**k_h [ft/day]**	**k_v [ft/day]**
1	Levee Fill	From 9.4 to -1.6	MC	130.0	37.0	**0.020**	**30.0**	**0.3**	0.1	0.1
2	Cracked Pavement	From -1.6 to -4.5	MC	150.0	35	**0.025**	**200**	**0.2**	1	1
3	Base Course	From -4.5 to -6.2	MC	Values are the same as Table 3.7a					1	1
4	BM Crust	From -6.2 to -10	MC	100.0	0.0	**0.580**	**116.0**	**0.3**	8.E-04	4.E-04
5	BM1	From -10 to -15	MC	Values are the same as Table 3.7a					8.E-04	4.E-04
6	BM2	From -15 to -20	MC						8.E-04	4.E-04
7	BM3	From -20 to -25	MC						8.E-04	4.E-04
8	BM4	From -25 to -30	MC						8.E-04	4.E-04
9	BM5	From -30 to -35	MC						8.E-04	4.E-04
10	BM6	From -35 t0 -40	MC						8.E-04	4.E-04
11	BM7	From -40 to -41.5	MC						8.E-04	4.E-04
12	Below BM	From -41.5 below	Linear Elastic							

Note: The Author replaced the lower portion of the pavement used by URS (2003) with a granular base course (Layer 3)

Table 3.7d Selected Undrained Shear Strength and Young's Modulus for Bay Mud for σ'_{vf} Calculation

Layer No.	Name	Thickness (ft)	Mid El. (ft)	σ'_{v0} (ksf)	σ'_{p}(ksf)	OCR	S_u[ksf]	E_u[ksf]
1	BM1	From -10 to -15	-12.5	0.797	1.765	2.215	0.392	78.3
2	BM2	From -15 to -20	-17.5	0.950	1.579	1.662	0.366	73.2
3	BM3	From -20 to -25	-22.5	1.103	1.740	1.578	0.406	81.2
4	BM4	From -25 to -30	-27.5	1.256	1.919	1.528	0.450	90.0
5	BM5	From -30 to -35	-32.5	1.409	2.081	1.477	0.491	98.1
6	BM6	From -35 to -40	-37.5	1.562	2.251	1.441	0.533	106.5
7	BM7	From -40 to -41.5	-40.75	1.661	2.357	1.419	0.559	111.8
8	BM Crust	From -6.2 to -10	-8.1	0.640	3.20	5.00	0.580	116.0

Notes: - Estimate undrained shear strength (s_u) using SHANSEP method (Ladd and Foott, 1974)

- SHANSEP Equation: $\frac{s_u}{\sigma'_{vo}} = S\left(OCR\right)^m$, with S = 0.25 and m =0.85
- Estimated undrained Young's Modulus $E_u = 200 s_u$

Table 3.8a Measured Excess Pore Pressure Data at TS3

Units: psi x 144 = psf/62.4 = ft ; psi x 2.308 = h (ft)

Test Section and Piezometer Location				Piezometer Readings		Excess Pore Pressure Calculation				
TS3	**Soil**	**Piezo. #**	**EL.Tip (ft)**	**Date**	**(psi)**	**h_p (ft)**	**h_t (ft)**	**Selected h_s (ft)**	**$h_{ex} = h_t - h_s$ (ft)**	**u_e (ksf)**
Under Levee Crest (Line 3)	BM Crust	SP3-1	-10.1	3/12/02	2.62	6.05	-4.05	-4.04	0.00	0.000
	BM	3-1	-10.1	2/28/02	2.63	6.07	-4.03	-4.04	0.01	0.001
		3-2	-17.1	3/12/02	7.21	16.64	-0.46	-4.16	3.70	0.231
		3-3	-24.1	3/12/02	11.61	26.79	2.69	-4.30	6.99	0.436
		3-4	-31.1	3/12/02	14.68	33.88	2.78	-4.40	7.18	0.448
		3-5	-38.1	3/12/02	15.995	36.91	-1.19	-4.53	3.34	0.209
	Alluvium	3-6	-45.1	3/12/02	17.535	40.47	-4.63	-4.65	0.00	0.000
Under Levee Toe (Line 2)	BM	2-1	-10.8	2/1/02	3.25	7.50	-3.30	-4.04	0.74	0.046
		2-2	-17.8	2/1/02	6.54	15.09	-2.71	-4.16	1.45	0.091
		2-3	-24.8	2/1/02	9.58	22.11	-2.69	-4.30	1.61	0.100
		2-4	-32.8	2/1/02	13.03	30.07	-2.73	-4.40	1.67	0.104
		2-5	-39.8	2/1/02	15.53	35.84	-3.96	-4.53	0.57	0.035
	Alluvium	2-6	-47.8	2/1/02	18.68	43.11	-4.69	-4.70	0.01	0.000

Note: h_s based on assumed linear variation in the minimum h_t measured near the top and bottom of the Bay Mud for line 3.

Table 3.8b Measured Excess Pore Pressure Data at TS5

Units: psi x 144 = psf/62.4 = ft ; psi x 2.308 = h (ft)

Test Section and Piezometer Location				Piezometer Readings		Excess Pore Pressure Calculation				
TS5	**Soil**	**Piezo. #**	**EL.Tip (ft)**	**Date**	**(psi)**	**h_p (ft)**	**h_t (ft)**	**Selected h_s (ft)**	**$h_{ex} = h_t - h_s$ (ft)**	**u_e (ksf)**
Under Levee Crest (Line 3)	BM	SP3-1	-11.1	3/12-27/02	2.92	6.74	-4.36	-4.35	0.00	0.000
		3-1	-11.6	3/10-20/02	4.535	10.47	-1.13	-4.35	3.22	0.201
		3-2	-17.6	3/10-20/02	6.955	16.05	-1.55	-4.30	2.75	0.172
		3-3	-24.1	3/10-20/02	11.17	25.78	1.68	-4.25	5.93	0.370
		3-4	-30.6	3/10-20/02	13.48	31.11	0.51	-4.20	4.71	0.294
		3-5	-36.6	3/10-20/02	15.56	35.91	-0.69	-4.15	3.46	0.216
	Alluvium	3-6	-43.1	3/10/02	16.9	39.00	-4.10	-4.00		0.000
Under Levee Toe (Line 2)										
	Crust	2-1	-9.8	1/25/02	2.08	4.80	-5.00	-5.00	0.00	0.000
	BM	2-2	-17.8	1/25/02	6.31	14.56	-3.24	-4.90	1.66	0.104
		2-3	-26.3	1/25/02	10.7	24.69	-1.61	-4.85	3.24	0.202
		2-4	-34.3	1/25/02	13.9	32.08	-2.22	-4.80	2.58	0.161
		2-5	-41.8	1/25/02	16.09	37.13	-4.67	-4.70	0.03	0.002
	Alluvium									

Note: h_s based on assumed linear variation in the minimum h_t measured near the top and bottom of the Bay Mud for line 3.

Table 3.9a Summary Results of 1-D Consolidation Settlement Calculations [SH1, SH2, and URS (2003)]

Computed with Preconsolidation Stress Profiles	Computed 1-D Consolidation Settlements at 1/31/02, ρ_c (ft)						Measured Settlements at 1/31/02, ρ_m, (ft)	
	(a) Stress History 1 (SH1) Case A &B, Fig. 3.12b		(b) Stress History 2 (SH2) Case C, Fig. 3.12c		(c) URS (2003)			
	TS3	TS5	TS3	TS5	TS3	TS5	TS3	TS5
σ'_p	0.761	0.81	1.043	1.141	0.61	0.58		
$0.9\sigma'_p$	0.963	1.186	1.42	1.548	1.06	0.99		
$0.8\sigma'_p$	1.229	1.501	1.713	1.865	1.65	1.5	**1.65**	**1.57**

Table 3.9b Comparison of Computed 1- D Consolidation Settlements (Computed with SH2) and Measured Settlements

Preconsolidation Stress Profile	ρ_c at 1/31/02 (ft)		% of Measured ρ_m		ρ_{cf} (ft)	Degree of Consolidation,U%	
	TS3	TS5	TS3	TS5	TS3=TS5	TS3	TS5
σ'_p	1.043	1.141	63	73	1.761	59	65
$0.9\sigma'_p$	1.42	1.548	86	99	2.169	65	71
$0.8\sigma'_p$	1.713	1.865	104	119	2.633	65	71
Measured (1/31/02)	**1.65**	**1.57**					

Table 3.10 Parameters for Simulations of Consolidation and Undrained Shear - Bay Mud

			1-D Consolidation		CK_0U PSC/E							CK_0U DSS	
Case			Case 1	Case 2	1	2	3	4	5	6	7	1	2
Name			BM1=URS	BM2=Nguyen									
Type			Undrained	Undrained	Undrained							Undrained	
SSM Property Name	**Symbol**	**Unit**											
Unit weight	γ_t	[klb/ft^3]	0.092	0.0927	0.0927							0.0927	
Horizontal hydraulic conductivity	k_x	[ft/day]	0.0008	0.0012	0.0012							0.0012	
Vertical hydraulic con.	k_y	[ft/day]	0.0004	0.0009	0.0009							0.0009	
Change of hydraulic con.	C_k	[-]	1.143	1.40	1.40							1.40	
Initial void ratio	e_0	[-]	1.00	2.50	2.50							2.50	
Modified compression index	λ^*	[-]	0.18 (CR=0.41)	0.174 (CR =0.40)	0.174 (CR =0.40)							0.174 (CR =0.40)	
Modified swelling index	κ^*	[-]	0.035 (RR=0.04)	0.104 (RR = 0.12)	0.104 (RR = 0.12)							0.104	0.002
Poisson's ratio for unloading/reloading	ν_{ur}	[-]	0.26	0.26	0.26							0.26	
Lateral stress ratio for NC BM	K_{0nc}	[-]	0.62	0.62	0.62			0.47				0.47	
Friction angle	φ'	[°]	30	30	20	30	46	20	25	30	46	25	
K_{0nc} - parameter	M	[-]	1.27	1.20	1.20			1.55				1.55	
Cohesion	c'	[klb/ft^2]	0.025	0.025	0.025							0.025	
Dilatancy angle	ψ'	[°]	0.001	0.0001	0.0001							0.0001	
Overconsolidation ratio	OCR	[-]	1.5	1.5	1, 1.5, 2, 3, and 5							1, 1.5, 2, and 4	

Table 3.11 Calculation Scheme for 1-D Consolidation Simulation of Incremental Oedometer Test

Phase ID	Cal. type	Loading input [ksf]	Time increment [day]	End time [day]	Notes
0	Initial Cal.	0.0	0	0	Initial phase, OCR = 1.5, K_{0OC}
1	Plastic	1.5	0	0	Loading to virgin compression
2	Consolidation	1.5	1	1	Check $u_e = 0$ at end of consolidation
3	Plastic	1.0	0	1	Unloading to 1.0 ksf (OCR =1.5)
4	Consolidation	1.0	1	2	Check $u_e = 0$ at end of consolidation
5	Plastic	2.5	0	2	Loading to virgin compression
6	Consolidation	2.5	2	4	Check $u_e = 0$ at end of consolidation

Table 3.12 Summary Results of PSC Simulations

(Sheet 1 of 2)

Case 1: With K_{0NC}=0.62 and Friction Angle = 20^0 (Line 1a)

OCR	K_0	σ'_p [ksf]	σ'_{vc} [ksf]	σ'_{hc} [ksf]	s_u [ksf]	s_u/σ'_p	$\mathbf{s_u/\sigma'_{vc}}$
1	**0.62**	1.5	1.50	0.93	0.428	0.28533	**0.285**
1.5	0.73	1.5	1.00	0.73	0.321	0.214	**0.321**
2	0.8181	1.5	0.75	0.61	0.258	0.172	**0.344**
3	0.9621	1.5	0.50	0.48	0.193	0.129	**0.386**
5	1.1803	1.5	0.30	0.35	0.138	0.092	**0.460**

Case 2: With K_{0NC}=0.62 and Friction Angle = 30^0 (Line 2a)

OCR	K_0	σ'_p [ksf]	σ'_{vc} [ksf]	σ'_{hc} [ksf]	s_u [ksf]	s_u/σ'_p	$\mathbf{s_u/\sigma'_{vc}}$
1	**0.62**	1.5	1.50	0.93	0.538	0.35867	**0.3587**
1.5	0.73	1.5	1.00	0.73	0.444	0.296	**0.444**
2	0.8181	1.5	0.75	0.61	0.396	0.264	**0.528**
3	0.9621	1.5	0.50	0.48	0.269	0.179	**0.538**
5	1.1803	1.5	0.30	0.35	0.186	0.124	**0.620**

Case 3: With K_{0NC}=0.62 and Friction Angle = 46^0 (Line 3a)

OCR	K_0	σ'_p [ksf]	σ'_{vc} [ksf]	σ'_{hc} [ksf]	s_u [ksf]	s_u/σ'_p	$\mathbf{s_u/\sigma'_{vc}}$
1	**0.62**	1.5	1.50	0.93	0.829	0.55267	**0.553**
1.5	0.73	1.5	1.00	0.73	0.614	0.40933	**0.614**
2	0.8181	1.5	0.75	0.61	0.515	0.34333	**0.687**
3	0.9621	1.5	0.50	0.48	0.375	0.250	**0.75**
5	1.1803	1.5	0.30	0.35	0.257	0.17133	**0.857**

Case 4: With K_{0NC}=0.47 and Friction Angle = 20^0 (Line 1b)

OCR	K_0	σ'_p [ksf]	σ'_{vc} [ksf]	σ'_{hc} [ksf]	s_u [ksf]	s_u/σ'_p	$\mathbf{s_u/\sigma'_{vc}}$
1	**0.47**	1.5	1.50	0.71	0.4	0.266667	**0.267**
1.5	0.552757	1.5	1.00	0.55	0.289	0.192667	**0.289**
2	0.620169	1.5	0.75	0.47	0.232	0.154667	**0.309**
3	0.729367	1.5	0.50	0.36	0.172	0.115	**0.344**
5	0.894717	1.5	0.30	0.27	0.123	0.082	**0.410**

Case 6: With K_{0NC}=0.47 and Friction Angle = 30^0 (Line 2b)

OCR	K_0	σ'_p [ksf]	σ'_{vc} [ksf]	σ'_{hc} [ksf]	s_u [ksf]	s_u/σ'_p	$\mathbf{s_u/\sigma'_{vc}}$
1	**0.47**	1.5	1.50	0.71	0.564	0.376	**0.376**
1.5	0.552757	1.5	1.00	0.55	0.412	0.275	**0.412**
2	0.620169	1.5	0.75	0.47	0.327	0.218	**0.436**
3	0.729367	1.5	0.50	0.36	0.239	0.159	**0.478**
5	0.894717	1.5	0.30	0.27	0.164	0.109	**0.547**

Case 7: With K_{0NC}=0.47 and Friction Angle = 46^0 (Line 3b)

OCR	K_0	σ'_p [ksf]	σ'_{vc} [ksf]	σ'_{hc} [ksf]	s_u [ksf]	s_u/σ'_p	$\mathbf{s_u/\sigma'_{vc}}$
1	**0.47**	1.5	1.50	0.71	0.741	0.494	**0.494**
1.5	0.552757	1.5	1.00	0.55	0.617	0.411	**0.617**
2	0.620169	1.5	0.75	0.47	0.458	0.305	**0.611**
3	0.729367	1.5	0.50	0.36	0.331	0.221	**0.662**
5	0.894717	1.5	0.30	0.27	0.222	0.148	**0.740**

Case 5: With K_{0NC}=0.47 and Friction Angle = 25^0 (Best Selected Line)

OCR	K_0	σ'_p [ksf]	σ'_{vc} [ksf]	σ'_{hc} [ksf]	s_u [ksf]	s_u/σ'_p	$\mathbf{s_u/\sigma'_{vc}}$
1	**0.47**	1.5	1.50	0.71	0.498	0.332	**0.332**
1.5	0.552757	1.5	1.00	0.55	0.352	0.235	**0.352**
2	0.620169	1.5	0.75	0.47	0.28	0.187	**0.373**
3	0.729367	1.5	0.50	0.36	0.206	0.137	**0.412**
5	0.894717	1.5	0.30	0.27	0.146	0.097	**0.487**

Table 3.13 Summary Results of DSS Simulations

Case 1 with measured κ* = 0.104								
OCR	K_0	σ'_p [ksf]	σ'_{vc} [ksf]	σ'_{hc} [ksf]	s_u [ksf]	s_u/σ'_p	$\mathbf{s_u/\sigma'_{vc}}$	$\mathbf{E_u/\sigma'_{vc}}$
1	**0.47**	1.5	1.500	0.705	0.486	0.324	**0.324**	**11**
1.5	0.5528	1.5	1.000	0.553	0.350	0.233	**0.35**	**16.1**
2	0.6202	1.5	0.750	0.465	0.279	0.186	**0.372**	**21.7**
4	0.8183	1.5	0.375	0.268	0.160	0.107	**0.427**	**42.8**

Case 2 with reduced κ* = 0.002								
OCR	K_0	σ'_p [ksf]	σ'_{vc} [ksf]	σ'_{hc} [ksf]	s_u [ksf]	s_u/σ'_p	$\mathbf{s_u/\sigma'_{vc}}$	$\mathbf{E_u/\sigma'_{vc}}$
1	**0.47**	1.5	1.500	0.705	0.458	0.305	**0.305**	**557.1**
1.5	0.5528	1.5	1.000	0.553	0.351	0.234	**0.351**	**835.7**
2	0.6202	1.5	0.750	0.465	0.279	0.186	**0.372**	**1114.2**
4	0.8183	1.5	0.375	0.268	0.158	0.105	**0.421**	**2228.5**

Table 3.14 Definition of Cases for NHPL FE Analyses

Case	Pavement	BAY MUD*				Alluvium k_{vo} (ft/day)	Effect of
		σ'_p	s_u (DSS) @ OCR =1.5	c_v(NC) (ft^2/day)	k_{vo}, k_{h0} (ft/day) and C_k		
A1	URS (2003) uncracked pavement	σ'_p(FV)	K_{onc}= 0.47, $\phi'=25^0$	0.06	9E-4, 12E-4, C_k = 1.40	0.001	Pavement
A2	Cracked Pavement (below and extended at toes of NHPL)	,,	,,	0.06	,,	,,	Cracked Pavement
B	,,	,,	,,	0.06	,,	1	u_e = 0 below BM
C1	,,	,,	,,	0.04	4E-4, 8E-4, C_k = 1.143	0.001	c_v(NC)
C2	,,	,,	,,	0.045	6E-4, 9E-4; C_k = 1.40	,,	,,
C3	,,	,,	,,	0.05	7E-4, 10.5E-4; C_k = 1.40	,,	,,
D1	,,	0.9σ'_p	,,	0.06	9E-4, 12E-4, C_k = 1.40	,,	σ'_p
D2	,,	0.8σ'_p	,,	0.06	9E-4, 12E-4, C_k = 1.40	,,	σ'_p and c_v(NC)
D3	,,	0.8σ'_p	,,	0.04	4E-4, 8E-4, C_k = 1.143	,,	σ'_p and c_v(NC)
D4	,,	0.8σ'_p	,,	0.04	4E-4, 8E-4, C_k = 1.143	0.005	σ'_p, c_v(NC), k_{v0} of Alluvium and Crust

Notes *

Nguyen's Selected CR = 0.40 for BM Crust and Bay Mud		
Nguyen's Selected RR	σ'_p	0.9σ'_p & 0.8σ'_p
From EL. -6.2 to -20	0.06	0.04
From EL. -20 to -41.5	0.12	0.08

Table 3.15 Soil and Pavement Properties Used in NHPL FE Analyses

SUBSOIL LAYER	NHPL Analysis Case	No.		1	2	3	4	5	6	7	8
		From EL.	[ft]	9.4	-1.6	-1.6	-4.5	-6.2	-10	-20	-41.5
		To EL.	[ft]	-1.6	-4.5	-4.5	-6.2	-10	-20	-41.5	-60
		Soil layer	-	**Levee Fill**	**Pavement**	**Cracked Pavement**	**Base Course**	**Bay Mud Crust**	**Bay Mud 1**	**Bay Mud 2**	**Alluvium**
		Soil Model	-	MC	MC	MC	MC	SSM	SSM	SSM	Linear Elastic
		Type		Drained	Drained	Drained	Drained	Undrained	Undrained	Undrained	Undrained
Constant parameters	All Cases	γ_t	[pcf]	130	150	150	145	99.8	92.7	92.7	130
		e_0	[-]	-	-	-	-	2.5	2.5	2.5	-
		ν_{ur}	[-]	0.3	0.15	0.2	0.2	0.26	0.26	0.26	0.3
		E_ref	[ksf]	30	1000	200	200	-	-	-	1000
		c'	[ksf]	0.02	0.02	0.025	0.025	0.025	0.025	0.025	-
		ϕ'	[°]	37	35	35	35	25	25	25	-
		ψ'	[°]	0	5	2	2	0	0	0	-
		K_{0NC}	[-]	0.5	0.5	0.5	0.5	0.47	0.47	0.47	0.7
		M	[-]	-	-	-	-	1.693	1.693	1.55	-
		λ*	[-]	-	-	-	-	0.174 (CR=0.40)	0.174 (CR=0.40)	0.174 (CR=0.40)	-
Varied parameters	D1, D2, D3, and D4	**κ***	[-]	-	-	-	-	0.035 (RR=0.04)	0.035 (RR=0.04)	0.07 (RR=0.08)	-
	Other Cases			-	-	-	-	0.052 (RR=0.06)	0.052 (RR=0.06)	0.104 (RR=0.12)	-
	A1, A2, D1, D2	k_{vo}, k_{ho}	[ft/day]	0.1	1.0	1.0	1.0	9E-4; 12E-4	9E-4; 12E-4	9E-4; 12E-4	0.001
	B			,,	,,	,,	,,	9E-4; 12E-4	9E-4; 12E-4	9E-4; 12E-4	1.0
	C1			,,	,,	,,	,,	4E-4; 8E-4	4E-4; 8E-4	4E-4; 8E-4	0.001
	C2			,,	,,	,,	,,	6E-4; 9E-4	6E-4; 9E-4	6E-4; 9E-4	,,
	C3			,,	,,	,,	,,	7E-4; 10.5E-4	7E-4; 10.5E-4	7E-4; 10.5E-4	,,
	D3			,,	,,	,,	,,	4E-4; 8E-4	4E-4; 8E-4	4E-4; 8E-4	,,
	D4			,,	,,	,,	,,	0.005	4E-4; 8E-4	4E-4; 8E-4	0.005
	Other Cases	C_k	[-]	,,	,,	,,	,,	1.40	1.40	1.40	-
	C1, D3, D4							1.143	1.143	1.143	-

Table 3.16 Imposed Initial OCR and K_0 in the Subsoil Layers for Plaxis Analyses of the NHP Levee

Sub-layer						Case A, B &C (σ'_p)		Case D1 ($0.9\sigma'_p$)		Case D2 ($0.8\sigma'_p$)	
Soil	**From EL. [ft]**	**To EL. [ft]**	**Average EL. [ft]**	**σ'_{v0} [ksf]**	**σ'_p [ksf]**	**OCR**	**K_0**	**OCR**	**K_0**	**OCR**	**K_0**
Bay Mud Crust	-6.2	-10	-8.1	0.647	3.300	5.104	0.826	4.594	0.801	4.083	0.769
BAY MUD	-10	-12	-11	0.748	2.224	2.974	0.694	2.677	0.663	2.379	0.637
	-12	-15	-13.5	0.824	1.623	1.971	0.596	1.774	0.574	1.577	0.551
	-15	-20	-17.5	0.945	1.584	1.676	0.561	1.509	0.543	1.341	0.521
	-20	-25	-22.5	1.096	1.752	1.598	0.551	1.438	0.534	1.278	0.512
	-25	-30	-27.5	1.248	1.920	1.539	0.545	1.385	0.527	1.231	0.505
	-30	-35	-32.5	1.399	2.088	1.492	0.539	1.343	0.521	1.194	0.500
	-35	-40	-37.5	1.551	2.256	1.455	0.534	1.309	0.516	1.164	0.496
	-40	-41.5	-40.75	1.649	2.365	1.434	0.531	1.291	0.514	1.147	0.493

Notes:

+ Estimate K_0 using method from Ladd et al. (1977) Tokyo SOA report: $K_{0OC} = K_{0NC}(OCR)^m$ selecting m = 0.35 (I_p = 50%) and K_{0NC} = 0.47;

+ WT. elevation = -4.5 ft

Table 3.17 Calculation phases in PLAXIS

Phase ID	Cal. type	Loading input	Layer thickness [ft]	∑H Levee [ft]	Time increment [day]	End time [day]	Construction Time	Remarks
1	Plastic	Layer 1	2	2	0	0		Start of Construction 4/11/96
2	Consolidation	Layer 1		2	45	45		
3	Plastic	+Layer 2	2	4	0	45	CD45	
4	Consolidation	+Layer 2		4	45	90		
5	Plastic	+Layer 3	2	6	0	90	CD90	
6	Consolidation	+Layer 3		6	30	120		
7	Plastic	+Layer 4	2	8	0	120	CD120	
8	Consolidation	+Layer 4		8	30	150		
9	Plastic	+Layer 5	2	10	0	150	CD150	
10	Consolidation	+Layer 5		10	30	180		
11	Plastic	+Layer 6	1	11	0	180	CD180	End of Construction (EOC)
12	Consolidation	Full Levee		11	1935	2115	CD2115	$t = t_c$ = 1/31/02

Table 3.18 Summary of Results of All Plaxis Analyses of the NHP Levee

(3.18a)

NHPL Case Prediction					ρ_c/ρ_mx100%		Maximum u_e (predicted)/u_e (measured) x100%		ρ_c(HQN)/ρ_c(URS)* x100%	Maximum u_e (HQN)/u_e (URS) x100%
Case	c_v(NC) (ft^2/day)	σ'_p Factor	ρ_c @CD2115 (ft)	Max. u_e (ksf)	TS3	TS5	TS3	TS5		
A1	0.06	1	1.477	0.23	89.5	94.1	47.9	63.9		
A2	0.06	1	1.46	0.2265	88.5	93.0	47.2	62.9		
B	0.06	1	1.49	0.104	90.3	94.9	21.7	28.9		
C1	0.04	1	1.252	0.458	75.9	79.7	95.4	127.2		
C2	0.045	1	1.271	0.331	77.0	81.0	69.0	91.9		
C3	0.05	1	1.336	0.291	81.0	85.1	60.6	80.8		
D1	0.06	0.9	1.53	0.2	92.7	97.5	41.7	55.6		
D2	0.06	0.8	1.89	0.263	114.5	120.4	54.8	73.1	119.4	66.4
D3	0.04	0.8	1.494	0.477	90.5	95.2	99.4	132.5	94.4 **	120.5
D4	0.04	0.8	1.70	0.373	103.0	108.3	77.7	103.6	107.4	94.2

* URS(2003) Plaxis ρ_c = 1.58 ft for Feb., 2002 and max. u_e = 0.396 ksf

** URS used free draining below BM (u_e =0), thus having higher rate of consolidation compared to Case D3

(3.18b)

Results	Construction Day	Analysis Cases										Measured	
		A1	A2	B	C1	C2	C3	D1	D2	D3	D4	TS3	TS5
ρ_t (ft)	CD180	2.367	2.30	2.529	2.508	2.678	2.709	1.806	1.843	1.84	1.936	1.0 to 1.5 *	
ρ_t (ft)	CD2115	3.844	3.76	4.019	3.76	3.949	4.045	3.336	3.733	3.334	3.636		
ρ_c (ft)	**CD(2115 - 180)**	**1.477**	**1.46**	**1.49**	**1.252**	**1.271**	**1.336**	**1.53**	**1.89**	**1.494**	**1.70**	**1.65**	**1.57**
h_{max} (ft) at toe	CD(180; 2115)**	1.09	1.15	1.09	1.09	1.17	1.15	0.79	0.87	0.87	0.86		
u_e max (ksf)	CD2115	0.23	0.2265	0.104	0.458	0.331	0.291	0.2	0.263	0.477	0.373	0.48	0.36

Note: ρ_t and ρ_c for point A at EL. - 3.0 ft

* Based on change in elevation of pavement surface (See Section 2.3)

** Case D2 hmax at CD2115

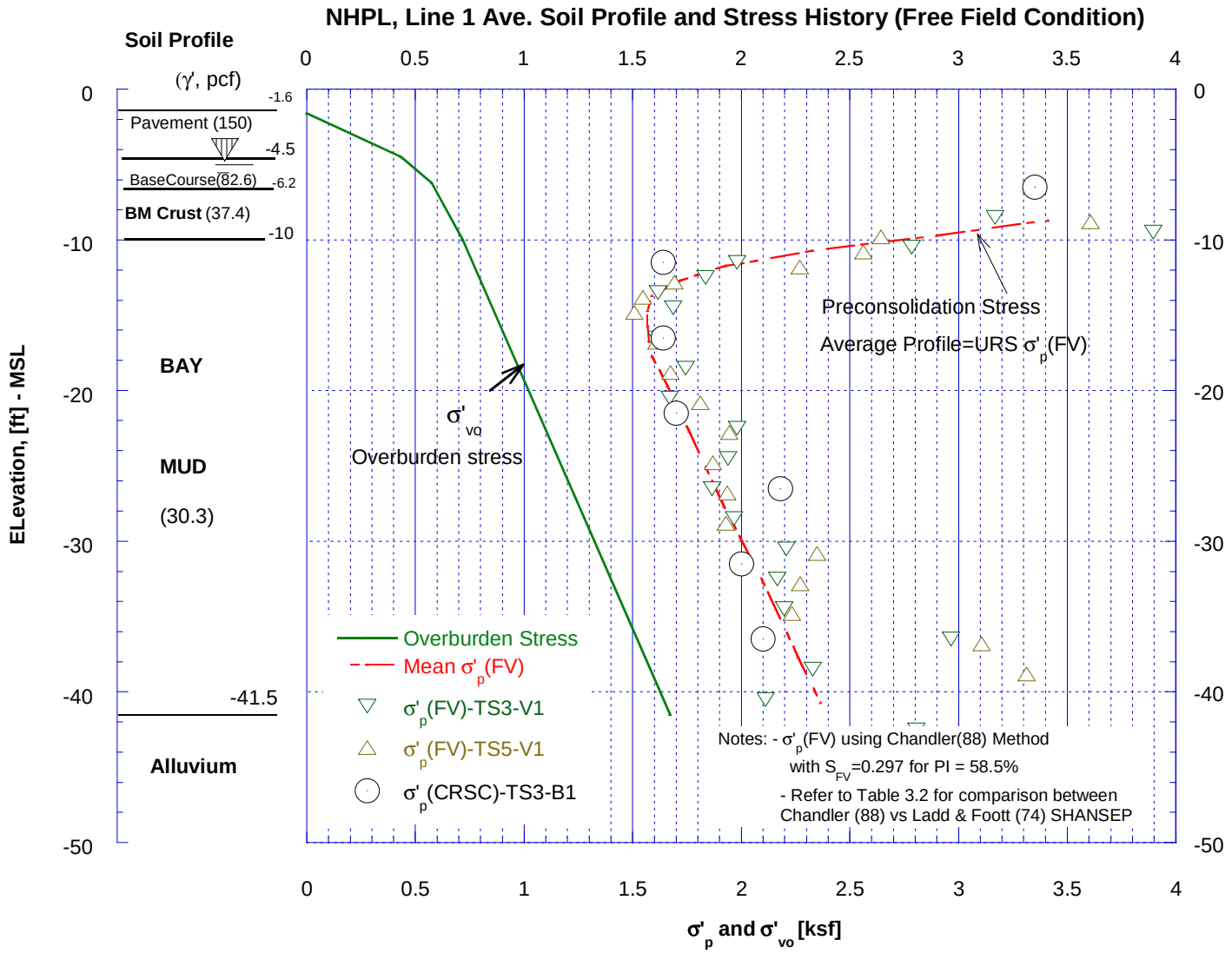

Figure 3.1 NHPL, Line 1 Average Soil Profile and Stress History – Free Field Conditions

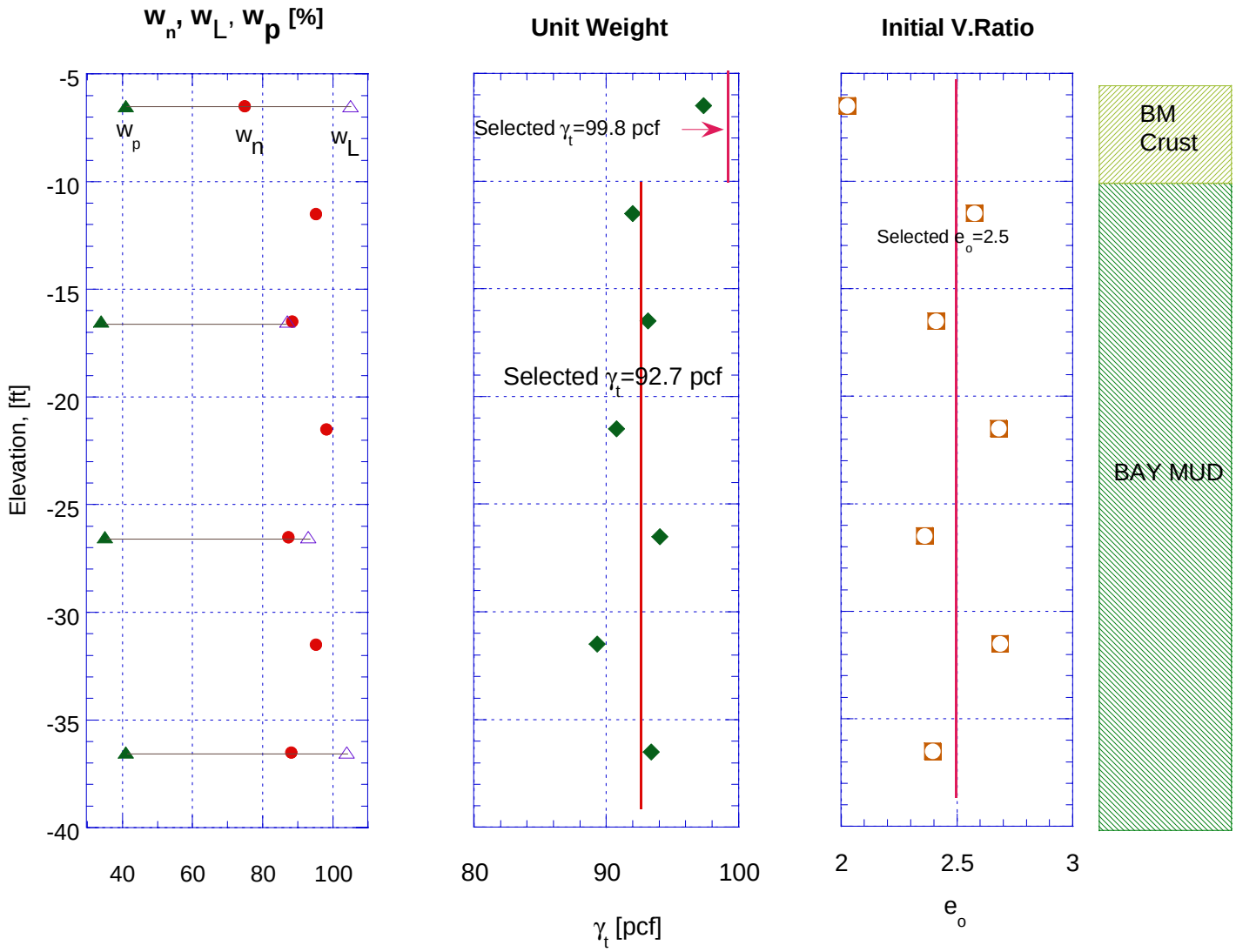

Figure 3.2 Index Properties of Bay Mud at Free Field Condition, TS3-B1

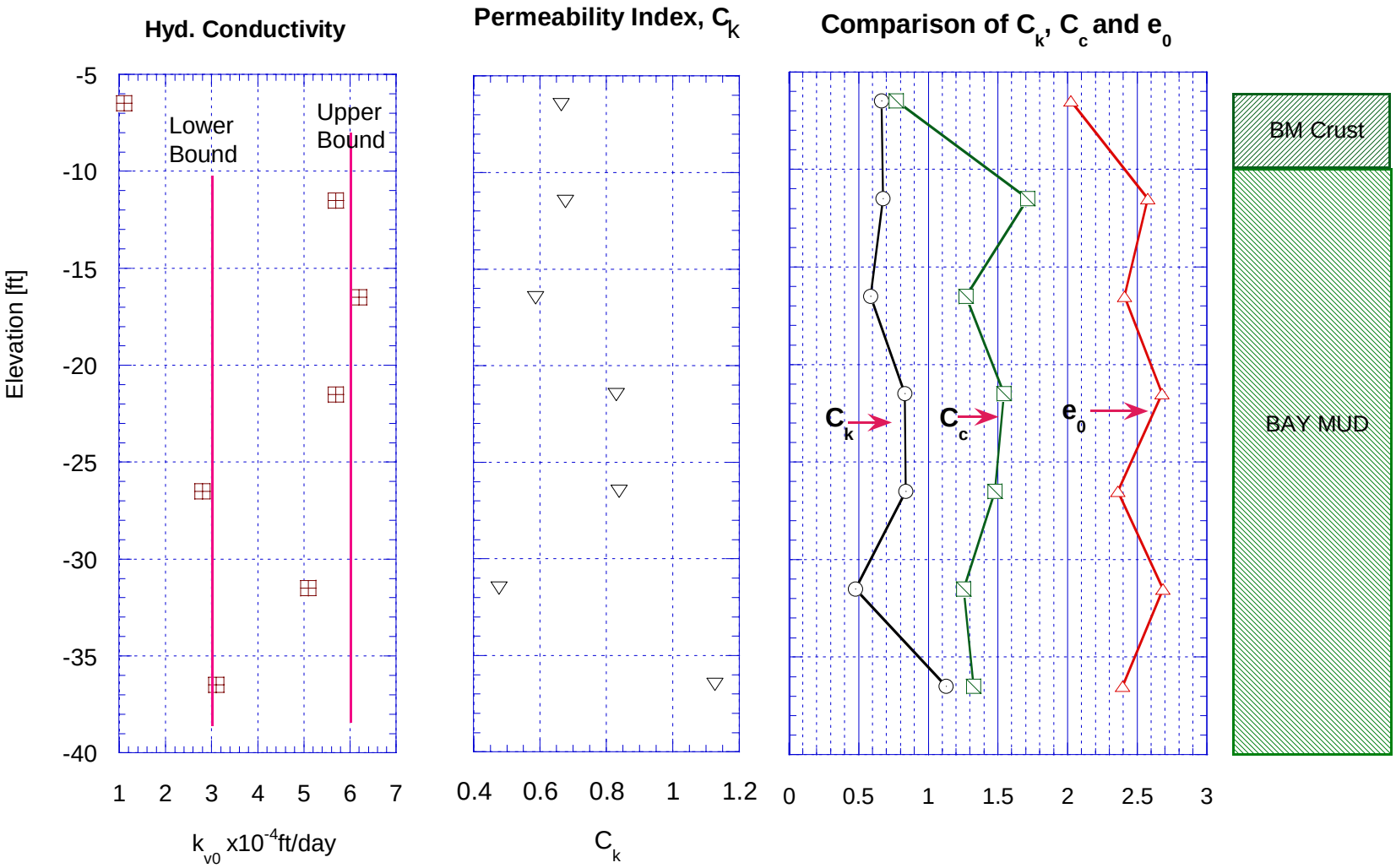

Figure 3.3a Hydraulic Conductivity Property of Bay Mud at TS3-B1

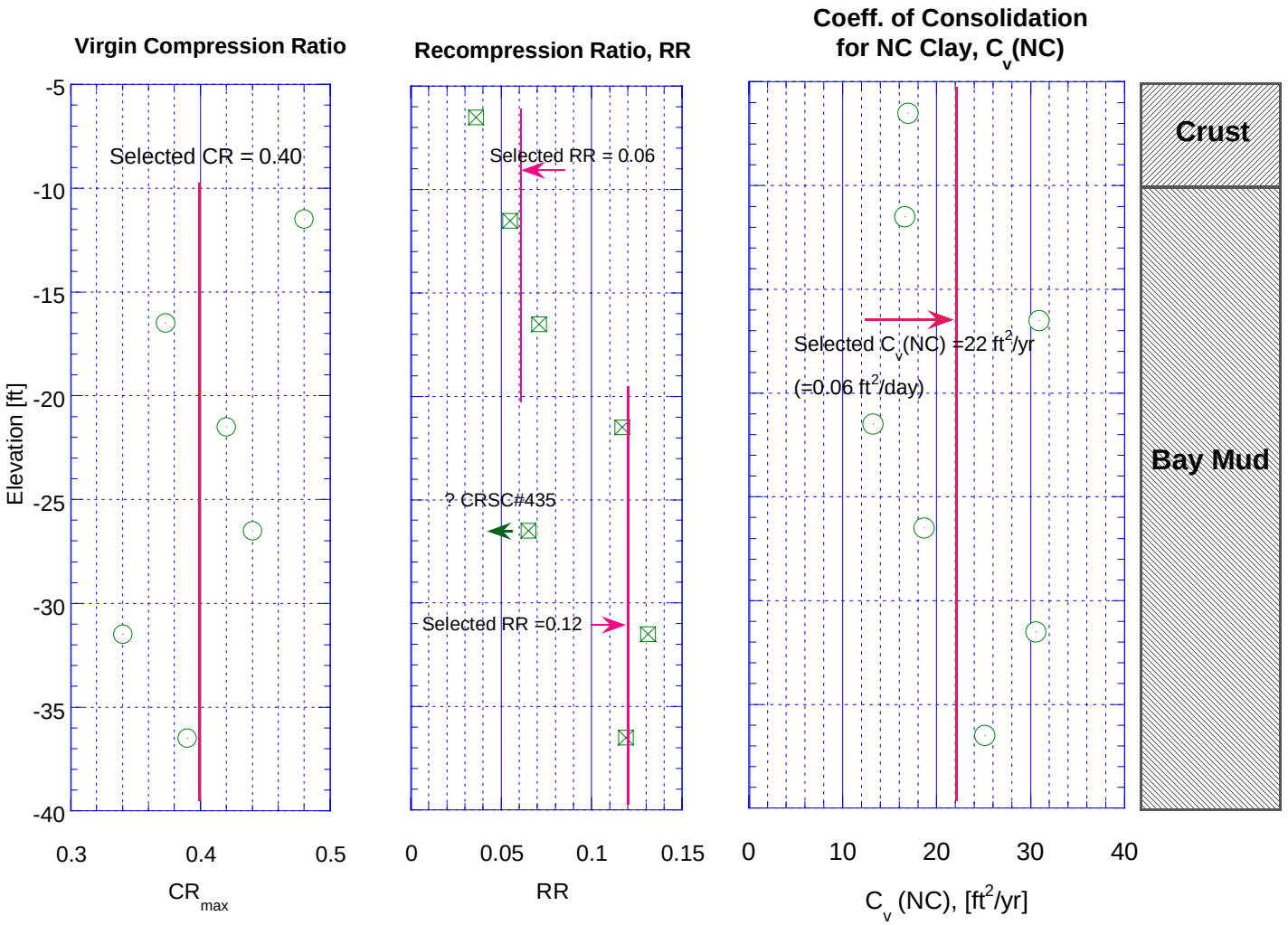

Figure 3.3b Selected Consolidation Properties for Virgin Bay Mud

(Values of RR based on mean σ'_p(FV) profile)

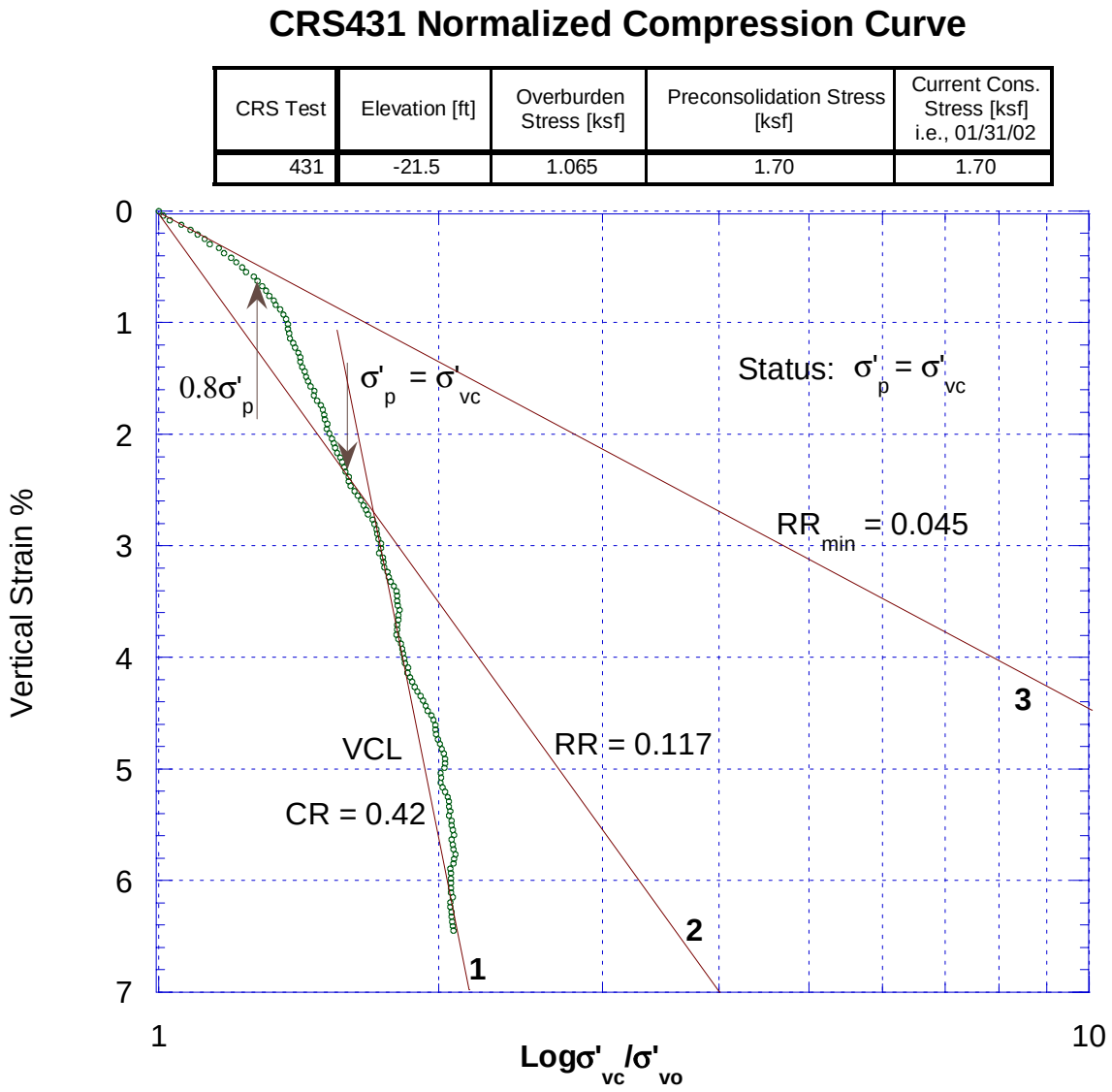

Figure 3.4a CRS431 Normalized Compression Curve in Log-Scale ($\sigma'_p \approx \sigma'_{vc}$)

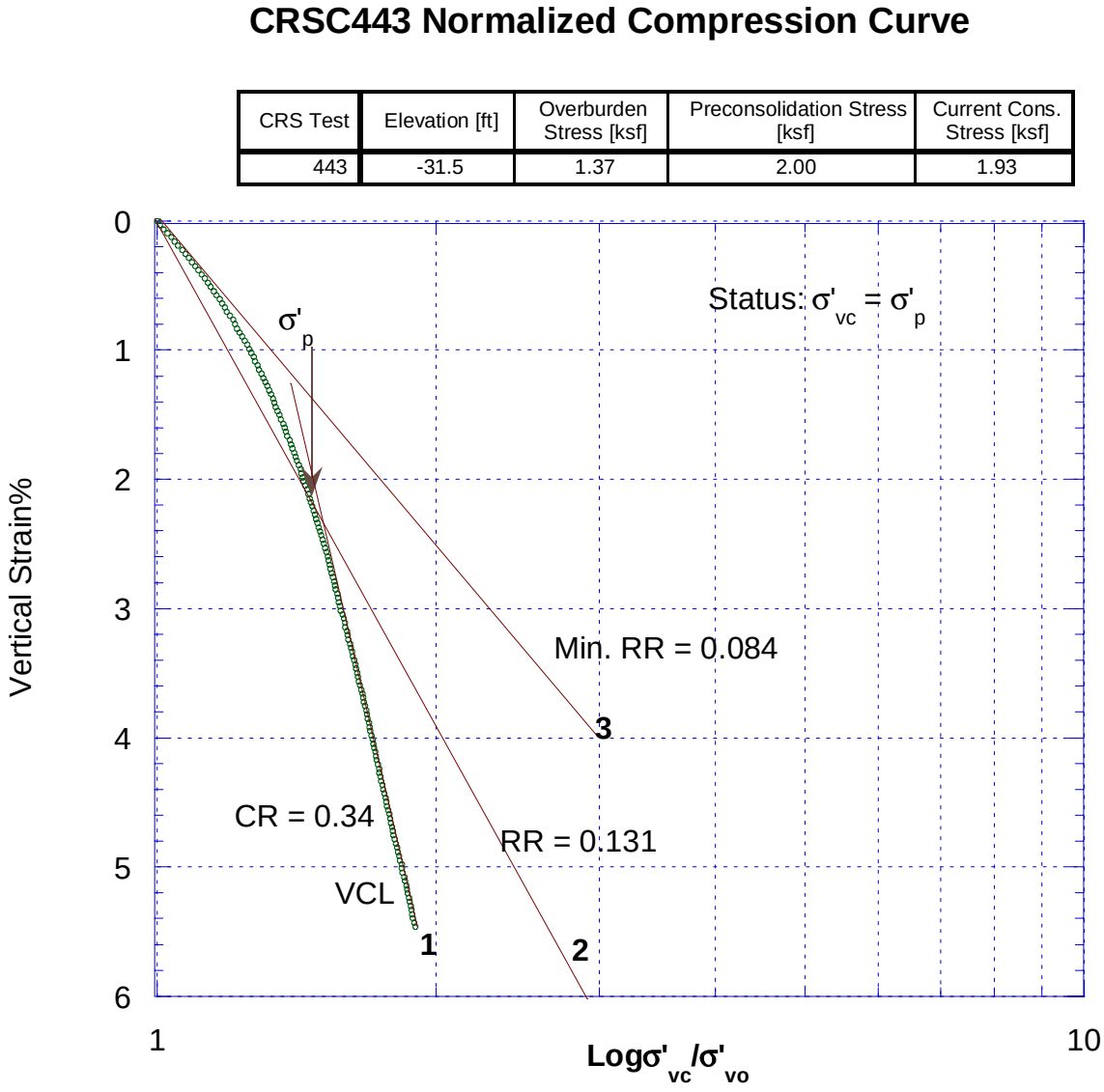

Figure 3.4b CRS443 Normalized Compression Curve in Log-scale ($\sigma'_{vc} \approx \sigma'_{p}$)

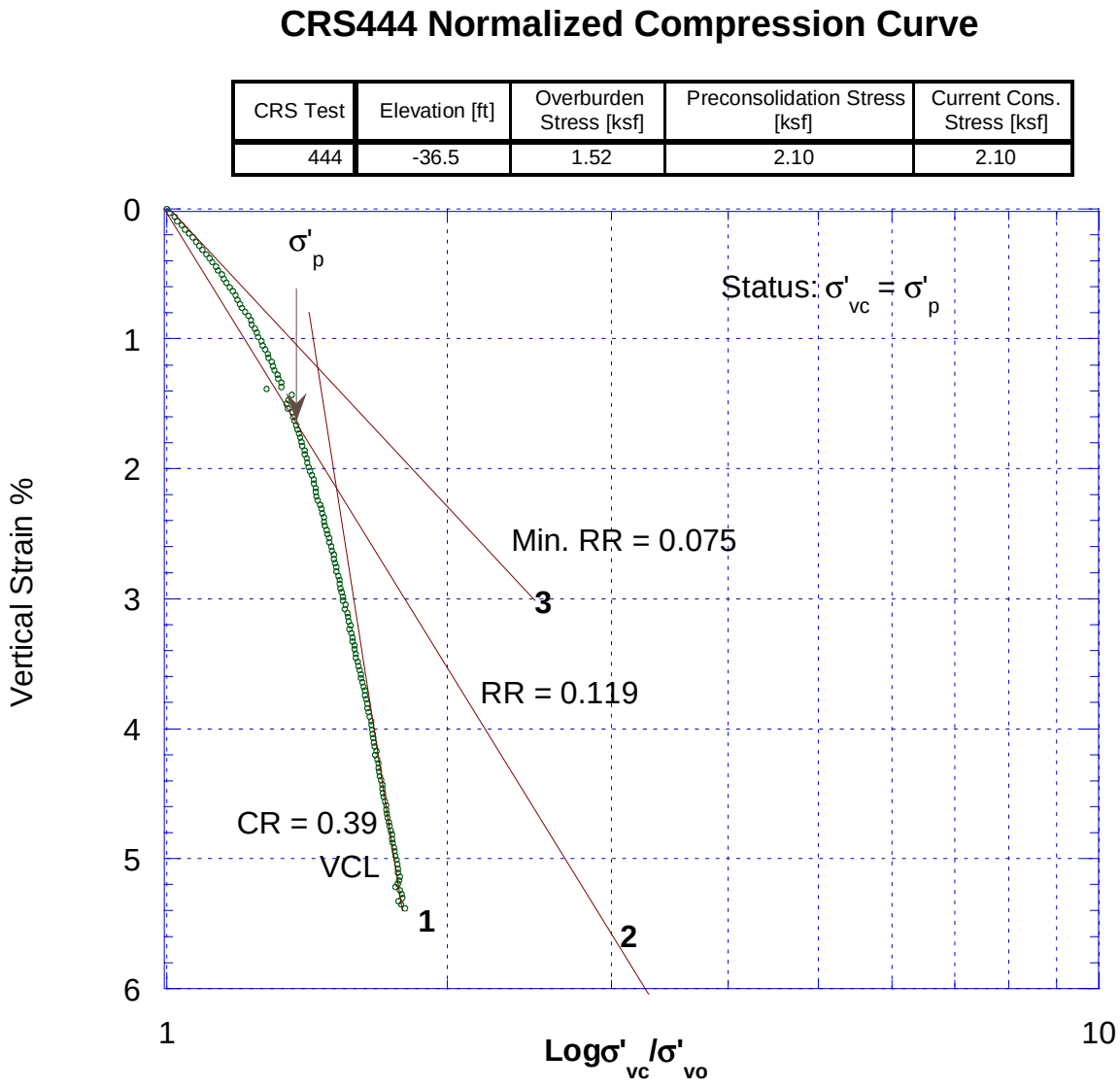

Figure 3.4c CRS444 Normalized Compression Curve in Log-scale ($\sigma'_{vc} \approx \sigma'_{p}$)

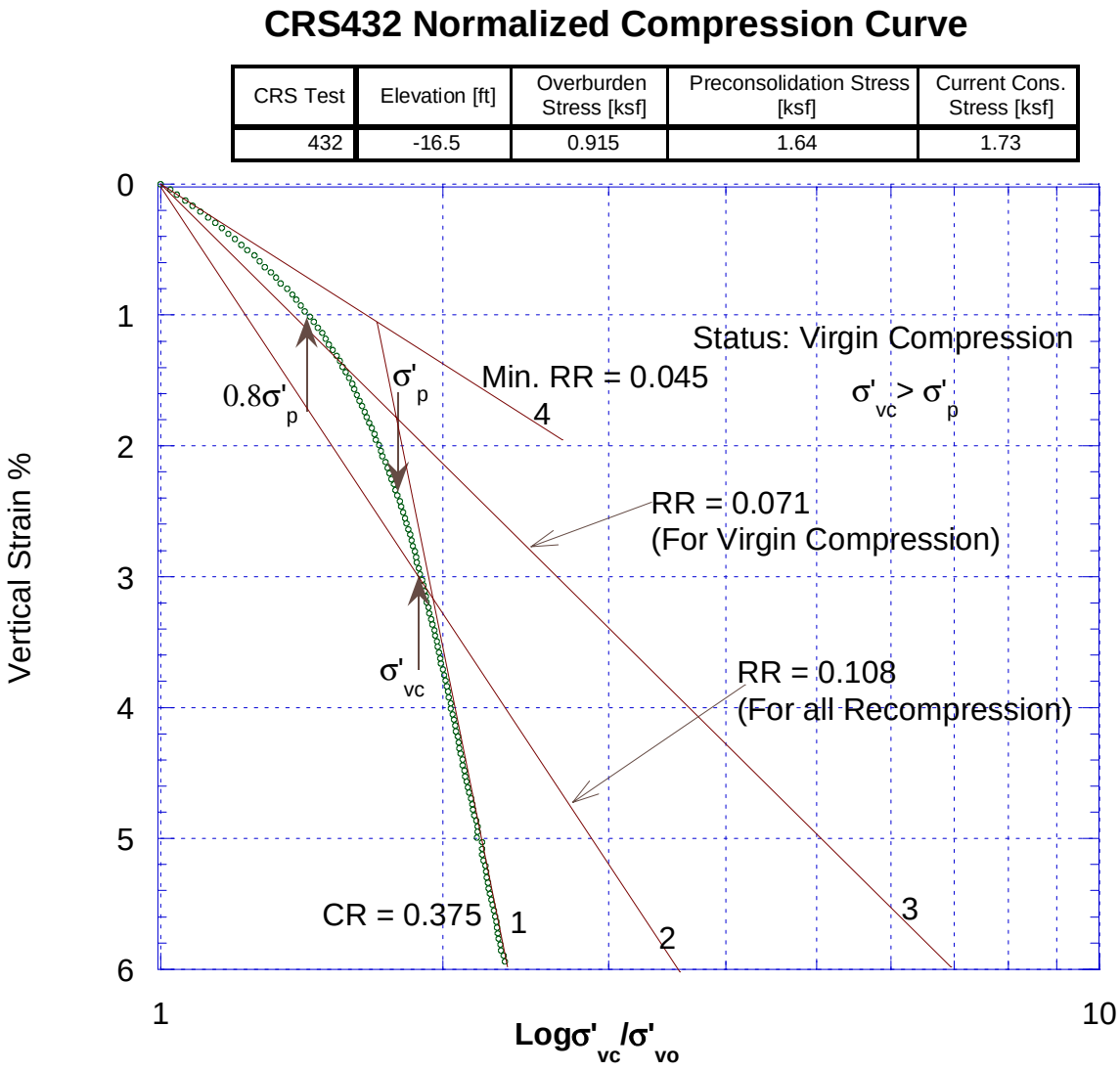

Figure 3.4d CRS432 Normalized Compression Curve in Log-scale ($\sigma'_{vc} > \sigma'_{p}$)

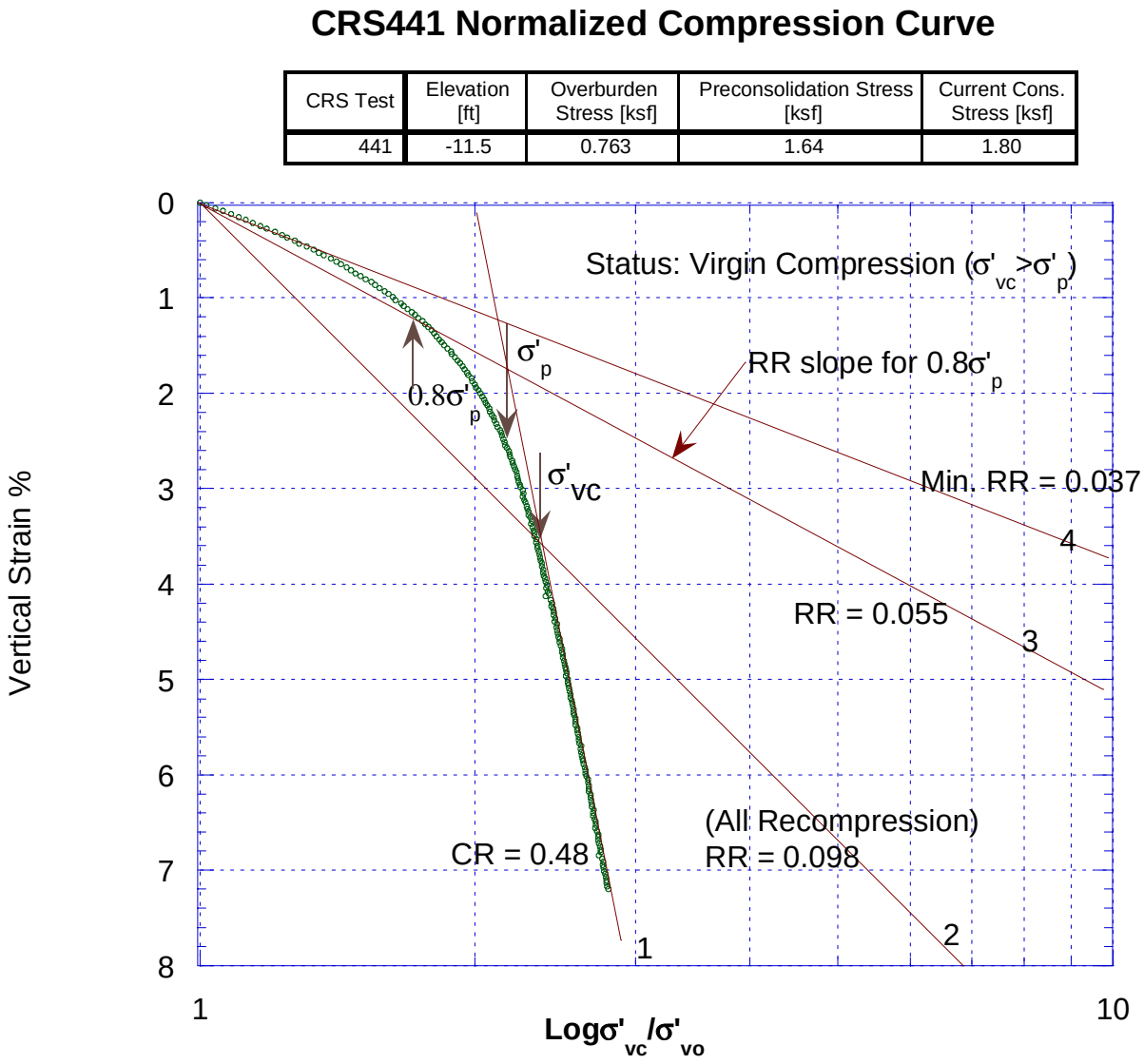

Figure 3.4e CRS441 Normalized Compression Curve in Log-scale ($\sigma'_{vc}>\sigma'_{p}$)

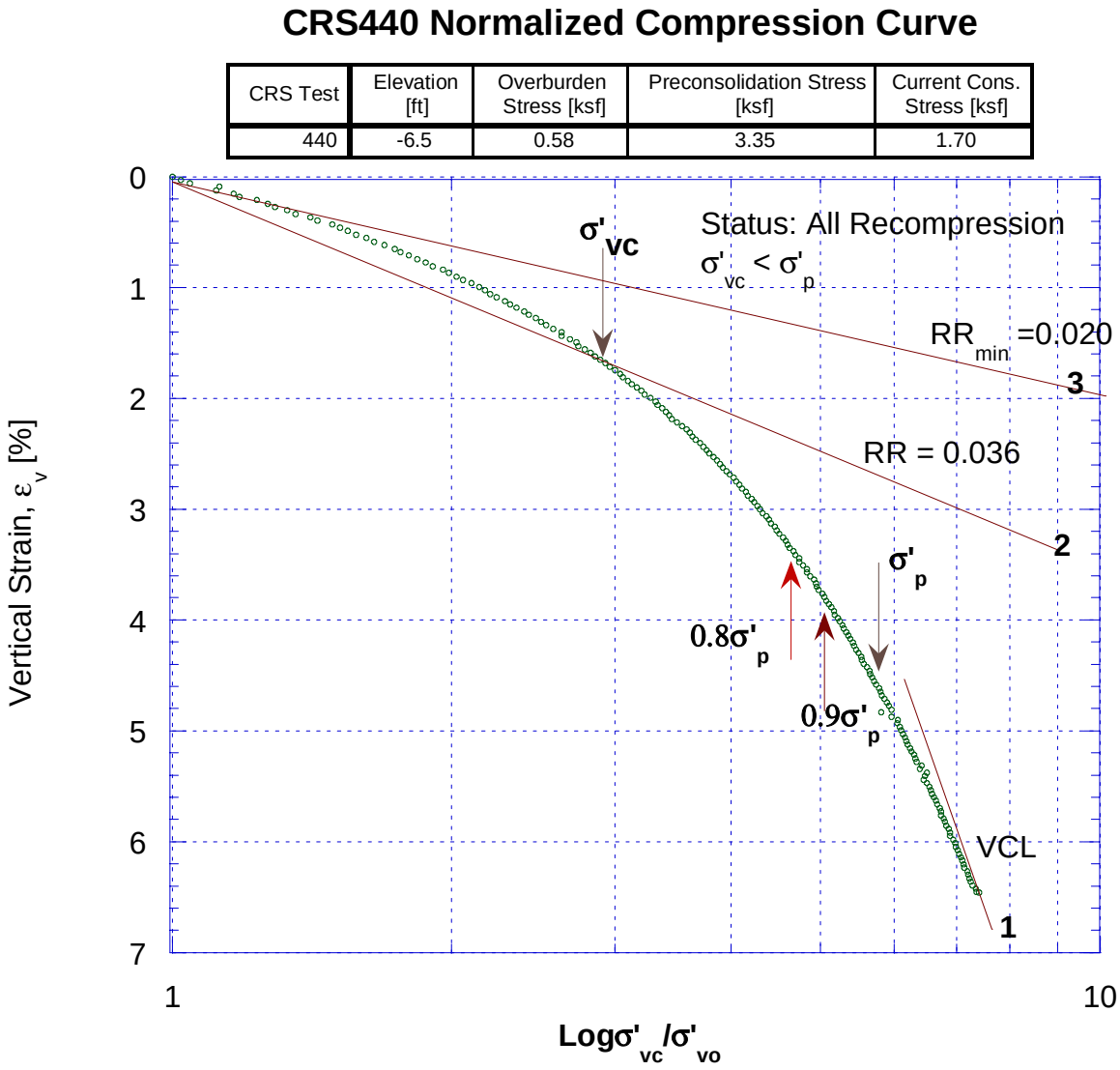

Figure 3.4f CRS440 Normalized Compression Curve in Log-scale ($\sigma'_{vc} < \sigma'_{p}$)

CRS435 Normalized Compression Curve

CRS Test	Elevation [ft]	Overburden Stress [ksf]	Preconsolidation Stress [ksf]	Current Cons. Stress [ksf]
435	-26.5	1.220	2.180	1.860

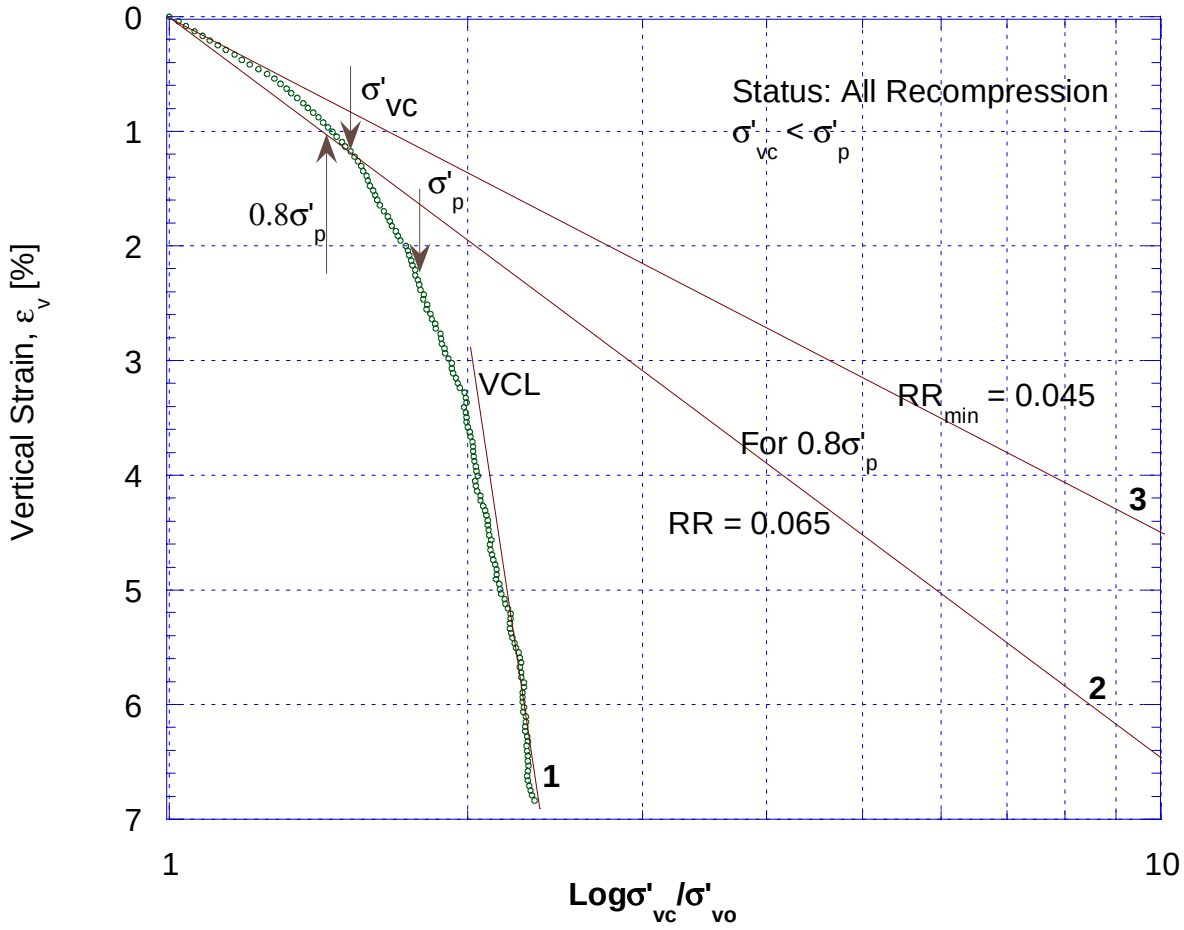

Figure 3.4g CRS435 Normalized Compression Curve in Log-scale ($\sigma'_{vc}<\sigma'_{p}$)

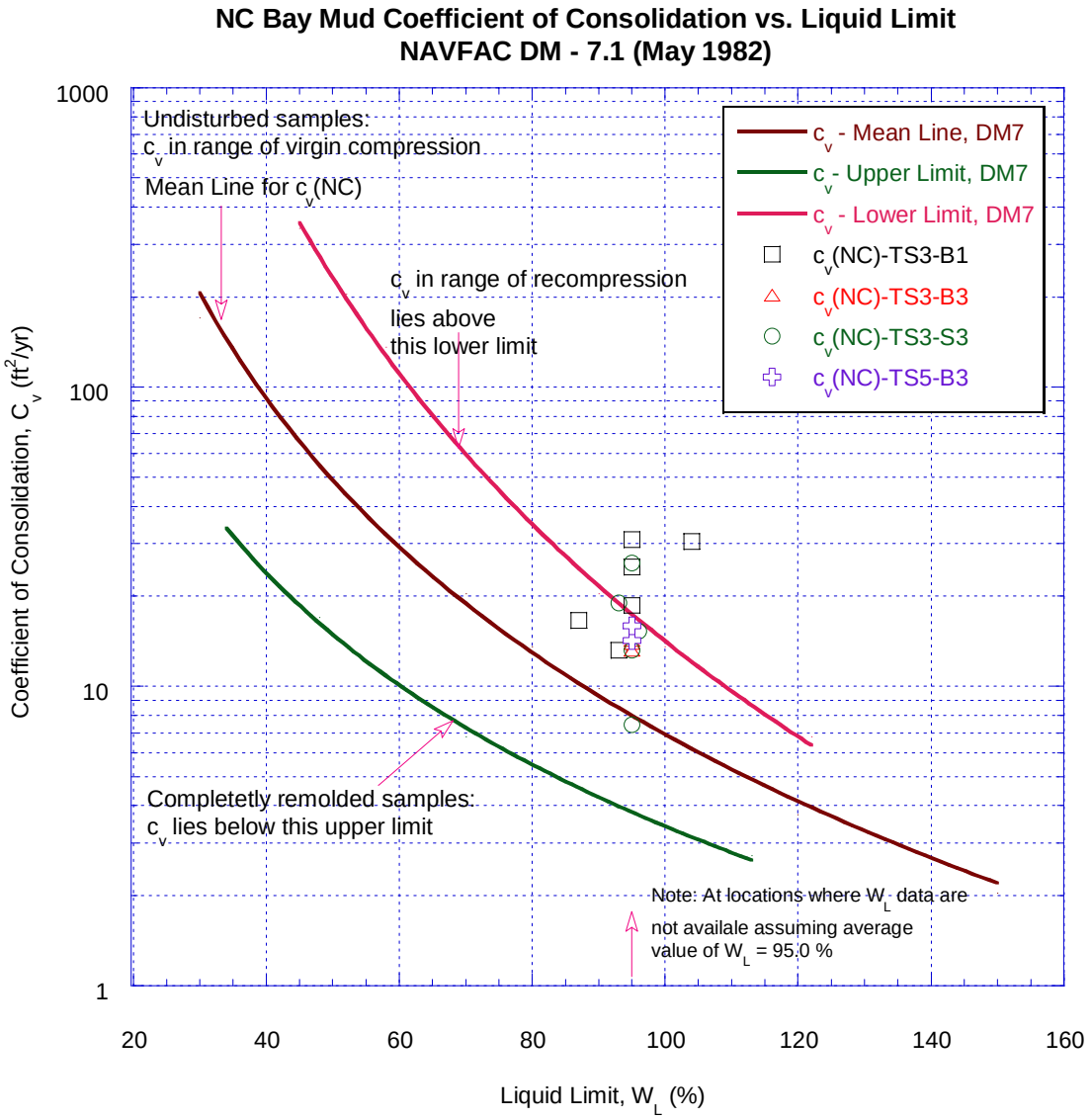

Figure 3.5 Comparison of NC Coefficient of Consolidation of Bay Mud with NAVFAC DM-7.1 (May1982) Chart

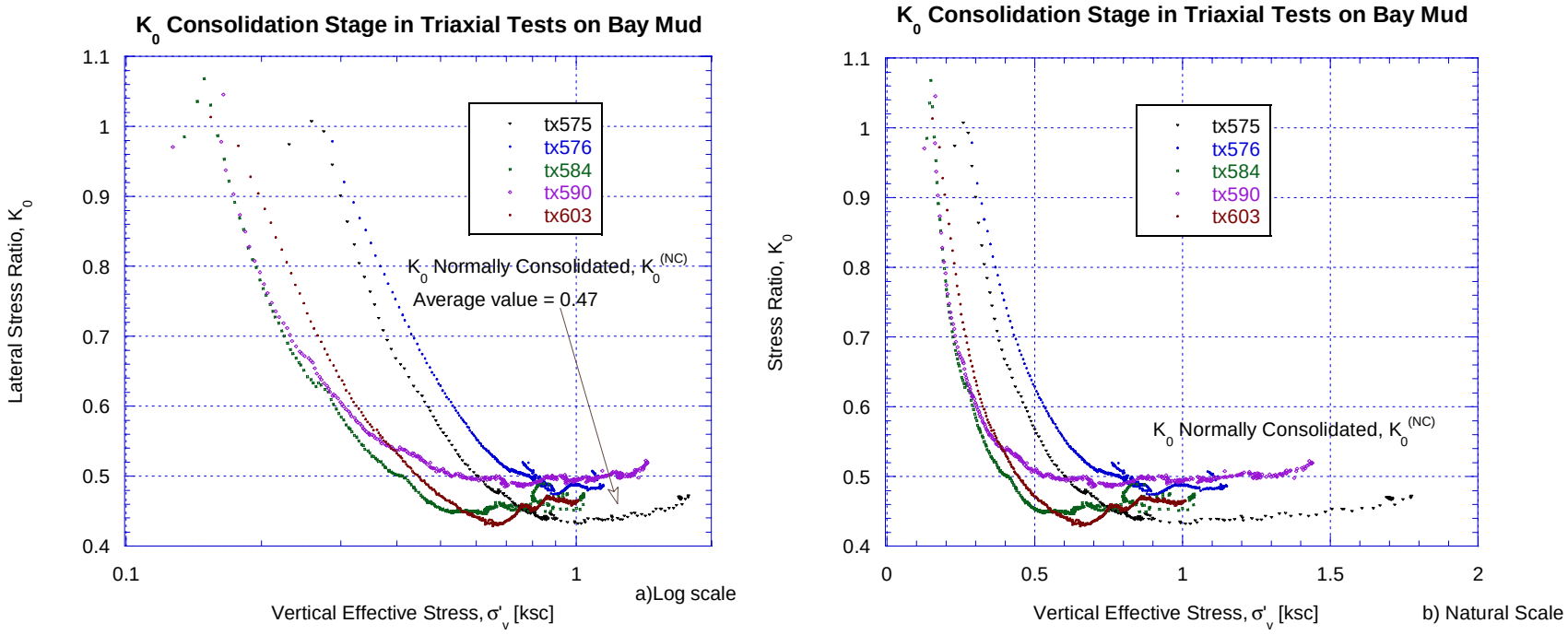

Figure 3.6 Coefficient of Earth Pressure at Rest for Normally Consolidated Bay Mud, K_0^{NC}

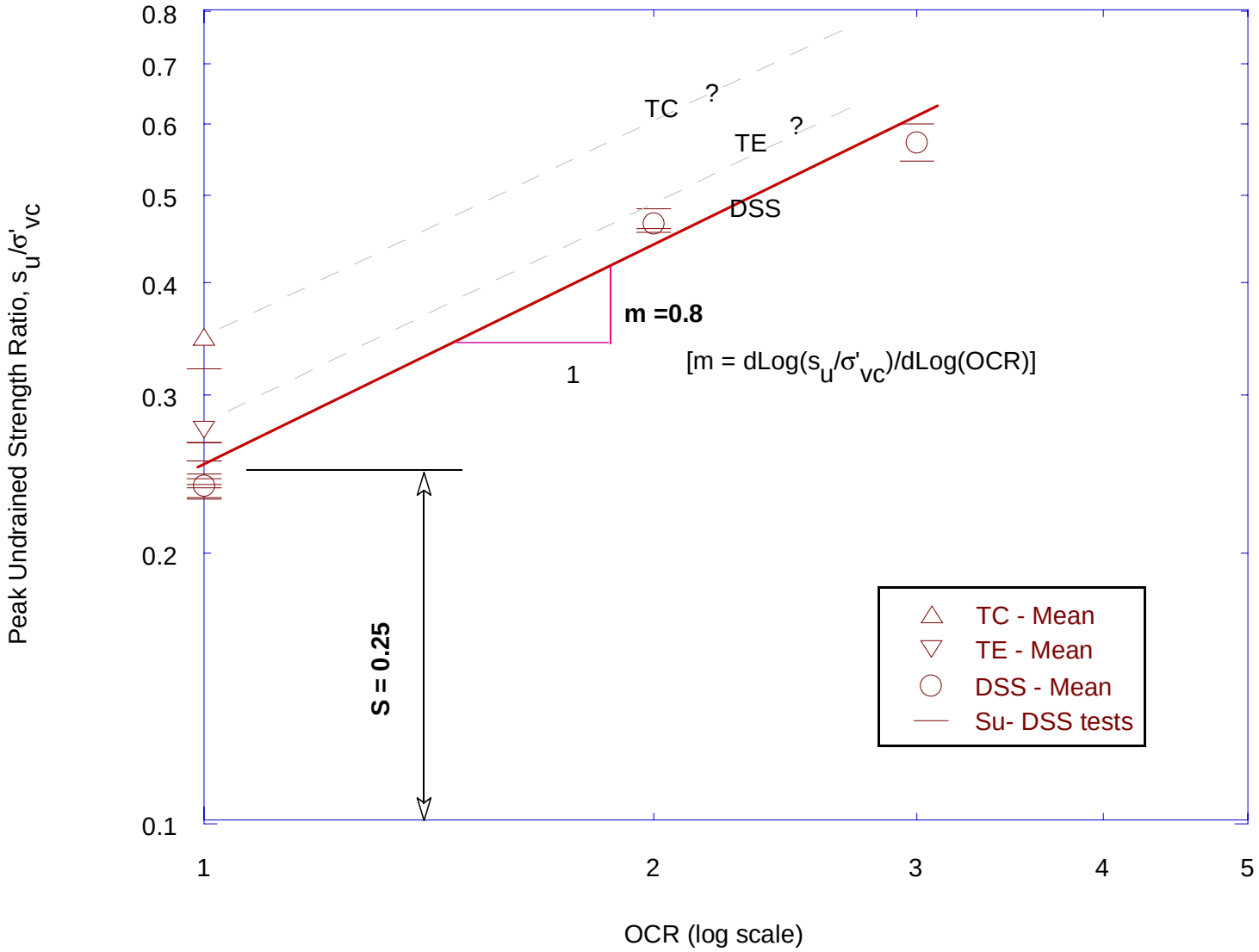

[Data from Germaine, 2002 & 2004 including DSS tests from North Levees]

Figure 3.7 Undrained Strength Ratio vs. Overconsolidation Ratio (Log s_u/σ'_{vc} vs. Log OCR)

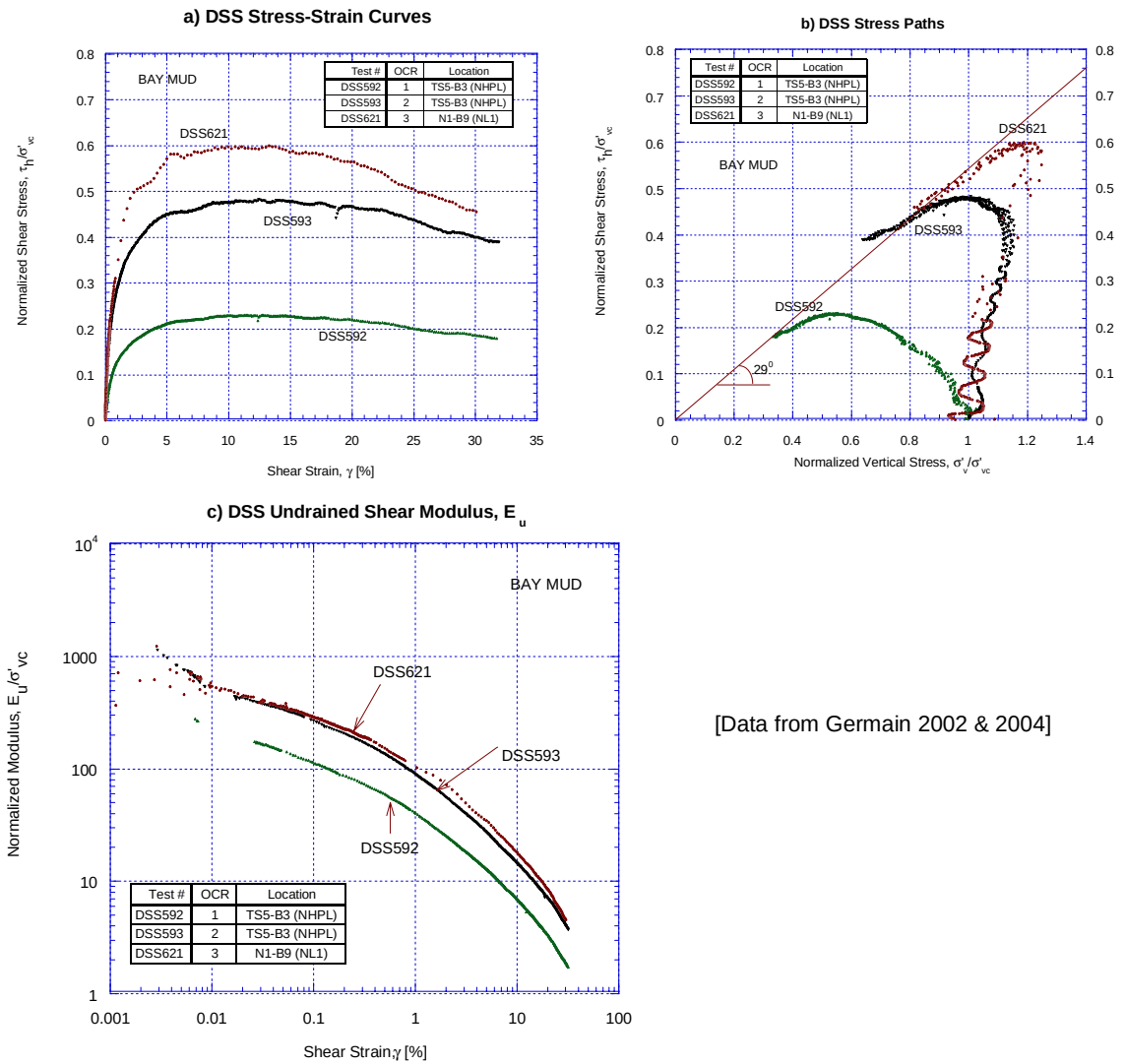

[Data from Germain 2002 & 2004]

Figure 3.8 Typical Results of CK_0UDSS Tests on Bay Mud at OCR = 1, 2 and 3.

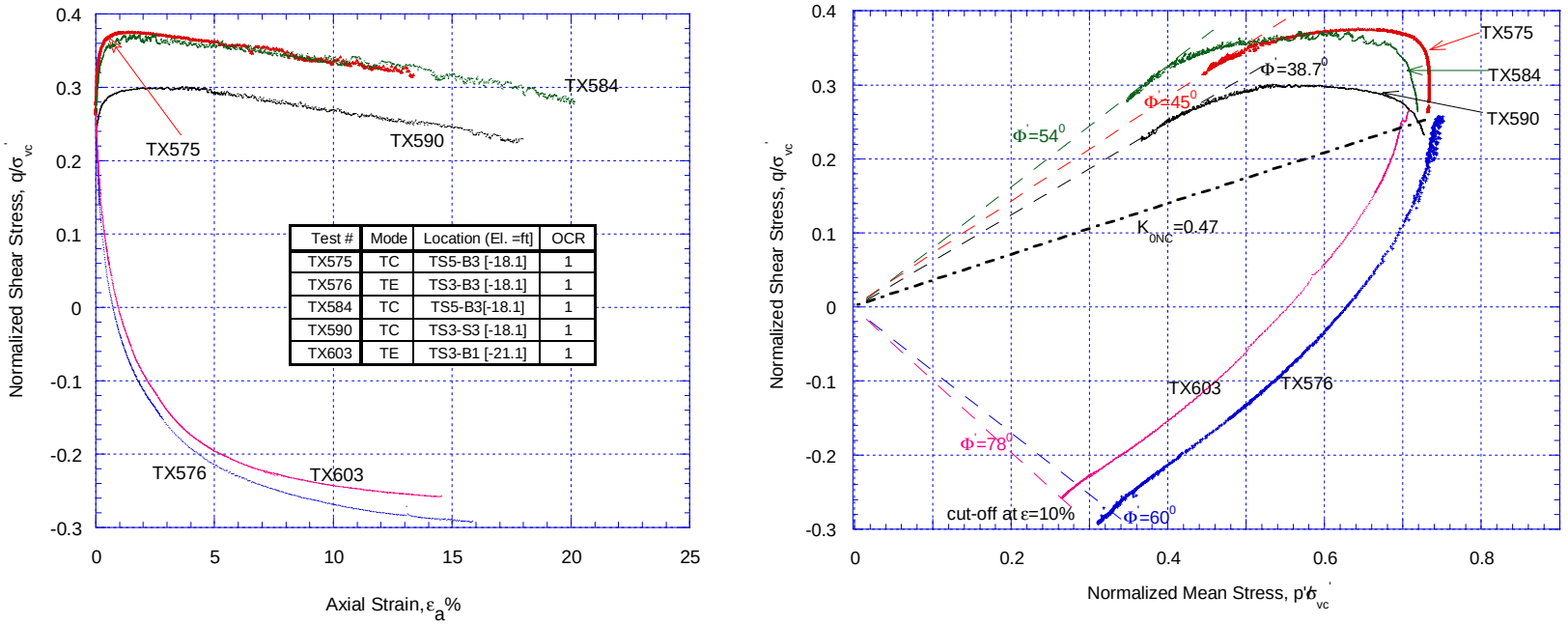

[Data from Germaine, 2002]

Figure 3.9a Results of CK_0UTX Tests on Bay Mud at OCR =1: Stress-Strain and Stress Path

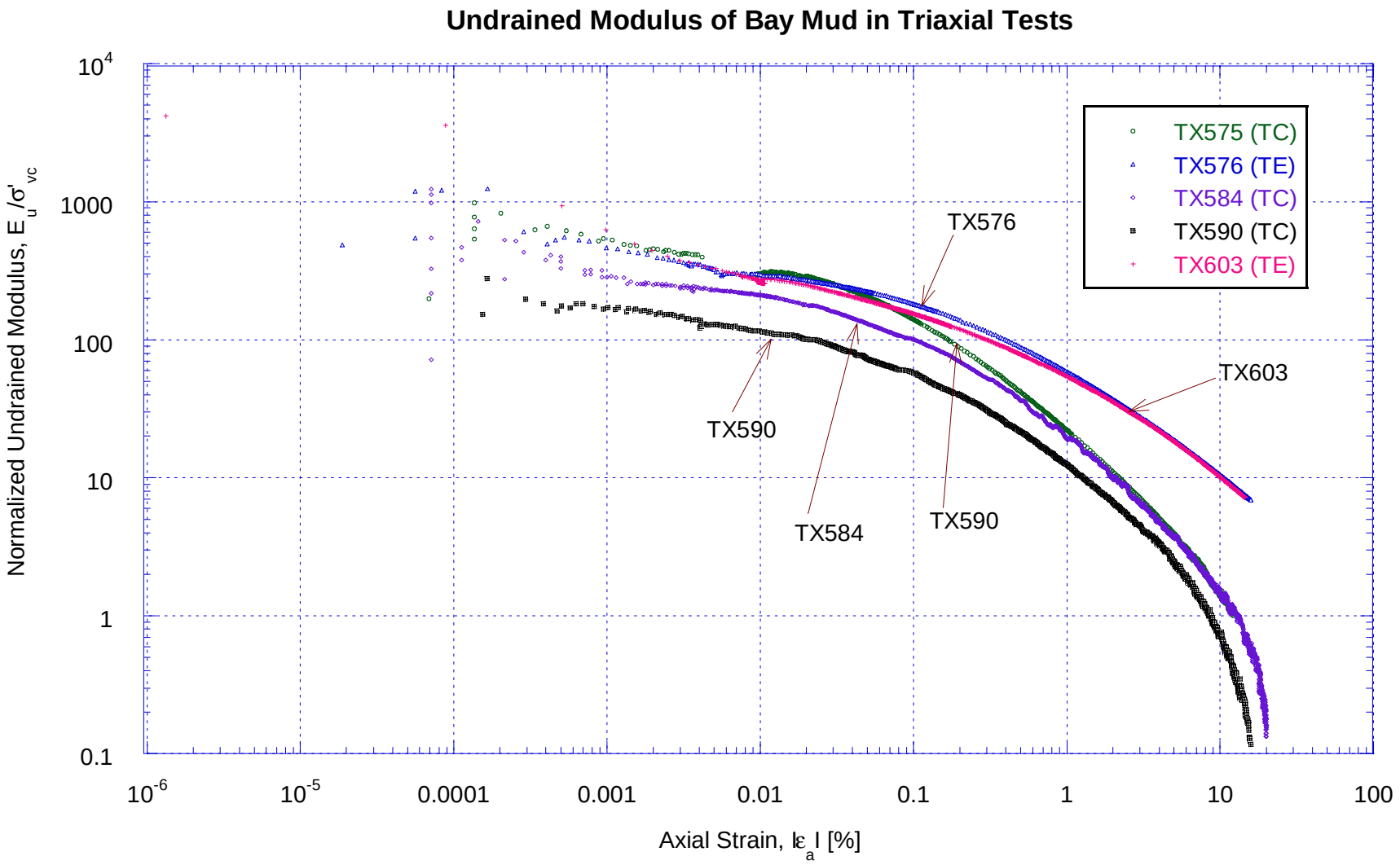

Figure 3.9b Results of CK_0UTX Tests on Bay Mud at OCR =1: Undrained Young's Modulus

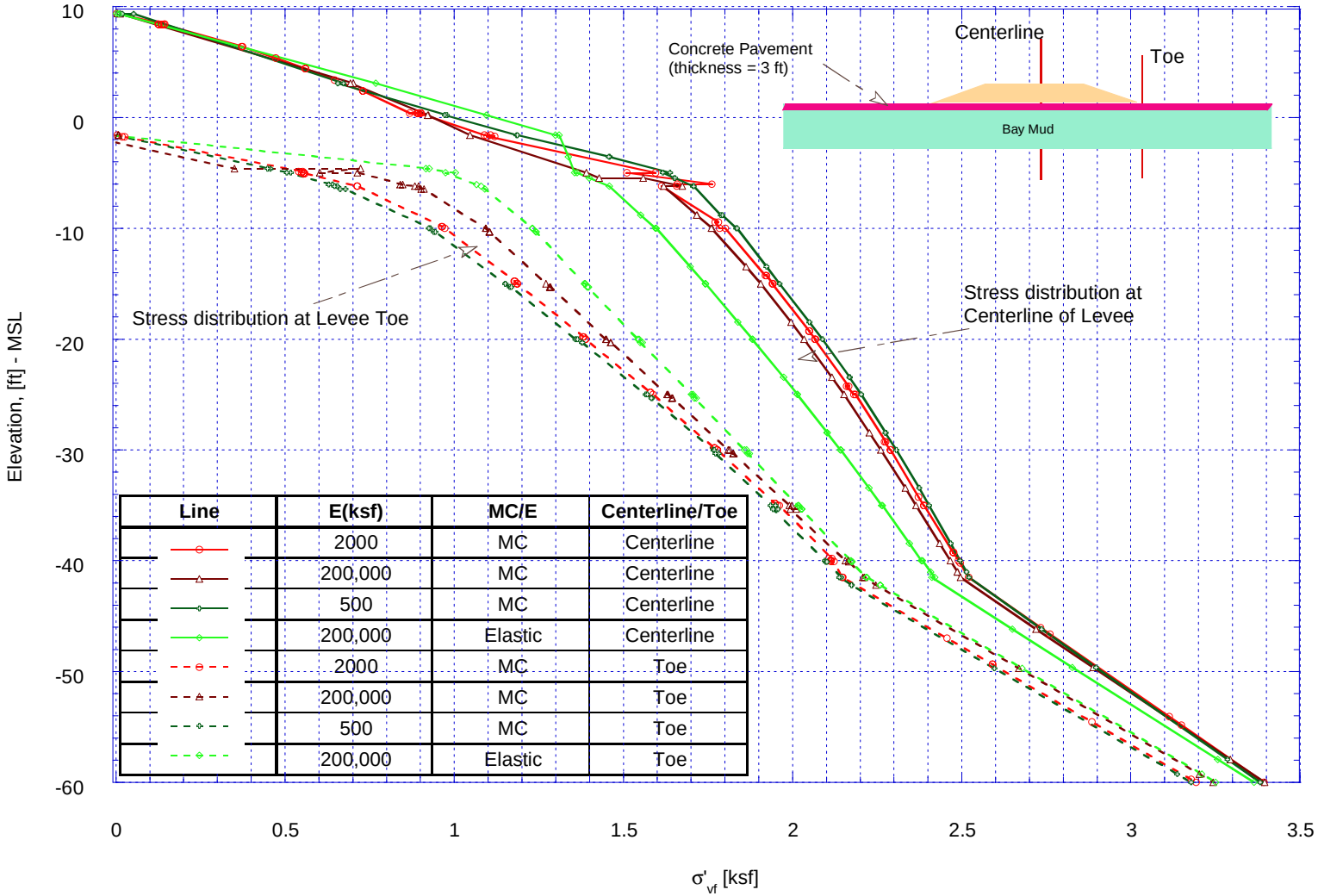

Figure 3.10 Influence of Young's Modulus and Strength of Uncracked, Continuous Concrete Pavement on Final Vertical Effective Stress Distribution in Bay Mud

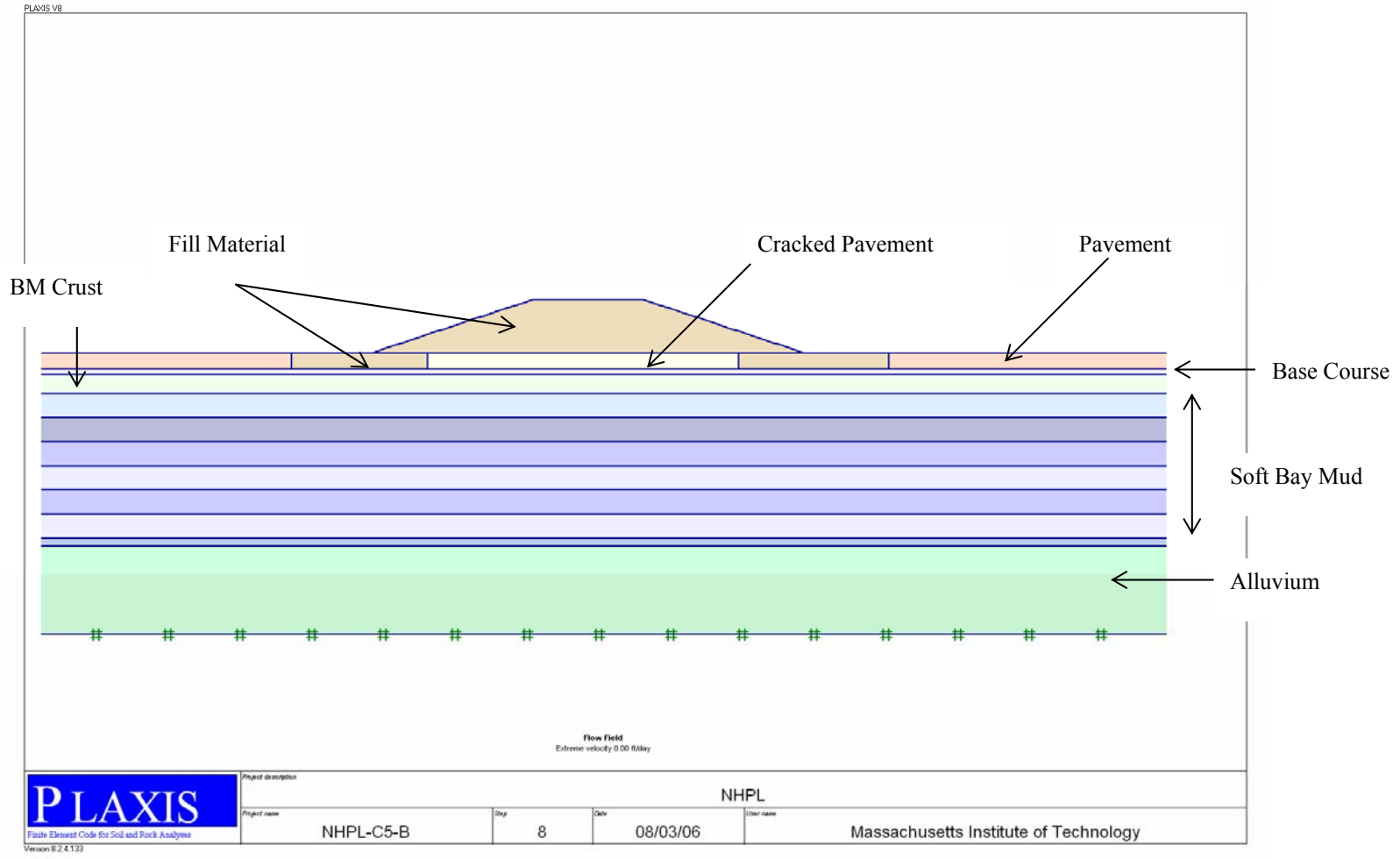

Figure 3.11a Geometry for CASE B&C Analyses of Final Vertical Stress, σ'_{vf}

(Note: For Case A, there is only an uncracked and continuous pavement below the NHPL)

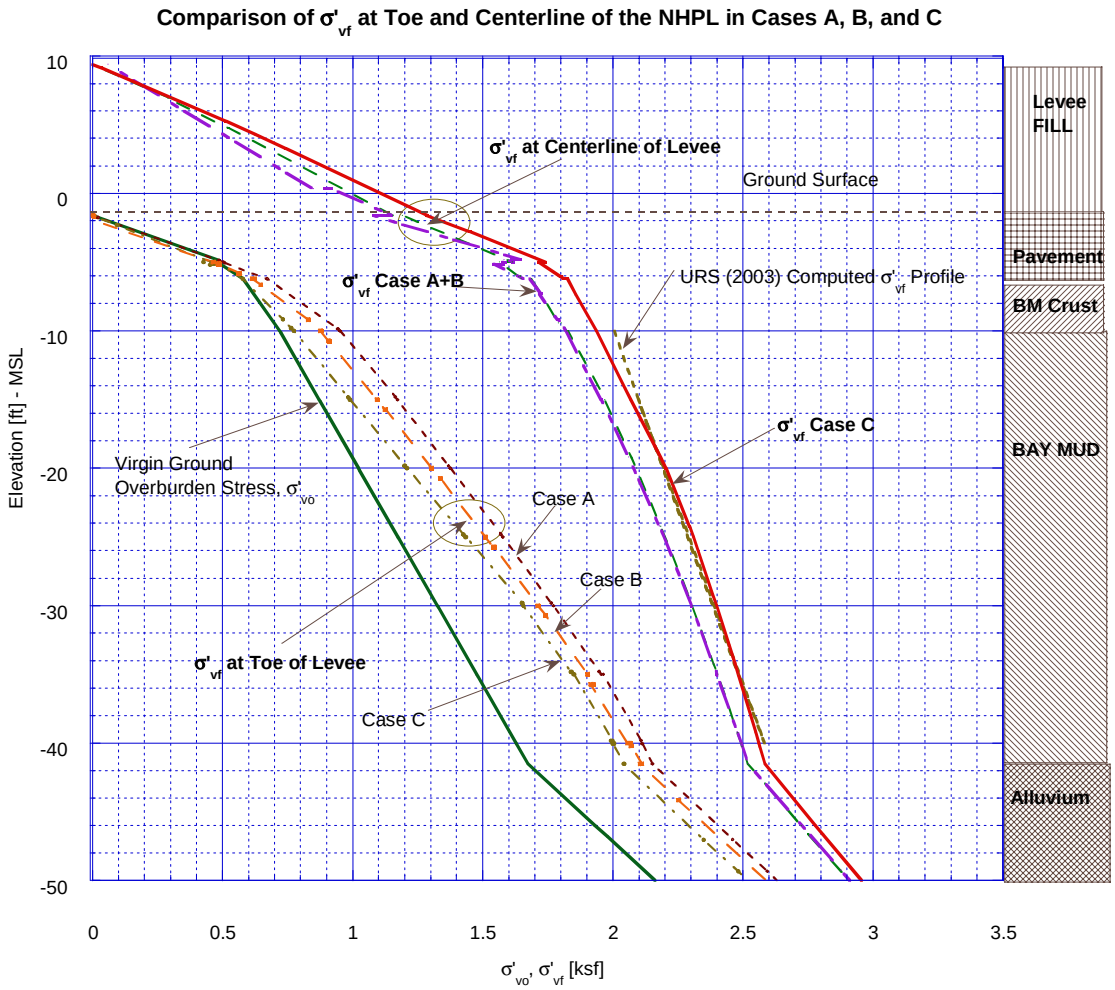

Cases	A	B	C
Condition	Intact concrete pavement	Cracked pavement	Cracked pavement
Fill Props	URS,2005	URS,2005	URS,2003
c' (ksf)	0.30	0.30	0.02
E (ksf)	300	300	20
(Cracked) Pavement Props.	URS, 2005	URS, 2005	URS, 2003
c' (ksf)	4.96	0.025	0.025
E (ksf)	2000	1500	200
BM Crust Props.	URS, 2005	URS, 2005	Nguyen, 2006
c' (ksf)	0.80	0.80	0.58
E_u (ksf)	300	300	116
Table 3.7	**a**	**b**	**c**

Note: URS = URS/ARUP (2005)

Figure 3.11b PLAXIS Predicted Final Consolidation Vertical Effective Stress at Centerline and Toe of Levee (Cases A, B and C)

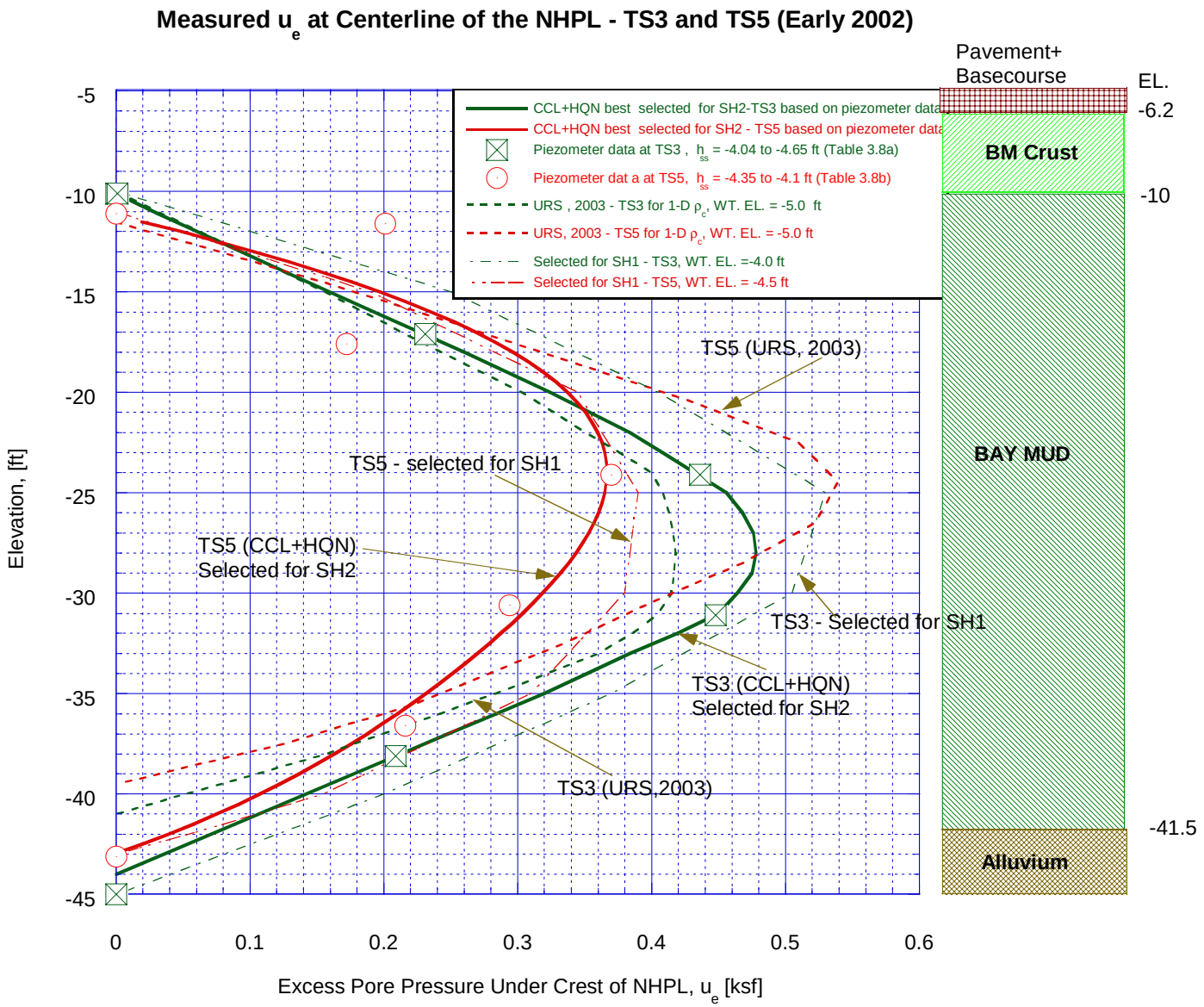

Figure 3.12a Selected Excess Pore Pressure Profiles under Centerline of Levee at TS3 and TS5

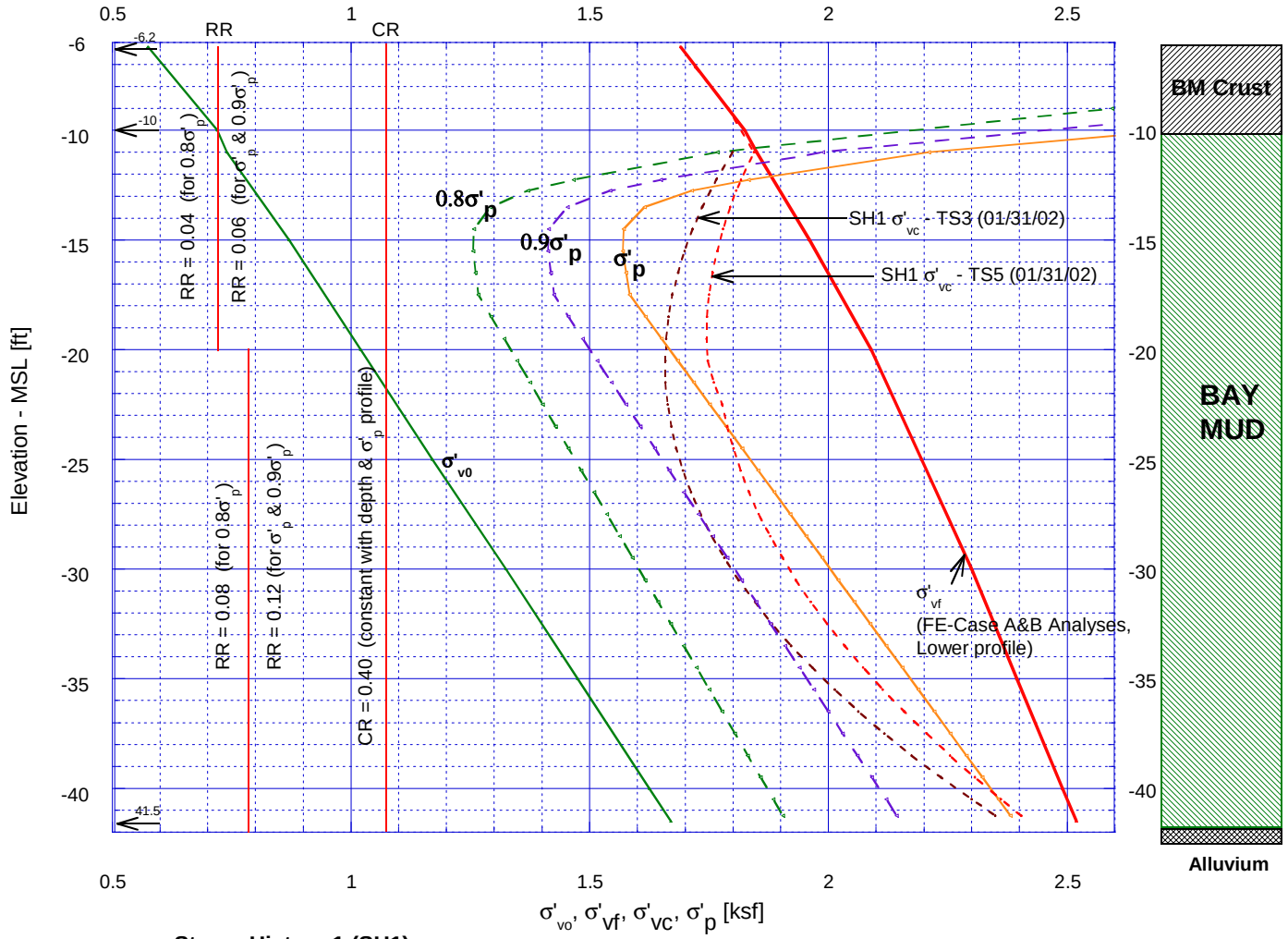

Stress History 1 (SH1)

NOTES: $\sigma'_{vc} = \sigma'_{vf} - u_e$ (measured u_e SH1 i.e., Fig. 3.12a) σ'_{vf} = FE PLAXIS 2-D Analysis Case A & B

Figure 3.12b TS3 & TS5, Line 3 Stress Histories for One-Dimensional Consolidation Analysis (SH1)

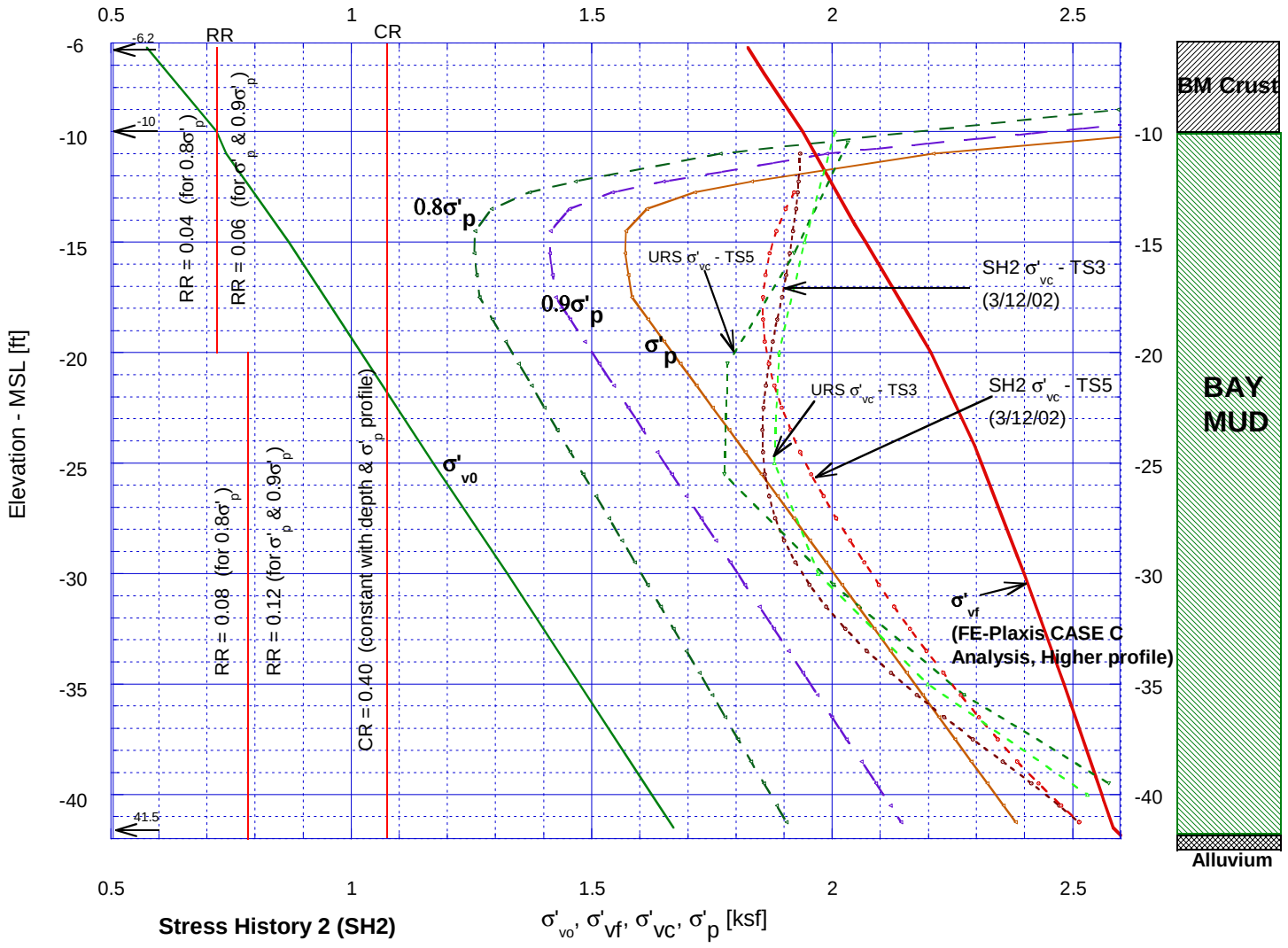

NOTES: $\sigma'_{vc} = \sigma'_{vf} - u_e$ (measured u_e SH2 i.e., Fig. 3.12a)

σ'_{vf} = FE PLAXIS 2-D Analysis in Case C, higher profile

Figure 3.12c TS3 & TS5, Line 3 Stress Histories for One –Dimensional Consolidation Analysis (SH2)

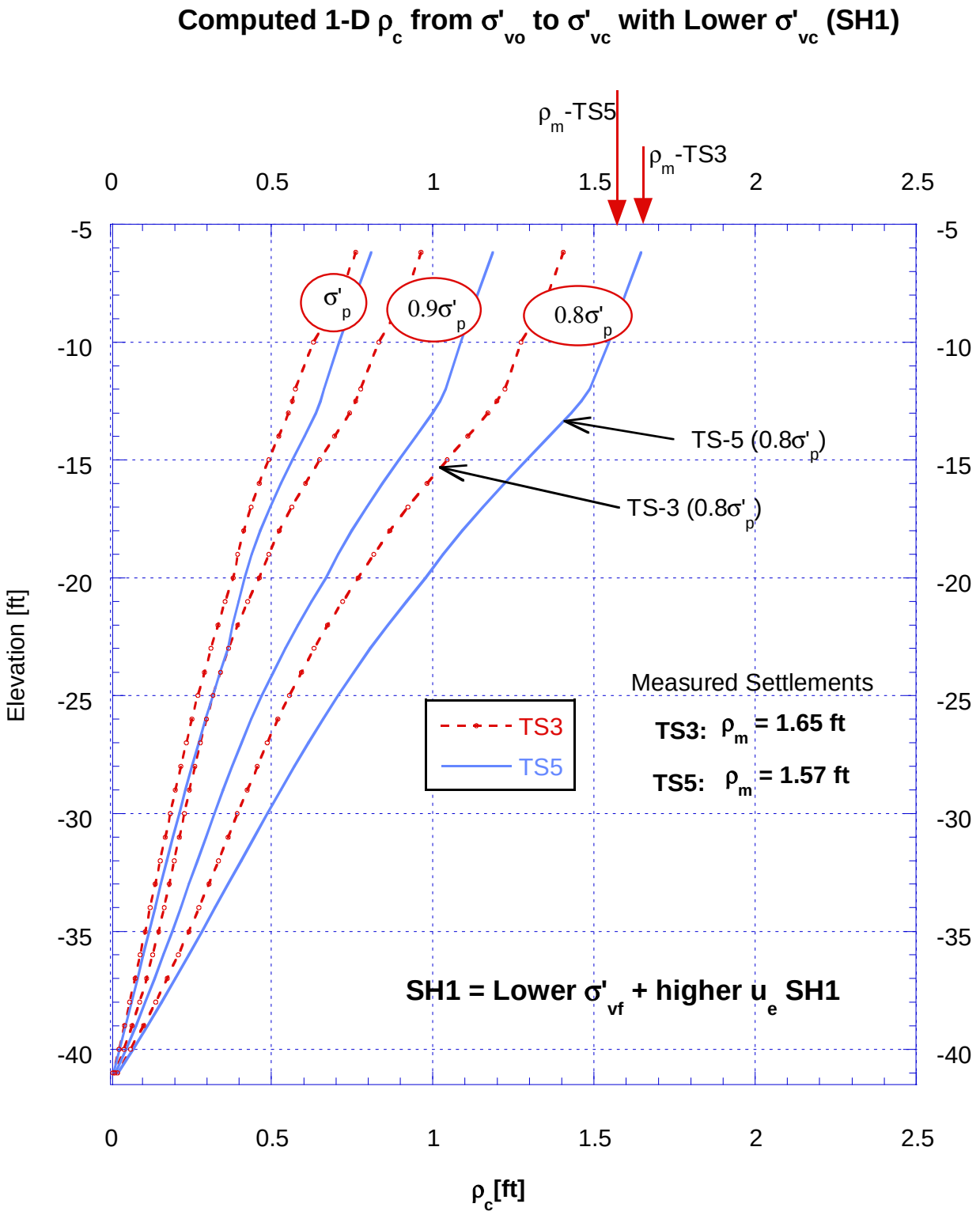

Figure 3.13a One-Dimensional Consolidation Settlements and Measured Settlements at TS3 & TS5 up to 01/31/02 (SH1)

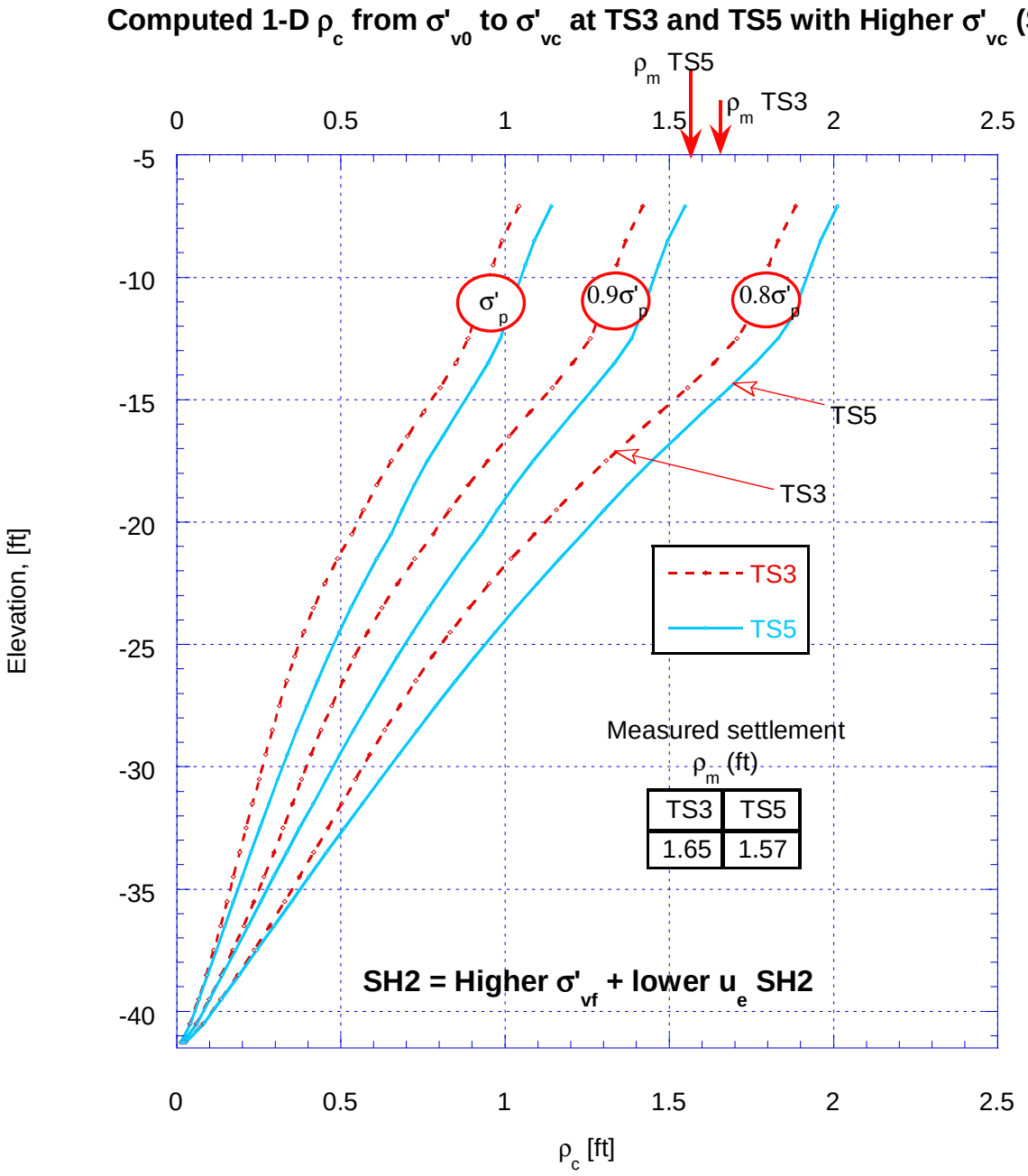

Figure 3.13b One-Dimensional Consolidation Settlements and Measured Settlements at TS3 & TS5 up to 01/31/02 (SH2)

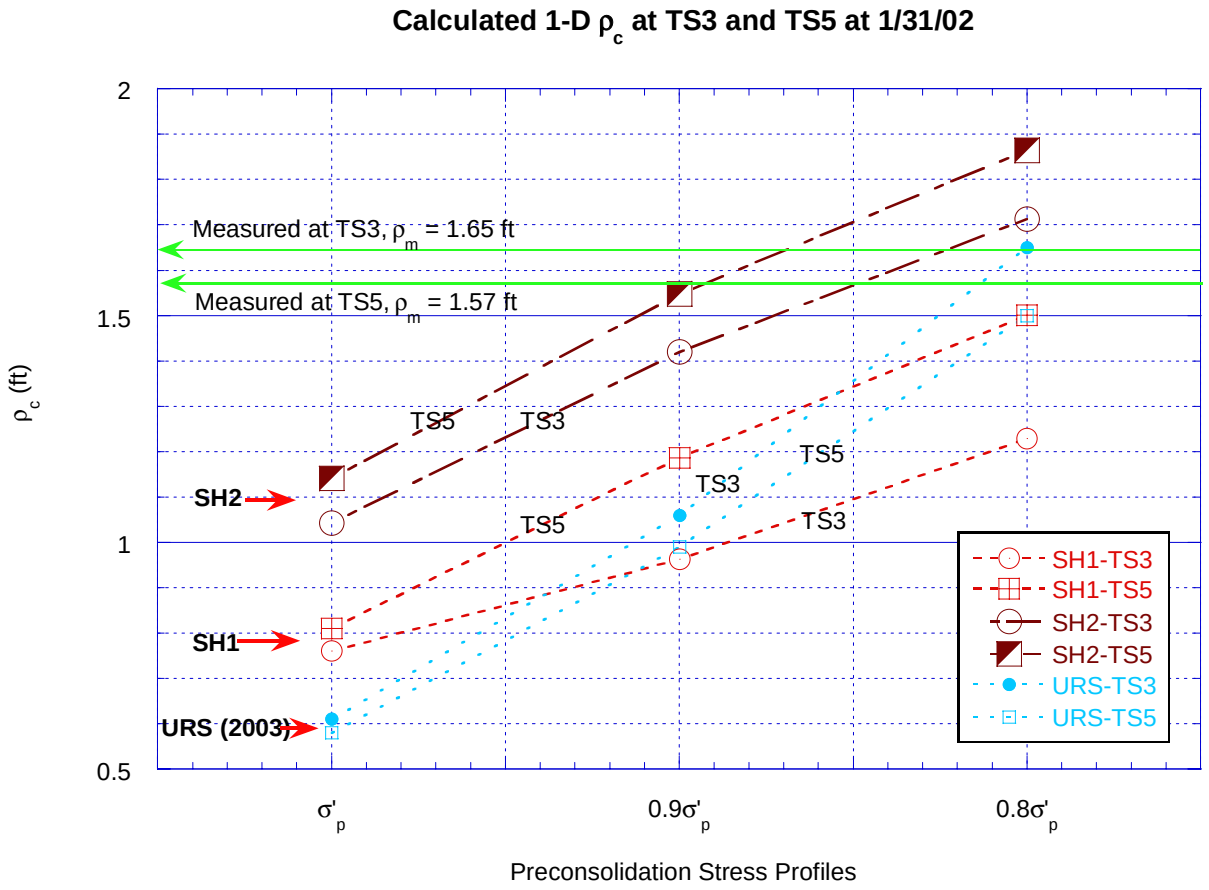

Figure 3.13c Comparison of 1-D Consolidation Settlements at TS3 and TS5 at 1/31/02 [SH1, SH2, and URS (2003)]

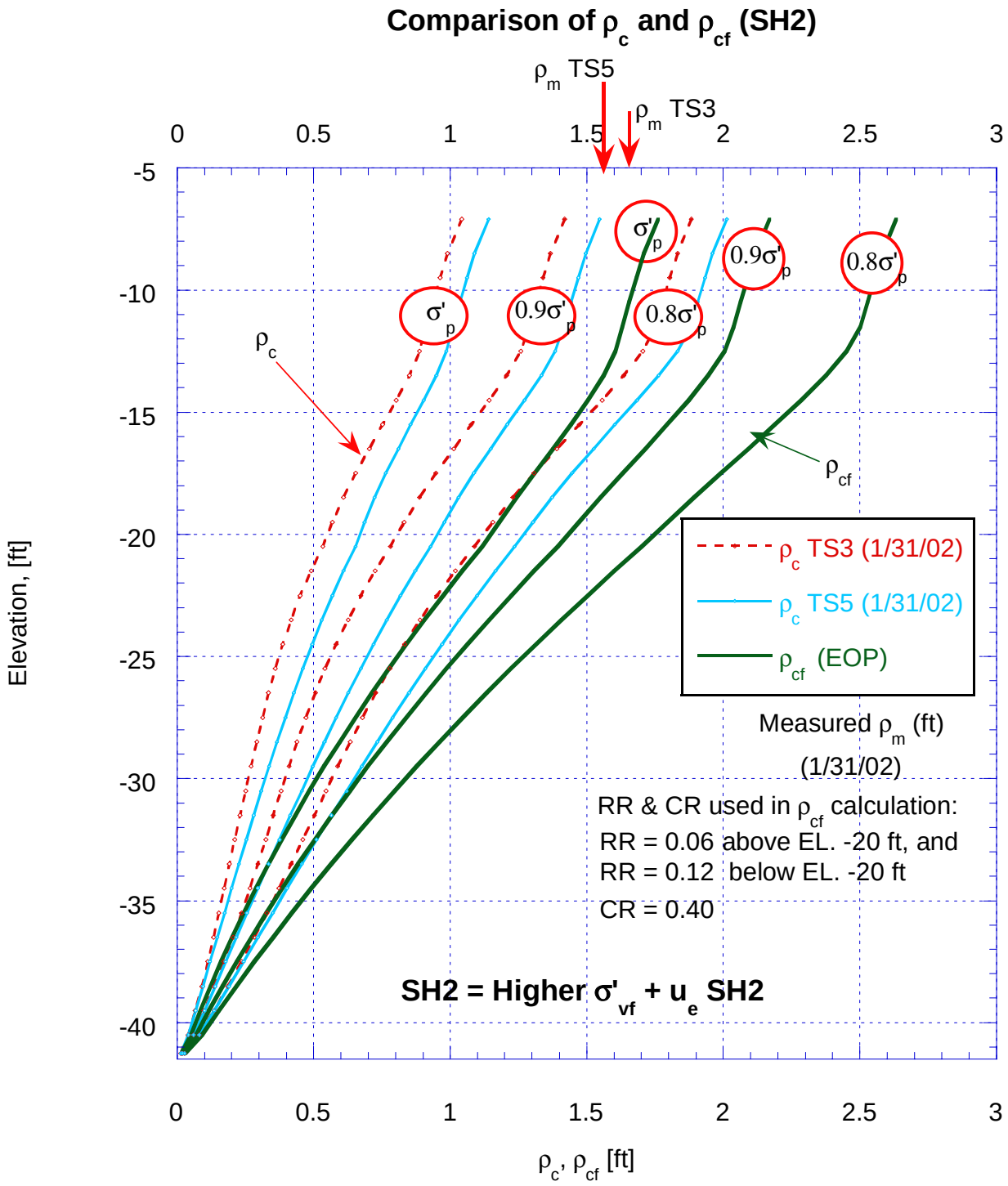

Figure 3.13d Predicted 1-D Consolidation Settlements at 1/02 and Final Consolidation Settlements with SH2

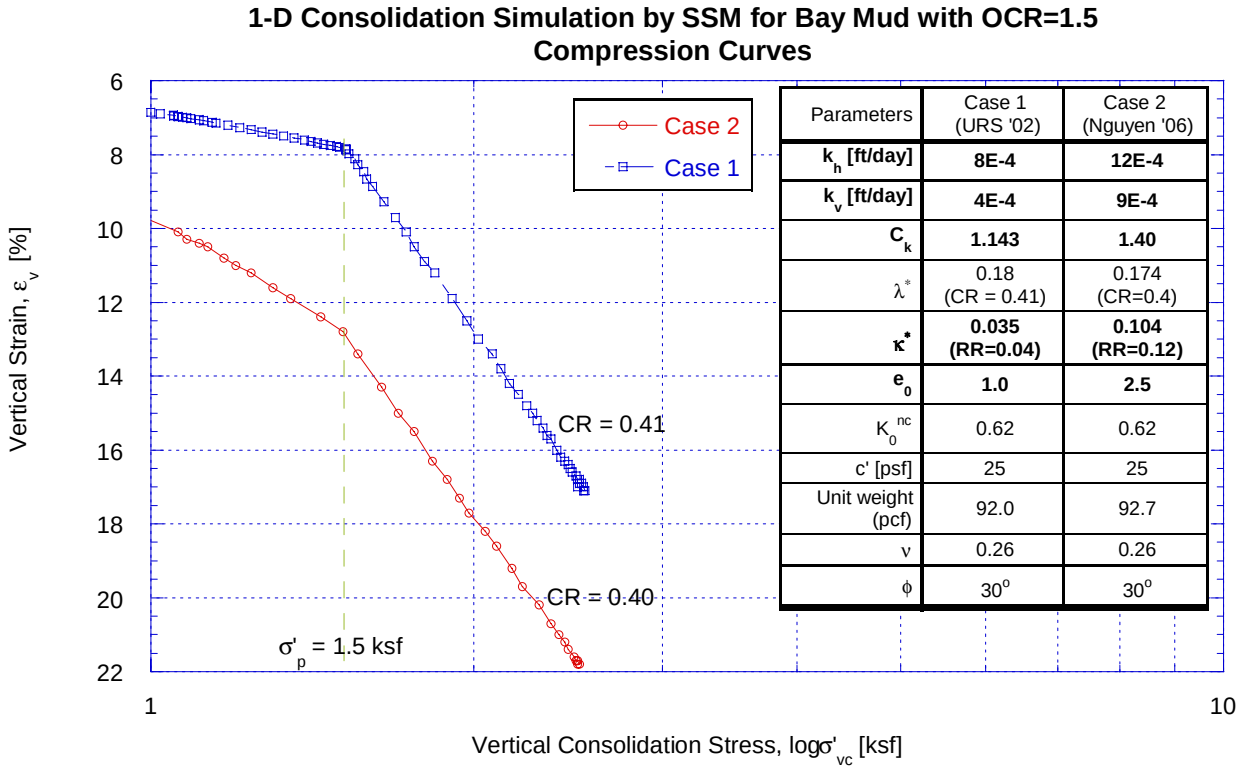

Parameters	Case 1 (URS '02)	Case 2 (Nguyen '06)
k_h [ft/day]	**8E-4**	**12E-4**
k_v [ft/day]	**4E-4**	**9E-4**
C_k	**1.143**	**1.40**
λ^*	0.18 (CR = 0.41)	0.174 (CR=0.4)
κ^*	**0.035 (RR=0.04)**	**0.104 (RR=0.12)**
e_0	**1.0**	**2.5**
K_0^{nc}	0.62	0.62
c' [psf]	25	25
Unit weight (pcf)	92.0	92.7
ν	0.26	0.26
ϕ	30^o	30^o

Figure 3.14a Stress-Strain Log Scale, 1-D Consolidation Model Test on Bay Mud SSM

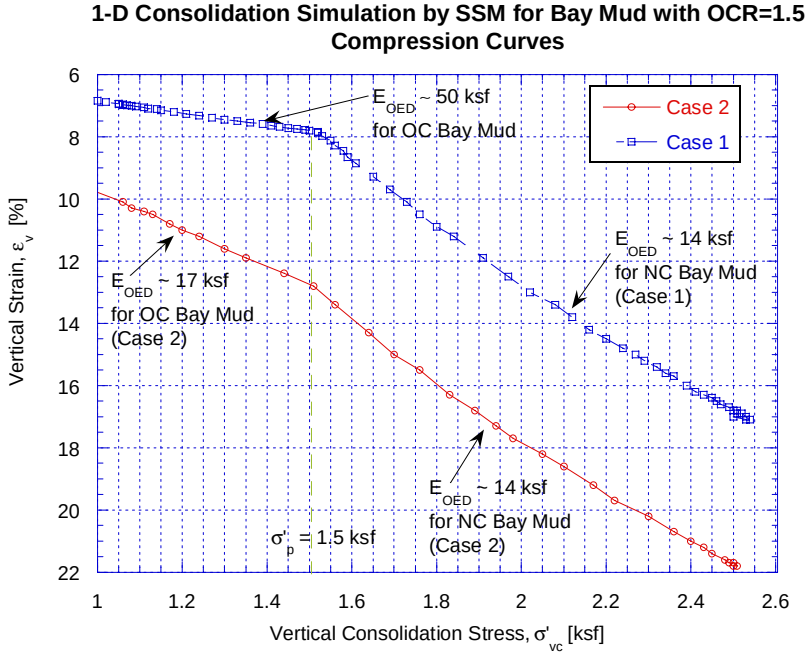

Parameters	Case 1 (URS '02)	Case 2 (Nguyen '06)
k_h [ft/day]	**8E-4**	**12E-4**
k_v [ft/day]	**4E-4**	**9E-4**
C_k	**1.143**	**1.40**
λ^*	0.18 (CR = 0.41)	0.174 (CR=0.4)
κ^*	**0.035 (RR=0.04)**	**0.104 (RR=0.12)**
e_0	**1.0**	**2.5**
K_0^{nc}	0.62	0.62
c' [psf]	25	25
Unit weight (pcf)	92.0	92.7
ν	0.26	0.26
ϕ	30^o	30^o

Figure 3.14b Stress-Strain Natural Scale, 1-D Consolidation Model Test on Bay Mud SSM

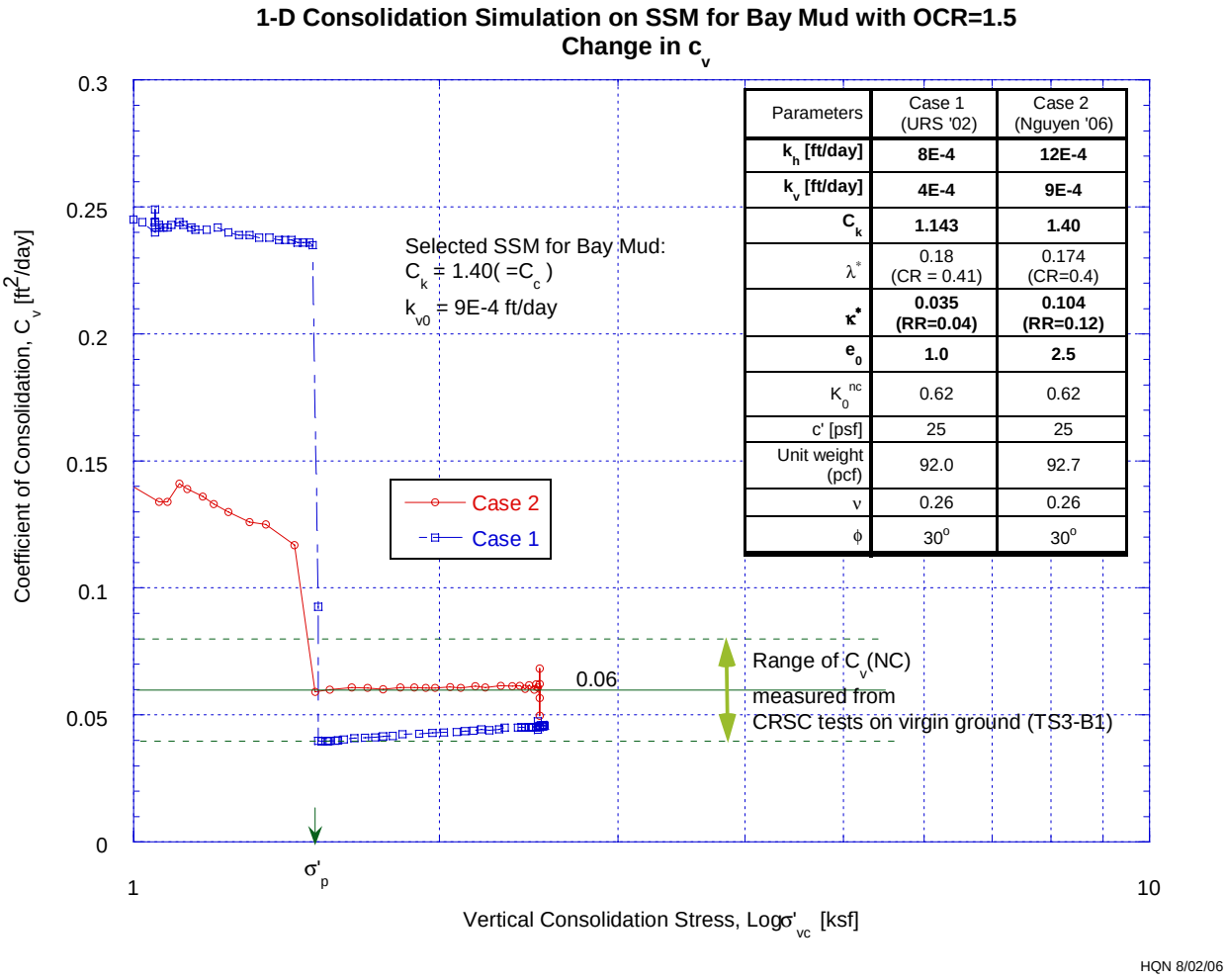

Parameters	Case 1 (URS '02)	Case 2 (Nguyen '06)
k_h [ft/day]	**8E-4**	**12E-4**
k_v [ft/day]	**4E-4**	**9E-4**
C_k	**1.143**	**1.40**
λ^*	0.18 (CR = 0.41)	0.174 (CR=0.4)
κ^*	**0.035 (RR=0.04)**	**0.104 (RR=0.12)**
e_0	**1.0**	**2.5**
K_0^{nc}	0.62	0.62
c' [psf]	25	25
Unit weight (pcf)	92.0	92.7
ν	0.26	0.26
ϕ	30^o	30^o

Figure 3.14c Coefficient of Consolidation, 1-D Consolidation Model Test on Bay Mud SSM

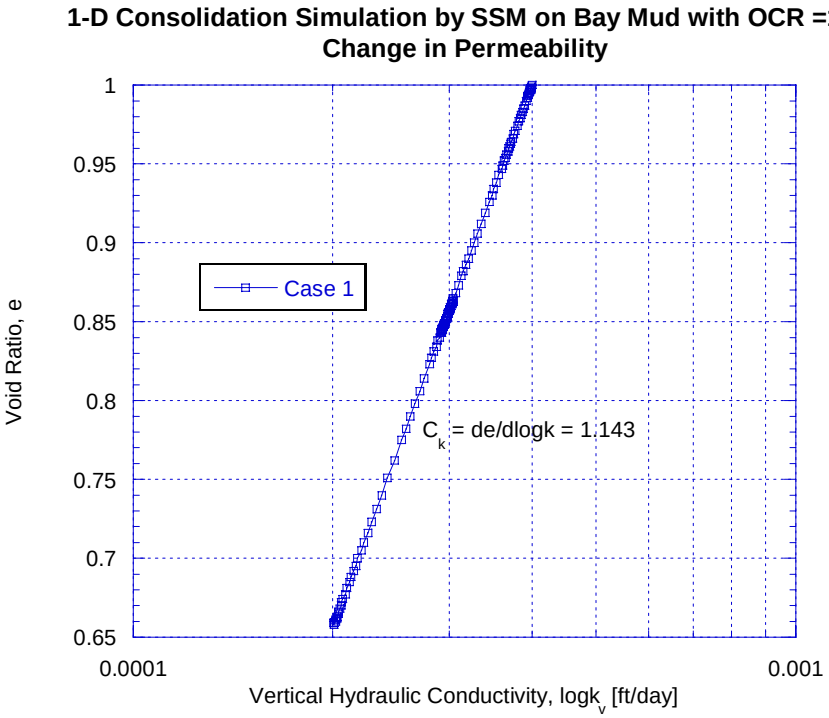

Figure 3.14d Change in Permeability, Case 1 1-D Consolidation Model Test on Bay Mud SSM

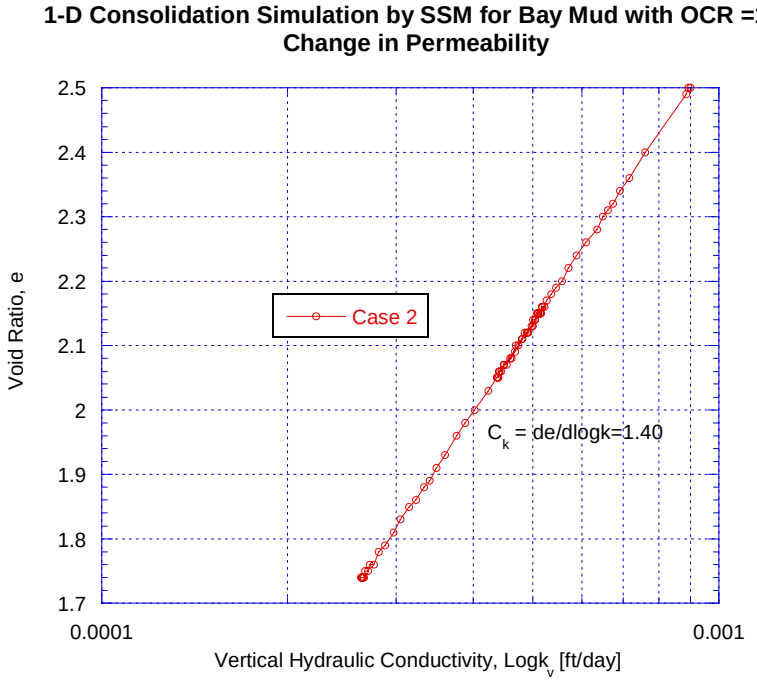

Figure 3.14e Change in Permeability, Case 2 1-D Consolidation Model Test on Bay Mud SSM

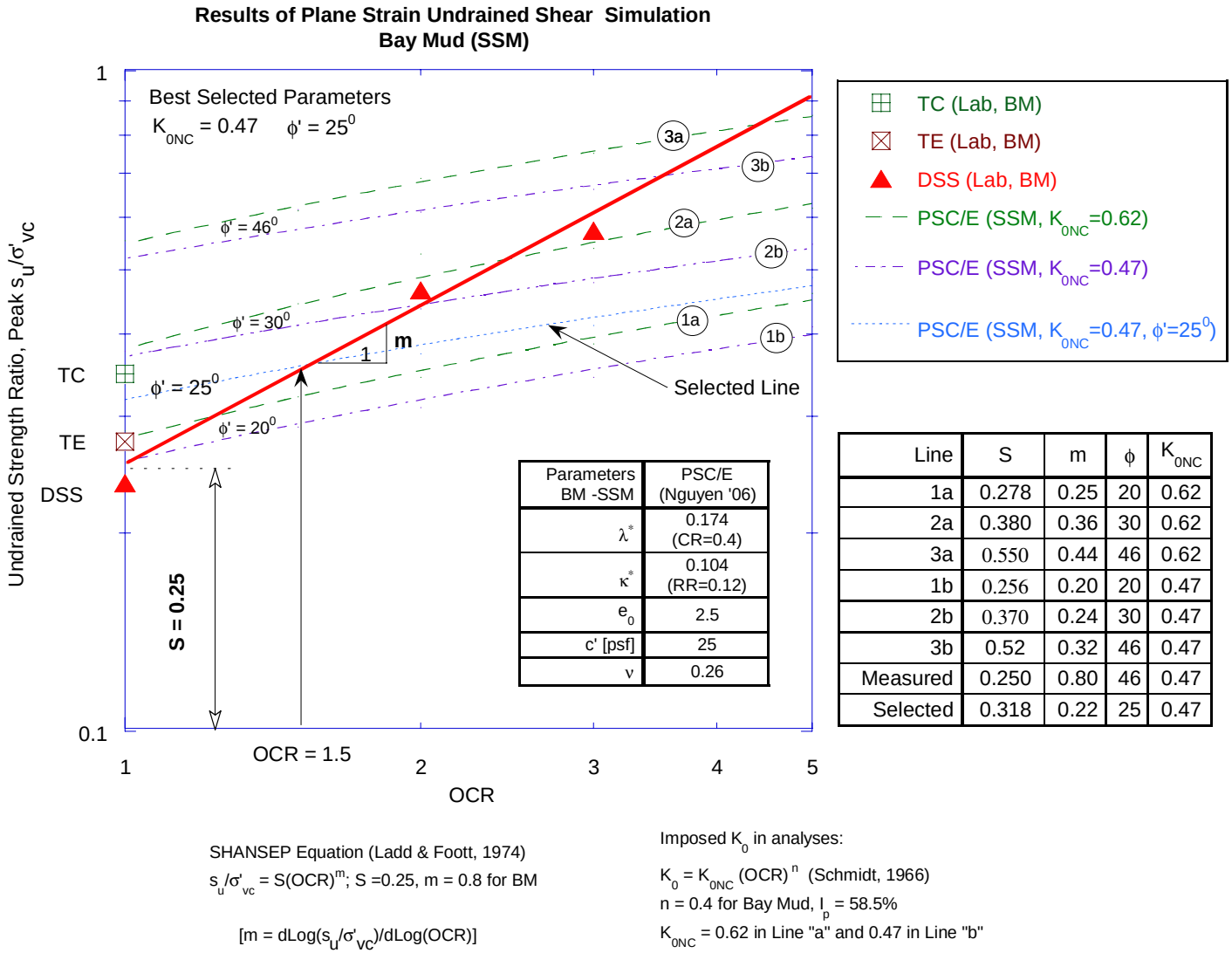

Parameters BM -SSM	PSC/E (Nguyen '06)
λ^*	0.174 (CR=0.4)
κ^*	0.104 (RR=0.12)
e_0	2.5
c' [psf]	25
ν	0.26

Line	S	m	ϕ	K_{0NC}
1a	0.278	0.25	20	0.62
2a	0.380	0.36	30	0.62
3a	0.550	0.44	46	0.62
1b	0.256	0.20	20	0.47
2b	0.370	0.24	30	0.47
3b	0.52	0.32	46	0.47
Measured	0.250	0.80	46	0.47
Selected	0.318	0.22	25	0.47

SHANSEP Equation (Ladd & Foott, 1974)

$s_u/\sigma'_{vc} = S(OCR)^m$; S =0.25, m = 0.8 for BM

[$m = dLog(s_u/\sigma'_{vc})/dLog(OCR)$]

Imposed K_0 in analyses:

$K_0 = K_{0NC}\,(OCR)^n$ (Schmidt, 1966)

n = 0.4 for Bay Mud, I_p = 58.5%

K_{0NC} = 0.62 in Line "a" and 0.47 in Line "b"

Figure 3.15 Undrained Shear Strength Ratio vs. OCR, CK_0U PSC/E Tests Simulation with SSM for Bay Mud

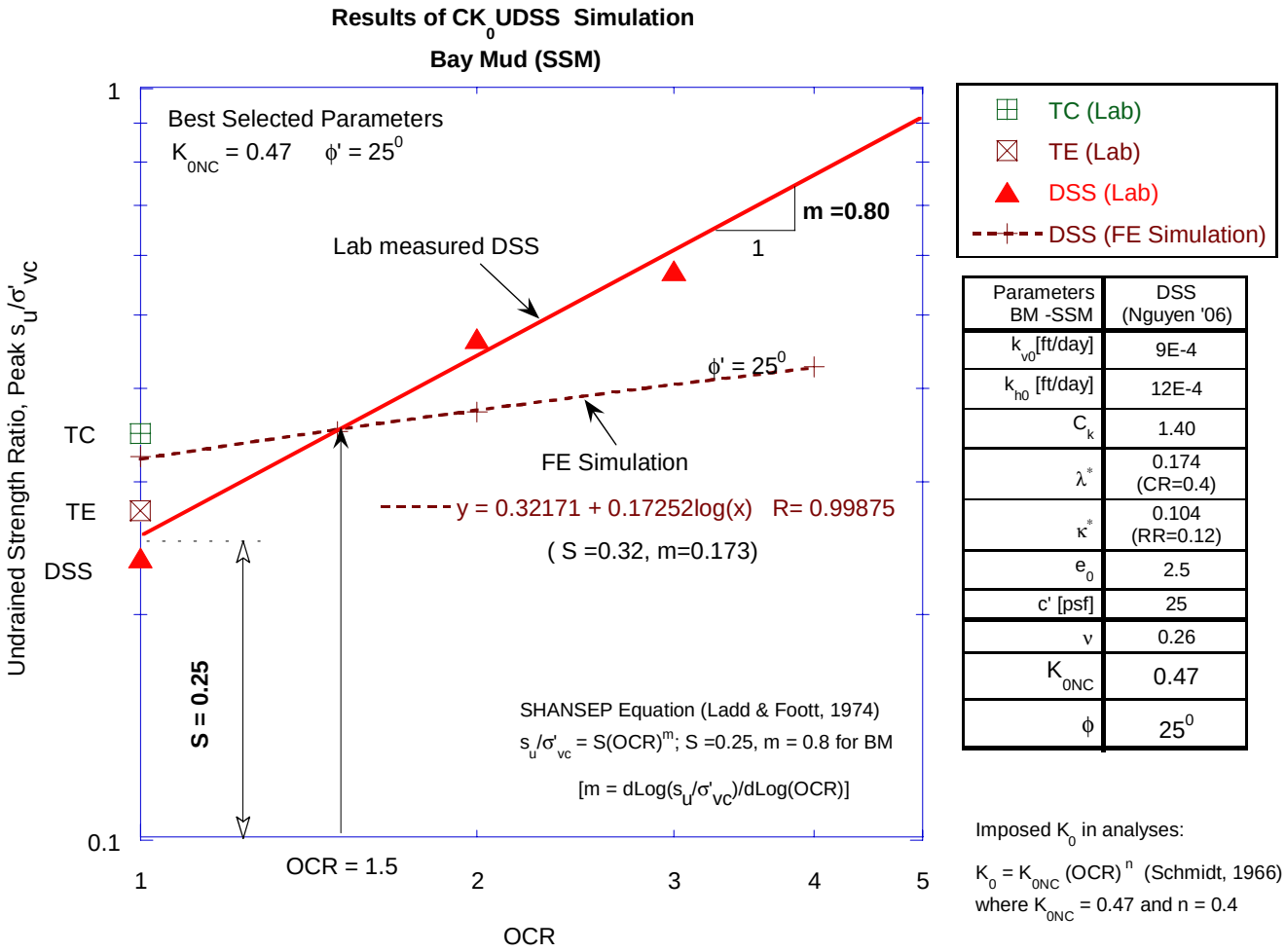

Parameters BM -SSM	DSS (Nguyen '06)
k_{v0} [ft/day]	9E-4
k_{h0} [ft/day]	12E-4
C_k	1.40
λ^*	0.174 (CR=0.4)
κ^*	0.104 (RR=0.12)
e_0	2.5
c' [psf]	25
ν	0.26
K_{0NC}	0.47
ϕ	25^0

Imposed K_0 in analyses:

$K_0 = K_{0NC} (OCR)^n$ (Schmidt, 1966)
where $K_{0NC} = 0.47$ and $n = 0.4$

Figure 3.16 Undrained Strength Ratio vs. OCR, DSS Simulation for Bay Mud (SSM), $\kappa^* = 0.104$ and 0.002

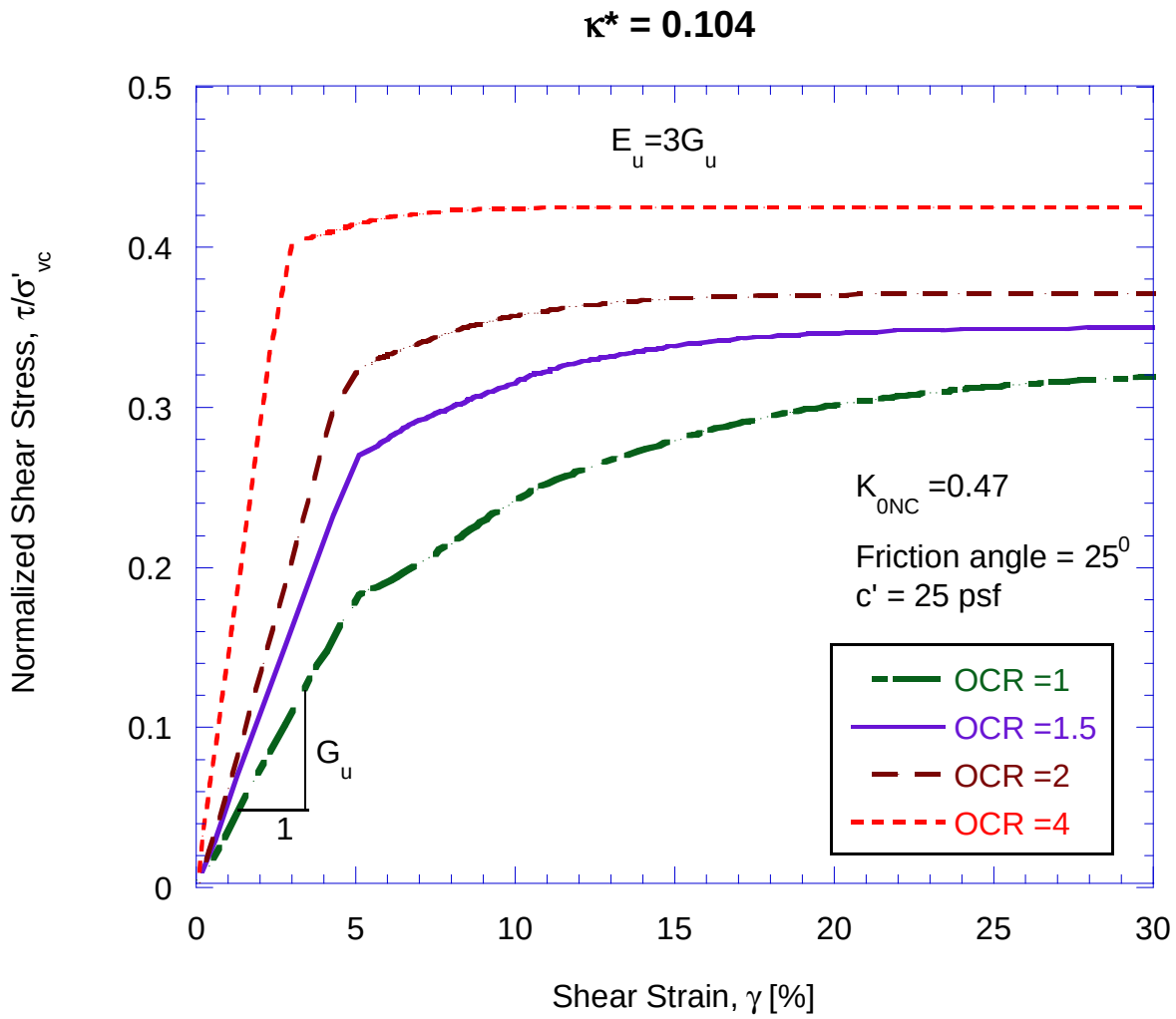

Figure 3.17a Normalized Undrained Shear Stress vs. Shear Strain, DSS Simulation on Bay Mud (SSM), κ*=0.104

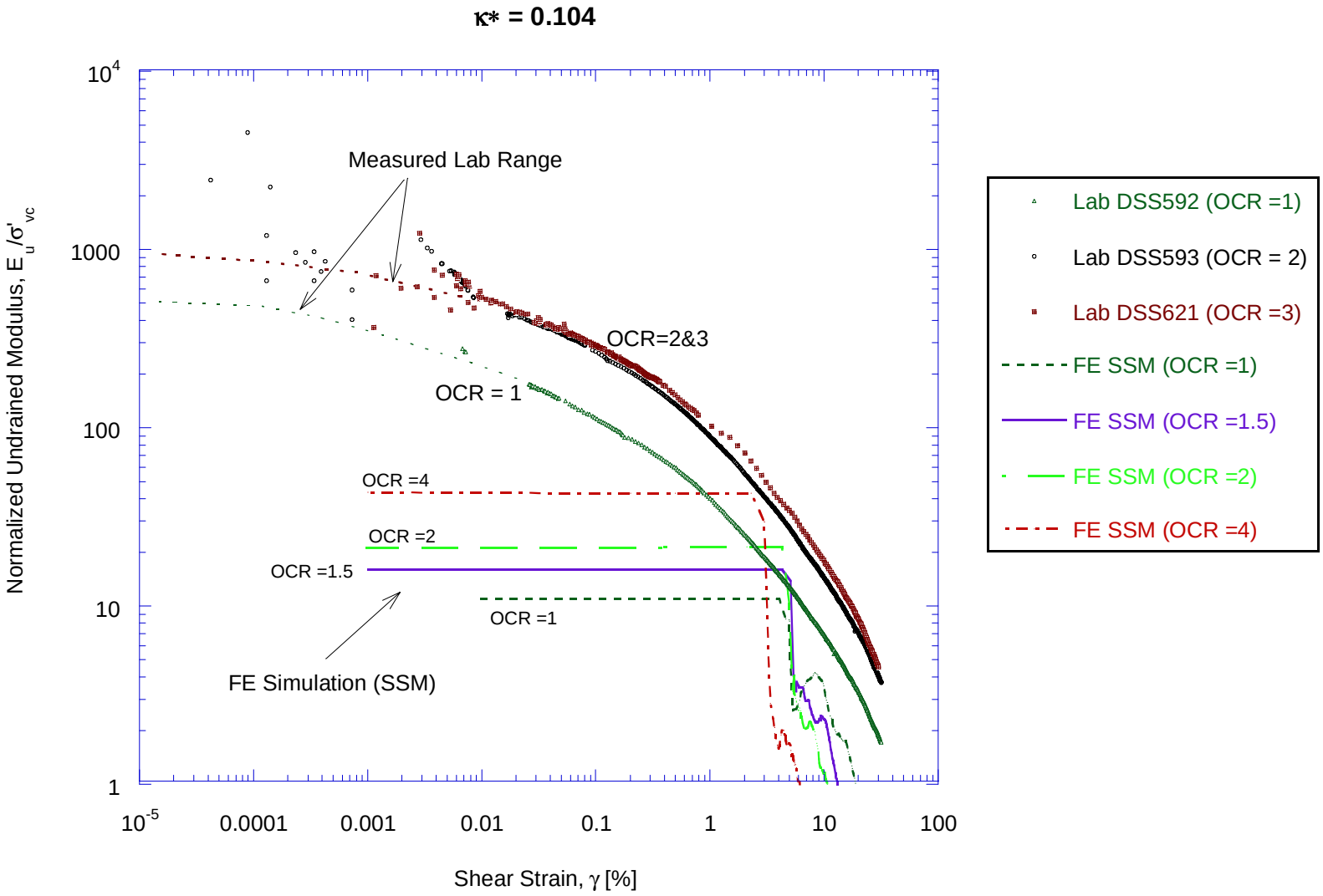

Figure 3.17b Normalized Undrained Modulus vs. Shear Strain, DSS Simulation on Bay Mud (SSM), κ*=0.104

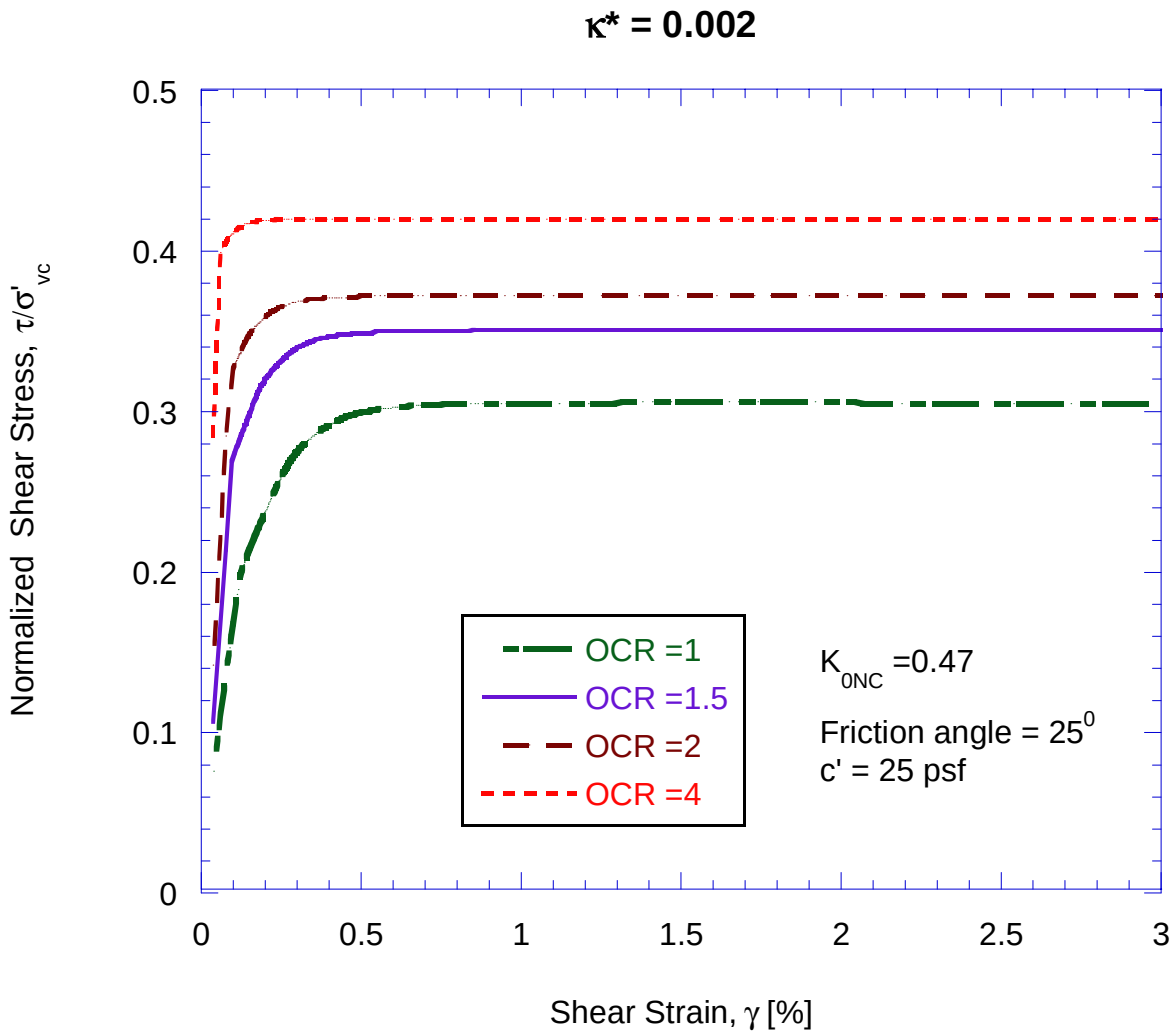

Figure 3.18a Normalized Undrained Shear Stress vs. Shear Strain, DSS Simulation on Bay Mud (SSM), κ*=0.002

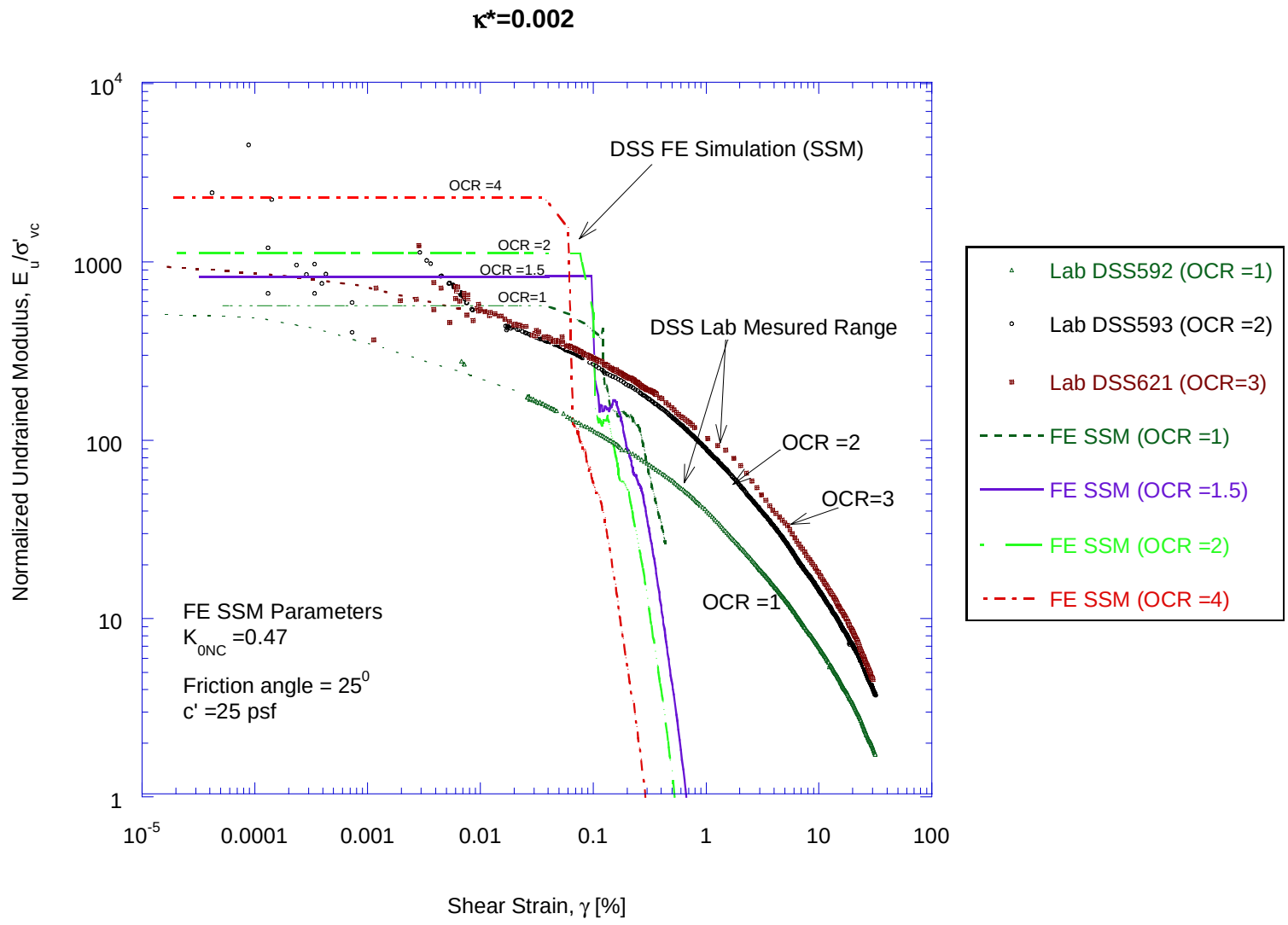

Figure 3.18b Normalized Undrained Modulus vs. Shear Strain, DSS Simulations on Bay Mud (SSM), κ*=0.002

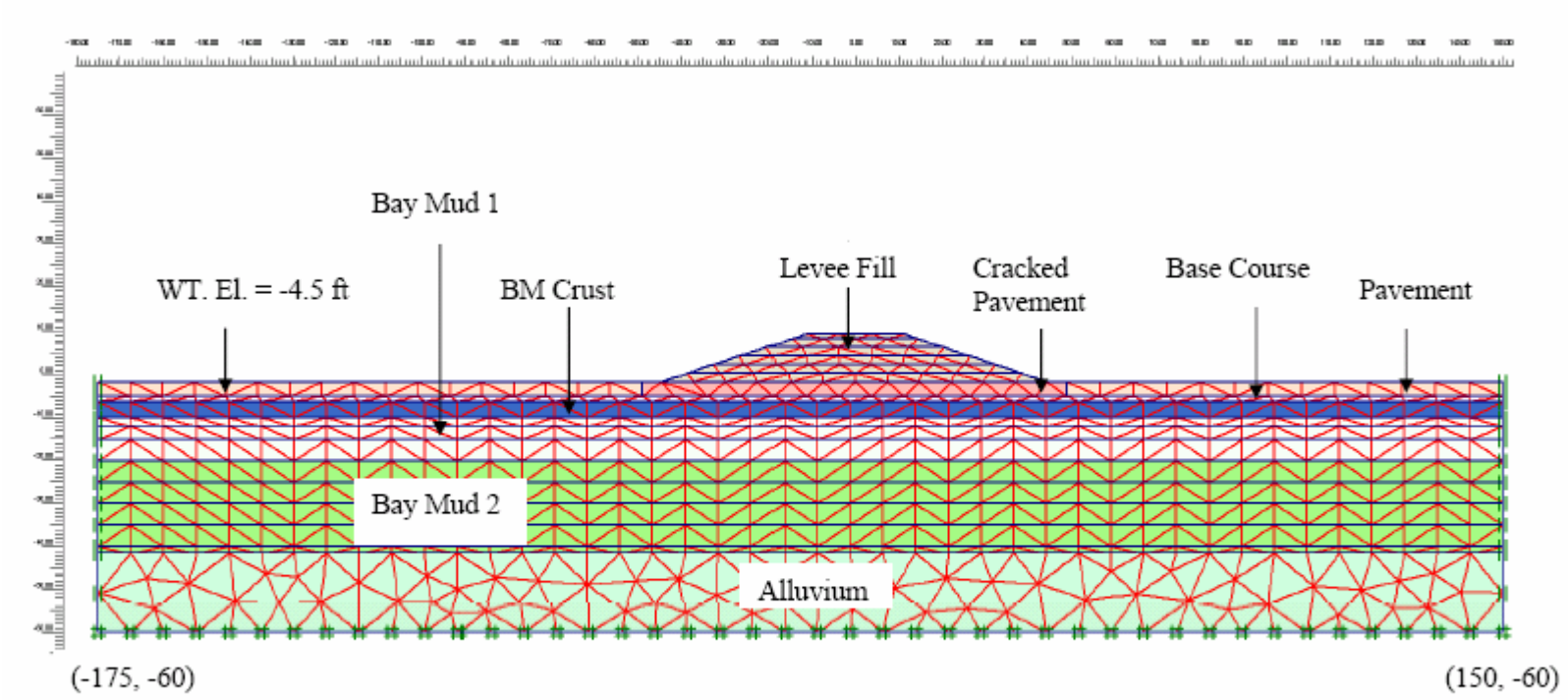

Note: - Cracked pavement under the NHPL and extended 4.5 ft from the toe except for Case A1 with a continuous pavement;
- Levee Crest El. = 9.4 ft;
- Pavement EL. = -1.6 ft.

Figure 3.19 Geometry of NHP Levee Model with FE Mesh and Soil Materials for Cracked Pavement

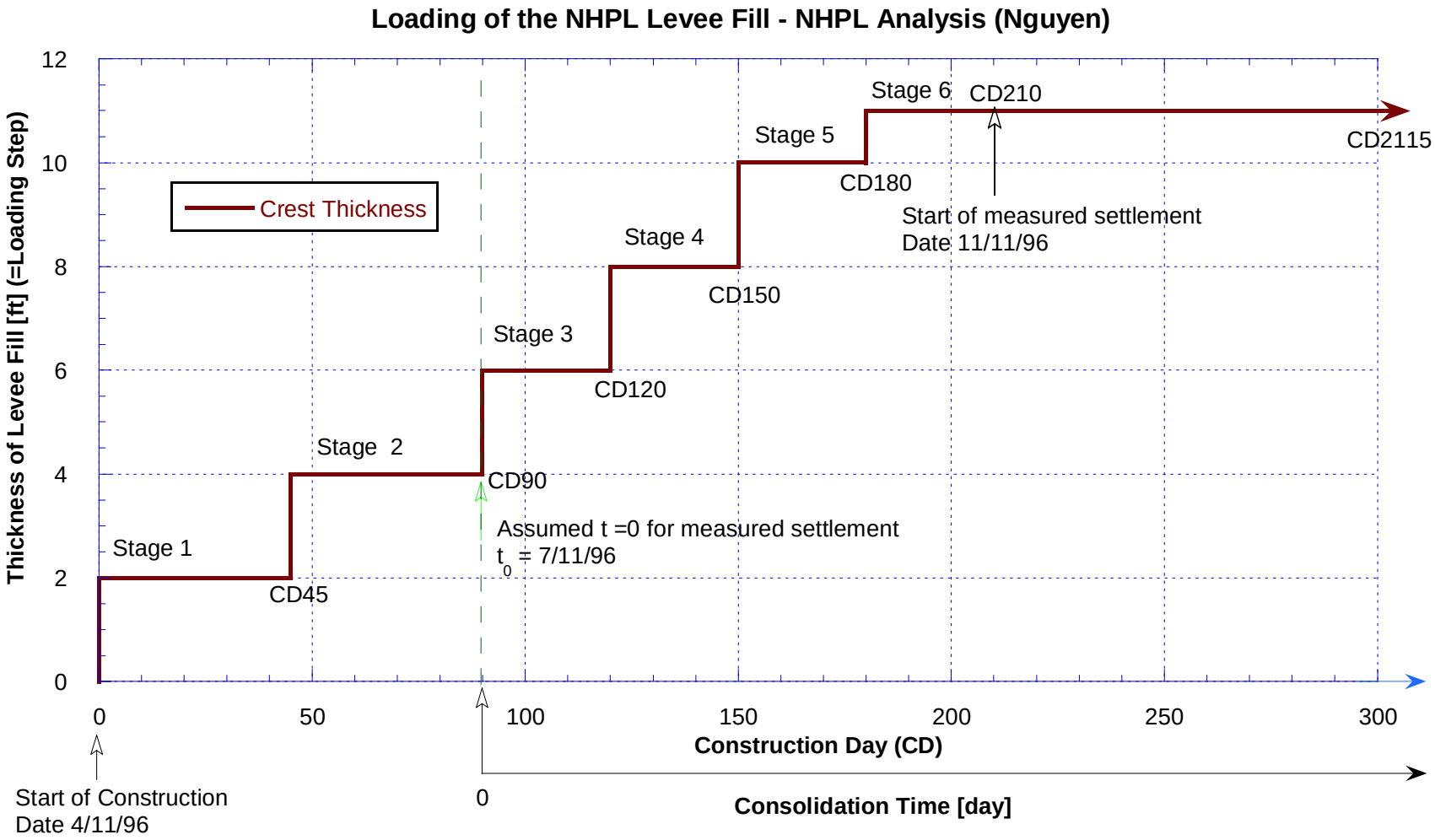

Figure 3.20 Staged Construction Modeling of NHP Levee

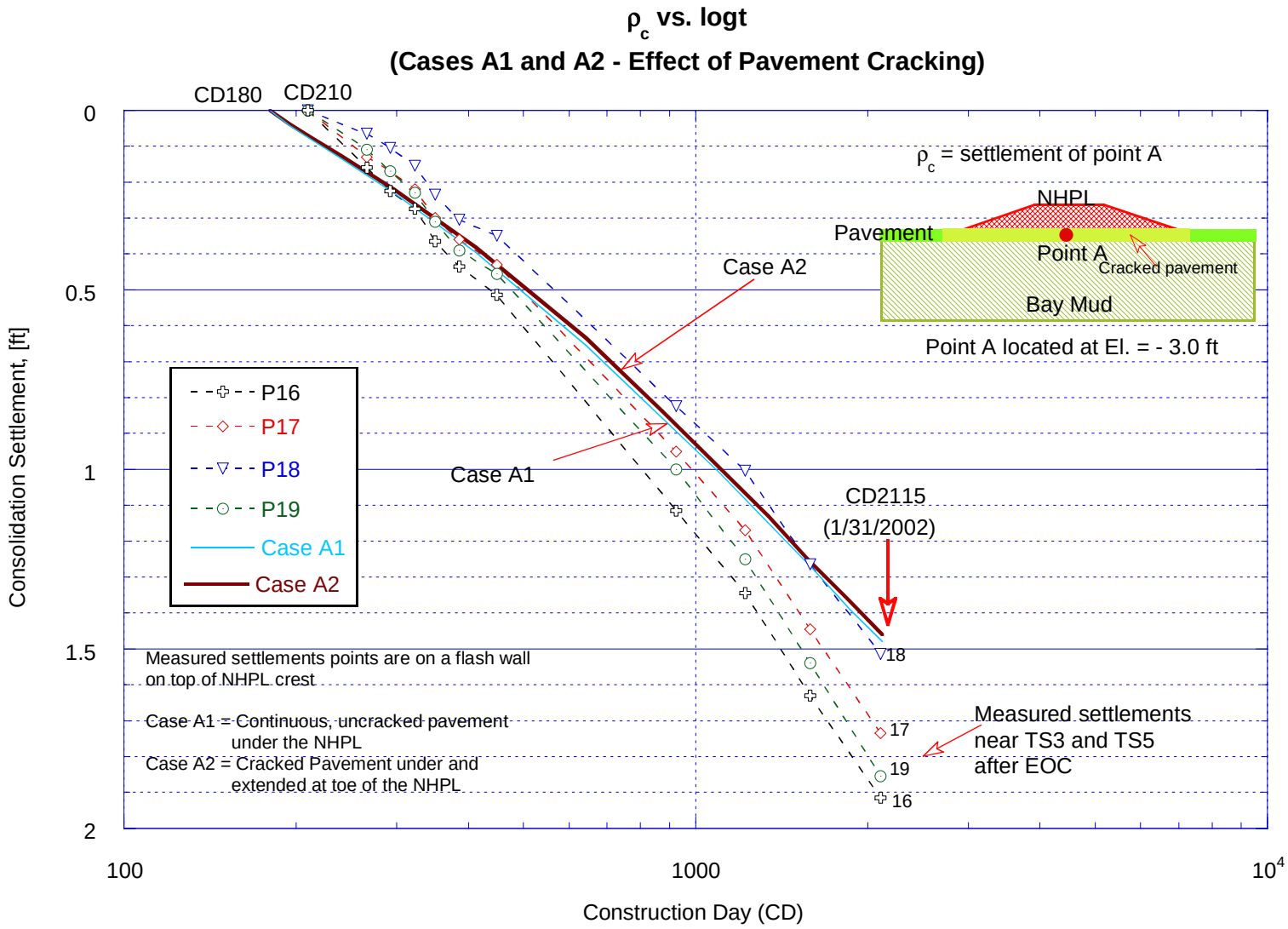

Figure 3.21a Predicted and Measured Consolidation Settlements of NHPL for Cases A1 and A2 Analyses: Effect of Pavement Cracking

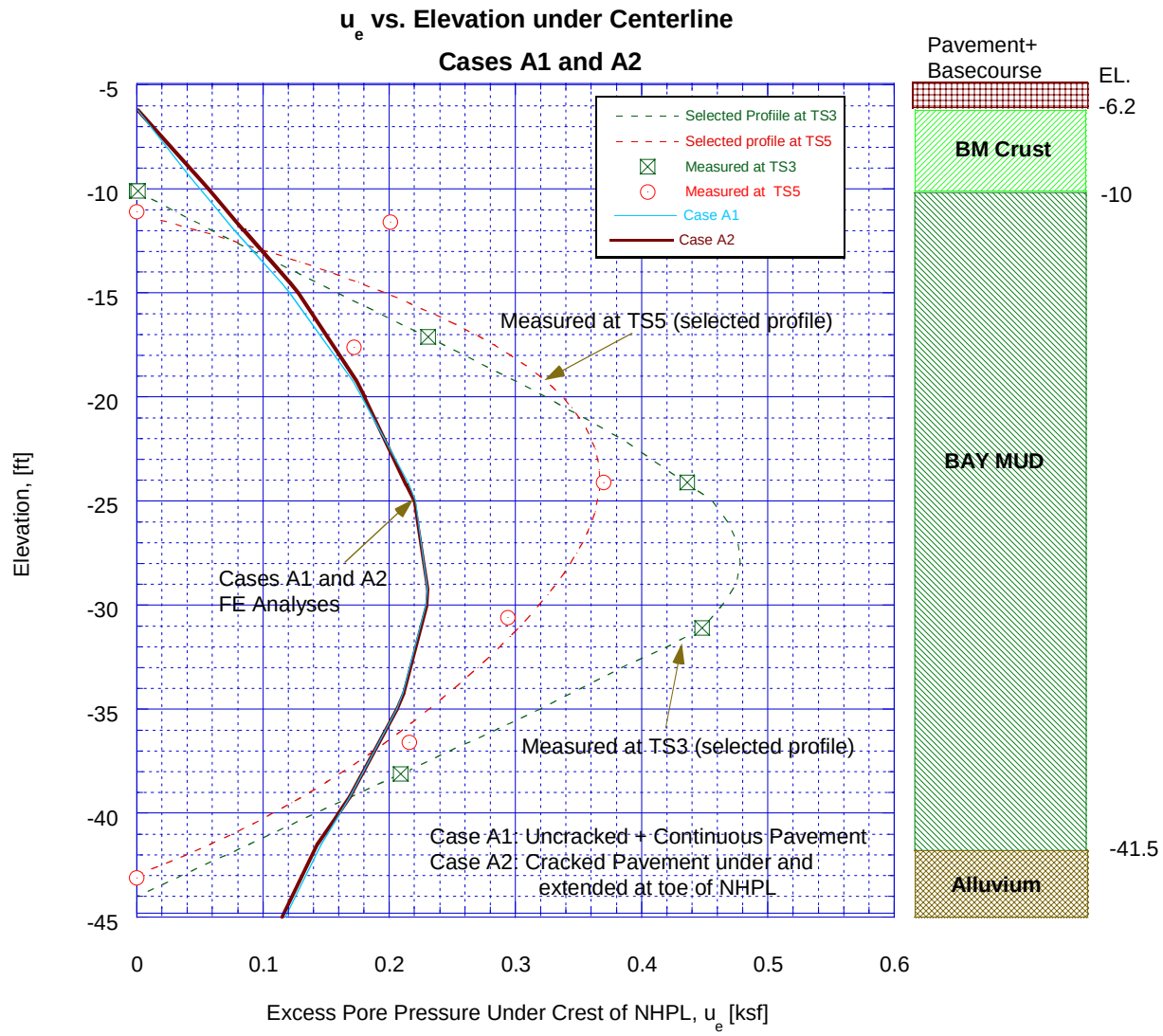

Figure 3.21b Predicted and Measured Excess Pore Pressure at Feb., 2002 under Centerline for Cases A1 and A2 Analyses: Effect of Pavement Cracking

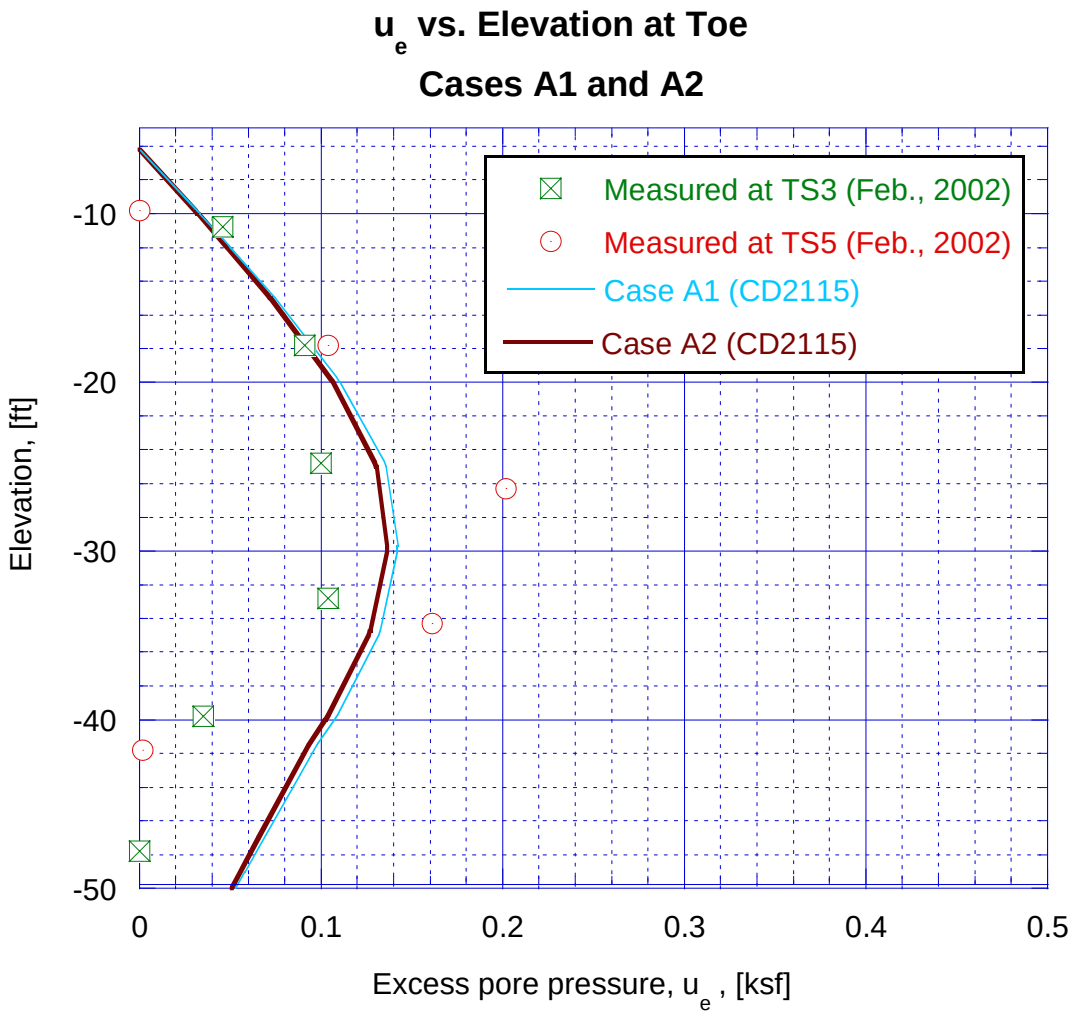

Figure 3.21c Predicted and Measured Excess Pore Pressure at Feb., 2002 under Toe for Cases A1 and A2 Analyses: Effect of Pavement Cracking

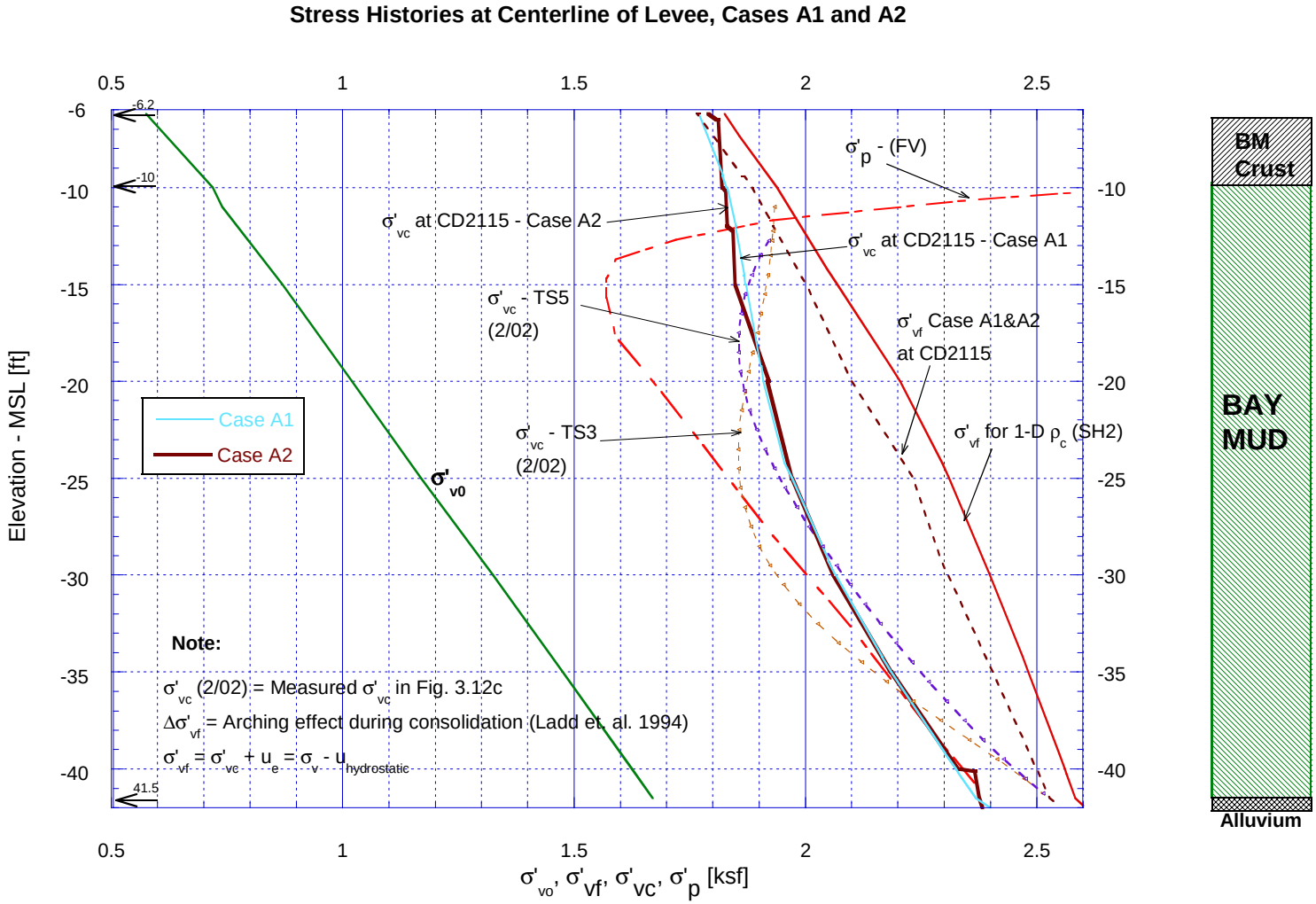

Figure 3.21d Comparison of Predicted and Measured Stress Histories under Centerline of NHPL at Feb. 2002 for Cases A1 and A2 Analyses: Effect of Pavement Cracking

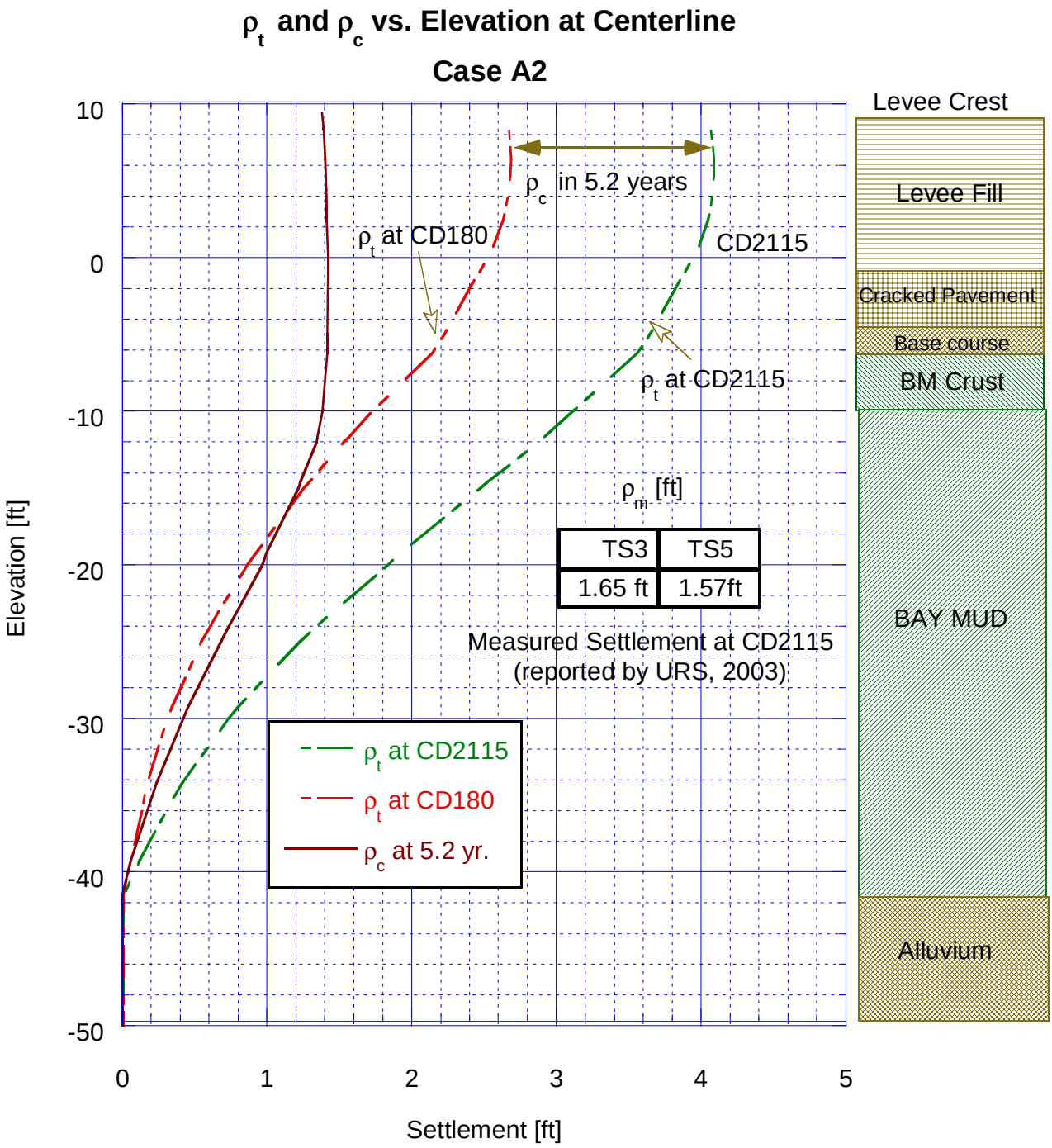

Figure 3.21e Predicted Total Settlement Profiles at CD180 and CD2115 under Centerline of the NHPL for Case A2 Analysis

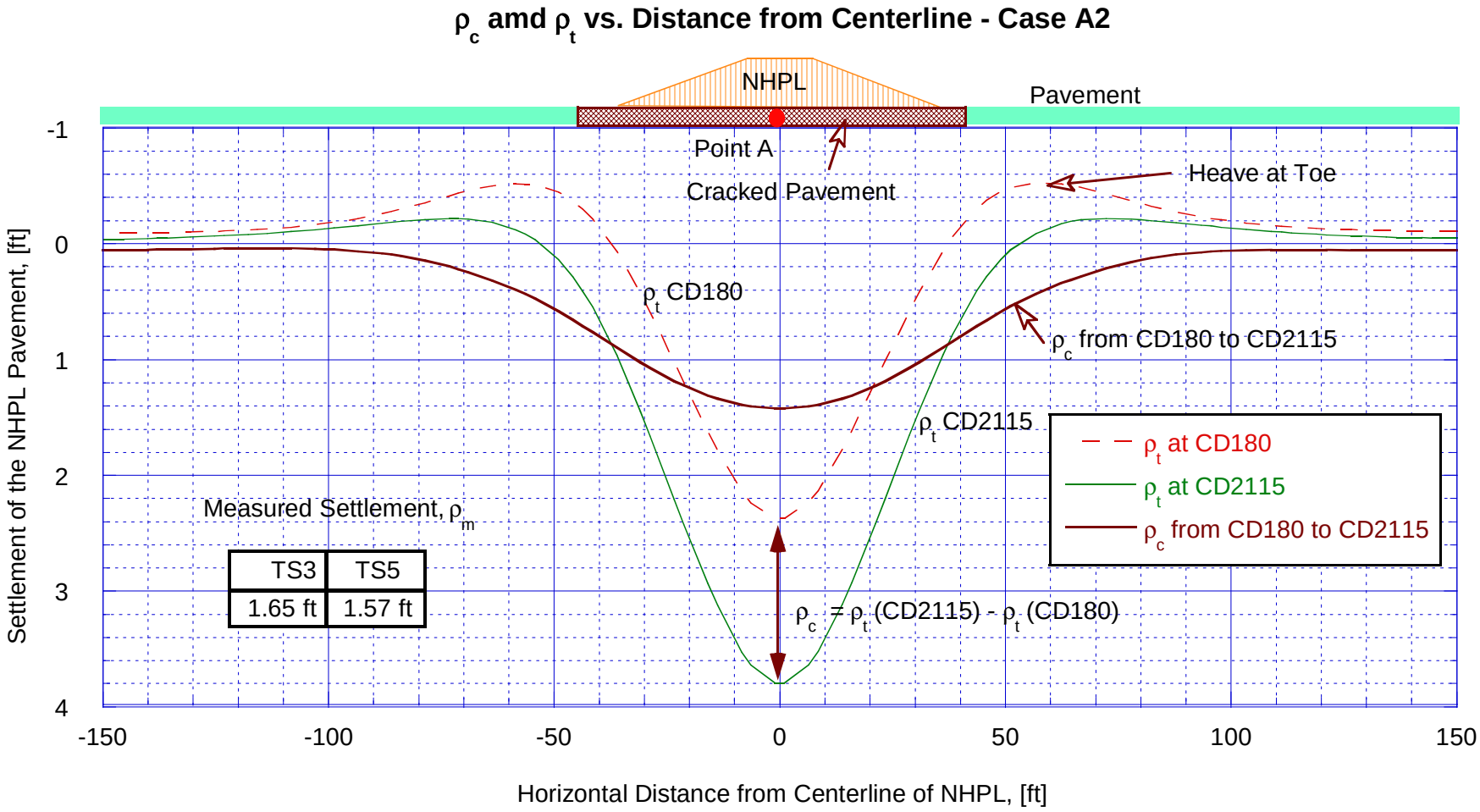

Figure 3.21f Predicted Settlement Profiles at CD180 and CD2115 of the Ground under the NHPL for Case A2 Analysis

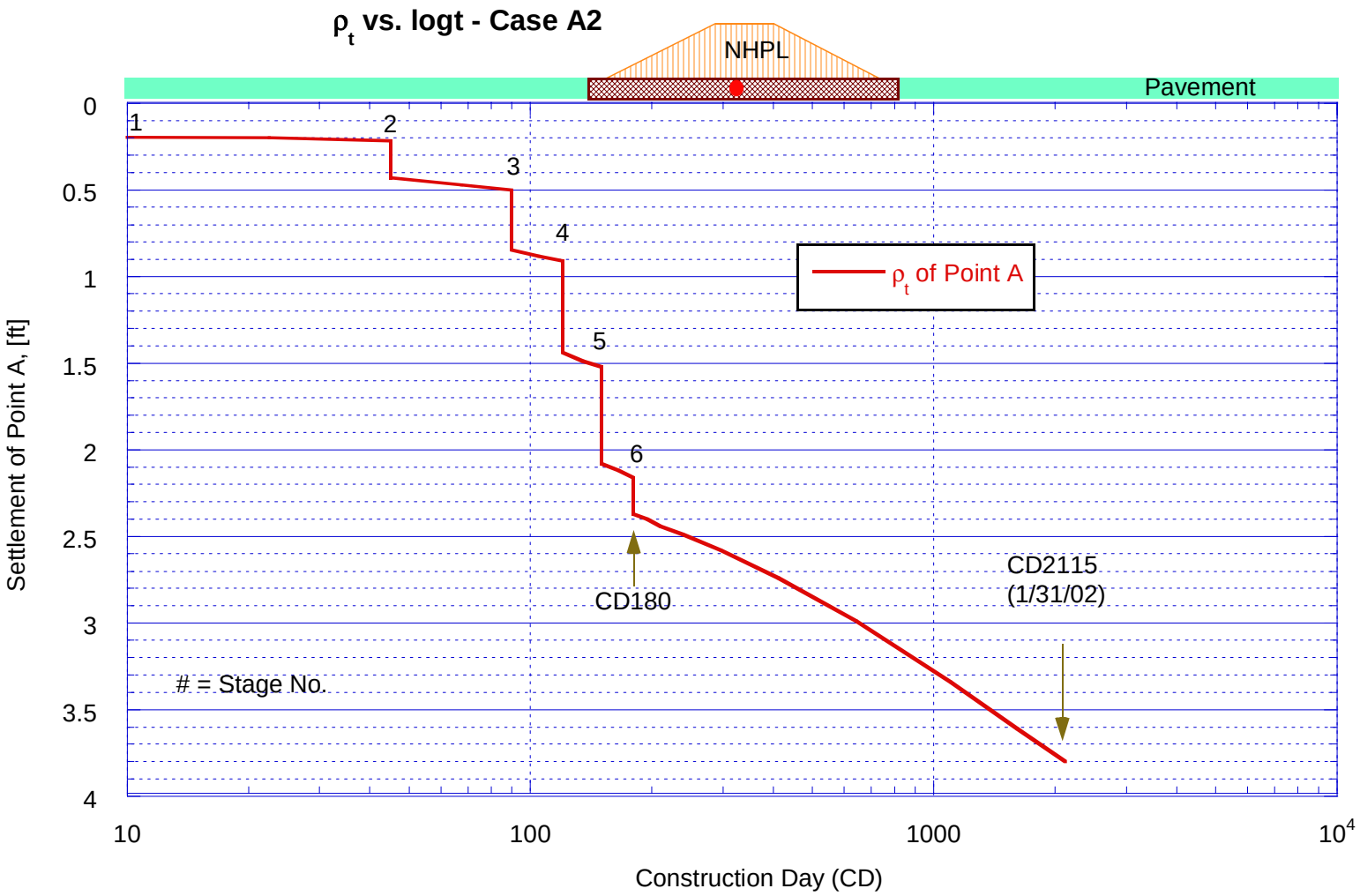

Figure 3.21g Predicted Settlement vs. logt for Case A2 Analysis

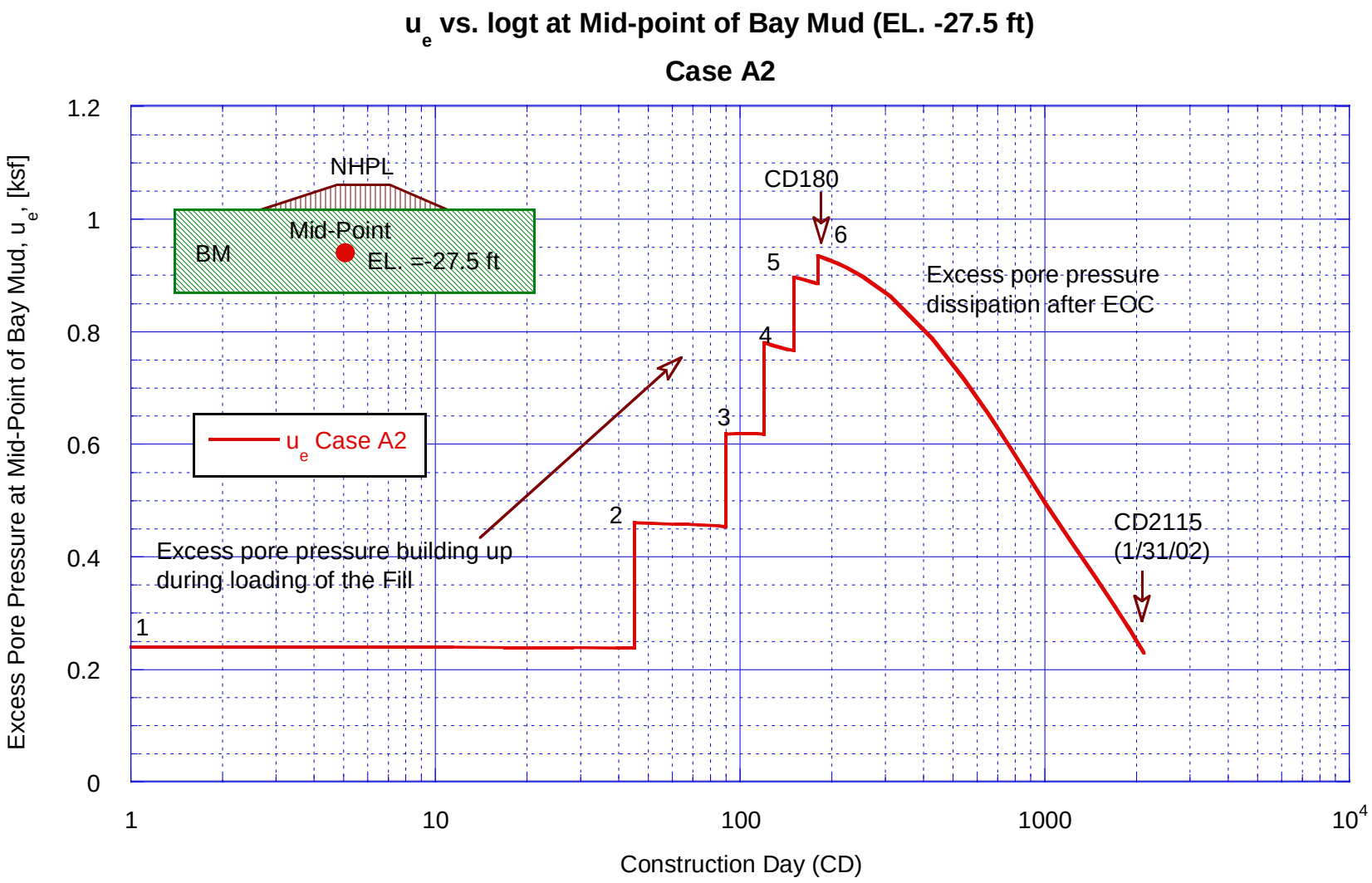

Figure 3.21h Predicted Excess Pore Pressure at Mid-point of Bay Mud vs. logt for Case A2 Analysis

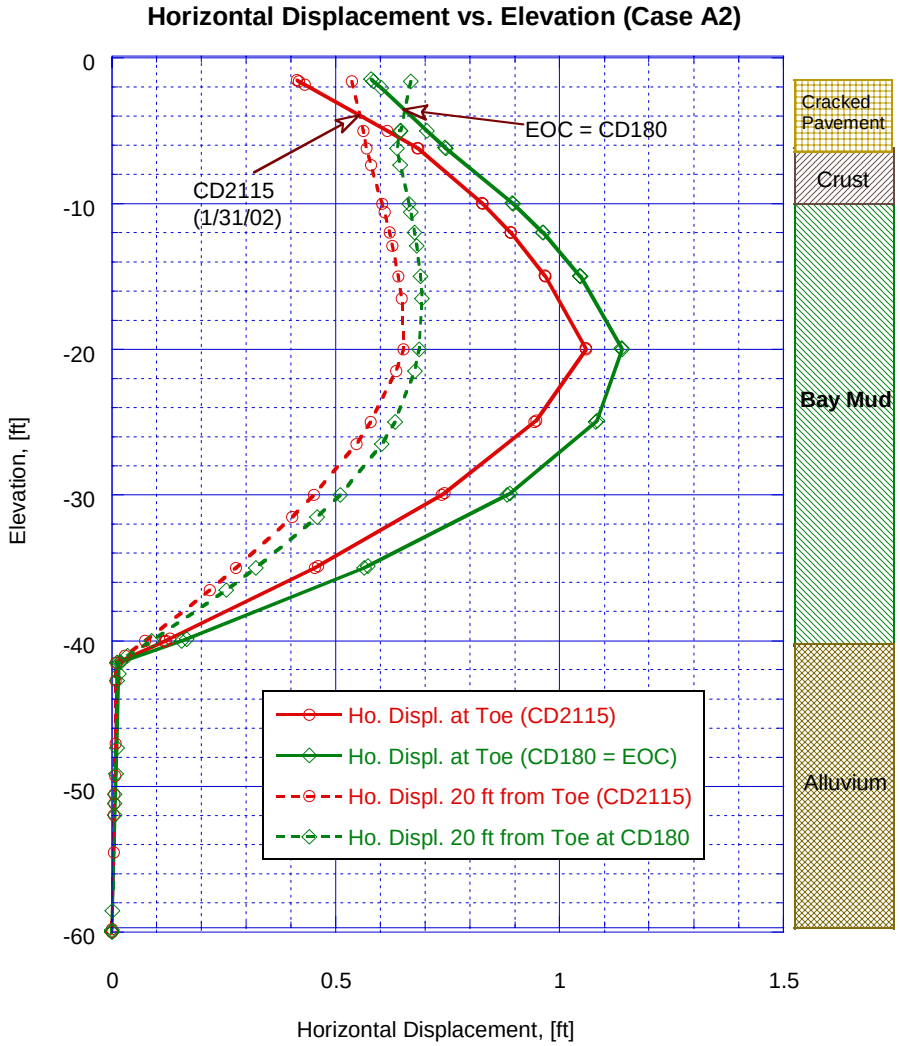

Figure 3.21i Horizontal Displacements at Toe of the NHPL for Case A2 Analysis

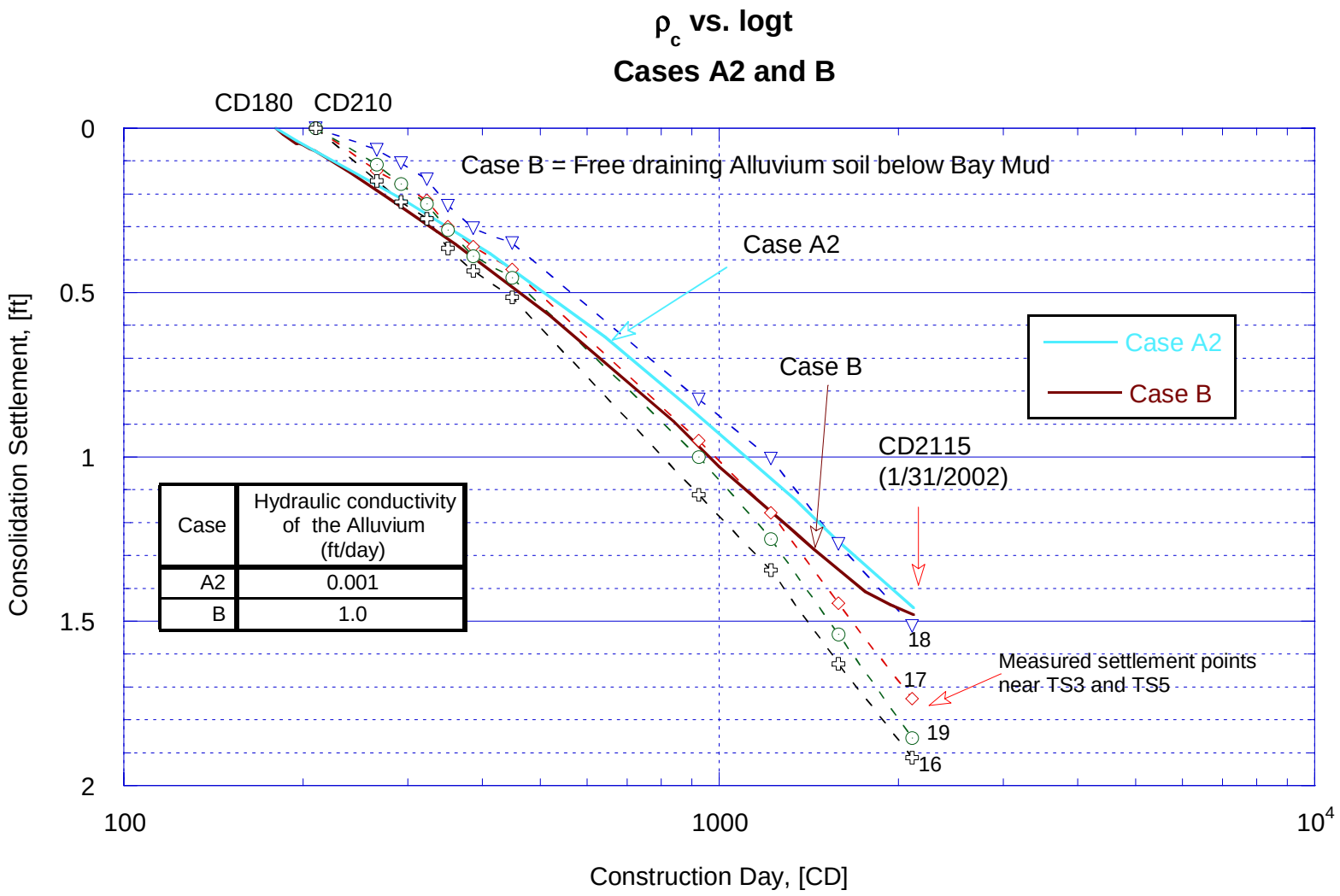

Figure 3.22a Predicted and Measured Consolidation Settlements of the NHPL for Cases A2 and B Analyses: Effect of Free Draining Alluvium

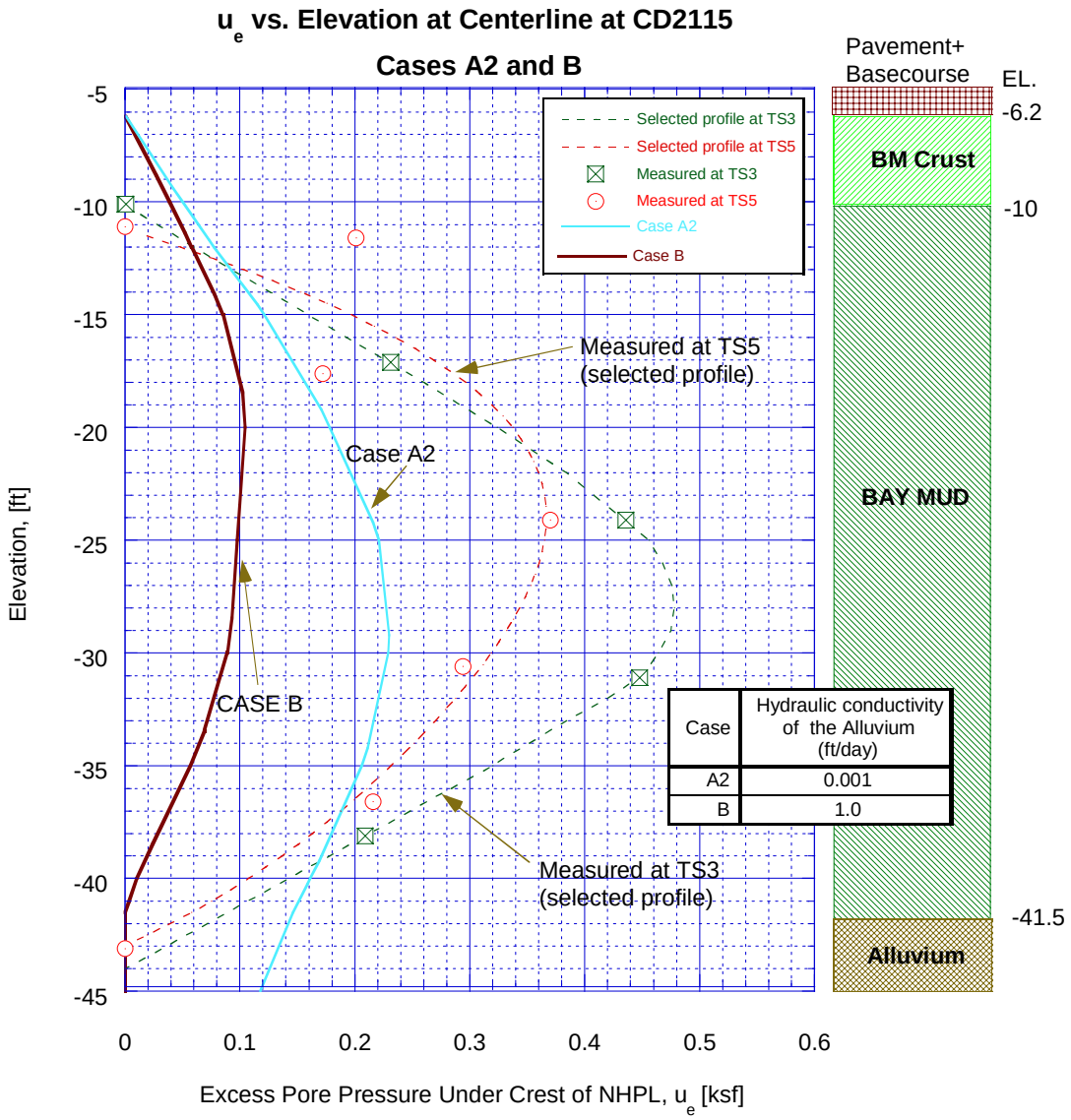

Figure 3.22b Predicted and Measured Excess Pore Pressure under Centerline of the NHPL at Feb. 2002 for Cases A2 and B Analyses: Effect of Free Draining at the Alluvium

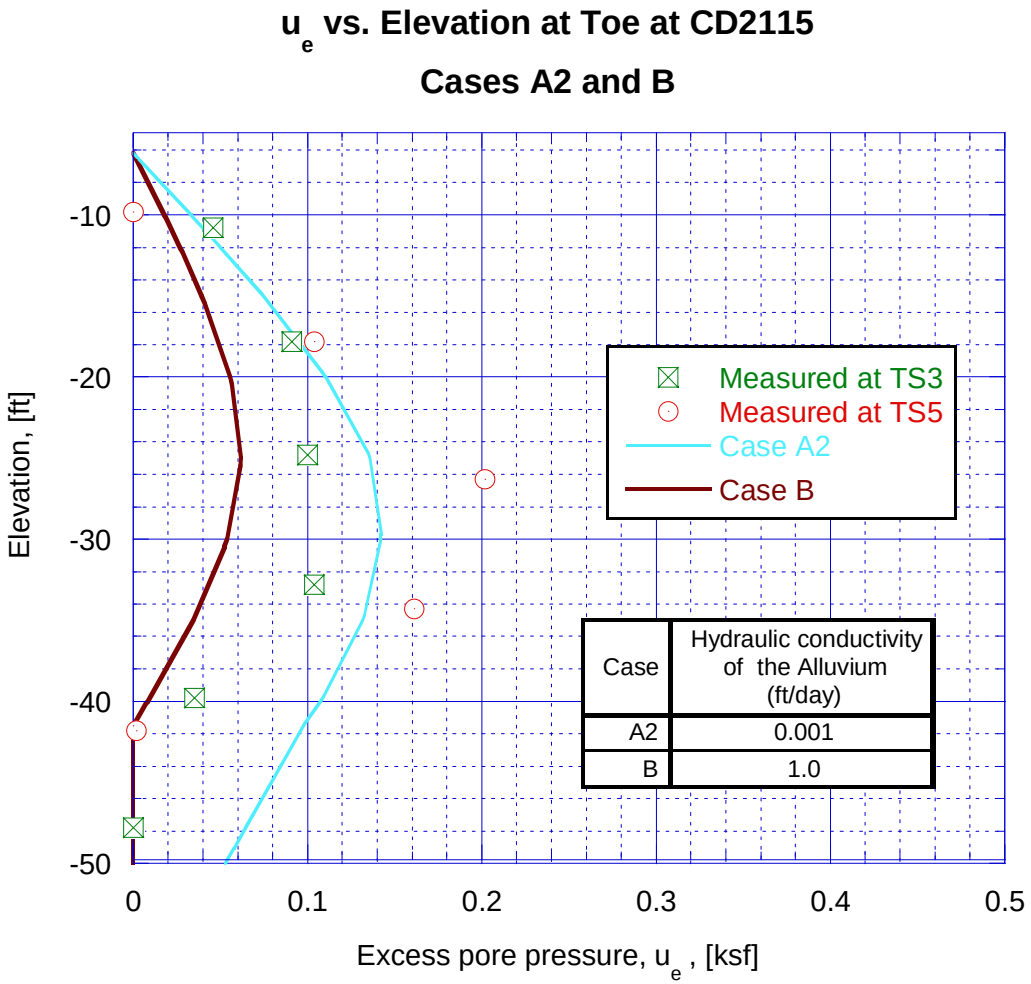

Figure 3.22c Predicted and Measured Excess Pore Pressure at Toe of the NHPL at Feb. 2002 for Cases A2 and B Analyses: Effect of Free Draining at the Alluvium

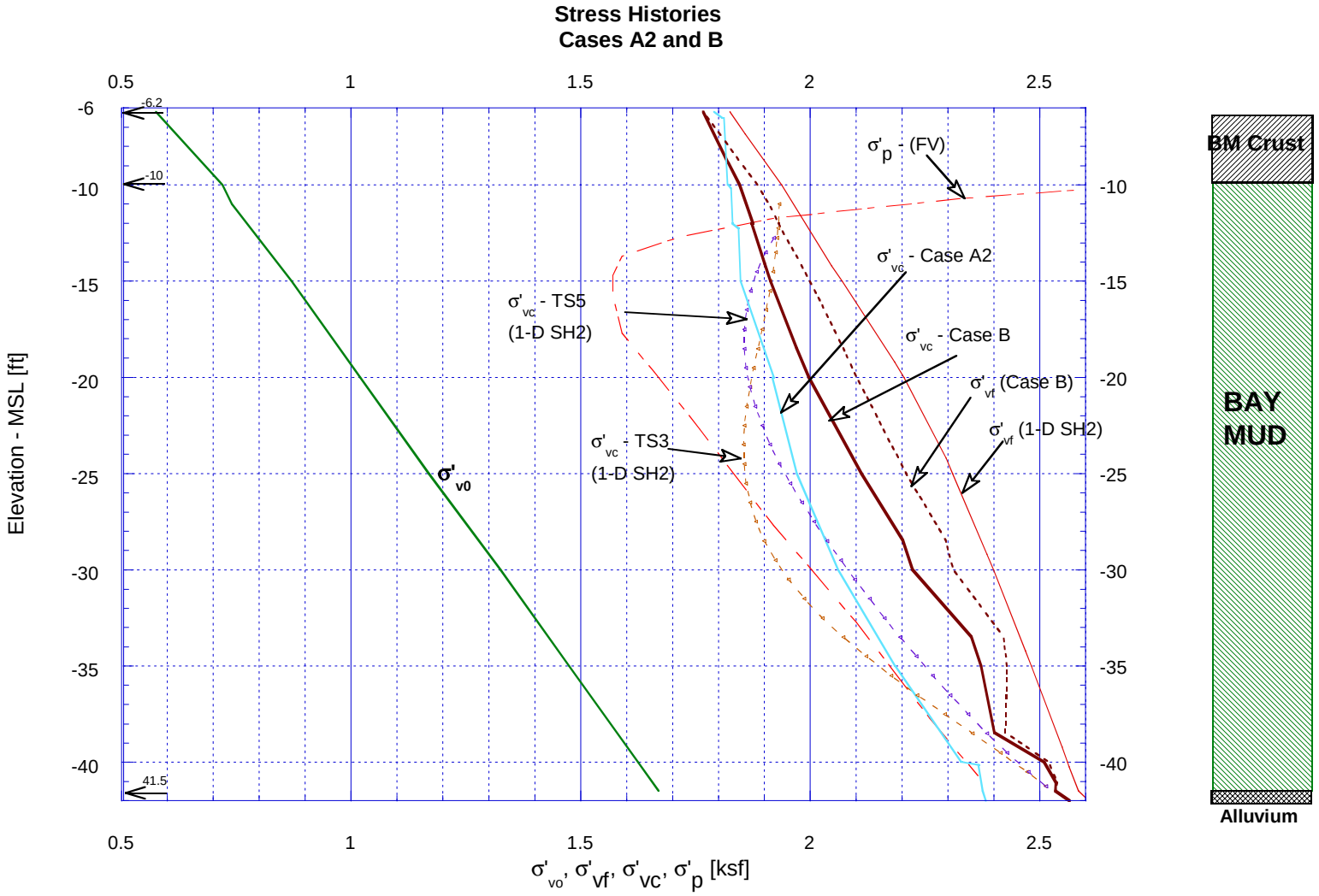

Figure 3.22d Comparison of Predicted and Measured Stress Histories under Centerline of the NHPL at Feb. 2002 for Cases A2 and B Analyses: Effect of Free Draining Alluvium

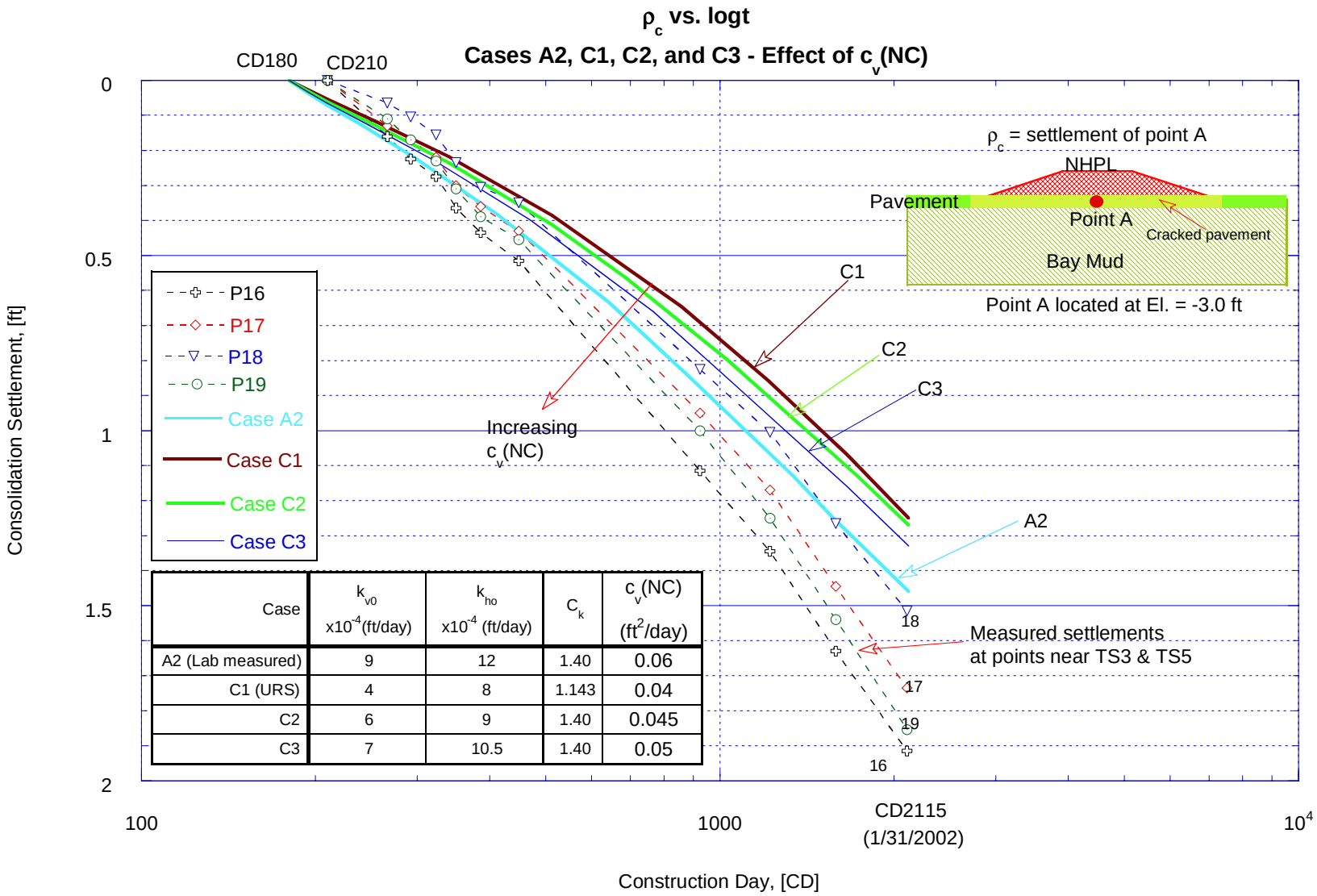

Case	k_{v0} x10^{-4}(ft/day)	k_{ho} x10^{-4} (ft/day)	C_k	c_v(NC) (ft^2/day)
A2 (Lab measured)	9	12	1.40	0.06
C1 (URS)	4	8	1.143	0.04
C2	6	9	1.40	0.045
C3	7	10.5	1.40	0.05

Figure 3.23a Predicted and Measured Consolidation Settlements of the NHPL for Cases A2, C1, C2, and C3 Analyses: Effect of c_v(NC) of Bay Mud

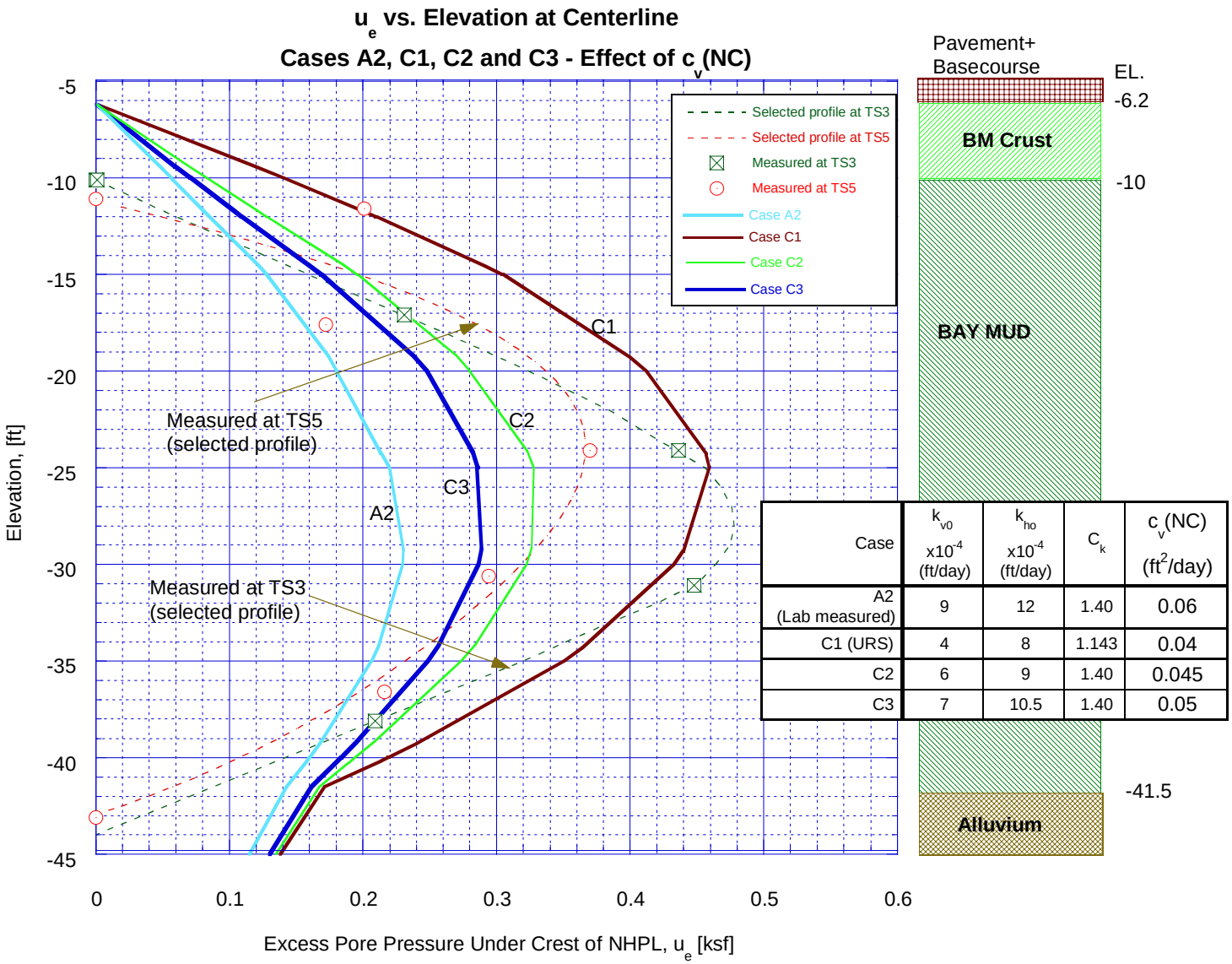

Figure 3.23b Predicted and Measured Excess Pore Pressure at Centerline of the NHPL for Cases A2, C1, C2 and C3 Analyses: Effect of c_v(NC) of Bay Mud

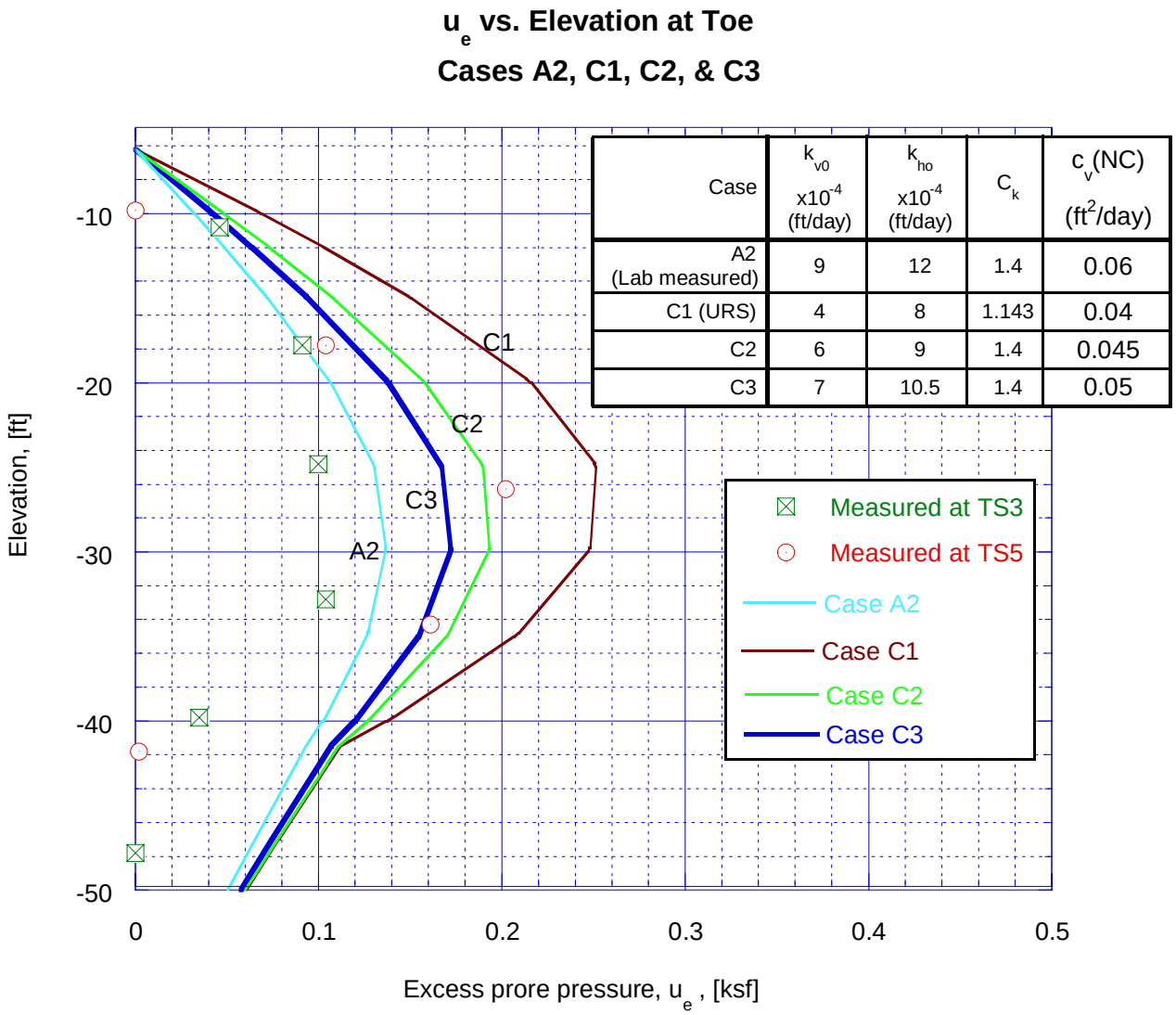

Figure 3.23c Predicted and Measured Excess Pore Pressure at Toe of the NHPL for Cases A2, C1, C2, and C3 Analyses: Effect of c_v(NC) of Bay Mud

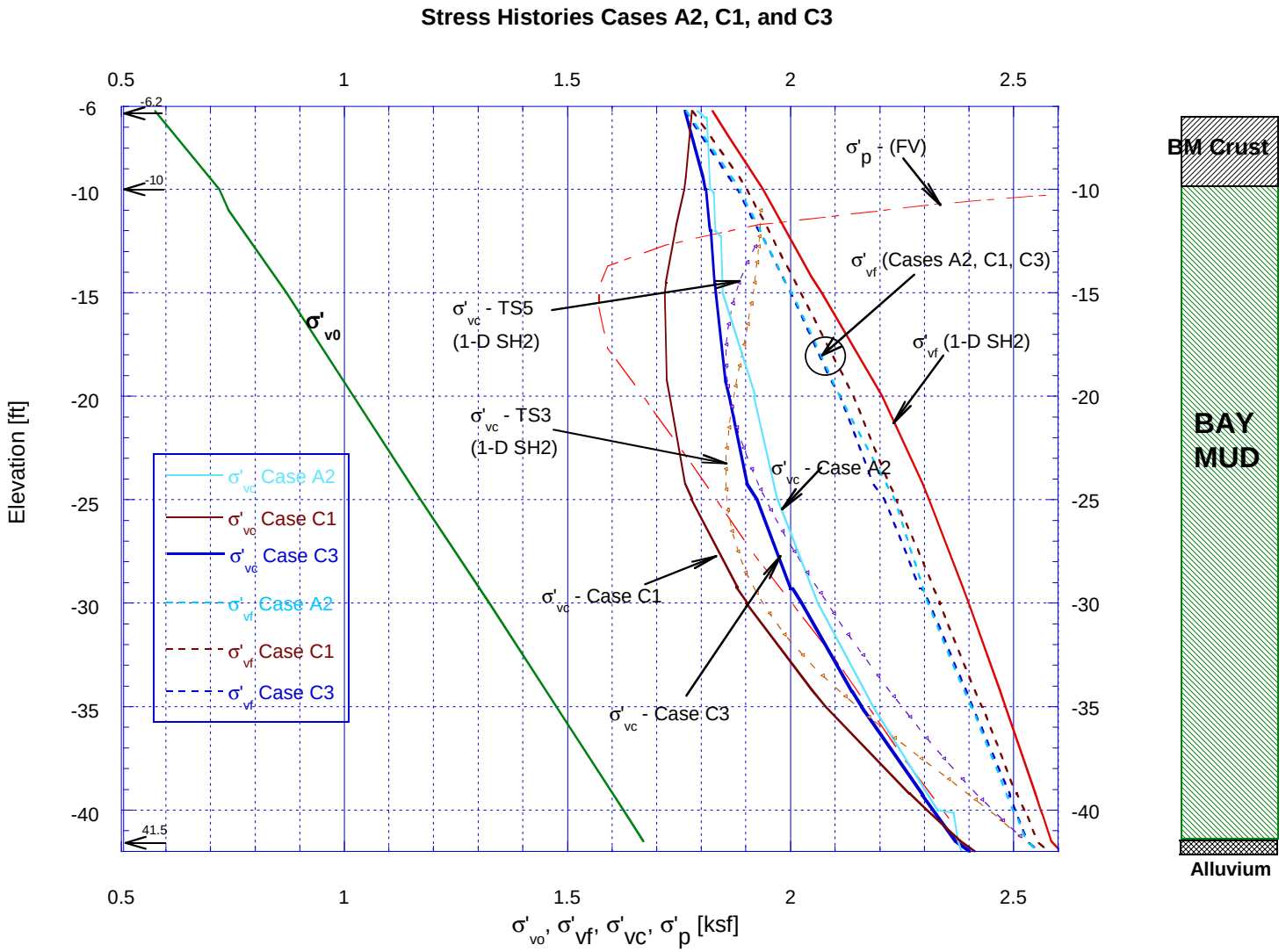

Figure 3.23d Comparison of Predicted and Measured Stress Histories for Cases A2, C1 and C3 Analyses: Effect of c_v(NC) of Bay Mud

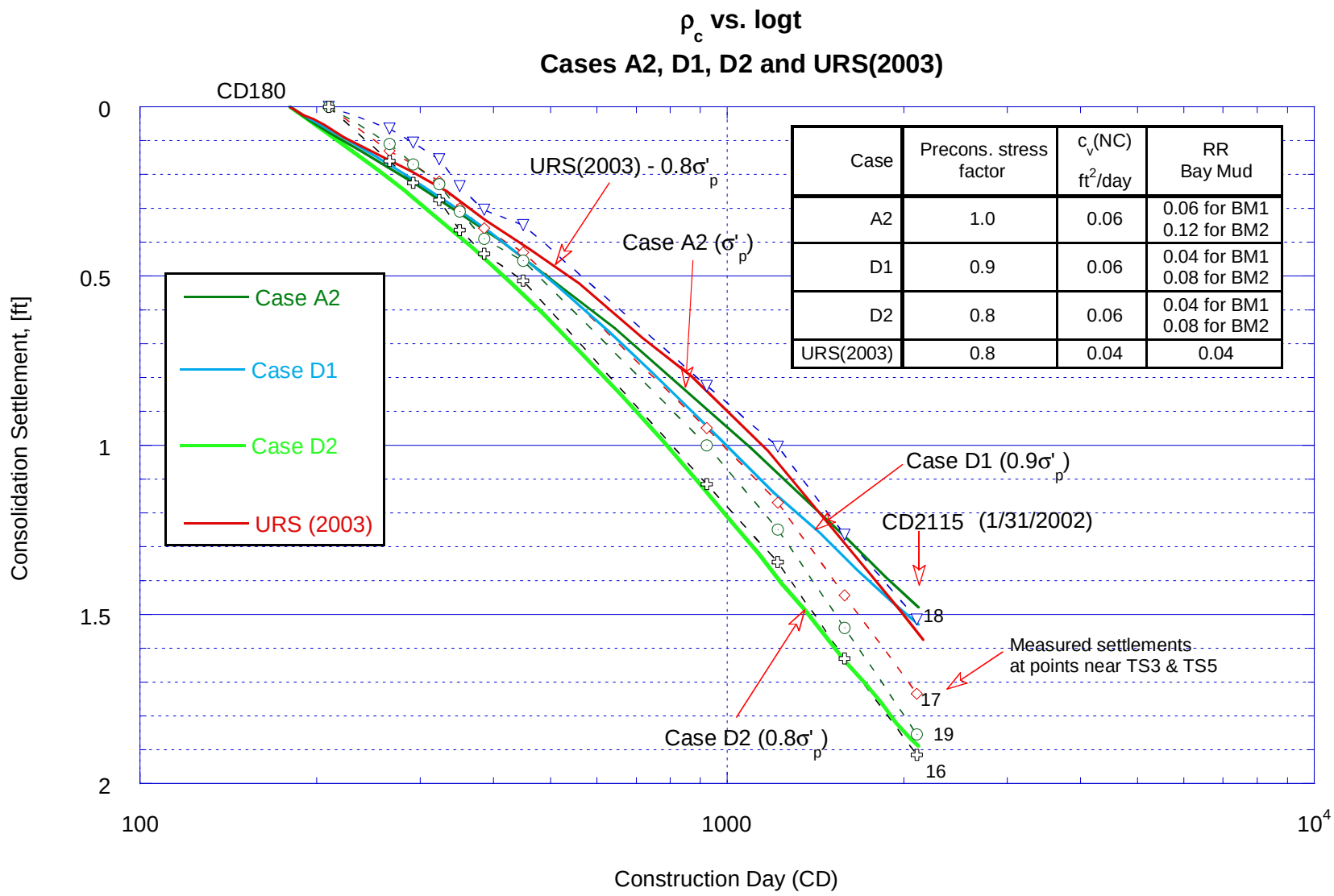

Figure 3.24a Predicted and Measured Consolidation Settlements of the NHPL for Case A2, D1, D2 and URS(2003) Analyses: Effect of Preconsolidation Stress

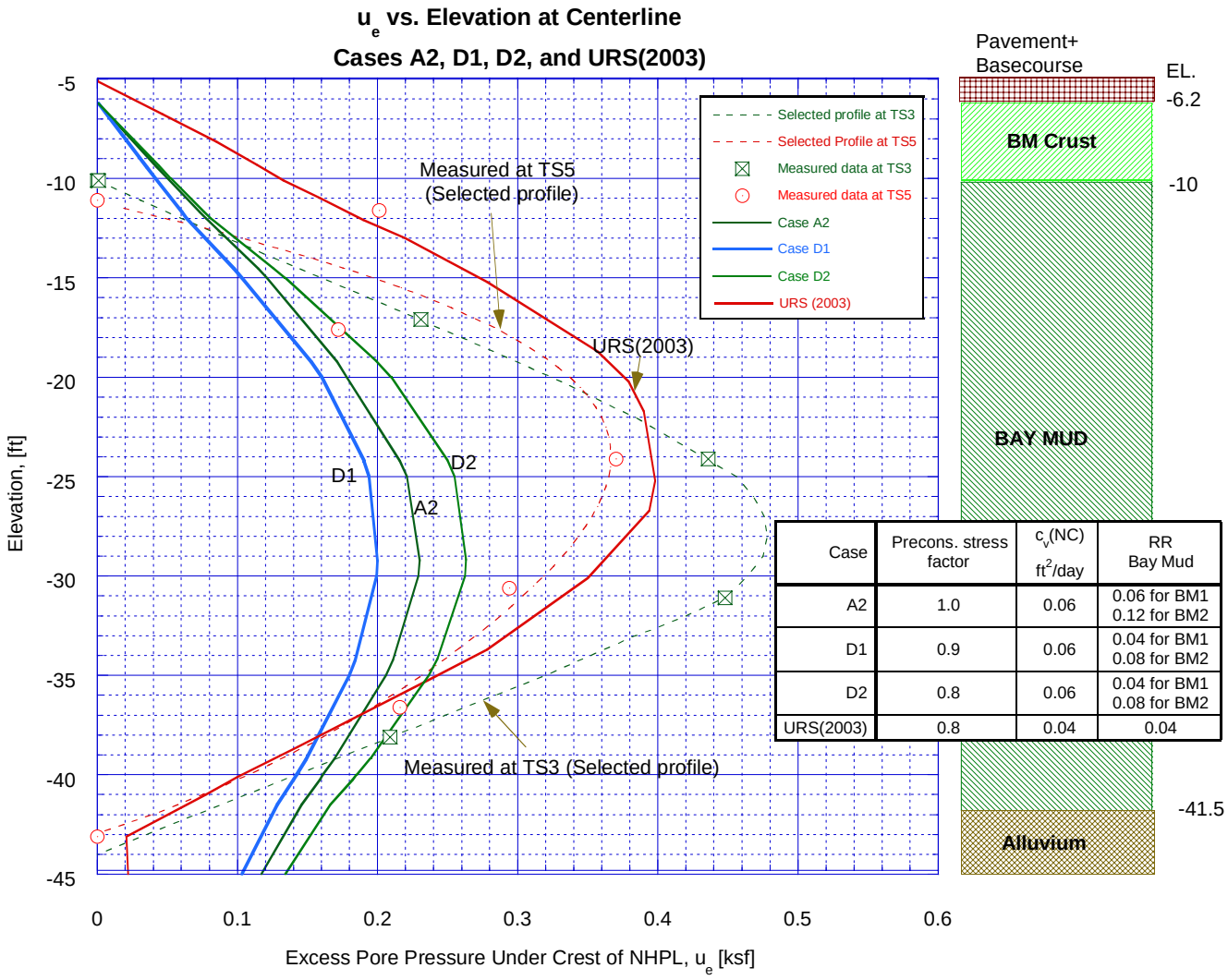

Case	Precons. stress factor	c_v(NC) ft^2/day	RR Bay Mud
A2	1.0	0.06	0.06 for BM1 0.12 for BM2
D1	0.9	0.06	0.04 for BM1 0.08 for BM2
D2	0.8	0.06	0.04 for BM1 0.08 for BM2
URS(2003)	0.8	0.04	0.04

Figure 3.24b Predicted and Measured Excess Pore Pressure at Centerline of the NHPL for Cases A2, D1, D2 and URS (2003) Analyses: Effect of Preconsolidation Stress

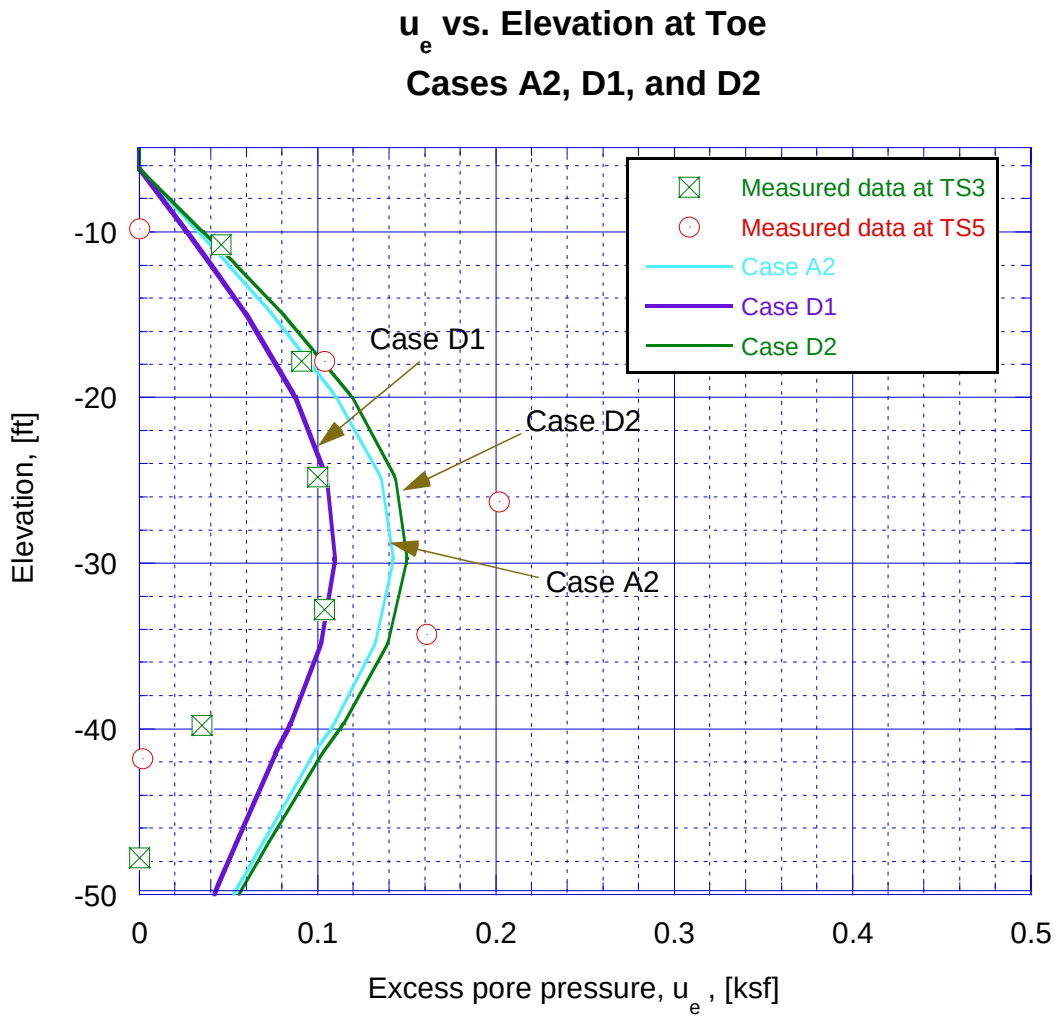

Figure 3.24c Predicted and Measured Excess Pore Pressure at Toe of the NHPL for Cases A2, D1, and D2 Analyses: Effect of Preconsolidation Stress

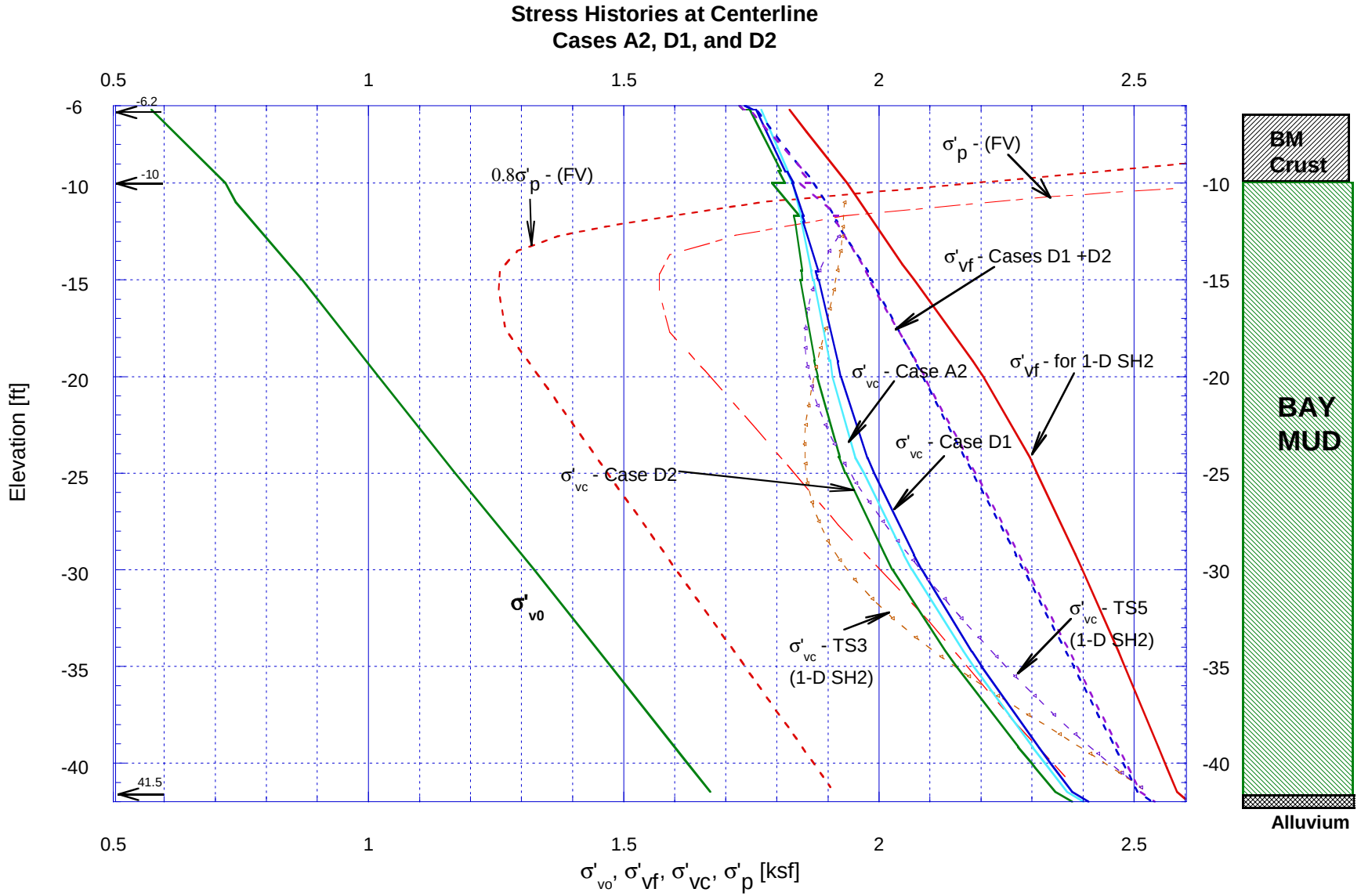

Figure 3.24d Predicted and Measured Stress Histories for Cases A2, D1 and D2 Analyses: Effect of Preconsolidation Stress

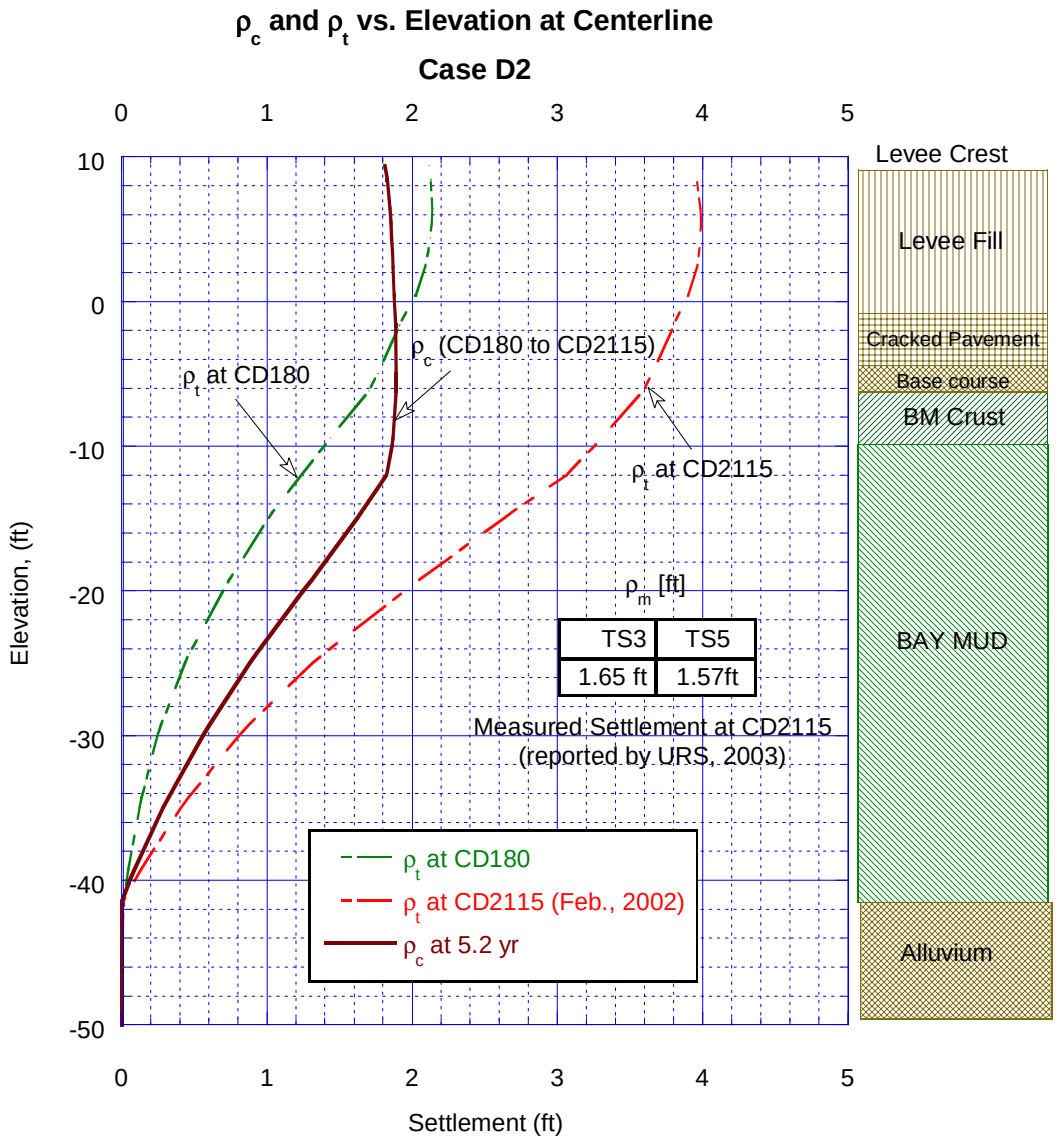

Figure 3.24e Predicted Settlement Profiles under Centerline of the NHPL for Case D2 Analysis: Effect of Preconsolidation Stress

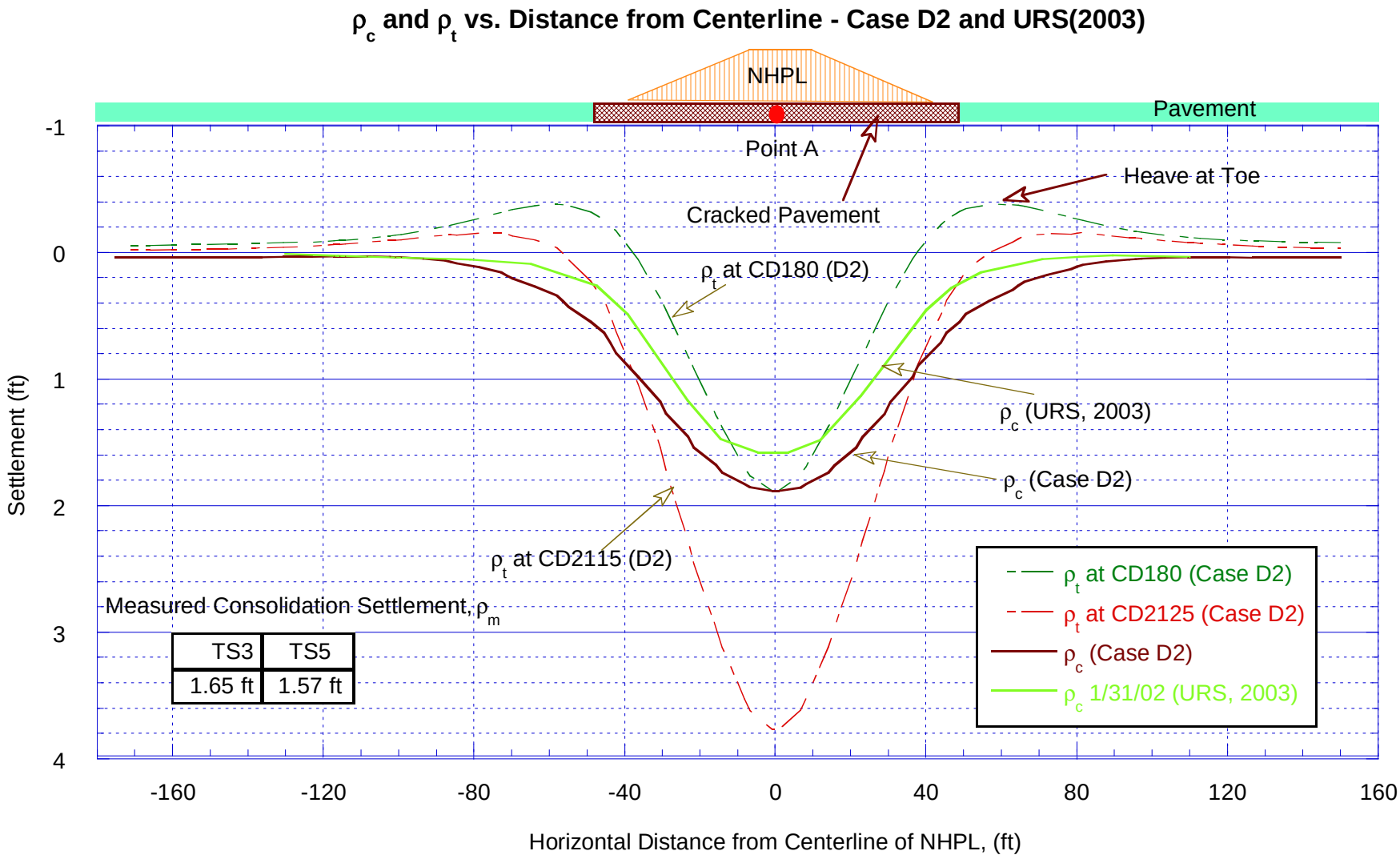

Figure 3.24f Predicted Settlement Profiles of the Ground under the NHPL for Cases D2 and URS (2003) Analyses

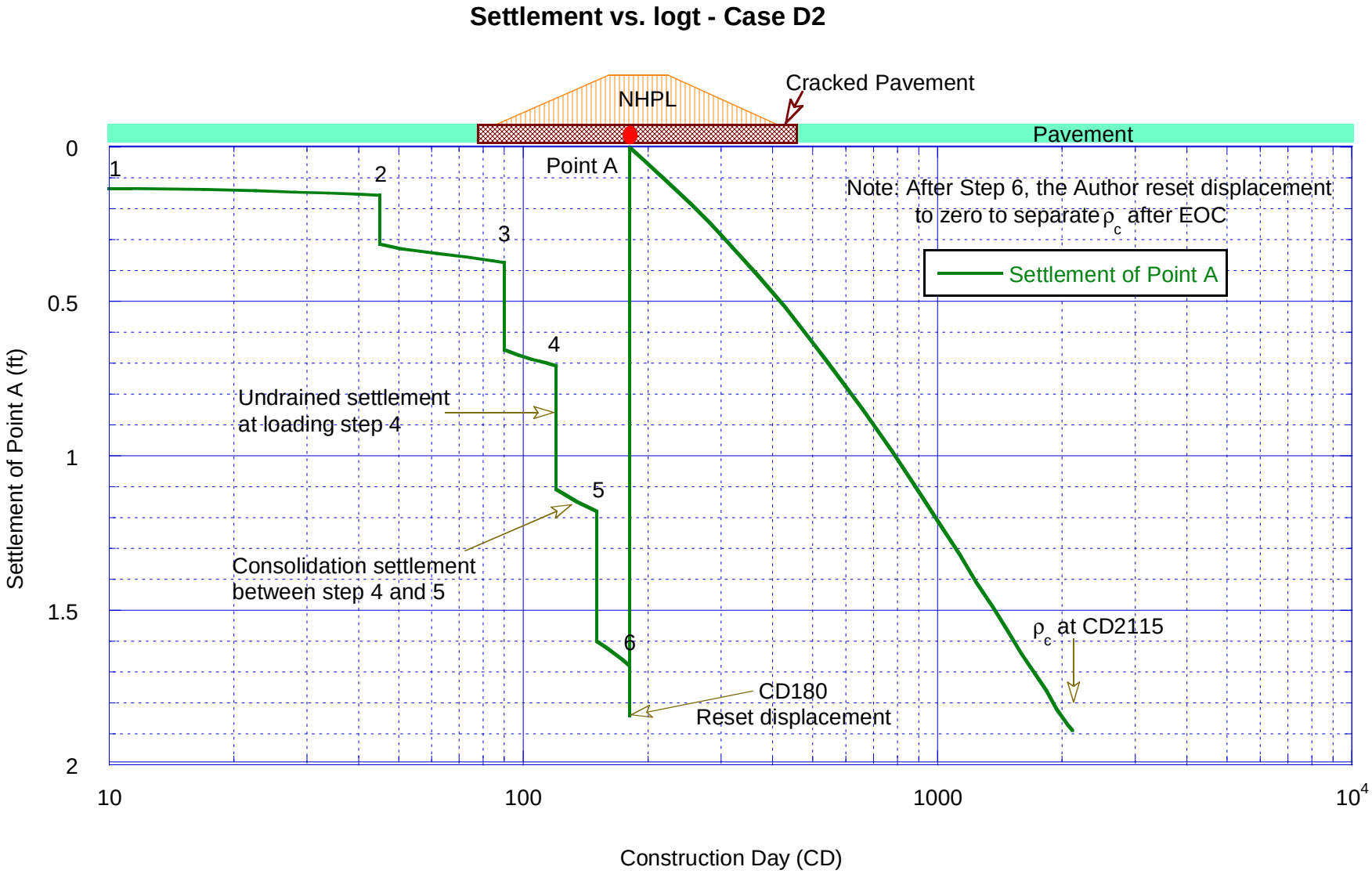

Figure 3.24g Predicted Settlement vs. logt for Case D2 Analysis: Effect of Preconsolidation Stress

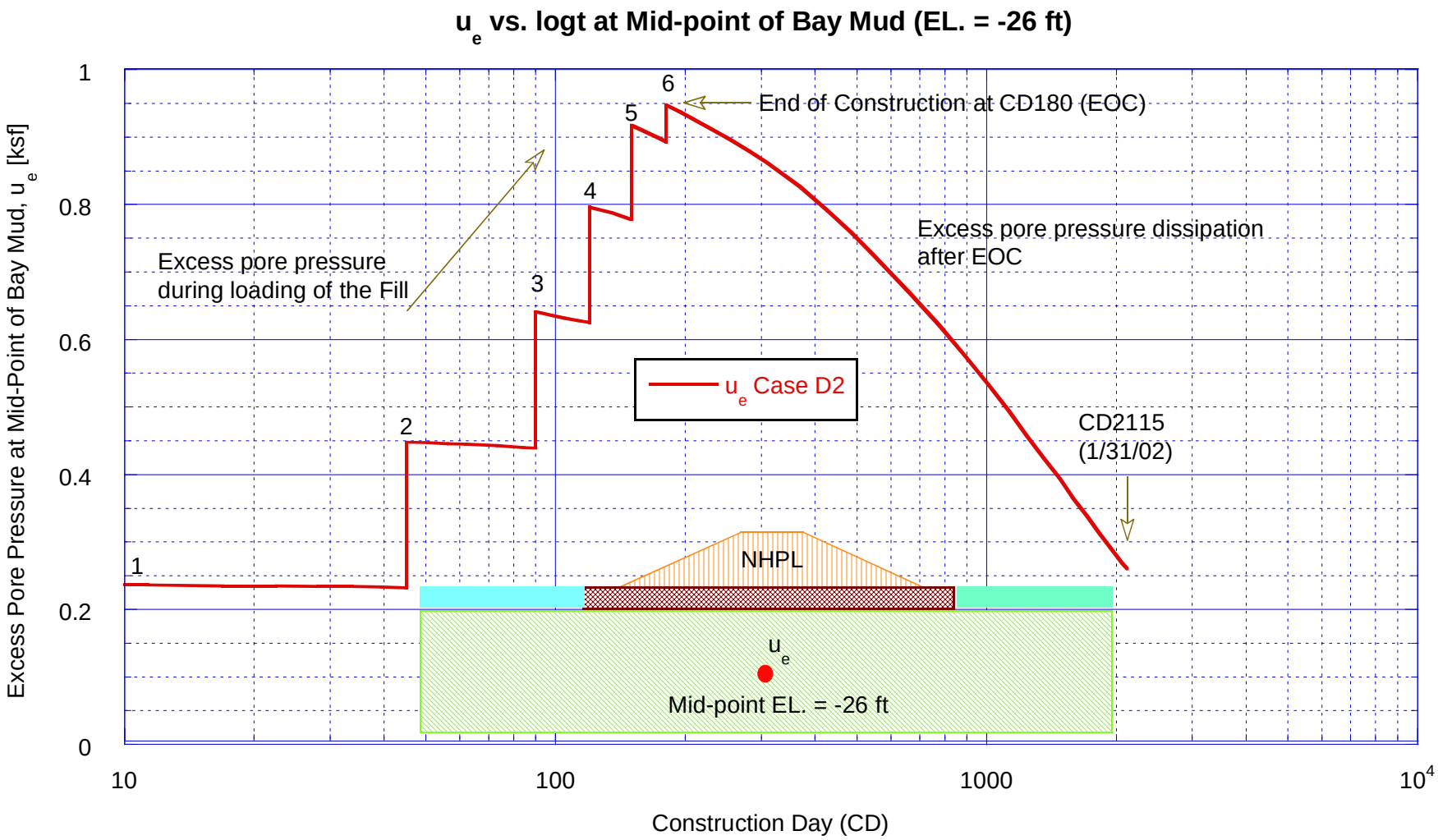

Figure 3.24h Predicted Excess Pore Pressure at Mid-point of Bay Mud vs. logt for Case D2 Analysis

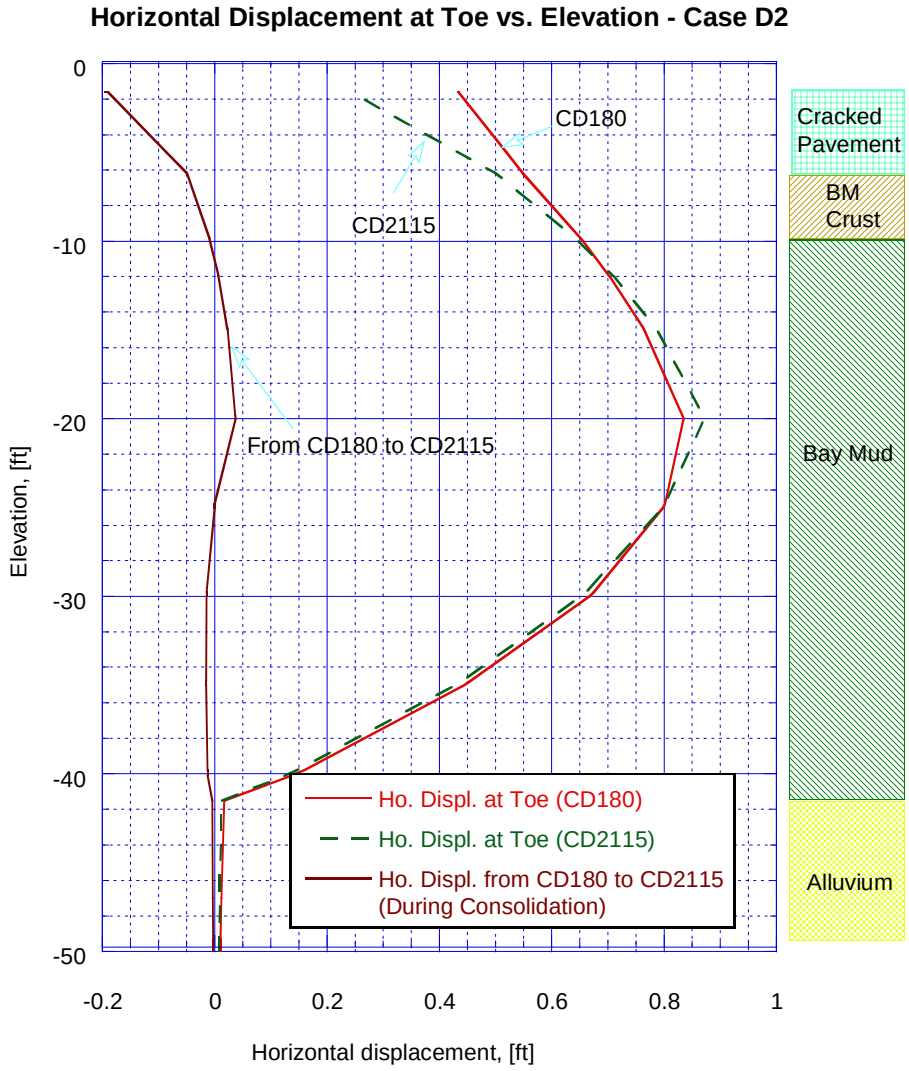

Figure 3.24i Predicted Horizontal Displacements at Toe of the NHPL for Case D2 Analysis

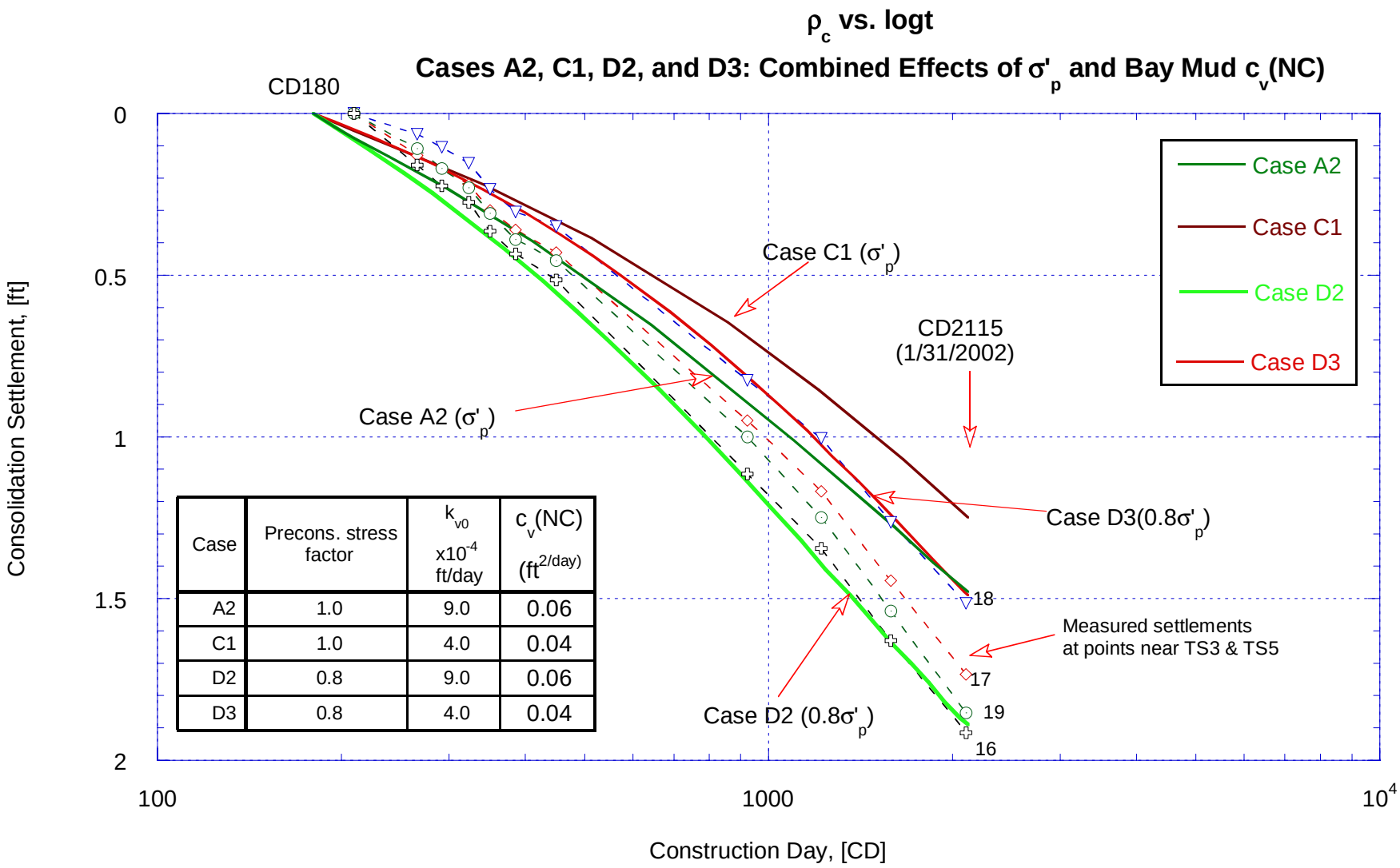

Case	Precons. stress factor	k_{v0} x10^{-4} ft/day	c_v(NC) (ft^{2}/day)
A2	1.0	9.0	0.06
C1	1.0	4.0	0.04
D2	0.8	9.0	0.06
D3	0.8	4.0	0.04

Figure 3.25a Predicted and Measured Consolidation Settlements of the NHPL for Cases A2, C1, D2 and D3 Analyses: Combined Effects of Preconsolidation Stress and Bay Mud c_v(NC)

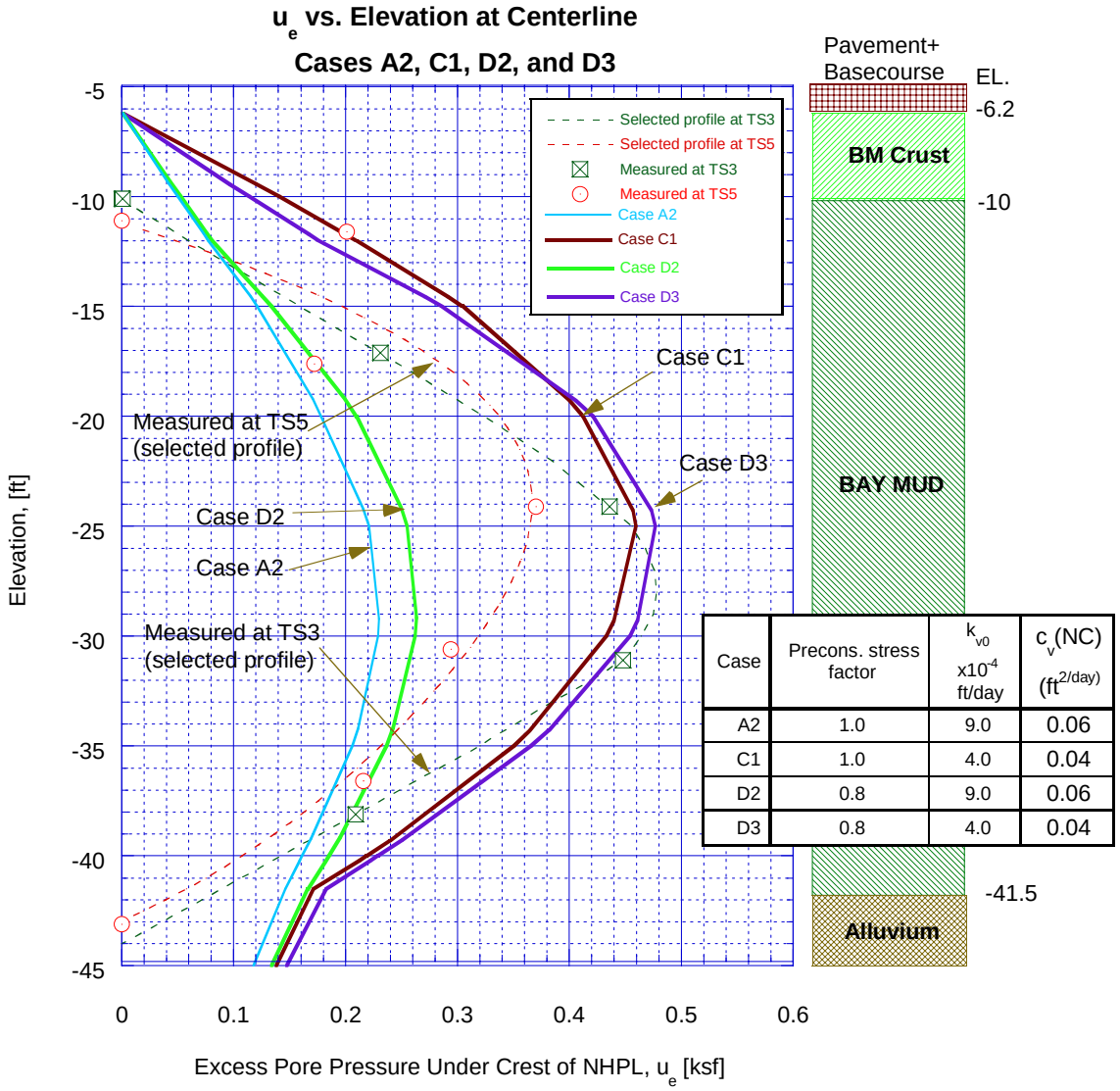

Case	Precons. stress factor	k_{v0} x10^{-4} ft/day	c_v(NC) (ft^{2}/day)
A2	1.0	9.0	0.06
C1	1.0	4.0	0.04
D2	0.8	9.0	0.06
D3	0.8	4.0	0.04

Figure 3.25b Predicted and Measured Excess Pore Pressure at Centerline of the NHPL for Cases A2, C1, D2 and D3 Analyses: Combined Effects of Preconsolidation Stress and Bay Mud c_v(NC)

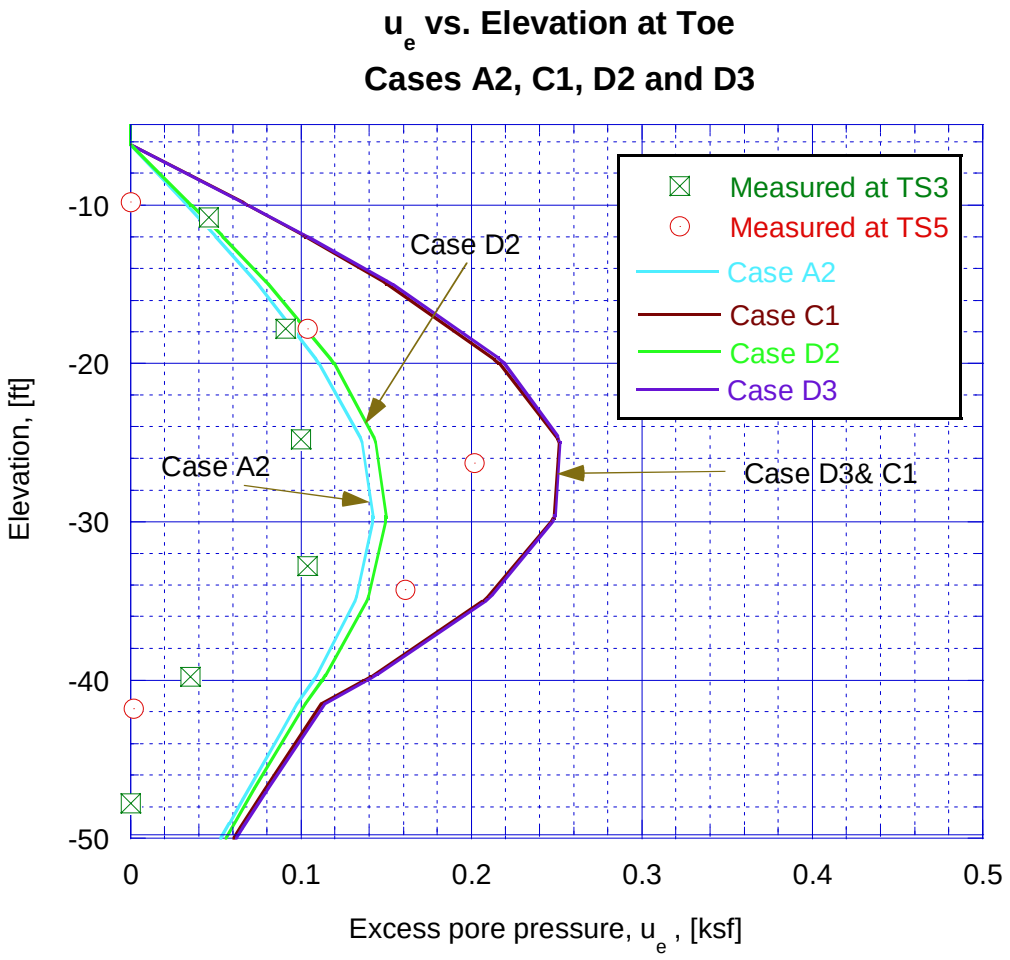

Figure 3.25c Predicted and Measured Excess Pore Pressure at Toe of the NHPL for Cases A2, C1, D2 and D3 Analyses: Combined Effects of Preconsolidation Stress and Bay Mud c_v(NC)

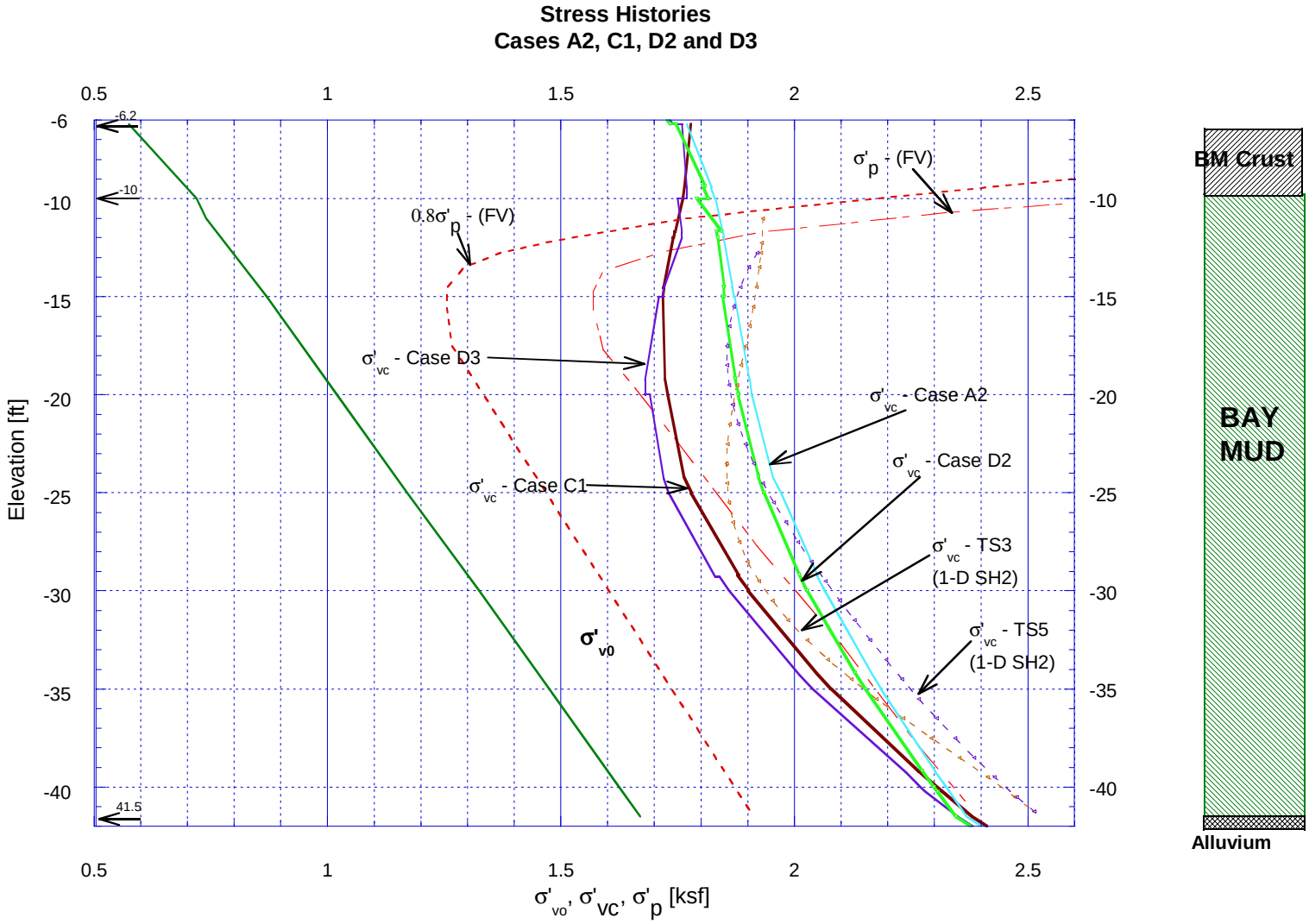

Figure 3.25d Predicted Stress Histories for Cases A2, C1, D2 and D3 Analyses

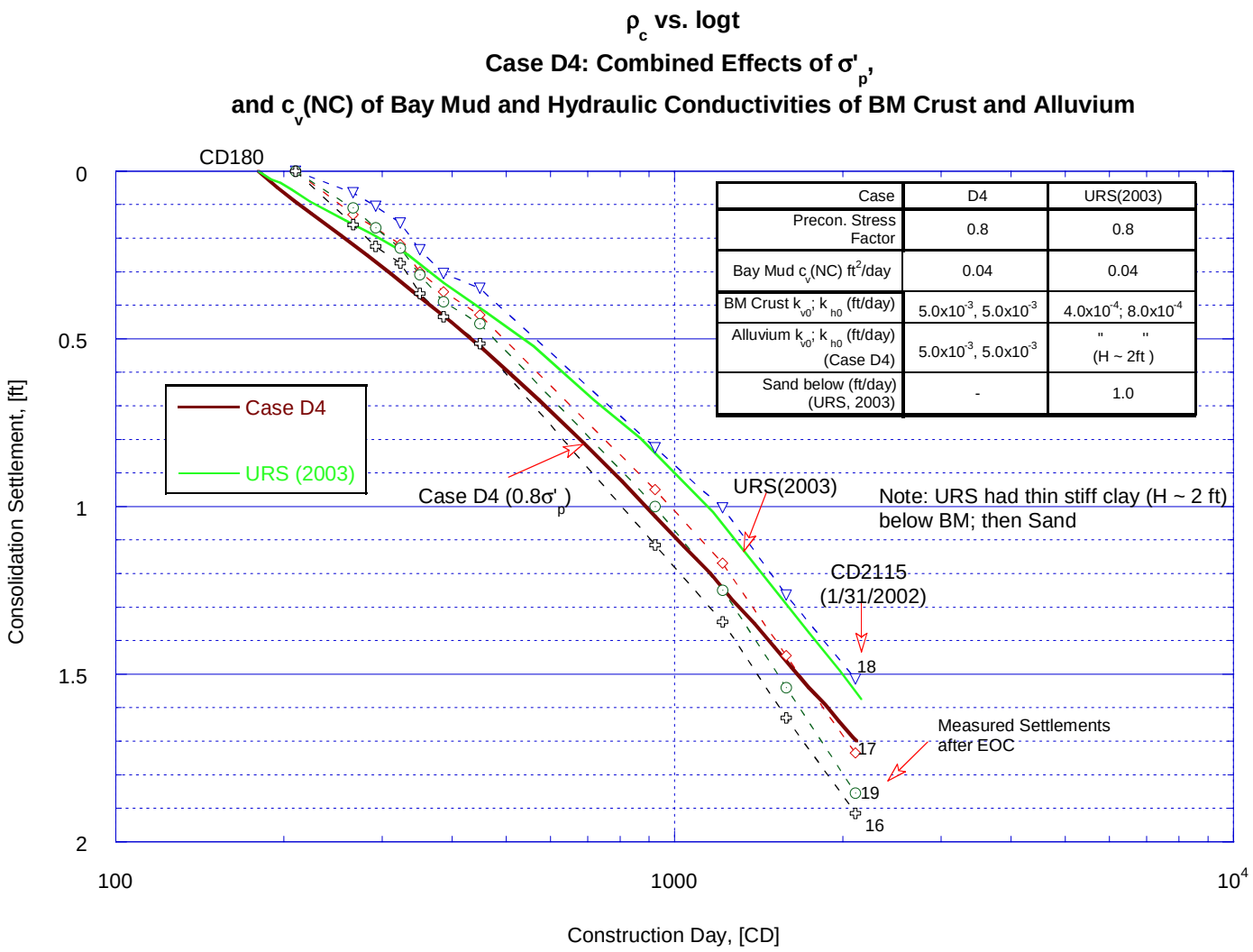

Figure 3.26a Predicted and Measured Consolidation Settlements of the NHPL for Case D4 and URS (2003): Combined Effects of Bay Mud c_v(NC), σ'_p Profile and Permeability of BM Crust and Alluvium

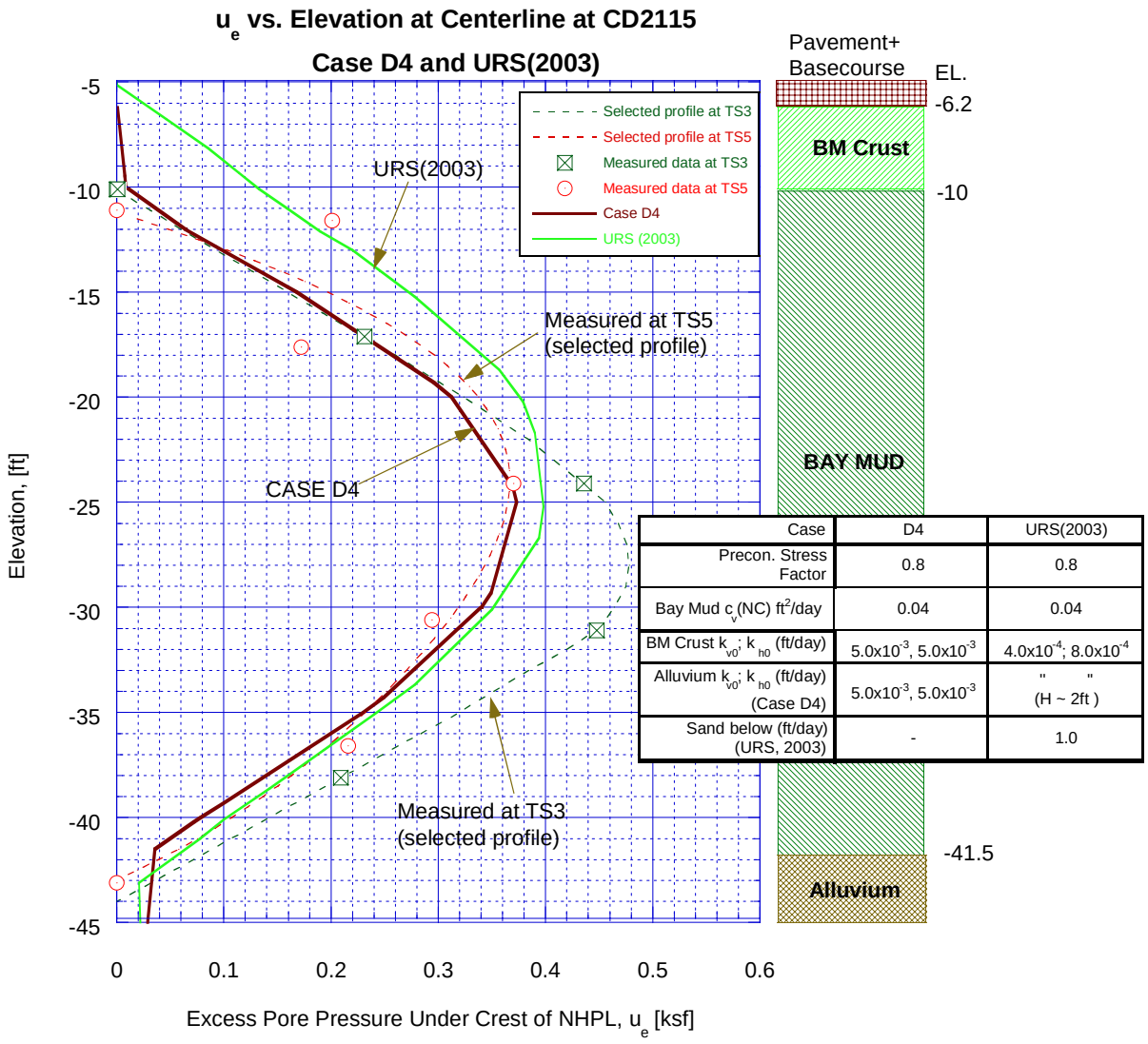

Case	D4	URS(2003)
Precon. Stress Factor	0.8	0.8
Bay Mud c_v(NC) ft^2/day	0.04	0.04
BM Crust k_{v0}; k_{h0} (ft/day)	5.0×10^{-3}, 5.0×10^{-3}	4.0×10^{-4}; 8.0×10^{-4}
Alluvium k_{v0}; k_{h0} (ft/day) (Case D4)	5.0×10^{-3}, 5.0×10^{-3}	" " (H ~ 2ft)
Sand below (ft/day) (URS, 2003)	-	1.0

Figure 3.26b Predicted and Measured Excess Pore Pressure at Centerline of the NHPL at CD2115 for Case D4 and URS (2003): Effects of Bay Mud c_v(NC), σ'_p Profile and Permeability of BM Crust and Alluvium

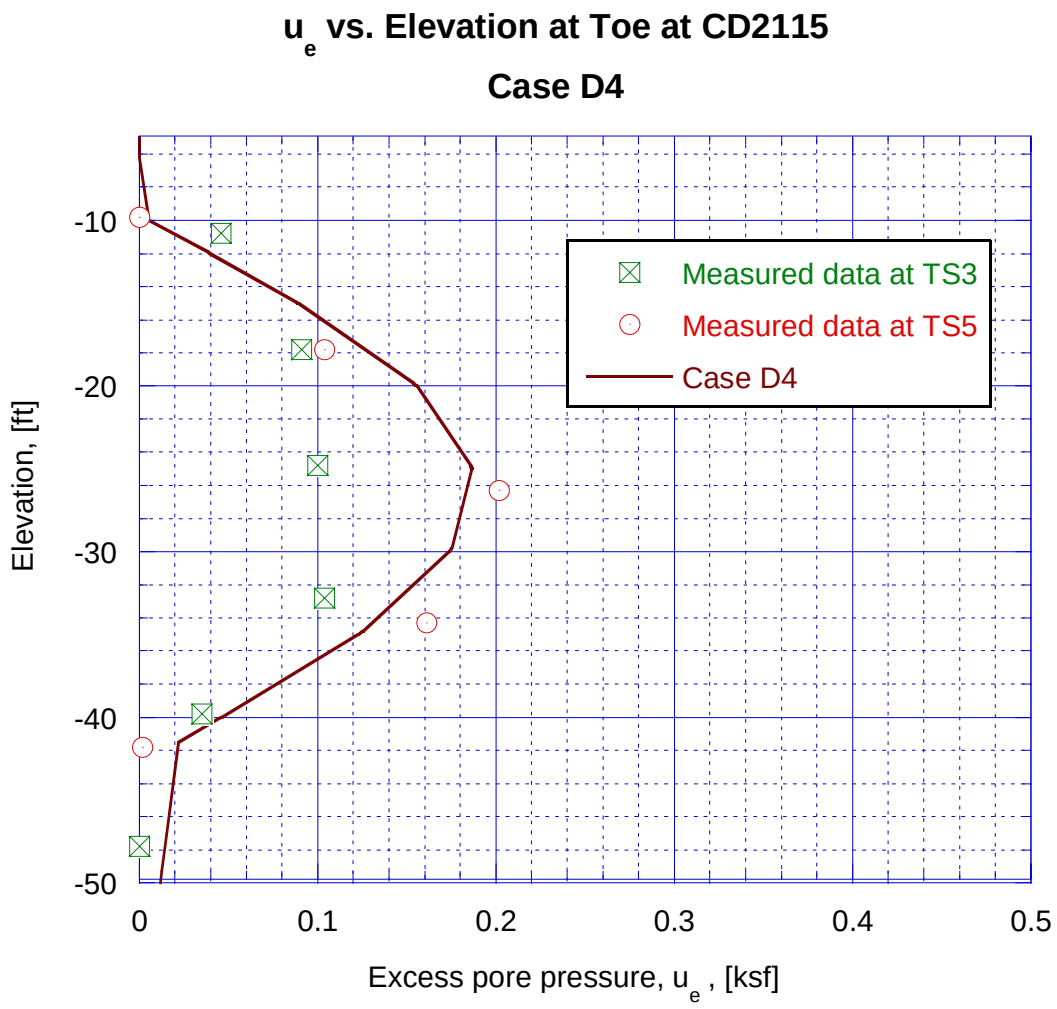

Figure 3.26c Predicted and Measured Excess Pore Pressure at Toe of the NHPL at CD2115 for Case D4

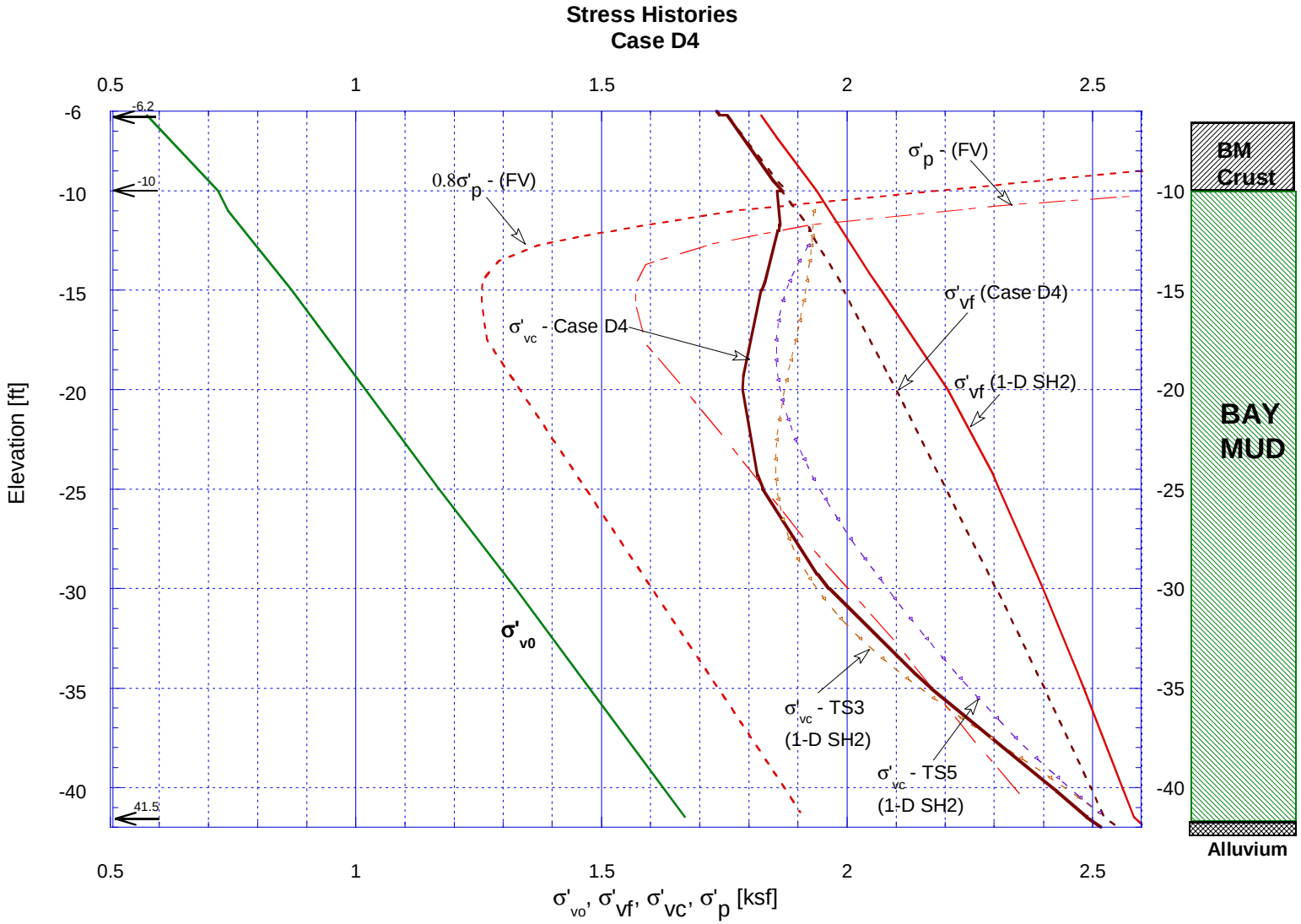

Figure 3.26d Predicted Stress Histories for Case D4

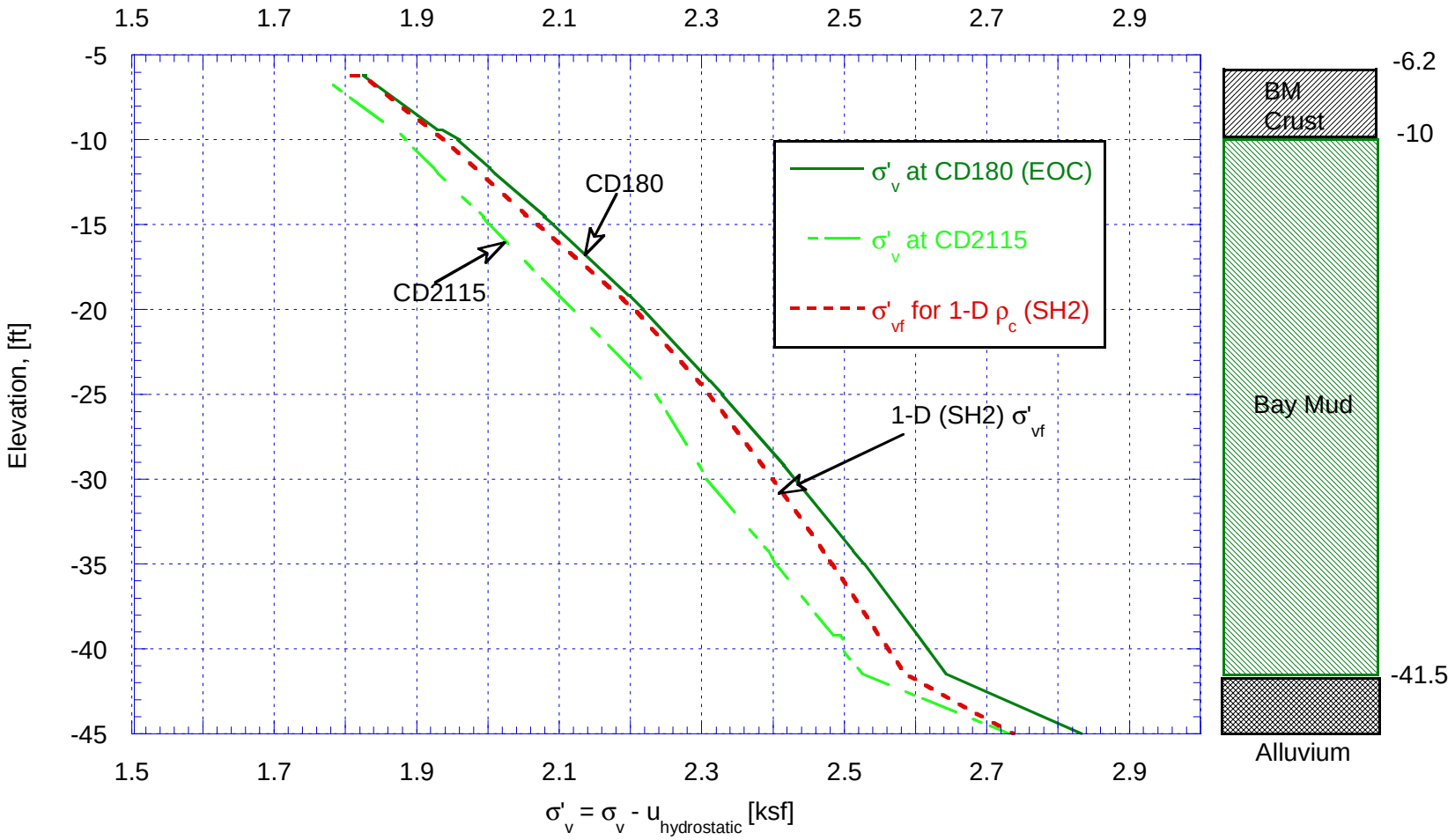

Figure 3.27a Predicted Reduction in Total Vertical Stress at Centerline of NHPL during Consolidation from CD180 (EOC) to CD2115 for Case A2 Analysis

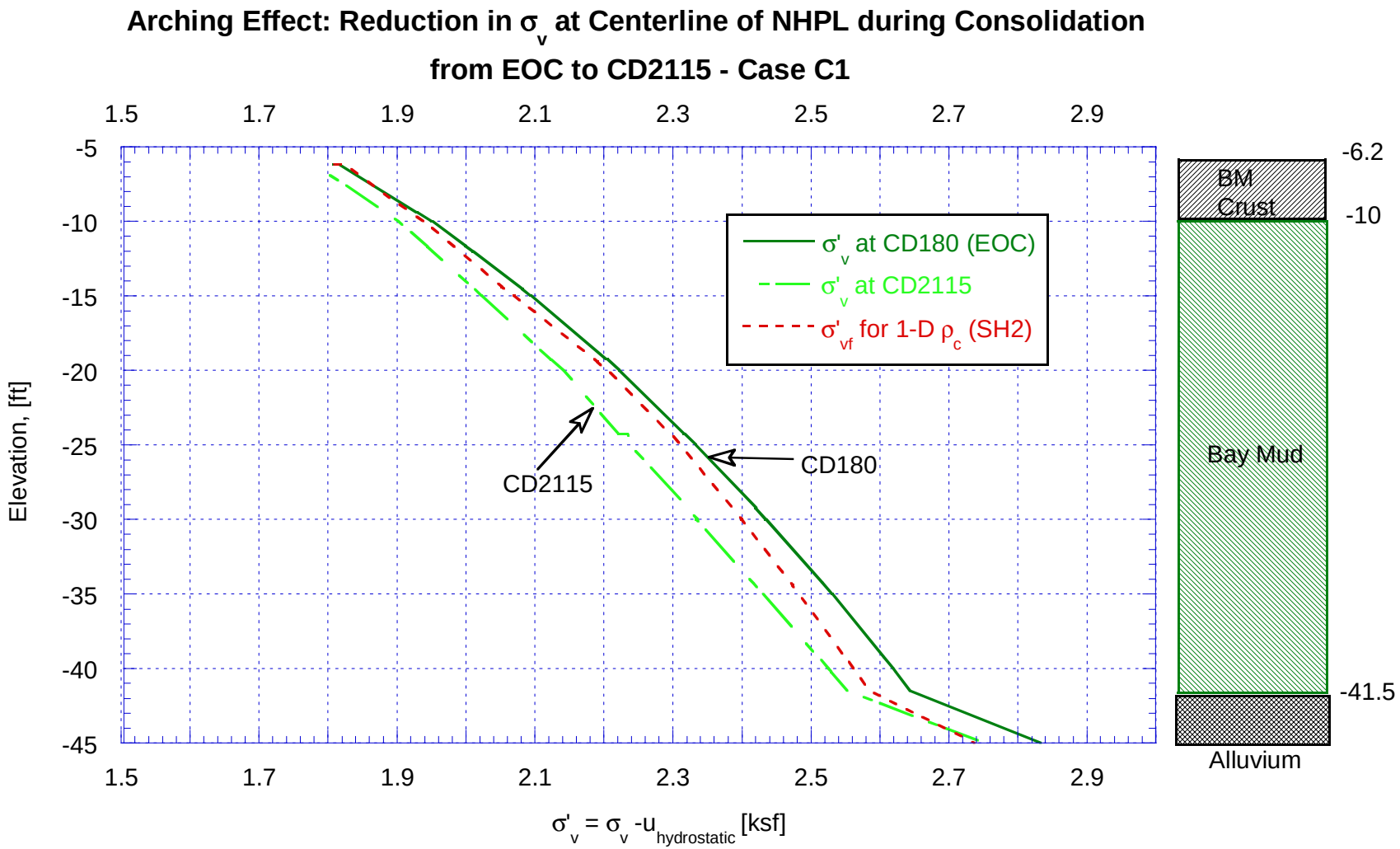

Figure 3.27b Predicted Reduction in Total Vertical Stress at Centerline of NHPL during Consolidation from CD180 (EOC) to CD2115 for Case C1 Analysis

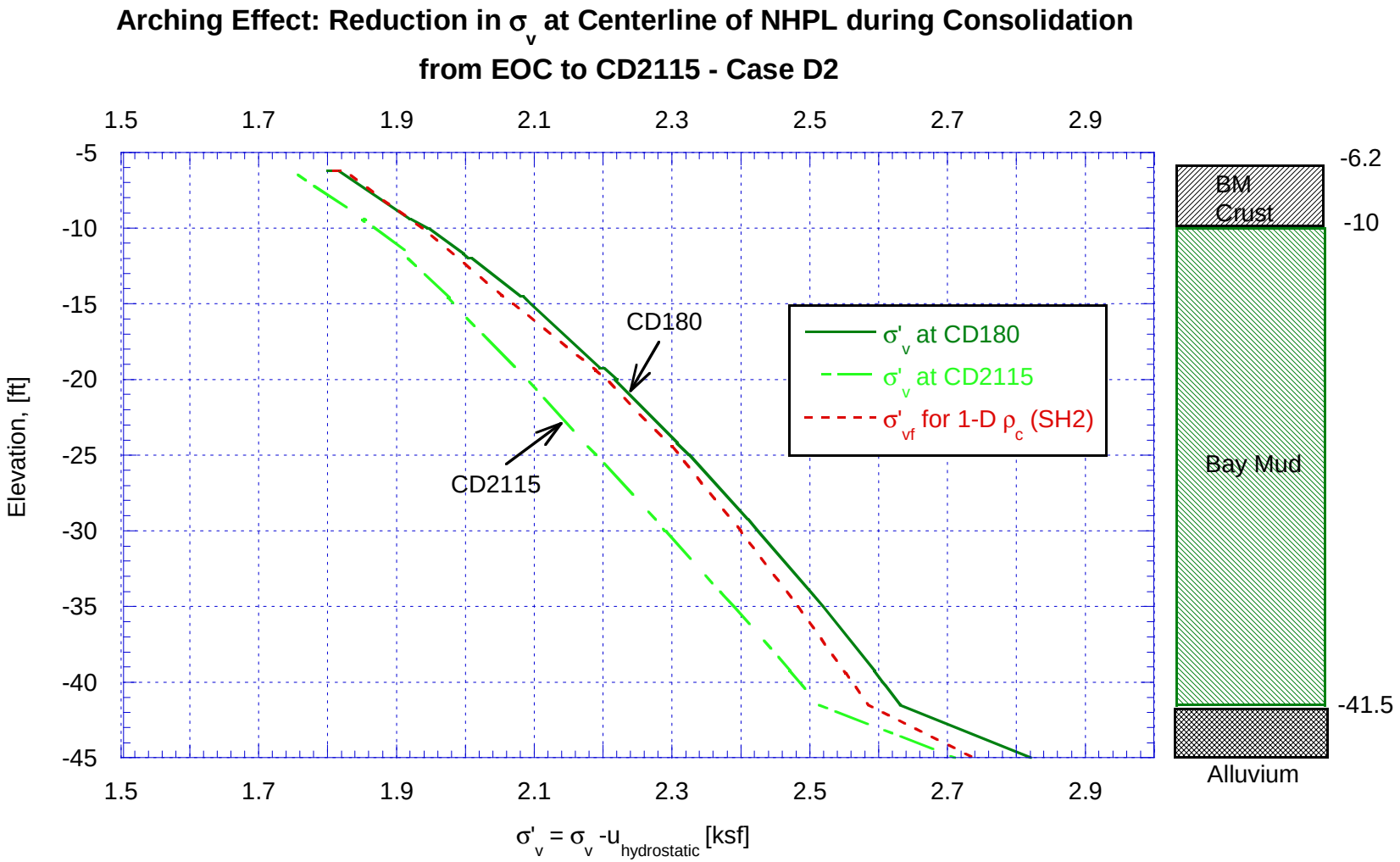

Figure 3.27c Predicted Reduction in Total Vertical Stress at Centerline of NHPL during Consolidation from CD180 (EOC) to CD2115 for Case D2 Analysis

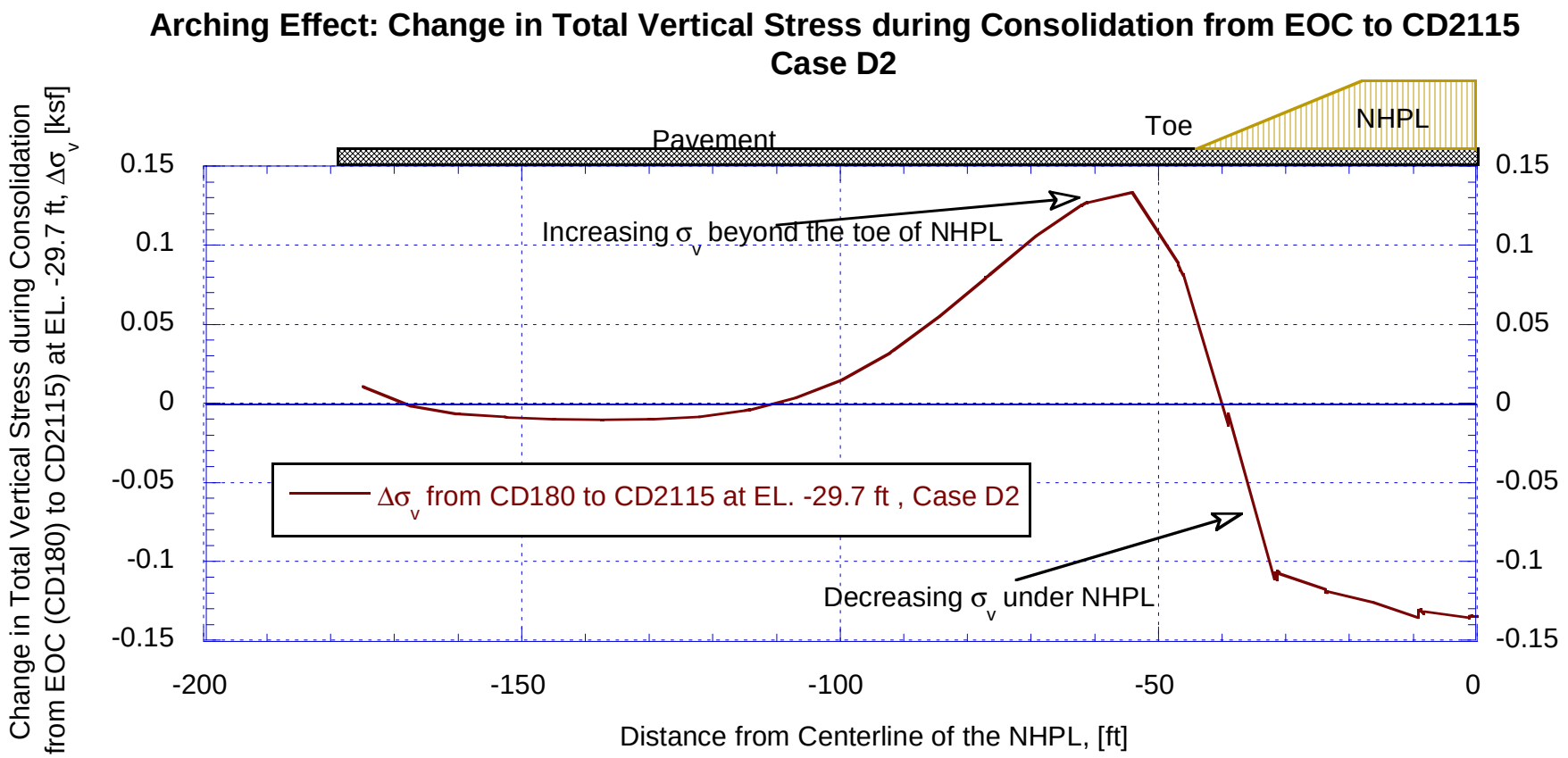

Figure 3.27d Predicted Changes in Total Vertical Stress ("Arching Effect") under the NHPL at El. -29.7 ft for Case D2 Analysis

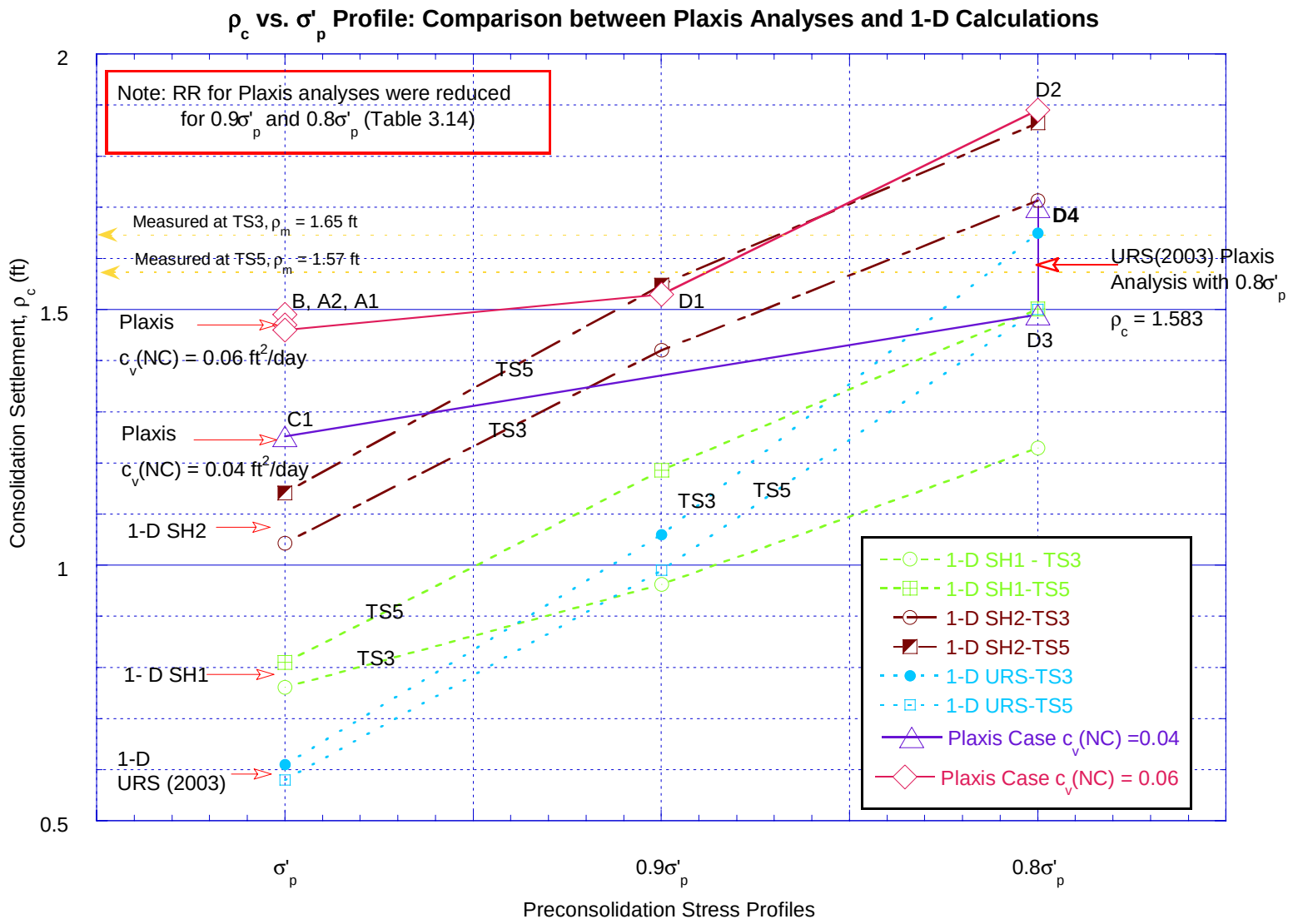

Figure 3.28a Summary and Comparison of Plaxis Predicted Consolidation Settlements at Feb. 2002 with URS (2003) and 1-D ρ_c Results

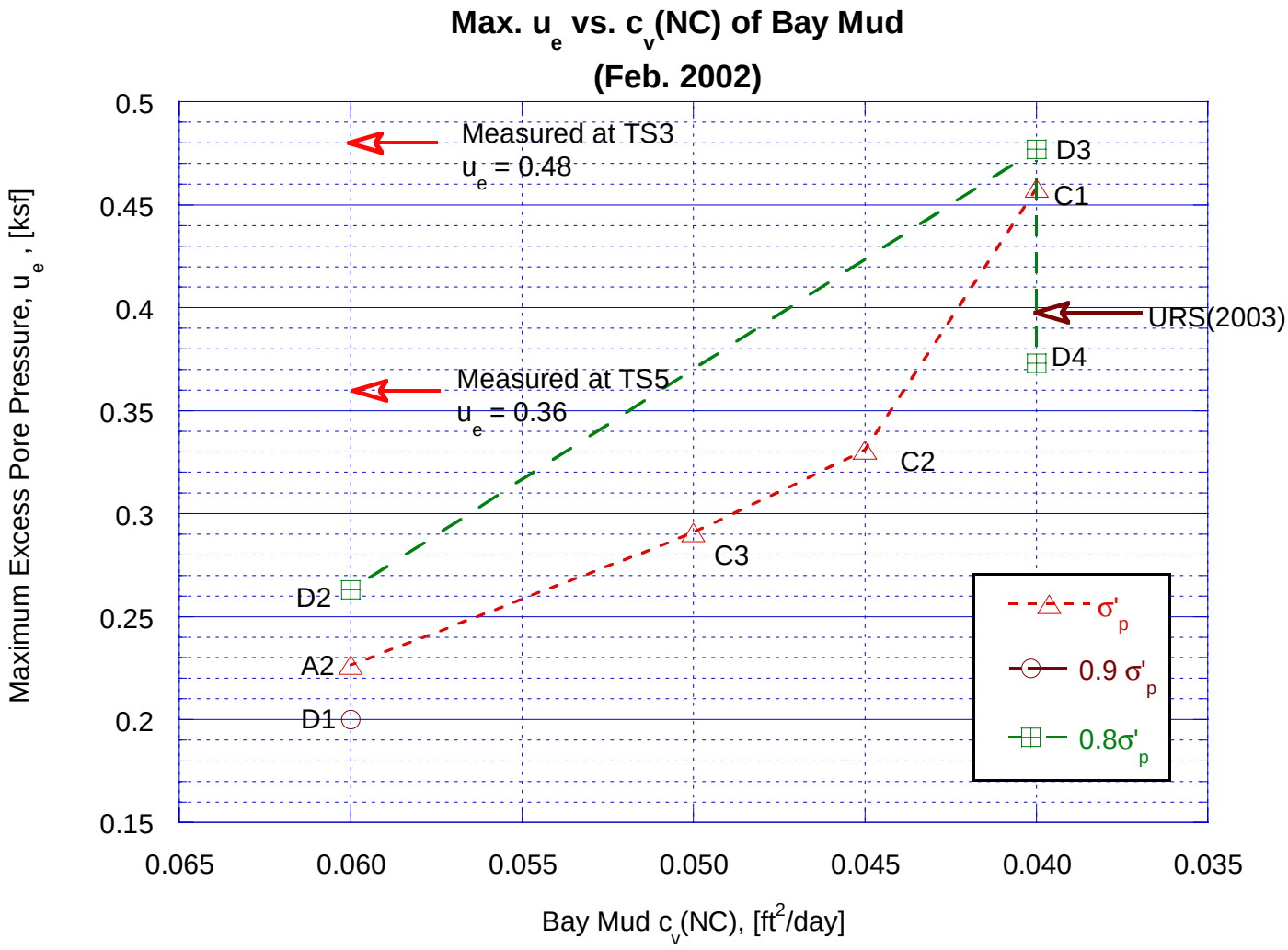

Figure 3.28b Summary and Comparison of Plaxis Predicted Maximum Excess Pore Pressure within Bay Mud at Feb. 2002

CHAPTER 4

SUMMARY, CONCLUSIONS AND RECOMMENDATIONS

4.1 Summary and Conclusions

This thesis presents results of a case history to interpret the performance of the New Hamilton Partnership Levee (NHPL) constructed on soft San Francisco Bay Mud. The thesis comprises five parts:

(1) Description of the project case history including: the geotechnical site conditions; levee construction; instrumentation and monitored performance (over a period of 5.2 years); and results of prior analyses by the geotechnical consultant for the project (URS, 2003).

(2) Reevaluation of soil properties for the Bay Mud (BM) from the field and laboratory data;

(3) Reanalysis of settlements of the NHP levee using the conventional 1-D consolidation settlement analysis (Eq. 2.3);

(4) Calibration of the Soft Soil model (SSM) parameters for Bay Mud by using element test simulations to match the laboratory measured data of consolidation and strength properties; and

(5) 2-D finite element analyses with the effective stress SSM to predict the performances of the NHP levee during and after construction.

This section summarizes the case history, major research results, and conclusions obtained from this research. The following section presents recommendations for further possible research.

4.1.1 Overview of Project

The NHP levee built on the San Francisco Bay Mud (SFBM) foundation soil is a levee section in a system of several levees containing the Hamilton Army Air Field (HAAF) Wetland Restoration project, which aims to restore an ecological system of seasonal and tidal wetlands for the region (Fig.1.4). A part of the restoration project is to modify the existing NHPL and construct new levees surrounding the new wetlands.

The existing NHPL was built between March and October 1996, with approximate dimension of 7,200 ft long and 11 to 12 ft high, to serve as a flood-control structure for the New Hamilton Partnership residential area. The foundation meterials under the levee are several feet of pavement, several feet of BM crust, 30 to 40 feet of soft recent BM, and alluvial soil strata of sand and stiff clay overlying bedrock (see cross-section of the NHP levee and underlying soil profile in Fig.1.5). The thick Bay Mud layer known, as the San Francisco Recent Bay Mud, is a soft, compressible, marine clay with a low undrained shear strength, and is slightly over-consolidated (i.e., OCR=1.5 within most of the deposit below the crust), which incurs problems of settlement and stability of the levees.

Starting shortly after construction of the NHP levee, (which occurred approximately from October to November, 1996), the City of Novato monitored the settlements of the levee crest along its alignment using 200 ft interval survey points located on the flood- wall on top of the levee. The measured settlements (ρ_m) of the levee in January 2002, which was approximately 5.2 years after construction, show that $\rho_m = 2.0 \pm 0.5$ ft along the levee alignment.

4.1.2 URS Site Characterization and Settlement Analyses

In 2002, URS, as the geotechnical consulting firm for the project, conducted a comprehensive geotechnical site investigation with "state-of-the art" field and laboratory testing programs and instrumentations (i.e., Table 2.1 and Table 2.2) in order to evaluate the performance of the existing NHP levee and to develop design recommendations for new levee construction. Detailed results of the site characterization and soil properties are presented in Chapter 2 and Section 3.2 of Chapter 3 at one location along the alignment, designated as test sections TS3 and TS5 (Figs. 2.1 and 2.2), that had extensive laboratory and field vane tests and instrumentation (especially piezometers).

Soil Properties

The 30 to 40 ft thick recent soft Bay Mud, which starts some 10 ft below original ground surface (Fig. 1.5), is an organic, highly plastic CH-OH material with Atterberg limits that plot near to well below the A-line with a typical $w_L = 97 \pm 9$ % and $I_P = 59 \pm 5$ % (Fig. 1.6). The Bay Mud is slightly overconsolidated with OCR ≈1.5 within most of the deposit.

The field and laboratory test programs have developed:

(1) Very well defined soil profile and initial stress history for the virgin soil, plus estimates of the "existing" (i.e., in early 2002) consolidation stress under the crest of the levee (Fig.2.5 to Fig.2.8 and Fig.3.1). In particular, there is good agreement between values of preconsolidation stress (σ'_p) measured by CRSC tests and those computed from field vane data, σ'_p(FV), using both the SHANSEP technique (Ladd and Foott, 1974) in Eq.3.3 and the Chandler(1988) method in Eq.3.4;

(2) Well defined values for the Bay Mud recompression and virgin compression ratios, RR and CR parameters (i.e., Fig.2.9, Fig.2.10 and Fig.3.3b). In particular, the Author's reinterpretation of RR presented in Section 3.2.2 (i.e., values of RR using normalized CRSC stress-strain curves) resulted in much higher values of RR for the Bay Mud (Fig.3.3b) as compared to the URS (2003) selected value of RR = 0.04.

(3) c_v(NC) values of the Bay Mud that exceed the DM-7 mean line for liquid limit w_L ≈ 95% (i.e., c_v(NC) = 20 ft^2/yr = 0.06 ft^2/day). The high value of c_v(NC) suggests that the Bay Mud deposit will experience relatively high rates of consolidation under the NHP levee compared to clays with similar index properties and drainage heights;

(4) Vertical hydraulic conductivity interpreted for the Bay Mud from CRSC tests, k_{v0} = 4.8 ± 1.5x10^{-4} ft/day, and C_k <1.0, which is much smaller than the mean C_c =1.40. The low values of C_k may in part be caused by the fact that most of CRSC tests did not yield linear plots of e vs. logk_v. However, there was a lack of prior investigation and interpretation of the hydraulic conductivity properties (k_{v0}, k_{h0} and C_k) of the Bay Mud and especially of the Alluvium soils below the Bay Mud. The flow properties of the Bay Mud Crust and the underlying Alluvium affect the predicted rate of consolidation of the soft Bay Mud.

(5) Well defined undrained shear strength (s_u) and undrained modulus (E_u) of Bay Mud (i.e., Fig.3.7 to 3.9) from laboratory CK_0U DSS tests.

URS 1- D Consolidation Settlement Analysis

URS used conventional 1-D consolidation analyses via Eqn.2.3 to compute consolidation settlements (ρ_c) from the initial overburden stress (σ'_{v0}) to the current (early 2002) consolidation stress (σ'_{vc}) under the crest of the levee with RR = 0.04 and CR=0.41. They estimated consolidation settlements of ρ_c = 0.55 ± 0.1 ft at five test sections along the

NHPL alignment (i.e., Fig. 2.15) for the mean σ'_p(FV) profile plotted in Fig. 3.1. These predicted "best-estimate" settlements are several times lower than the measured settlements of the flood-wall ($\rho_m = 2.0 \pm 0.5$ ft). In addition, changes in pavement elevation from the boring logs located at the levee crest and the free field indicate that an additional settlement of approximately 1.0 to 1.5 ft to occurred before starting the measurements of wall settlement. Hence, the URS (2003) predictions significantly underestimated the measured settlements of the levee. For the design purpose, URS reduced the best-estimate σ'_p (FV) = σ'_p(EOP) profile by a factor of 0.8 in order to obtain agreement between predicted and measured settlements along the NHPL.

URS (2003) also performed finite element Plaxis analyses with the SSM for Bay Mud and using the reduced preconsolidation stress $0.8\sigma'_p$. The URS predicted $\rho_c \approx 1.58$ ft and maximum $u_e \approx 0.4$ ksf at 1/31/02 are in reasonable agreement with the measured data.

4.1.3 Hypothesis A versus Hypothesis B

The URS settlement analyses assumed that there is negligible secondary compression (drained creep) during primary consolidation as discussed in Section 1.2, this follows accepted US practice that consolidation in the field has a unique EOP compression curve independent of the clay thickness and hence the time required for dissipation of excess pore pressures (so-called Hypothesis A). However, others believe that secondary compression also occurs during primary consolidation at a rate equal to that measured in lab oedometer tests (so-called Hypothesis B), which results in decreased values of the in situ σ'_p and larger settlements throughout the period of pore pressure dissipation.

Professor C.C. Ladd, as an independent consultant to URS, evaluated possible reasons for the large discrepancies between the predicted and measured settlements (Ladd, 2002). He concluded that use of Hypothesis B was consistent with the larger measured settlements at 5.2 years for the NHP levee soil conditions. However, he also thought that the plastic nature of the clay might have caused a large initial settlement plus ongoing creep, thus increased settlements due to lateral deformations [e.g., Foott and Ladd (1981)] during the 5.2 years settlement monitoring period. Using undrained modulus data from CK_0U DSS tests on Bay Mud, the procedure for estimating initial settlement (ρ_i) presented in Foott and Ladd (1981), Ladd (2002) predicted $\rho_i \approx 0.3$ ft for the NHP levee. However, this value is far less than the estimated value of 1.0 to 1.5 ft of "short-term" settlement in the period between the start of construction and the start of the first settlement measurements.

4.1.4 Reanalysis of One-Dimensional (1-D) Consolidation Settlements

The Author computed 1-D consolidation settlements (ρ_c) for the NHP levee using the same methodology as URS described in Section 2.7. The two stress histories (SH1 and SH2) used for the 1-D consolidation settlements are shown in Figs. 3.12b and 3.12c. Detailed calculations are contained in Appendix B. There are three variables (i.e., RR, σ'_{vf} and u_e) other than σ'_p that cause uncertainties in the calculations. The Author devoted significant studies to these three variables to come up with the "best estimates".

As seen in Fig.3.12b, the "measured" vertical consolidation stresses, $\sigma'_{vc} = \sigma'_{vf} - u_e$, under the Crest of the levee are close to the mean σ'_p profile within most of the Bay Mud. Hence, the value of RR, and how it varies as a function of the ratio σ'_{vc}/σ'_p, are very

important. Evaluation of RR based on normalized compression curves from CRSC tests were used to select appropriate RR values for the 1-D consolidation settlement calculations.

FE analyses to compute σ'_{vf} were carried out to address the effects of the concrete pavement, the levee fill and BM Crust strength and stiffness properties on the stress distribution (i.e., σ'_{vf} profile) under the NHP levee. A strong, uncracked pavement with high stiffness properties (i.e., c', E') give a low centerline σ'_{vf} profile, and therefore lower σ'_{vc} profiles for the 1-D ρ_c calculation. On the other hand, a cracked, low stiffness material will result in higher σ'_{vf}. The Author's SH2 stress history used the higher σ'_{vf} profile, which is close to the σ'_{vf} profile adopted by URS (2003).

The reexamination of the measured u_e from piezometers at TS3 and TS5 shows that the Author's selected u_e at TS3 for SH2 is slightly higher than that of URS (2003), but the Author's selected u_e at TS5 is much less than that of URS (2003) as per Fig. 3.12a. Thus, the Author's σ'_{vc} at TS3 is slightly lower than that of URS (2003), whereas his σ'_{vc} at TS5 is much larger than that of URS (2003) as per in Fig. 3.12c.

The results of the 1-D consolidation settlement (ρ_c) calculation with SH2 and comparisons with the measured settlements (ρ_m) at TS3 and TS5 are presented in Table 3.9 and Figs. 3.13c and 3.13d for values of σ'_p equal to σ'_p(FV) and 0.9 and 0.8 times σ'_p(FV).

Agreement between measured and computed consolidation settlements was achieved by reducing the σ'_p profile by about 10% to 15%. A 5 to 10% reduction in σ'_p is considered reasonable based on correcting the σ'_p(CRSC) values for strain rate effects to obtain σ'_p (EOP) as recommended by Mesri and Feng (1992).

The values of 1-D ρ_c computed with the SH2 profile are about twice as large as reported by URS (2003) for the measured σ'_p(FV), i.e., as in Fig. 3.13c. Therefore, the

technique of selecting RR as a function of σ'_{vc}/σ'_{p} ratio for soft ground conditions plays a critical role in 1-D consolidation settlement calculations.

4.1.5 Simulated Bay Mud Behavior in Plaxis SSM

To model the consolidation and undrained strength behavior of Bay Mud in SSM, the Author simulated OED, CK_0UPS DSS and CK_0UPSC/E tests for Bay Mud in the FE code Plaxis to evaluate appropriate SSM material parameters for the Bay Mud. These calibrated consolidation and strength parameters were then used in the Author's 2-D analyses of the NHPL.

The 1-D consolidation simulations (Section 3.4) show that using SSM, the URS selected k_{v0} =4x10^{-4} ft/day and C_k =1.143 result in a low c_v(NC) = 0.04 ft^2/day compared to the average measured c_v(NC) = 0.06 ft^2/day from the CRSC tests. To obtain c_v(NC) = 0.06 ft^2/day, the SSM requires k_{v0} = 9x10^{-4} ft/day, and $C_k = C_c$ = 1.40 (i.e., Fig.3.14c).

The shear lab test simulations have shown some very important facts such as SSM requires an artificially low friction angle ϕ' = 25^0 (with measured K_{0NC} = 0.47) in order to achieve agreement with the measured s_u(DSS) at OCR = 1.5 for the Bay Mud (e.g., Fig 3.15 and 3.16). In addition, the SSM predicts the same undrained shear strength in plane strain compression/extension and DSS shear modes, i.e., it ignores s_u anisotropy. The selected κ^* for SSM for ρ_c predictions results in a much too low E_u (by a factor about 45 to 50 at OCR =1.5). To predict reasonable E_u, therefore the initial settlement ρ_i, one should reduce κ^* by a factor of about 45. Hence, one cannot use the same value of κ^* for realistic predictions of both ρ_i and ρ_c. However, one can use two values of κ^* i.e., low values to predict ρ_i and much higher values to predict ρ_c.

4.1.6 Two-Dimensional (2-D) Finite Element Analyses

Two-dimensional finite element analyses of the NHP levee were carried out with the application of the Soft Soil Model (SSM) in Plaxis for the Bay Mud and BM Crust. Staged construction of the NHP levee was simulated as in Fig. 3.20, where relevant construction days (CD) are CD=180 at the EOC and CD = 2115 at 1/31/02.

The Author did analyses with basically four group of cases (A, B, C, and D in Table 3.14) in order to evaluate the effects of: (1) the pavement under the NHPL (Cases A1 and A2); (2) the Alluvium hydraulic conductivity (Case B); (3) rate of consolidation, i.e., c_v(NC) of Bay Mud (Cases C1, C2, and C3); (4) the effect of preconsolidation stress profiles, σ'_p (Cases D1 and D2); and (5) the combined effects of σ'_p, c_v(NC), and hydraulic conductivities of Bay Mud Crust and Alluvium (Cases D3 and D4). Parameters selected for each case are specified in Table 3.15.

Case A1 and A2 , with the "best estimate" parameters, analyses show no change in σ'_{vc}, ρ_c and u_e predictions when using an uncracked pavement (E = 1000 ksf) for Case A1 and a cracked pavement (E=200 ksf) for Case A2. The analyses predict a consolidation settlement at 5.2 year after EOC of ρ_c = 89% and 94% ρ_m at TS3 and TS5, respectively. The predicted maximum excess pore pressure within Bay Mud u_e = 64% and 48% u_e measured at TS5 and TS3, respectively. The two cases predict a rate of settlement close to the lowest of the four measured ρ_m curves near TS3 and TS5 (Fig. 3.21a).

Case B uses the same parameters as Case A2 except for a much higher hydraulic conductivity of the Alluvium below Bay Mud (i.e., $k_{v0} = k_{h0}$ = 1.0 ft/day), such that u_e = 0 below the Bay Mud in early 2002. Case B slightly increases the rate of settlement (Fig. 3.22a),

but predicts much too low u_e at CD2115 compared with the measured u_e at TS3 and TS5 (Fig. 3.22b).

Cases C1, C2 and C3 use the same properties as Case A2 except for the reduced values of c_v(NC) of Bay Mud (i.e., = 0.04, 0.045, and 0.05 ft^2/day, respectively). The lower c_v(NC) of Bay Mud results in lower rates of consolidation, thus smaller predicted ρ_c at CD2115 (Fig. 3.23a) and increased u_e below the NHPL (Fig. 3.23b and 3.23c). Case C1 and C2 approximately bracket the measured u_e data under the centerline.

Cases D1 and D2 use the reduced σ'_p profiles (i.e., $0.9\sigma'_p$ and $0.8\sigma'_p$, respectively) and also values of RR reduced by one-third. The ρ_c vs. logt curves for these cases bracket the four ρ_m curves (Fig. 3.24a). However, using c_v(NC) = 0.06 ft^2/day in these two cases results in two low u_e at centerline (Fig. 3.24b), but can predict very well u_e at toe of the NHP levee (Fig. 3.24c).

Therefore, both σ'_p and c_v(NC) have significant effects on the predictions of ρ_c and u_e (Figs. 3.25a to 3.25c). Case D4 presents the "best predicted" case that takes into account the combined effects of σ'_p, c_v(NC), and hydraulic conductivities of Bay Mud Crust and Alluvium. Case D4 matches rather well both ρ_c and u_e with the measured data (Figs. 3.26). This case illustrates that there are several important factors controlling the consolidation behavior of the NHP levee other than the pavement and the preconsolidation stress profile, i.e., c_v(NC) of Bay Mud, and hydraulic conductivities of BM Crust and the Alluvium.

The Plaxis SSM cannot describe the increasing horizontal displacements (h) during consolidation after EOC. In fact, the analysis results show that h remains almost constant or reduces slightly during consolidation (i.e., Fig.3.21i and 3.24.i).

The undrained shear induced settlements (i.e., initial settlements, ρ_i) predicted using SSM in the analysis cases are unrealistic because of the much too low E_u due to the selected κ^* for consolidation analysis (i.e., as discussed in Section 3.4). Therefore, the horizontal displacement results are much too large. One can better predict ρ_i and h_x, when using SSM by greatly lowering κ^* to obtain more realistic values of undrained modulus E_u.

The two-dimensional FE analyses using SSM also show an important "arching effect" associated with coupled consolidation in which the total vertical stress decreases under the centerline and increases at toe of the levee by a significant amount (Figs. 3.27a, b, c, d). Reductions in σ_v below NHP levee during consolidation affect (reduce) the predicted consolidation settlement (ρ_c) and final consolidation settlement (ρ_{cf}). In contrast, a 1-D consolidation analysis assumes that σ_v remains constant after EOC. Further research should focus on the identification of factors that control the arching effect and its role on the overall behavior of an embankment after EOC.

In conclusion, the results of the 1-D and Plaxis consolidation analyses both suggest that the in situ σ'_p is probably less than derived from the CRSC and field vane tests, and hence less than σ'_p (EOC) for the NHP levee site. However, it is very likely that continued lateral deformations during consolidation also caused increases in settlement. Thus, one cannot assess the actual reduction in the in situ σ'_p and hence the validity of Hypothesis B.

4.2 Recommendations for Further Research

The Author has the following recommendations:

- Perform 2-D FE analyses with more advanced soil models that can better simulates soil behavior [e.g., MIT-E3, Whittle and Kavvadas (1994); MIT-S1, Pestana and Whittle (1999)] with respect to initial settlement, lateral deformations and consolidation behavior when σ'_{vc}/σ'_{p} is near or slightly larger than unity;
- Perform further research on the arching effect under an embankment to identify factors controlling the reduction in σ_v and its effects on the consolidation behavior of the embankment;
- Perform further experimental research on secondary compression behavior of Bay Mud to identify its creep behavior and its effects on consolidation and undrained shear.

CHAPTER 5

REFERENCES

ARUP(2006). "Report: Numerical analysis of proposed revised design of seasonal wetland fill along the existing NHP levee, Hamilton wetlands restoration project." Submitted to URS Corporation, San Francisco, CA.

Becker, D.E., Crooks, J.H.A., Been, K. and Jefferies, M.G. (1987). " Work as a criterion for determining in situ and yield stresses in clays." *Canadian Geotech. J.,* 24(4), 549-564.

Bejerrum, L. (1972). "Embankments on soft ground: SOA report." *Proc. Specialty Conf. of Earth and Earth-Supported Structures,* ASCE, Lafayette, Indiana, Vol.2, 1-54.

Bejerrum, L. (1973). "Problems of soil mechanics on construction on soft clays: SOA report." *Proc. 8th Int. Conf. on Soil Mech. And Found. Engr.*, Moscow, U.S.S.R., Vol.3, 111-159.

Brinkgreve, R.B.J. (2002). Editor: "PLAXIS 8.v – User's manual." Delft University of Technology & PLAXIS b.v., The Netherlands.

Casagrande, A. (1936). " The determination of the pre-consolidation load and its practical significance." *Proc. 1st Int. Conf. on Soil Mech. And Found. Engr.*, Cambridge, MA., Vol.3, 60-64.

Chandler, R.J. (1988). "The in-situ measurement of the undrained shear strength of clays using the field vane: SOA paper." *Vane Shear Strength Testing in Soils: Field and Laboratory Studies,* ASTM, STP 1014, 13-44.

DeGroot, D.J. (2003). "Laboratory measurement and interpretation of soft clay mechanical behavior." *Proc. of the 2001 Ladd Symposium on Soil Behavior and Soft Ground Construction,* MIT, Cambridge, MA, ASCE GSP No. 119, Editors: Germaine J.T., Sheahan, T.C., and Whitman, R.V., 167-200.

Foott, R. and Ladd, C.C. (1981). " Undrained settlement of plastic and organic clays." *J. Geotech. Engr. Div.,* ASCE, 107(8), 1079-1094.

Germaine, J.T. (2002, 2004). *Database of laboratory tests on Bay Mud.* Dept. of Civil and Environmental Engineering, MIT, Cambridge, MA.

Germaine, J.T. (2005, 2006). Personal communications.

Germaine, J.T., and Ladd, C.C. (1988). " Triaxial testing of saturated cohesive soils: SOA paper." *Advances in Triaxial Testing of Soil and Rock,* ASTM STP 977, 421-459.

Germaine, J.T., Sheahan, T.C., and Whitman, R.V. (2003). " Soil behavior and soft ground construction" *2001 Ladd Symposium on Soil Behavior and Soft Ground Construction* ASCE GSP No.119.

Hight, D.W. (2003). "Sampling effects in soft clay: An update on Ladd and Lambe (1963)." *Proc. of the 2001 Ladd Symposium on Soil Behavior and Soft Ground Construction,* MIT, Cambridge, MA, ASCE GSP No. 119, Editors: Germaine, J.T., Sheahan, T.C., and Whitman, R.V., pp 191-196.

Jamiolkowski, M., Ladd, C.C., Germaine, J.T., Lancellotta, R., (1985). "New Developments in field and laboratory testing of soils: SOA report" *Proc. 11th Int. Conf. on Soil Mech. And Found. Engr.,* San Francisco, Vol.1, 57-153.

Koutsoftas, D.C., and Ladd, C.C. (1985). " Design strengths for an offshore clay." *J. of Geotech. Engr.*, ASCE, 111(3), 337-355.

Ladd, C.C. (1973). "Settlement analysis for cohesive soils." Res. Report R71-2, No.272, Dept. of Civil Engineering, MIT, Cambridge, MA

Ladd, C.C. (1991). "Stability evaluation during staged construction, 22nd Terzaghi Lecture." *J. Geotech. Engr.,* ASCE, 117(4), 537-615.

Ladd, C.C. (1998). *Soil Behavior*. MIT Class notes

Ladd, C.C. (2002). "Technical memorandum on discrepancies between predicted and measured settlement of New Hamilton Partnership Levee, HAAFB wetlands restoration project, Novato, CA.", Prepared for URS Corp., August 19, 2002.

Ladd, C.C., and DeGroot, D.J.(2003). "Recommended practice for soft ground site characterization: Arthur Casagrande Lecture." *Proc. 12th Panamerican Conf. on Soil Mech. And Geotech. Engr.,* MIT, Cambridge, MA, Vol.1, 3-57.

Ladd, C.C., Foott, R. (1974). "New design procedure for stability of soft clays." *J. of Geotech. Engr.,* ASCE, 100 (7), 763 -786.

Ladd, C.C., Foott, R., Ishihara, K., Schlosser, F. Poulos, H.G. (1977). "Stress-deformation and strength characteristics: SOA report." *Proc. 9th Int. Conf. on Soil Mech. And Found. Engr.,* Tokyo, Vol.2, 421-494.

Ladd, C.C., Whittle, A.J., and Legaspi. D.E.(1994). "Stress-deformation behavior of an embankment on Boston Blue Clay." *Vertical and horizontal deformations of foundations and embankments. Proc. Settlement '94,* ASCE GSP No.40, College Station, Texas, Vol. 2, 1730-1759.

Lee, S-M. (1995). "Stability and deformation during staged construction of an offshore breakwater on soft clay." *Sc.D. Thesis*, Dept. of Civil and Environmental Engineering, MIT, Cambridge, MA.

Leroueil, S. (1994). "Compressibility of clays: fundamental and practical aspects." *Vertial and horizontal deformations of foundations and embankments. Proc. Settlement '94,* ASCE GSP. No.40, College Station, Texas, Vol.1, 57-76.

Leroueil, S., Kabbaj, M., Tavenas, F. and Bouchard, R. (1985). " Stress-strain-strain rate relation for compressibility of sensitive natural clays." *Geotechnique,* 35(2), 159-180.

Mesri, G. (2003). "Primary compression and secondary compression." *Proc. of the Ladd Symposium on Soil Behavior and Soft Ground Construction,* MIT, Cambridge, MA, ASCE GSP No. 119, Editors: Germaine, J.T., Sheahan, T.C., and Whitman, R.V., 122-166.

Mesri, G., and Choi, Y.K. (1985). "The uniqueness of the end-of-primary (EOP) void ratio-effective stress relationship." *Proc. 11th Int. Conf. On Soil Mech. And Found. Engr.,* San Francisco, Vol.2, 587-590.

Mesri, G., and Feng, T.W. (1986). Discussion, *Geotechnique*, 36 (2), 283-290.

Mesri, G., and Feng, T.W. (1992). "Constant rate of strain consolidation tests of soft clays, Invited Lecture." *Raul J. Marsal Volume,* Mexican Society of Soil Mechanics., 49-59.

Mesri, G., and Godlewski, P.M. (1977). " Time-and stress-compressibility interrelationship." *J. of Geotech. Engr.,* Div., ASCE, Vol.105, GT5, 417-430.

Mesri, G., and Rokhsar, A. (1974). "Theory of consolidation for clays." *J. Geotech. Engrg.,* ASCE, 100(8), 889-904.

NAVFAC. (1982). Naval Facilities Engineering Command. Design Manual 7.01, Soil Mechanics. Fig. 4, pp 7.1-144

Neher, H.P., Wehnert, M., and Bonnier, P.G. (2001). "An evaluation of soft soil models based on trial embankments" *Journal of Computer Methods and Advances in Geomechanics*, *Desai et al.*

Pestana, J. M. (1994) "A unified constitutive model for clays and sands." *Sc.D. Thesis,* Dept. of Civil and Environmental Engineering, MIT, Cambridge, MA.

Pestana, J. M. and Whittle A. J. (1999) " Formulation of a unified constitutive model for clays and sands" *Int. J. Numer. Anal. Meth. Geomech.,* 23. 1215-1243.

PLAXIS 2-D v.8.2 (2002). *Finite Element Code for Soil and Rock Analyses,* Plaxis B.V., The Netherlands.

Poulos, H.G., and Davis, E.H. (1974). *Elastic Solutions for Soil and Rock Mechanics.* John Wiley and Sons, Inc., New York, NY.

Roscoe, K.H., and Burland, J.B. (1968). "On the generalized stress-strain behavior of 'Wet' clay." *Engineering Plasticity,* Ed.J. Heyman and F.A. Leckie, Cambridge University Press, Cambrdige, U.K., 535-609.

Schmitdt, B. (1966). Discussion of "Earth pressure at rest related to stress history" *Canadian Geotechnical Journal,* Vol.3, No. 4, pp. 239-242.

Schofield, A.N., and Wroth, C.P. (1968). *Critical State Soil Mechanics.* McGraw Hill, London.

Singh, A., and Mittchell, J.K. (1969). " Creep potential and creep rupture of soils." *Proc. 7th Int. Conf. Soil Mech. And Found. Engr.,* Mexico, Vol.1 379-384.

Terzaghi, K., Peck, R.B. and Mesri, G. (1996). *Soil Mechanics in Engineering Practice,* 3rd Edition, John Wiley & Son, New York, 549 p.

URS (2003). "Report: Geotechnical investigation and design recommendations for the New Hamilton partnership levee, Hamilton army air field base, wetlands restoration project." URS Corporation, San Francisco, CA. Draft report dated February 14, 2003 (Note: the final draft report was issued April 30, 2004).

URS/ARUP (2005). "Report: Test fill construction, monitoring, and evaluation. Part 1: Performance during construction, Hamilton Wetland Restoration Project". Submitted to USACE San Francisco District, CA.

Whittle, A.J. (1987). "A constitutive model for overconsolidated clays with application to the cyclic loading of tension piles in clay." *Sc.D. Thesis,* Dept. of Civil and Environmental Engineering, MIT, Cambridge, MA.

Whittle, A.J. (2004). 1.364 Advanced Geotechnical Engineering, MIT Class note 8.

Whittle, A.J. and Kavvadas, M.J. (1994). "Formulation of MIT-E3 constitutive model for overconsolidated clays." *J. Geotech. Engr.* ASCE, 120 (10), 173-189.

Wissa, A.E.Z., Christian, J.T., Davis, E.H., and Heiberg, S. (1971). "Consolidation at constant rate of strain." *J. Soil Mech. And Found. Div.,* ASCE, 97(10), 1393-1413.

CHAPTER 6

APPENDIXES

6.1 Appendix A: MIT Laboratory Tests on Bay Mud

6.1.1 CRSC Tests on Bay Mud at TS3-B1(From Germaine, 2002)

Table A1 Summary of CRSC Tests at TS3-B1

(From Germaine, 2002)

Last Revised: 04/24/02

Spec. Location		Index Tests			Specimen Data		Test Conditions				Remarks
Test #	Depth (ft)	T_v	ω_c	ω_p	ω_n	e_i			.	$\Delta u/\sigma_v$	
Boring		SD	SD	ω_l	I_p	S_i (%)	σ_s	u_b	ε	@ σ'_{vm}	
Sample	Markers	# obs	# obs	%2μ	γ_t	G_s	(ksc)	(ksc)	(%/hr)	(%)	
CRS430		0.26	94.2		85.87	2.318					Control failure-no data-soil extruded from ring
TS3-B1		0.03	9.5			100.0					water content and void ratio computed
S-3	4-5	5	4		1.512	2.70					based on assume S=100%
CRS431		0.25	96.0		98.16	2.678					
TS3-B1		0.04	3.5			99.0					
S-4	3-4	6	4		1.455	2.70					
CRS432		0.21	88.2		88.35	2.407					
TS3-B1		0.03	4.8			99.1					
S-3	8-9	4	3		1.493	2.70					
CRS435		0.32	86.7		87.37	2.358					
TS3-B1		0.05	3.5			100.0					
S-5	3-4	6	4		1.507	2.70					
CRS440		0.70	74.9		74.88	2.026					
TS3-B1		0.09	0.7			99.8					
S-1	3.5-4.5	8	4		1.560	2.70					
CRS441		0.36	91.1		95.17	2.574					
TS3-B1		0.01	2.0			99.8					
S-2	10-11	7	4		1.474	2.70					
CRS443		0.48	100.5		95.22	2.684					Organic material, specific gravity too high
TS3-B1		0.04	9.9			95.8					
S-6	6-7	6	4		1.431	2.70					
CRS444		0.30	86.6		88.12	2.393					
TS3-B1		0.05	2.8			99.4					
S-7	5.5-6.5	3	4		1.497	2.70					

a) Markers - Location within tube b) Stresses in kg/cm^2 c) 1 kg/cm^2 = 2048 psf d) Water Contents in %

URS Corp.
CRS 440: TS3-B1 S-1

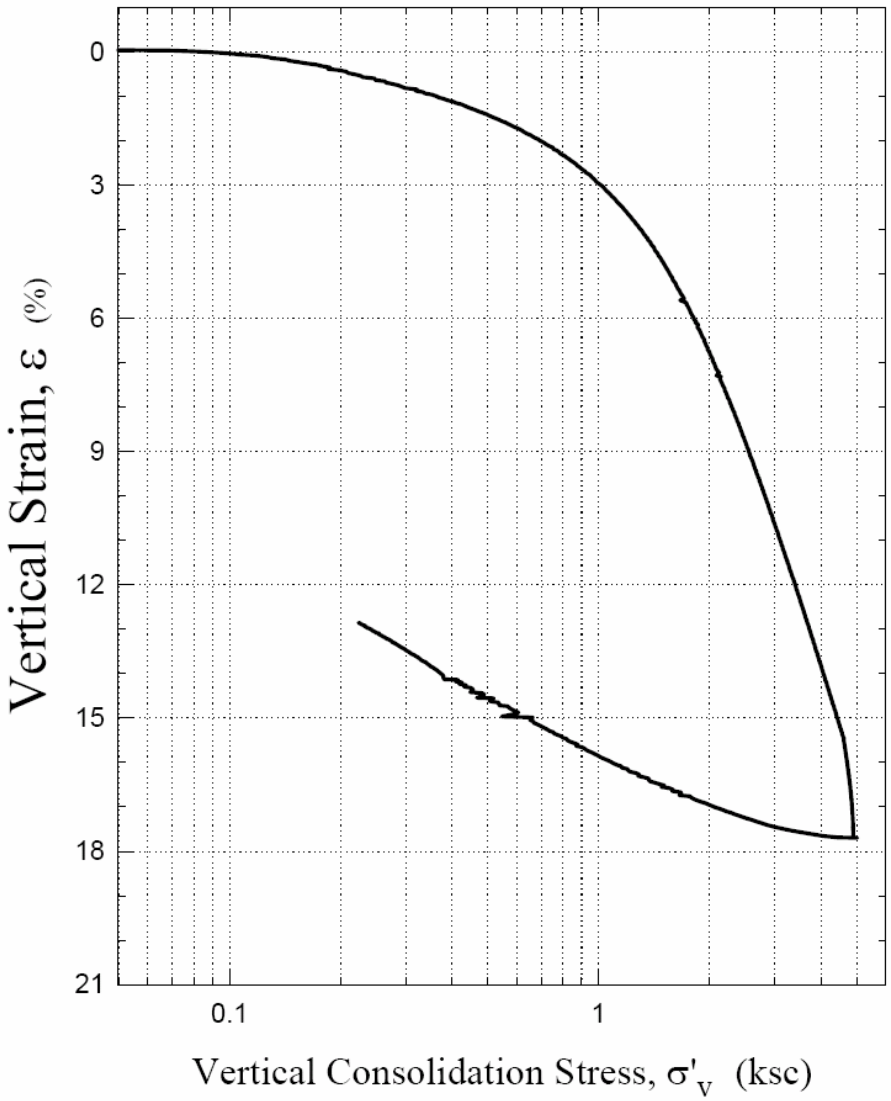

2/21/02 JTG

URS Corp.
CRS 440: TS3-B1 S-1

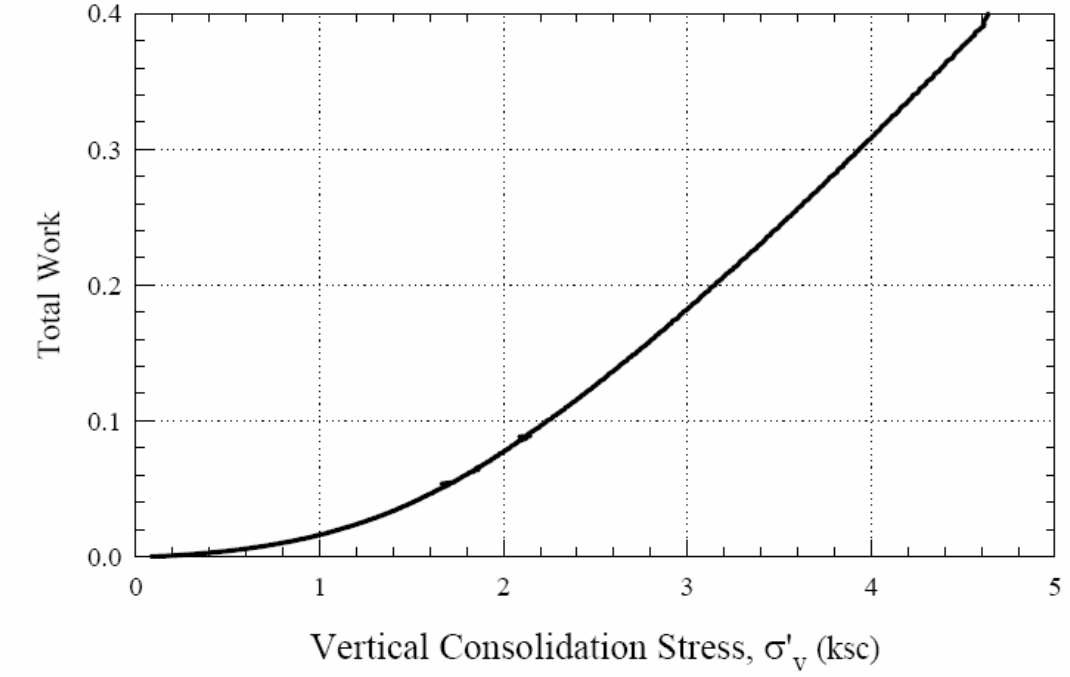

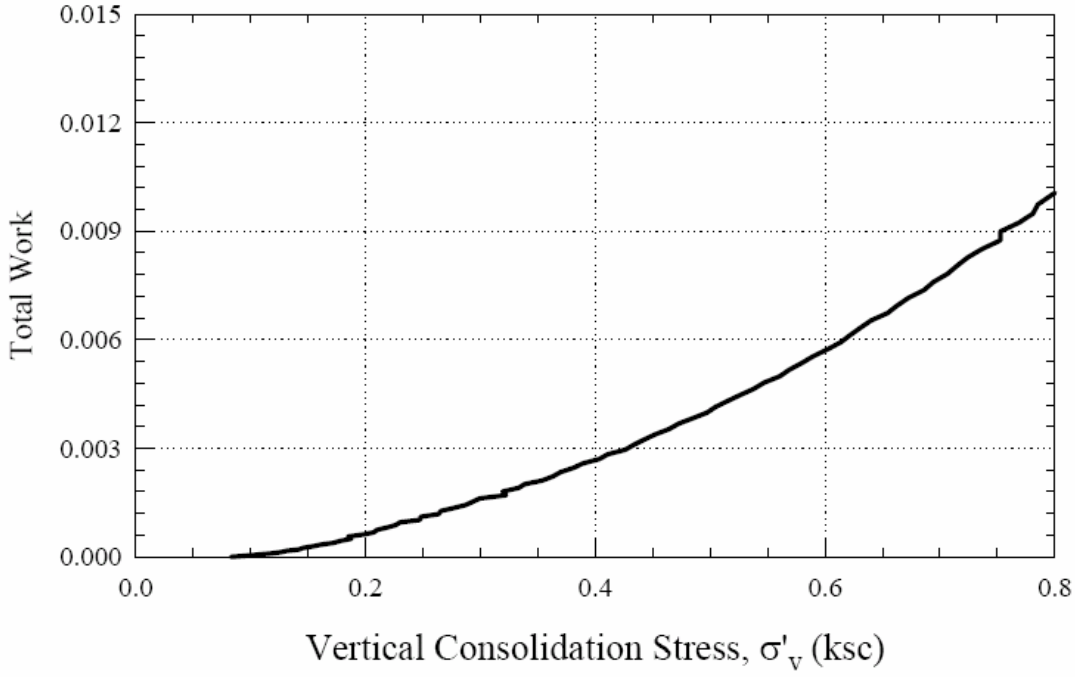

URS Corp.
CRS 440: TS3-B1 S-1

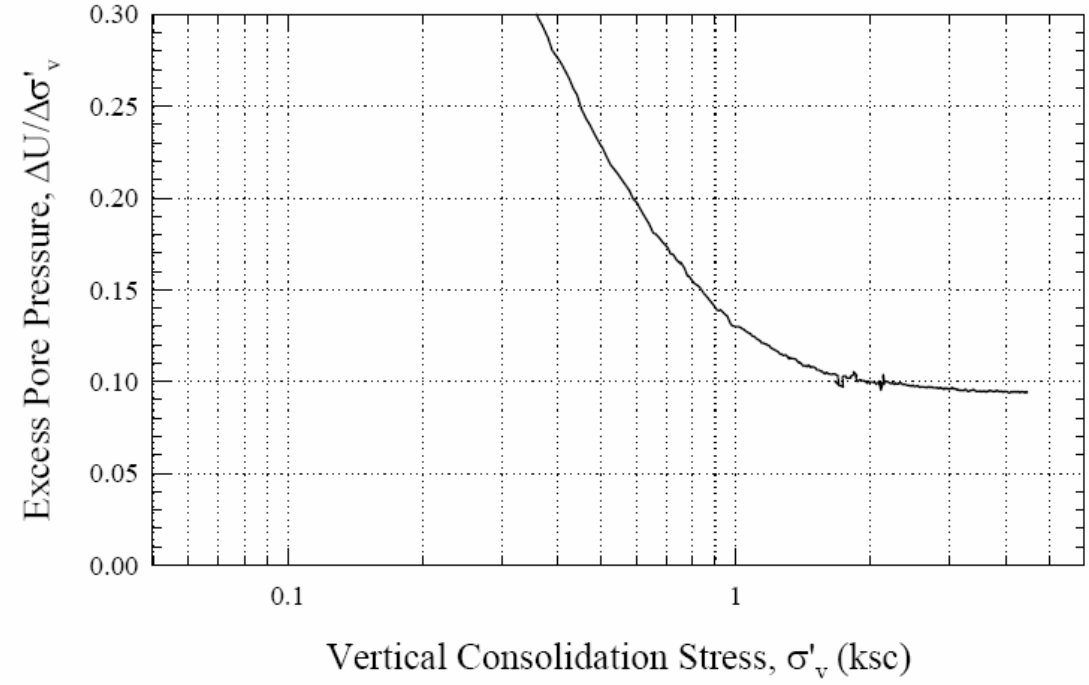

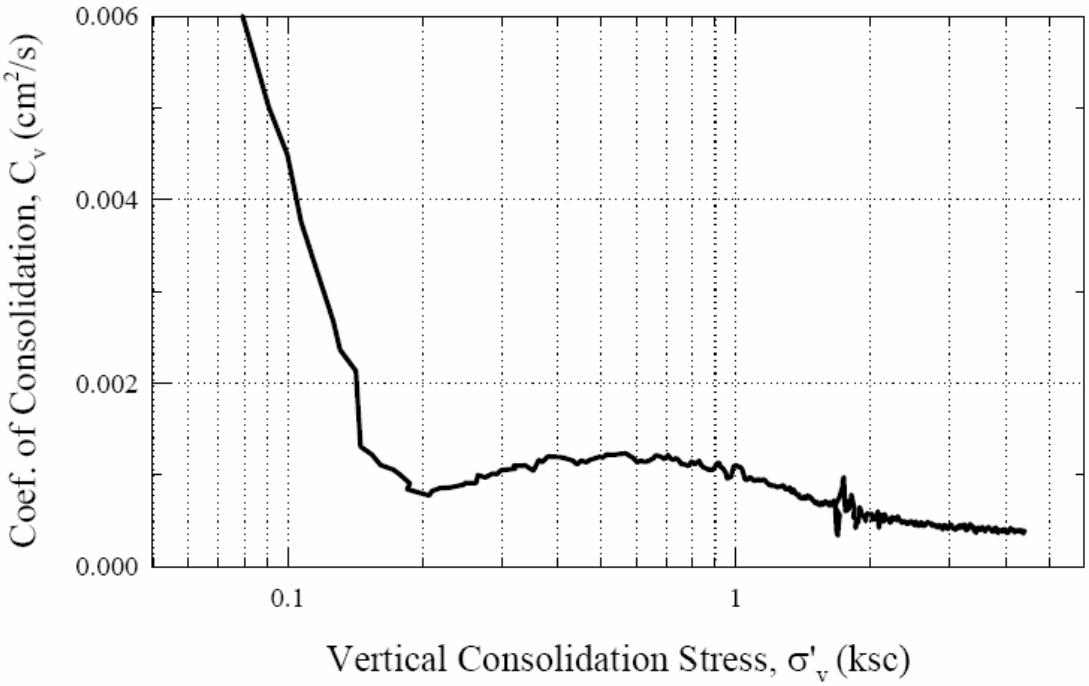

URS Corp.
CRS 440: TS3-B1 S-1

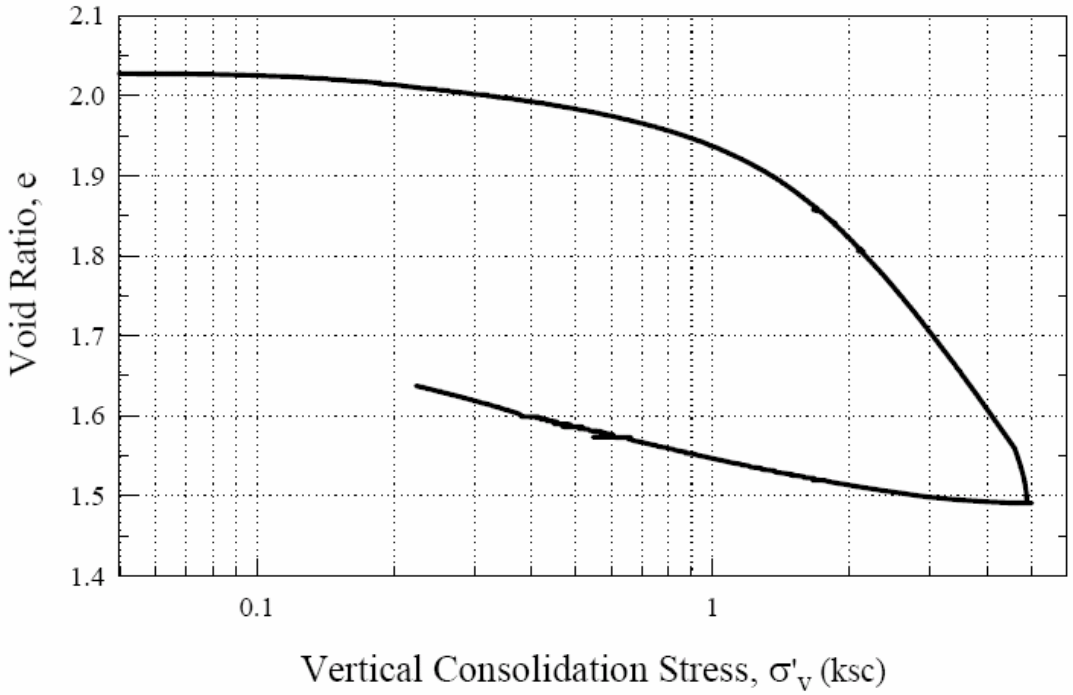

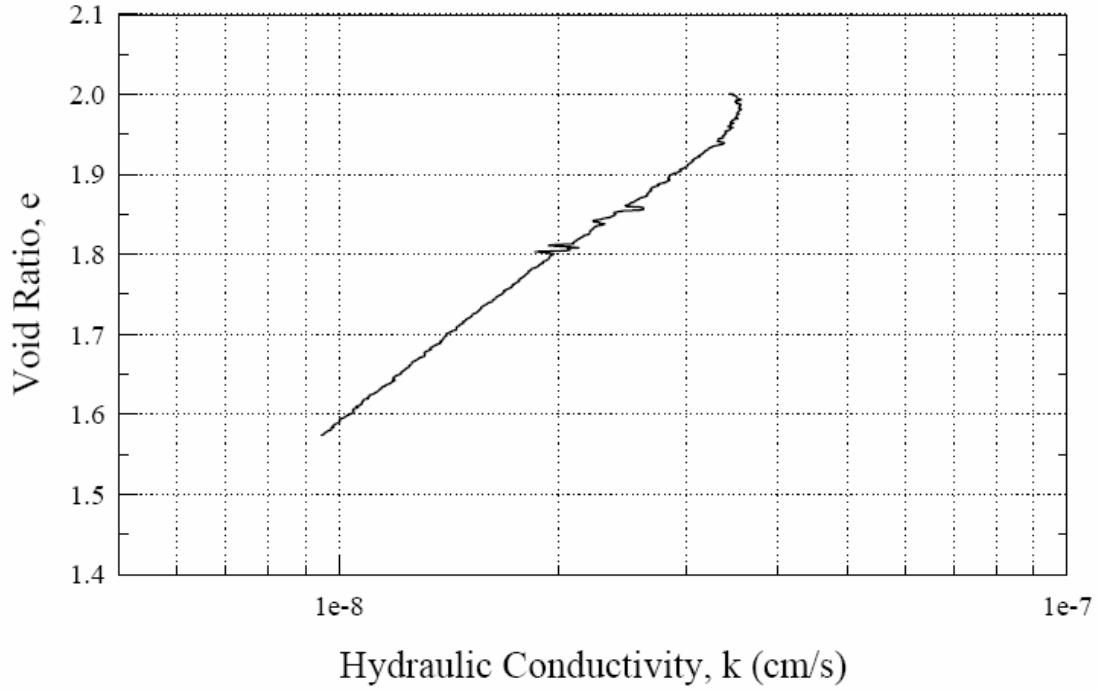

URS Corp.
CRS 441: TS3-B1 S-2

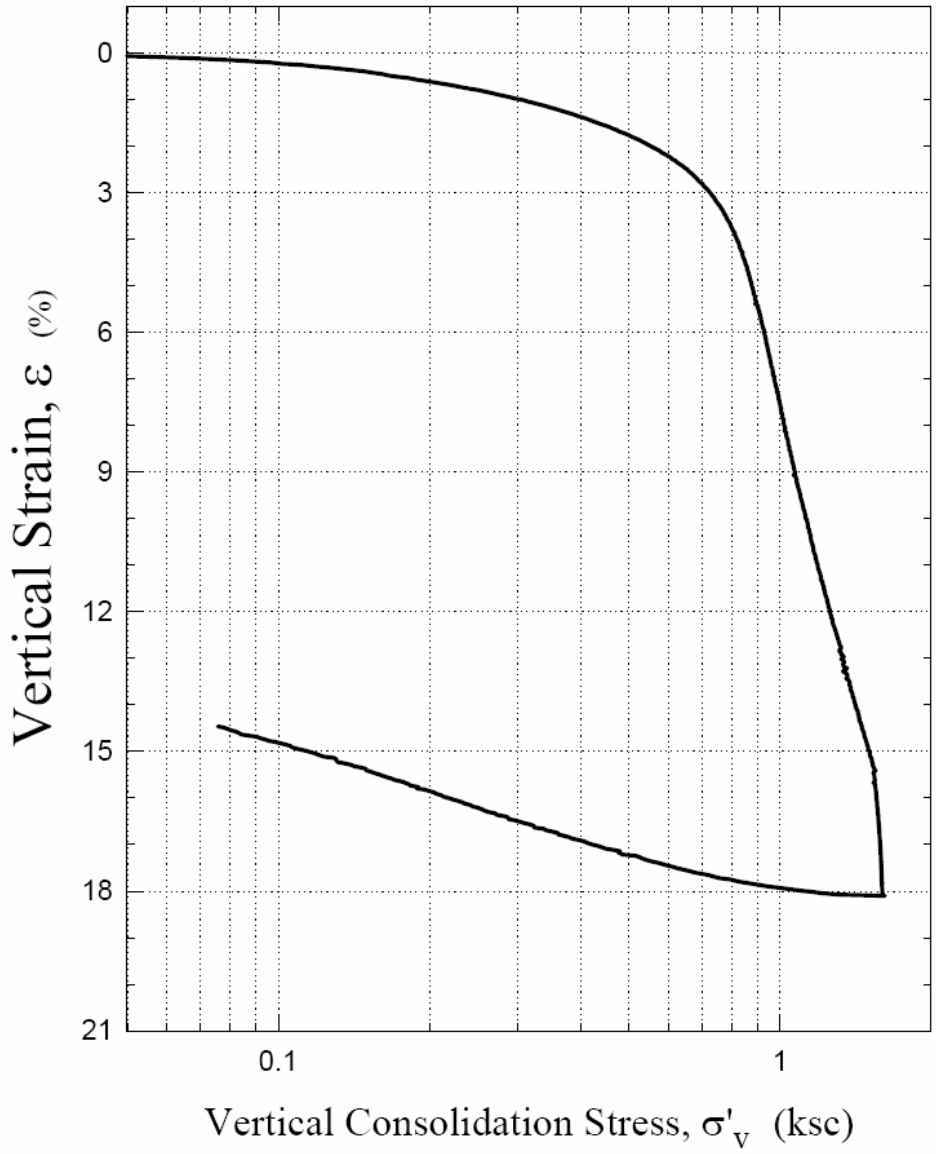

URS Corp.
CRS 441: TS3-B1 S-2

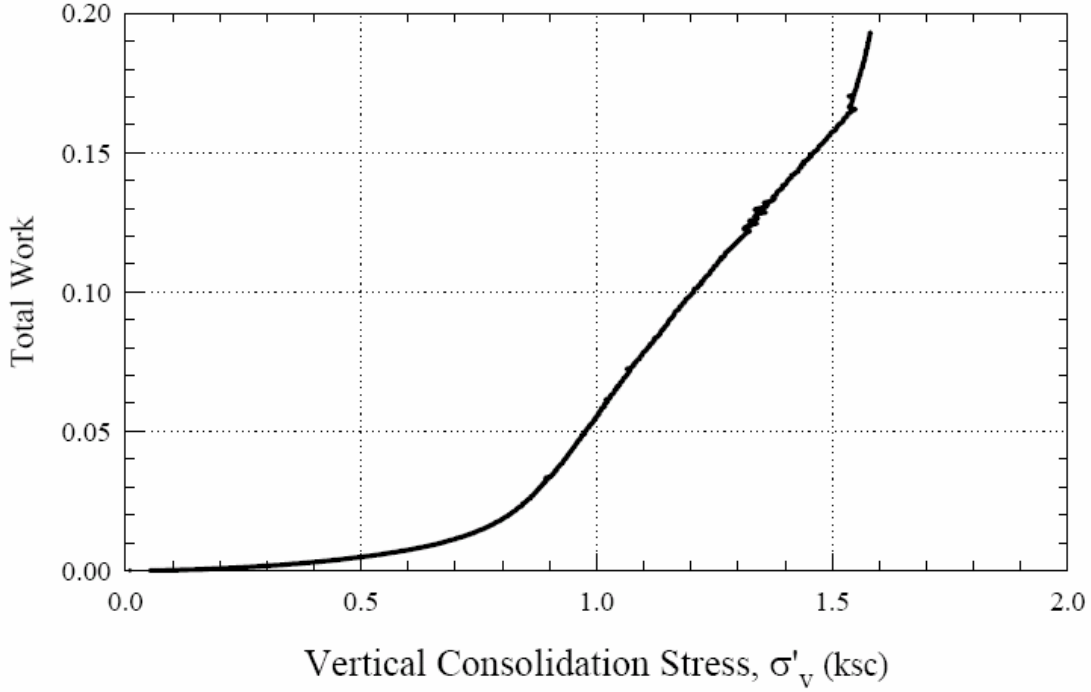

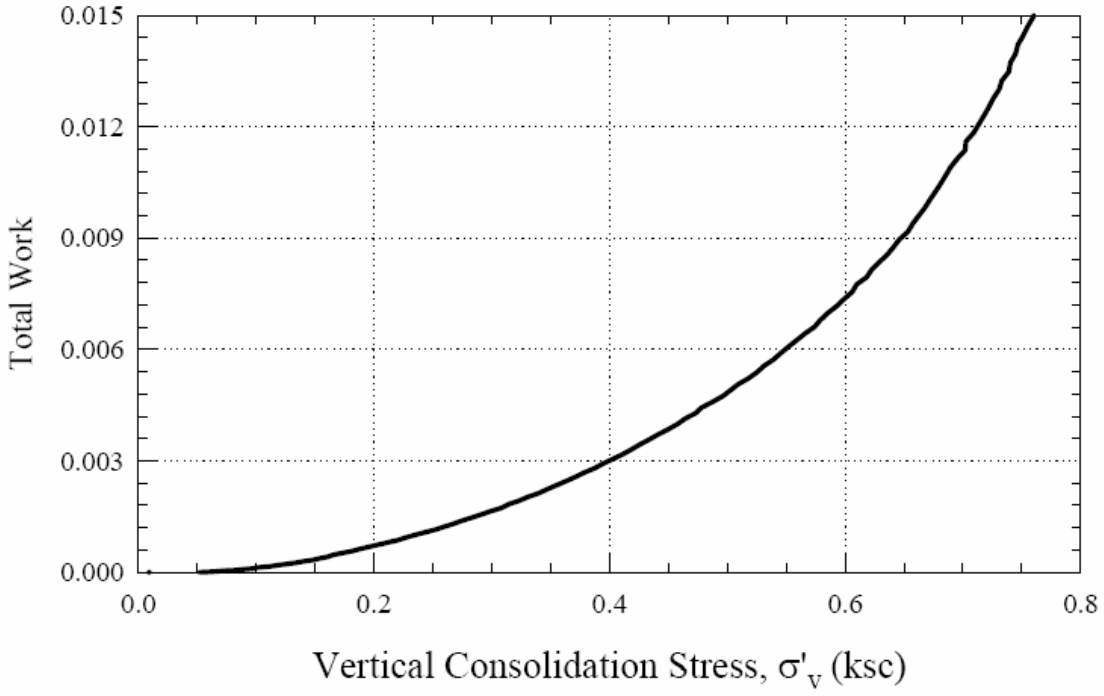

URS Corp.
CRS 441: TS3-B1 S-2

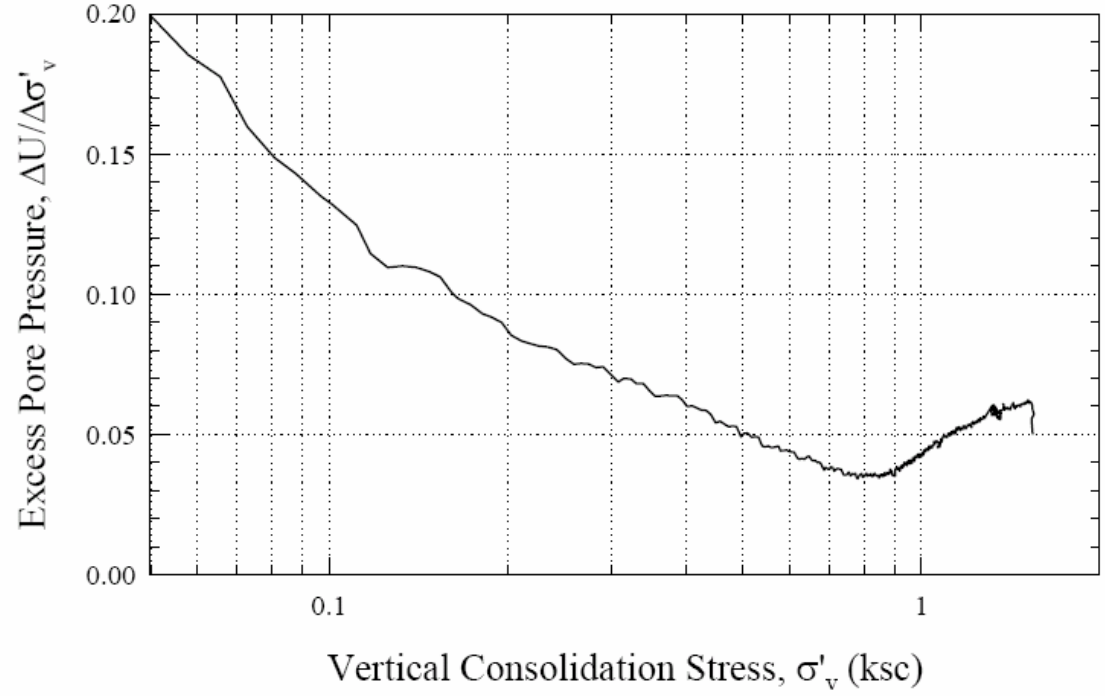

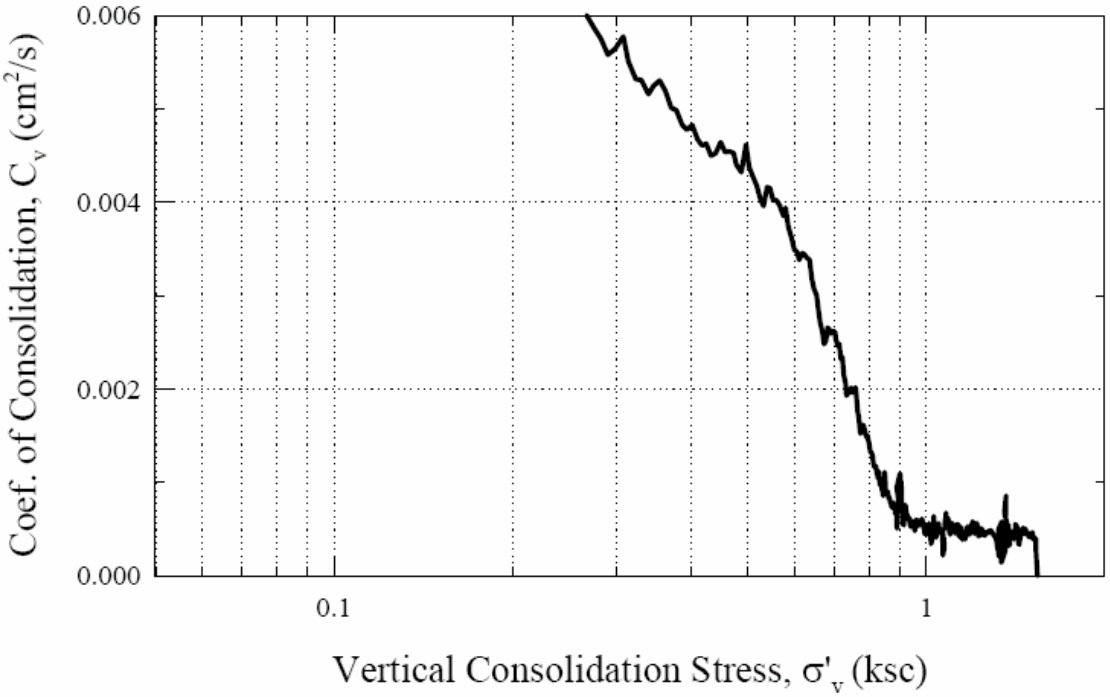

URS Corp.
CRS 441: TS3-B1 S-2

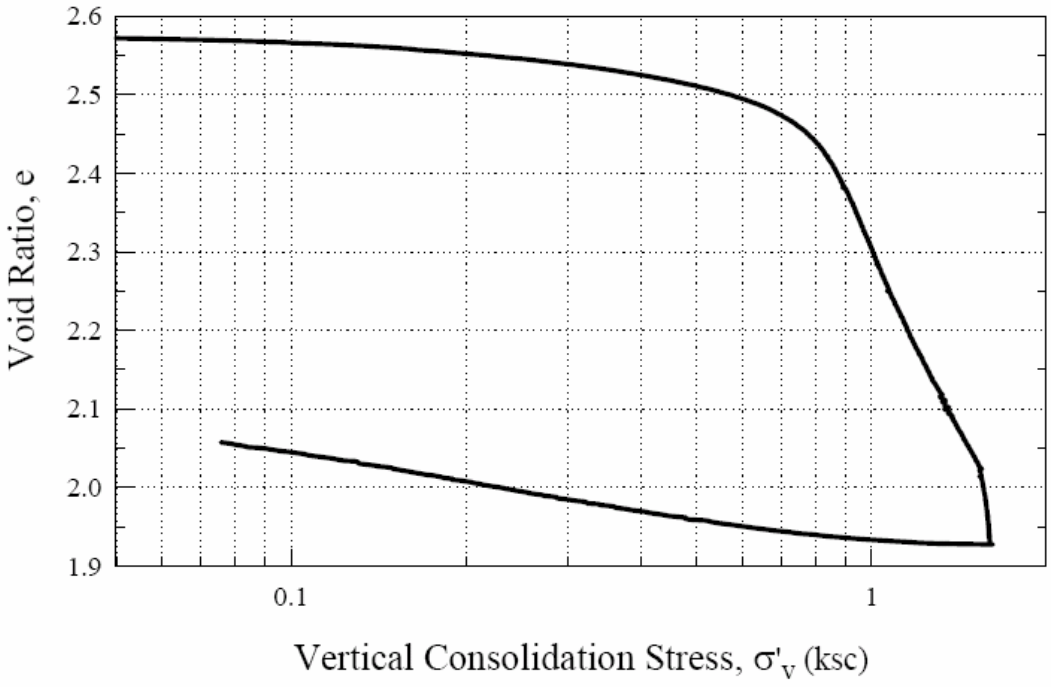

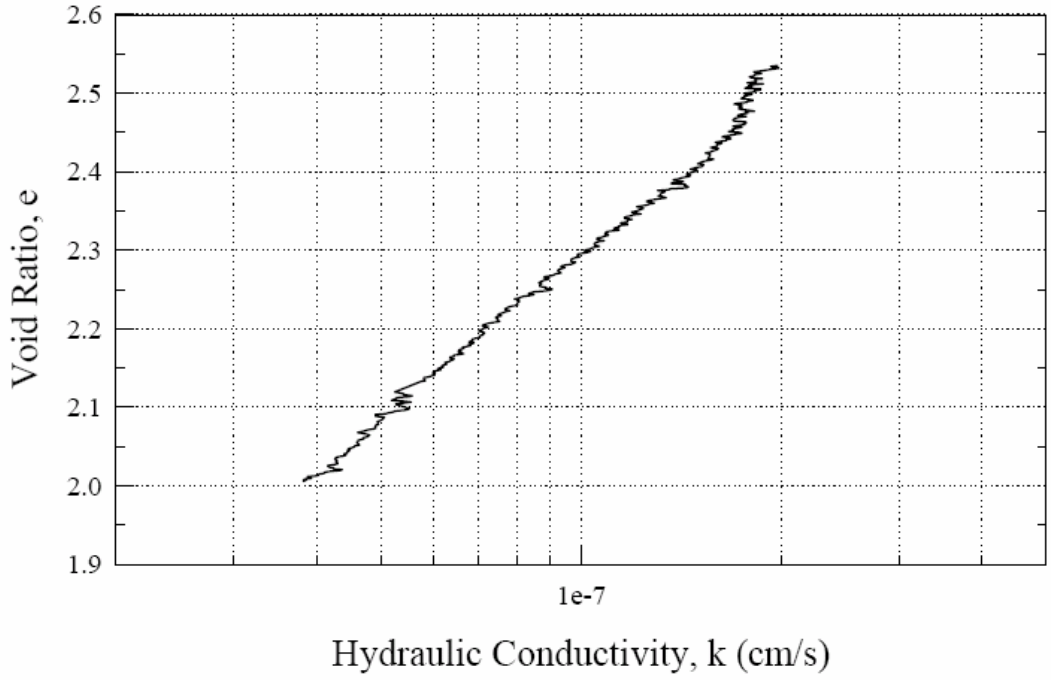

URS Corp.
CRS 432: TS3-B1 S-3

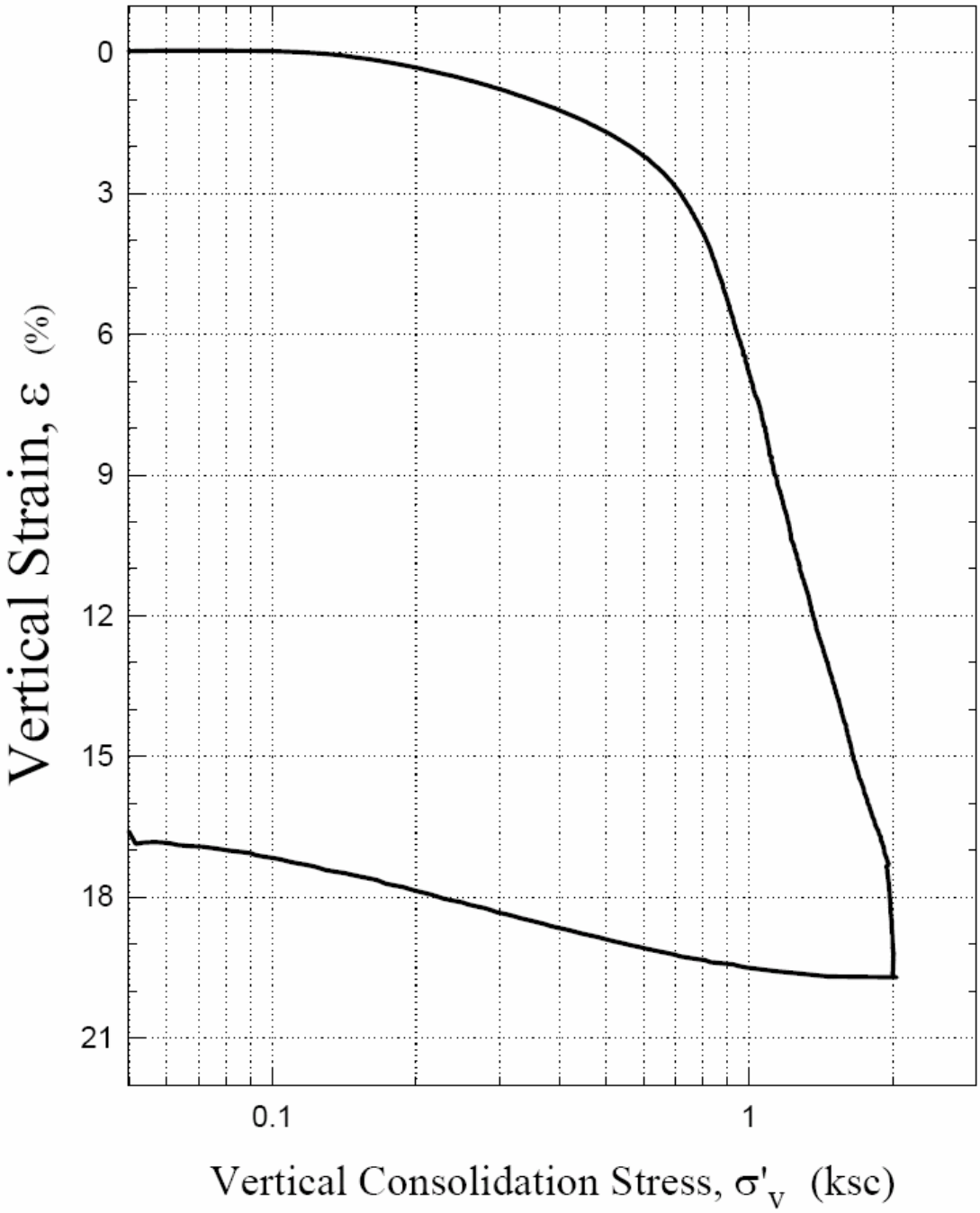

URS Corp.
CRS 432: TS3-B1 S-3

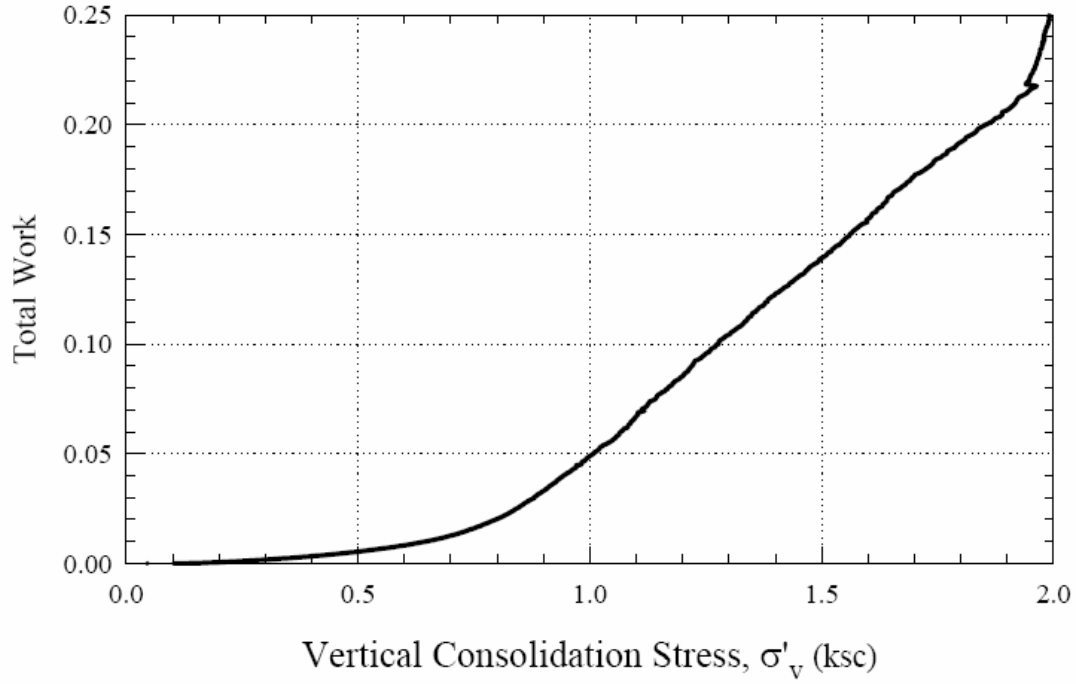

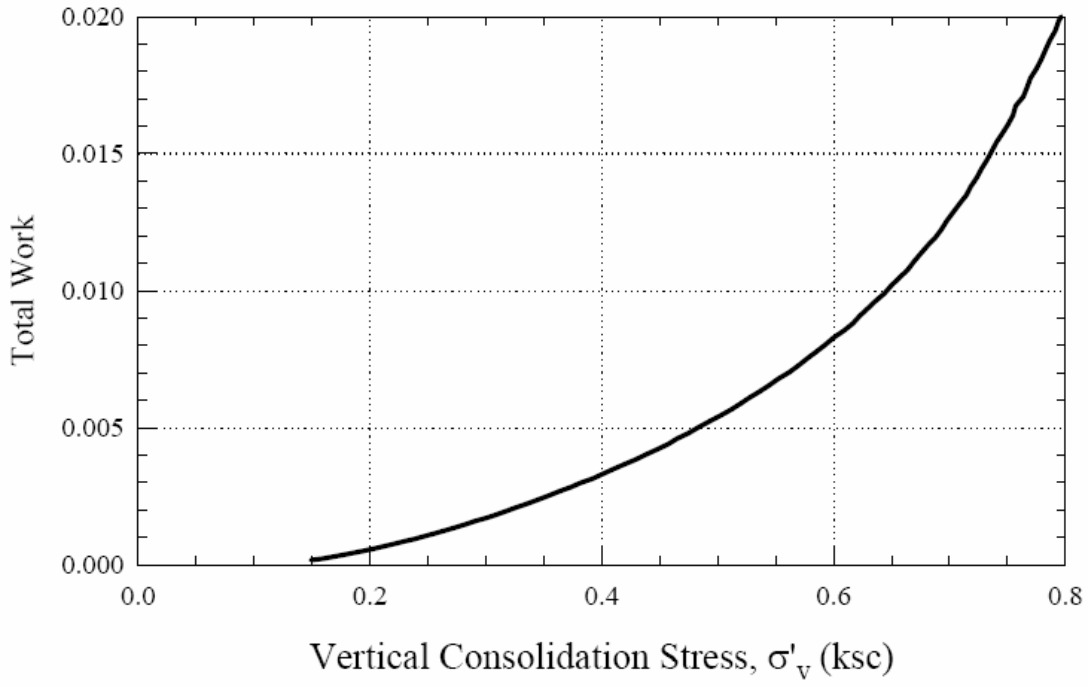

URS Corp.
CRS 432: TS3-B1 S-3

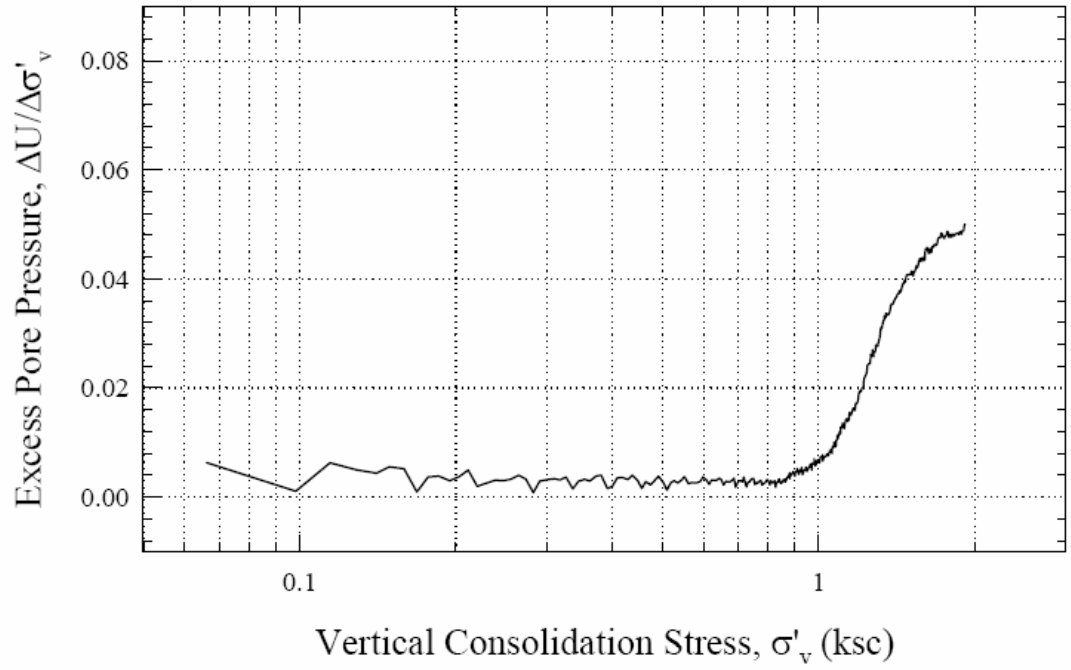

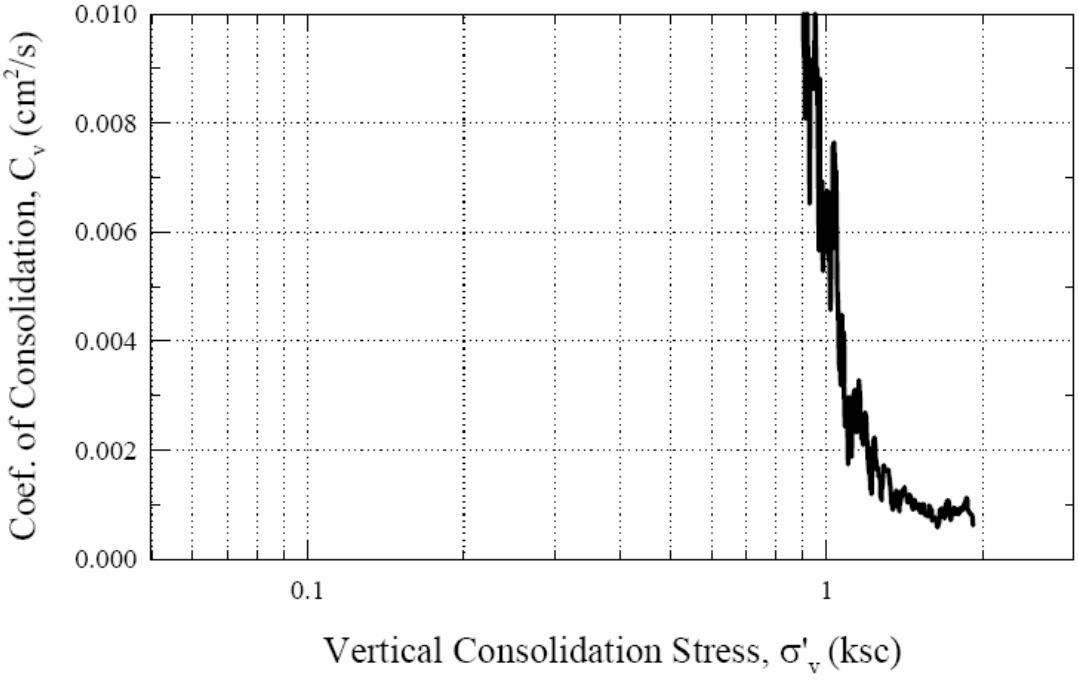

URS Corp.
CRS 432: TS3-B1 S-3

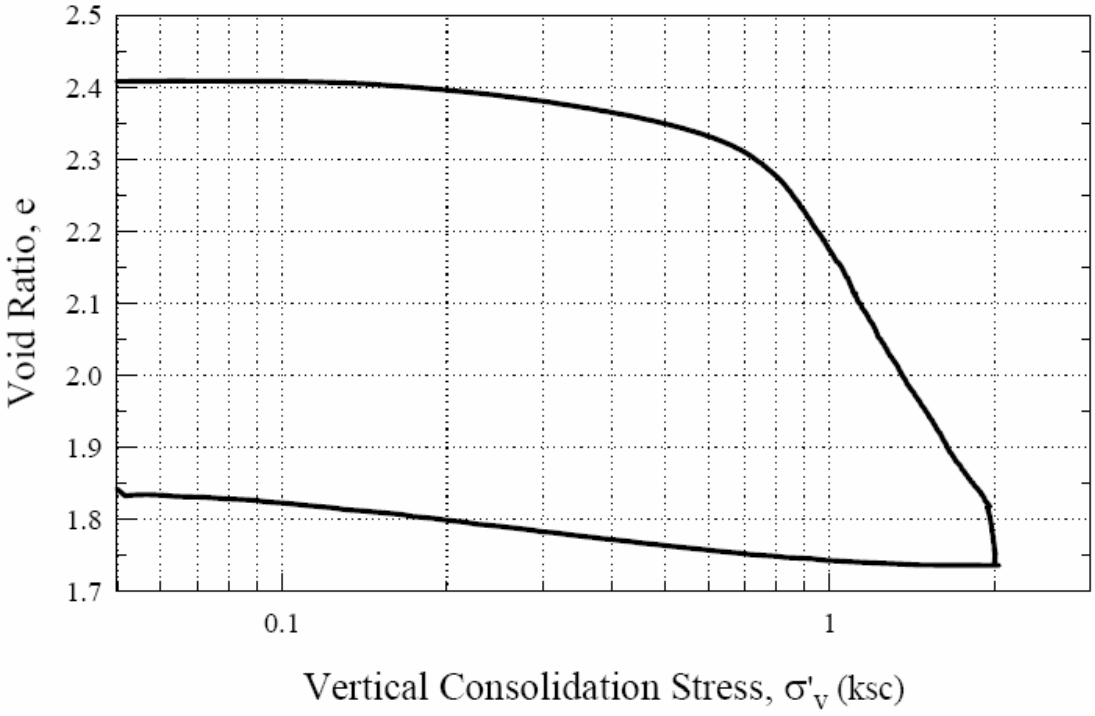

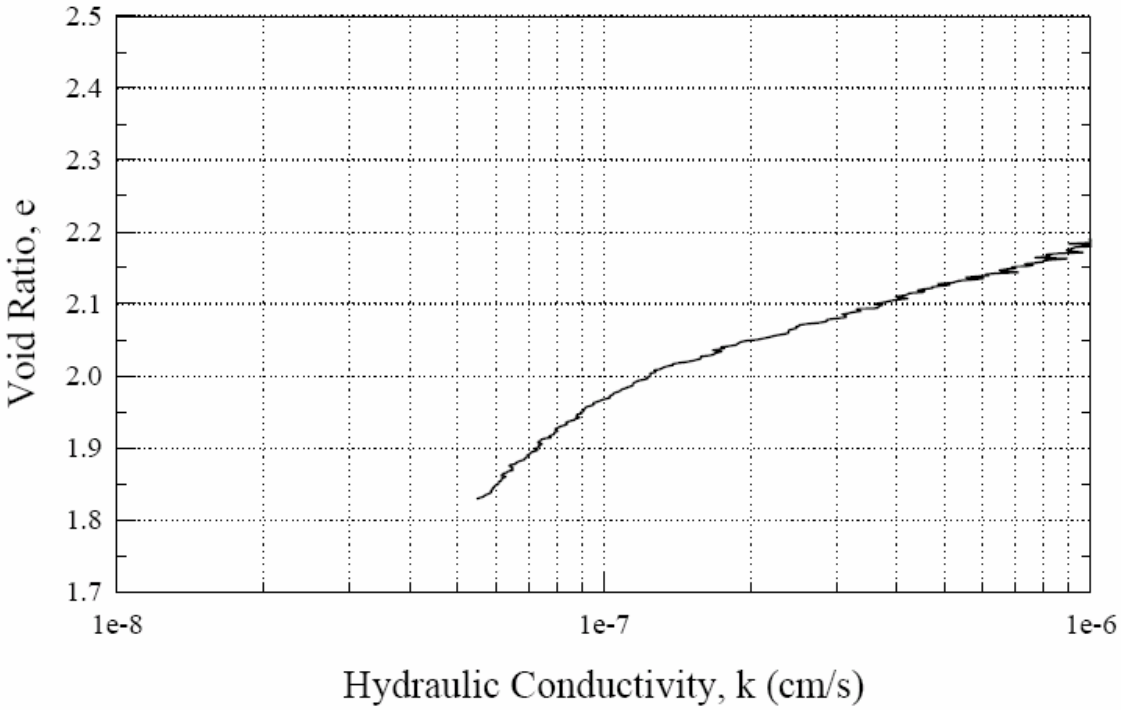

URS Corp.
CRS 431: TS3-B1 S-4

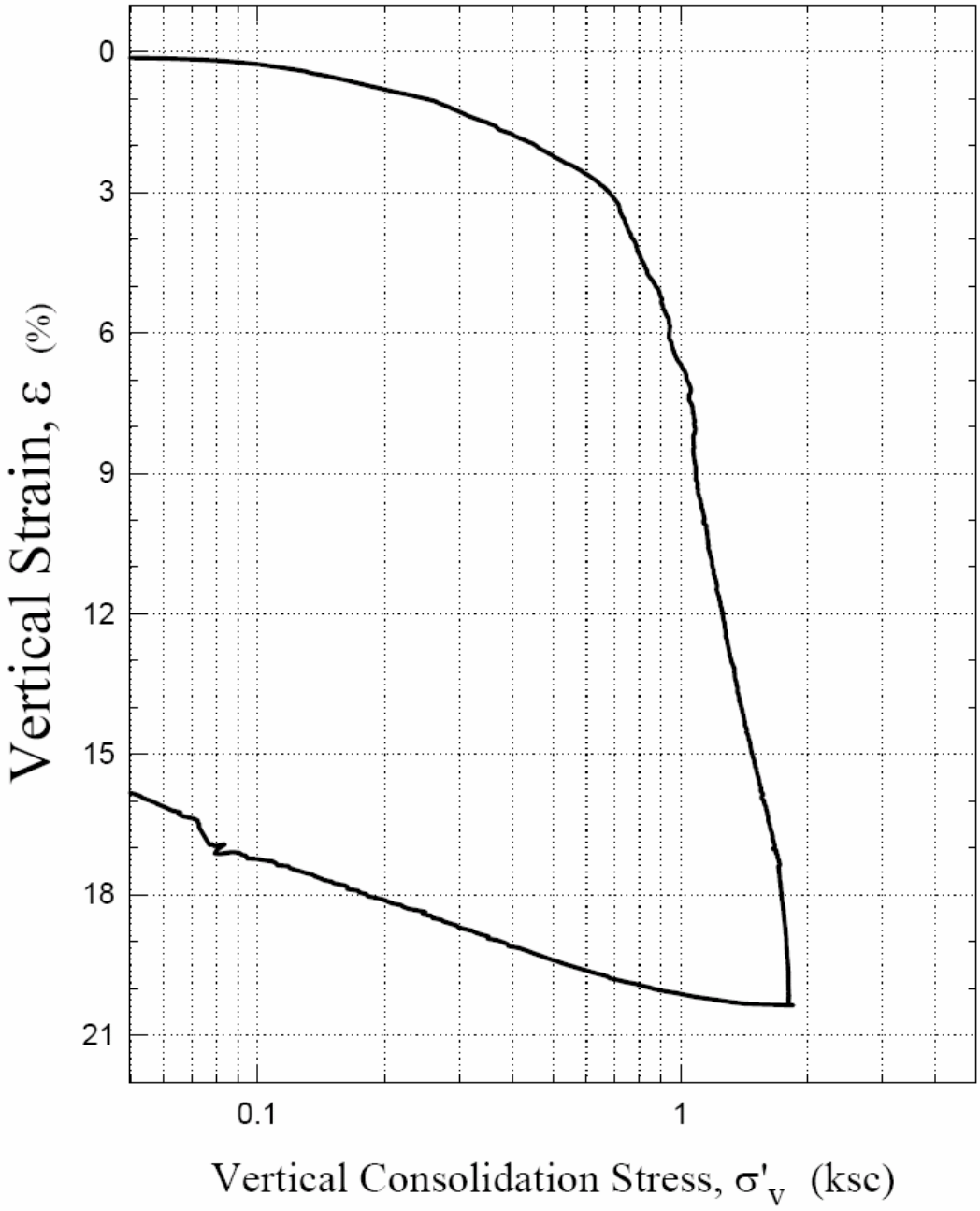

URS Corp.
CRS 431: TS3-B1 S-4

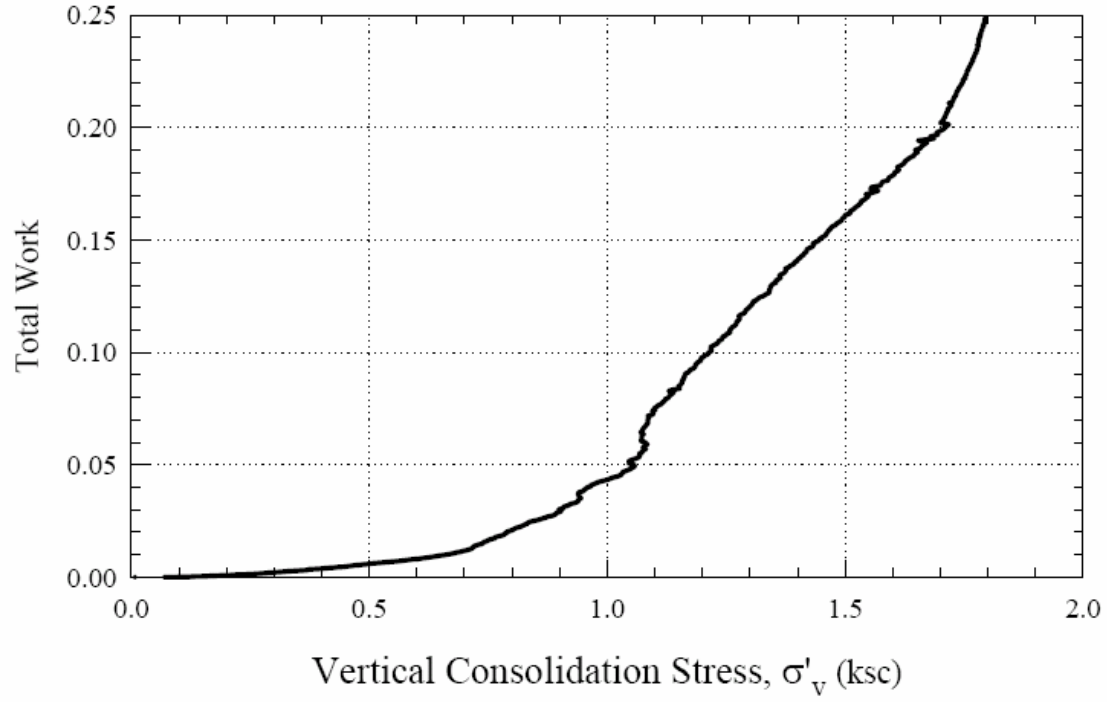

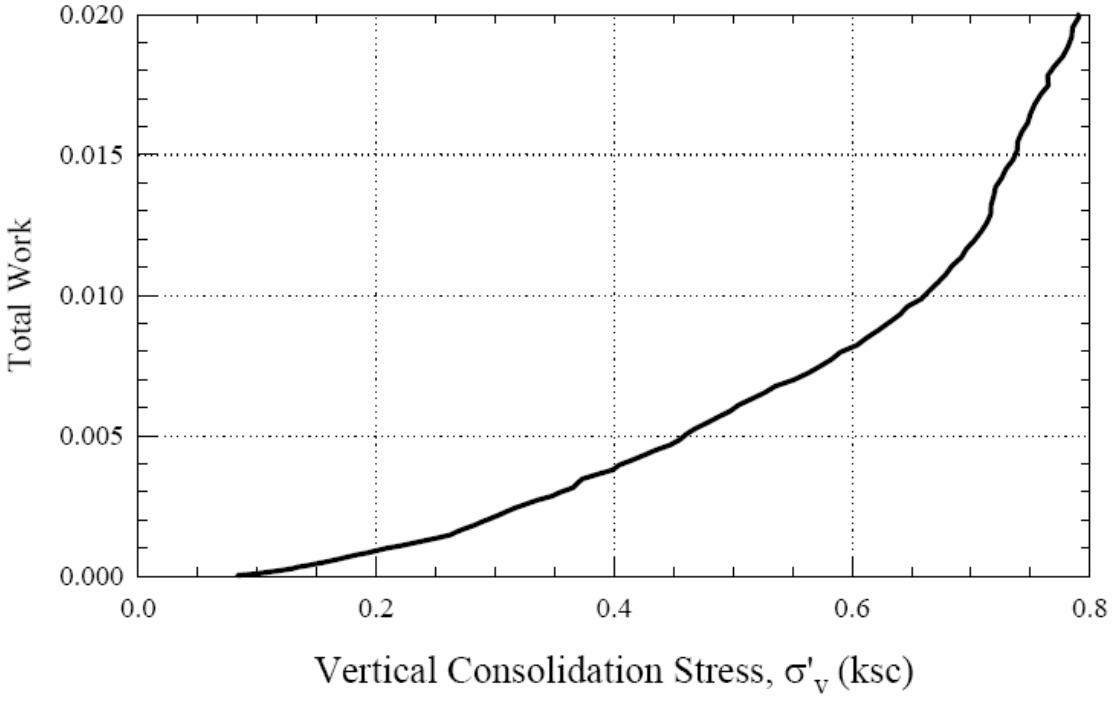

URS Corp.
CRS 431: TS3-B1 S-4

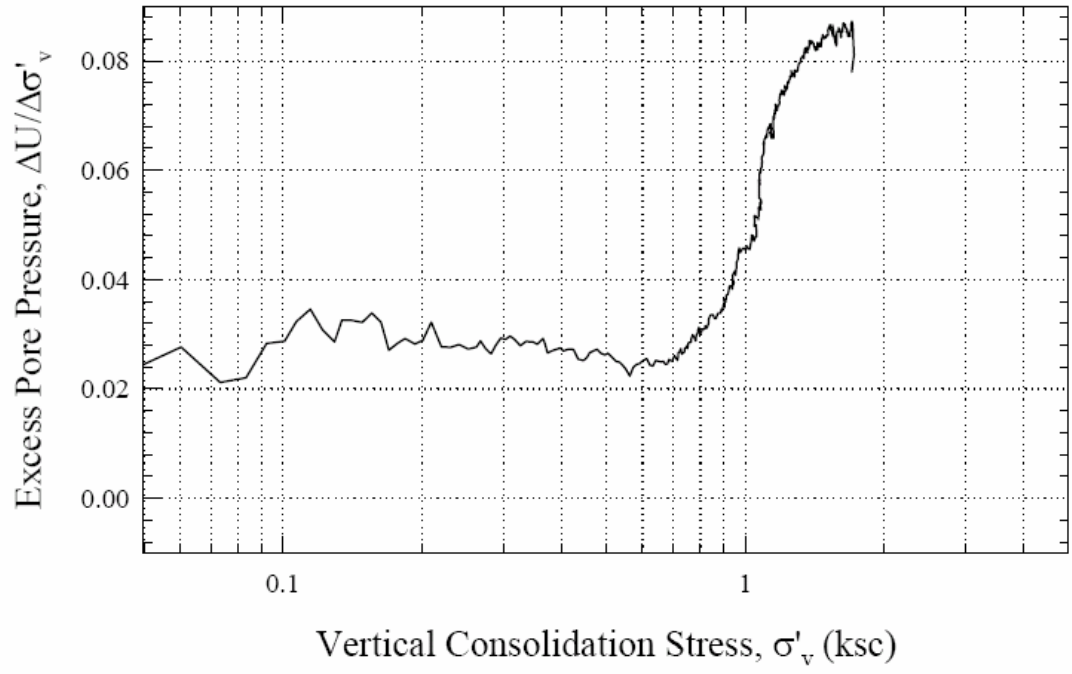

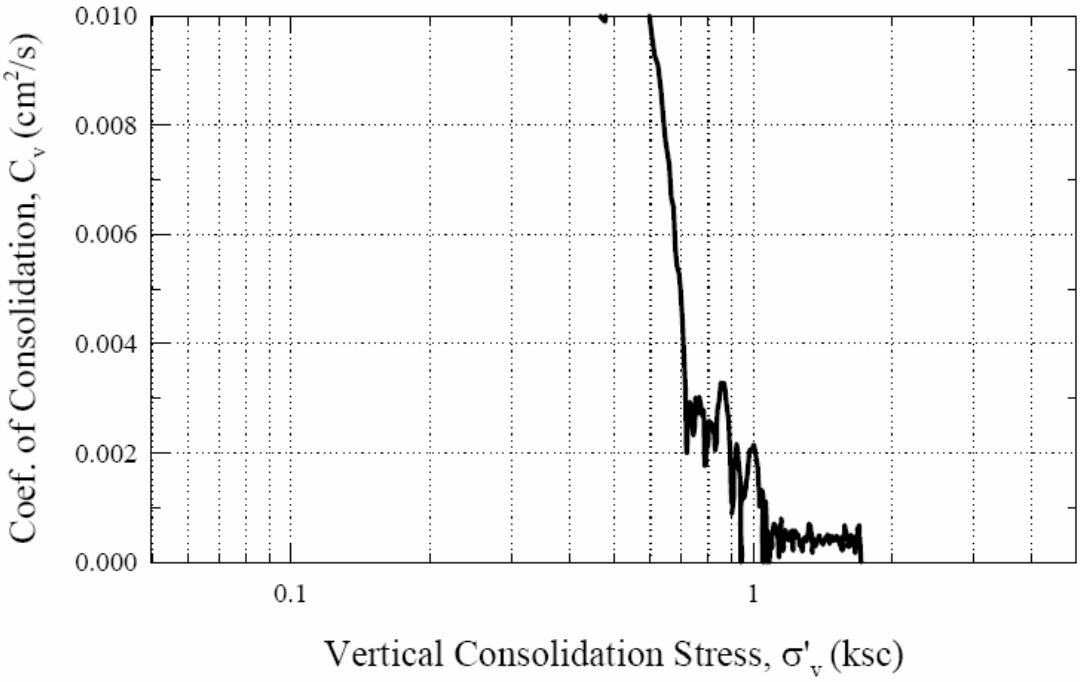

URS Corp.
CRS 431: TS3-B1 S-4

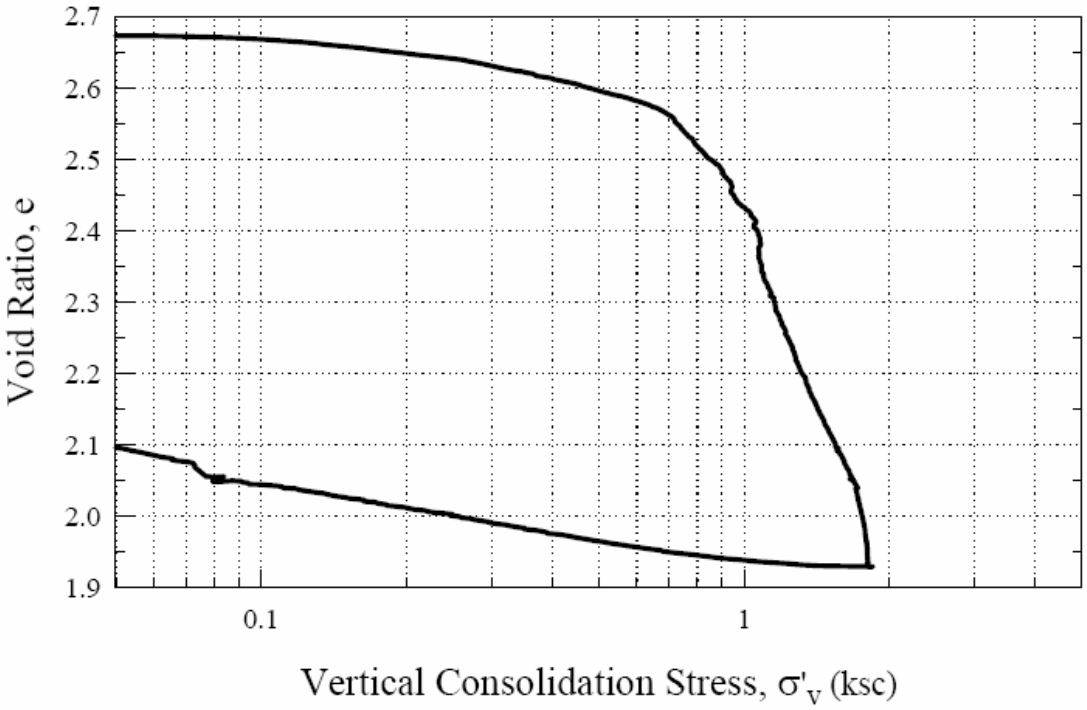

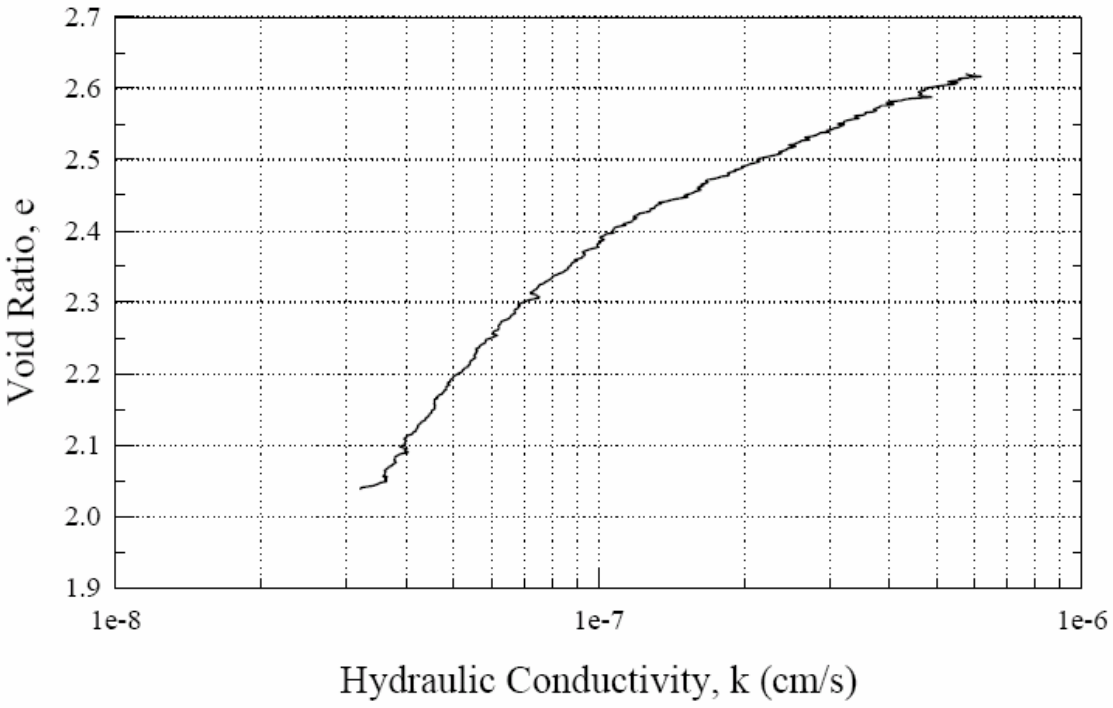

URS Corp.
CRS 435: TS3-B1 S-5

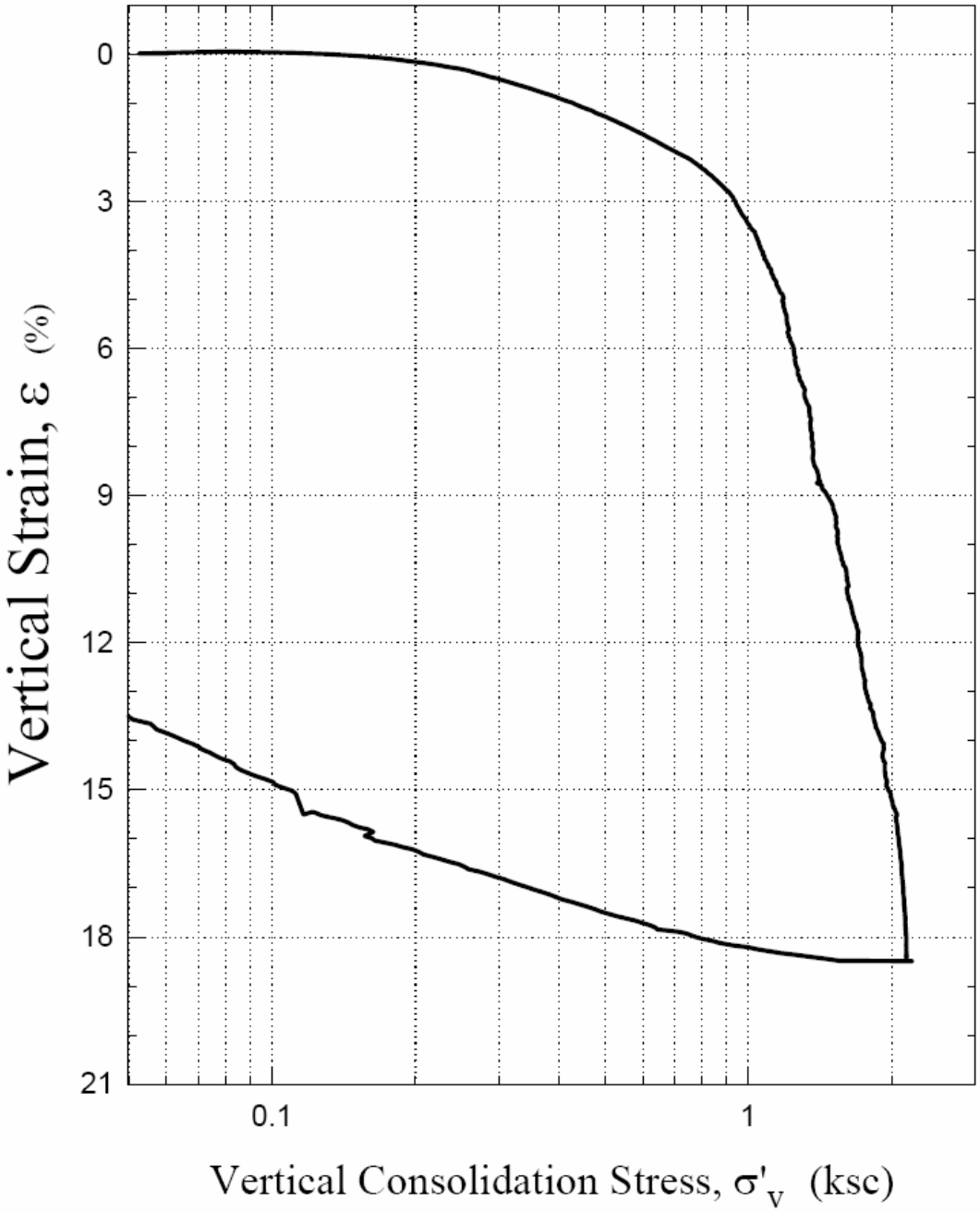

URS Corp.
CRS 435: TS3-B1 S-5

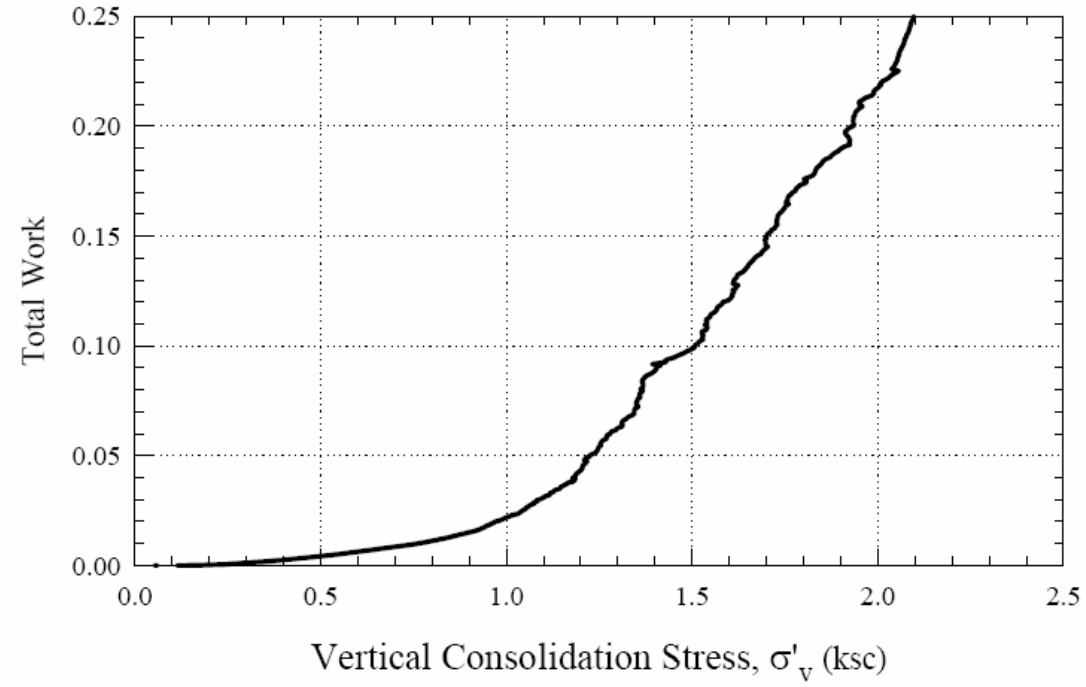

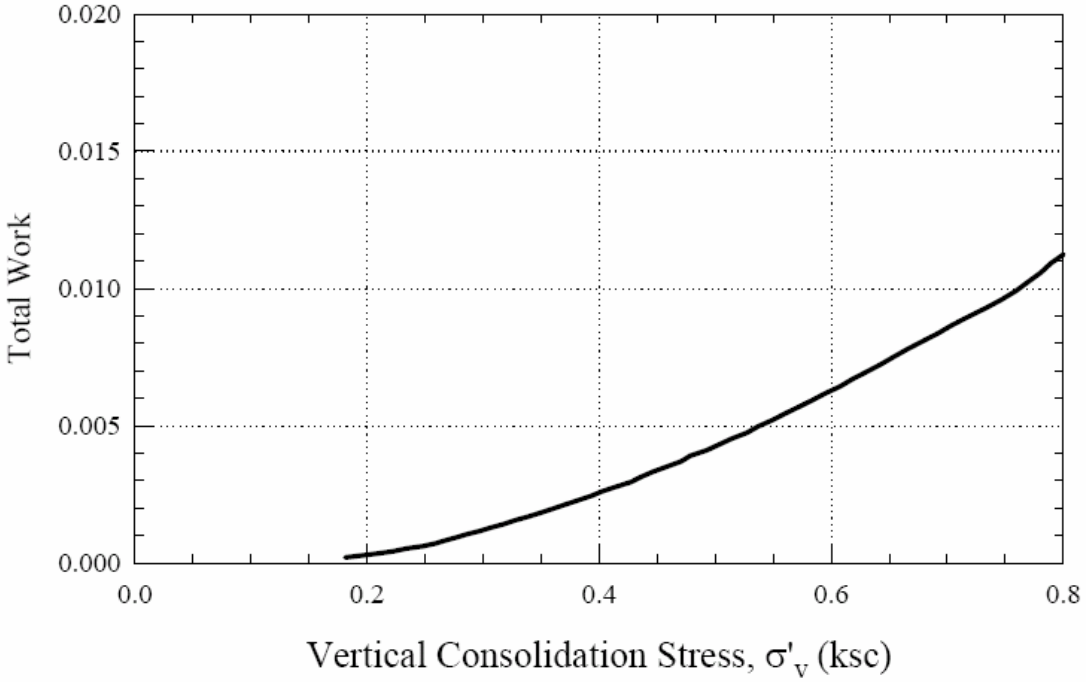

URS Corp.
CRS 435: TS3-B1 S-5

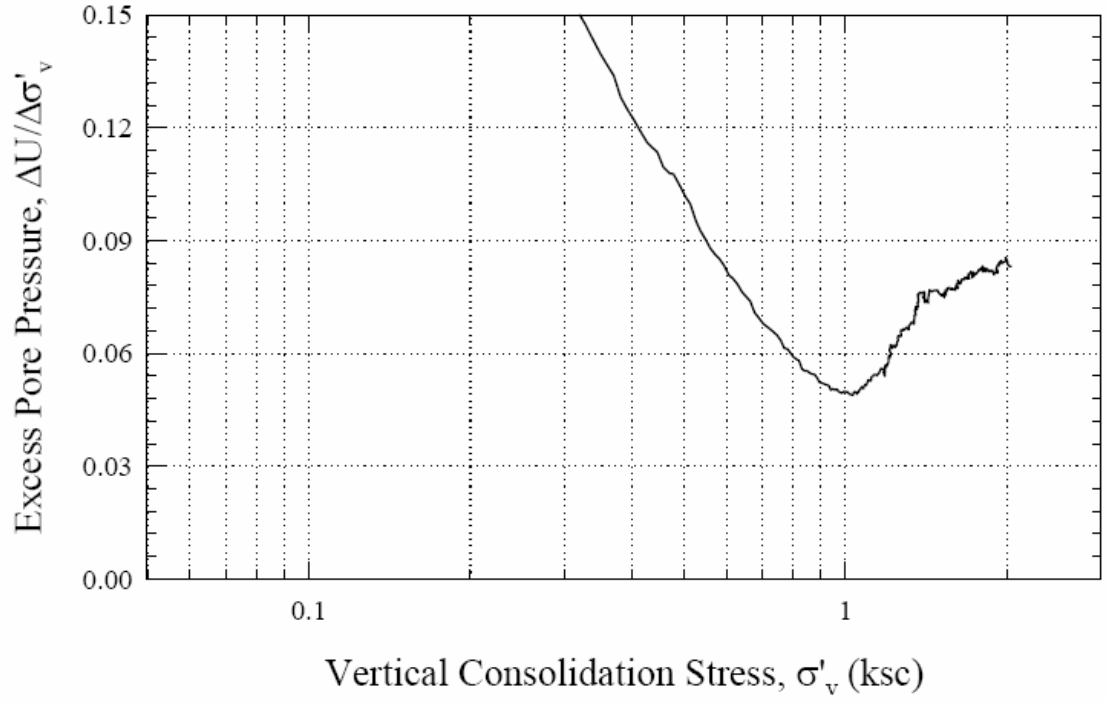

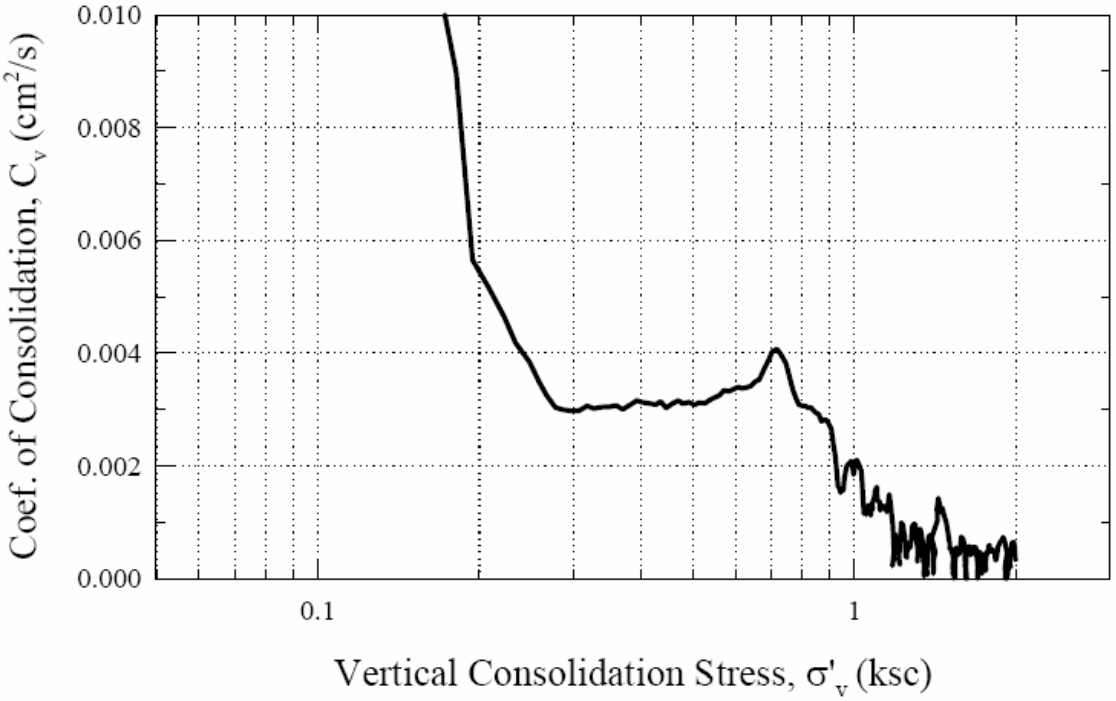

URS Corp.
CRS 435: TS3-B1 S-5

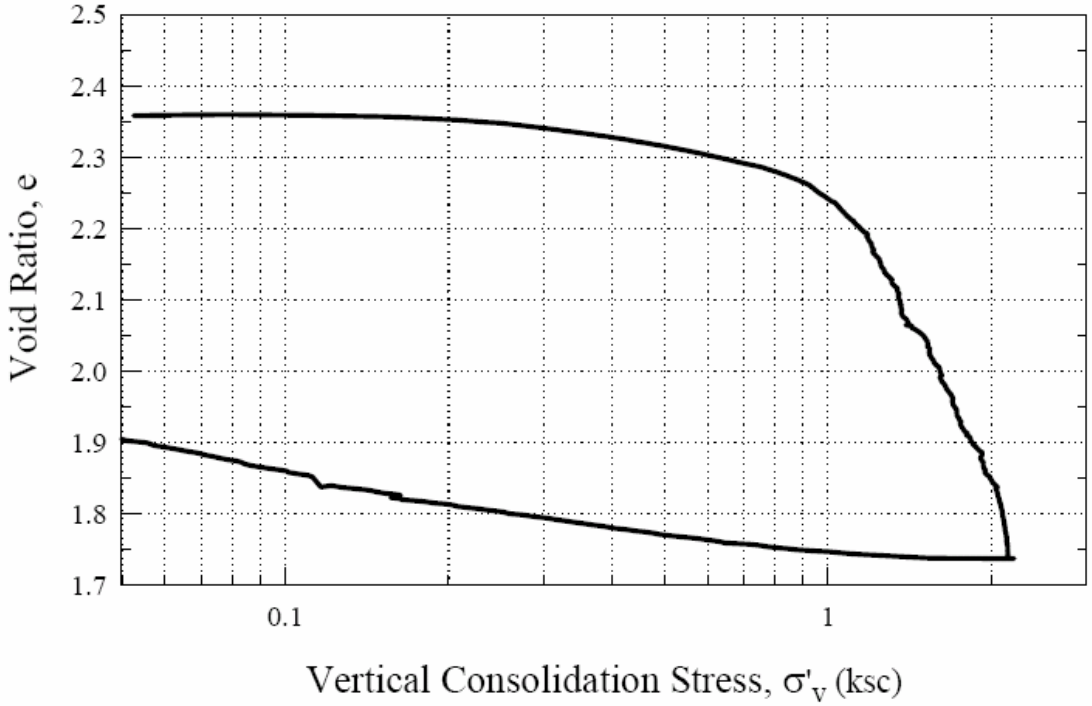

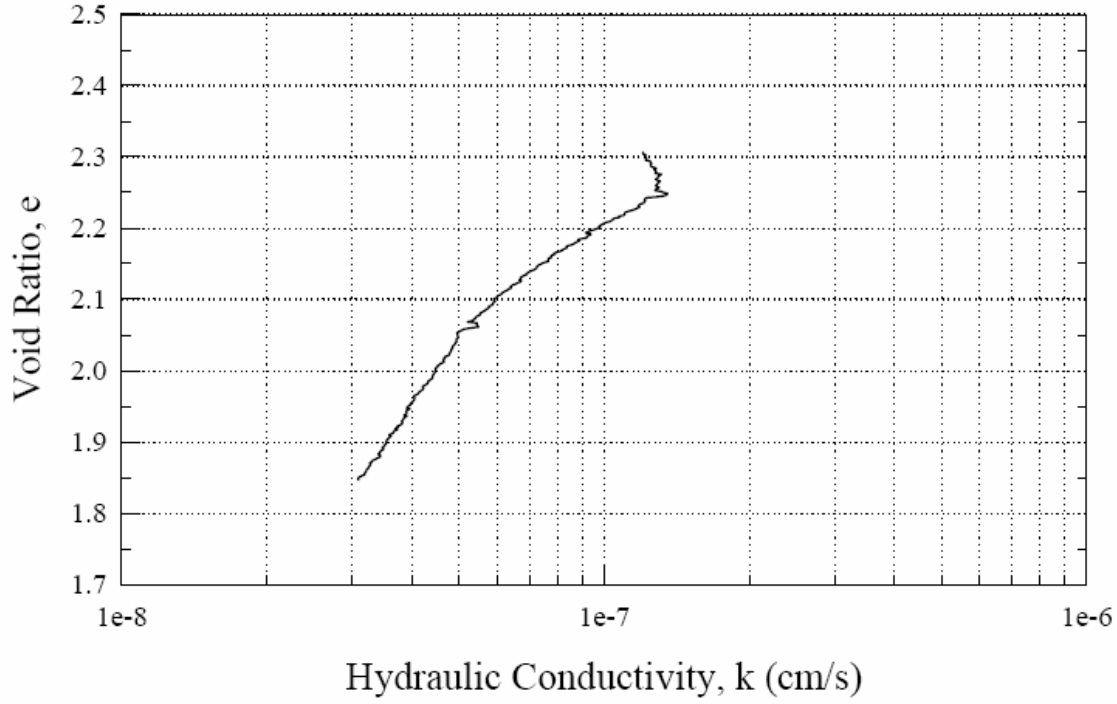

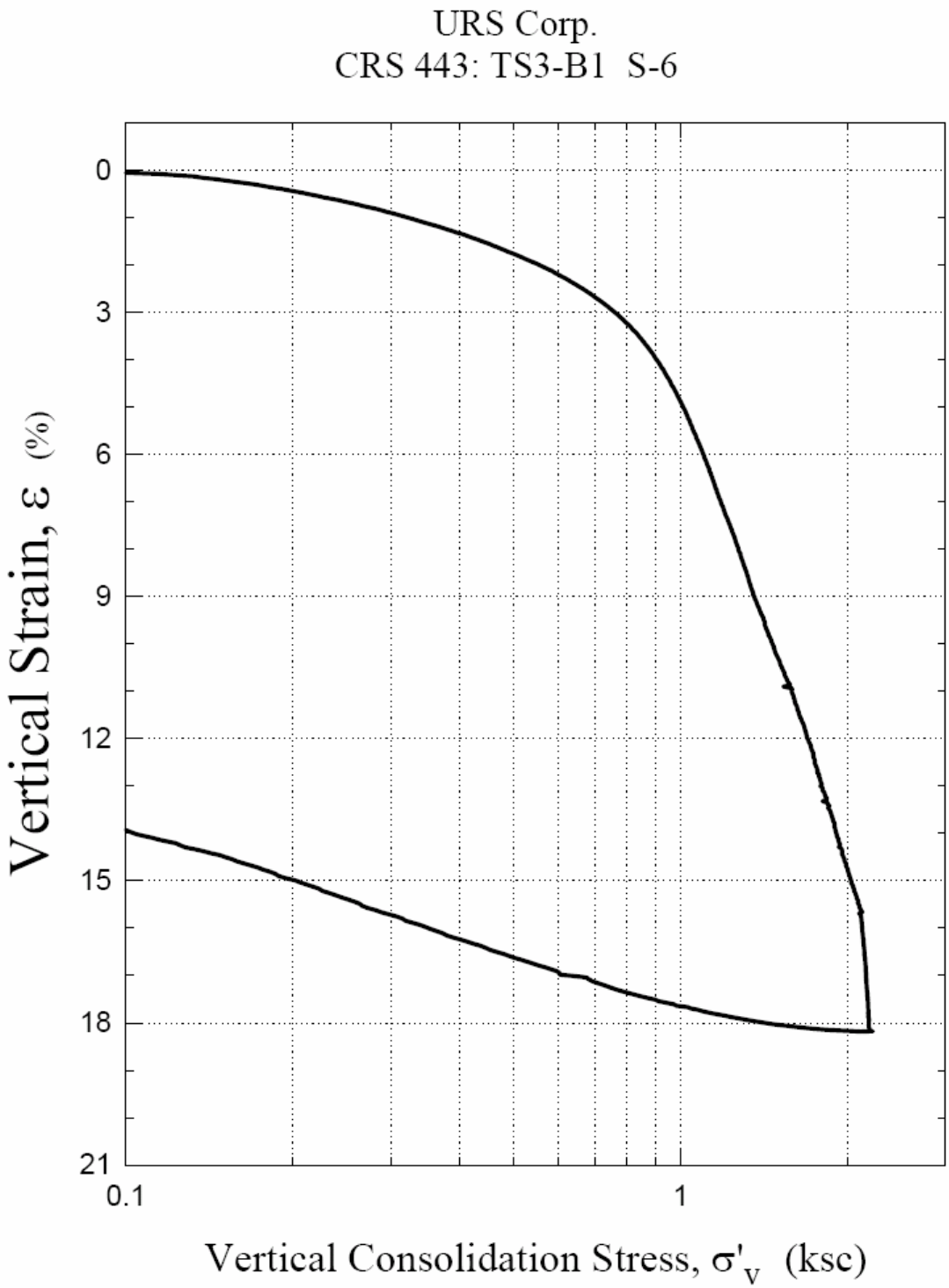
URS Corp.
CRS 443: TS3-B1 S-6
0
3
6
9
12
15
18
21
Vertical Strain, ε (%)
0.1
1
Vertical Consolidation Stress, σ'v (ksc)

URS Corp.
CRS 443: TS3-B1 S-6

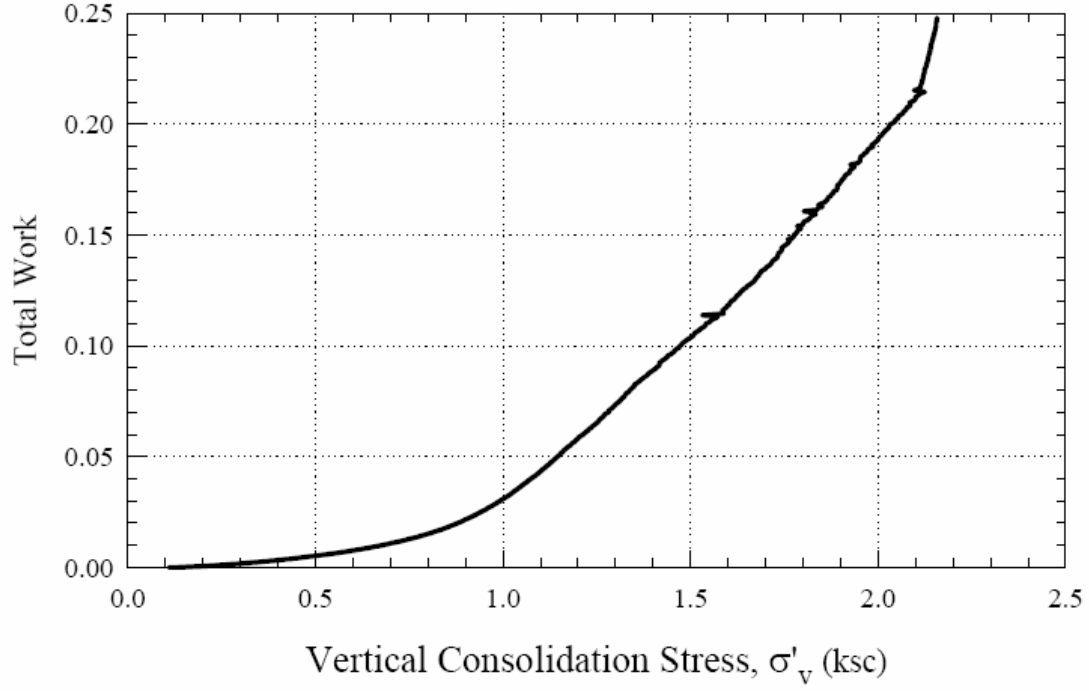

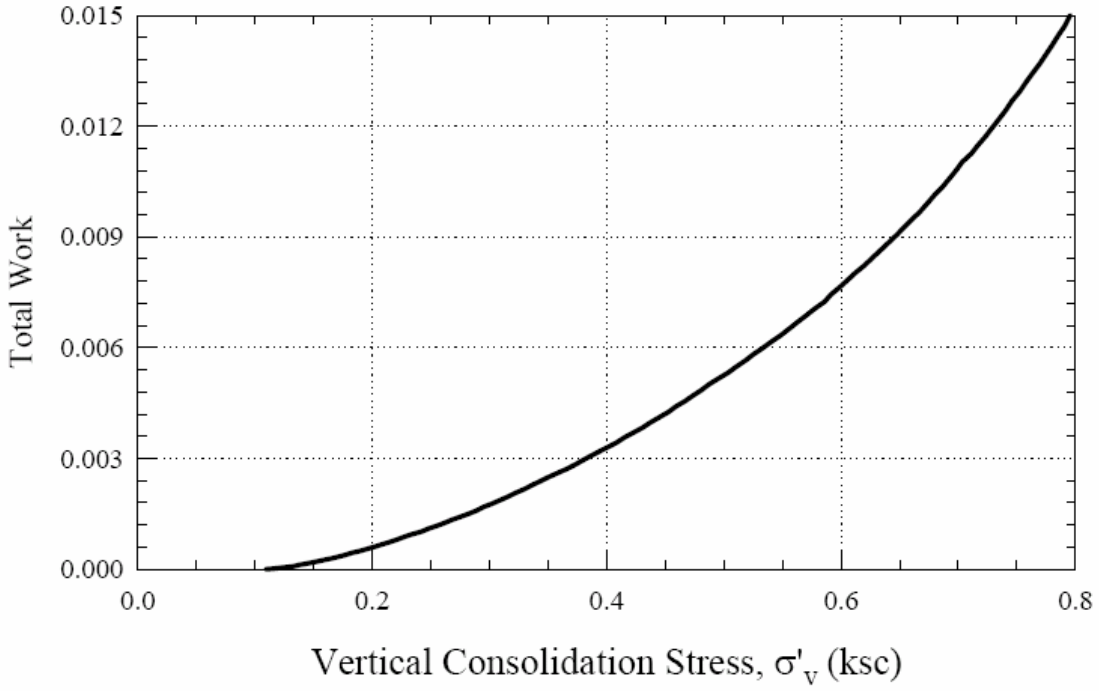

URS Corp.
CRS 443: TS3-B1 S-6

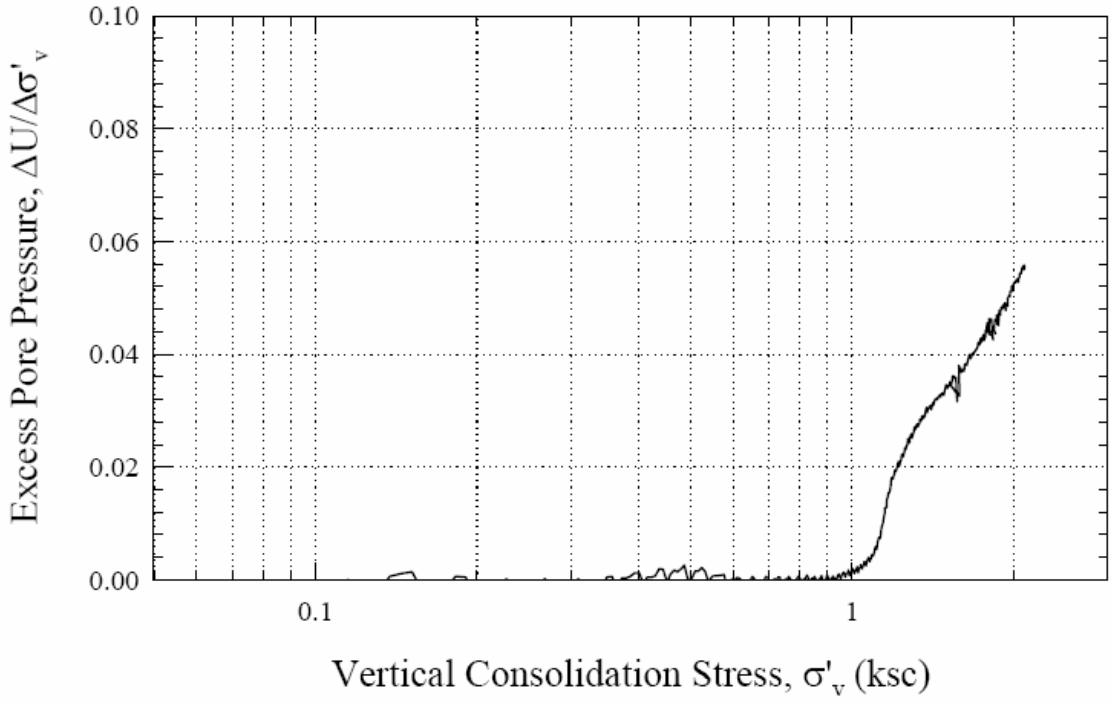

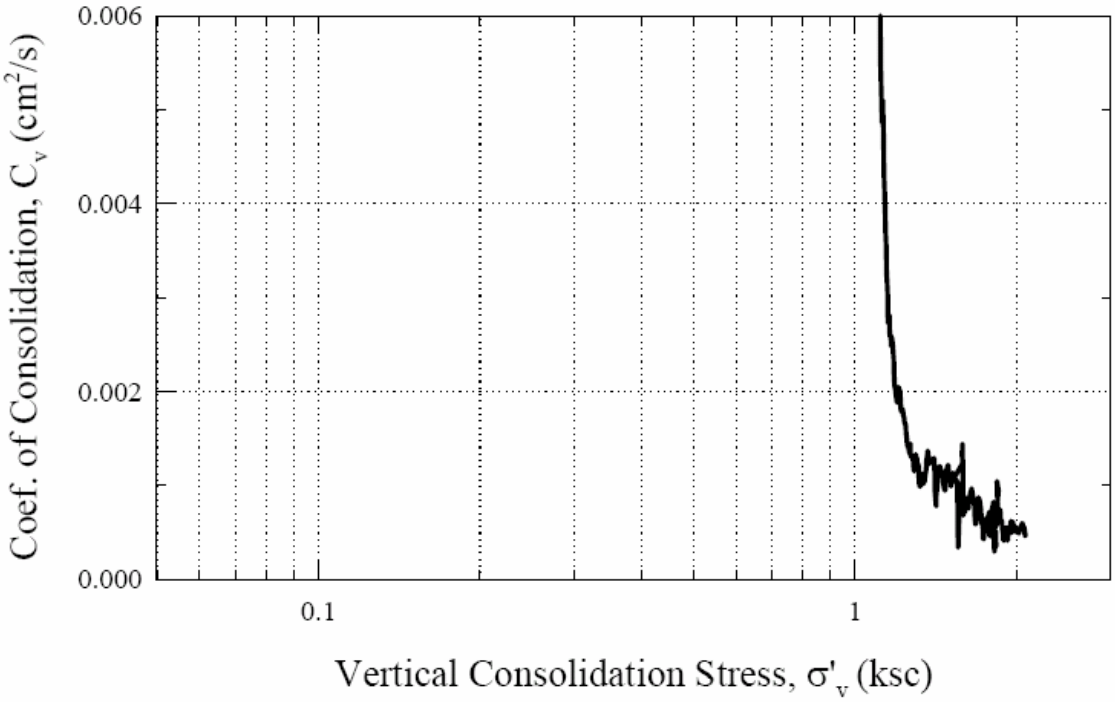

URS Corp.
CRS 443: TS3-B1 S-6

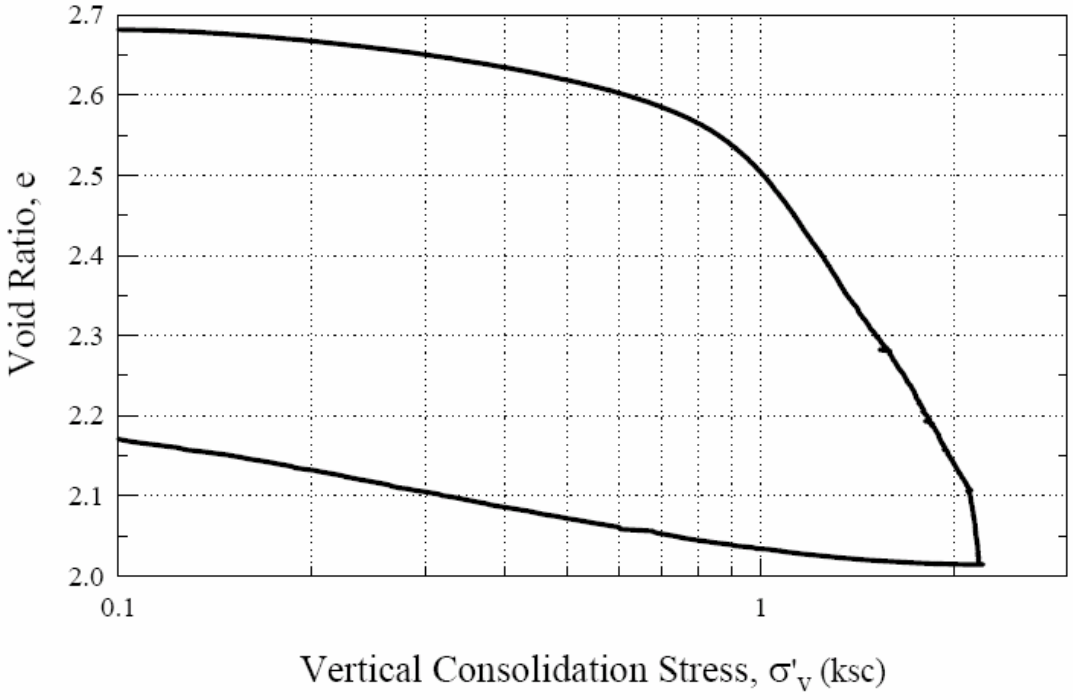

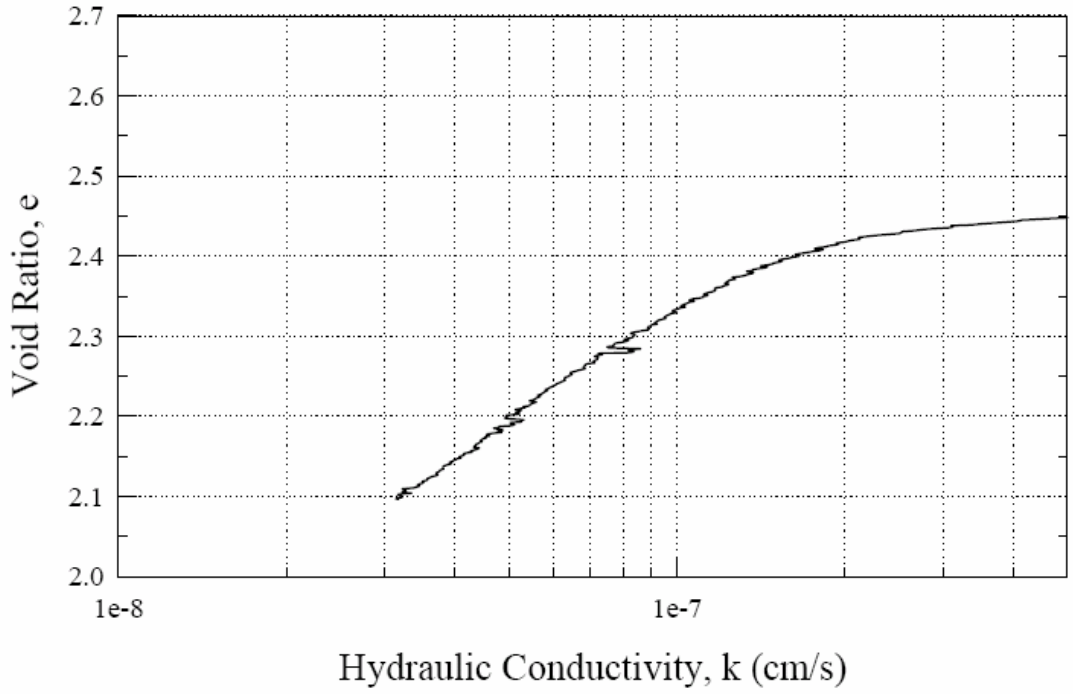

URS Corp.
CRS 444: TS3-B1 S-7

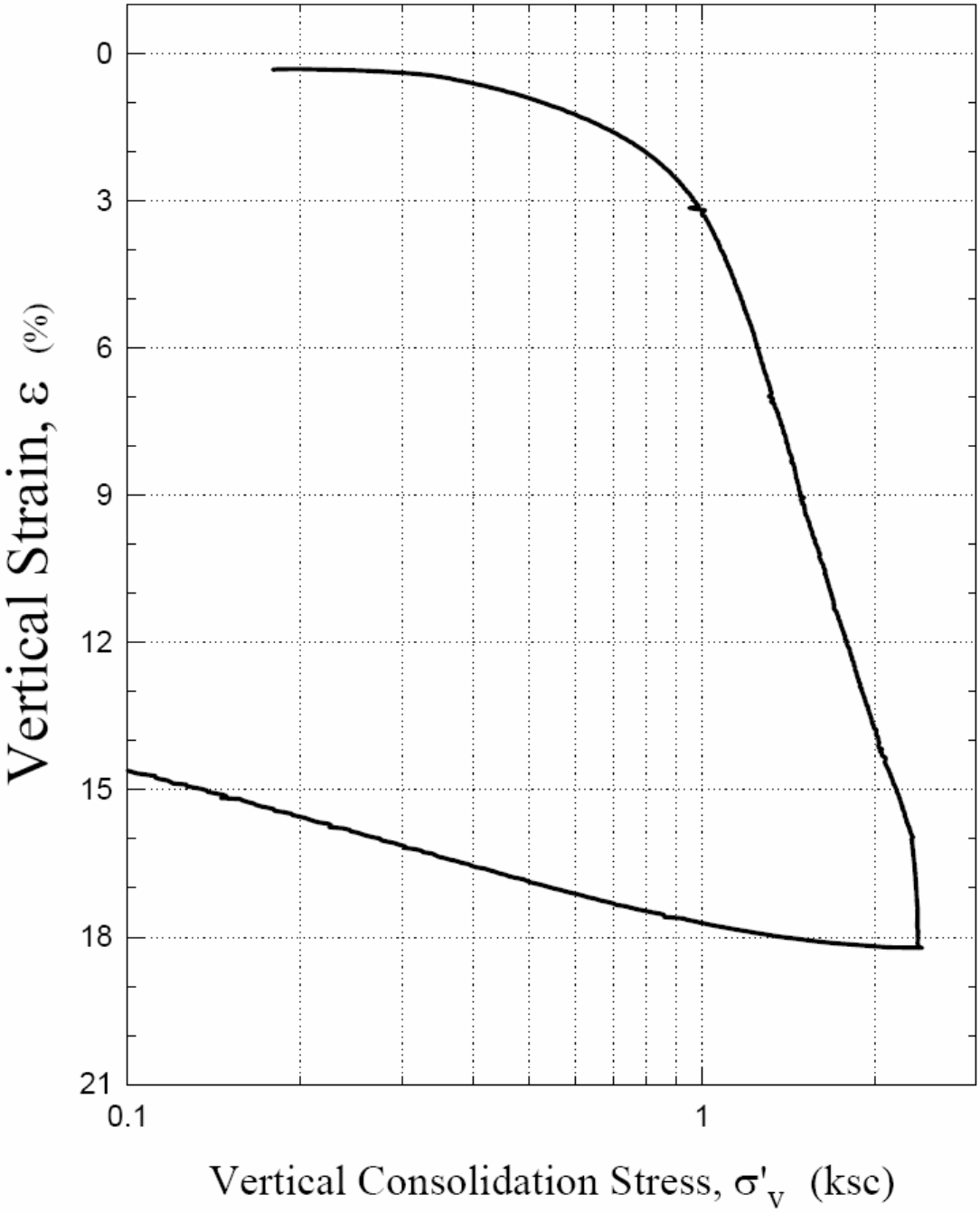

URS Corp.
CRS 444: TS3-B1 S-7

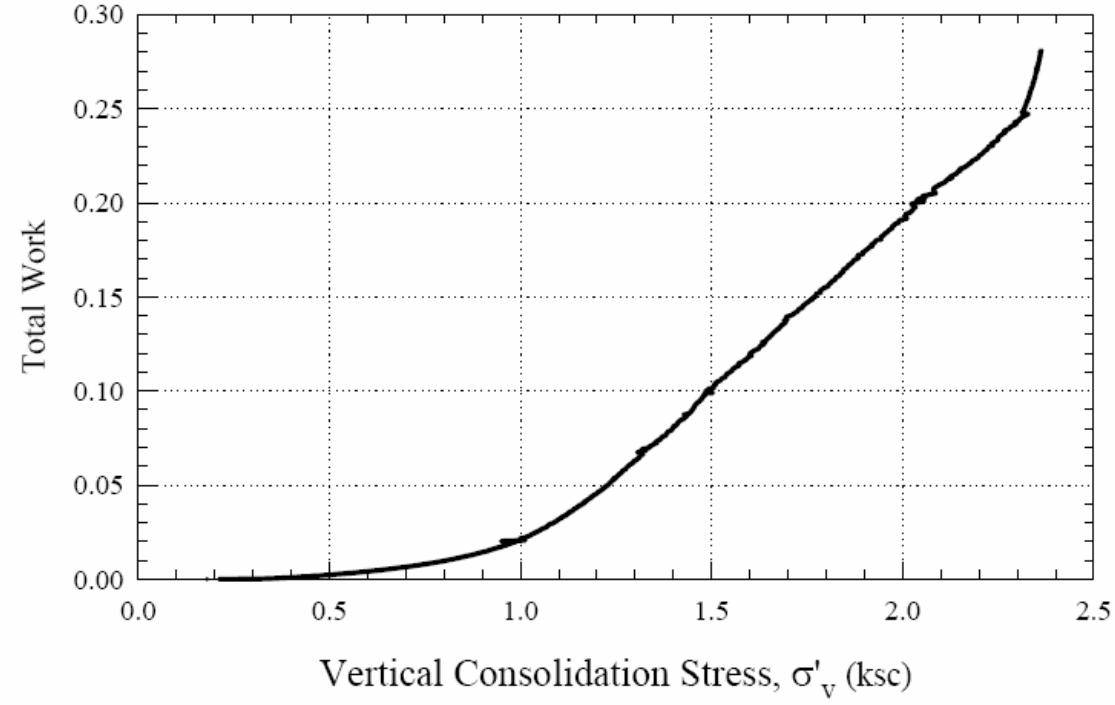

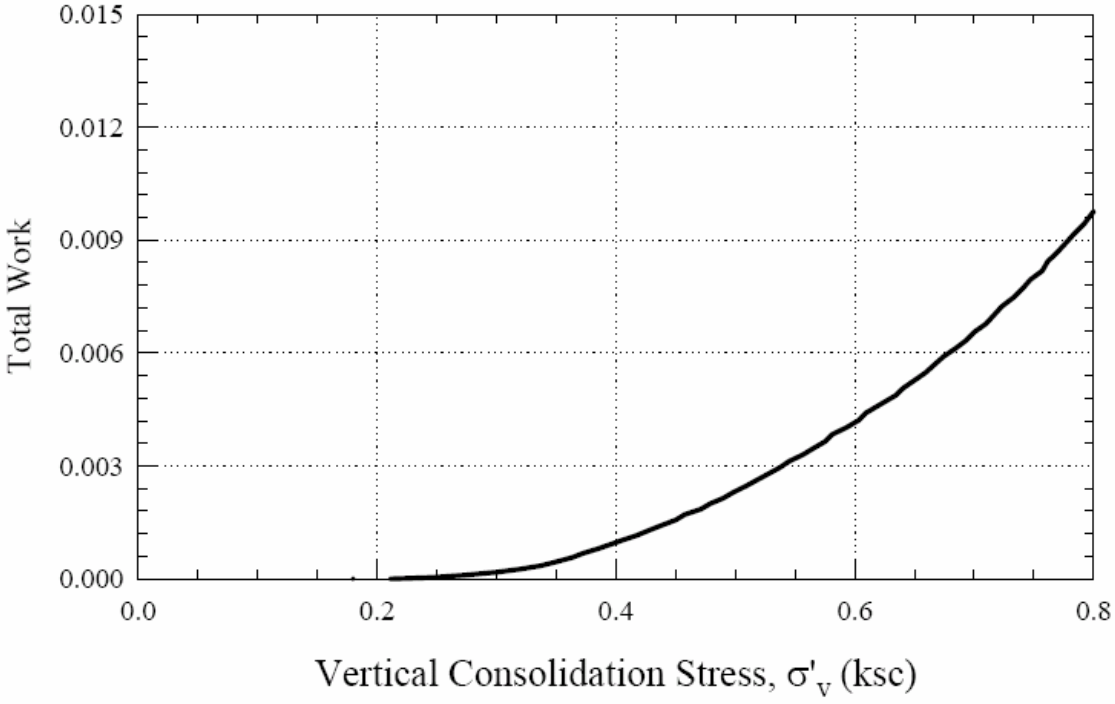

URS Corp.
CRS 444: TS3-B1 S-7

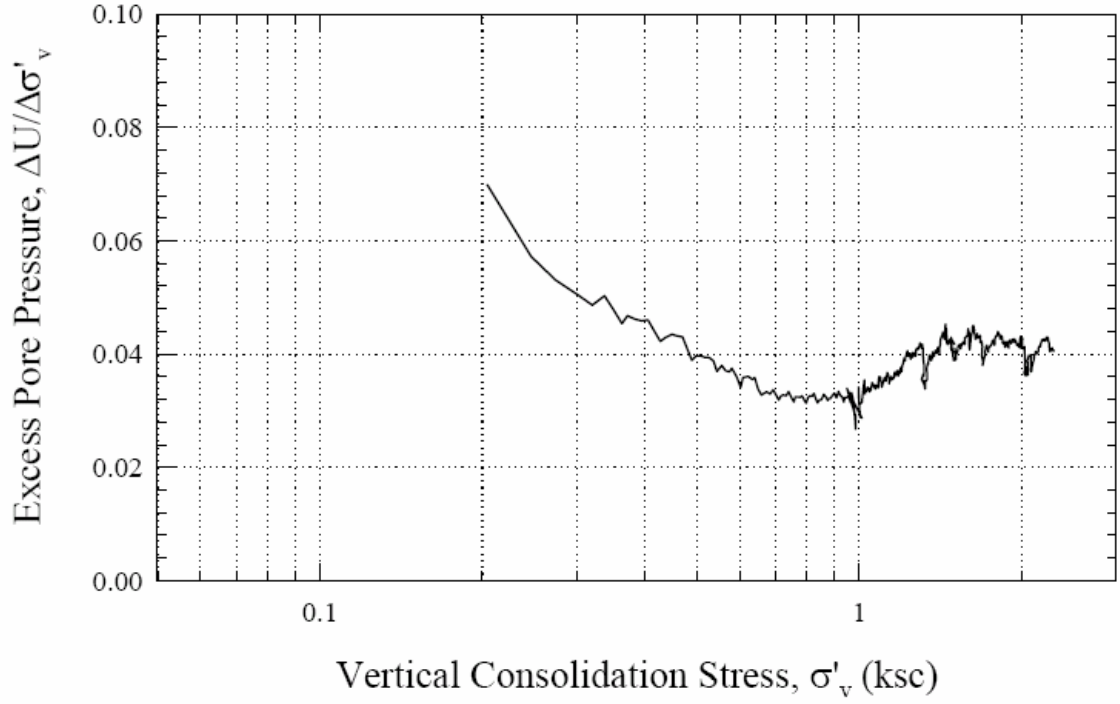

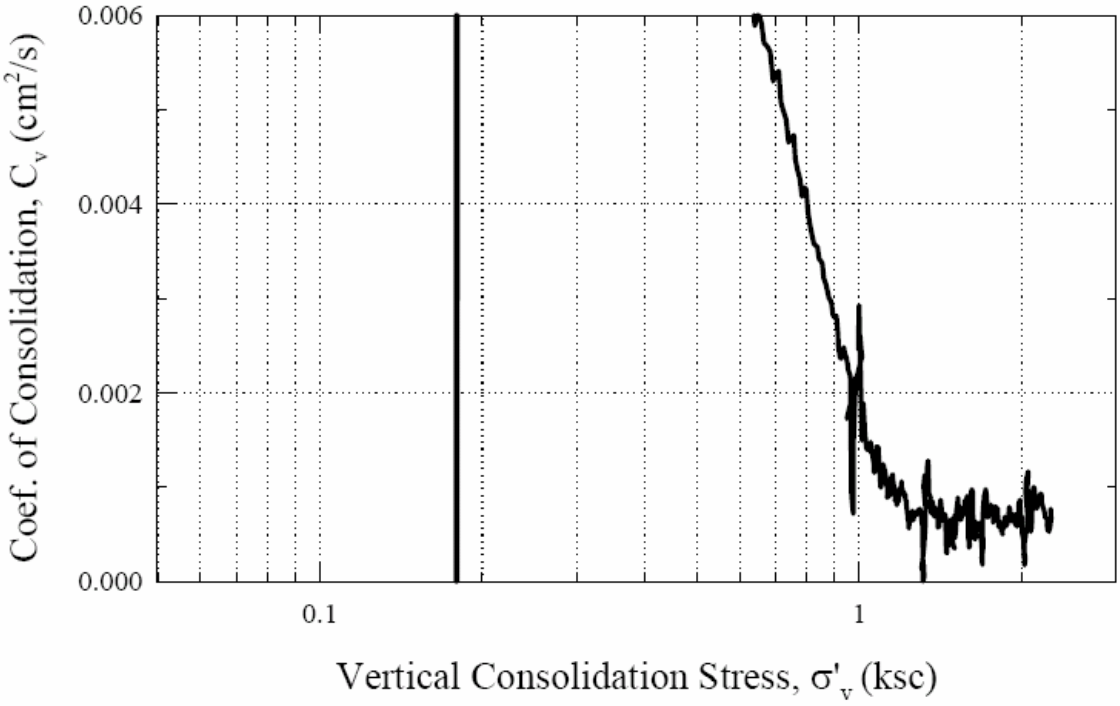

URS Corp.
CRS 444: TS3-B1 S-7

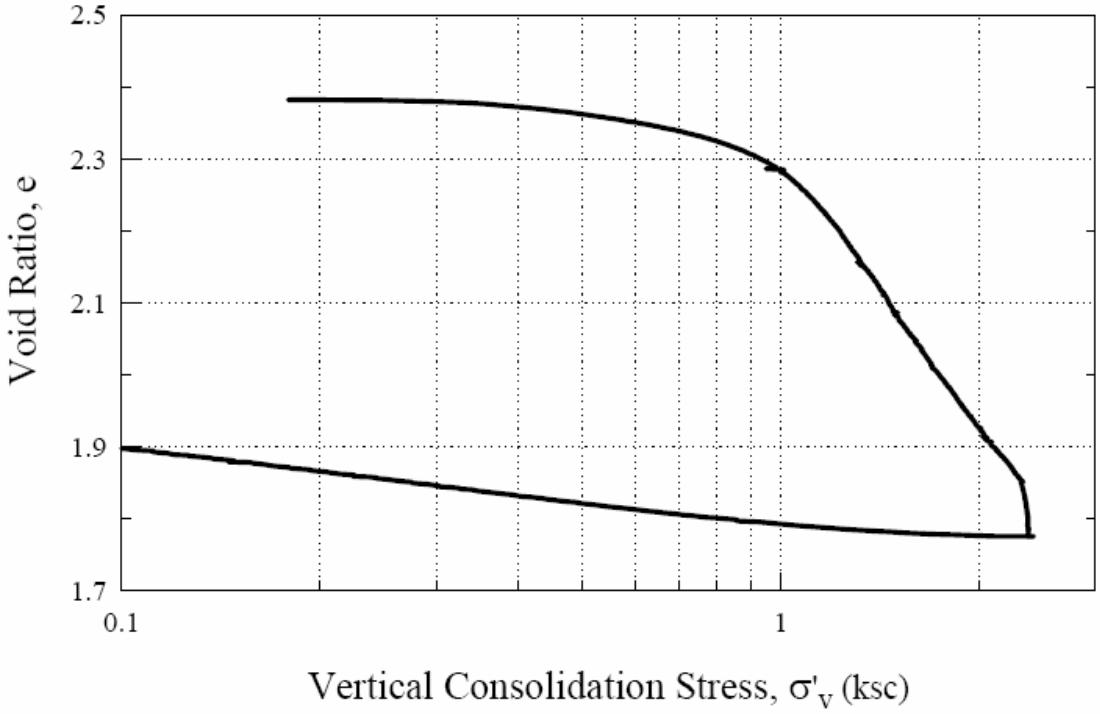

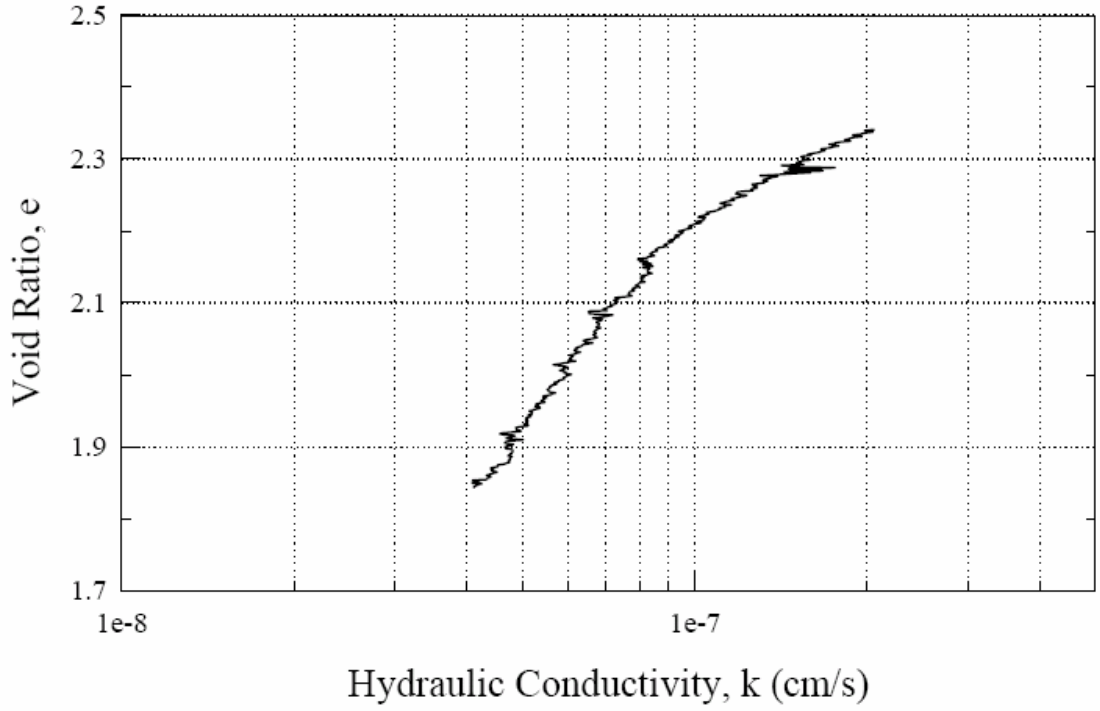

Natural-Scale Plots of Normalized Compression Curves to Overburden Stress of CRSC Tests at TS3-B1

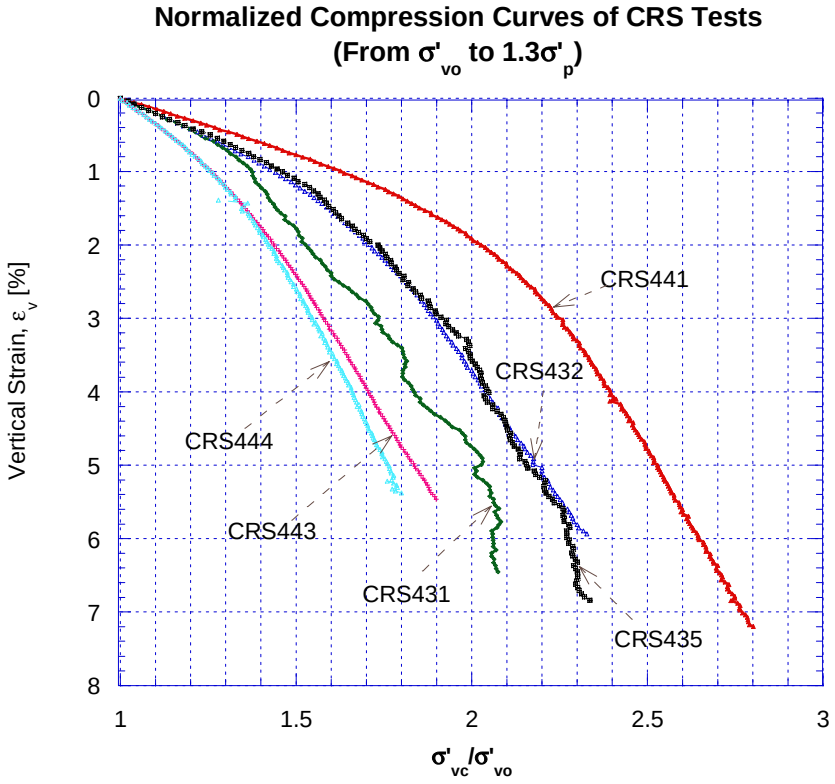

CRS440 Normalized Compression Curve

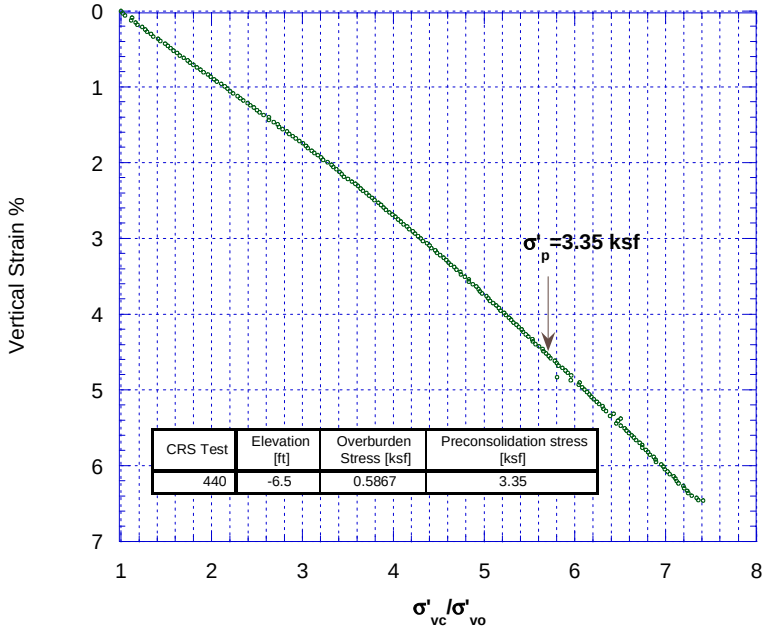

CRS441 Normalized Compression Curve

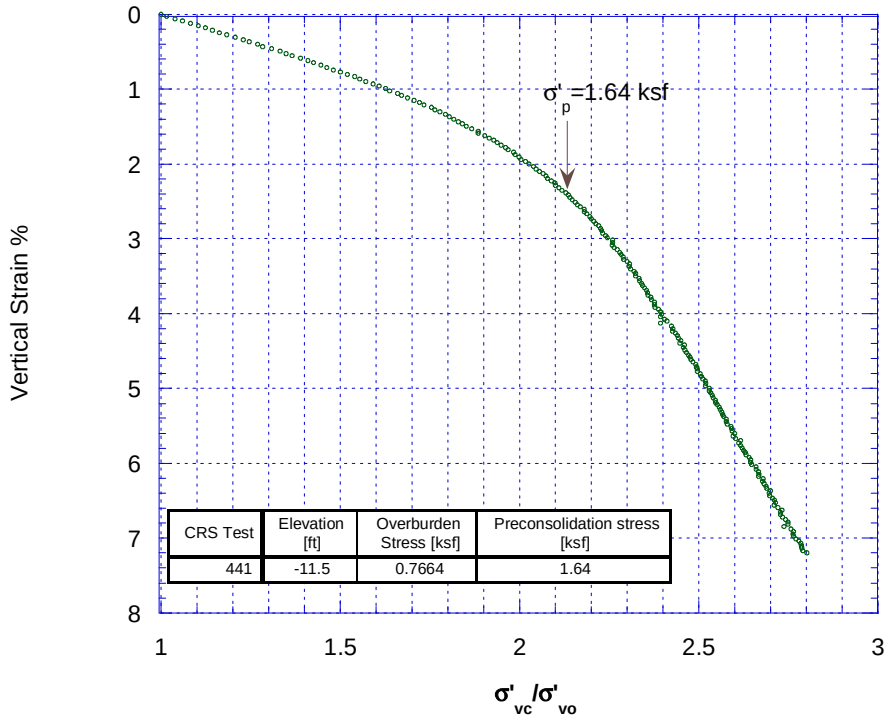

CRS432 Normalized Compression Curve

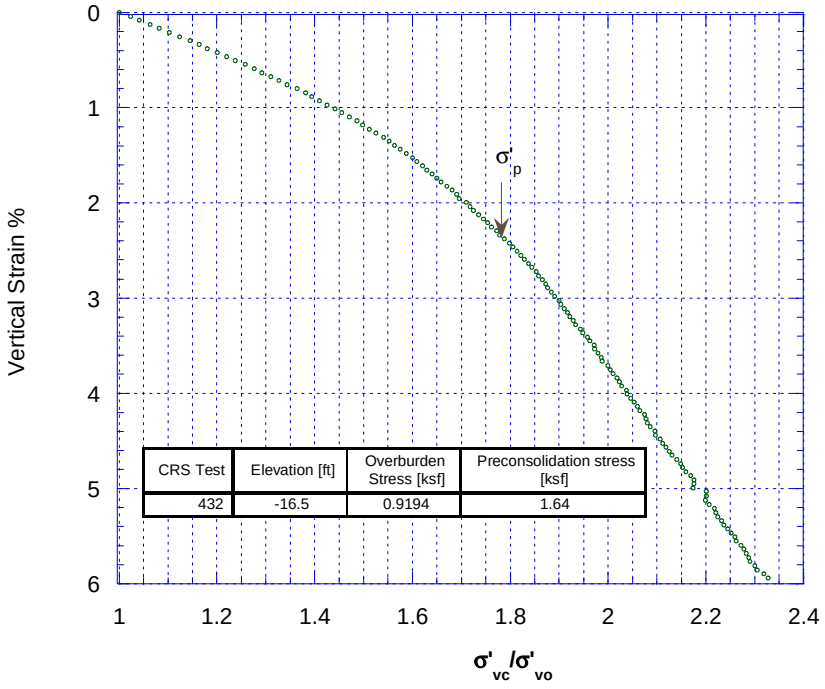

CRS431 Normalized Compression Curve

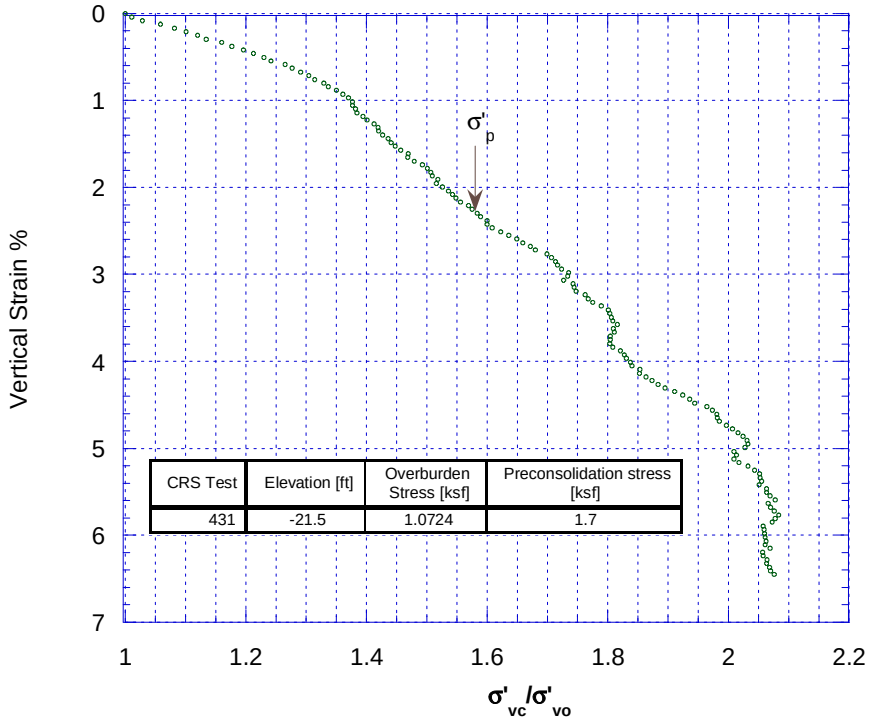

CRS435 Normalized Compression Curve

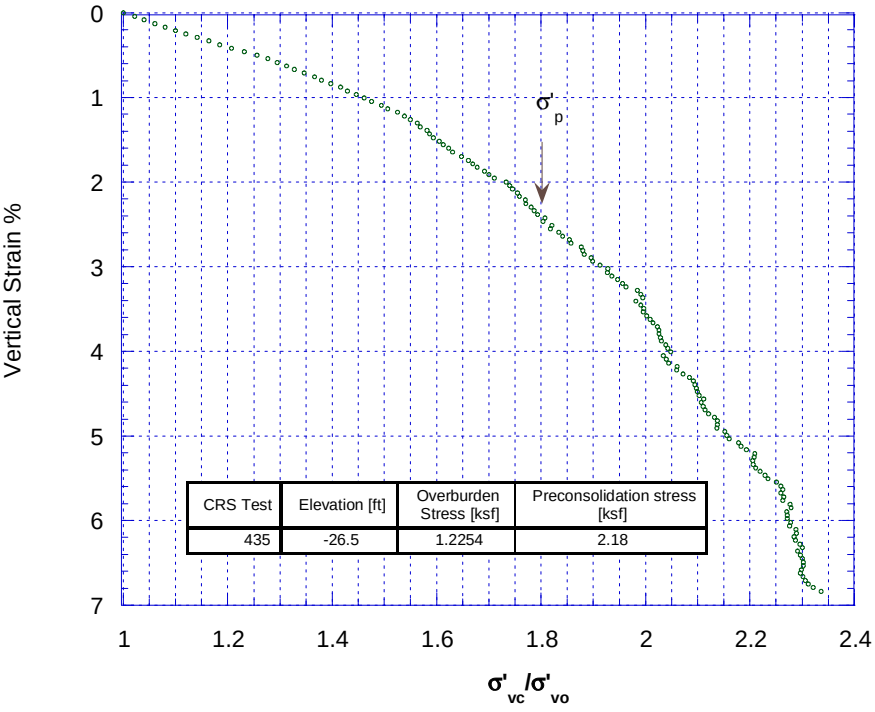

CRSC443 Normalized Compression Curve

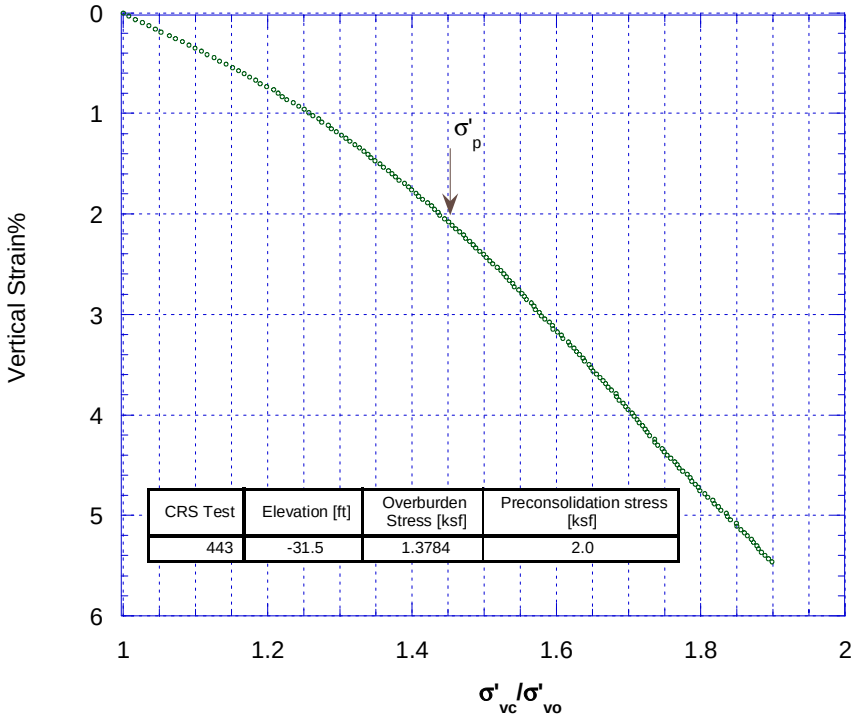

CRS Test	Elevation [ft]	Overburden Stress [ksf]	Preconsolidation stress [ksf]
443	-31.5	1.3784	2.0

CRS444 Normalized Compression Curve

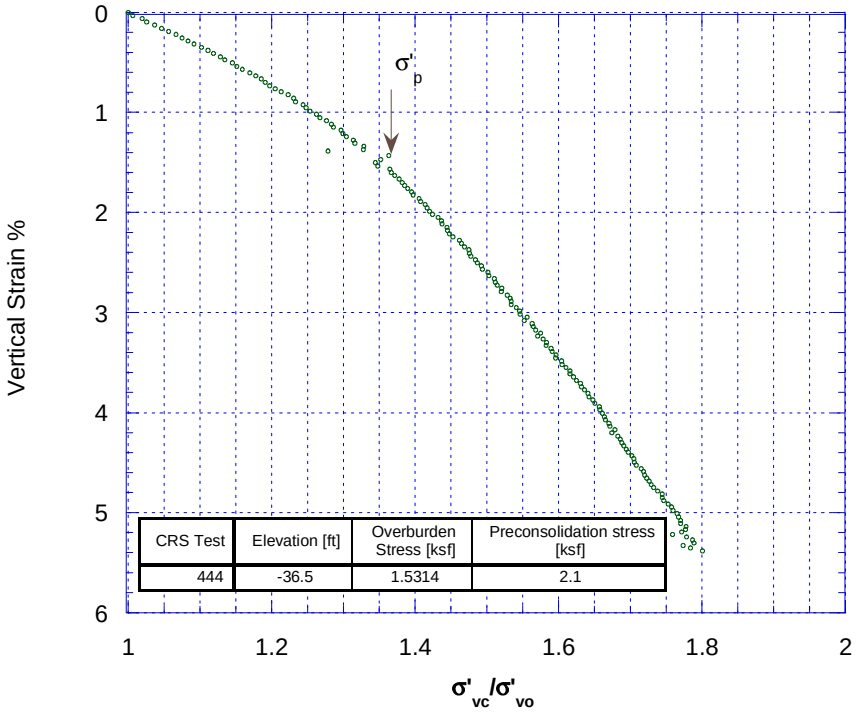

CRS Test	Elevation [ft]	Overburden Stress [ksf]	Preconsolidation stress [ksf]
444	-36.5	1.5314	2.1

6.1.2 CK_0U-DSS Tests at OCR =1, 2, & 3 on Bay Mud (From Germaine, 2002 & 2004)

Table A2 Details of Direct Simple Shear Test Results of Bay Mud at NHPL and North Levees (N1 and N2)

Spec. Location		Index Tests			Specimen		Lab Consolidation					At Max Stress			At Final Point			E_u/σ'_{vc}: @		Remarks
Test No. Boring Sample	El. Loc.[a]	T_v SD # obs	ω_h SD # obs	%2μ	ω_h γ_i	e_i S_i (%) G_s	σ'_p CR RR	C_α $_o$ ε_a	σ'_{vm} ε_a t_s	σ'_{vc} ε_a t_s	ω_c e_c OCR	γ $_o$ γ	τ_h/σ'_{vc} σ'_v/σ'_{vc}	τ_h/σ'_v ψ^u	γ γ	τ_h/σ'_{vc} σ'_v/σ'_{vc}	τ_h/σ'_v ψ^u	$\gamma =$ 0.01 0.1	$\Delta\tau_h =$ 30% 50%	
DSS583 N2-B7 S-5	 4.5-5.5	0.39 0 8	73.1 2.0 4		77.38 1.565	2.060 101.4 2.70		 0.79	1.554 14.23 29.5	1.554 14.23 29.5	 1.00	11.00 5.3	0.2653 0.5937	0.447 24.1	 30.0 	0.2111 0.3824	0.552 28.9	320 161	132 83	
DSS584 N2-B7 S-5	 6-7	0.43 0.04 3	74.4 2.6 4		77.97 1.567	2.067 101.9 2.70		 0.74	2.444 20.17 21.7	2.444 20.17 21.7	 1.00	11.12 5.3	0.2420 0.5781	0.419 22.7	 30.0 	0.1958 0.3583	0.546 28.7	170 125	103 69	Stepped rate after peak shear
DSS585 N2-B7 S-7	 3.5-4.5	0.40 0.02 4	76.3 0.5 3		78.10 1.555	2.092 100.8 2.70		 0.74	1.336 12.87 24.4	1.336 12.87 24.4	 1.00	9.81 4.9	0.2523 0.5896	0.428 23.2	 30.0 	0.1913 0.3397	0.563 29.4	240 156	122 77	
DSS586 N2-B7 S-9	 7.5-8.5	0.38 0 8	65.4 2.8 4		69.73 1.602	1.860 101.2 2.70		 0.77	1.434 13.71 23.9	1.434 13.71 23.9	 1.00	12.40 4.9	0.2448 0.5234	0.468 25.1	 30.0 	0.1778 0.2776	0.640 32.6	336 161	130 84	
DSS587 N2-B7 S-13	 5.3-6.3	0.50 0 6	90.3 2.1 4		93.74 1.486	2.519 100.5 2.70		 0.77	1.760 13.95 26.8	1.760 13.95 26.8	 1.00	13.57 5.0	0.2654 0.5692	0.466 25.0	 30.0 	0.2074 0.3703	0.560 29.3	220 139	108 66	
DSS588 TS5-B3 S-6	-18.1 2.5-3.5	0.41 0 8	86.5 4.1 4		86.01 1.514	2.316 100.3 2.70		 0.75	1.249 15.10 26.0	1.249 15.10 26.0	 1.00	13.02 5.1	0.2533 0.5512	0.460 24.7	 30.0 	0.1927 0.3352	0.575 29.9	220 136	108 70	
DSS589 TS5-B3 S-8	-28.1 3.5-4.5	0.40 0 6	85.8 2.7 4		88.14 1.508	2.369 100.4 2.70		 0.76	1.529 15.32 27.5	1.529 15.32 27.5	 1.00	9.02 5.0	0.2295 0.5989	0.383 21.0	 30.0 	0.1634 0.3102	0.527 27.8	170 125	106 70	
DSS590 TS3-S3 S-3	-18.1 4 - 5	0.34 0 3	91.0 6.4 3		95.41 1.487	2.548 101.1 2.70		 0.76	1.124 15.27 24.4	1.124 15.27 24.4	 1.00	11.47 5.1	0.2383 0.5780	0.412 22.4	 30.0 	0.1840 0.3549	0.518 27.4	256 138	106 70	
DSS591 TS3-S3 S-5	-28.1 H.5-I.5	0.74 0 3	171.8 20.4 3		163.9 1.267	4.625 95.7 2.70		 0.76	1.473 16.12 29.6	1.473 16.12 29.6	 1.00	19.90 5.2	0.3205 0.6210	0.516 27.3	 30.0 	0.3024 0.5467	0.553 28.9	120 82	49 30	Organic clay Gs too high

a) Loc. - marker location in tube

b) Stresses in kg/cm^2

c) 1 kg/cm^2 = 2048 psf

d) Water content and strain in %

e) Time in hours

f) Elevation in Feet

g) t_s time for secondary compression

h) Shear strain rate from 10% to 100% of peak stress

(Table A2 Continued)

Spec. Location		Index Tests			Specimen		Lab Consolidation					At Max Stress			At Final Point			E_u/σ'_{vc}: @		Remarks
Test No. Boring Sample	EL. Loc.[a]	T_v SD # obs	ω_h SD # obs	%2μ	ω_h γ_i	e_i S_i(%) G_s	σ'_p CR RR	C_α o ε_a	σ'_{vm} ε_a t_s	σ'_{vc} ε_a t_s	ω_c e_c OCR	γ o γ	τ_h/σ'_{vc} σ'_v/σ'_{vc}	τ_h/σ'_v ψ^υ	γ	τ_h/σ'_{vc} σ'_v/σ'_{vc}	τ_h/σ'_v ψ^υ	$\gamma =$ 0.01 0.1	$\Delta\tau_h =$ 30% 50%	
DSS592 TS5-B3 S-6	 6.5-7.5	0.38 0 3	87.6 3.4 3		90.63 1.487	2.461 99.4 2.70		 0.76	1.195 12.63 2.3	1.195 12.63 2.3	 1.00	11.40 5.0	0.2306 0.5512	0.418 22.7	 30.0 	0.1867 0.3475	0.537 28.2	230 112	78 50	
DSS593 TS5-B3 S-6	 8.5-9.5	0.39 0.01 4	88.7 1.7 3		92.04 1.491	2.478 100.3 2.70		 0.77	1.181 14.28 24.0	0.604 13.37 7.7	 1.96	12.45 5.1	0.4828 1.0070	0.479 25.6	 30.0 	0.3995 0.6958	0.574 29.9	500 265	197 122	
DSS594 N2-B7 S-7	 5.5-6.5	0.26 0.02 4	74.0 0.9 3		76.67 1.572	2.034 101.8 2.70		 0.75	1.447 13.47 24.0	0.737 12.84 9.6	 1.96	8.59 4.8	0.4589 1.0220	0.449 24.2	 30.0 	0.3385 0.5342	0.634 32.4	470 255	202 134	
DSS596 N2-B7 S-13	 7-8	0.25 0 4	87.9 2.1 3		89.65 1.498	2.418 100.1 2.70		 0.76	1.882 15.53 24.0	0.954 14.54 9.2	 1.97	12.78 5.0	0.4546 0.9744	0.467 25.0	 30.0 	0.3493 0.6430	0.543 28.5	360 227	170 110	
DSS601 TS3-S3 S-3	 11-12	0.40 0 4	88.1 4.4 3		94.49 1.48	2.549 100.1 2.70		 0.72	1.171 15.26 24.5	1.171 15.26 24.5	 1.00	10.00 0.83	0.2366 0.5917	0.400 21.8	 30.0 	0.1801 0.3422	0.526 27.8	200 135	106 66	
DSS621 N1-B9 S-6	 G.5-H.5	0.21 0.02 6	75.3 8.4 4		85.43 1.512	2.311 99.8 2.70		 1.47	1.633 19.85 2.0	0.564 18.29 17.5	 2.89	13.26 5.3	0.5999 1.1880	0.505 26.79	 30.0 	0.4558 0.8290	0.550 28.80	550 290	200 125	
DSS622 N1-B4 S-9	 6.5-7.5	0.25 0.00 6	78.0 2.3 4		85.97 1.510	2.324 99.9 2.70		 3.10	3.237 24.34 1.0	1.103 22.80 33.3	 2.94	n/a 5.5	0.5454 1.1813	0.462 24.78	 n/a 	 	 	800 350	250 150	Top cap slip

a) Loc. - marker location in tube
b) Stresses in kg/cm^2
c) 1 kg/cm^2 = 2048 psf
d) Water content and strain in %
e) Time in hours
f) ELevation in Feet
g) t_s time for secondary compression
h) Shear strain rate from 10% to 100% of peak stress

[Data from Germaine, (2002, 2004)]

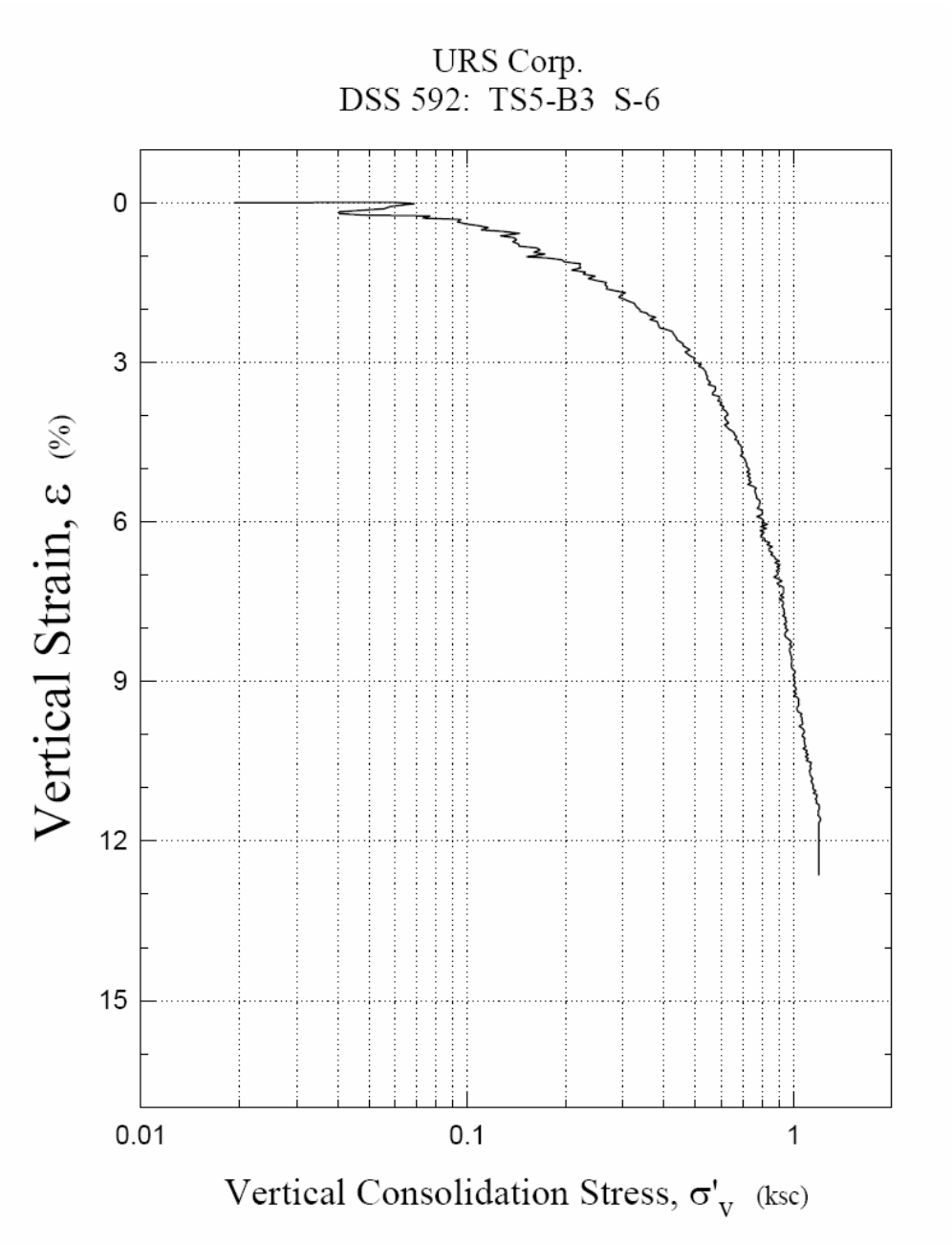
URS Corp.
DSS 592: TS5-B3 S-6
Vertical Strain, ε (%)
0
3
6
9
12
15
0.01
0.1
1
Vertical Consolidation Stress, σ'v (ksc)

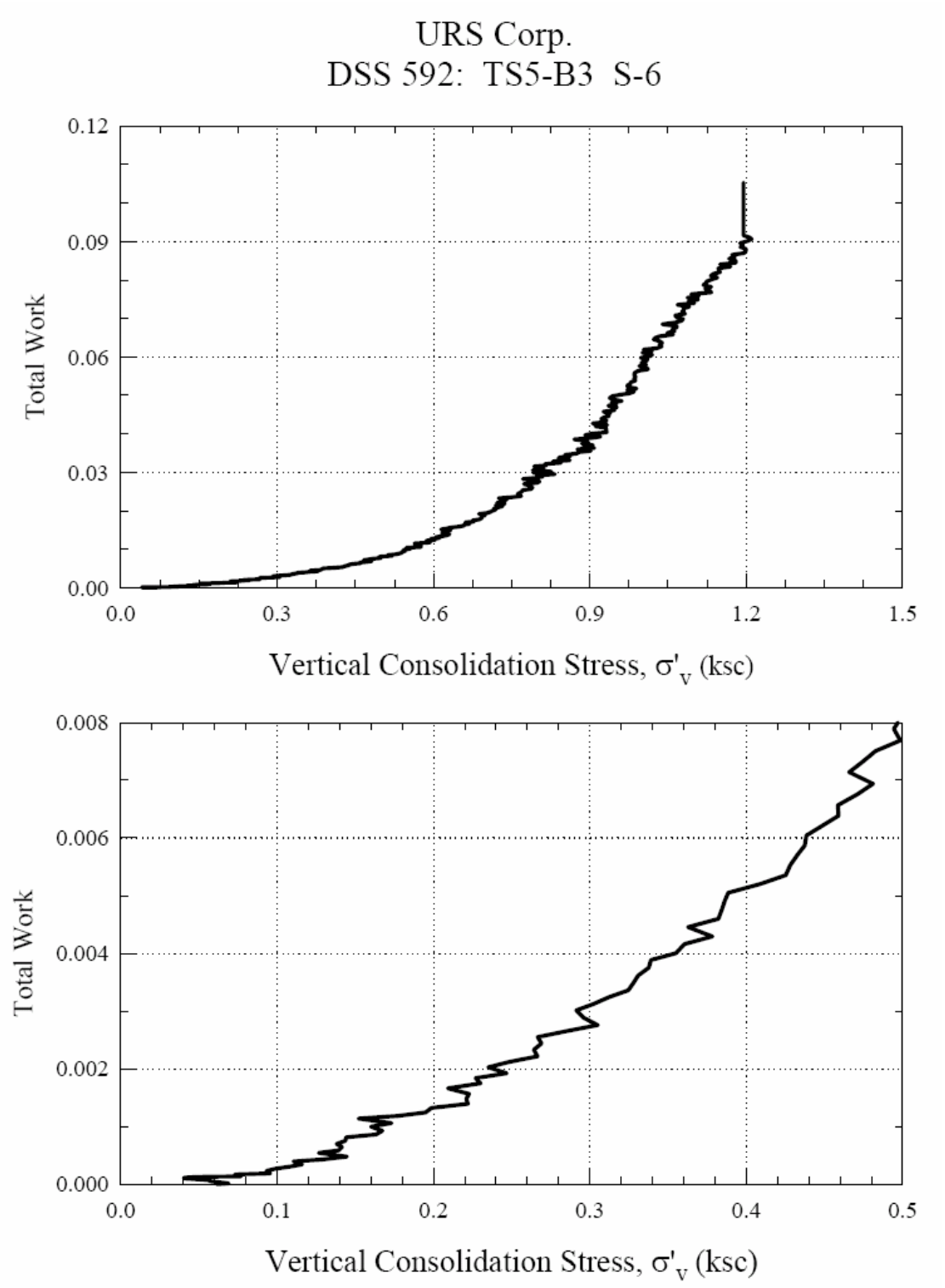
URS Corp.
DSS 592: TS5-B3 S-6
Total Work
0.12
0.09
0.06
0.03
0.00
0.0
0.3
0.6
0.9
1.2
1.5
Vertical Consolidation Stress, σ'v (ksc)
Total Work
0.008
0.006
0.004
0.002
0.000
0.0
0.1
0.2
0.3
0.4
0.5
Vertical Consolidation Stress, σ'v (ksc)

URS Corp.
DSS 592: TS5-B3 S-6

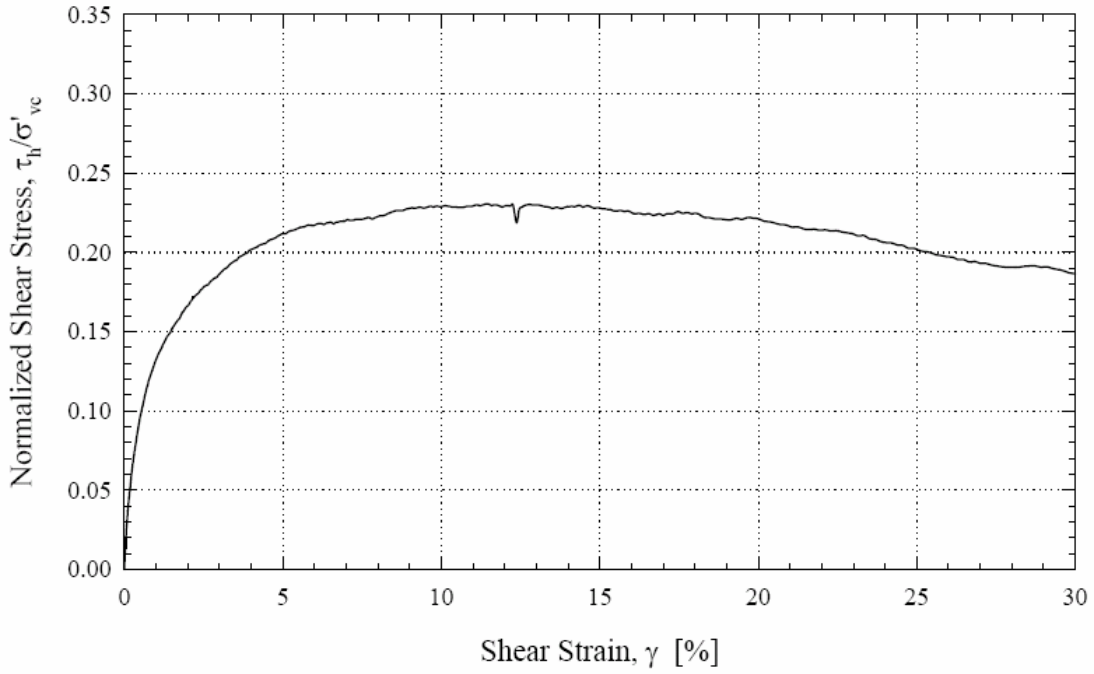

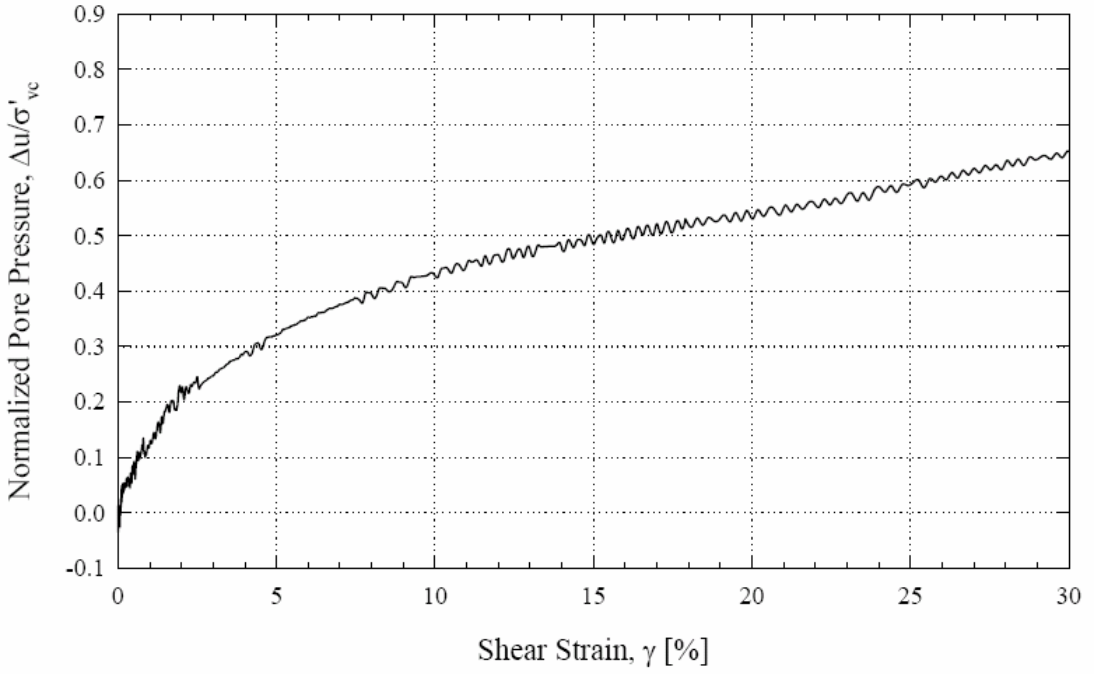

URS Corp.
DSS 592: TS5-B3 S-6

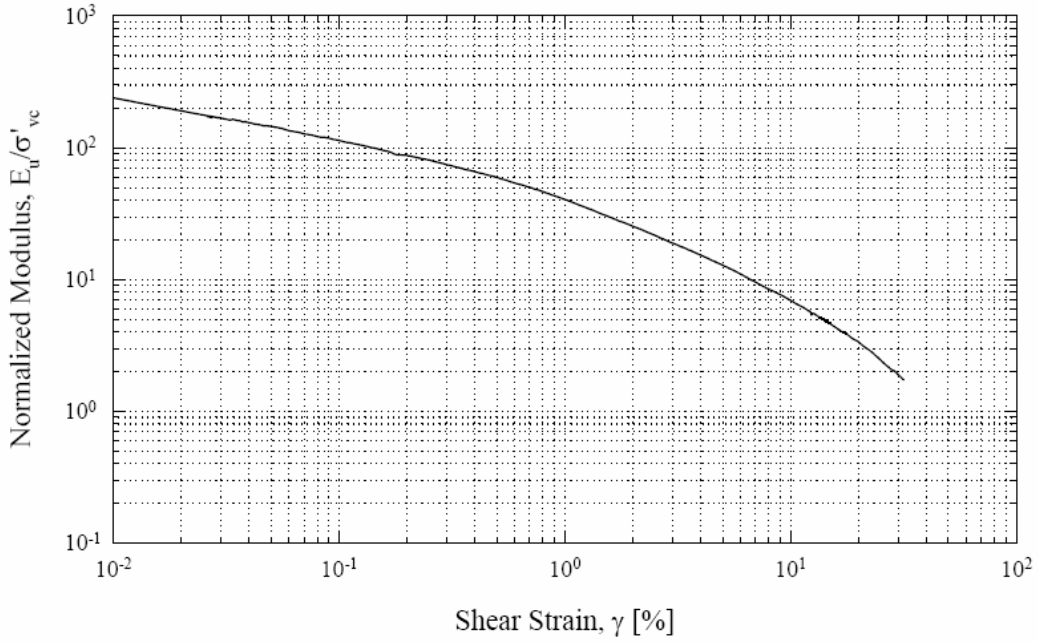

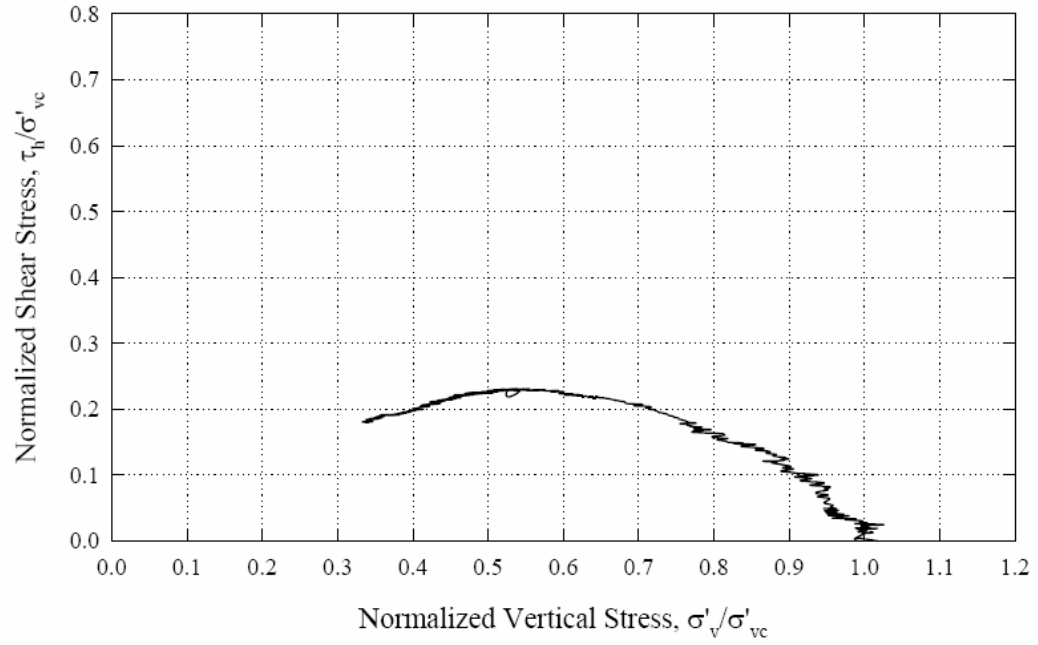

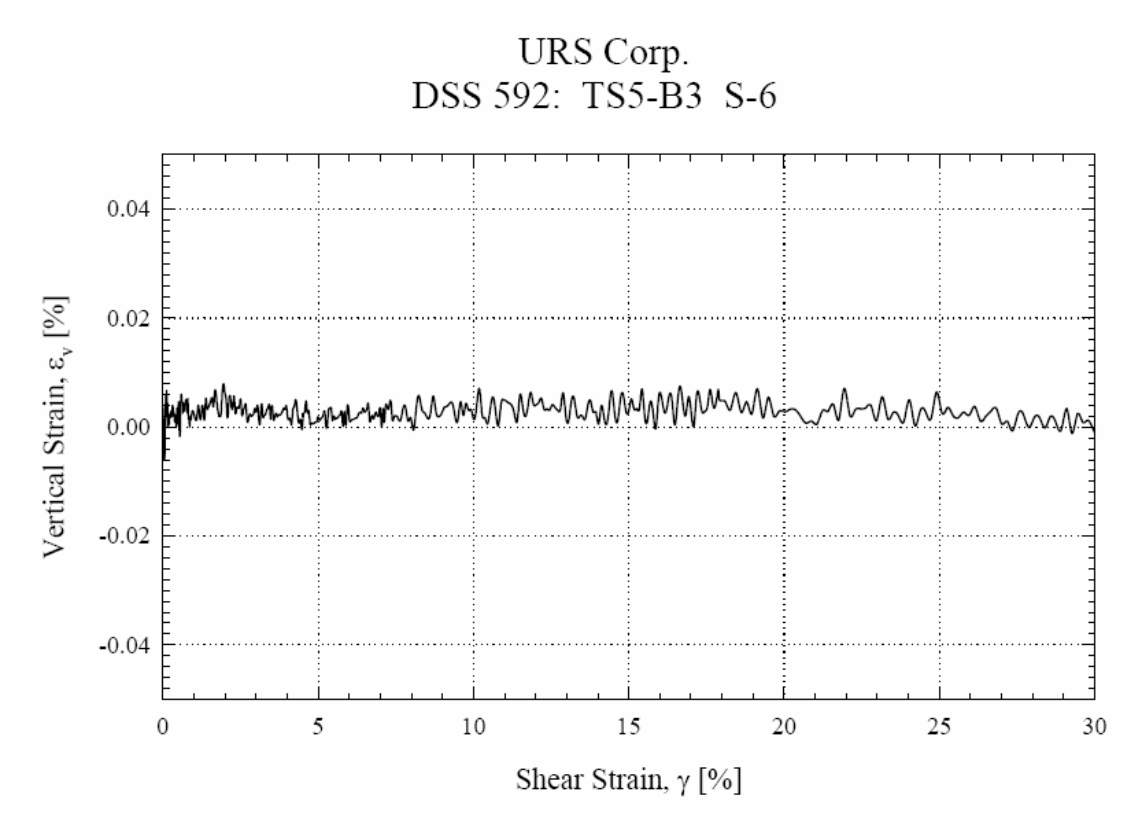
URS Corp.
DSS 592: TS5-B3 S-6
0.04
0.02
0.00
-0.02
-0.04
Vertical Strain, ε_v [%]
0
5
10
15
20
25
30
Shear Strain, γ [%]

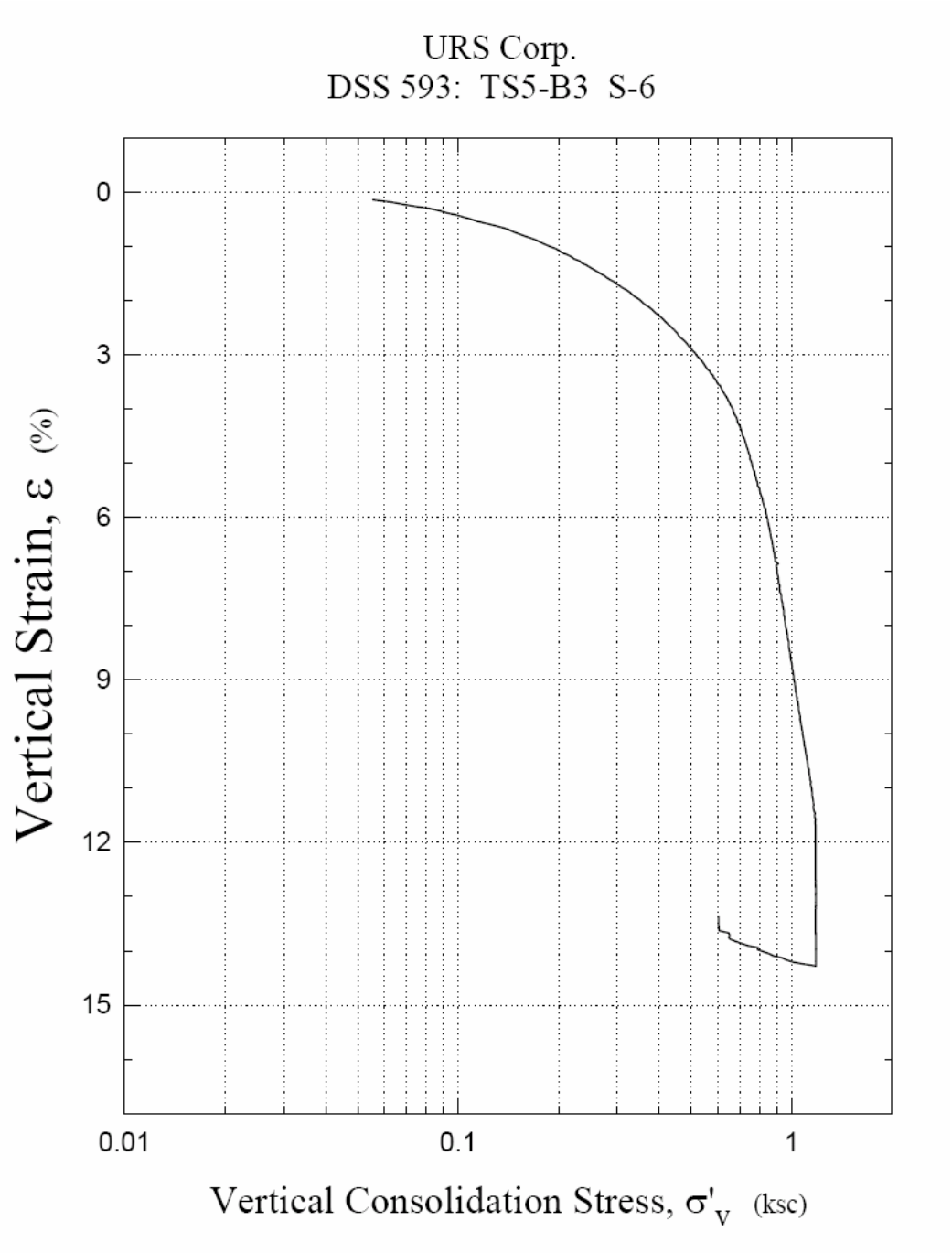
URS Corp.
DSS 593: TS5-B3 S-6
0
3
6
9
12
15
Vertical Strain, ε (%)
0.01
0.1
1
Vertical Consolidation Stress, σ'v (ksc)

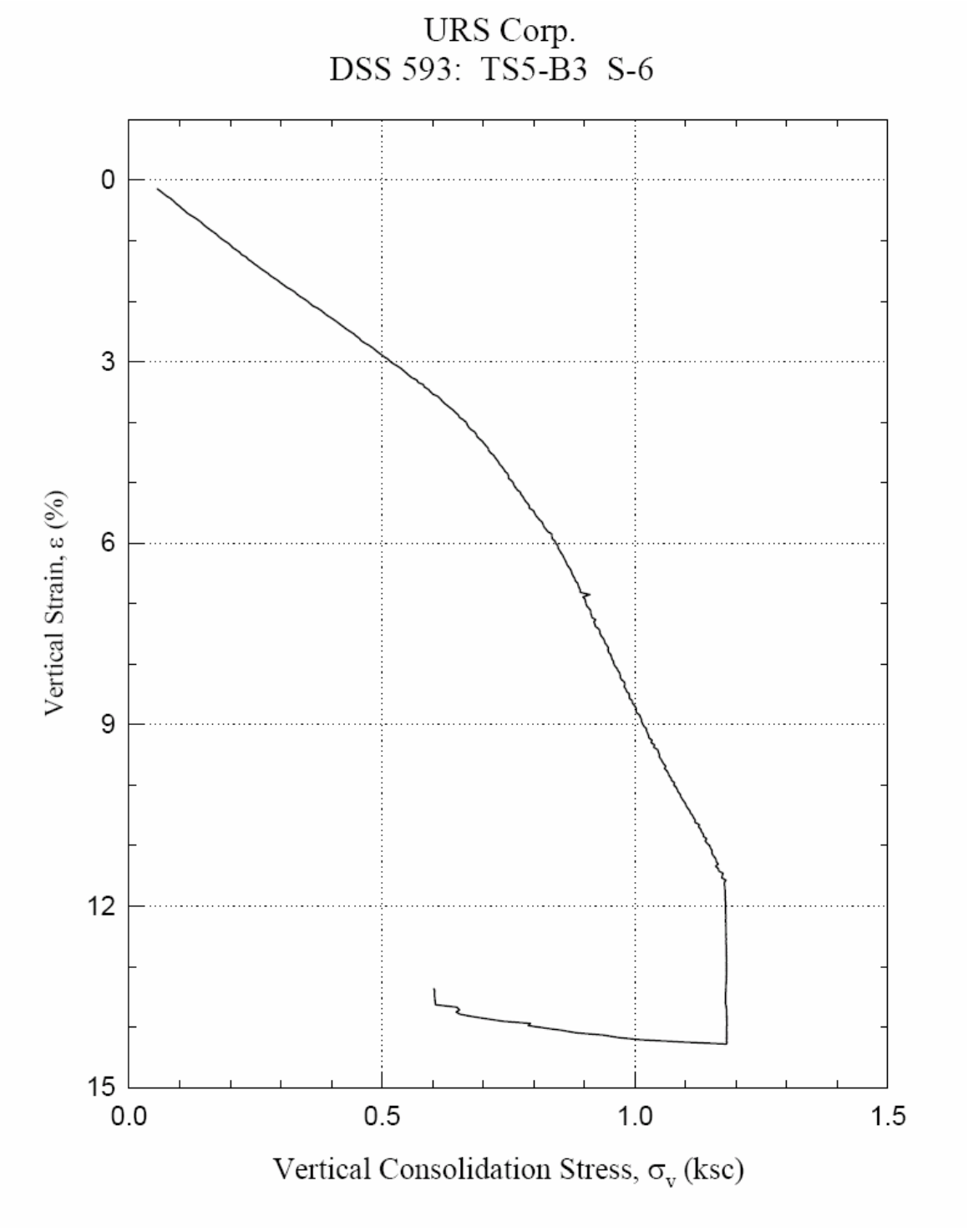
URS Corp.
DSS 593: TS5-B3 S-6
0
3
6
9
12
15
Vertical Strain, ε (%)
0.0
0.5
1.0
1.5
Vertical Consolidation Stress, σv (ksc)

URS Corp.
DSS 593: TS5-B3 S-6

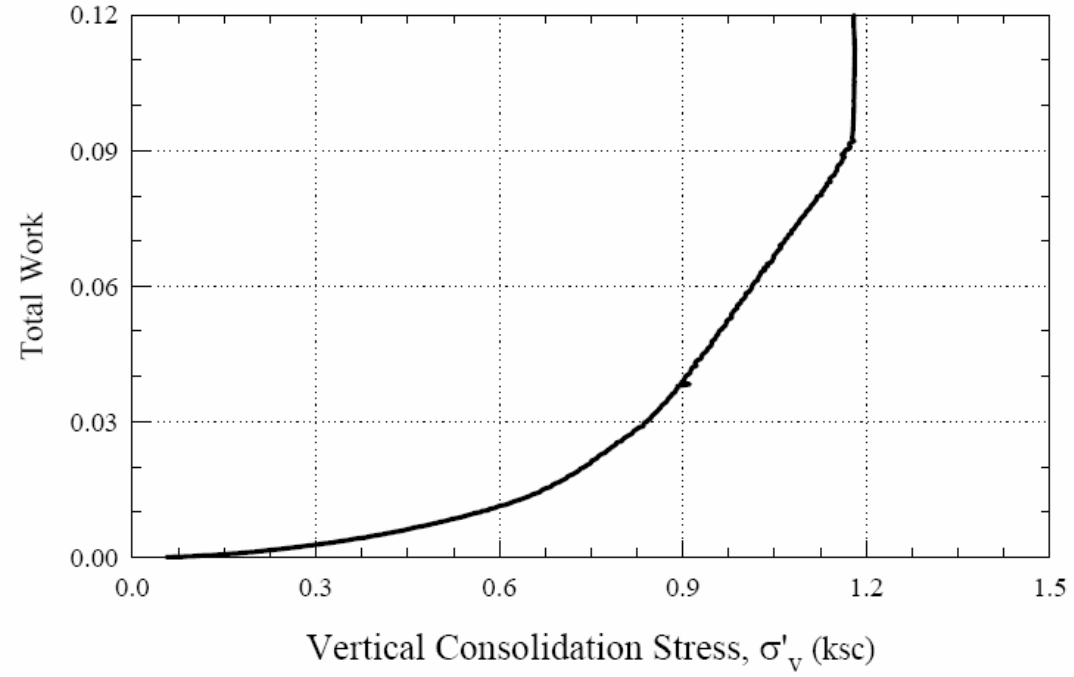

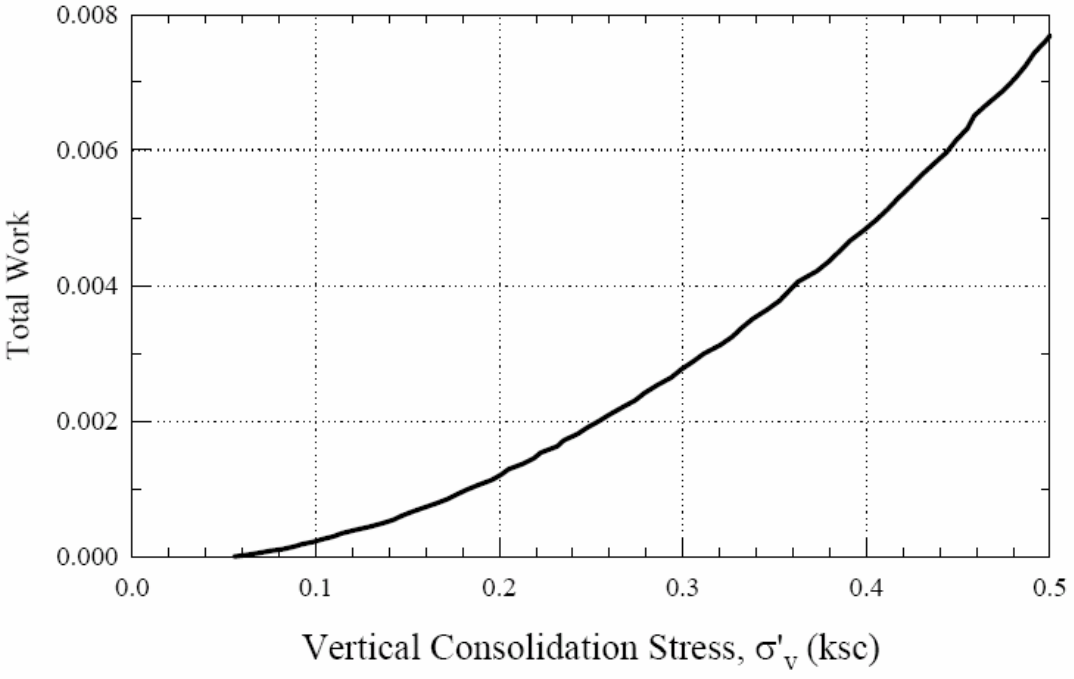

URS Corp.
DSS 593: TS5-B3 S-6

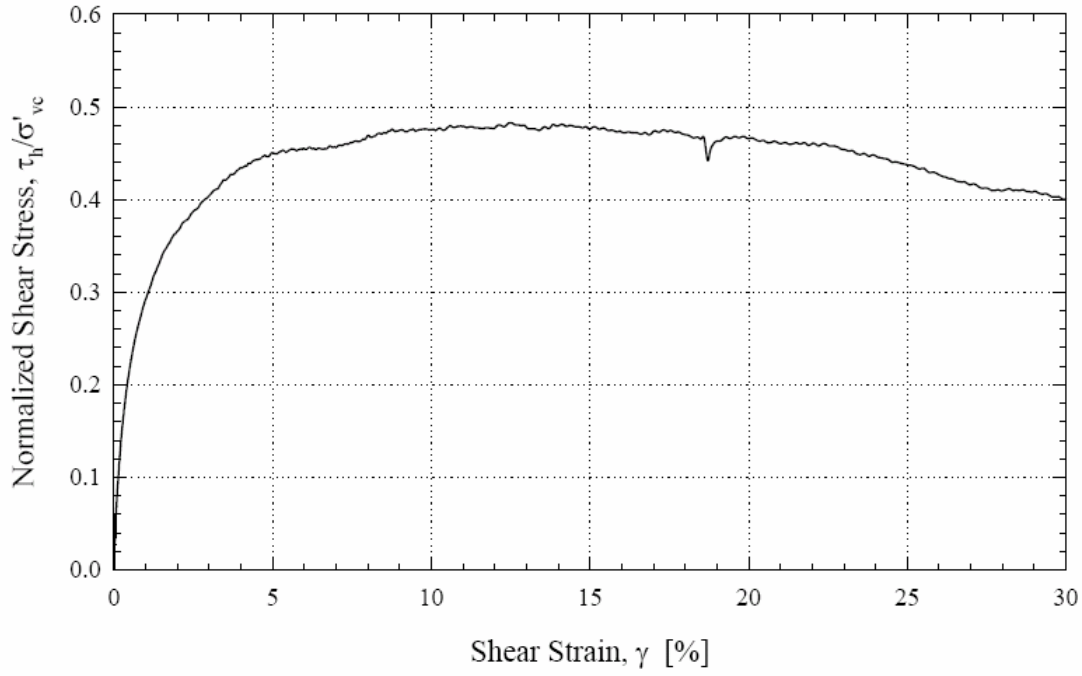

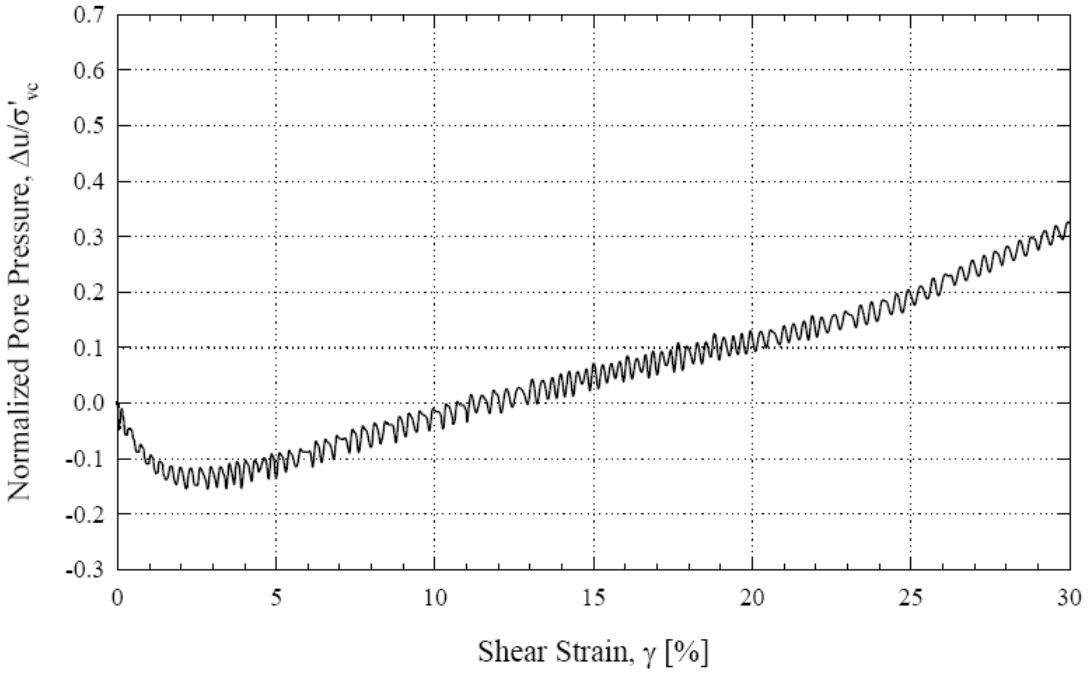

URS Corp.
DSS 593: TS5-B3 S-6

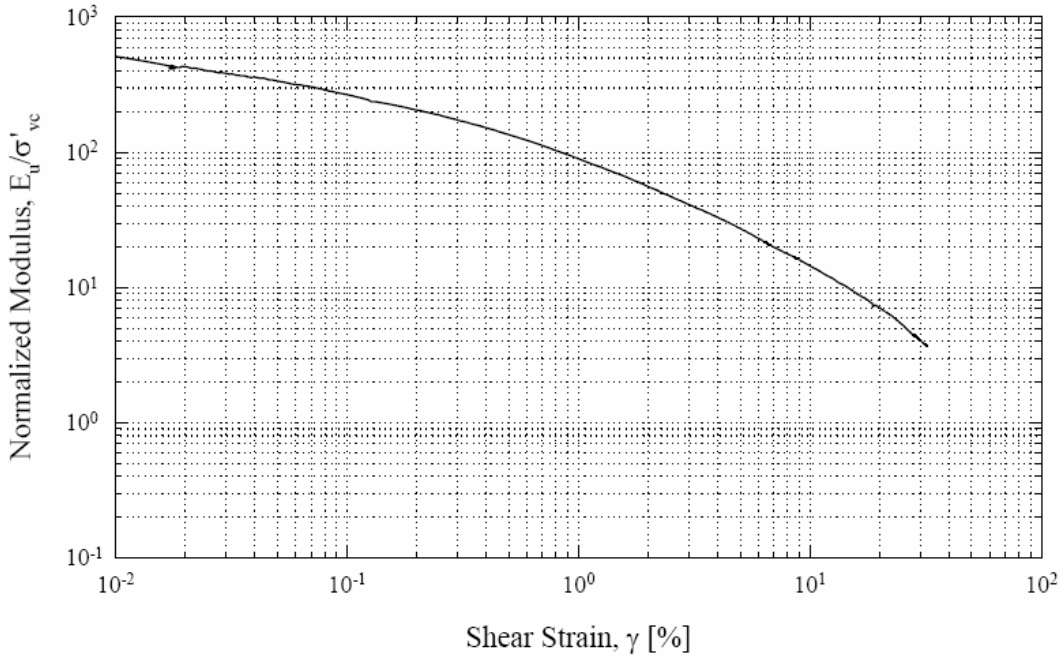

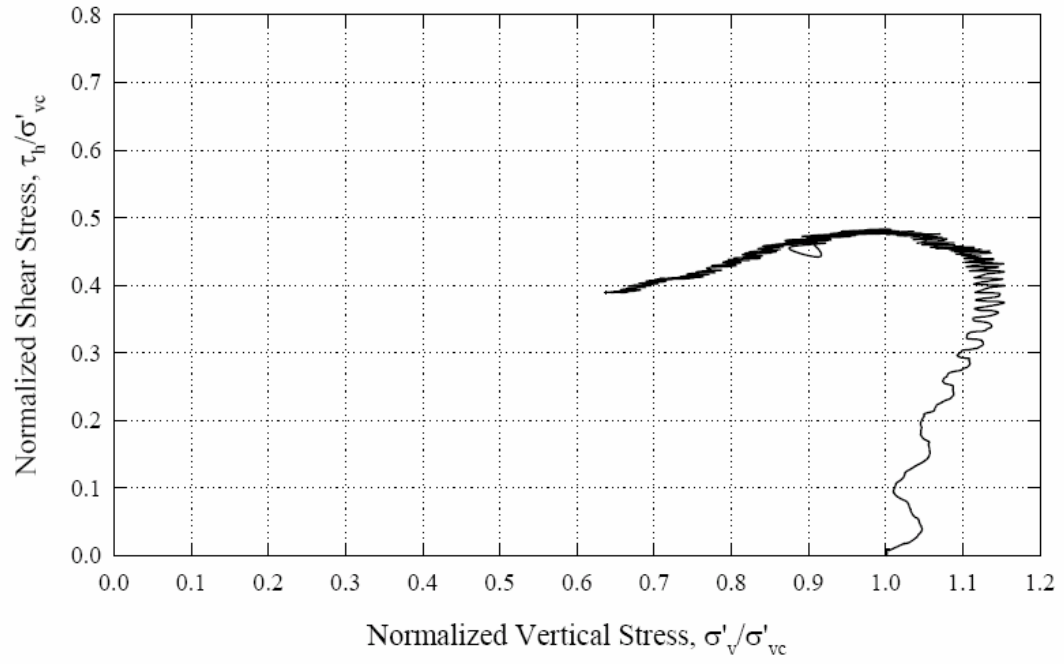

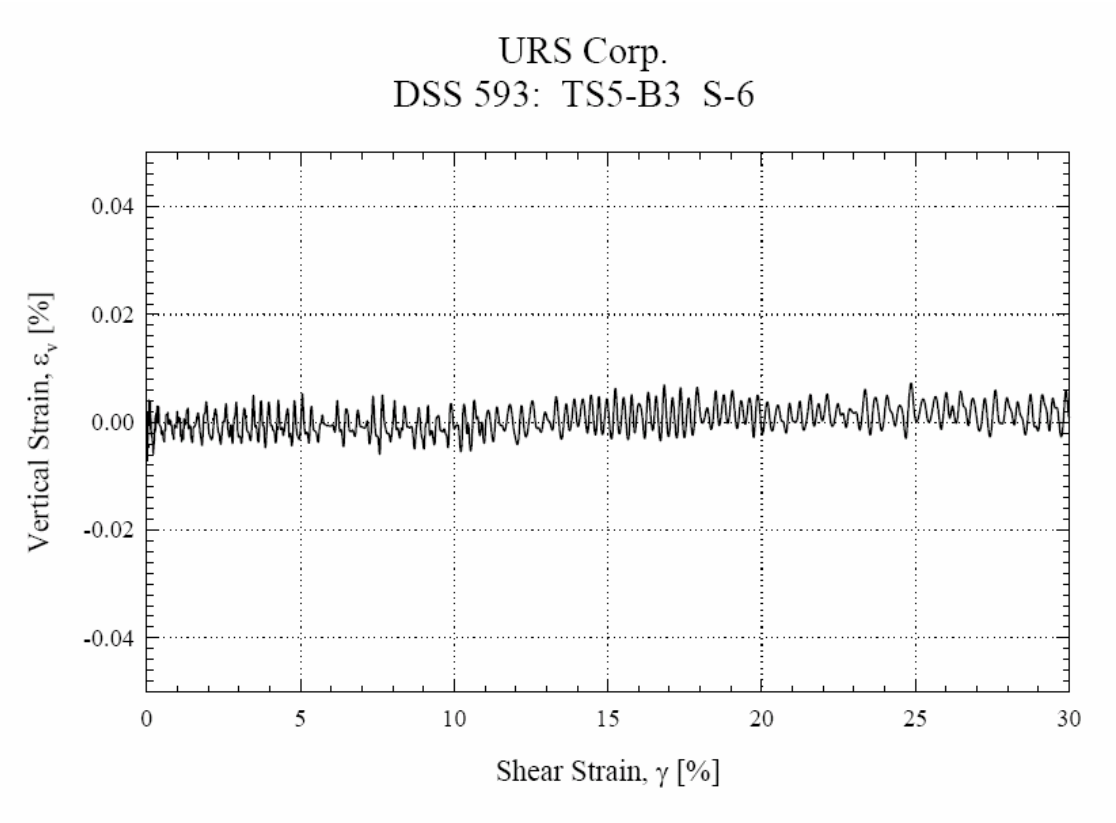
URS Corp.
DSS 593: TS5-B3 S-6
0.04
0.02
0.00
-0.02
-0.04
Vertical Strain, ε_v [%]
0
5
10
15
20
25
30
Shear Strain, γ [%]

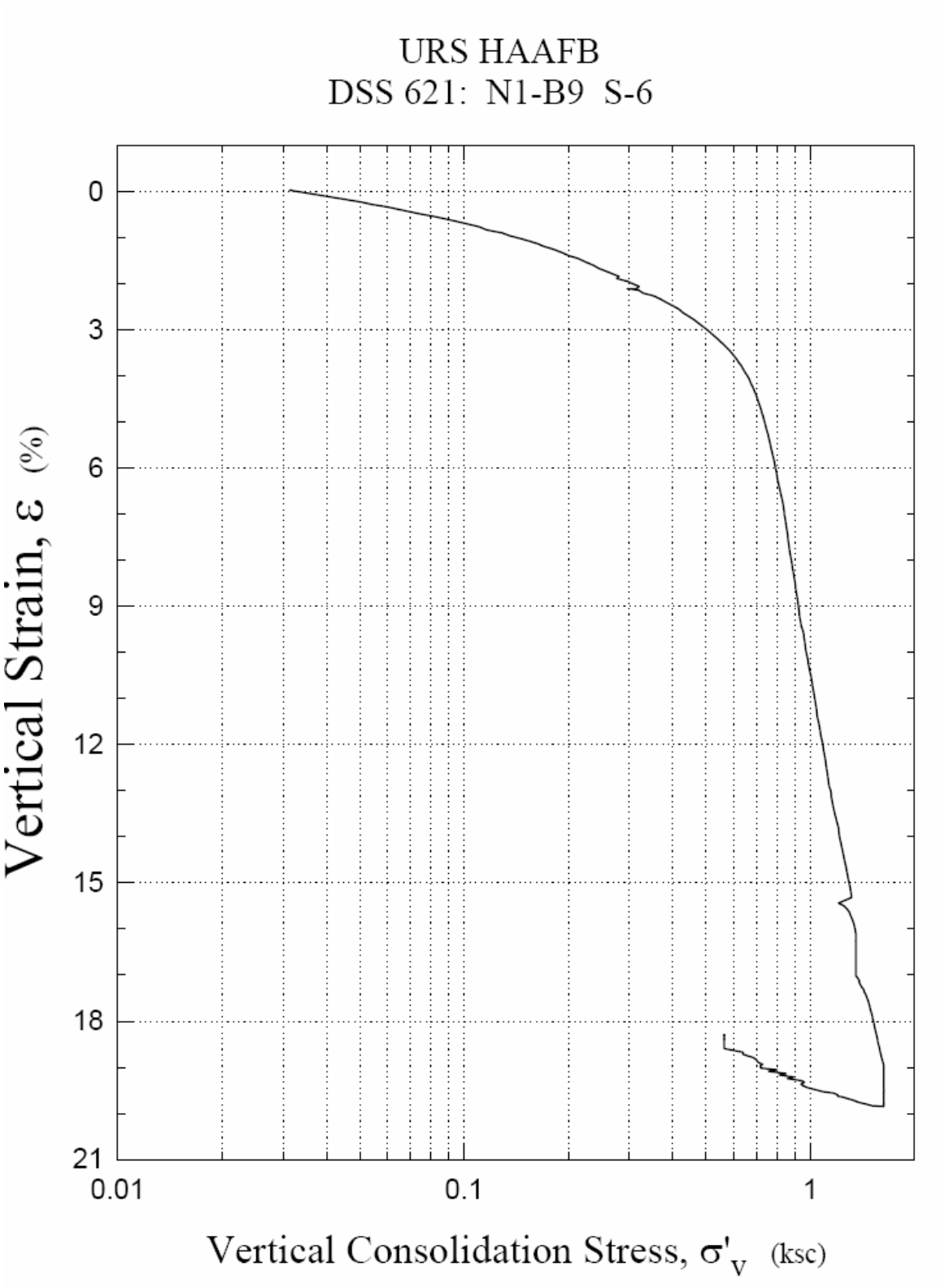
URS HAAFB
DSS 621: N1-B9 S-6
Vertical Strain, ε (%)
0
3
6
9
12
15
18
21
0.01
0.1
1
Vertical Consolidation Stress, σ'v (ksc)

URS HAAFB
DSS 621: N1-B9 S-6

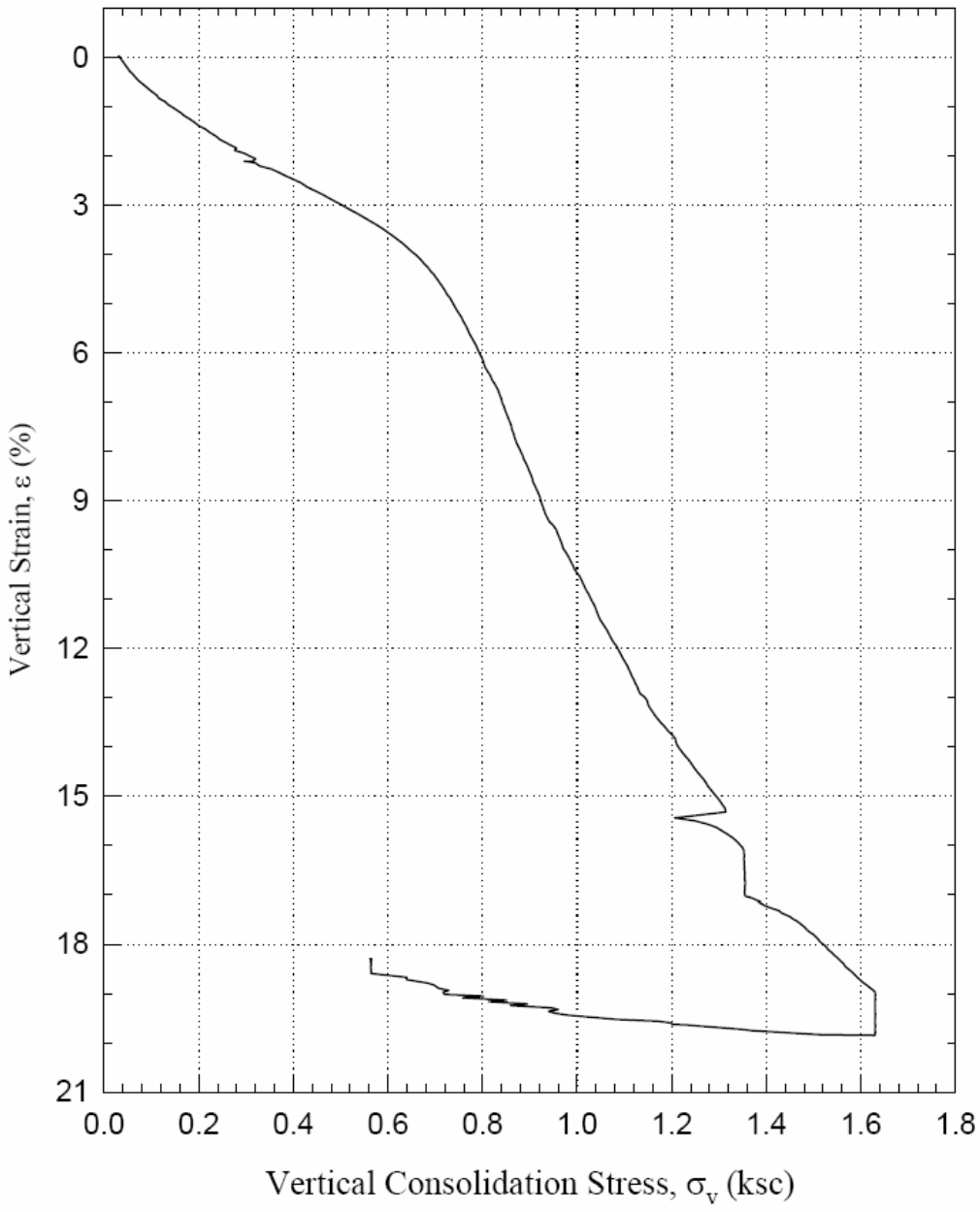

URS HAAFB
DSS 621: N1-B9 S-6

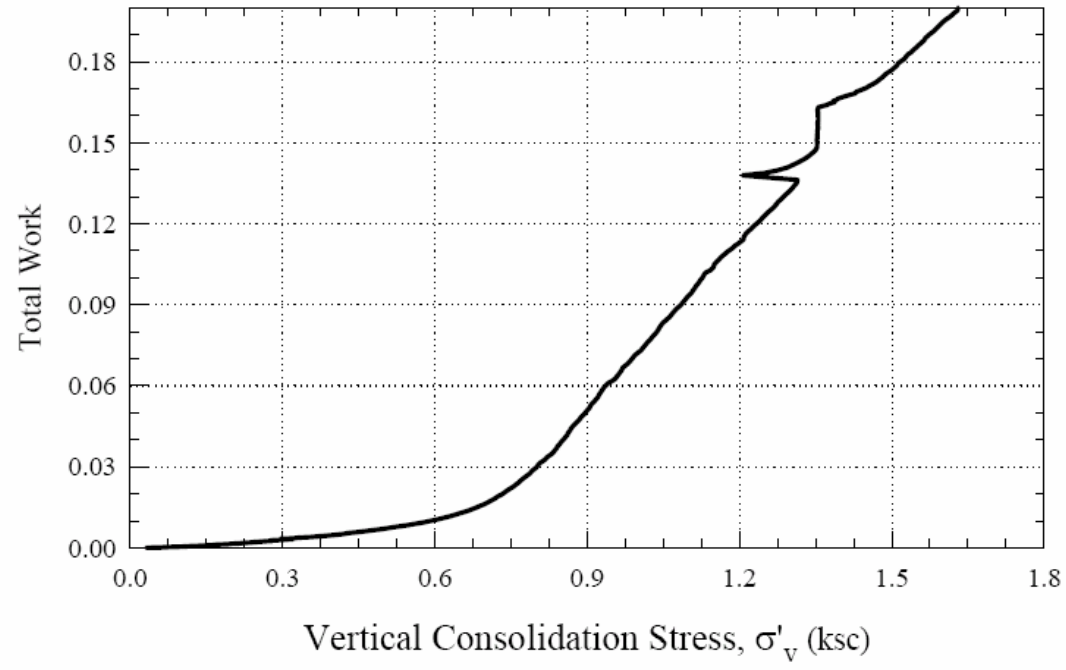

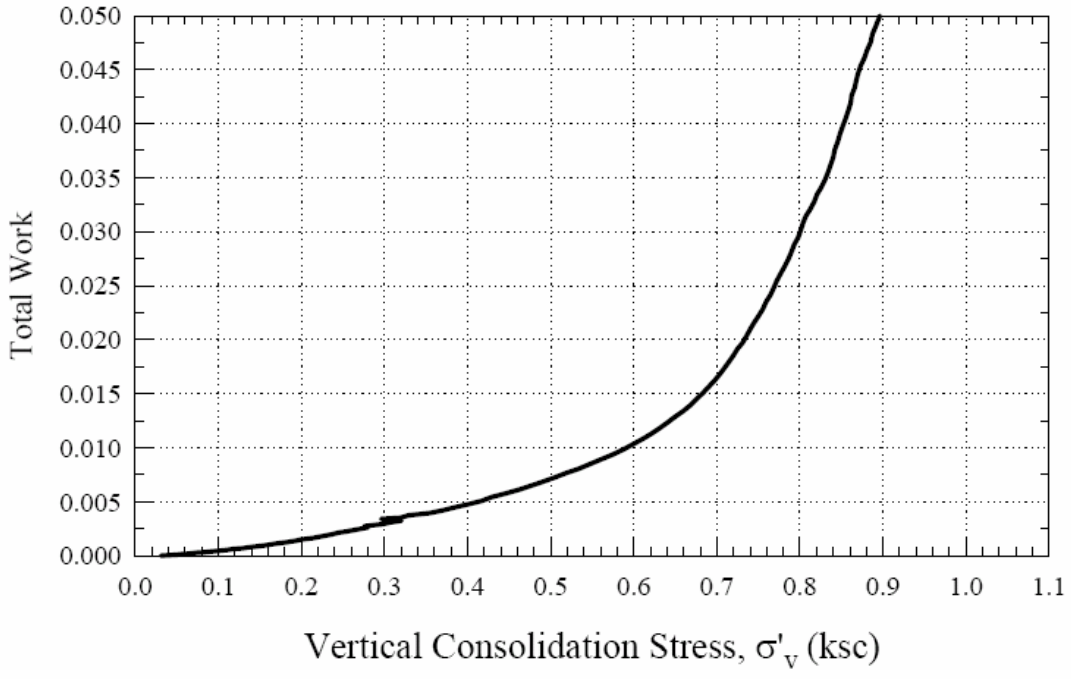

URS HAAFB
DSS 621: N1-B9 S-6

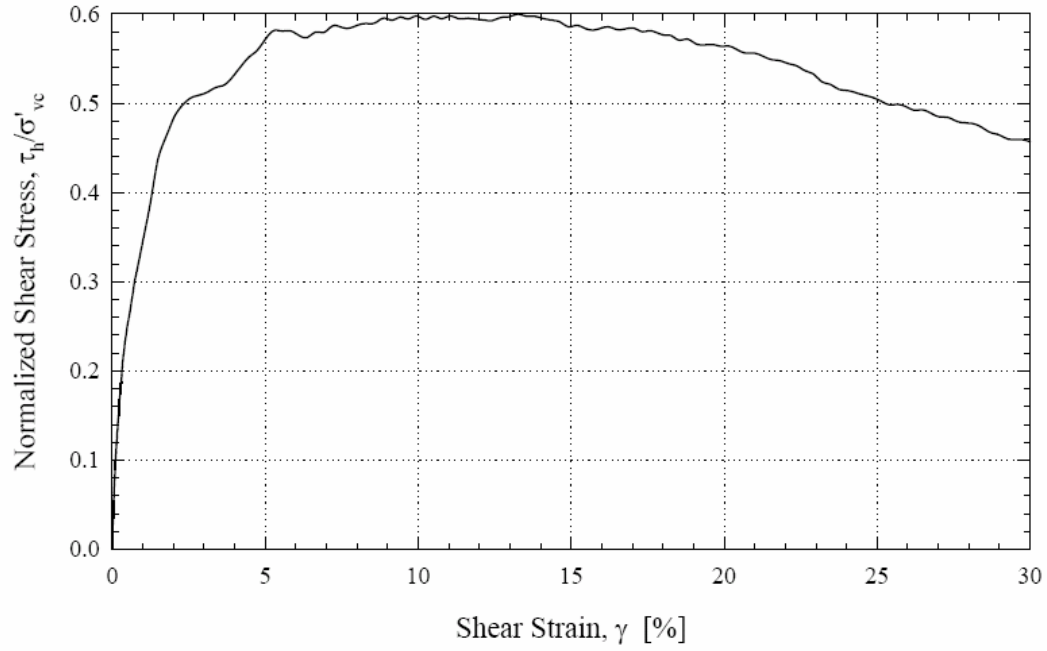

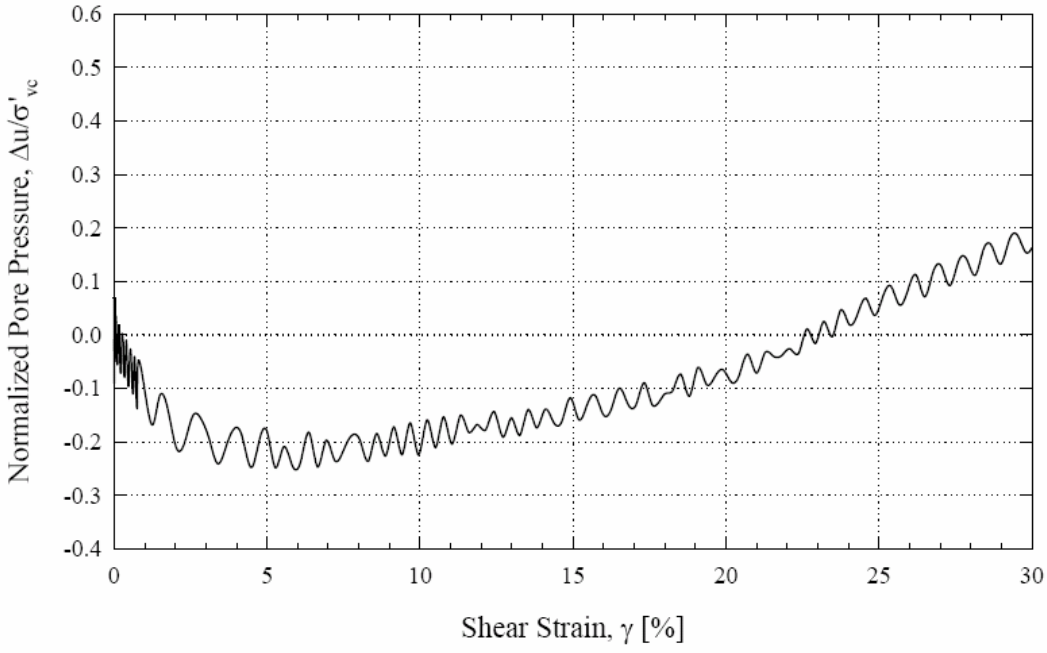

URS HAAFB
DSS 621: N1-B9 S-6

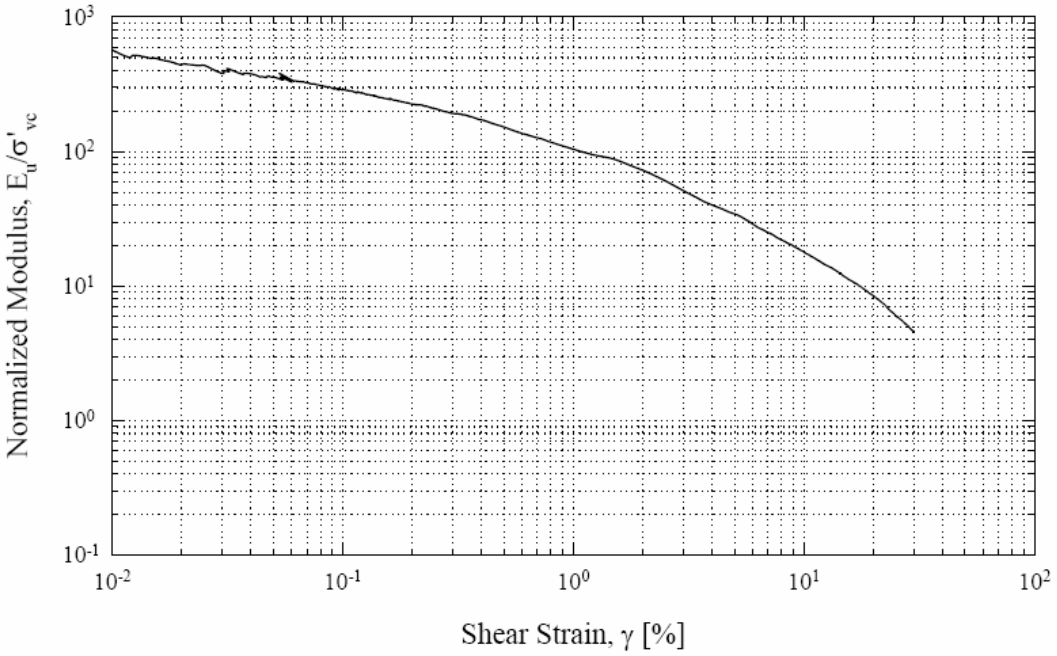

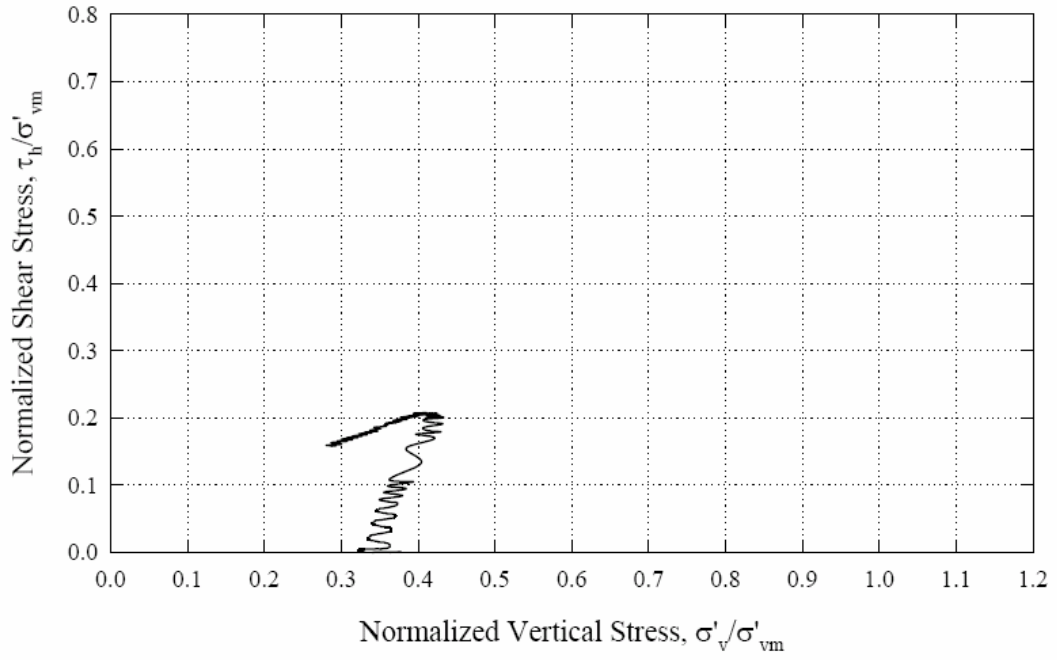

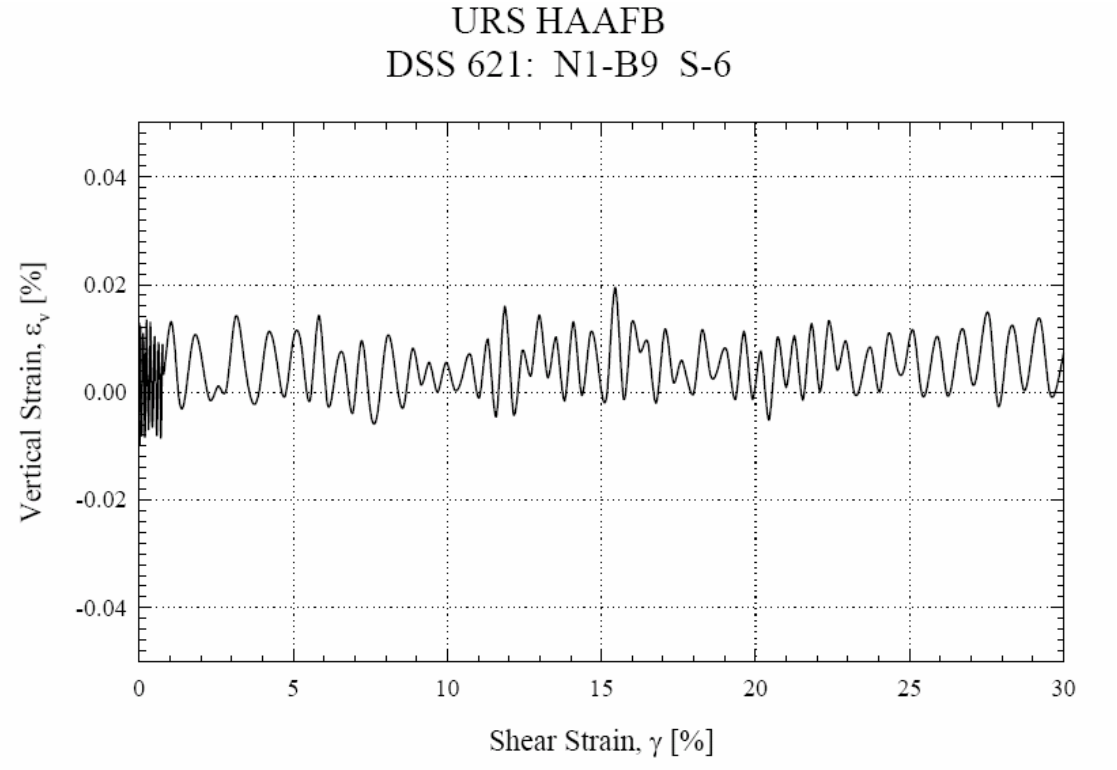
URS HAAFB
DSS 621: N1-B9 S-6
Vertical Strain, ε_v [%]
0.04
0.02
0.00
-0.02
-0.04
0
5
10
15
20
25
30
Shear Strain, γ [%]

6.1.3 CK_0UTC/TE tests on Bay Mud at OCR =1 (From Germaine, 2002)

Table A3 Detail Results of CK_0U Triaxial Tests on Bay Mud at NHPL

Specimen Location		Specimen Data		Preshear Conditions			At Max Shear			At Max Obliquity			E_{u}/σ'_{vc} @		Remarks
													ε_a =	$\Delta q/\Delta q_m$	
Test #	Depth	ω_n	e_i	t_s	ε_v	σ'_{vc}	ε_a	$\Delta u_e/\sigma'_{vc}$	q/p'	ε_a	$\Delta u_e/\sigma'_{vc}$	q/p'	0.001%	0.3	
Boring		I_p	S_i					$\Delta u_s/\sigma'_{vc}$	ϕ'		$\Delta u_s/\sigma'_{vc}$	ϕ'	0.01%		
Sample	Markers	γ_t	G_s		K_c	OCR	q/σ'_{vc}	p'/σ'_{vc}	A	q/σ'_{vc}	p'/σ'_{vc}	A	0.1%	0.5	
TX575		85.23	2.276	42.5	15.86	1.699	1.53	0.2038	0.5843	13.02	0.3430	0.7201	550	270	
TS5-B3			101.1					0.1260	35.8		0.2978	46.1	300		
S-6	11-14	1.527	2.70		0.469	1.00	0.3757	0.643	0.895	0.3278	0.4552	2.65	140	190	
TX576		91.26	2.434	41.5	11.70	1.132	-15.00	-0.1149	-0.9312				460	120	Internal strain yoke
TS5-B3			101.3					0.2509	-68.6	Same as Max Shear			295		strength taken at
S-6	15-18	1.504	2.70		0.486	1.00	-0.2908	0.3123	0.104				180	65	15% strain
TX584		91.62	2.474	11.8	13.06	1.029	2.41	0.2585	0.6543	15.00	0.3864	0.8205	290	130	
TS5-B3			100.0					0.1855	40.9		0.3484	55.1	210		
S-6	19.5-22.5	1.489	2.70		0.470	1.00	0.3725	0.5693	1.19	0.3187	0.3884	3.51	100	94	
TX590		86.29	2.322	3.0	11.40	1.427	3.84	0.2628	0.5645	13.43	0.3460	0.6345	170	67	
TS3-S3			100.3					0.2167	34.4		0.3325	39.4	115		
S-6	8-11	1.514	2.70		0.517	1.00	0.3009	0.533	1.91	0.2543	0.4008	8.72	58	45	
TX603				5.2	11.28	1.000	-14.5	-0.0841	-0.9799				N/A	97	Internal strain yoke
TS3-B1								0.2704	-78.5	Same as Max Shear			265		SS Modulus NG due
S-4	10-13				0.463	1.00	-0.2580	0.2633	0.0745				155	57	to sec. Strain rate

a) Marker location in tube
b) Stresses in kg/cm^2
c) 1 kg/cm^2 = 2048 psf
d) Depth in Feet
e) Time in hours
f) Water content, saturation, and strain in %
g) density in gm/cm^3

[Data from Germaine, (2002)]

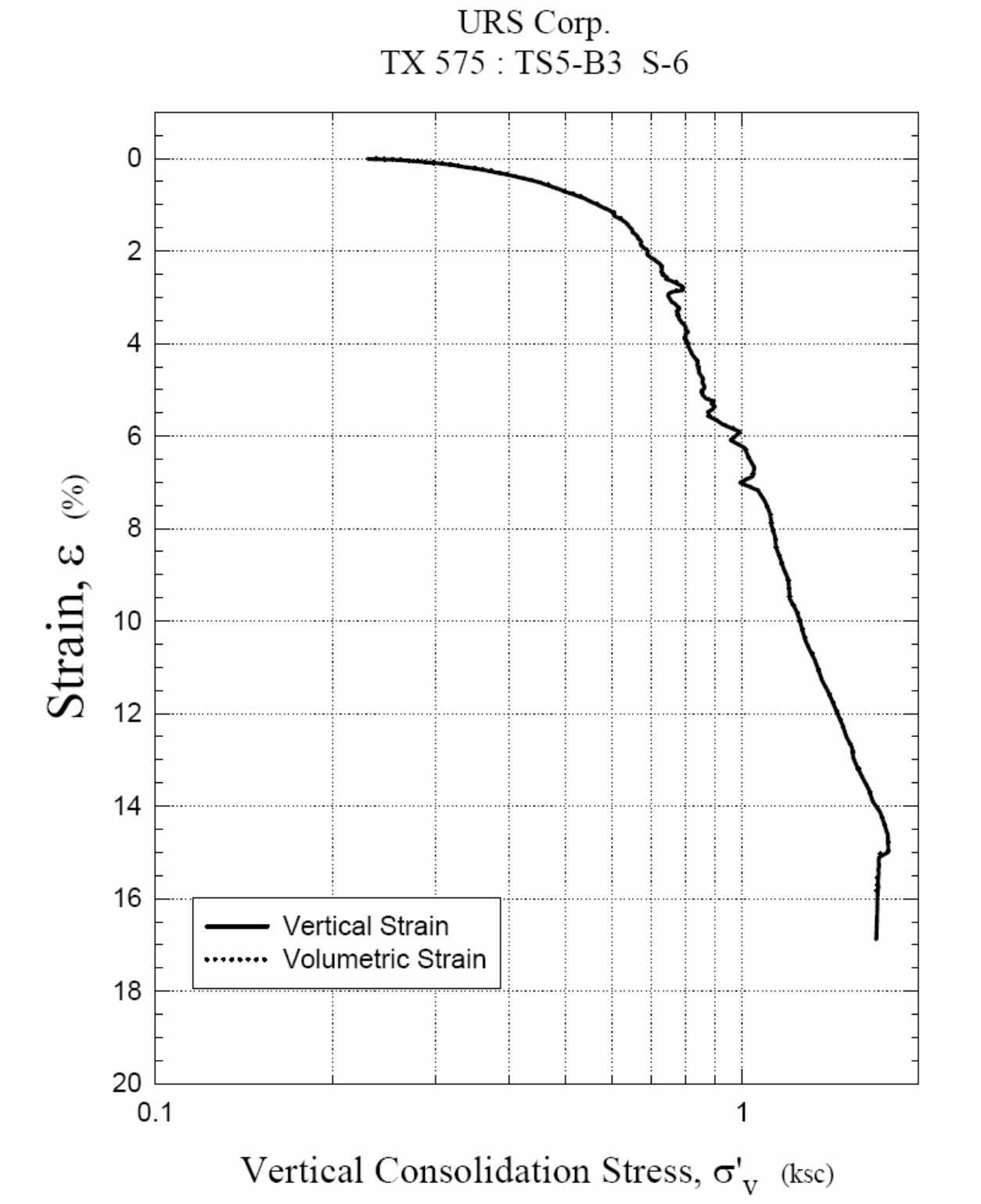
URS Corp.
TX 575 : TS5-B3 S-6
Strain, ε (%)
0
2
4
6
8
10
12
14
16
18
20
0.1
1
Vertical Strain
Volumetric Strain
Vertical Consolidation Stress, σ'v (ksc)

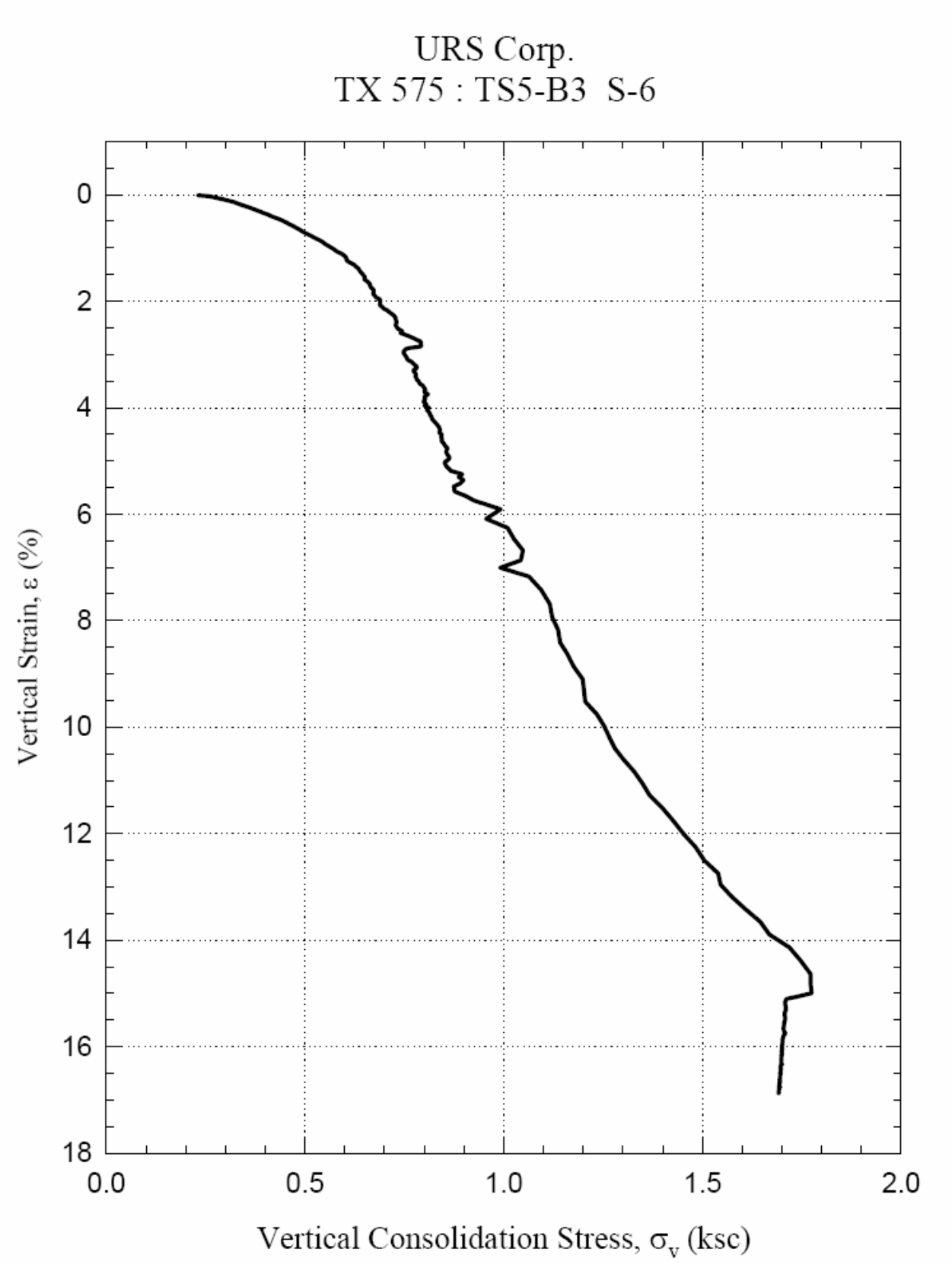
URS Corp.
TX 575 : TS5-B3 S-6
Vertical Strain, ε (%)
0
2
4
6
8
10
12
14
16
18
0.0
0.5
1.0
1.5
2.0
Vertical Consolidation Stress, σv (ksc)

URS Corp.
TX 575 : TS5-B3 S-6

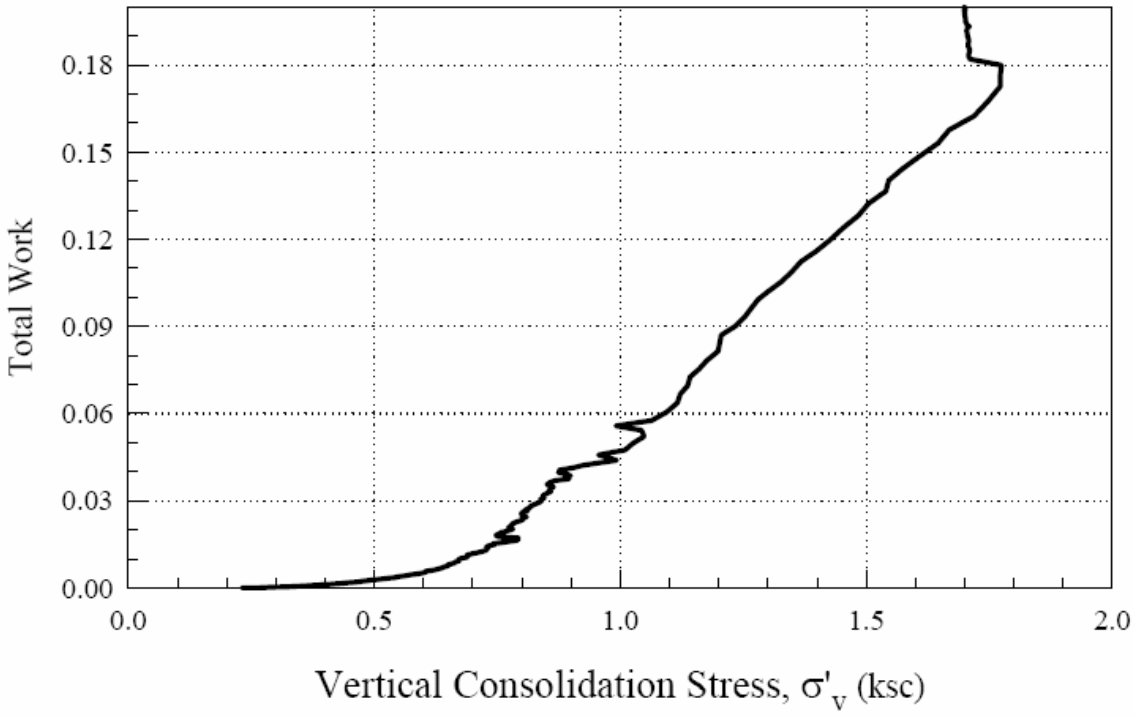

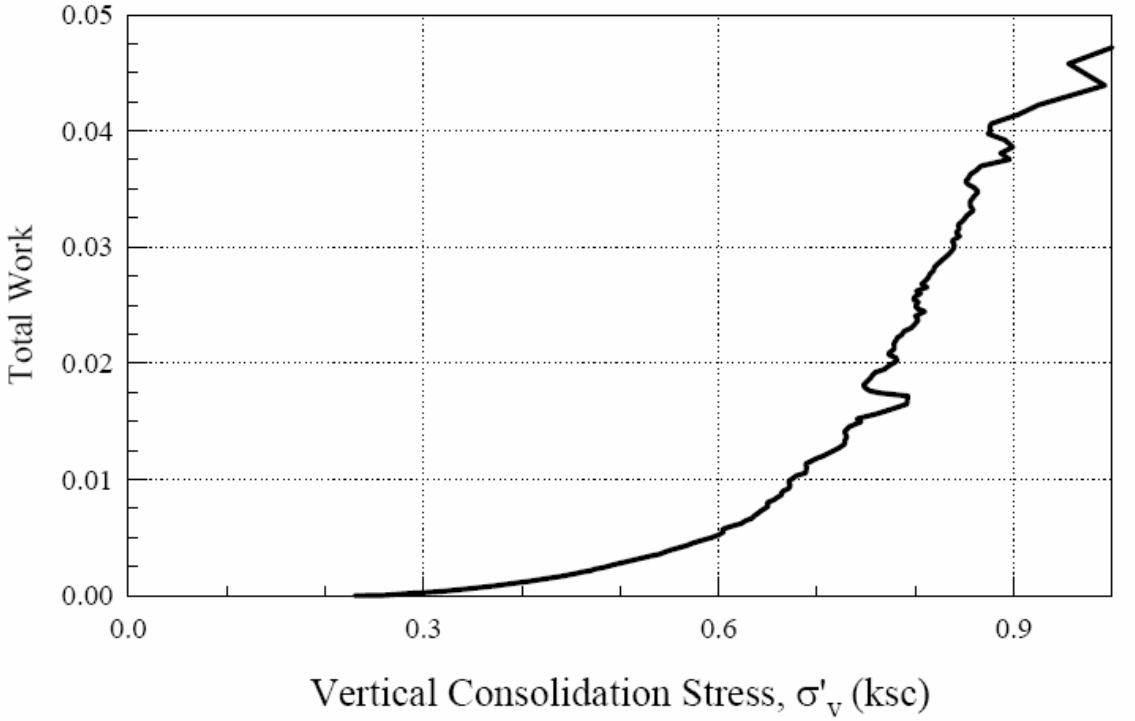

URS Corp.
TX 575 : TS5-B3 S-6

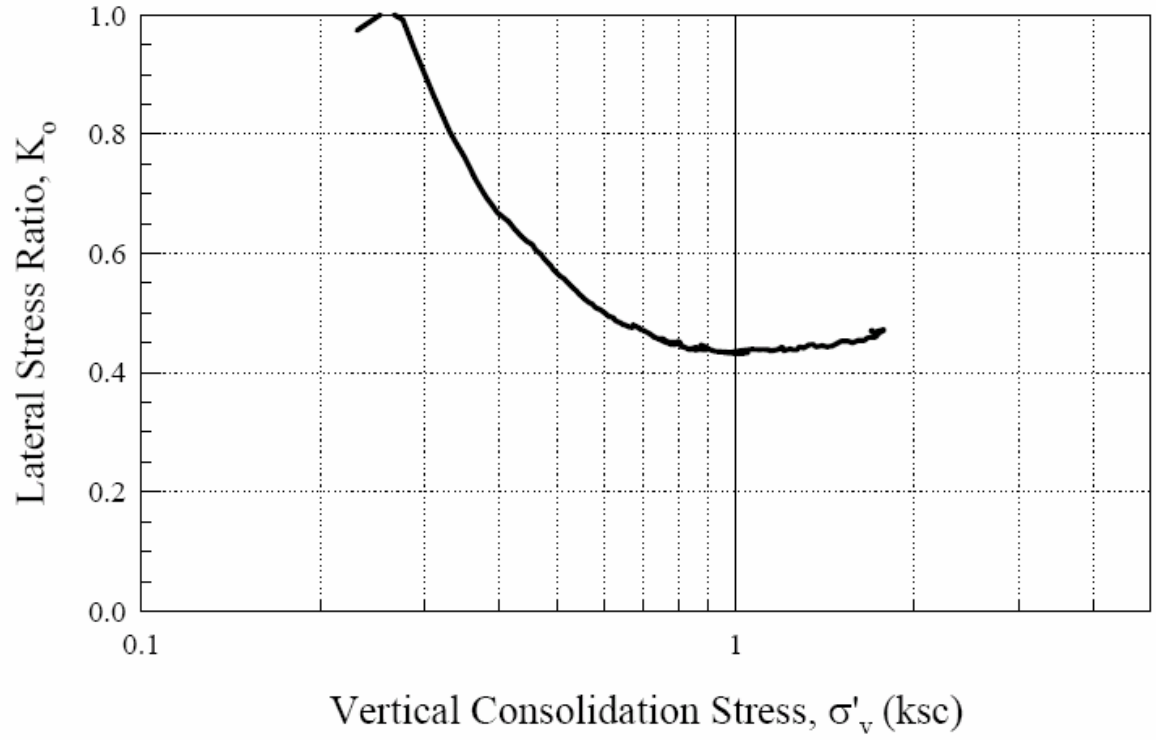

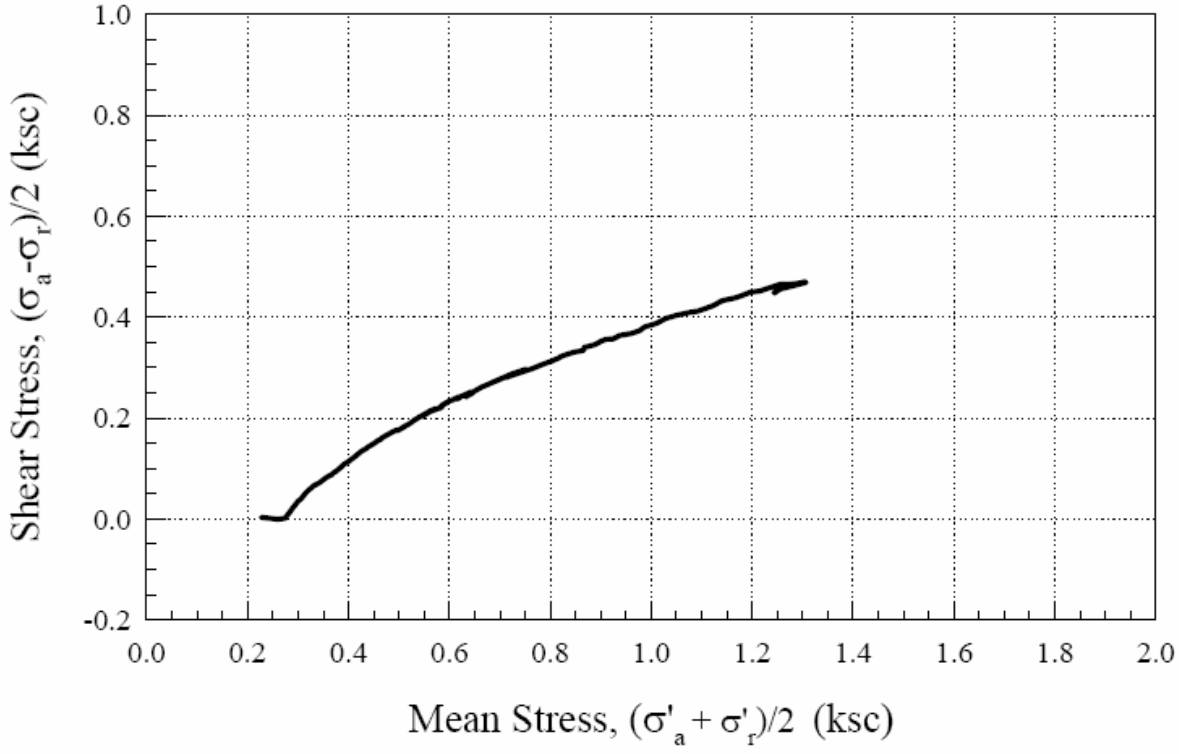

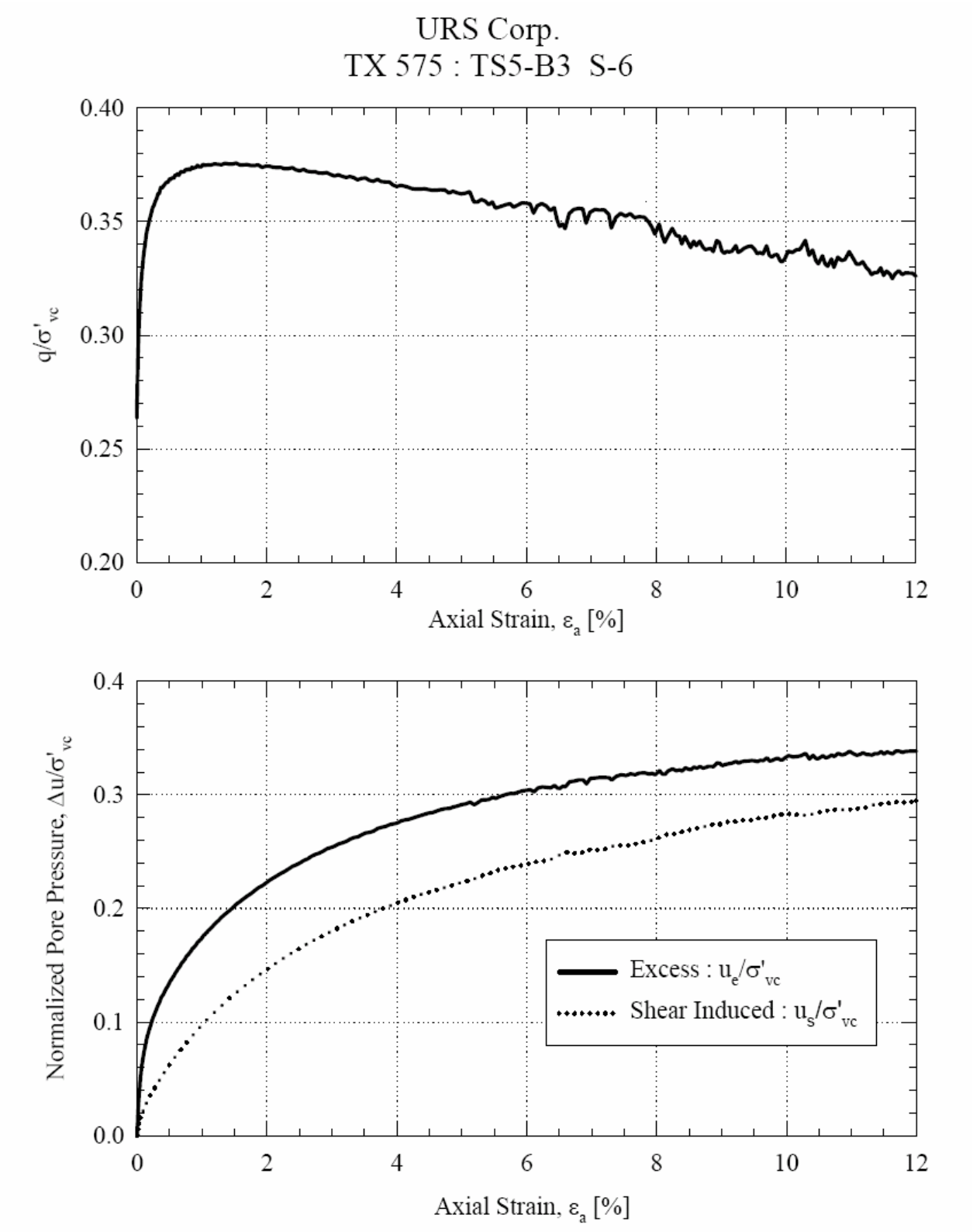
URS Corp.
TX 575 : TS5-B3 S-6
q/σ'vc
0.40
0.35
0.30
0.25
0.20
0
2
4
6
8
10
12
Axial Strain, εa [%]
Normalized Pore Pressure, Δu/σ'vc
0.4
0.3
0.2
0.1
0.0
Excess : ue/σ'vc
Shear Induced : us/σ'vc
0
2
4
6
8
10
12
Axial Strain, εa [%]

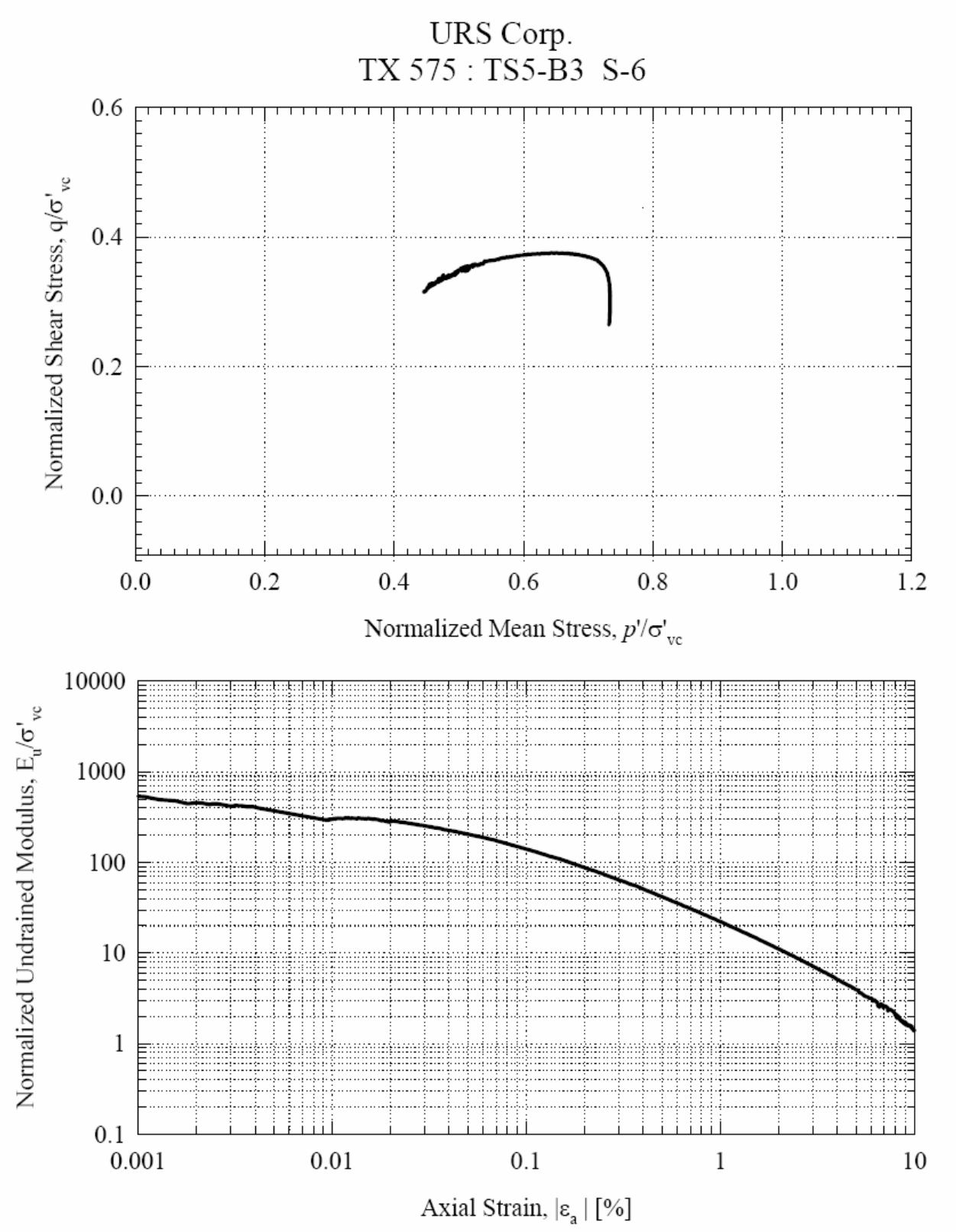
URS Corp.
TX 575 : TS5-B3 S-6
Normalized Shear Stress, q/σ'vc
0.6
0.4
0.2
0.0
0.0
0.2
0.4
0.6
0.8
1.0
1.2
Normalized Mean Stress, p'/σ'vc
Normalized Undrained Modulus, Eu/σ'vc
10000
1000
100
10
1
0.1
0.001
0.01
0.1
1
10
Axial Strain, |εa| [%]

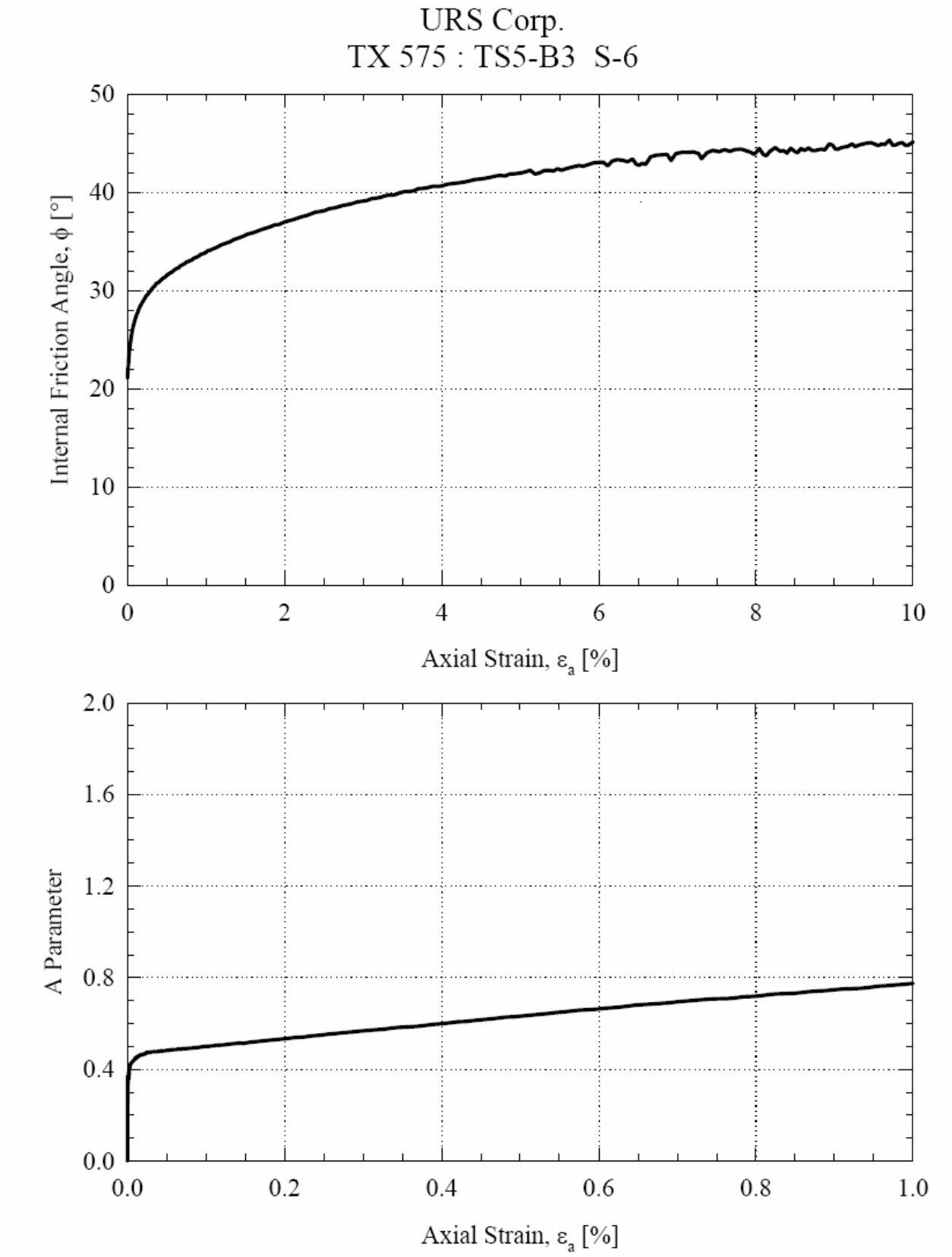
URS Corp.
TX 575 : TS5-B3 S-6
Internal Friction Angle, ϕ [°]
50
40
30
20
10
0
0
2
4
6
8
10
Axial Strain, ε_a [%]
A Parameter
2.0
1.6
1.2
0.8
0.4
0.0
0.0
0.2
0.4
0.6
0.8
1.0
Axial Strain, ε_a [%]

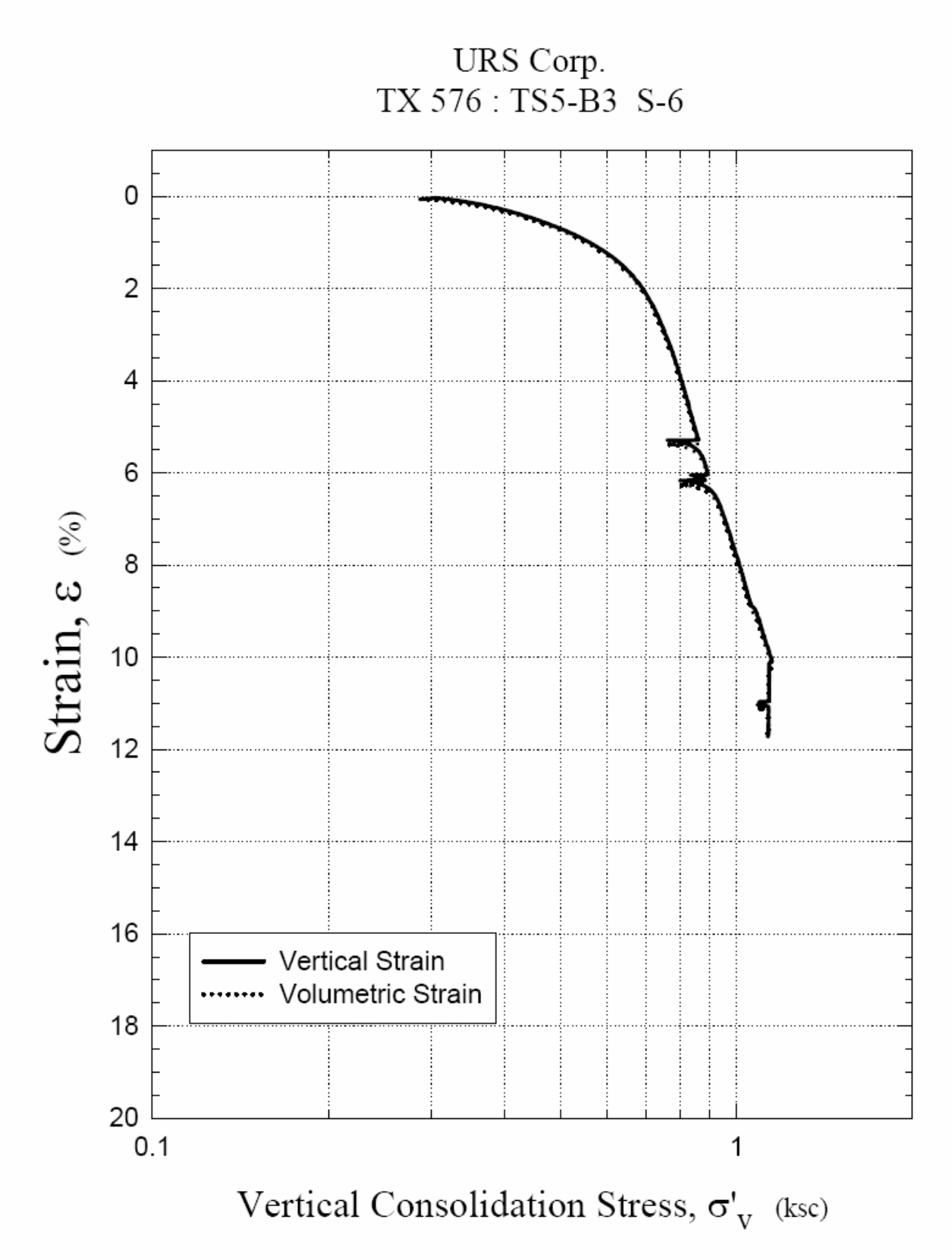
URS Corp.
TX 576 : TS5-B3 S-6
Strain, ε (%)
0
2
4
6
8
10
12
14
16
18
20
0.1
1
Vertical Strain
Volumetric Strain
Vertical Consolidation Stress, σ'v (ksc)

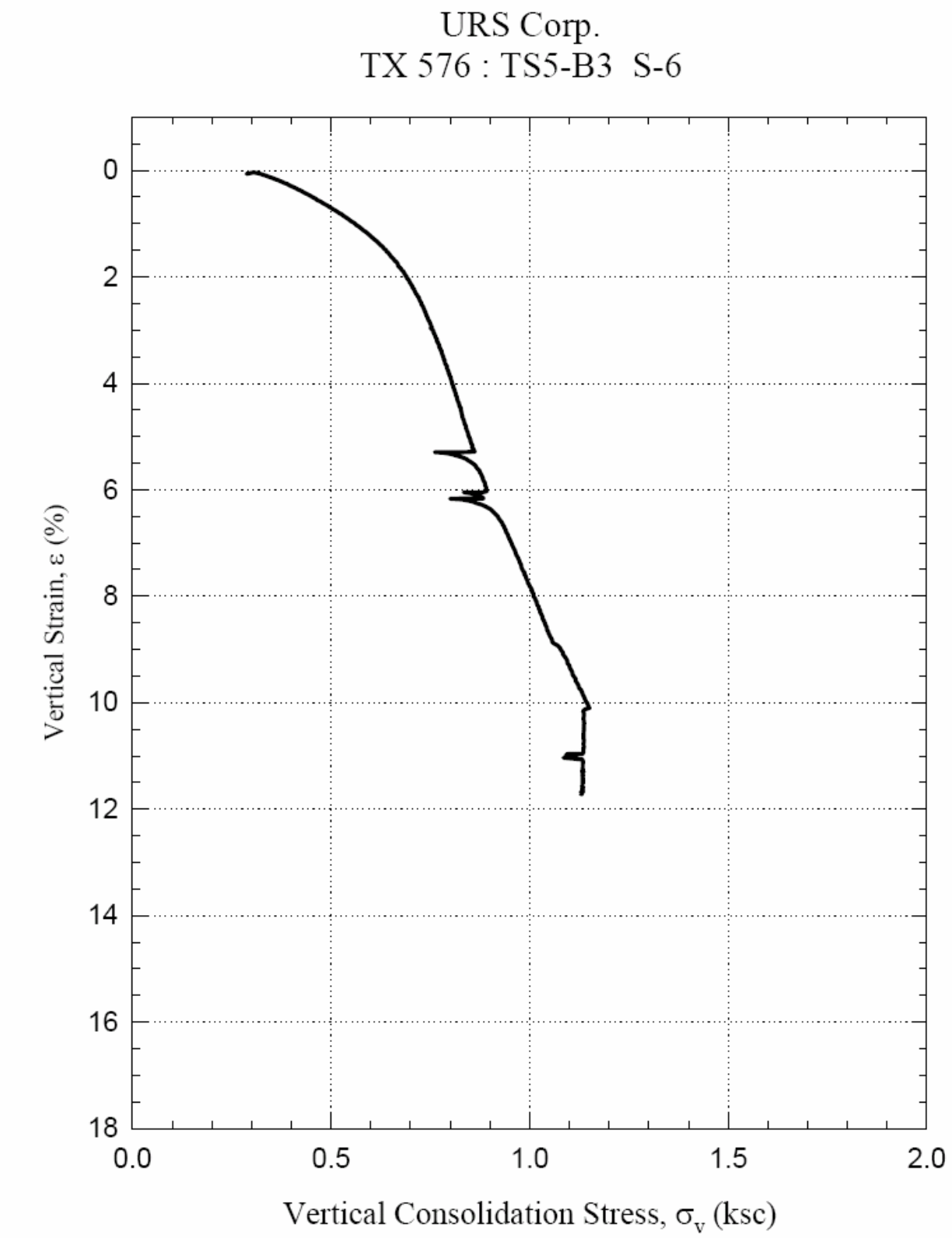
URS Corp.
TX 576 : TS5-B3 S-6
Vertical Strain, ε (%)
0
2
4
6
8
10
12
14
16
18
0.0
0.5
1.0
1.5
2.0
Vertical Consolidation Stress, σv (ksc)

URS Corp.
TX 576 : TS5-B3 S-6

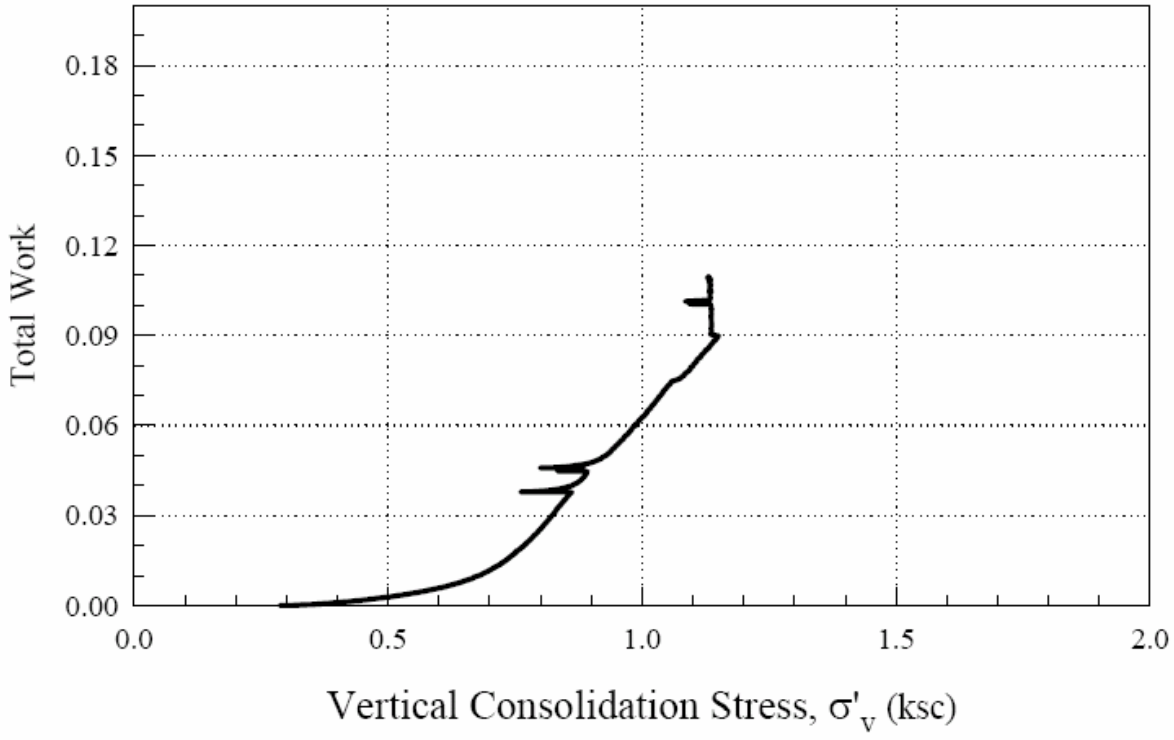

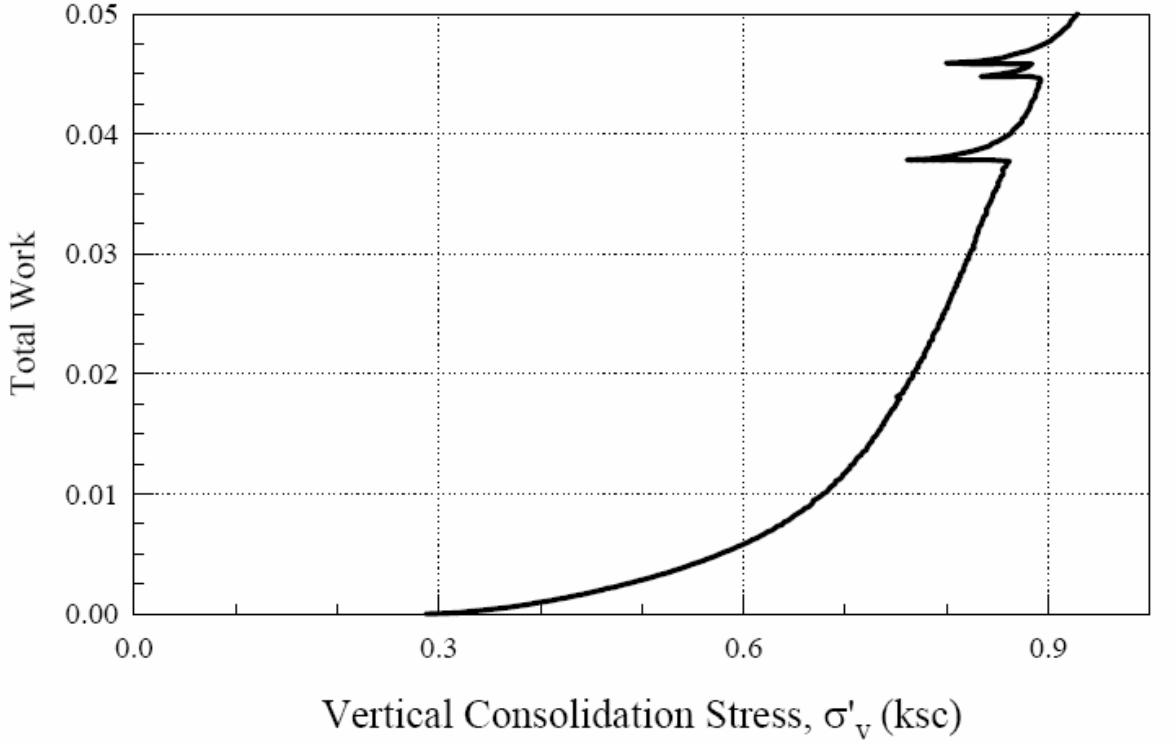

URS Corp.
TX 576 : TS5-B3 S-6

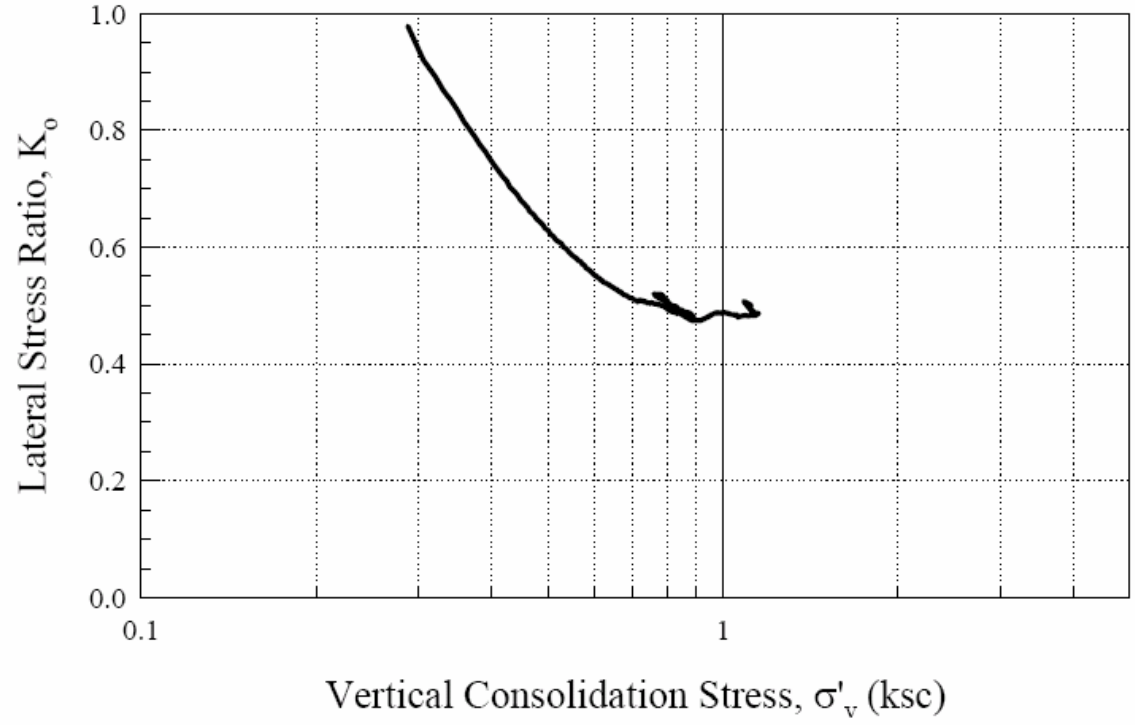

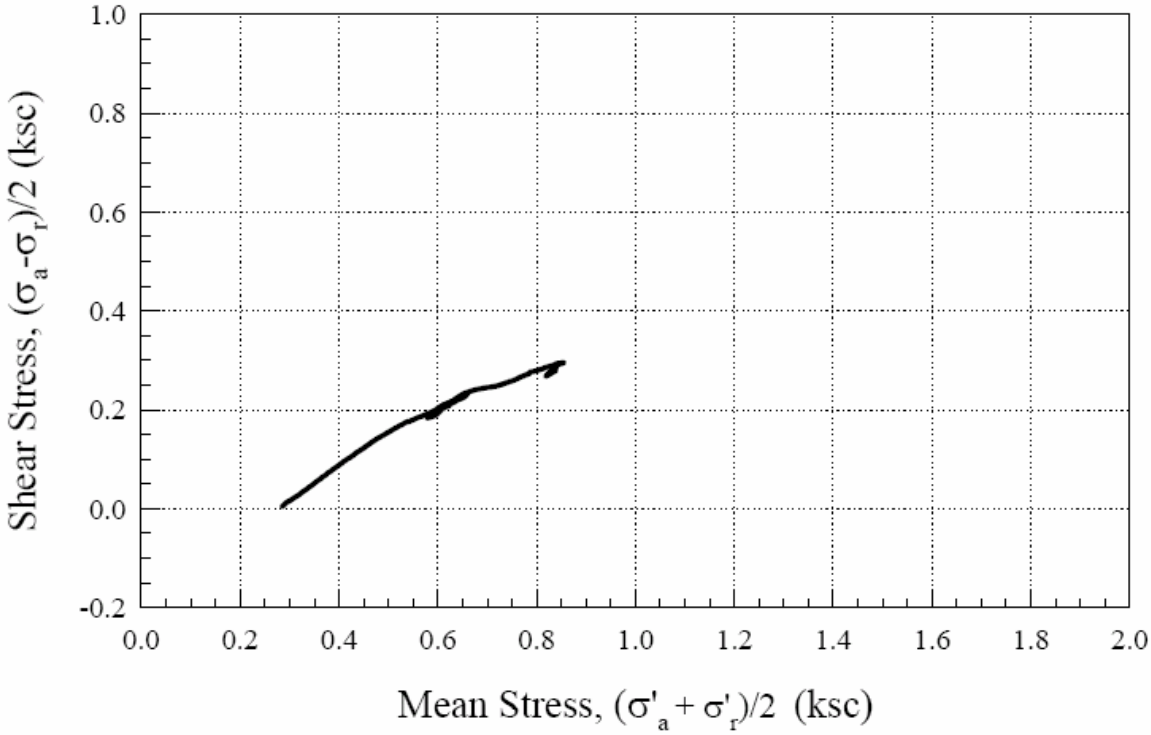

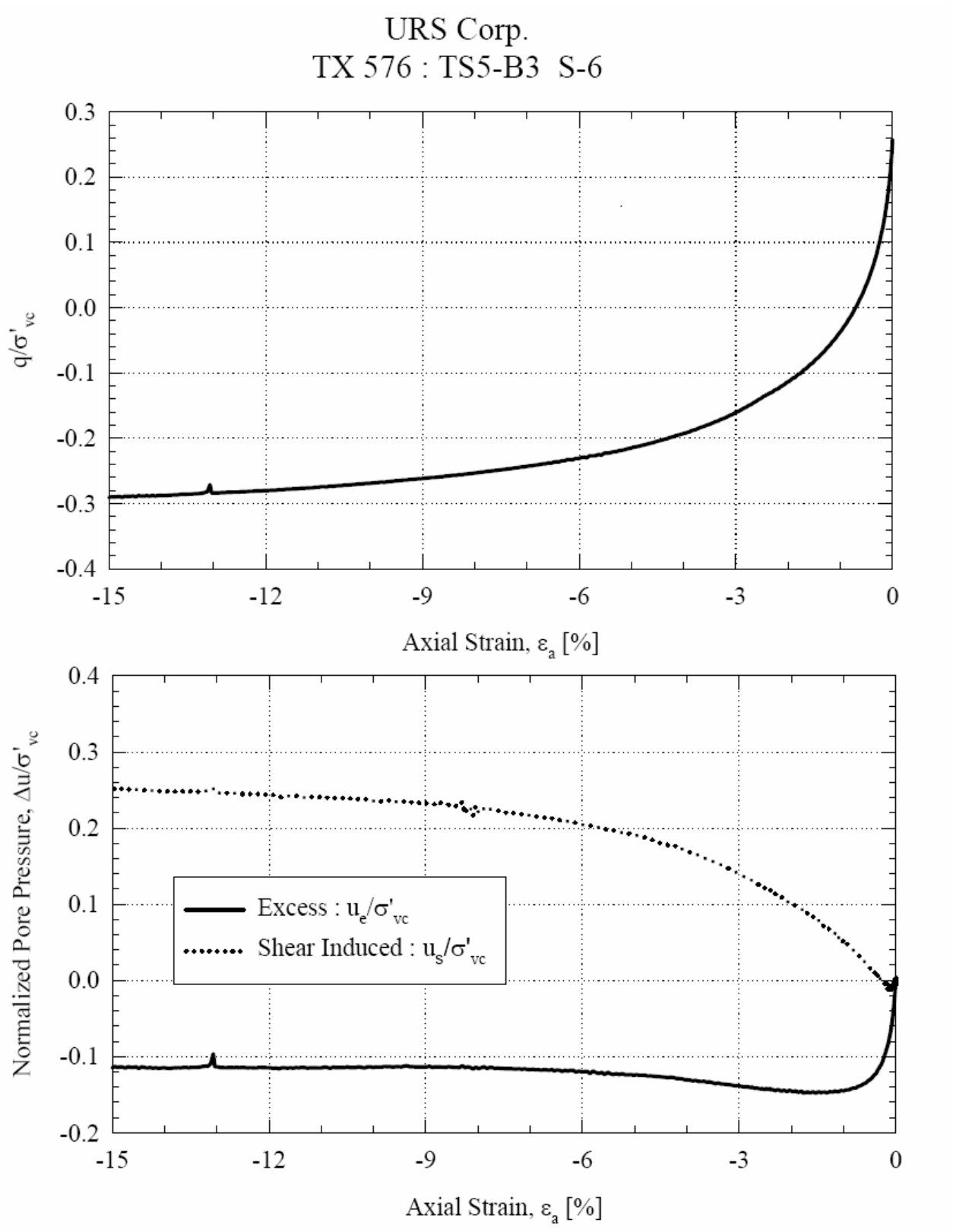
URS Corp.
TX 576 : TS5-B3 S-6
q/σ'vc
0.3
0.2
0.1
0.0
-0.1
-0.2
-0.3
-0.4
-15
-12
-9
-6
-3
0
Axial Strain, εa [%]
Normalized Pore Pressure, Δu/σ'vc
0.4
0.3
0.2
0.1
0.0
-0.1
-0.2
Excess : ue/σ'vc
Shear Induced : us/σ'vc
-15
-12
-9
-6
-3
0
Axial Strain, εa [%]

URS Corp.
TX 576 : TS5-B3 S-6

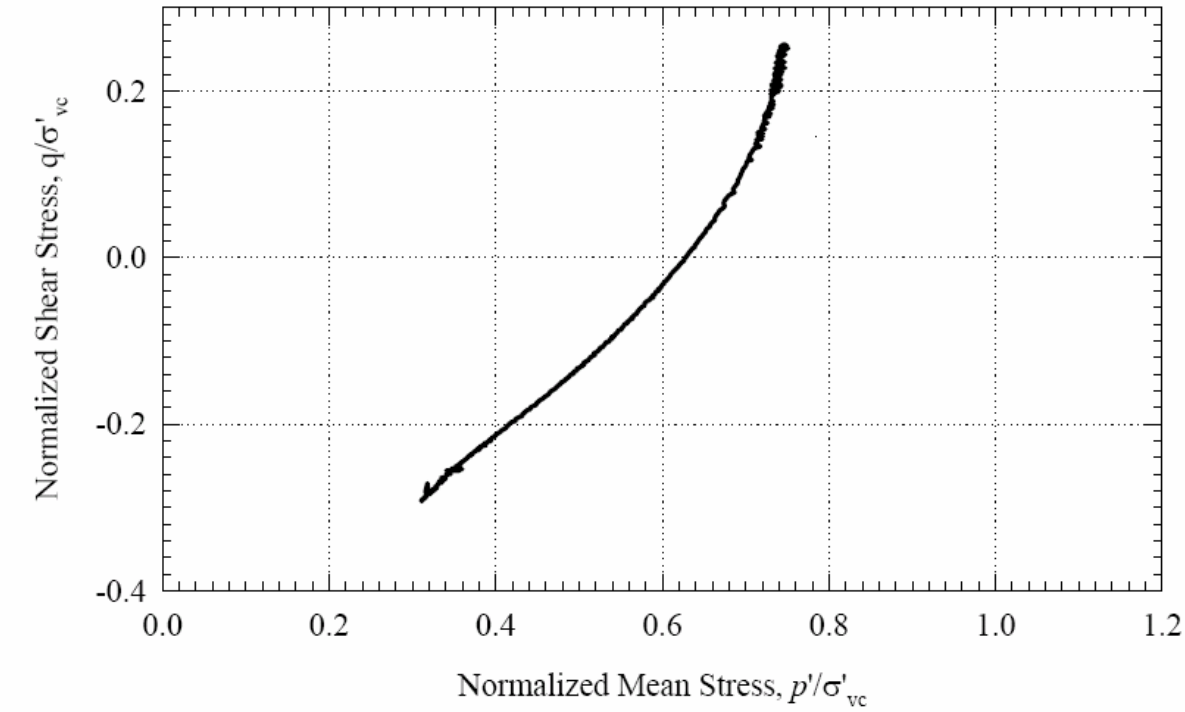

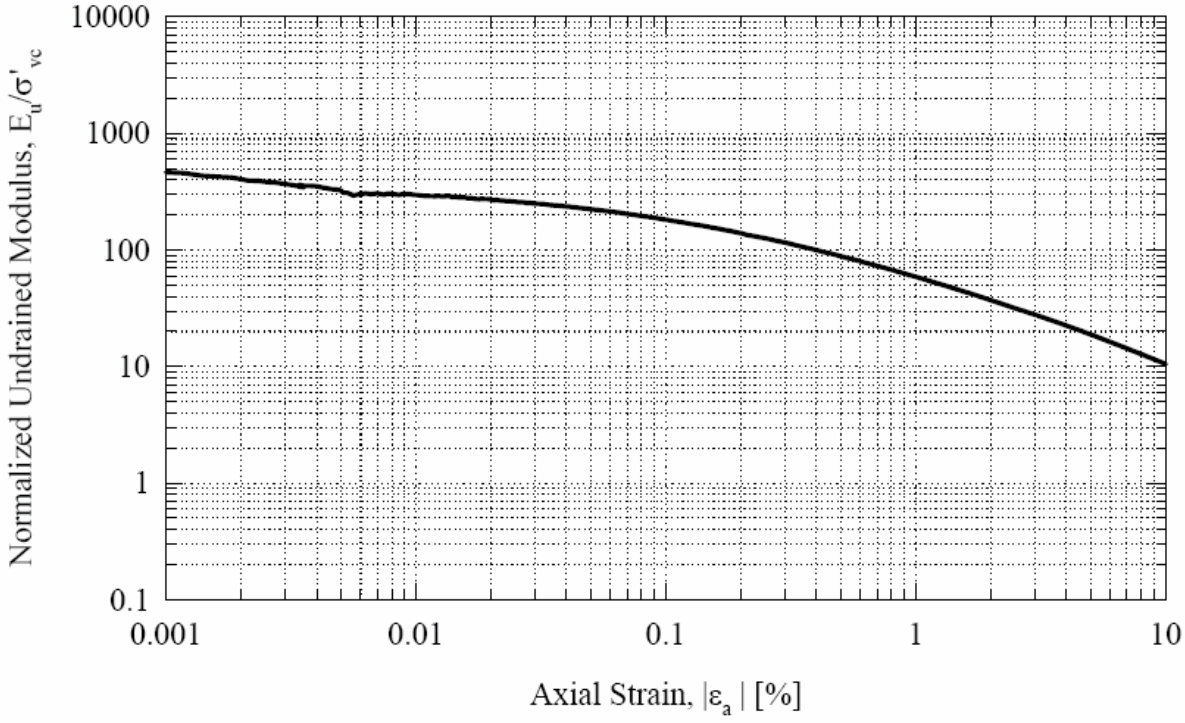

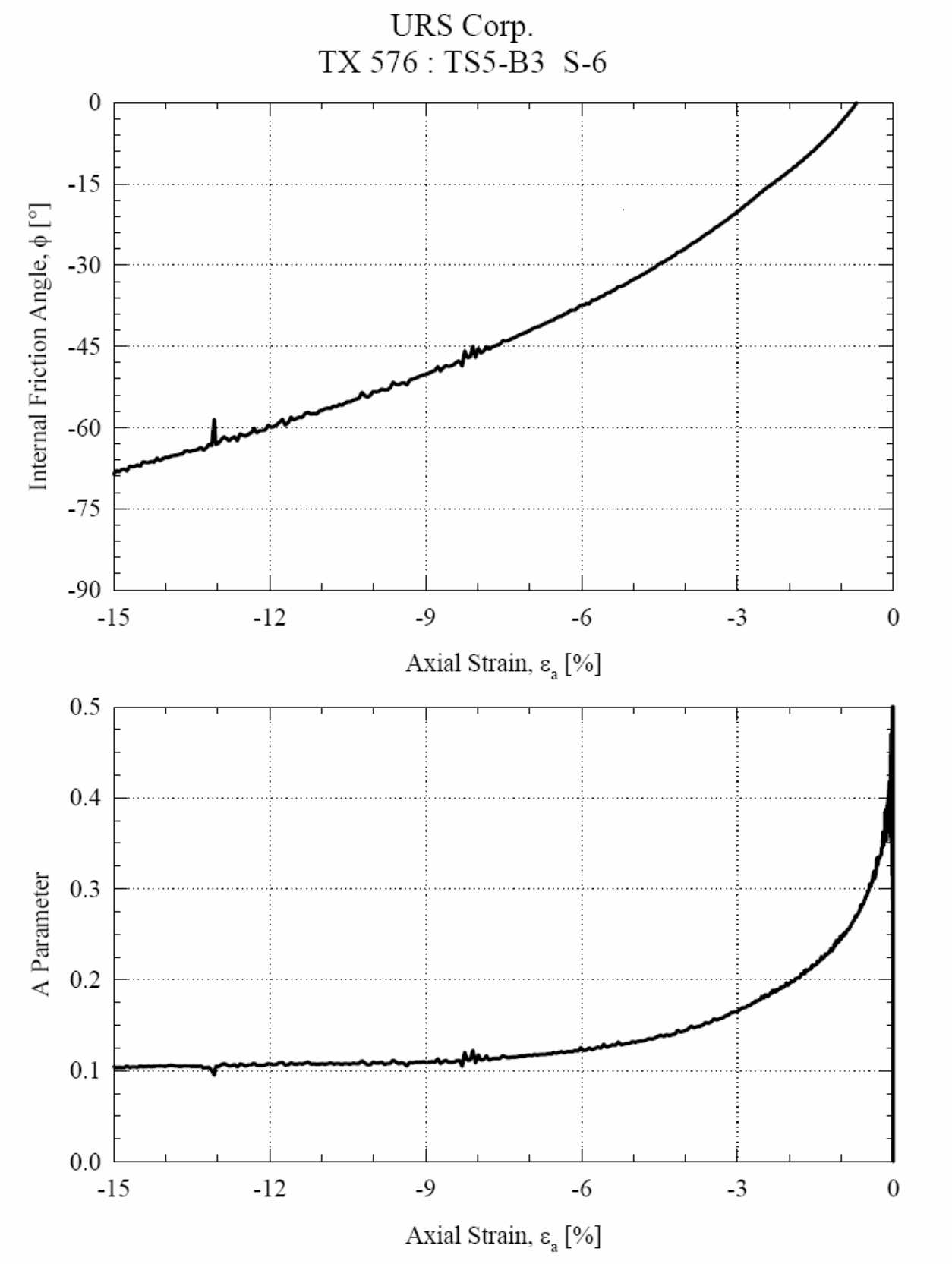
URS Corp.
TX 576 : TS5-B3 S-6
Internal Friction Angle, ϕ [°]
0
-15
-30
-45
-60
-75
-90
-15
-12
-9
-6
-3
0
Axial Strain, ε_a [%]
A Parameter
0.5
0.4
0.3
0.2
0.1
0.0
-15
-12
-9
-6
-3
0
Axial Strain, ε_a [%]

6.2 Appendix B: 1-D Consolidation Settlement Calculation

Note: For Stress History 2 (Case C σ'_{vf} and SH2 u_e)

Table B-1 1-D Consolidation Settlement Prediction at TS3 (computed with σ'_p profile)

TS3 -σ'_p

Layers			Cons. Status	Computed Settlement : $\sigma'_{vo} \rightarrow \sigma'_{vc}$ TS3 with σ'_p								
From EL. (ft)	To EL. (ft)	Soil type		Average EL. (ft)	Thickness of soil H_i[ft]	σ'_{v0} (ksf)	σ'_p(FV) (ksf)	σ'_{vc} TS3 (ksf)	ε	ε[%]	$\Delta\rho_c$ (ft)	ρ_c [ft]
-1.6	-4.5	Pavement										
-4.5	-6.2	Basecourse										
-6.2	-8	BM Crust	RR=0.06	-7.1	1.8	0.609	5.0689	1.851	0.0290	2.90	0.0521	**1.0430**
-8	-9	BM Crust	RR=0.06	-8.5	1	0.662	3.300	1.890	0.0274	2.74	0.0274	0.9909
-9	-10	BM Crust	RR=0.06	-9.5	1	0.699	2.747	1.918	0.0263	2.63	0.0263	0.9635
-10	-11	BM	RR=0.06	-10.5	1	0.733	2.469	1.947	0.0255	2.55	0.0255	0.9372
-11	**-12**	BM	RR=0.06	-11.5	1	0.763	2.080	1.932	0.0242	2.42	0.0242	0.9118
-12	-13	BM	RR=0.06, CR=0.40	-12.5	1	0.793	1.760	1.929	0.0367	3.67	0.0367	0.8875
-13	-14	BM	RR=0.06, CR=0.40	-13.5	1	0.824	1.615	1.925	0.0480	4.80	0.0480	0.8508
-14	-15	BM	RR=0.06, CR=0.40	-14.5	1	0.854	1.572	1.919	0.0506	5.06	0.0506	0.8028
-15	-16	BM	RR=0.06, CR=0.40	-15.5	1	0.884	1.569	1.912	0.0493	4.93	0.0493	0.7522
-16	-17	BM	RR=0.06, CR=0.40	-16.5	1	0.914	1.550	1.904	0.0495	4.95	0.0495	0.7029
-17	-18	BM	RR=0.06, CR=0.40	-17.5	1	0.945	1.584	1.895	0.0446	4.46	0.0446	0.6535
-18	-19	BM	RR=0.06, CR=0.40	-18.5	1	0.975	1.617	1.886	0.0399	3.99	0.0399	0.6088
-19	-20	BM	RR=0.06, CR=0.40	-19.5	1	1.005	1.651	1.877	0.0352	3.52	0.0352	0.5690
-20	-21	BM	RR=0.12, CR=0.40	-20.5	1	1.036	1.685	1.869	0.0434	4.34	0.0434	0.5337
-21	-22	BM	RR=0.12, CR=0.40	-21.5	1	1.066	1.718	1.862	0.0389	3.89	0.0389	0.4903
-22	-23	BM	RR=0.12, CR=0.40	-22.5	1	1.096	1.752	1.857	0.0346	3.46	0.0346	0.4515
-23	-24	BM	RR=0.12, CR=0.40	-23.5	1	1.127	1.785	1.855	0.0306	3.06	0.0306	0.4169
-24	-25	BM	RR=0.12, CR=0.40	-24.5	1	1.157	1.819	1.856	0.0271	2.71	0.0271	0.3862
-25	-26	BM	RR=0.12, CR=0.40	-25.5	1	1.187	1.853	1.860	0.0239	2.39	0.0239	0.3592
-26	-27	BM	RR=0.12	-26.5	1	1.217	1.886	1.869	0.0223	2.23	0.0223	0.3353
-27	-28	BM	RR=0.12	-27.5	1	1.248	1.920	1.882	0.0214	2.14	0.0214	0.3130
-28	-29	BM	RR=0.12	-28.5	1	1.278	1.953	1.900	0.0207	2.07	0.0207	0.2915
-29	-30	BM	RR=0.12	-29.5	1	1.308	1.987	1.924	0.0201	2.01	0.0201	0.2709
-30	-31	BM	RR=0.12	-30.5	1	1.339	2.021	1.953	0.0197	1.97	0.0197	0.2508
-31	-32	BM	RR=0.12	-31.5	1	1.369	2.054	1.987	0.0194	1.94	0.0194	0.2311
-32	-33	BM	RR=0.12	-32.5	1	1.399	2.088	2.027	0.0193	1.93	0.0193	0.2117
-33	-34	BM	RR=0.12	-33.5	1	1.430	2.121	2.072	0.0193	1.93	0.0193	0.1924
-34	-35	BM	RR=0.12	-34.5	1	1.460	2.155	2.122	0.0195	1.95	0.0195	0.1730
-35	-36	BM	RR=0.12	-35.5	1	1.490	2.189	2.176	0.0197	1.97	0.0197	0.1536
-36	-37	BM	RR=0.12, CR=0.40	-36.5	1	1.520	2.222	2.233	0.0206	2.06	0.0206	0.1338
-37	-38	BM	RR=0.12, CR=0.40	-37.5	1	1.551	2.256	2.293	0.0223	2.23	0.0223	0.1132
-38	-39	BM	RR=0.12, CR=0.40	-38.5	1	1.581	2.289	2.353	0.0241	2.41	0.0241	0.0909
-39	-40	BM	RR=0.12, CR=0.40	-39.5	1	1.611	2.323	2.414	0.0257	2.57	0.0257	0.0668
-40	-41	BM	RR=0.12, CR=0.40	-40.5	1	1.642	2.357	2.472	0.0271	2.71	0.0271	0.0411
-41	-41.5	BM	RR=0.12, CR=0.40	-41.25	0.5	1.664	2.382	2.512	0.0280	2.80	0.0140	0.0140

Table B-2 1-D Consolidation Settlement Prediction at TS3 (computed with $0.9\sigma'_p$ profile)

TS3 -0.9σ'p

Layers			Cons. Status	Computed Settlement : $\sigma'_{vo} \rightarrow \sigma'_{vc}$ TS3 with $0.9\sigma'_p$									
From EL. (ft)	To EL. (ft)	Soil type		Average EL. (ft)	Thickness of soil H_i[ft]	σ'_{v0} (ksf)	σ'_p(FV) (ksf)	$0.9\sigma'_p$(FV) (ksf)	σ'_{vc} TS3 (ksf)	ε	ε[%]	$\Delta\rho_c$ (ft)	ρ_c [ft]
-1.6	-4.5	Pavement											
-4.5	-6.2	Basecourse											
-6.2	-8	BM Crust	RR=0.06	-7.1	1.8	0.609	5.0689	4.5620	1.852	0.0290	2.90	0.0522	**1.4197**
-8	-9	BM Crust	RR=0.06	-8.5	1	0.662	3.300	2.9700	1.892	0.0274	2.74	0.0274	1.3675
-9	-10	BM Crust	RR=0.06	-9.5	1	0.699	2.747	2.4723	1.925	0.0264	2.64	0.0264	1.3401
-10	-11	BM	RR=0.06	-10.5	1	0.733	2.469	2.2221	1.952	0.0255	2.55	0.0255	1.3137
-11	**-12**	BM	RR=0.06, CR=0.40	-11.5	1	0.763	2.080	1.8720	1.932	0.0289	2.89	0.0289	1.2882
-12	-13	BM	RR=0.06, CR=0.40	-12.5	1	0.793	1.760	1.5840	1.929	0.0523	5.23	0.0523	1.2593
-13	-14	BM	RR=0.06, CR=0.40	-13.5	1	0.824	1.615	1.4537	1.925	0.0636	6.36	0.0636	1.2070
-14	-15	BM	RR=0.06, CR=0.40	-14.5	1	0.854	1.572	1.4145	1.919	0.0662	6.62	0.0662	1.1435
-15	-16	BM	RR=0.06, CR=0.40	-15.5	1	0.884	1.569	1.4125	1.912	0.0648	6.48	0.0648	1.0773
-16	-17	BM	RR=0.06, CR=0.40	-16.5	1	0.914	1.550	1.3952	1.904	0.0650	6.50	0.0650	1.0125
-17	-18	BM	RR=0.06, CR=0.40	-17.5	1	0.945	1.584	1.4254	1.895	0.0602	6.02	0.0602	0.9475
-18	-19	BM	RR=0.06, CR=0.40	-18.5	1	0.975	1.617	1.4557	1.886	0.0554	5.54	0.0554	0.8873
-19	-20	BM	RR=0.06, CR=0.40	-19.5	1	1.005	1.651	1.4859	1.877	0.0508	5.08	0.0508	0.8318
-20	-21	BM	RR=0.12, CR=0.40	-20.5	1	1.036	1.685	1.5161	1.869	0.0562	5.62	0.0562	0.7810
-21	-22	BM	RR=0.12, CR=0.40	-21.5	1	1.066	1.718	1.5464	1.862	0.0517	5.17	0.0517	0.7248
-22	-23	BM	RR=0.12, CR=0.40	-22.5	1	1.096	1.752	1.5766	1.857	0.0474	4.74	0.0474	0.6732
-23	-24	BM	RR=0.12, CR=0.40	-23.5	1	1.127	1.785	1.6069	1.855	0.0434	4.34	0.0434	0.6258
-24	-25	BM	RR=0.12, CR=0.40	-24.5	1	1.157	1.819	1.6371	1.856	0.0399	3.99	0.0399	0.5823
-25	-26	BM	RR=0.12, CR=0.40	-25.5	1	1.187	1.853	1.6673	1.860	0.0367	3.67	0.0367	0.5424
-26	-27	BM	RR=0.12, CR=0.40	-26.5	1	1.217	1.886	1.6976	1.869	0.0340	3.40	0.0340	0.5057
-27	-28	BM	RR=0.12, CR=0.40	-27.5	1	1.248	1.920	1.7278	1.882	0.0318	3.18	0.0318	0.4717
-28	-29	BM	RR=0.12, CR=0.40	-28.5	1	1.278	1.953	1.7581	1.900	0.0301	3.01	0.0301	0.4399
-29	-30	BM	RR=0.12, CR=0.40	-29.5	1	1.308	1.987	1.7883	1.924	0.0290	2.90	0.0290	0.4098
-30	-31	BM	RR=0.12, CR=0.40	-30.5	1	1.339	2.021	1.8185	1.953	0.0283	2.83	0.0283	0.3808
-31	-32	BM	RR=0.12, CR=0.40	-31.5	1	1.369	2.054	1.8488	1.987	0.0282	2.82	0.0282	0.3525
-32	-33	BM	RR=0.12, CR=0.40	-32.5	1	1.399	2.088	1.8790	2.027	0.0285	2.85	0.0285	0.3243
-33	-34	BM	RR=0.12, CR=0.40	-33.5	1	1.430	2.121	1.9093	2.072	0.0293	2.93	0.0293	0.2958
-34	-35	BM	RR=0.12, CR=0.40	-34.5	1	1.460	2.155	1.9395	2.122	0.0304	3.04	0.0304	0.2665
-35	-36	BM	RR=0.12, CR=0.40	-35.5	1	1.490	2.189	1.9697	2.176	0.0318	3.18	0.0318	0.2361
-36	-37	BM	RR=0.12, CR=0.40	-36.5	1	1.520	2.222	2.0000	2.233	0.0334	3.34	0.0334	0.2043
-37	-38	BM	RR=0.12, CR=0.40	-37.5	1	1.551	2.256	2.0302	2.293	0.0352	3.52	0.0352	0.1709
-38	-39	BM	RR=0.12, CR=0.40	-38.5	1	1.581	2.289	2.0605	2.353	0.0369	3.69	0.0369	0.1357
-39	-40	BM	RR=0.12, CR=0.40	-39.5	1	1.611	2.323	2.0907	2.414	0.0385	3.85	0.0385	0.0988
-40	-41	BM	RR=0.12, CR=0.40	-40.5	1	1.642	2.357	2.1209	2.472	0.0399	3.99	0.0399	0.0603
-41	-41.5	BM	RR=0.12, CR=0.40	-41.25	0.5	1.664	2.382	2.1436	2.512	0.0408	4.08	0.0204	0.0204

Table B-3 1-D Consolidation Settlement Prediction at TS3 (computed with $0.8\sigma'_p$ profile)

TS3 -$0.8\sigma'_p$

Layers			Cons. Status	Computed Settlement : $\sigma'_{vo} \rightarrow \sigma'_{vc}$ TS3 with $0.8\sigma'_p$									
From EL. (ft)	To EL. (ft)	Soil type	(Reduced RR)	Average EL. (ft)	Thickness of soil H_i[ft]	σ'_{v0} (ksf)	σ'_p(FV) (ksf)	$0.8\sigma'_p$(FV) (ksf)	σ'_{vc} TS3 (ksf)	ε	ε[%]	$\Delta\rho_c$ (ft)	ρ_c [ft]
-1.6	-4.5	Pavement											
-4.5	-6.2	Basecourse											
-6.2	-8	BM Crust	RR=0.04	-7.1	1.8	0.609	5.0689	4.0551	1.852	0.0193	1.93	0.0348	**1.7133**
-8	-9	BM Crust	RR=0.04	-8.5	1	0.662	3.300	2.6400	1.892	0.0183	1.83	0.0183	1.6785
-9	-10	BM Crust	RR=0.04	-9.5	1	0.699	2.747	2.1976	1.925	0.0176	1.76	0.0176	1.6602
-10	-11	BM	RR=0.04	-10.5	1	0.733	2.469	1.9752	1.952	0.0170	1.70	0.0170	1.6426
-11	**-12**	BM	RR=0.04	-11.5	1	0.763	2.080	1.6640	1.932	0.0161	1.61	0.0161	1.6256
-12	-13	BM	RR=0.04, CR=0.40	-12.5	1	0.793	1.760	1.4080	1.929	0.0647	6.47	0.0647	1.6095
-13	-14	BM	RR=0.04, CR=0.40	-13.5	1	0.824	1.615	1.2922	1.925	0.0771	7.71	0.0771	1.5448
-14	-15	BM	RR=0.04, CR=0.40	-14.5	1	0.854	1.572	1.2574	1.919	0.0802	8.02	0.0802	1.4677
-15	-16	BM	RR=0.04, CR=0.40	-15.5	1	0.884	1.569	1.2555	1.912	0.0792	7.92	0.0792	1.3875
-16	-17	BM	RR=0.04, CR=0.40	-16.5	1	0.914	1.550	1.2402	1.904	0.0798	7.98	0.0798	1.3084
-17	-18	BM	RR=0.04, CR=0.40	-17.5	1	0.945	1.584	1.2670	1.895	0.0750	7.50	0.0750	1.2286
-18	-19	BM	RR=0.04, CR=0.40	-18.5	1	0.975	1.617	1.2939	1.886	0.0704	7.04	0.0704	1.1536
-19	-20	BM	RR=0.04, CR=0.40	-19.5	1	1.005	1.651	1.3208	1.877	0.0658	6.58	0.0658	1.0832
-20	-21	BM	RR=0.08, CR=0.40	-20.5	1	1.036	1.685	1.3477	1.869	0.0660	6.60	0.0660	1.0174
-21	-22	BM	RR=0.08, CR=0.40	-21.5	1	1.066	1.718	1.3746	1.862	0.0616	6.16	0.0616	0.9514
-22	-23	BM	RR=0.08, CR=0.40	-22.5	1	1.096	1.752	1.4014	1.857	0.0575	5.75	0.0575	0.8898
-23	-24	BM	RR=0.08, CR=0.40	-23.5	1	1.127	1.785	1.4283	1.855	0.0536	5.36	0.0536	0.8324
-24	-25	BM	RR=0.08, CR=0.40	-24.5	1	1.157	1.819	1.4552	1.856	0.0502	5.02	0.0502	0.7787
-25	-26	BM	RR=0.08, CR=0.40	-25.5	1	1.187	1.853	1.4821	1.860	0.0472	4.72	0.0472	0.7285
-26	-27	BM	RR=0.08, CR=0.40	-26.5	1	1.217	1.886	1.5090	1.869	0.0446	4.46	0.0446	0.6814
-27	-28	BM	RR=0.08, CR=0.40	-27.5	1	1.248	1.920	1.5358	1.882	0.0425	4.25	0.0425	0.6368
-28	-29	BM	RR=0.08, CR=0.40	-28.5	1	1.278	1.953	1.5627	1.900	0.0409	4.09	0.0409	0.5942
-29	-30	BM	RR=0.08, CR=0.40	-29.5	1	1.308	1.987	1.5896	1.924	0.0399	3.99	0.0399	0.5533
-30	-31	BM	RR=0.08, CR=0.40	-30.5	1	1.339	2.021	1.6165	1.953	0.0394	3.94	0.0394	0.5134
-31	-32	BM	RR=0.08, CR=0.40	-31.5	1	1.369	2.054	1.6434	1.987	0.0393	3.93	0.0393	0.4740
-32	-33	BM	RR=0.08, CR=0.40	-32.5	1	1.399	2.088	1.6702	2.027	0.0398	3.98	0.0398	0.4347
-33	-34	BM	RR=0.08, CR=0.40	-33.5	1	1.430	2.121	1.6971	2.072	0.0406	4.06	0.0406	0.3949
-34	-35	BM	RR=0.08, CR=0.40	-34.5	1	1.460	2.155	1.7240	2.122	0.0418	4.18	0.0418	0.3543
-35	-36	BM	RR=0.08, CR=0.40	-35.5	1	1.490	2.189	1.7509	2.176	0.0433	4.33	0.0433	0.3125
-36	-37	BM	RR=0.08, CR=0.40	-36.5	1	1.520	2.222	1.7778	2.233	0.0450	4.50	0.0450	0.2691
-37	-38	BM	RR=0.08, CR=0.40	-37.5	1	1.551	2.256	1.8046	2.293	0.0468	4.68	0.0468	0.2241
-38	-39	BM	RR=0.08, CR=0.40	-38.5	1	1.581	2.289	1.8315	2.353	0.0487	4.87	0.0487	0.1772
-39	-40	BM	RR=0.08, CR=0.40	-39.5	1	1.611	2.323	1.8584	2.414	0.0504	5.04	0.0504	0.1286
-40	-41	BM	RR=0.08, CR=0.40	-40.5	1	1.642	2.357	1.8853	2.472	0.0518	5.18	0.0518	0.0782
-41	-41.5	BM	RR=0.08, CR=0.40	-41.25	0.5	1.664	2.382	1.9054	2.512	0.0527	5.27	0.0264	0.0264

Table B-4 1-D Consolidation Settlement Prediction at TS5 (computed with σ'_p profile)

TS5 -σ'_p

Layers			Cons. Status	Computed Settlement : $\sigma'_{vo} \rightarrow \sigma'_{vc}$ TS5 with σ'_p								
From EL. (ft)	To EL. (ft)	Soil type		Average EL. (ft)	Thickness of soil H_i[ft]	σ'_{v0} (ksf)	σ'_p(FV) (ksf)	σ'_{vc} TS5 (ksf)	ε	ε[%]	$\Delta\rho_c$ (ft)	ρ_c [ft]
-1.6	-4.5	Pavement										
-4.5	-6.2	Basecourse										
-6.2	-8	BM Crust	RR=0.06	-7.1	1.8	0.609	5.0689	1.852	0.0290	2.90	0.0522	**1.1414**
-8	-9	BM Crust	RR=0.06	-8.5	1	0.662	3.300	1.892	0.0274	2.74	0.0274	1.0893
-9	-10	BM Crust	RR=0.06	-9.5	1	0.699	2.747	1.925	0.0264	2.64	0.0264	1.0619
-10	-11	BM	RR=0.06	-10.5	1	0.733	2.469	1.952	0.0255	2.55	0.0255	1.0355
-11	**-12**	BM	RR=0.06	-11.5	1	0.763	2.080	1.957	0.0245	2.45	0.0245	1.0100
-12	-13	BM	RR=0.06, CR=0.40	-12.5	1	0.793	1.760	1.928	0.0366	3.66	0.0366	0.9854
-13	-14	BM	RR=0.06, CR=0.40	-13.5	1	0.824	1.615	1.903	0.0461	4.61	0.0461	0.9489
-14	-15	BM	RR=0.06, CR=0.40	-14.5	1	0.854	1.572	1.884	0.0474	4.74	0.0474	0.9028
-15	-16	BM	RR=0.06, CR=0.40	-15.5	1	0.884	1.569	1.870	0.0454	4.54	0.0454	0.8554
-16	-17	BM	RR=0.06, CR=0.40	-16.5	1	0.914	1.550	1.861	0.0455	4.55	0.0455	0.8100
-17	-18	BM	RR=0.06, CR=0.40	-17.5	1	0.945	1.584	1.856	0.0410	4.10	0.0410	0.7645
-18	-19	BM	RR=0.06, CR=0.40	-18.5	1	0.975	1.617	1.856	0.0371	3.71	0.0371	0.7235
-19	-20	BM	RR=0.06, CR=0.40	-19.5	1	1.005	1.651	1.860	0.0337	3.37	0.0337	0.6864
-20	-21	BM	RR=0.12, CR=0.40	-20.5	1	1.036	1.685	1.868	0.0433	4.33	0.0433	0.6528
-21	-22	BM	RR=0.12, CR=0.40	-21.5	1	1.066	1.718	1.880	0.0405	4.05	0.0405	0.6094
-22	-23	BM	RR=0.12, CR=0.40	-22.5	1	1.096	1.752	1.895	0.0381	3.81	0.0381	0.5689
-23	-24	BM	RR=0.12, CR=0.40	-23.5	1	1.127	1.785	1.913	0.0360	3.60	0.0360	0.5309
-24	-25	BM	RR=0.12, CR=0.40	-24.5	1	1.157	1.819	1.933	0.0342	3.42	0.0342	0.4949
-25	-26	BM	RR=0.12, CR=0.40	-25.5	1	1.187	1.853	1.956	0.0327	3.27	0.0327	0.4607
-26	-27	BM	RR=0.12, CR=0.40	-26.5	1	1.217	1.886	1.982	0.0314	3.14	0.0314	0.4280
-27	-28	BM	RR=0.12, CR=0.40	-27.5	1	1.248	1.920	2.008	0.0303	3.03	0.0303	0.3966
-28	-29	BM	RR=0.12, CR=0.40	-28.5	1	1.278	1.953	2.037	0.0294	2.94	0.0294	0.3663
-29	-30	BM	RR=0.12, CR=0.40	-29.5	1	1.308	1.987	2.066	0.0286	2.86	0.0286	0.3370
-30	-31	BM	RR=0.12, CR=0.40	-30.5	1	1.339	2.021	2.097	0.0279	2.79	0.0279	0.3084
-31	-32	BM	RR=0.12, CR=0.40	-31.5	1	1.369	2.054	2.129	0.0274	2.74	0.0274	0.2805
-32	-33	BM	RR=0.12, CR=0.40	-32.5	1	1.399	2.088	2.162	0.0269	2.69	0.0269	0.2531
-33	-34	BM	RR=0.12, CR=0.40	-33.5	1	1.430	2.121	2.196	0.0266	2.66	0.0266	0.2261
-34	-35	BM	RR=0.12, CR=0.40	-34.5	1	1.460	2.155	2.231	0.0263	2.63	0.0263	0.1995
-35	-36	BM	RR=0.12, CR=0.40	-35.5	1	1.490	2.189	2.267	0.0262	2.62	0.0262	0.1732
-36	-37	BM	RR=0.12, CR=0.40	-36.5	1	1.520	2.222	2.305	0.0261	2.61	0.0261	0.1470
-37	-38	BM	RR=0.12, CR=0.40	-37.5	1	1.551	2.256	2.344	0.0262	2.62	0.0262	0.1209
-38	-39	BM	RR=0.12, CR=0.40	-38.5	1	1.581	2.289	2.385	0.0264	2.64	0.0264	0.0947
-39	-40	BM	RR=0.12, CR=0.40	-39.5	1	1.611	2.323	2.429	0.0268	2.68	0.0268	0.0683
-40	-41	BM	RR=0.12, CR=0.40	-40.5	1	1.642	2.357	2.476	0.0274	2.74	0.0274	0.0415
-41	-41.5	BM	RR=0.12, CR=0.40	-41.25	0.5	1.664	2.382	2.514	0.0281	2.81	0.0140	0.0140

Table B-5 1-D Consolidation Settlement Prediction at TS5 (computed with $0.9\sigma'_p$ profile)

TS5 $-0.9\sigma'_p$

Layers			Cons. Status	Computed Settlement : $\sigma'_{v0} \rightarrow \sigma'_{vc}$ TS5 with $0.9\sigma'_p$									
From EL. (ft)	To EL. (ft)	Soil type		Average EL. (ft)	Thickness of soil H_i[ft]	σ'_{v0} (ksf)	σ'_p(FV) (ksf)	$0.9\sigma'_p$(FV) (ksf)	σ'_{vc} TS5 (ksf)	ε	ε[%]	$\Delta\rho_c$ (ft)	ρ_c [ft]
-1.6	-4.5	Pavement											
-4.5	-6.2	Basecourse											
-6.2	-8	BM Crust	RR=0.06	-7.1	1.8	0.609	5.0689	4.5620	1.852	0.0290	2.90	0.0522	**1.5479**
-8	-9	BM Crust	RR=0.06	-8.5	1	0.662	3.300	2.9700	1.892	0.0274	2.74	0.0274	1.4957
-9	-10	BM Crust	RR=0.06	-9.5	1	0.699	2.747	2.4723	1.925	0.0264	2.64	0.0264	1.4684
-10	-11	BM	RR=0.06	-10.5	1	0.733	2.469	2.2221	1.952	0.0255	2.55	0.0255	1.4420
-11	**-12**	BM	RR=0.06, CR=0.40	-11.5	1	0.763	2.080	1.8720	1.957	0.0311	3.11	0.0311	1.4164
-12	-13	BM	RR=0.06, CR=0.40	-12.5	1	0.793	1.760	1.5840	1.928	0.0521	5.21	0.0521	1.3853
-13	-14	BM	RR=0.06, CR=0.40	-13.5	1	0.824	1.615	1.4537	1.903	0.0616	6.16	0.0616	1.3332
-14	-15	BM	RR=0.06, CR=0.40	-14.5	1	0.854	1.572	1.4145	1.884	0.0629	6.29	0.0629	1.2716
-15	-16	BM	RR=0.06, CR=0.40	-15.5	1	0.884	1.569	1.4125	1.870	0.0609	6.09	0.0609	1.2086
-16	-17	BM	RR=0.06, CR=0.40	-16.5	1	0.914	1.550	1.3952	1.861	0.0610	6.10	0.0610	1.1477
-17	-18	BM	RR=0.06, CR=0.40	-17.5	1	0.945	1.584	1.4254	1.856	0.0566	5.66	0.0566	1.0867
-18	-19	BM	RR=0.06, CR=0.40	-18.5	1	0.975	1.617	1.4557	1.856	0.0527	5.27	0.0527	1.0301
-19	-20	BM	RR=0.06, CR=0.40	-19.5	1	1.005	1.651	1.4859	1.860	0.0492	4.92	0.0492	0.9774
-20	-21	BM	RR=0.12, CR=0.40	-20.5	1	1.036	1.685	1.5161	1.868	0.0561	5.61	0.0561	0.9282
-21	-22	BM	RR=0.12, CR=0.40	-21.5	1	1.066	1.718	1.5464	1.880	0.0533	5.33	0.0533	0.8721
-22	-23	BM	RR=0.12, CR=0.40	-22.5	1	1.096	1.752	1.5766	1.895	0.0509	5.09	0.0509	0.8188
-23	-24	BM	RR=0.12, CR=0.40	-23.5	1	1.127	1.785	1.6069	1.913	0.0488	4.88	0.0488	0.7679
-24	-25	BM	RR=0.12, CR=0.40	-24.5	1	1.157	1.819	1.6371	1.933	0.0470	4.70	0.0470	0.7191
-25	-26	BM	RR=0.12, CR=0.40	-25.5	1	1.187	1.853	1.6673	1.956	0.0455	4.55	0.0455	0.6721
-26	-27	BM	RR=0.12, CR=0.40	-26.5	1	1.217	1.886	1.6976	1.982	0.0442	4.42	0.0442	0.6266
-27	-28	BM	RR=0.12, CR=0.40	-27.5	1	1.248	1.920	1.7278	2.008	0.0431	4.31	0.0431	0.5824
-28	-29	BM	RR=0.12, CR=0.40	-28.5	1	1.278	1.953	1.7581	2.037	0.0422	4.22	0.0422	0.5393
-29	-30	BM	RR=0.12, CR=0.40	-29.5	1	1.308	1.987	1.7883	2.066	0.0414	4.14	0.0414	0.4971
-30	-31	BM	RR=0.12, CR=0.40	-30.5	1	1.339	2.021	1.8185	2.097	0.0407	4.07	0.0407	0.4557
-31	-32	BM	RR=0.12, CR=0.40	-31.5	1	1.369	2.054	1.8488	2.129	0.0402	4.02	0.0402	0.4150
-32	-33	BM	RR=0.12, CR=0.40	-32.5	1	1.399	2.088	1.8790	2.162	0.0398	3.98	0.0398	0.3748
-33	-34	BM	RR=0.12, CR=0.40	-33.5	1	1.430	2.121	1.9093	2.196	0.0394	3.94	0.0394	0.3350
-34	-35	BM	RR=0.12, CR=0.40	-34.5	1	1.460	2.155	1.9395	2.231	0.0391	3.91	0.0391	0.2956
-35	-36	BM	RR=0.12, CR=0.40	-35.5	1	1.490	2.189	1.9697	2.267	0.0390	3.90	0.0390	0.2565
-36	-37	BM	RR=0.12, CR=0.40	-36.5	1	1.520	2.222	2.0000	2.305	0.0389	3.89	0.0389	0.2175
-37	-38	BM	RR=0.12, CR=0.40	-37.5	1	1.551	2.256	2.0302	2.344	0.0390	3.90	0.0390	0.1786
-38	-39	BM	RR=0.12, CR=0.40	-38.5	1	1.581	2.289	2.0605	2.385	0.0392	3.92	0.0392	0.1396
-39	-40	BM	RR=0.12, CR=0.40	-39.5	1	1.611	2.323	2.0907	2.429	0.0396	3.96	0.0396	0.1003
-40	-41	BM	RR=0.12, CR=0.40	-40.5	1	1.642	2.357	2.1209	2.476	0.0403	4.03	0.0403	0.0607
-41	-41.5	BM	RR=0.12, CR=0.40	-41.25	0.5	1.664	2.382	2.1436	2.514	0.0409	4.09	0.0204	0.0204

Table B-6 1-D Consolidation Settlement Prediction at TS5 (computed with $0.8\sigma'_p$ profile)

TS5 -0.8σ'$_p$

Layers			Cons. Status	Computed Settlement : $\sigma'_{vo} \rightarrow \sigma'_{vc}$ TS5 with $0.8\sigma'_p$									
From EL. (ft)	To EL. (ft)	Soil type		Average EL. (ft)	Thickness of soil H_i[ft]	σ'_{v0} (ksf)	σ'_p(FV) (ksf)	$0.8\sigma'_p$(FV) (ksf)	σ'_{vc} TS5 (ksf)	ε	ε[%]	$\Delta\rho_c$ (ft)	ρ_c [ft]
-1.6	-4.5	Pavement											
-4.5	-6.2	Basecourse											
-6.2	-8	BM Crust	RR=0.04	-7.1	1.8	0.609	5.0689	4.0551	1.852	0.0193	1.93	0.0348	**1.8648**
-8	-9	BM Crust	RR=0.04	-8.5	1	0.662	3.300	2.6400	1.892	0.0183	1.83	0.0183	1.8301
-9	-10	BM Crust	RR=0.04	-9.5	1	0.699	2.747	2.1976	1.925	0.0176	1.76	0.0176	1.8118
-10	-11	BM	RR=0.04	-10.5	1	0.733	2.469	1.9752	1.952	0.0170	1.70	0.0170	1.7942
-11	**-12**	BM	RR=0.04, CR=0.40	-11.5	1	0.763	2.080	1.6640	1.957	0.0417	4.17	0.0417	1.7772
-12	-13	BM	RR=0.04, CR=0.40	-12.5	1	0.793	1.760	1.4080	1.928	0.0645	6.45	0.0645	1.7355
-13	-14	BM	RR=0.04, CR=0.40	-13.5	1	0.824	1.615	1.2922	1.903	0.0751	7.51	0.0751	1.6710
-14	-15	BM	RR=0.04, CR=0.40	-14.5	1	0.854	1.572	1.2574	1.884	0.0770	7.70	0.0770	1.5959
-15	-16	BM	RR=0.04, CR=0.40	-15.5	1	0.884	1.569	1.2555	1.870	0.0753	7.53	0.0753	1.5189
-16	-17	BM	RR=0.04, CR=0.40	-16.5	1	0.914	1.550	1.2402	1.861	0.0758	7.58	0.0758	1.4436
-17	-18	BM	RR=0.04, CR=0.40	-17.5	1	0.945	1.584	1.2670	1.856	0.0714	7.14	0.0714	1.3678
-18	-19	BM	RR=0.04, CR=0.40	-18.5	1	0.975	1.617	1.2939	1.856	0.0676	6.76	0.0676	1.2964
-19	-20	BM	RR=0.04, CR=0.40	-19.5	1	1.005	1.651	1.3208	1.860	0.0642	6.42	0.0642	1.2288
-20	-21	BM	RR=0.08, CR=0.40	-20.5	1	1.036	1.685	1.3477	1.868	0.0659	6.59	0.0659	1.1646
-21	-22	BM	RR=0.08, CR=0.40	-21.5	1	1.066	1.718	1.3746	1.880	0.0632	6.32	0.0632	1.0987
-22	-23	BM	RR=0.08, CR=0.40	-22.5	1	1.096	1.752	1.4014	1.895	0.0609	6.09	0.0609	1.0355
-23	-24	BM	RR=0.08, CR=0.40	-23.5	1	1.127	1.785	1.4283	1.913	0.0590	5.90	0.0590	0.9745
-24	-25	BM	RR=0.08, CR=0.40	-24.5	1	1.157	1.819	1.4552	1.933	0.0573	5.73	0.0573	0.9155
-25	-26	BM	RR=0.08, CR=0.40	-25.5	1	1.187	1.853	1.4821	1.956	0.0559	5.59	0.0559	0.8582
-26	-27	BM	RR=0.08, CR=0.40	-26.5	1	1.217	1.886	1.5090	1.982	0.0548	5.48	0.0548	0.8022
-27	-28	BM	RR=0.08, CR=0.40	-27.5	1	1.248	1.920	1.5358	2.008	0.0538	5.38	0.0538	0.7475
-28	-29	BM	RR=0.08, CR=0.40	-28.5	1	1.278	1.953	1.5627	2.037	0.0530	5.30	0.0530	0.6936
-29	-30	BM	RR=0.08, CR=0.40	-29.5	1	1.308	1.987	1.5896	2.066	0.0523	5.23	0.0523	0.6406
-30	-31	BM	RR=0.08, CR=0.40	-30.5	1	1.339	2.021	1.6165	2.097	0.0518	5.18	0.0518	0.5883
-31	-32	BM	RR=0.08, CR=0.40	-31.5	1	1.369	2.054	1.6434	2.129	0.0514	5.14	0.0514	0.5365
-32	-33	BM	RR=0.08, CR=0.40	-32.5	1	1.399	2.088	1.6702	2.162	0.0510	5.10	0.0510	0.4851
-33	-34	BM	RR=0.08, CR=0.40	-33.5	1	1.430	2.121	1.6971	2.196	0.0507	5.07	0.0507	0.4341
-34	-35	BM	RR=0.08, CR=0.40	-34.5	1	1.460	2.155	1.7240	2.231	0.0506	5.06	0.0506	0.3834
-35	-36	BM	RR=0.08, CR=0.40	-35.5	1	1.490	2.189	1.7509	2.267	0.0505	5.05	0.0505	0.3328
-36	-37	BM	RR=0.08, CR=0.40	-36.5	1	1.520	2.222	1.7778	2.305	0.0505	5.05	0.0505	0.2823
-37	-38	BM	RR=0.08, CR=0.40	-37.5	1	1.551	2.256	1.8046	2.344	0.0507	5.07	0.0507	0.2318
-38	-39	BM	RR=0.08, CR=0.40	-38.5	1	1.581	2.289	1.8315	2.385	0.0510	5.10	0.0510	0.1811
-39	-40	BM	RR=0.08, CR=0.40	-39.5	1	1.611	2.323	1.8584	2.429	0.0515	5.15	0.0515	0.1301
-40	-41	BM	RR=0.08, CR=0.40	-40.5	1	1.642	2.357	1.8853	2.476	0.0522	5.22	0.0522	0.0786
-41	-41.5	BM	RR=0.08, CR=0.40	-41.25	0.5	1.664	2.382	1.9054	2.514	0.0529	5.29	0.0264	0.0264

Table B-7 1-D Final Consolidation Settlement Prediction at TS3 & TS5 (computed with σ'_p profile)

TS3&TS5 -σ'_p

Layers			Cons. Status	Computed Final Consolidation Settlement : $\sigma'_{vo} \rightarrow \sigma'_{vf}$ with σ'_p								
From EL. (ft)	To EL. (ft)	Soil type		Average EL. (ft)	Thickness of soil H_i[ft]	σ'_{v0} (ksf)	σ'_p(FV) (ksf)	σ'_{vf} (ksf)	ε	ε[%]	$\Delta\rho_c$ (ft)	ρ_c [ft]
-1.6	-4.5	Pavement										
-4.5	-6.2	Basecourse										
-6.2	-8	BM Crust	RR=0.06	-7.1	1.8	0.609	5.0689	1.851	0.0290	2.90	0.0521	**1.7611**
-8	-9	BM Crust	RR=0.06	-8.5	1	0.662	3.300	1.890	0.0274	2.74	0.0274	1.7090
-9	-10	BM Crust	RR=0.06	-9.5	1	0.699	2.747	1.918	0.0263	2.63	0.0263	1.6816
-10	-11	BM	RR=0.06	-10.5	1	0.733	2.469	1.947	0.0255	2.55	0.0255	1.6553
-11	**-12**	BM	RR=0.06	-11.5	1	0.763	2.080	1.975	0.0248	2.48	0.0248	1.6298
-12	-13	BM	RR=0.06, CR=0.40	-12.5	1	0.793	1.760	2.004	0.0433	4.33	0.0433	1.6050
-13	-14	BM	RR=0.06, CR=0.40	-13.5	1	0.824	1.615	2.032	0.0574	5.74	0.0574	1.5617
-14	-15	BM	RR=0.06, CR=0.40	-14.5	1	0.854	1.572	2.060	0.0629	6.29	0.0629	1.5043
-15	-16	BM	RR=0.06, CR=0.40	-15.5	1	0.884	1.569	2.087	0.0645	6.45	0.0645	1.4415
-16	-17	BM	RR=0.06, CR=0.40	-16.5	1	0.914	1.550	2.114	0.0676	6.76	0.0676	1.3770
-17	-18	BM	RR=0.06, CR=0.40	-17.5	1	0.945	1.584	2.140	0.0657	6.57	0.0657	1.3094
-18	-19	BM	RR=0.06, CR=0.40	-18.5	1	0.975	1.617	2.165	0.0638	6.38	0.0638	1.2437
-19	-20	BM	RR=0.06, CR=0.40	-19.5	1	1.005	1.651	2.189	0.0619	6.19	0.0619	1.1799
-20	-21	BM	RR=0.12, CR=0.40	-20.5	1	1.036	1.685	2.213	0.0727	7.27	0.0727	1.1179
-21	-22	BM	RR=0.12, CR=0.40	-21.5	1	1.066	1.718	2.236	0.0706	7.06	0.0706	1.0452
-22	-23	BM	RR=0.12, CR=0.40	-22.5	1	1.096	1.752	2.258	0.0685	6.85	0.0685	0.9745
-23	-24	BM	RR=0.12, CR=0.40	-23.5	1	1.127	1.785	2.279	0.0664	6.64	0.0664	0.9060
-24	-25	BM	RR=0.12, CR=0.40	-24.5	1	1.157	1.819	2.300	0.0643	6.43	0.0643	0.8396
-25	-26	BM	RR=0.12, CR=0.40	-25.5	1	1.187	1.853	2.320	0.0622	6.22	0.0622	0.7753
-26	-27	BM	RR=0.12, CR=0.40	-26.5	1	1.217	1.886	2.339	0.0602	6.02	0.0602	0.7130
-27	-28	BM	RR=0.12, CR=0.40	-27.5	1	1.248	1.920	2.357	0.0581	5.81	0.0581	0.6528
-28	-29	BM	RR=0.12, CR=0.40	-28.5	1	1.278	1.953	2.375	0.0561	5.61	0.0561	0.5947
-29	-30	BM	RR=0.12, CR=0.40	-29.5	1	1.308	1.987	2.392	0.0540	5.40	0.0540	0.5387
-30	-31	BM	RR=0.12, CR=0.40	-30.5	1	1.339	2.021	2.409	0.0520	5.20	0.0520	0.4847
-31	-32	BM	RR=0.12, CR=0.40	-31.5	1	1.369	2.054	2.426	0.0500	5.00	0.0500	0.4326
-32	-33	BM	RR=0.12, CR=0.40	-32.5	1	1.399	2.088	2.442	0.0481	4.81	0.0481	0.3826
-33	-34	BM	RR=0.12, CR=0.40	-33.5	1	1.430	2.121	2.457	0.0461	4.61	0.0461	0.3346
-34	-35	BM	RR=0.12, CR=0.40	-34.5	1	1.460	2.155	2.473	0.0442	4.42	0.0442	0.2885
-35	-36	BM	RR=0.12, CR=0.40	-35.5	1	1.490	2.189	2.489	0.0424	4.24	0.0424	0.2442
-36	-37	BM	RR=0.12, CR=0.40	-36.5	1	1.520	2.222	2.504	0.0405	4.05	0.0405	0.2019
-37	-38	BM	RR=0.12, CR=0.40	-37.5	1	1.551	2.256	2.520	0.0388	3.88	0.0388	0.1613
-38	-39	BM	RR=0.12, CR=0.40	-38.5	1	1.581	2.289	2.536	0.0371	3.71	0.0371	0.1226
-39	-40	BM	RR=0.12, CR=0.40	-39.5	1	1.611	2.323	2.552	0.0354	3.54	0.0354	0.0855
-40	-41	BM	RR=0.12, CR=0.40	-40.5	1	1.642	2.357	2.568	0.0338	3.38	0.0338	0.0501
-41	-41.5	BM	RR=0.12, CR=0.40	-41.25	0.5	1.664	2.382	2.581	0.0326	3.26	0.0163	0.0163

Table B-8 1-D Final Consolidation Settlement Prediction at TS3 & TS5 (computed with $0.9\sigma'_p$ profile)

TS3&TS5 -0.9σ'$_p$

Layers			Cons. Status	Computed Final Consolidation Settlement : $\sigma'_{vo} \rightarrow \sigma'_{vf}$ with $0.9\sigma'_p$									
From EL. (ft)	To EL. (ft)	Soil type		Average EL. (ft)	Thickness of soil H_i[ft]	σ'_{v0} (ksf)	σ'_p(FV) (ksf)	$0.9\sigma'_p$(FV) (ksf)	σ'_{vf} (ksf)	ε	ε[%]	$\Delta\rho_c$ (ft)	ρ_c [ft]
-1.6	-4.5	Pavement											
-4.5	-6.2	Basecourse											
-6.2	-8	BM Crust	RR=0.06	-7.1	1.8	0.609	5.0689	4.5620	1.851	0.0290	2.90	0.0521	**2.1689**
-8	-9	BM Crust	RR=0.06	-8.5	1	0.662	3.300	2.9700	1.890	0.0274	2.74	0.0274	2.1168
-9	-10	BM Crust	RR=0.06	-9.5	1	0.699	2.747	2.4723	1.918	0.0263	2.63	0.0263	2.0894
-10	-11	BM	RR=0.06	-10.5	1	0.733	2.469	2.2221	1.947	0.0255	2.55	0.0255	2.0631
-11	**-12**	BM	RR=0.06, CR=0.40	-11.5	1	0.763	2.080	1.8720	1.975	0.0327	3.27	0.0327	2.0377
-12	-13	BM	RR=0.06, CR=0.40	-12.5	1	0.793	1.760	1.5840	2.004	0.0589	5.89	0.0589	2.0050
-13	-14	BM	RR=0.06, CR=0.40	-13.5	1	0.824	1.615	1.4537	2.032	0.0730	7.30	0.0730	1.9461
-14	-15	BM	RR=0.06, CR=0.40	-14.5	1	0.854	1.572	1.4145	2.060	0.0784	7.84	0.0784	1.8731
-15	-16	BM	RR=0.06, CR=0.40	-15.5	1	0.884	1.569	1.4125	2.087	0.0800	8.00	0.0800	1.7947
-16	-17	BM	RR=0.06, CR=0.40	-16.5	1	0.914	1.550	1.3952	2.114	0.0832	8.32	0.0832	1.7147
-17	-18	BM	RR=0.06, CR=0.40	-17.5	1	0.945	1.584	1.4254	2.140	0.0813	8.13	0.0813	1.6315
-18	-19	BM	RR=0.06, CR=0.40	-18.5	1	0.975	1.617	1.4557	2.165	0.0794	7.94	0.0794	1.5503
-19	-20	BM	RR=0.06, CR=0.40	-19.5	1	1.005	1.651	1.4859	2.189	0.0775	7.75	0.0775	1.4709
-20	-21	BM	RR=0.12, CR=0.40	-20.5	1	1.036	1.685	1.5161	2.213	0.0856	8.56	0.0856	1.3934
-21	-22	BM	RR=0.12, CR=0.40	-21.5	1	1.066	1.718	1.5464	2.236	0.0834	8.34	0.0834	1.3078
-22	-23	BM	RR=0.12, CR=0.40	-22.5	1	1.096	1.752	1.5766	2.258	0.0813	8.13	0.0813	1.2244
-23	-24	BM	RR=0.12, CR=0.40	-23.5	1	1.127	1.785	1.6069	2.279	0.0792	7.92	0.0792	1.1430
-24	-25	BM	RR=0.12, CR=0.40	-24.5	1	1.157	1.819	1.6371	2.300	0.0771	7.71	0.0771	1.0638
-25	-26	BM	RR=0.12, CR=0.40	-25.5	1	1.187	1.853	1.6673	2.320	0.0751	7.51	0.0751	0.9867
-26	-27	BM	RR=0.12, CR=0.40	-26.5	1	1.217	1.886	1.6976	2.339	0.0730	7.30	0.0730	0.9116
-27	-28	BM	RR=0.12, CR=0.40	-27.5	1	1.248	1.920	1.7278	2.357	0.0709	7.09	0.0709	0.8386
-28	-29	BM	RR=0.12, CR=0.40	-28.5	1	1.278	1.953	1.7581	2.375	0.0689	6.89	0.0689	0.7677
-29	-30	BM	RR=0.12, CR=0.40	-29.5	1	1.308	1.987	1.7883	2.392	0.0668	6.68	0.0668	0.6988
-30	-31	BM	RR=0.12, CR=0.40	-30.5	1	1.339	2.021	1.8185	2.409	0.0648	6.48	0.0648	0.6320
-31	-32	BM	RR=0.12, CR=0.40	-31.5	1	1.369	2.054	1.8488	2.426	0.0628	6.28	0.0628	0.5672
-32	-33	BM	RR=0.12, CR=0.40	-32.5	1	1.399	2.088	1.8790	2.442	0.0609	6.09	0.0609	0.5043
-33	-34	BM	RR=0.12, CR=0.40	-33.5	1	1.430	2.121	1.9093	2.457	0.0589	5.89	0.0589	0.4435
-34	-35	BM	RR=0.12, CR=0.40	-34.5	1	1.460	2.155	1.9395	2.473	0.0570	5.70	0.0570	0.3846
-35	-36	BM	RR=0.12, CR=0.40	-35.5	1	1.490	2.189	1.9697	2.489	0.0552	5.52	0.0552	0.3275
-36	-37	BM	RR=0.12, CR=0.40	-36.5	1	1.520	2.222	2.0000	2.504	0.0534	5.34	0.0534	0.2723
-37	-38	BM	RR=0.12, CR=0.40	-37.5	1	1.551	2.256	2.0302	2.520	0.0516	5.16	0.0516	0.2190
-38	-39	BM	RR=0.12, CR=0.40	-38.5	1	1.581	2.289	2.0605	2.536	0.0499	4.99	0.0499	0.1674
-39	-40	BM	RR=0.12, CR=0.40	-39.5	1	1.611	2.323	2.0907	2.552	0.0482	4.82	0.0482	0.1175
-40	-41	BM	RR=0.12, CR=0.40	-40.5	1	1.642	2.357	2.1209	2.568	0.0466	4.66	0.0466	0.0693
-41	-41.5	BM	RR=0.12, CR=0.40	-41.25	0.5	1.664	2.382	2.1436	2.581	0.0454	4.54	0.0227	0.0227

Table B-9 1-D Final Consolidation Settlement Prediction at TS3 & TS5 (computed with $0.8\sigma'_p$ profile)

TS3&TS5 -$0.8\sigma'_p$

Layers			Cons. Status	Computed Final Consolidation Settlement : $\sigma'_{vo} \rightarrow \sigma'_{vf}$ with $0.8\sigma'_p$									
From EL. (ft)	To EL. (ft)	Soil type		Average EL. (ft)	Thickness of soil H_i[ft]	σ'_{v0} (ksf)	σ'_p(FV) (ksf)	$0.8\sigma'_p$(FV) (ksf)	s'vf (ksf)	ε	ε[%]	$\Delta\rho_c$ (ft)	ρ_c [ft]
-1.6	-4.5	Pavement											
-4.5	-6.2	Basecourse											
-6.2	-8	BM Crust	RR=0.06	-7.1	1.8	0.609	5.0689	4.0551	1.851	0.0290	2.90	0.0521	**2.6334**
-8	-9	BM Crust	RR=0.06	-8.5	1	0.662	3.300	2.6400	1.890	0.0274	2.74	0.0274	2.5813
-9	-10	BM Crust	RR=0.06	-9.5	1	0.699	2.747	2.1976	1.918	0.0263	2.63	0.0263	2.5539
-10	-11	BM	RR=0.06	-10.5	1	0.733	2.469	1.9752	1.947	0.0255	2.55	0.0255	2.5276
-11	**-12**	BM	RR=0.06, CR=0.40	-11.5	1	0.763	2.080	1.6640	1.975	0.0501	5.01	0.0501	2.5021
-12	-13	BM	RR=0.06, CR=0.40	-12.5	1	0.793	1.760	1.4080	2.004	0.0762	7.62	0.0762	2.4520
-13	-14	BM	RR=0.06, CR=0.40	-13.5	1	0.824	1.615	1.2922	2.032	0.0904	9.04	0.0904	2.3758
-14	-15	BM	RR=0.06, CR=0.40	-14.5	1	0.854	1.572	1.2574	2.060	0.0958	9.58	0.0958	2.2854
-15	-16	BM	RR=0.06, CR=0.40	-15.5	1	0.884	1.569	1.2555	2.087	0.0974	9.74	0.0974	2.1896
-16	-17	BM	RR=0.06, CR=0.40	-16.5	1	0.914	1.550	1.2402	2.114	0.1006	10.06	0.1006	2.0922
-17	-18	BM	RR=0.06, CR=0.40	-17.5	1	0.945	1.584	1.2670	2.140	0.0987	9.87	0.0987	1.9916
-18	-19	BM	RR=0.06, CR=0.40	-18.5	1	0.975	1.617	1.2939	2.165	0.0968	9.68	0.0968	1.8930
-19	-20	BM	RR=0.06, CR=0.40	-19.5	1	1.005	1.651	1.3208	2.189	0.0949	9.49	0.0949	1.7962
-20	-21	BM	RR=0.12, CR=0.40	-20.5	1	1.036	1.685	1.3477	2.213	0.0999	9.99	0.0999	1.7013
-21	-22	BM	RR=0.12, CR=0.40	-21.5	1	1.066	1.718	1.3746	2.236	0.0978	9.78	0.0978	1.6014
-22	-23	BM	RR=0.12, CR=0.40	-22.5	1	1.096	1.752	1.4014	2.258	0.0957	9.57	0.0957	1.5037
-23	-24	BM	RR=0.12, CR=0.40	-23.5	1	1.127	1.785	1.4283	2.279	0.0936	9.36	0.0936	1.4080
-24	-25	BM	RR=0.12, CR=0.40	-24.5	1	1.157	1.819	1.4552	2.300	0.0915	9.15	0.0915	1.3144
-25	-26	BM	RR=0.12, CR=0.40	-25.5	1	1.187	1.853	1.4821	2.320	0.0894	8.94	0.0894	1.2230
-26	-27	BM	RR=0.12, CR=0.40	-26.5	1	1.217	1.886	1.5090	2.339	0.0873	8.73	0.0873	1.1336
-27	-28	BM	RR=0.12, CR=0.40	-27.5	1	1.248	1.920	1.5358	2.357	0.0852	8.52	0.0852	1.0463
-28	-29	BM	RR=0.12, CR=0.40	-28.5	1	1.278	1.953	1.5627	2.375	0.0832	8.32	0.0832	0.9611
-29	-30	BM	RR=0.12, CR=0.40	-29.5	1	1.308	1.987	1.5896	2.392	0.0812	8.12	0.0812	0.8779
-30	-31	BM	RR=0.12, CR=0.40	-30.5	1	1.339	2.021	1.6165	2.409	0.0791	7.91	0.0791	0.7967
-31	-32	BM	RR=0.12, CR=0.40	-31.5	1	1.369	2.054	1.6434	2.426	0.0772	7.72	0.0772	0.7176
-32	-33	BM	RR=0.12, CR=0.40	-32.5	1	1.399	2.088	1.6702	2.442	0.0752	7.52	0.0752	0.6404
-33	-34	BM	RR=0.12, CR=0.40	-33.5	1	1.430	2.121	1.6971	2.457	0.0733	7.33	0.0733	0.5652
-34	-35	BM	RR=0.12, CR=0.40	-34.5	1	1.460	2.155	1.7240	2.473	0.0714	7.14	0.0714	0.4920
-35	-36	BM	RR=0.12, CR=0.40	-35.5	1	1.490	2.189	1.7509	2.489	0.0695	6.95	0.0695	0.4206
-36	-37	BM	RR=0.12, CR=0.40	-36.5	1	1.520	2.222	1.7778	2.504	0.0677	6.77	0.0677	0.3511
-37	-38	BM	RR=0.12, CR=0.40	-37.5	1	1.551	2.256	1.8046	2.520	0.0659	6.59	0.0659	0.2834
-38	-39	BM	RR=0.12, CR=0.40	-38.5	1	1.581	2.289	1.8315	2.536	0.0642	6.42	0.0642	0.2175
-39	-40	BM	RR=0.12, CR=0.40	-39.5	1	1.611	2.323	1.8584	2.552	0.0625	6.25	0.0625	0.1533
-40	-41	BM	RR=0.12, CR=0.40	-40.5	1	1.642	2.357	1.8853	2.568	0.0609	6.09	0.0609	0.0908
-41	-41.5	BM	RR=0.12, CR=0.40	-41.25	0.5	1.664	2.382	1.9054	2.581	0.0598	5.98	0.0299	0.0299

6.3 Appendix C: NHPL Plaxis Analysis Control Parameters

REPORT

September 14, 2006

User:	Massachusetts Institute of Technology
Title:	NHPL-A2
Comments:	8/08/06 NHPL – A2 Cracked Pavement,

Table of Contents

1. General Information 346
2. Geometry 347
3. Mesh data 349
4. Material data 350
5. Calculation phases 352

1. General Information

Table [1] Units

Type	Unit
Length	ft
Force	klb
Time	day

Table [2] Model dimensions

	min.	max.
X	-175.000	150.000
Y	-60.000	9.400

Table [3] Model

Model	Plane strain
Element	15-Noded

2. Geometry

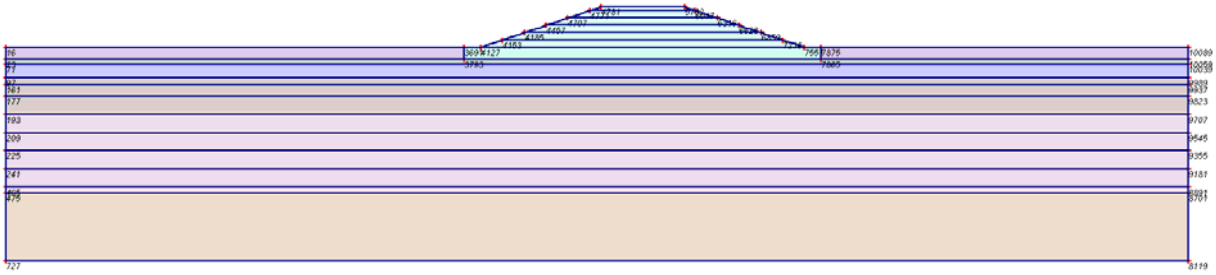

Fig. 1 Plot of geometry model with significant nodes

Table [4] Table of significant nodes

Node no.	x-coord.	y-coord.	Node no.	x-coord.	y-coord.
727	-175.000	-60.000	9707	150.000	-20.000
8119	150.000	-60.000	209	-175.000	-25.000
475	-175.000	-41.500	9545	150.000	-25.000
8701	150.000	-41.500	225	-175.000	-30.000
465	-175.000	-40.000	9355	150.000	-30.000
8891	150.000	-40.000	241	-175.000	-35.000
97	-175.000	-10.000	9181	150.000	-35.000
9989	150.000	-10.000	4153	-38.500	0.400
23	-175.000	-5.000	7216	38.500	0.400
10059	150.000	-5.000	4185	-32.500	2.400
16	-175.000	-1.600	6859	32.500	2.400
10089	150.000	-1.600	6628	26.500	4.400
4127	-44.500	-1.600	4457	-26.500	4.400
7551	44.500	-1.600	6316	20.500	6.400
4781	-11.500	9.400	4707	-20.500	6.400
5702	11.500	9.400	4771	-14.500	8.400
71	-175.000	-6.200	6017	14.500	8.400
10039	150.000	-6.200	161	-175.000	-12.000
9937	150.000	-12.000	3691	-49.000	-1.600
177	-175.000	-15.000	3793	-49.000	-5.000
9823	150.000	-15.000	7875	49.000	-1.600
193	-175.000	-20.000	7865	49.000	-5.000

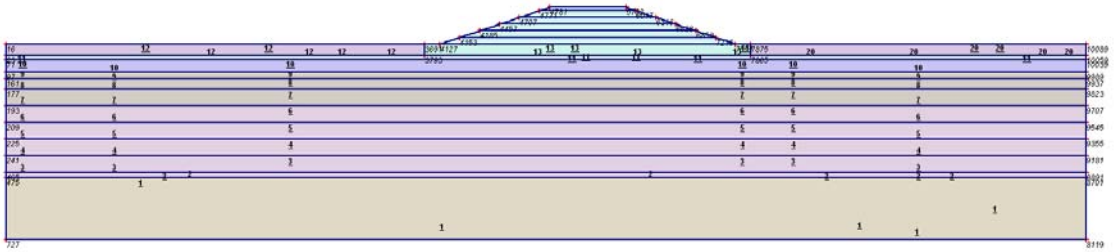

Fig. 2 Plot of geometry model with cluster numbers

Table [5] Table of clusters

Cluster no.	Nodes
1	727, 8119, 475, 8701.
2	475, 8701, 465, 8891.
3	465, 8891, 241, 9181.
4	225, 9355, 241, 9181.
5	209, 9545, 225, 9355.
6	193, 9707, 209, 9545.
7	177, 9823, 193, 9707.
8	9937, 177, 9823, 161.
9	97, 9989, 9937, 161.
10	97, 9989, 71, 10039.
11	23, 10059, 71, 10039, 3793, 7865.
12	23, 16, 3691, 3793.
13	4127, 7551, 3691, 3793, 7875, 7865.
14	4127, 7551, 4153, 7216.
15	4153, 7216, 4185, 6859.
16	4185, 6859, 6628, 4457.
17	6628, 4457, 6316, 4707.
18	6316, 4707, 4771, 6017.
19	4781, 5702, 4771, 6017.
20	10059, 10089, 7875, 7865.

3. Mesh data

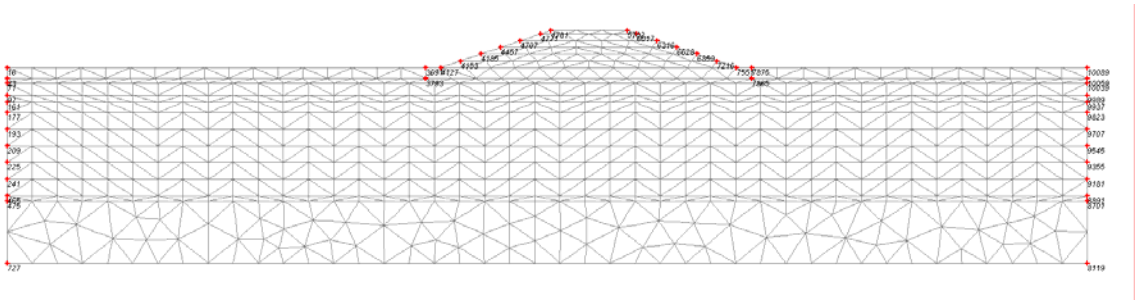

Fig. 3 Plot of the mesh with significant nodes

Table [6] Numbers, type of elements, integrations

Type	Type of element	Type of integration	Total no.
Soil	15-noded	12-point Gauss	1232

4. Material data

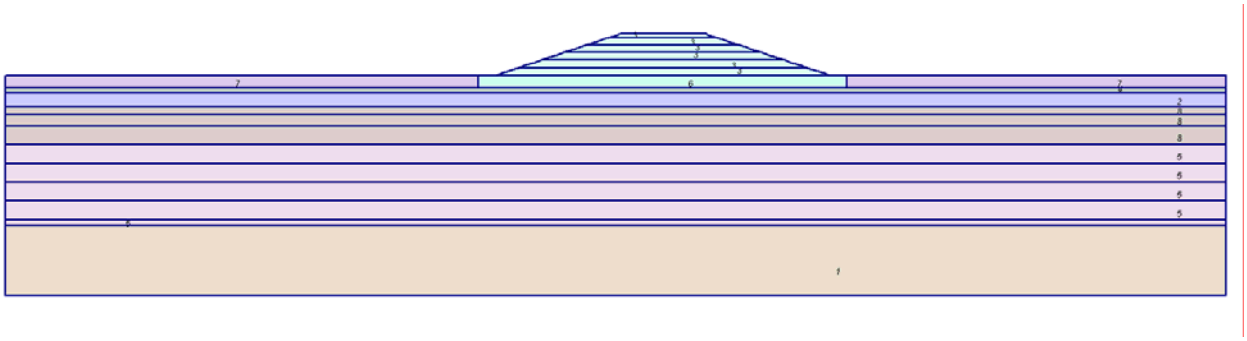

Fig. 4 Plot of geometry with material data sets

Table [7] Soil data sets parameters

Linear Elastic		1 Alluvium (below BM)
*Type		Undrained
γ_{unsat}	[klb/ft³]	0.13
γ_{sat}	[klb/ft³]	0.13
k_x	[ft/day]	0.001
k_y	[ft/day]	0.001
e_{init}	[-]	2.200
c_k	[-]	1E15
E_{ref}	[klb/ft²]	1000.00
ν	[-]	0.300
G_{ref}	[klb/ft²]	384.615
E_{oed}	[klb/ft²]	1346.154
E_{incr}	[klb/ft²/ft]	0.00
y_{ref}	[ft]	0.000
R_{inter}	[-]	1.000
Interface permeability		Neutral

Mohr-Coulomb		3 Levee Fill	4 Base Course	6 Cracked Pavement	7 Pavement
Type		Drained	Drained	Drained	Drained
γ_{unsat}	[klb/ft³]	0.13	0.15	0.15	0.15
γ_{sat}	[klb/ft³]	0.13	0.15	0.15	0.15
k_x	[ft/day]	0.100	1.000	1.000	1.000
k_y	[ft/day]	0.100	1.000	1.000	1.000
e_{init}	[-]	1.000	0.500	0.500	0.500
c_k	[-]	1E15	1E15	1E15	1E15
E_{ref}	[klb/ft²]	30.000	200.000	200.000	1000.000
ν	[-]	0.300	0.200	0.200	0.150
G_{ref}	[klb/ft²]	11.538	83.333	83.333	434.783
E_{oed}	[klb/ft²]	40.385	222.222	222.222	1055.901
c_{ref}	[klb/ft²]	0.02	0.03	0.03	0.02
φ	[°]	37.00	35.00	35.00	35.00
ψ	[°]	0.00	2.00	2.00	5.00
E_{inc}	[klb/ft²/ft]	0.00	0.00	0.00	0.00
y_{ref}	[ft]	0.000	0.000	0.000	0.000

Mohr-Coulomb		3 Levee Fill	4 Base Course	6 Cracked Pavement	7 Pavement
$c_{increment}$	[klb/ft²/ft]	0.00	0.00	0.00	0.00
$T_{str.}$	[klb/ft²]	0.00	0.00	0.00	0.00
$R_{inter.}$	[-]	1.00	1.00	1.00	1.00
Interface permeability		Neutral	Neutral	Neutral	Neutral

Soft-Soil		2 Bay Mud Crust	5 Bay Mud B	8 Bay Mud A
Type		Undrained	Undrained	Undrained
γ_{unsat}	[klb/ft³]	0.10	0.09	0.09
γ_{sat}	[klb/ft³]	0.10	0.09	0.09
k_x	[ft/day]	0.001	0.001	0.001
k_y	[ft/day]	0.001	0.001	0.001
e_{init}	[-]	2.50	2.50	2.50
c_k	[-]	1.40	1.40	1.40
λ^*	[-]	0.174	0.174	0.174
κ^*	[-]	0.052	0.104	0.052
c	[klb/ft²]	0.03	0.03	0.03
φ	[°]	25.00	25.00	25.00
ψ	[°]	0.00	0.00	0.00
ν_{ur}	[-]	0.260	0.260	0.260
K_0^{nc}	[-]	0.47	0.47	0.47
R_{inter}	[-]	1.00	1.00	1.00
Interface permeability		Neutral	Neutral	Neutral

5. Calculation phases

Table [8] List of phases

Phase	Ph-No.	Start phase	Calculation type	Load input	First step	Last step
Initial phase	0	0		-	0	0
1 st layer	1	0	Plastic	Staged construction	1	13
Consolidating 45 days	2	1	Consolidation	Staged Construction	14	20
2 nd layer	3	2	Plastic	Staged construction	21	36
Consolidating 45 days	4	3	Consolidation	Staged Construction	37	43
3 rd	5	4	Plastic	Staged construction	44	70
Consolidating 30 days	6	5	Consolidation	Staged Construction	71	74
4th	7	6	Plastic	Staged construction	75	102
Consolidating 30 days	8	7	Consolidation	Staged Construction	103	106
5th	9	8	Plastic	Staged construction	107	139
Consolidating 30 days	10	9	Consolidation	Staged Construction	140	142
6th	11	10	Plastic	Staged construction	143	164
Consolidating 30 days	12	11	Consolidation	Staged Construction	165	166
Consolidating to 2115	13	12	Consolidation	Staged Construction	167	175

Table [9] Staged construction info

Ph-No.	Active clusters	Inactive clusters	Active beams	Active geotextiles	Active anchors
0	1, 2, 3, 4, 5, 6, 7, 8, 9, 10, 11, 12, 13, 20.	14, 15, 16, 17, 18, 19.			
1	1, 2, 3, 4, 5, 6, 7, 8, 9, 10, 11, 12, 13, 14, 20.	15, 16, 17, 18, 19.			
3	1, 2, 3, 4, 5, 6, 7, 8, 9, 10, 11, 12, 13, 14, 15, 20.	16, 17, 18, 19.			
5	1, 2, 3, 4, 5, 6, 7, 8, 9, 10, 11, 12, 13, 14, 15, 16, 20.	17, 18, 19.			
7	1, 2, 3, 4, 5, 6, 7, 8, 9, 10, 11, 12, 13, 14, 15, 16, 17, 20.	18, 19.			
9	1, 2, 3, 4, 5, 6, 7, 8, 9, 10, 11, 12, 13, 14, 15, 16, 17, 18, 20.	19.			
11	1, 2, 3, 4, 5, 6, 7, 8, 9, 10, 11, 12, 13, 14, 15, 16, 17, 18, 19, 20.				

Table [10] Control parameters 1

Ph-No.	Additional steps	Reset displacements to zero	Ignore undrained behaviour	Delete intermediate steps
1	250	No	No	Yes
2	250	No	No	Yes
3	250	No	No	Yes
4	250	No	No	Yes
5	250	No	No	Yes
6	250	No	No	Yes
7	250	No	No	Yes
8	250	No	No	No
9	250	No	No	Yes
10	250	No	No	Yes
11	250	No	No	Yes
12	250	Yes	No	No
13	500	No	No	Yes

Table [11] Control parameters 2

Ph-No.	Iterative procedure	Tolerated error	Over relaxation	Max. iterations	Desired min.	Desired max.	Arc-Length control
1	Manual	0.001	1.200	60	6	15	Yes
2	Manual	0.001	1.200	60	6	15	Yes
3	Manual	0.001	1.200	60	6	15	Yes
4	Manual	0.001	1.200	60	6	15	Yes
5	Manual	0.001	1.200	60	6	15	Yes
6	Manual	0.001	1.200	60	6	15	Yes
7	Manual	0.001	1.200	60	6	15	Yes
8	Manual	0.001	1.200	60	6	15	Yes
9	Manual	0.001	1.200	60	6	15	Yes
10	Manual	0.001	1.200	60	6	15	Yes
11	Manual	0.001	1.200	60	6	15	Yes
12	Manual	0.001	1.200	60	6	15	Yes
13	Standard	0.010	1.200	60	6	15	Yes

Table [12] Incremental multipliers (input values)

Ph-No.	Displ.	Load A	Load B	Weight	Accel	Time	s-f
0	0.0000	0.0000	0.0000	0.0000	0.0000	0.0000	0.0000
1	0.0000	0.0000	0.0000	0.0000	0.0000	0.0000	0.0000
2	0.0000	0.0000	0.0000	0.0000	0.0000	45.0000	0.0000
3	0.0000	0.0000	0.0000	0.0000	0.0000	0.0000	0.0000
4	0.0000	0.0000	0.0000	0.0000	0.0000	45.0000	0.0000
5	0.0000	0.0000	0.0000	0.0000	0.0000	0.0000	0.0000
6	0.0000	0.0000	0.0000	0.0000	0.0000	30.0000	0.0000
7	0.0000	0.0000	0.0000	0.0000	0.0000	0.0000	0.0000
8	0.0000	0.0000	0.0000	0.0000	0.0000	30.0000	0.0000
9	0.0000	0.0000	0.0000	0.0000	0.0000	0.0000	0.0000
10	0.0000	0.0000	0.0000	0.0000	0.0000	30.0000	0.0000
11	0.0000	0.0000	0.0000	0.0000	0.0000	0.0000	0.0000
12	0.0000	0.0000	0.0000	0.0000	0.0000	30.0000	0.0000
13	0.0000	0.0000	0.0000	0.0000	0.0000	1905.0000	0.0000

Table [13] Total multipliers - input values

Ph-No.	Displ.	Load A	Load B	Weight	Accel	Time	s-f
0	1.0000	1.0000	1.0000	1.0000	0.0000	0.0000	1.0000
1	1.0000	1.0000	1.0000	1.0000	0.0000	0.0000	1.0000
2	1.0000	1.0000	1.0000	1.0000	0.0000	45.0000	1.0000
3	1.0000	1.0000	1.0000	1.0000	0.0000	45.0000	1.0000
4	1.0000	1.0000	1.0000	1.0000	0.0000	90.0000	1.0000
5	1.0000	1.0000	1.0000	1.0000	0.0000	90.0000	1.0000
6	1.0000	1.0000	1.0000	1.0000	0.0000	120.0000	1.0000
7	1.0000	1.0000	1.0000	1.0000	0.0000	120.0000	1.0000
8	1.0000	1.0000	1.0000	1.0000	0.0000	150.0000	1.0000
9	1.0000	1.0000	1.0000	1.0000	0.0000	150.0000	1.0000
10	1.0000	1.0000	1.0000	1.0000	0.0000	180.0000	1.0000
11	1.0000	1.0000	1.0000	1.0000	0.0000	180.0000	1.0000
12	1.0000	1.0000	1.0000	1.0000	0.0000	210.0000	1.0000
13	1.0000	1.0000	1.0000	1.0000	0.0000	2115.0000	1.0000

Table [14] Total multipliers - reached values

Ph-No.	Displ.	Load A	Load B	Weight	Accel	Time	s-f
0	1.0000	1.0000	1.0000	1.0000	0.0000	0.0000	1.0000
1	1.0000	1.0000	1.0000	1.0000	0.0000	0.0000	1.0000
2	1.0000	1.0000	1.0000	1.0000	0.0000	45.0000	1.0000
3	1.0000	1.0000	1.0000	1.0000	0.0000	45.0000	1.0000
4	1.0000	1.0000	1.0000	1.0000	0.0000	90.0000	1.0000
5	1.0000	1.0000	1.0000	1.0000	0.0000	90.0000	1.0000
6	1.0000	1.0000	1.0000	1.0000	0.0000	120.0000	1.0000
7	1.0000	1.0000	1.0000	1.0000	0.0000	120.0000	1.0000
8	1.0000	1.0000	1.0000	1.0000	0.0000	150.0000	1.0000
9	1.0000	1.0000	1.0000	1.0000	0.0000	150.0000	1.0000
10	1.0000	1.0000	1.0000	1.0000	0.0000	180.0000	1.0000
11	1.0000	1.0000	1.0000	1.0000	0.0000	180.0000	1.0000
12	1.0000	1.0000	1.0000	1.0000	0.0000	210.0000	1.0000
13	1.0000	1.0000	1.0000	1.0000	0.0000	2115.0000	1.0000

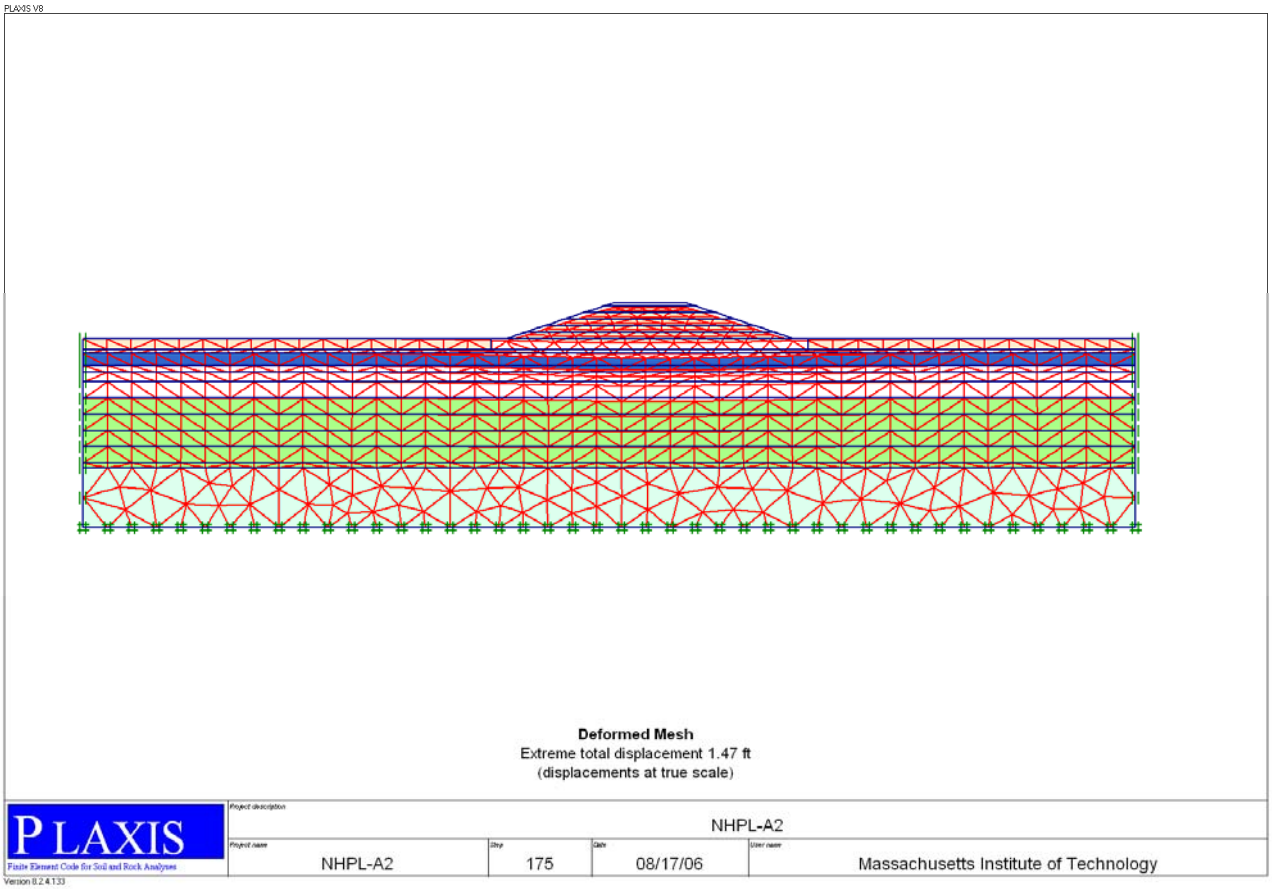

Fig. 5 Plot of geometry with deformed mesh & boundary conditions at CD2115

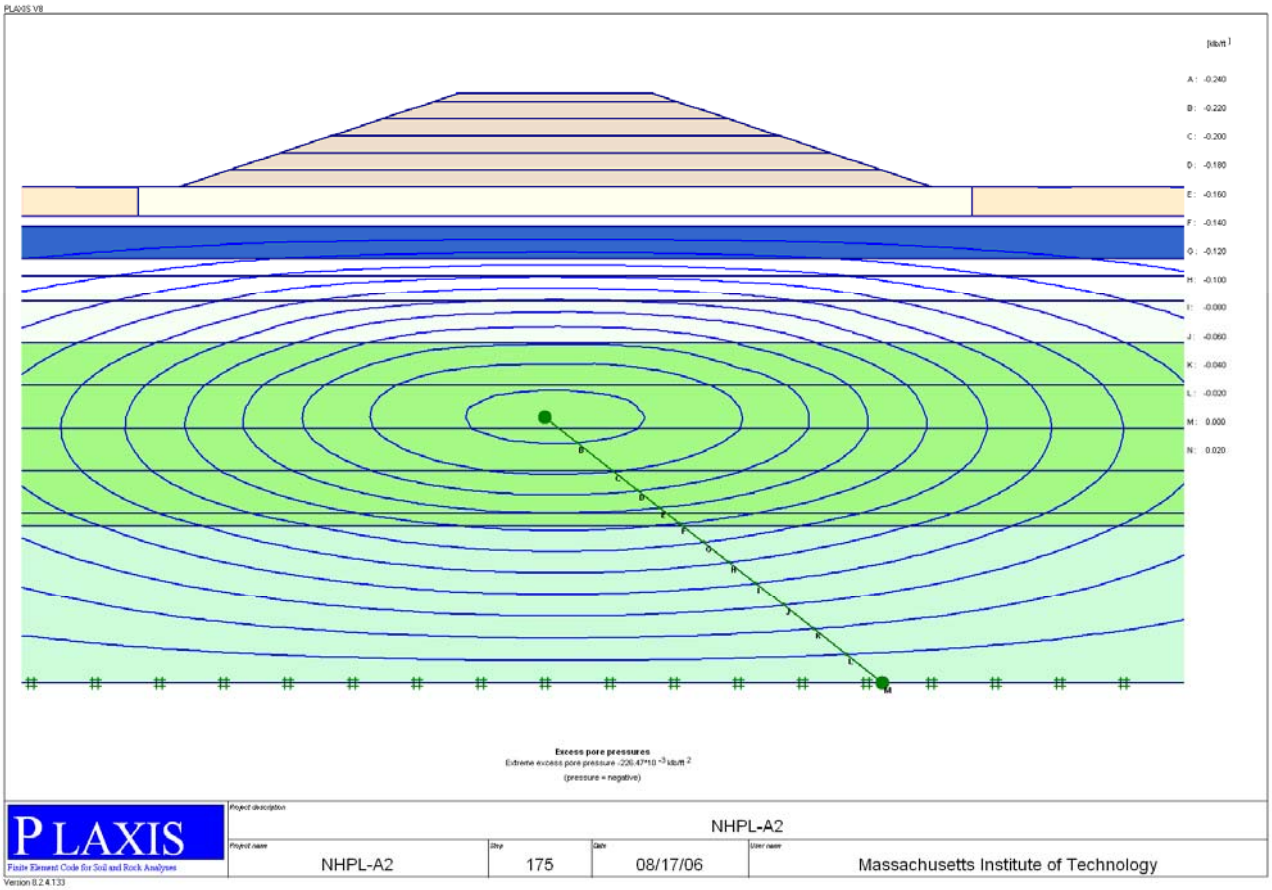

Fig. 6 Plot of geometry with excess pore pressure contours at CD2115

6.4 Appendix D: Author's Replication of URS (2003) Plaxis Analysis of NHPL

This Appendix presents a brief summary of an analysis performed by the Author to replicate finite element results presented by URS (2003) using Plaxis program. This work was done at the beginning of the current study prior to independent evaluation of the site conditions, soil properties and load history of the NHP levee. The results are included for completeness in documenting the research done on the NHP levee project.

Tables D1 through D5 summarize the input parameters for the Plaxis finite element (FE) model: The Bay Mud and Bay Mud Crust are modeled using the Soft Soil Model [Plaxis 2-D v. 8.2 (2002)], while other soil and pavement layers are treated as linearly elastic or linearly-elastic perfectly plastic (i.e., Mohr Coulomb) materials. Figures D1 and D2 give full details of the FE model geometry which includes the stiff clay, dense sand and Old Bay Mud beneath the soft Bay Mud. Note that the analysis was done for the reduced preconsolidation stress profile $0.8\sigma'_p$ (FV) for the Bay Mud and BM Crust.

Construction and consolidation of the NHP levee are simulated by staged construction as in table D6. The construction of the levee is implemented in two stages with two fill layers. The first fill layer is loaded and consolidated in 120 days following by the loading of second fill layer and consolidating in 90 days. The total construction time is 7 months. Note that URS (2003) did not present details of their simulation sequence. The Author selected 7 months for construction of the NHP levee based on the reported construction information.

Consolidation after end of construction are simulated in stages according to the reported results by URS (2003) in construction day (CD) after EOC, i.e., CD365= 1 yr, CD2035 ≈ 1/31/02 etc. Detailed construction phases are presented in Table D6.

The following results of the Author's replicate analysis are compared with URS (2003), including: consolidation settlement after EOC at the centerline of the levee (ρ_c vs. logt, Figure D3); horizontal profile of consolidation settlement of the pavement (ρ_c vs. distance from the centerline, Figure D4); excess pore pressure at the centerline of the levee, mid-depth of Bay Mud (u_e vs. logt at El. ≈ -26 ft, Figure D5); and vertical profiles of excess pore pressure at the centerline of the levee (Elevation vs. u_e, Figures D6). In conclusion, the comparisons of ρ_c and u_e show that the Author's replicate analysis results match well with those of URS (2003).

Table D1 Units

Type	Unit
Length	ft
Force	lb
Time	day

Table D2 Model dimensions

	min.	max.
X	-175.000	150.000
Y	-60.000	9.000

Table D3 Model

Model	Plane strain
Element	15-Noded

Table D4 URS (2003) Selected Soil Properties for Analysis

SUBSOIL LAYER	**No.**		**1**	**2**	**3**	**4**	**5**	**6**	**7**
	From EL.	[ft]	9	-2	-5	-10	-40	-44	-50
	To EL.	[ft]	-2	-5	-10	-40	-44	-50	-60
	Soil layer	-	**Levee Fill**	**Pavement**	**Bay Mud Crust**	**Bay Mud**	**Stiff Clay**	**Dense Sand**	**Old Bay Mud**
	Soil Model	-	MC	MC	SSM	SSM	Linear Elastic	Linear Elastic	Linear Elastic
	Type		Drained	Drained	Undrained	Undrained	Undrained	Drained	Undrained
Input parameters	γ_t	[pcf]	130	150	100	92	120	130	130
	e_0	[-]	-	-	1	1	-	-	-
	ν_{ur}	[-]	0.3	0.2	0.26	0.26	0.3	0.3	0.3
	E_ref	[ksf]	30	1000	-	-	1000	1000	2640
	c'	[ksf]	0.02	0.02	0.025	0.025			-
	ϕ'	[°]	37	35	30	30			-
	ψ'	[°]	0	5	0	0			-
	K_{0NC}	[-]			0.62	0.62			-
	M	[-]	-	-					-
	λ*	[-]	-	-	0.18 (CR=0.41)	0.18 (CR=0.41)			-
	κ*	[-]	-	-	0.035 (RR=0.04)	0.035 (RR=0.04)			-
	k_{vo}, k_{ho}	[ft/day]	0.1	1.0	4E-4; 8E-4	4E-4; 8E-4	4E-4; 8E-4	1.0; 1.0	4E-4; 8E-4
	C_k	[-]			1.14	1.14			

Table D5

Imposed OCR and K_0 in Sub-layers for Plaxis Analyses of the NHP Levee URS (2003)

Sub-layer					URS (2003)	
Soil	**From EL. [ft]**	**To EL. [ft]**	**Average EL. [ft]**	**σ'_p [ksf]**	**OCR**	**K_0**
Levee Fill	9	4	6.5		NA	0.5
	4	-2	1		NA	0.5
Pavement	-2	-4	-3		NA	0.5
	-4	-5	-4.5		NA	0.5
Bay Mud Crust	-5	-8	-6.5	3.520	6.000	1.68
	-8	-10	-9	2.886	4.200	1.3
BAY MUD	-10	-12	-11	2.019	2.700	1.08
	-12	-15	-13.5	1.449	1.760	0.82
	-15	-20	-17.5	1.584	1.550	0.77
	-20	-25	-22.5	1.752	1.410	0.73
	-25	-30	-27.5	1.920	1.320	0.71
	-30	-35	-32.5	2.088	1.250	0.69
	-35	-40	-37.5	2.256	1.200	0.67
Stiff Clay	-40	-44	-42		NA	1
Dense Sand	-44	-50	-47		NA	1
Old BM	-50	-60	-55		NA	1

Note: Water table EL. = -4.0 ft

Bay Mud K_0(NC) = 0.62

Table D6 Construction Phases

Phase	Ph-No.	Start phase	Calculation type	Load input	Time (Day)	Construction Time (Day)
Initial phase	0	0		-	0	0
Loading 1st Fill layer	1	0	Consolidation	Staged Construction	120	120
Loading 2nd Fill Layer	2	1	Consolidation	Staged Construction	90	210
1yr	3	2	Consolidation	Staged Construction	365	575
2yr	4	3	Consolidation	Staged Construction	365	940
5yr	5	4	Consolidation	Staged Construction	1095	2035
10yr	6	5	Consolidation	Staged Construction	1825	3860
20yr	7	6	Consolidation	Staged Construction	3650	7510
50yr	8	7	Consolidation	Staged Construction	10950	18460

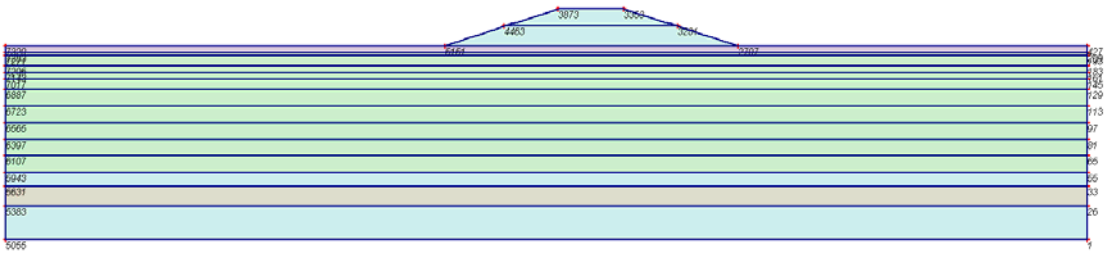

Fig. D1 Plot of geometry model with significant nodes

Table of significant nodes

Node no.	x-coord.	y-coord.	Node no.	x-coord.	y-coord.
5055	-175.000	-60.000	4463	-25.170	4.000
1	150.000	-60.000	3281	26.918	4.000
26	150.000	-50.000	7205	-175.000	-8.000
5383	-175.000	-50.000	183	150.000	-8.000
5631	-175.000	-44.000	7017	-175.000	-12.000
33	150.000	-44.000	145	150.000	-12.000
5943	-175.000	-40.000	6887	-175.000	-15.000
55	150.000	-40.000	129	150.000	-15.000
7143	-175.000	-10.000	6723	-175.000	-20.000
161	150.000	-10.000	113	150.000	-20.000
7271	-175.000	-5.000	6565	-175.000	-25.000
193	150.000	-5.000	97	150.000	-25.000
7320	-175.000	-2.000	6397	-175.000	-30.000
427	150.000	-2.000	81	150.000	-30.000
5151	-43.000	-2.000	6107	-175.000	-35.000
2707	45.000	-2.000	65	150.000	-35.000
3873	-9.000	9.000	7283	-175.000	-4.000
3353	10.628	9.000	209	150.000	-4.000

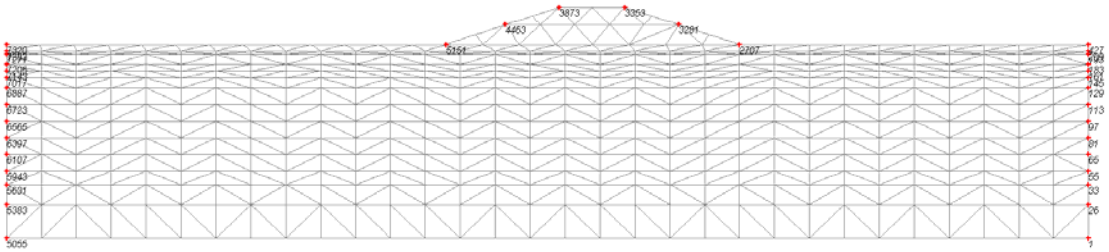

Fig.D2 Plot of the mesh with significant nodes

Numbers, type of elements, integrations

Type	Type of element	Type of integration	Total no.
Soil	15-noded	12-point Gauss	892

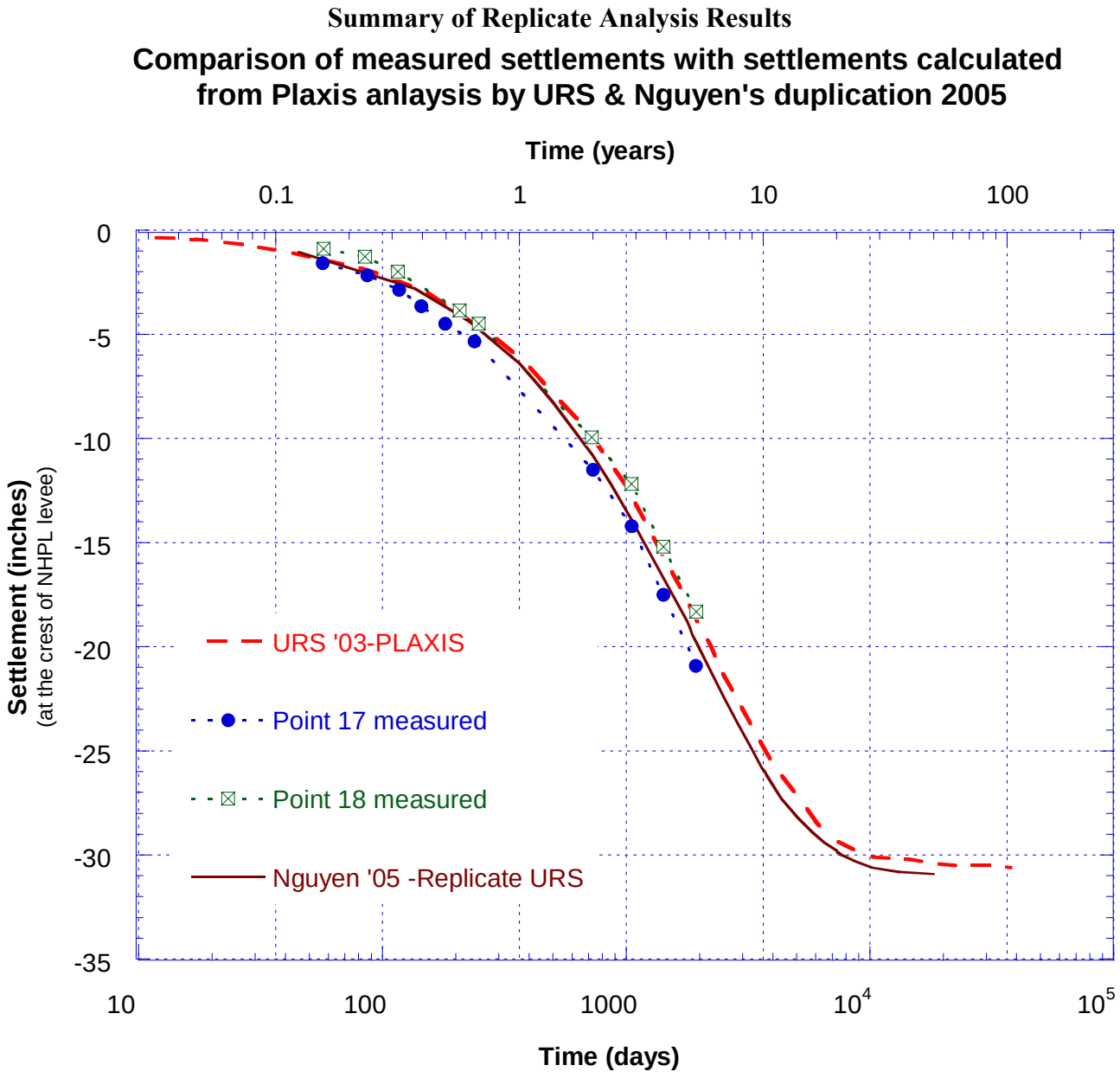

Data used for analysis at test section TS-3, NHPL Levee
Point 17 & 18 are adjacent to section TS-3

Figure D3: URS Plaxis Analysis Replicate – Settlement vs. log (time)

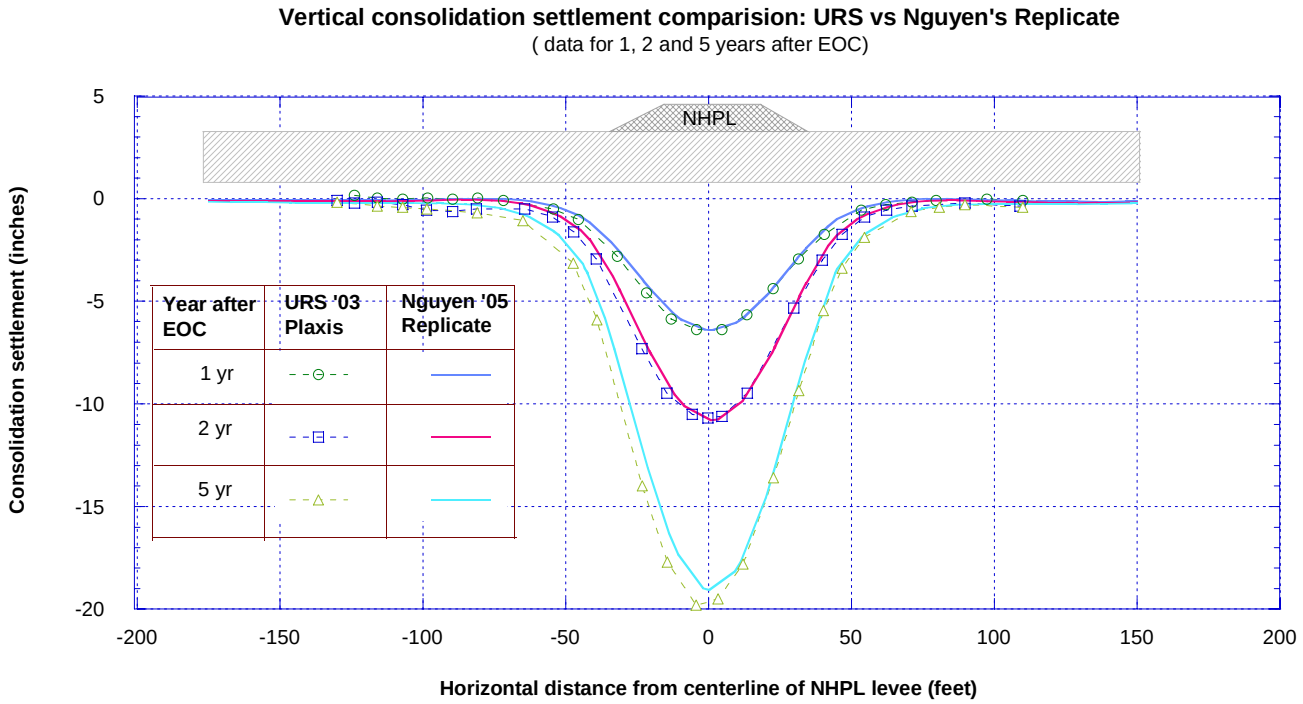

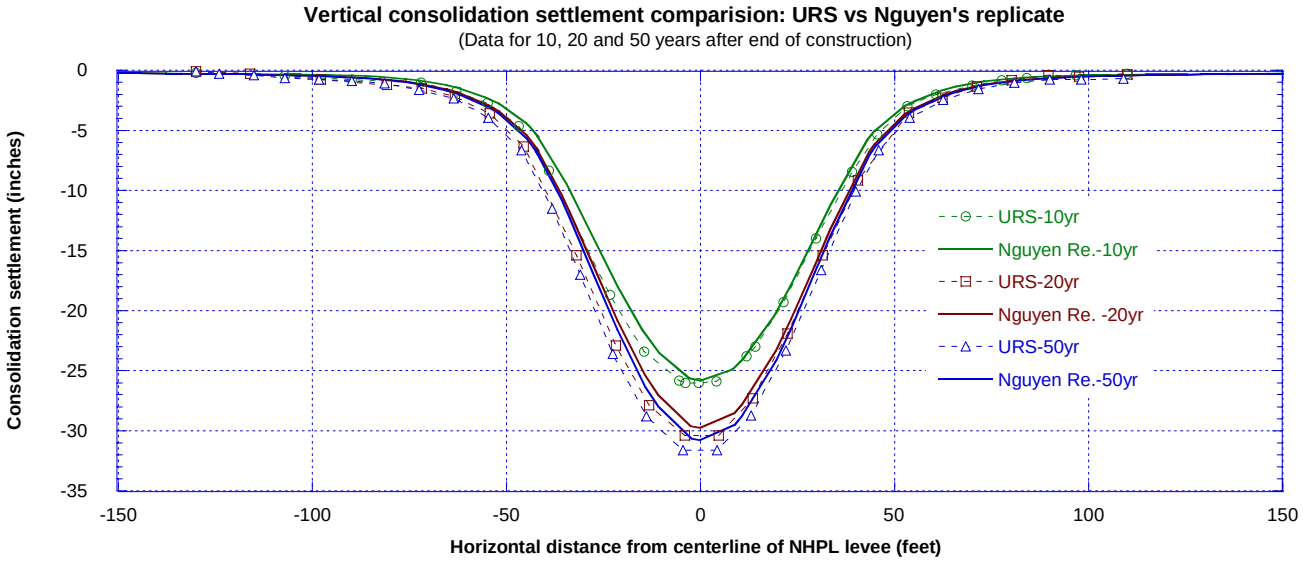

Figure D4: URS vs. Nguyen Replicate Plaxis Analysis - Comparison of Settlement

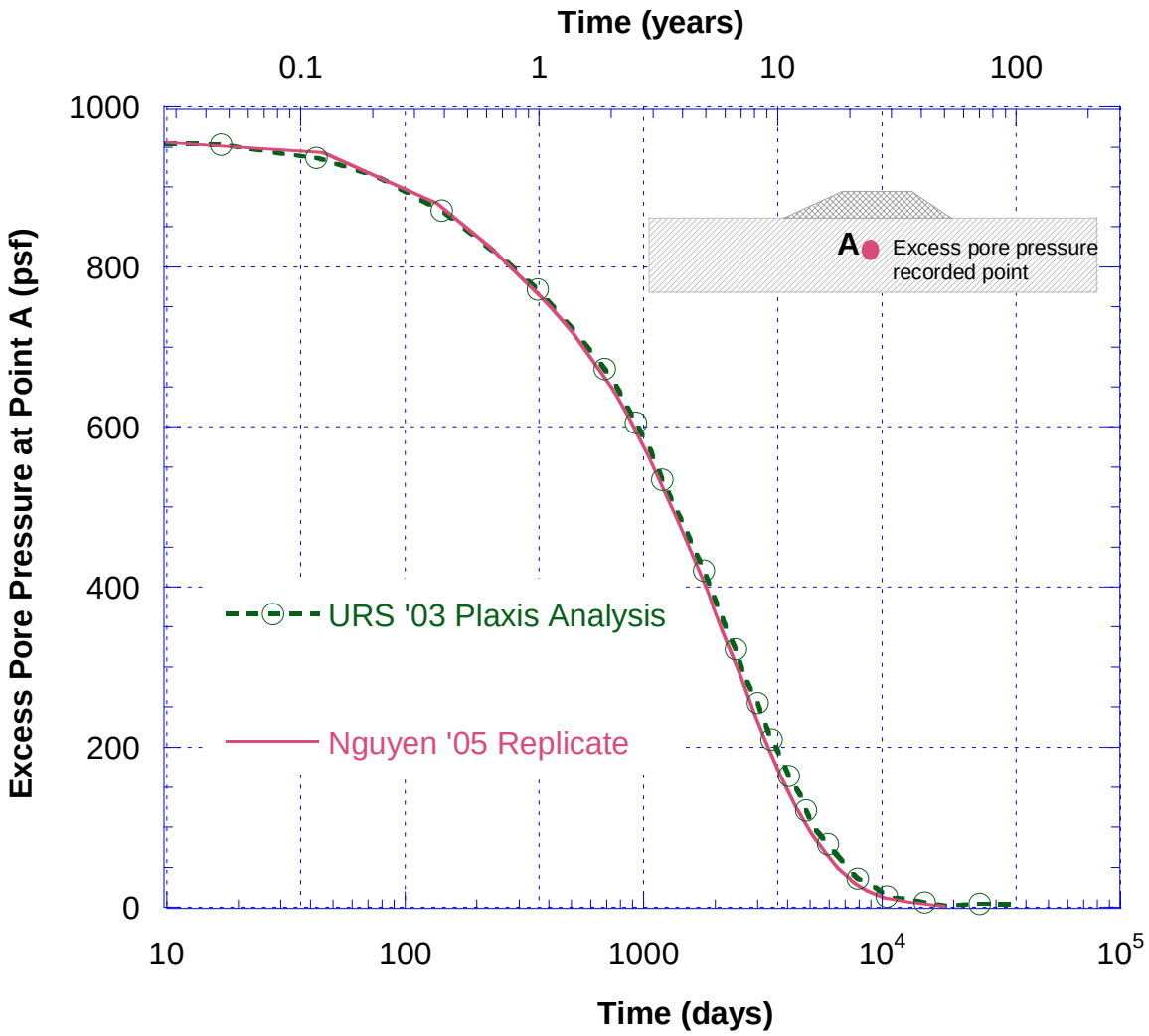

Figure D5: URS vs. Nguyen Replicate Plaxis Analysis - Comparison of Excess Pore Pressure Dissipation at Middle Point of Bay Mud

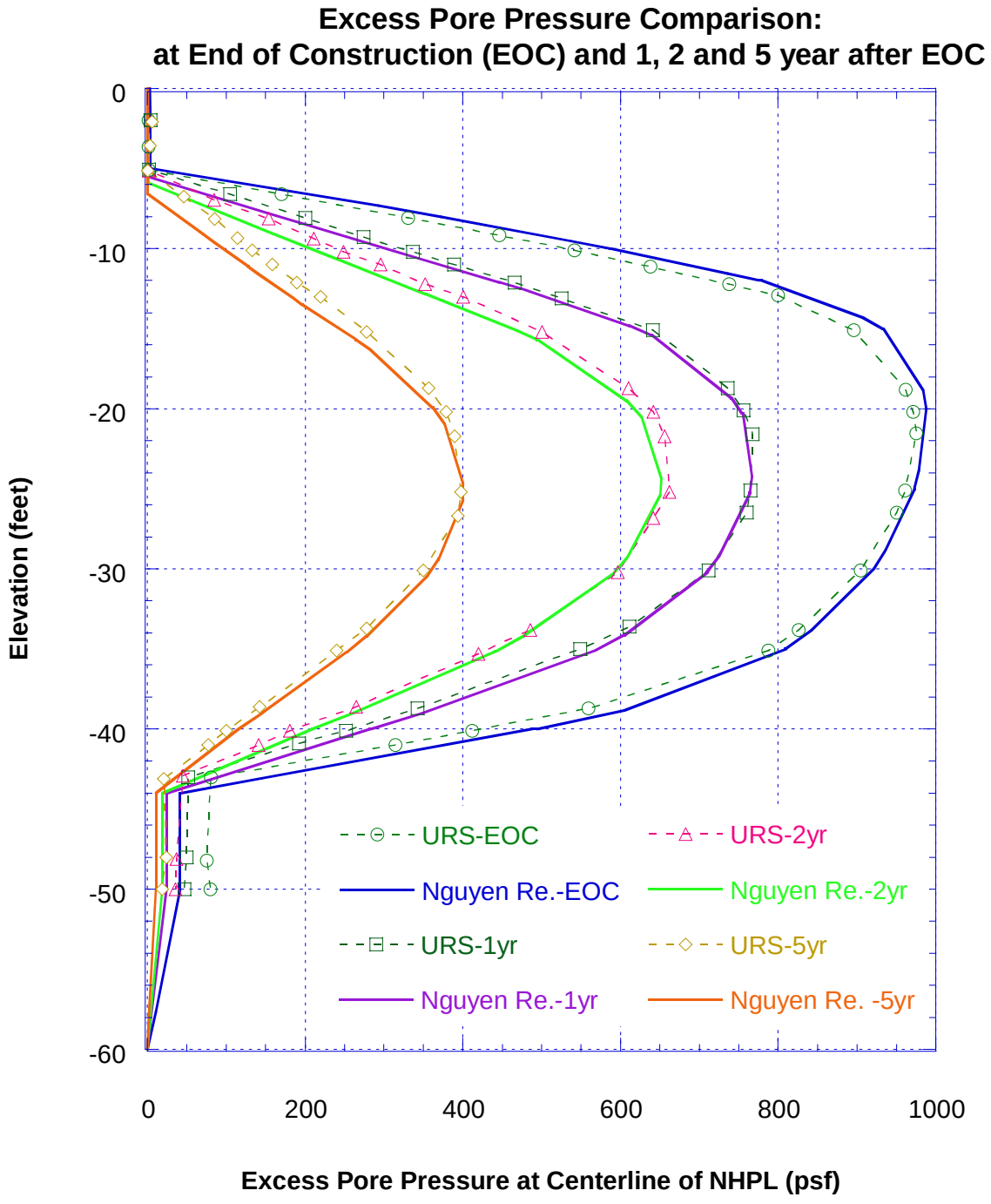

(a) Excess Pore Pressure Profile at Centerline of NHPL at End of Construction (EOC), 1, 2 and 5 years after EOC

Figure D6a: URS vs. Nguyen Replicate Plaxis Analysis - Comparison of Excess Pore Pressure in Bay Mud at Centerline of NHPL

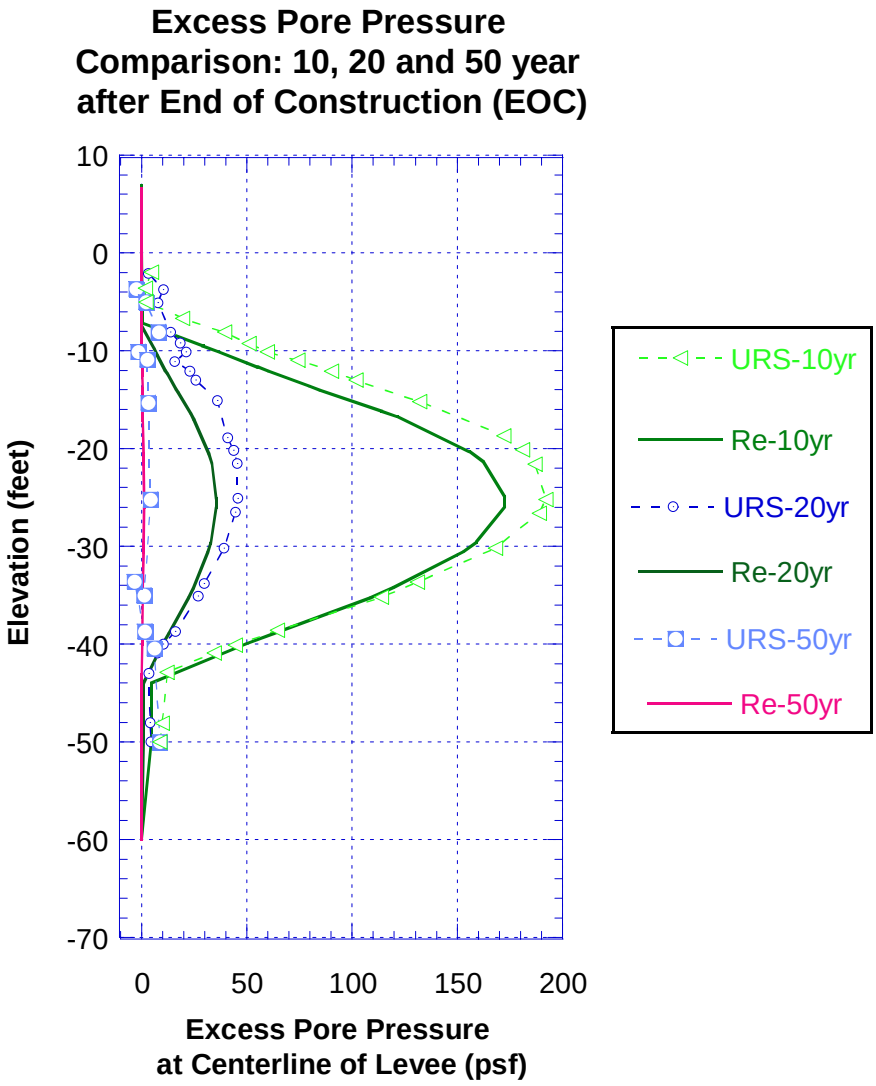

(b) Excess Pore Pressure Profile at Centerline of NHPL in 10, 20, and 50 years after EOC

Figure D6b: URS vs. Nguyen Replicate Plaxis Analysis - Comparison of Excess Pore Pressure Dissipation at Middle Point of Bay Mud